# Micro-grid design and dispatch co-optimisation considering uncertainties and demand response – Cases in New Zealand

by

Soheil Mohseni

A thesis
submitted to Victoria University of Wellington
in fulfilment of the requirements for the degree of
Doctor of Philosophy in Engineering.

Victoria University of Wellington
2021

# Abstract

One in eight people around the world, approximately one billion people, lack access to reliable electricity. Also, a great majority of people with access to electricity are experiencing some form of energy hardship – around a third (29%) of New Zealand households struggle to afford their electricity bills, spend a major part of their income on power, or often feel cold in winter. In this light, the ever-falling costs and continued efficiency improvements of renewable energy technologies are facilitating the 'clean energy for all' initiatives globally. Whilst considerable effort has been devoted to a range of interventions to address the underlying technological, institutional, and regulatory barriers, less attention has been given to address the glaring technical knowledge gaps in quantitative energy planning research, in terms of investment planning and capacity optimisation modelling; for the design of renewable energy systems, and specifically micro-grid systems. In response, this thesis addresses four notable gaps in the literature, namely: (i) the underrepresented usage of state-of-the-art meta-heuristic optimisation algorithms to determine the configurations of components, (ii) the lack of application of game-theoretic frameworks to the study of aggregator-mediated demand-side flexibility procurement, (iii) the limited number of approaches that quantify multiple parametric uncertainties simultaneously, and (iv) the narrow focus on joint micro-grid investment planning and energy scheduling optimisation.

To this end, the thesis introduces a novel strategic, meta-heuristic-based, demand response-integrated, uncertainty-aware, long-term micro-grid energy planning and capacity optimisation model, featuring the following key novel generalisations, each addressing one of the above-mentioned gaps: (i) utilising a state-of-the-art meta-heuristic optimisation algorithm, moth-flame optimiser, which is found to have superior performance to a wide variety of well-established and state-of-the-art meta-heuristics in minimising micro-grid life-cycle costs, (ii) characterising the utility-aggregator-customer interactions in interruptible load programmes using non-cooperative game theory in an equitable, market-based

approach, (iii) expanding the number of model-inherent parametric uncertainties quantified concurrently without excessive computational demands, and (iv) integrating a dynamic, forward-looking scheduling design framework for the co-optimisation of investment and operational planning costs.

To demonstrate the effectiveness of the model in yielding the cost-minimal mix of candidate renewable energy technologies considered for integration into a micro-grid system, the model was applied to four previously unexplored test cases. Four on- and off-grid 100%-renewable and -reliable micro-grid systems were specifically conceptualised for the following cases in New Zealand: (i) the community of 400 permanent inhabitants on Stewart Island, (ii) a rural community of about 350 people near Feilding, (iii) the eight-lot Totarabank Subdivision located in the Wairarapa District, and (iv) a 1,000-strong community in Ohakune that swells to 8,000 people during skiing season. Crucially, the case studies, undertaken on different scales and with different degrees of topological complexity, provide a robust evidence base to support the main research proposition that not only is it technically feasible to implement the smart, integrated renewable energy systems optimised by the proposed model, but they also surpass unsubsidised retail parity.

In particular, the thesis demonstrates that using the moth-flame optimisation algorithm, capturing the real flexibility potential of small- to medium-scale end-users, characterising multiple sources of data uncertainty, and adopting look-ahead, predictive dispatch strategies during the investment planning phases of stand-alone and grid-connected micro-grid systems, can pave the way toward achieving greater energy independence, -democracy, -resilience, and -security in rural and semi-urban areas in a cost-effective and environmentally efficient way. Most of all, the developed model provides in-depth, accurate, and robust strategic infrastructure planning decision-making support by adopting a holistic and comprehensive approach to energy planning optimisation. The approach enables a high-level, realistic analysis of the financial implications of the clean energy transition, especially in community-scale installations, necessary to cost-effectively promote private sector investment in the green economy – in the efforts to advance global electrification and economy-wide deep decarbonisation.

# Publications

A major part of this thesis draws on work from the author's published articles. In addition, an intellectual property (IP) disclosure has been submitted to Victoria University of Wellington's commercialisation office Wellington Univentures – Te Paewai and a patent application is scheduled to be filed.

## Author's contribution

For all articles, the author single-handedly executed the formulation of ideas, design of methodologies, gathering of input data, application of the proposed methods to test-case systems via numerical simulations, as well as formal analyses and model validations (>95% of the work). The co-authors contributed by minor wording and language editing before submission (<5% of the work). All the articles are therefore based on original research the author conducted under supervision during the period of enrolment.

## Peer-reviewed journal publications

1. **S. Mohseni**, A.C. Brent, and D. Burmester, "Off-Grid Multi-Carrier Microgrid Design Optimisation: The Case of Rakiura–Stewart Island, Aotearoa–New Zealand," *Energies* (Impact Factor = 3.0),[1] vol. 14, no. 20. p. 6522, 2021. Available at: https://doi.org/10.3390/en14206522

2. **S. Mohseni**, A.C. Brent, S. Kelly, W. Browne, and D. Burmester, "Strategic design optimisation of multi-energy-storage-technology micro-grids considering a two-stage game-theoretic market for demand response aggregation," *Applied Energy* (Impact Factor = 9.7), vol. 287, p. 116563, 2021. Available at: https://doi.org/10.1016/j.apenergy.2021.116563

[1] The impact factors presented in this thesis are based on the 2021 Journal Citation Reports.

3. **S. Mohseni**, A.C. Brent, S. Kelly, W. Browne, and D. Burmester, "Modelling utility-aggregator-customer interactions in interruptible load programmes using non-cooperative game theory," *International Journal of Electrical Power and Energy Systems* (Impact Factor = 4.6), vol. 133, p. 107183, 2021. Available at: https://doi.org/10.1016/j.ijepes.2021.107183

4. **S. Mohseni**, A.C. Brent, D. Burmester, and W. Browne, "Lévy-flight moth-flame optimisation algorithm-based micro-grid equipment sizing: An integrated investment and operational planning approach," *Energy and AI* (Impact Factor = N/A),[2] vol. 3, p. 100047, 2021. Available at: https://doi.org/10.1016/j.egyai.2021.100047

5. **S. Mohseni**, A.C. Brent, and D. Burmester, "A comparison of metaheuristics for the optimal capacity planning of an isolated, battery-less, hydrogen-based micro-grid," *Applied Energy* (Impact Factor = 9.7), vol. 259, p. 114224, 2020. Available at: https://doi.org/10.1016/j.apenergy.2019.114224

6. **S. Mohseni** and A.C. Brent, "Economic viability assessment of sustainable hydrogen production, storage, and utilisation technologies integrated into on- and off-grid micro-grids: A performance comparison of different meta-heuristics," *International Journal of Hydrogen Energy* (Impact Factor = 5.8), vol. 45, no. 59, pp. 34412–34436, 2020. Available at: https://doi.org/10.1016/j.ijhydene.2019.11.079

7. **S. Mohseni**, A.C. Brent, and D. Burmester, "Community Resilience-Oriented Optimal Micro-Grid Capacity Expansion Planning: The Case of Totarabank Eco-Village, New Zealand," *Energies* (Impact Factor = 3.0), vol. 13, no. 15. p. 3970, 2020. Available at: https://doi.org/10.3390/en13153970

8. **S. Mohseni**, A.C. Brent, and D. Burmester, "A demand response-centred approach to the long-term equipment capacity planning of grid-independent

[2] The newly established journal *Energy and AI* is the first journal dedicated to the current and future applications of AI in the energy and utilities sector, across the entire energy industry value chain. This made this journal the first choice for this article, despite it not having been assigned an impact factor yet.

micro-grids optimized by the moth-flame optimization algorithm," *Energy Conversion and Management* (Impact Factor = 9.7), vol. 200, p. 112105, 2019. Available at: https://doi.org/10.1016/j.enconman.2019.112105

## Peer-reviewed conference publications

1. **S. Mohseni**, A.C. Brent, D. Burmester, W. Browne, and S. Kelly "Adding a Computationally-Tractable Probabilistic Dimension to Meta-Heuristic-Based Microgrid Sizing," In: *Proceedings of the 2021 IEEE Region 10 Conference (TENCON)* (H-index = 38),[3] Auckland, New Zealand, 7–10 Dec. 2021, Accepted, In Press.
2. **S. Mohseni** and A.C. Brent, "Communications Technologies and Systems to Implement Coordinated, Aggregator-Mediated Demand Response in New Zealand," In: *Proceedings of the 2021 Electricity Engineers' Association (EEA) Conference & Exhibition* (H-index = N/A),[4] Wellington, New Zealand, 2–4 Aug. 2021, Accepted, In Press.
3. **S. Mohseni**, A.C. Brent, and S. Kelly, "A hierarchical, market-based, non-cooperative game-theoretic approach to projecting flexible demand-side resources: Towards more realistic demand response-integrated, long-term energy planning models," In: *Proceedings of the 2020 17th International Conference on the European Energy Market (EEM)* (H-index = 15), Stockholm, Sweden, 16–18 Sep. 2020, pp. 1–6. Available at: https://doi.org/10.1109/EEM49802.2020.9221977
4. **S. Mohseni**, A.C. Brent, D. Burmester, and W. Browne, "A Game-Theoretic Approach to Model Interruptible Loads: Application to Micro-Grid Planning," In: *Proceedings of the 2020 IEEE Power & Energy Society General Meeting (PESGM)* (H-index = 47), Montreal, Canada, 3–7 Aug. 2020, pp. 1–5. Available at: https://doi.org/10.1109/PESGM41954.2020.9281836

[3] The H-index values of the conference proceedings are reported from the SCImago Journal & Country Rank portal and refer to all the full proceedings of the conferences since their inceptions.

[4] The EEA Conference is New Zealand's largest technical power industry event. This made this conference the first choice for this article, despite the lack of information about its citation statistics.

5. **S. Mohseni**, A.C. Brent, and D. Burmester, "Power Quality Considerations in the Planning Phase of Stand-Alone Wind-Powered Micro-Grids," In: *Proceedings of the 2020 International Conference on Harmonics & Quality of Power* (H-index = 26), Dubai, UAE, 6–7 Jul. 2020, pp. 1–6. Available at: https://doi.org/10.1109/ICHQP46026.2020.9177937

6. **S. Mohseni**, A.C. Brent, D. Burmester, and A. Chatterjee, "Stochastic optimal sizing of micro-grids using the moth-flame optimization algorithm," In: *Proceedings of the 2019 IEEE Power & Energy Society General Meeting (PESGM)* (H-index = 47), Atlanta, GA, USA, 4–8 Aug. 2019, pp. 1–5. Available at: https://doi.org/10.1109/PESGM40551.2019.8973570

7. **S. Mohseni**, A.C. Brent, and D. Burmester, "A sustainable energy investment planning model based on the micro-grid concept using recent metaheuristic optimization algorithms," In: *Proceedings of the 2019 IEEE Congress on Evolutionary Computation (CEC)* (H-index = 46), Wellington, New Zealand, 10–13 Jun. 2019, pp. 219–226. Available at: https://doi.org/10.1109/CEC.2019.8790007

8. **S. Mohseni**, A.C. Brent, and D. Burmester, "A Reliability-Oriented Cost Optimisation Method for Capacity Planning of a Multi-Carrier Micro-Grid: A Case Study of Stewart Island, New Zealand," In: *Proceedings of the 2019 Electricity Engineers' Association (EEA) Conference & Exhibition* (H-index = N/A), Auckland, New Zealand, 25–27 Jun. 2019, pp. 1–10. Available at: https://arxiv.org/abs/1906.09544

9. **S. Mohseni**, A.C. Brent, D. Burmester, and A. Chatterjee, "Optimal sizing of an islanded micro-grid using meta-heuristic optimization algorithms considering demand-side management," In: *Proceedings of the 2018 Australasian Universities Power Engineering Conference (AUPEC)* (H-index = 13), Auckland, New Zealand, 27–30 Nov. 2018, pp. 1–6. Available at: https://doi.org/10.1109/AUPEC.2018.8757882

# Acknowledgements

First and foremost, I wish to thank my wife, Maral Mehdizad. Thank you for your continued support during this PhD journey. For your time, patience, understanding, and love I am truly grateful. This research would not have completed as it did without you.

I would like to thank my Mum and Dad, Lida and Hamid – both of whom are excellent teachers in their own rights – for their love and support. It is astounding how you quietly taught me that hard work, determination, and perseverance always win out. To me, this means that this thesis is not my, but your accomplishment.

I would like to thank my supervisors, Professor Alan Brent, Doctor Daniel Burmester, and Professor Will Browne, for their willingness to take on the supervision of my PhD proposal, as well as their wisdom, guidance, and feedback throughout this PhD. Thank you, Alan, for your pragmatic way of removing all the hurdles I needed to be removed, and for always having my back in Wellington. Living in Wellington has opened many doors that would not have been achievable without your support.

I also would like to thank my master's thesis supervisor, Associate Professor Seyed Masoud Moghaddas-Tafreshi, who set me on the road to where I am now – and whose expertise in modelling renewable and sustainable energy systems I have dwelled on materially over the last five years.

I wish to acknowledge Associate Professor Scott Kelly for being an accomplished and enthusiastic co-author of several of my academic papers; his input, ideas, and insights have benefitted the overall presentation and clarity of those papers, whilst additionally opening up new research avenues for me to explore in future studies.

I also wish to acknowledge all anonymous reviewers of my academic papers, as well as the various conference audiences I presented to, for their insightful comments, which improved the quality of this research.

Finally, I would like to thank the Victoria Doctoral Scholarship for the financial support that allowed me to devote time to my research interests.

# Table of Contents

# List of figures

# List of tables

# List of acronyms

| | |
|---|---|
| *ABC* | Artificial Bee Colony |
| *ACO* | Ant Colony Optimisation |
| *AI* | Artificial Intelligence |
| *ALO* | Ant Lion Optimiser |
| *AMI* | Advanced Metering Infrastructure |
| *BA* | Bat Algorithm |
| *BAU* | Business-As-Usual |
| *BB-BC* | Big Bang-Big Crunch |
| *BESS* | Battery Energy Storage System |
| *CHP* | Combined Heat and Power |
| *CPP* | Critical Peak Pricing |
| *CSA* | Cuckoo Search Algorithm |
| *DA* | Dragonfly Algorithm |
| *DERs* | Distributed Energy Resources |
| *DOD* | Depth of Discharge |
| *DPI* | Discounted Profitability Index |
| *DPP* | Discounted Payback Period |
| *DR* | Demand Response |
| *DRA* | Demand Response Aggregator |
| *DSM* | Demand-Side Management |
| *EaaS* | Energy-as-a-Service |
| *EDLC* | Electrochemical Double-Layer Capacitor |
| *EP* | Evening Peak |
| *EV* | Electric Vehicle |
| *FA* | Firefly Algorithm |
| *FCEV* | Fuel Cell Electric Vehicle |
| *FCEV2G* | Fuel cell Electric Vehicle in Vehicle-to-Grid Operation |
| *FRMP* | Financially Responsible Market Participant |

| | |
|---|---|
| *GA* | Genetic Algorithm |
| *GHG* | Green-House Gas |
| *GOA* | Grasshopper Optimisation Algorithm |
| *GSA* | Gravitational Search Algorithm |
| *GWO* | Grey Wolf Optimiser |
| *HABC-ACO* | Hybrid Artificial Bee Colony-Ant Colony Optimisation |
| *HGA-PSO* | Hybrid Genetic Algorithm-Particle Swarm Optimisation |
| *HSA* | Harmony Search Algorithm |
| *ICTs* | Information and Communication Technologies |
| *IEA* | International Energy Agency |
| *IHSA* | Improved Harmony Search Algorithm |
| *IRENA* | International Renewable Energy Agency |
| *IRR* | Internal Rate of Return |
| *LCOE* | Levelised Cost of Energy |
| *LCOEE* | Levelised Cost of Electric Energy |
| *LCOH* | Levelised Cost of Hydrogen |
| *LP* | Linear Programming |
| *LPSP* | Loss of Power Supply Probability |
| *Li-ion* | Lithium-ion |
| *MBI* | Market-Based Integration |
| *MCS* | Monte Carlo Simulation |
| *MFOA* | Moth-Flame Optimisation Algorithm |
| *MG* | Micro-Grid |
| *MH* | Micro-Hydro |
| *MILP* | Mixed-Integer Linear Programming |
| *MINLP* | Mixed-Integer Nonlinear Programming |
| *MIP* | Mixed-Integer Programming |
| *MIRR* | Modified Internal Rate of Return |
| *MP* | Morning Peak |
| *MSW* | Municipal Solid Waste |
| *MVO* | Multi-Verse Optimiser |
| *NFL* | No-Free-Lunch |

| | |
|---|---|
| *NIWA* | National Institute of Water and Atmospheric research |
| *NP-hard* | Non-deterministic Polynomial time-hard |
| *NPC* | Net Present Cost |
| *NPV* | Net Present Value |
| *NSGA-II* | Non-dominated Sorting Genetic Algorithm-II |
| *O&M* | Operation and Maintenance |
| *P2P* | Peer-to-Peer |
| *PCC* | Point of Common Coupling |
| *PDF* | Probability Distribution Function |
| *PEM* | Polymer Electrolyte Membrane |
| *PI* | Profitability Index |
| *PRISMA* | Preferred Reporting Items for Systematic reviews and Meta-Analyses |
| *PRO* | Primary Research Objective |
| *PSO* | Particle Swarm Optimisation |
| *PV* | Photovoltaic |
| *PtG* | Power-to-Gas |
| *QoI* | Quantity of Interest |
| *RESs* | Renewable Energy Sources |
| *RG* | Research Gap |
| *RSESs* | Renewable and Sustainable Energy Systems |
| *RTP* | Real-Time Pricing |
| *SA* | Simulated Annealing |
| *SC* | Super-Capacitor |
| *SCA* | Sine-Cosine Algorithm |
| *SOC* | State-of-Charge |
| *SRO* | Secondary Research Objective |
| *SSA* | Salp Swarm Algorithm |
| *SSR* | Self-Sufficiency Ratio |
| *STC* | Standard Test Conditions |
| *STDEC* | Share of the Total Discounted Equipment-related Costs |
| *ToU* | Time-of-Use |

| | |
|---|---|
| *V2G* | Vehicle-to-Grid |
| *VSS* | Value of the Stochastic Solution |
| *WEO* | Water Evaporation Optimisation |
| *WT* | Wind Turbine |
| *WoS* | Web of Science |
| *WtE* | Waste-to-Energy |

# Chapter 1: Introduction

## 1.1. The need for accelerating the deployment of smart, integrated renewable and sustainable energy systems

With around two-thirds of global greenhouse gas (GHG) emissions stemming from energy production and use, the energy sector is a key contributor to climate change [1]. Accordingly, accelerated decarbonisation of the energy sector is an integral part of the efforts to limit global warming to well below 2°C – preferably to 1.5°C – compared to pre-industrial levels, in line with the aims of the Paris Agreement [2]. To this end, large-scale renewable energy electrification has been recognised as an effective intervention to unlock transformational synergies between substantial increases in the use of electricity and renewable power generation [3].

The transition toward reliable, affordable, clean electricity as a principal energy vector has been enabled by recent advances in information and communications technologies (ICTs) – and, in particular, advanced metering infrastructure (AMI) technologies – within the evolving smart grid context [4]. As shown in Fig. 1.1, the International Renewable Energy Agency (IRENA) GET2050 analysis [3] estimates that a fundamental shift to deep renewable energy electrification is able to reduce total energy sector GHG emissions by at least 44% by 2050, relative to a base case, where a "business-as-usual" perspective is adopted on governments' current and planned energy interventions. This percentage increases to more than 70% if direct uses of renewable energy (such as solar heat-driven ventilation and biofuels for transportation), as well as energy efficiency and conservation measures, are additionally accounted for.

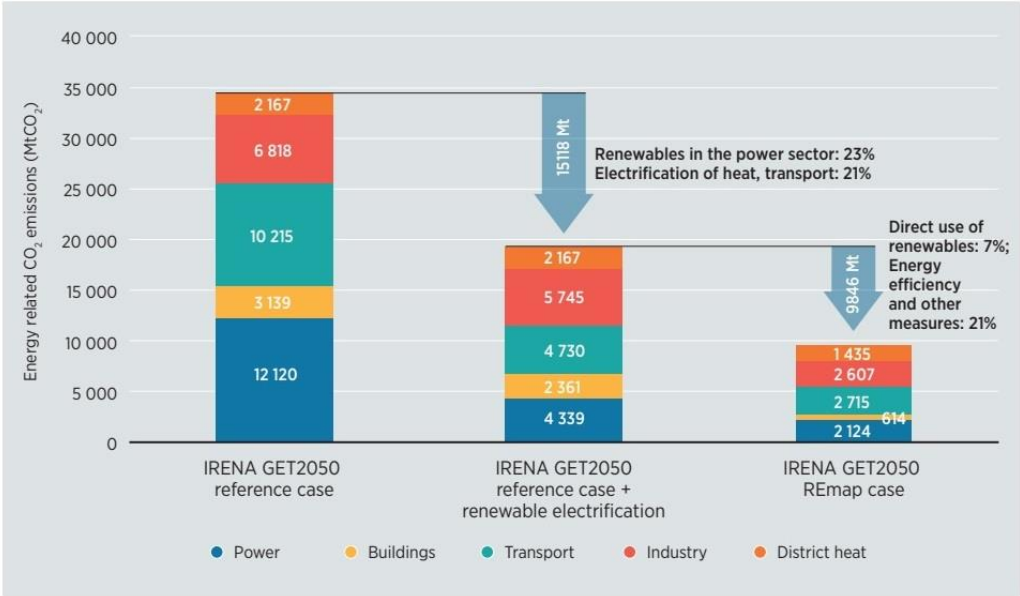


*Notes: $CO_2$ = carbon dioxide; $MtCO_2$ = million tonnes of carbon dioxide.*

Figure 1.1: Contribution of renewable electrification to global decarbonisation efforts [3].

In this context, the IRENA REmap analysis [5] estimates that the share of electricity in total global energy demand would approximately triple by 2050, where non-dispatchable renewable energy sources (RESs) make up around 66% of total electricity generated (see Fig. 1.2). A considerable portion of the projected increases in electricity demand is attributable to the so-called '*end-use sector coupling*' activities – that involve the electrification of energy demand across different sectors (mainly heat and transport) with the primary goal of increasing the share of renewable energy in other sectors [6].

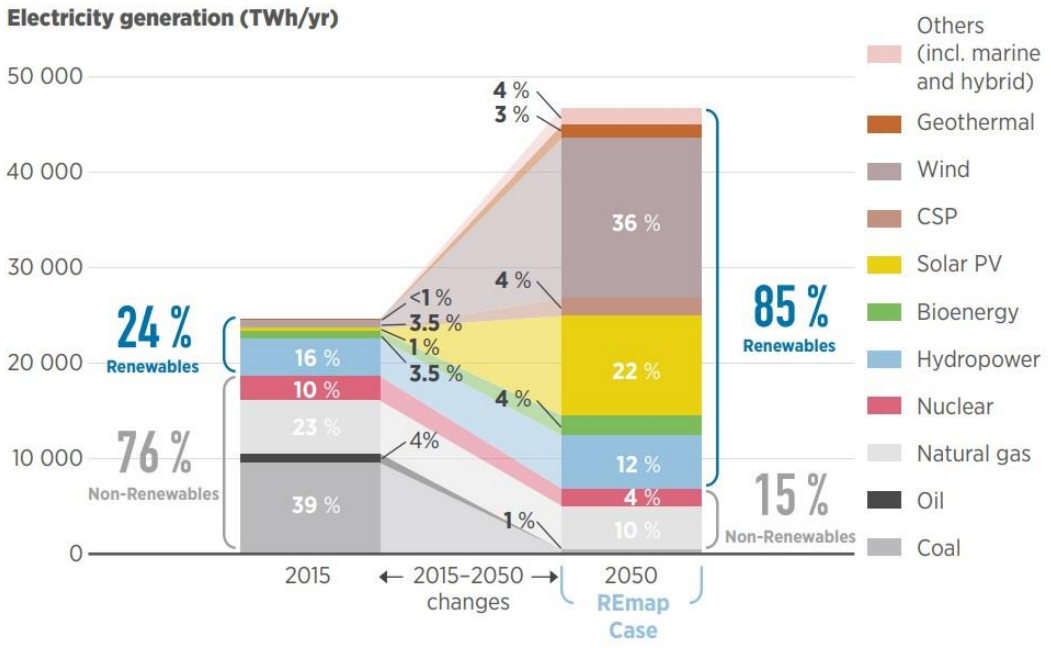


Figure 1.2: 2°C scenario for electricity generation, REmap case, 2015–2050 [5].

In traditional power grids, supply-side infrastructure – thermal power plants with advanced cycling capabilities, hydropower plants, and pumped hydro storage – have been utilised to address demand variability [7]. However, to effectively accommodate the associated weather-driven stochasticity, increasing the penetration of non-dispatchable renewables into the electricity supply mix requires additional flexibility capacities. Accordingly, grid modernisation and decarbonisation efforts are driving the deployment of demand-side flexibility resources using innovative solutions, such as end-use sector-coupling – power-to-heat, power-to-gas, coordinated charging of electric vehicles (EVs), and vehicle-to-grid (V2G) interventions – and smart operation of behind-the-meter batteries, as well as the procurement of demand response (DR) provisions across various end-use segments – residential, commercial, industrial, agricultural (see Fig. 1.3).

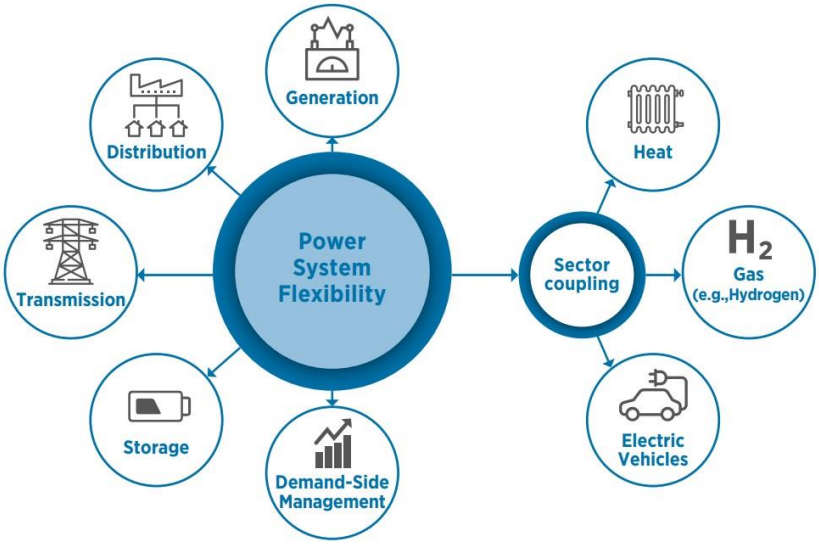


Figure 1.3: Sources of power system flexibility in modernised grids [5].

Furthermore, the major shift from synchronous, centralised generation to a diversified, heterogeneous combination of technologies with ever-increasing penetrations of distributed energy resources (DERs) presents potentially significant system balancing challenges given the critical lack of visibility of distribution network operational conditions by system operators [8]. In this setting, decentralised smart energy system-based integration of variable renewable energy and adopting bottom-up approaches to energy system operation have been identified as the most promising ways of increasing the resilience and reliability of variable renewables-dominated electrical grids. That is, smart, integrated, decentralised renewable energy systems are the building blocks of smart grids of the future [9]. On the other hand, off-grid smart, integrated, renewable energy systems are at the core of 'energy for all' initiatives, which are aimed at providing modern energy services to coastal, island and mountain village communities, as well as, more broadly, rural/peripheral communities [10].

In this light, this research was motivated by the dire need to improve the economics and operational efficiency of grid-connected and isolated smart, integrated renewable energy systems, and particularly micro-grid (MG) systems, which is not only central to the roll-out of variable RESs as part of global efforts to address climate change and energy decentralisation, but is also essential for accelerating universal energy access [10].

## 1.2. Scope

Aimed at cost-optimally addressing the mismatch of electricity supply and demand, energy system operation and investment planning optimisation has been defined in various degrees of comprehensiveness over a multitude of timescales ranging from fractions of a second to several decades. Accordingly, energy system planning optimisation studies can be grouped broadly into two classes, depending on whether they focus on [11]: (i) the control, operation, scheduling, dispatch and energy management, or (ii) the strategic long-term investment planning and designing. Fig. 1.4 categorises energy planning optimisation studies across different time horizons [12].

Furthermore, there exist several inter-relationships between the sizing and dispatching sub-disciplines of energy planning optimisation. That is, on the one hand, equipment sizing decisions have a significant impact on the optimal schedules of dispatchable components during the operation phase. On the other hand, failure to factoring the optimal system dispatch into long-term investment planning decision-making processes has the potential to oversize the components. In this light, a well-coordinated energy system planning method needs to consider inter-temporal constraints governing both the operation and investment planning problems. To capture the principal inter-linkages between energy system operations and investment planning (in pursuit of generating potentially significant savings), an optimal dispatch strategy decision-making problem is embedded in this thesis within the associated renewable energy investment portfolio management and asset allocation optimisation problem. Accordingly, the spectrum of the decision-making time horizon addressed in the thesis encompasses both the operational scheduling and investment planning decision horizons.

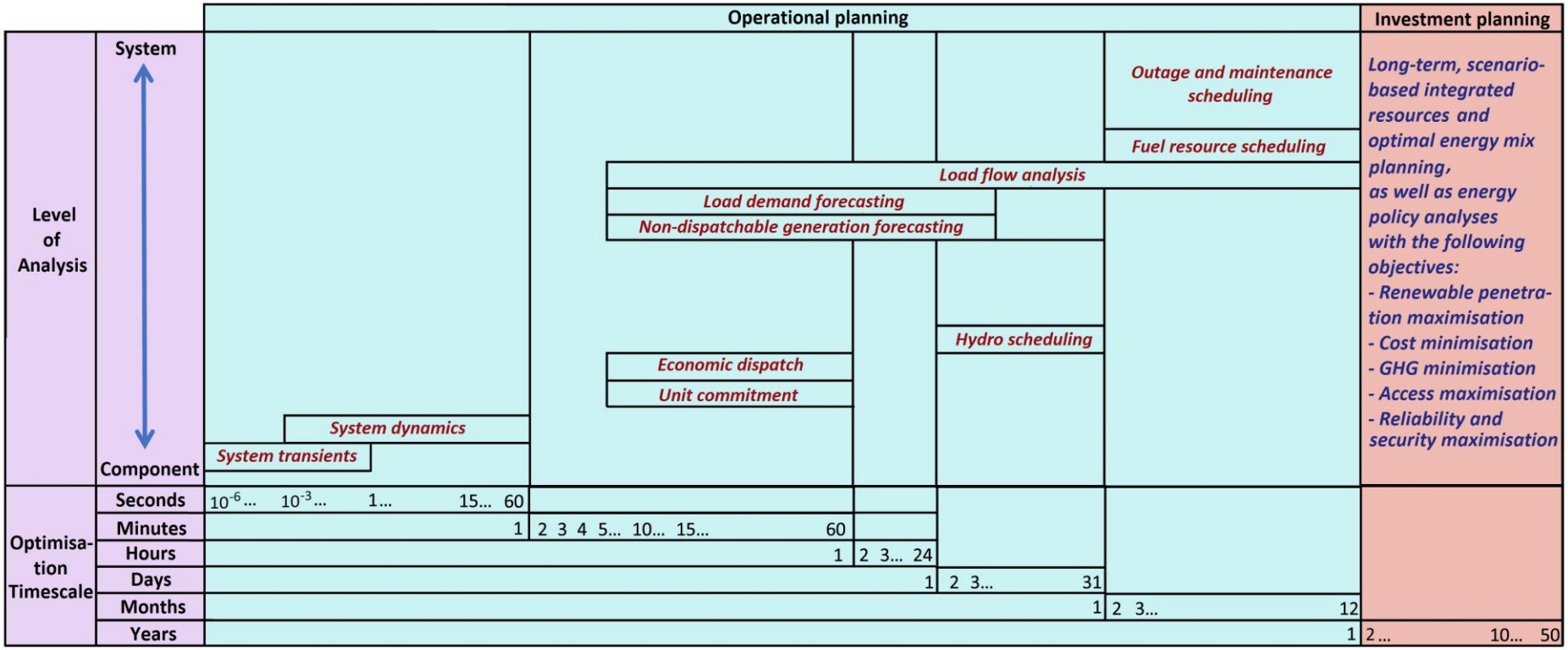


Figure 1.4: Time horizon of different energy system planning analyses (adapted from [12]).

In terms of geographical coverage, this thesis primarily focuses on the optimal resource allocation and strategic planning of autonomous and semi-autonomous clean, low-voltage, low-inertia, local energy networks.[1] More specifically, to ensure greater focus and achievability, the thesis studies the subset of problems related to the optimal strategic long-term equipment capacity sizing of on- and off-grid community-scale MG systems. The MG infrastructure capacity planning optimisation involves determining the whole-life cost-optimal mix of the sizes of the candidate DERs and power conversion devices, as well as the volumes and timing of energy trades with the main power grid (in case of grid-connected systems), so as to meet the energy requirements at a prescribed reliability level subject to a set of operational and planning constraints. That is, a solution to the optimal MG design problem identifies the least-cost combination of the sizes of the components of the system and energy flows over a decades-long – often spanning 20–30 years – investment planning horizon to meet the projected demand for energy [13].

In this setting, this thesis considers bulk power flows (in hourly time intervals). That is, it does not address ultra-short timescale simulation (~1 ms to 1 sec) necessary for voltage and frequency regulation analyses, as well as transient stability and power quality control. Also, scenario-led investment planning models often tailored to the entire national or continental energy systems lie beyond the scope of the thesis. Notably, different geographical and temporal scales warrant different levels of technical details (given the computational complexity concerns), as well as different decision objectives consistent with the relevant scope of the analysis. Yet, although it is sub-optimal to do so and yields less accurate approximations of reality, the proposed energy planning optimisation modelling framework – tailored specifically towards small- to medium-scale MGs – has the potential for application to the integrated, strategic resource planning for electric utilities, as well as the long-term power system capacity expansion planning

[1] The geographical span of the areas intended to be serviced using the community MGs range in size from a few houses in a subdivision or a village (usually less than 1 square mile) to rural territories (usually from 1 square mile to 5 square miles) to towns (usually from 5 square miles to 25 square miles) with the associated characteristics in terms of the population size and the proximity, or degree of remoteness, to larger urban areas.

problems, provided that bulk power system infrastructure such as transmission lines are adequately modelled and the inter- and intra-hour dynamics of thermal and hydropower generators are appropriately accounted for. Moreover, the modelling framework proposed to solve the coordinated, system-level design and dispatch problem of community MGs is non-specific with regard to the technologies considered in the candidate pool. Accordingly, the model allows supporting community energy system-level energy management interventions and business case analyses and can be applied to MGs of any architecture and topology.

It should also be highlighted that the prior feasibility evaluation and business case analyses carried out in this thesis study the costs associated with delivering a technically reliable service using a set of optimally-sized DERs. That is, the institutional, regulatory, and management costs, as well as the costs associated with advanced metering and control systems, are not necessarily covered.

## 1.3. Research rationale

As discussed above, while a combination of dramatic cost reductions, technology advancements, and enabling policies have driven the implementation of local 100%-renewable energy systems in recent years, the global deployment rate of non-dispatchable renewables – principally solar photovoltaic (PV) and wind – has failed to grow proportionately. The inadequate methodological energy planning development needed to address the increasing complexity of the portfolios of variable renewable energy-integrated energy systems has been widely recognised as a key factor underpinning the relatively slow deployment rate of non-dispatchable renewables on a global scale [3], [5], [12], [13].

The most salient modelling complexities of optimal long-term, strategic planning of renewable and sustainable energy systems (RSESs), especially when dealing with the sector-coupled MG capacity planning and design optimisation problem, can be categorised along the following four factors:

1. The optimisation technique used in the solution algorithm for the given energy planning and asset allocation model.

2. Integrating large-scale, distributed, sectoral DR capacities of heterogenous willingness-to-supply in the associated resource portfolios.

3. Quantifying the most salient parametric sources of forecast uncertainty necessary to produce accurate representations of real-world scenarios.

4. Nesting an optimal operational scheduling problem – tailored to the system-level dispatch of controllable DERs, DR resources, and grid energy trades.

Adding large volumes of non-dispatchable DERs to energy systems alters the nature of the associated operational and investment planning decision-making problems. More specifically, the associated simplifying assumptions commonly made in the operational and planning phases of conventional power systems – that the inter- and intra-hour dynamics of thermal generators can be neglected – do not hold for energy systems with high shares of renewables, where the outputs vary both inter- and intra-hourly. This is even more critical when dispatching and planning sector-coupled systems incorporating several integrated energy vectors, which are associated with higher levels of inter-dependency among decision variables involved. In mathematical terms, the associated highly dimensional objective functions of the problems under discussion cannot be approximated with functions that are strongly convex, linear, and differentiable with Lipschitz gradients [14]. In particular, the associated objective functions are commonly non-deterministic polynomial time-hard (NP-hard) [15], which are not amenable to exact mathematical analysis without strong simplifying assumptions. In this light, a recent, emerging strand of the long-term MG investment planning literature has proposed using artificial intelligence (AI)-based meta-heuristic optimisation algorithms as an alternative to classical optimisation methods [16]. This necessitates a comprehensive, high-level comparative performance evaluation of the well-established and state-of-the-art meta-heuristics for application to energy planning optimisation problems. Fig. 1.5 provides an overview of the most widely-used optimisation approaches in the larger literature on the capacity planning of RSESs, which, as illustrated above, can be categorised as either based on the exact mathematical or AI optimisation algorithms.

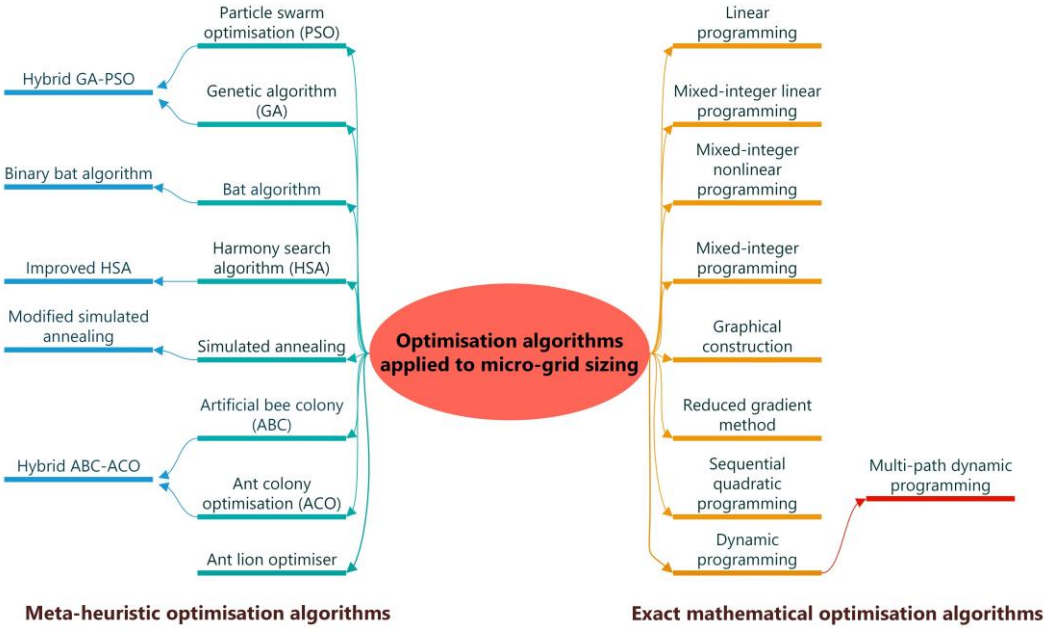


Figure 1.5: Categorisation of the optimisation techniques applied to the MG capacity allocation problem.

Compounding the complexity of sector-coupled energy planning optimisation is the integration of small- to medium-scale sectoral demand-side flexibility resources. These distributed DR resources are integrated into resource portfolios of utilities using dedicated third-party responsive load aggregators, who enlist end-users of the same load segment and give them enough scale to participate in DR provisioning services and sell the bundled load reduction to utilities [17]. Accordingly, a long-term, DR-integrated energy planning approach needs to model the involvement of aggregator-mediated sectoral customers in DR programmes in a market-driven approach. The approach needs to effectively capture the dynamic nature of strategic interactions between instrumentally rational, utility-maximising active economic agents in a liquid, aggregator-mediated demand-side management (DSM) market. More specifically, the approach needs to identify the reaction and commitment of different classes of customers activated by third-party demand response aggregators (DRAs) when exposed to variations in the economic incentives for load curtailment/shifting, whilst additionally promoting consumer choice and competition consistent with their expected utilities [18], [19].[2] This

[2] In economics, the term ‘utility’ refers to the wants-satisfying capacity of goods or services [314].

brings to light the importance of developing an efficient investment decision-making framework that systematically embeds end-users' flexibility preferences, aggregators' expected profits, and utilities' costs within the long-term energy system capital investment plans in a realistic manner.

Also, quantifying the parametric uncertainties in input data time-series – notably (i) weather forecasts and meteorological data that dictate power outputs from non-dispatchable generation technologies, (ii) energy demands, and (iii) wholesale electricity prices – using analytical and data-driven approaches adds new layers of theoretical, methodological, and computational complexity to producing an optimal solution to the sector-coupled energy system planning problem. The reason lies in the need to solve the problem for all possible combinations of data forecasts to represent a multi-variate scenario tree, with the nodes visited by each path (scenario) corresponding to values assumed for uncertain variables in the model. Even a moderate dimension for data uncertainty, when coupled with a large number of time slots in the planning horizon, can lead to an intractably high number of the above-mentioned paths that represent pseudo-random values the parameters take on. It is, therefore, imperative to employ efficient scenario clustering heuristics to derive relatively small subsets of discrete scenarios that adequately represent multi-variate stochastic processes for key uncertain parameters, while maintaining the associated statistical properties of the original scenario sets [20].

Moreover, the business-as-usual operational approach accommodated in optimal MG sizing methods is to use rule-based (fixed-controller) energy dispatch strategies to schedule the operation of MG systems based on a set of pre-defined control logics – which entail: (i) charging the energy storage systems and/or exporting to the upstream grid when excess power is available, and (ii) discharging the storage devices and/or importing from the main grid to meet onsite net energy deficits [21]. This has led to conservative designs for 100%-renewable MG systems given the lack of strategic foresight in business-as-usual operational strategies employed during the planning phases, which has severe long-term negative implications in terms of the overall system cost and efficiency. Accordingly, more advanced, optimisation-based energy dispatch strategies – that solve for the optimal schedules with respect to the upcoming system conditions on a day-ahead basis –

need to be systematically integrated into long-term energy planning models. Importantly, co-optimisation of the MG planning and dispatching in a predictive, look-ahead manner to effectively capture the system dynamics, whilst adhering to a set of inter-temporal constraints governing the system operation and design – by decomposing them into separate, coordinated sub-problems and optimising the short-term energy scheduling objectives simultaneously to the system design – plays a potentially significant role in minimising simulation-to-reality gaps.

In addition, to support the stakeholder decision-making process on the cost-optimal mix of energy generation, storage, and conversion technologies, a number of MG design optimisation and long-term investment planning software tools exist in the literature and industry [22]–[25]. The solution approaches used in the available tools can be broadly classified into two groups. The first class of the tools takes a simplistic full-factorial approach to solving the optimal design problem. The most notable software packages in this group are HOMER [26] and RETScreen [27]. Given that the full-factorial approach selects component sizes at a limited number of fixed intervals, it cannot be formally considered an 'optimal' solution [28]. Furthermore, it leads to the 'combinatorial explosion' when increasing the granularity of the search space and/or increasing the number of candidate technologies above a low critical value. The second, more algorithmically complex class of the existing tools employ a linearized approach to equipment capacity planning, such as mixed-integer linear programming (MILP) [29]. The notable software packages in this group include: HOMER Pro [30], Hybrid2 [31], SAM [32], XENDEE [33], REOpt [34], and DER-CAM [35]. A simplified exact mathematical problem formulation is used in these tools by providing convex constraints. That is, these tools are plagued by the same significant deficiencies as exact mathematical optimisation-based solution algorithms discussed above.

Furthermore, practically none of the available tools tailored to the optimal energy planning and equipment sizing of MGs have any standard uncertainty characterisation, operational scheduling optimisation, or aggregator-mediated sectoral DR procurement features. Consequently, they commonly produce sub-optimal solutions with the associated strategic plans falling under either risk-averse or risk-seeking strategies, depending on the model-inherent simplifications made.

This highlights the need for the development of a fundamentally new MG equipment capacity planning tool that is able to yield globally optimum, variability-aware solutions with forward-looking, dynamic operational schedules tailored to various uncertainty budgets, whilst effectively integrating small- to medium-scale DR resources into the associated resource plans.

## 1.4. Systematic literature review: DR-integrated energy planning optimisation under parametric uncertainty

This section presents an in-depth literature review of long-term, DR-centred energy planning optimisation in the presence of data uncertainty. It pursues four prime goals. First, it aims to characterise the optimisation methods used in the stochastic, DR-aware energy planning literature. To this end, the selected papers are categorised by optimisation timescales, meta-heuristic against exact mathematical optimisation approaches, and optimisation (decision) criteria that have been shown to be relevant and suitable for energy planning. Second, it examines different uncertainty quantification techniques used, uncertainty factors treated, DR programmes implemented, and responsive loads addressed. Third, it studies the operational strategies used during the planning phases of RSESs. Fourth, it surveys the geographical scope of the systems modelled and technologies considered in the given candidate pools.

These four points together then serve as a foundation for drawing conclusions regarding the gaps in the resulting body of literature and a high-level analysis of state-of-the-art energy planning optimisation methods in general. They, additionally, allow for positioning this research within the identified gaps. It is also noteworthy that each chapter that presents a novel contribution of the thesis (Chapters 2–4) begins with a separate literature review relating to the focus of the chapter. This ensures that the articles that have not met the selection criteria used in the systematic literature search approach – in terms of addressing both the DR and uncertainty management aspects simultaneously – are reviewed critically. Accordingly, while the systematic literature review, as well as the associated meta-analyses and thematic syntheses, reveal the overarching trends and aspects for improving the most holistic and integrative energy planning approaches present in

the literature, the literature review at the beginning of each of the above-mentioned chapters establishes the key ideas that the chapter's analysis develops and shows how the specific contribution of the chapter adds to the relevant strand of the literature – in addition to the collective goal of broadening the scope and level of analysis of the long-term energy planning problem.

There exist several review studies discussing approaches and trends for MG energy planning and capacity optimisation. Gamarra and Guerrero [36], Fathima and Palanisamy [37], as well as, more recently, Emad et al. [38] analyse the MG design optimisation literature; Sinha and Chandel [39], Hannan et al. [40], as well as Yang et al. [41], review the methods and algorithms for sizing energy storage systems; while Mellit and Kalogirou [42] discuss various AI-based optimisation techniques used for the optimal sizing of solar PV systems. There are also several review papers around the potential financial implications of DR procurement – as a power system resource – and uncertainty quantification in the design and feasibility analysis, as well as energy scheduling, of RSESs. For example, Shoreh et al. [43] have investigated the potentially significant role of industrial customers in delivering large-scale DR resources. They have also identified the most important barriers to the large-scale deployment of industrial DR services. Jordehi [44] has presented a review of optimisation methods utilised for the efficient operation of DR resources. Shariatzadeh et al. [45] have presented a classification scheme for different DR arrangements. They have also discussed the leading research and development projects worldwide. Furthermore, Mavromatidis et al. [46] have presented a review of different uncertainty treatment approaches in the optimal planning phase of RSESs. Zubo et al. [47] have focused on reviewing the literature on uncertainty-aware operation and planning of distribution grids with high penetration of renewables. Moreover, Aien et al. [48] have classified the emerging methods employed to capture different sources of uncertainties associated with various levels of power system analysis.

While several attempts have been made to review specific methods applied to either (i) uncertainty impact estimation, or (ii) DR scheduling in the realm of smart grid alone, the literature on long-term investment planning of RSESs is

lacking a review of research discussing the models incorporating both the model-inherent parametric uncertainty quantification and DR resource planning techniques.[3] Supporting the associated stochastic decision-making processes during the long-term investment planning of RSESs in the presence of distributed demand-side flexibility resources is of paramount importance in order to develop a deeper understanding of the optimal designs and dispatch strategies within the smart grid paradigm. Importantly, if demand-side flexibility resources are to become a core part of the utilities' resource portfolios, it is necessary to advance the existing DR-centred energy planning models under uncertainty such that they minimise the associated simulation-to-reality gaps under the assumptions that are realistic and appropriate. This has resulted in a substantial gap in the understanding and awareness of the wider renewable energy system modelling community of the new methodological opportunities that are able to give a more realistic grounding to research on renewable energy planning and dispatching optimisation – and particularly, the more robust optimal design alternatives of sustainable energy projects.

### 1.4.1. Search strategy and study selection criteria

To carry out an in-depth, systematic review of the state-of-the-art methods developed for the joint management of DR and uncertainty sources while optimally planning RSESs, this systematic review follows the method proposed by Glock and Hochrein [49]. Accordingly, the literature review method comprises of three stages, namely: (i) searching for the peer-reviewed journal and conference papers using a list of appropriate strings of search terms in the online literature databases;[4] (ii) scanning the obtained results for relevance, first by scanning the titles, abstracts and

[3] Note that this systematic review does not attempt to merely focus on reviewing the studies that have characterised the uncertainty inherent in implementing DR programmes; rather, it aims to systematically identify, review, and synthesise the existing studies in the wider field of optimal planning, designing, and scheduling of RSESs, which not only quantify at least one source of model-inherent parametric uncertainty, but also develop a framework for the procurement of DR provisions.

[4] Accordingly, grey literature (including technical or research reports from government departments, international energy agencies, working and white papers from private companies and consultants, as well as reports from civil societies and non-governmental organisations), unpublished studies, and non-English documents were considered as excluded publication types.

keywords, and then by a thorough analysis of the full papers deemed eligible for inclusion in the review; and (iii) using a snowballing approach – which refers to utilising the reference list of a paper or the citations to that paper to find additional relevant papers. The following online literature databases were used: (i) Thomson Reuters's Web of Science (WoS), (ii) Elsevier's Scopus, and (iii) Google Scholar.

Furthermore, the defined strings of search terms are listed in Fig. 1.6. In the figure, the column titled "Category 2" includes the frequently used terms as synonyms and/or the various subsets of the core terms listed in the column titled "Category 1", which were identified in the course of the literature search procedure. It is also noteworthy that the search queries under "Category 2" for energy system architecture are used to particularly search for sector-coupled systems.

The defined search queries were employed to search the title, abstract, and keywords fields of the papers when using the WoS and Scopus databases, whereas they were allowed to occur anywhere in the papers when using the Google Scholar search engine. The search results are effective as of April 2021.

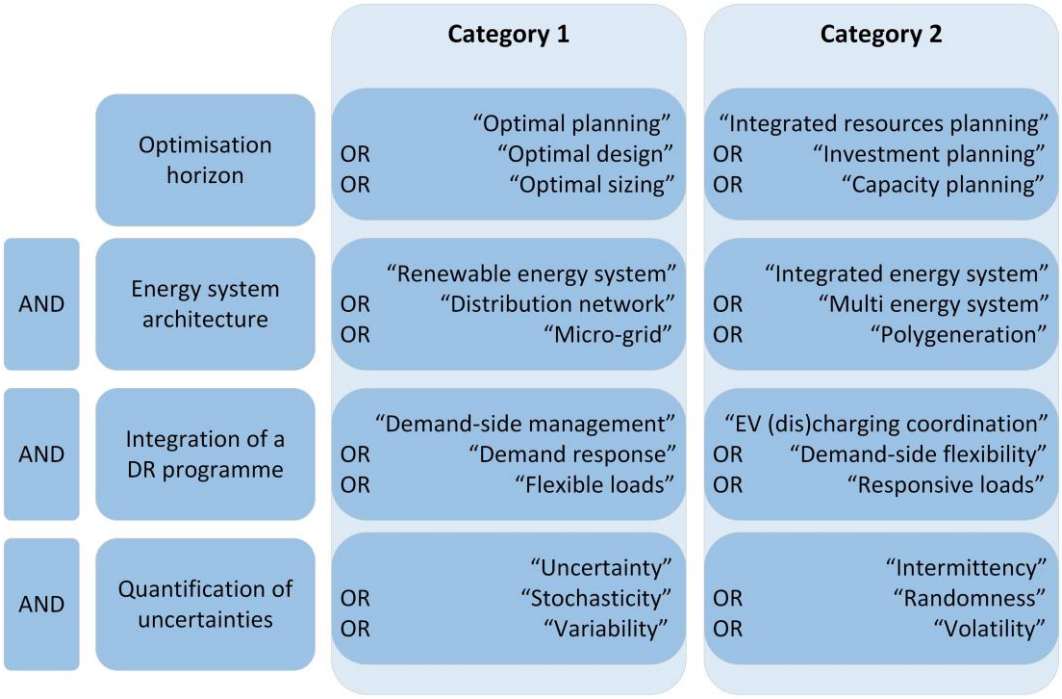


Figure 1.6: Outline of the search queries utilised to search within the selected databases.

### 1.4.2. Primary question-led content mapping

The contents of the reviewed literature were mapped by extracting information utilising a set of key questions. The following primary questions drove the literature review process and identified the wider trends and the aspects for renewable energy system design modelling improvement:

- PQ1. What is the technological and geographical scope addressed in the stochastic planning studies of RSESs in the presence of responsive loads?[5]
- PQ2. What are the wider optimisation methods and trends, as well as relevant decision criteria for stochastic, DR-centred energy system scheduling and designing?
- PQ3. What are the methodological trends and most salient sources of parametric uncertainty in DR-integrated energy system optimisation studies aimed at narrowing the model-inherent uncertainty bounds?
- PQ4. What are the research trends in terms of applied techniques and DR sources for integrating distributed demand-side flexibility resources into the utilities' uncertainty-aware resource portfolios?
- PQ5. What are the computational barriers to using super-resolved time-series, as well as increasing the number of uncertainty parameters and the response fidelity (time resolution) of DR programmes during the design phases of RSESs?
- PQ6. How energy scheduling management optimisation could be leveraged to improve the estimates of the capacity needed to meet coincident peaks (onsite and utility-wide), while addressing the variability in non-dispatchable generation, loads, and electricity prices?

[5] For the purposes of this systematic review, any energy system architecture featuring a high penetration of renewables, including those within the smart grid paradigm (such as active distribution networks, micro-grids, nano-grids, energy hubs, and virtual power plants), as well as conventional radial distribution grids equipped with distributed renewable generation, fall under the category of renewable and sustainable energy systems.

### 1.4.3. Identification of the studies meeting the inclusion criteria

The PRISMA (preferred reporting items for systematic reviews and meta-analyses) [50] flowchart of the adopted strategy to search for, filter out, and select the papers is shown in Fig. 1.7. As can be seen in the figure, 3,098 documents fitted the initial survey using the extended strings of search terms within the selected databases, which reduced to 2,065 after duplicates (n = 1,033) were eliminated. The remaining papers were then filtered out by the title, bringing about the exclusion of 1,892 papers as a result of lying outside the defined boundaries of the review paper (n = 1,828) and excluded publication types (n = 64). As detailed in Fig. 1.7, 1,828 papers did not fall within the scope of the review, with the summary of irrelevant research areas as follows: optimal short-term operational planning of both conventional and renewables-integrated power systems (n = 920); optimal equipment capacity planning and designing of conventional, non-renewables-integrated power systems (n = 338); short- or long-term forecasting of the load power demand and/or power outputs from weather-dependent renewable energy generators (n = 215); economic energy and/or reserve dispatching of electricity markets (n = 160); economic load dispatching, as well as optimal active and/or reactive power flow analysis (n = 63); stochastic and/or security-constrained unit commitment (n = 38); transmission network expansion planning or transmission congestion management (n = 29); power quality enhancement and analysis of harmonic disturbances in distribution grids (n = 26); optimal voltage and/or load-frequency control in distribution grids (n = 17); dynamic or static state estimation in power systems (n = 7); optimal spinning and/or non-spinning reserve procurement (n = 7); dynamic and transient analysis of bulk and distribution power systems (n = 4); failure analysis, optimal restoration, as well as reliability, adequacy and security evaluation of bulk power systems (n = 3); and risk-based maintenance scheduling of distribution networks (n = 1).

This left 173 papers for the abstract and keywords-based screening. A total of 92 papers were excluded at this filtering stage due to more context-specific reasons including: focusing on the management of uncertainties (n = 45) and DR programmes (n = 37) in other energy planning domains/horizons (for example, load restoration dynamics), rather than long-term investment planning, as well as

eliciting DR resources from natural gas end-users, rather than electricity end-consumers (n = 10). The remaining 81 papers progressed to the full-text assessment phase, which narrowed down the number of eligible papers (for the full review) to 39 by removing 42 further papers due to more discerning factors, including: (i) focusing solely on the uncertainty characterisation (n = 23), (ii) dealing solely with DR scheduling (n = 15), and (iii) addressing peer-to-peer (P2P) energy transaction management, rather than the investment planning optimisation of RSESs (n = 4). Finally, a forward and backward snowballing search procedure found 3 additional papers and increased the total number of the eligible papers for the final review to 42.

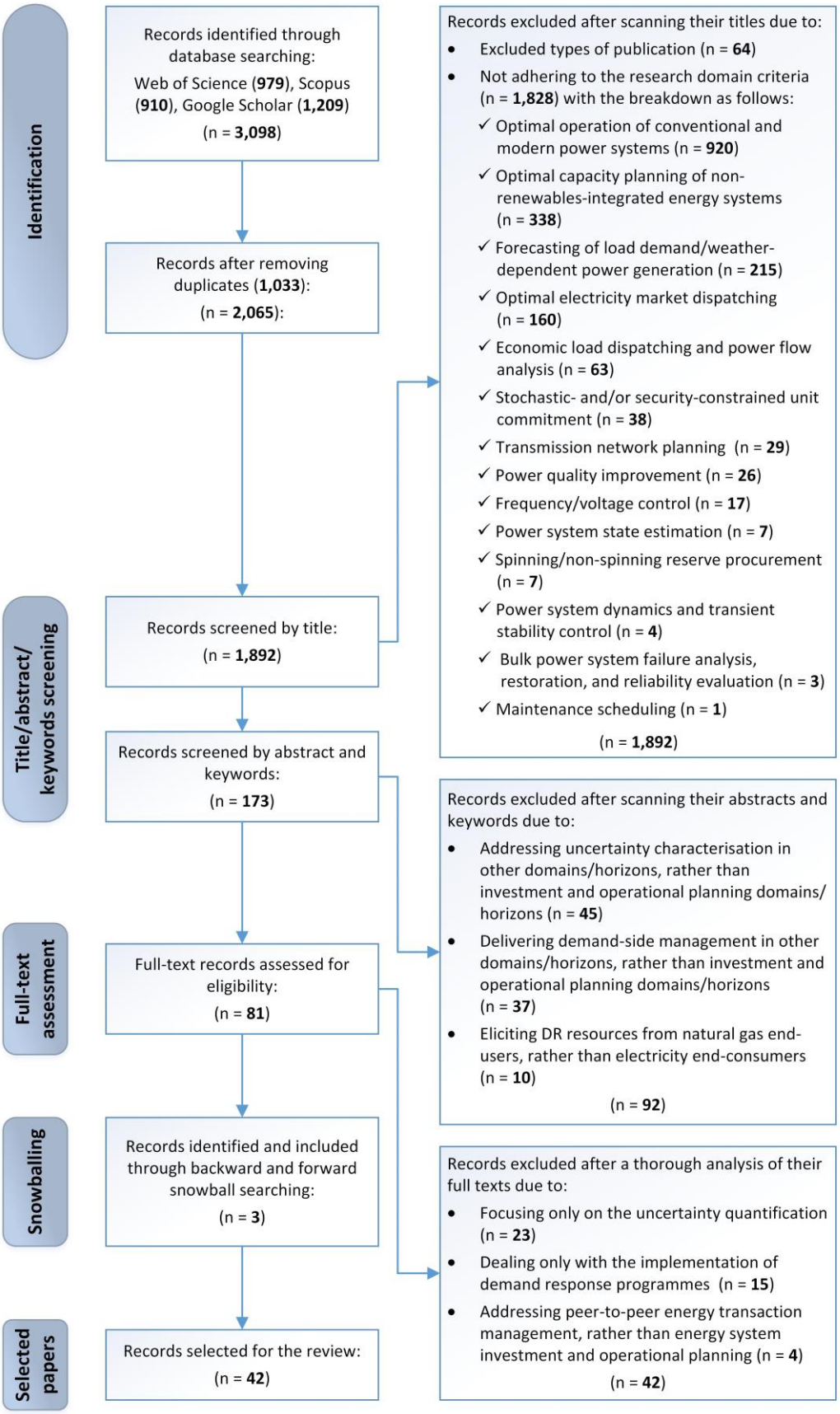


Figure 1.7: PRISMA-compliant flowchart of the literature search process.

### 1.4.3.1. Temporal development

Fig. 1.8 displays the number of papers addressed in this review per year over time. As it can be seen from the figure, the studies included in the review span eleven years, with the earliest study dating back to 2011. This indicates that the stochastic energy system optimisation in the presence of DR interventions is a relatively new research topic that aims to bridge a key methodological gap between purely uncertainty-aware and purely DR-oriented strands of the literature – towards a more integrated approach to energy planning that is realistic and appropriate. Additionally, Fig. 1.8 depicts a visible upward trend in publications on DR-aided optimisation of renewable energy systems considering the model-inherent uncertainties with a salient, continuing spike in 2016.

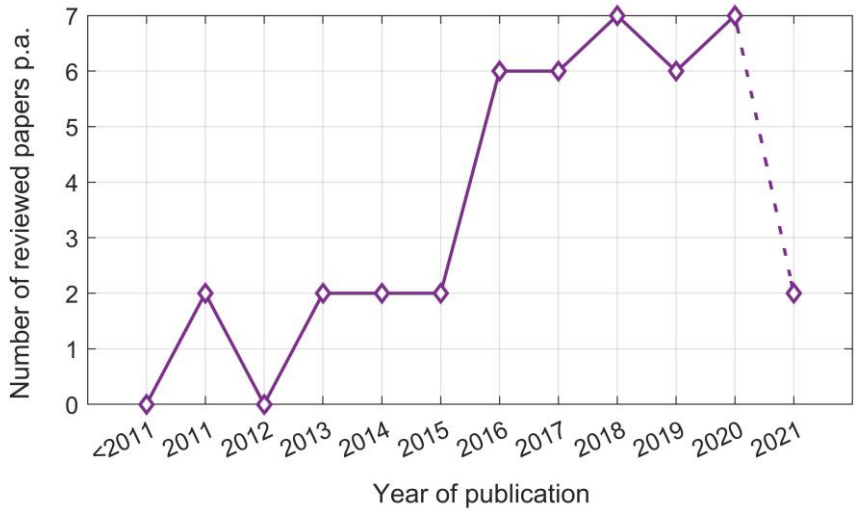


Figure 1.8: Number of included articles in the review per year over time: (- -) represents partial results for the year 2021.

### 1.4.4. Overview of the identified articles

Table SM1.1 in the Supplementary Material accompanying the main text (Supplementary Material 1) summarises the identified studies on the long-term, strategic, DR-integrated, uncertainty-aware capacity optimisation models tailored to RSESs.

### 1.4.5. Thematic synthesis of the literature: Research gaps and questions

The systematic review enables a thematic analysis and categorisation of the resulting body of literature along the contextual characteristics of the test-case systems optimised and the mathematical formulations put forward, which give rise to a number of glaring methodological and content gaps and previously neglected factors in optimal, DR-integrated, uncertainty-aware sector-coupled MG equipment capacity planning and designing tailored to community-scale installations. Indeed, the severity of existing research gaps is substantially greater than what a single PhD thesis would cover. Rather, based on the author's judgement of relative importance and effect size on improving MG life-cycle cost estimates, the following seven research gaps are prioritised and selected to be addressed in this study, from which arise a number of relevant key research questions, as follows:

***RG1. Narrow focus on state-of-the-art meta-heuristics:*** Although their superiority to conventional meta-heuristics and exact mathematical optimisation algorithms has been demonstrated in numerous engineering optimisation problem instances, fundamentally new meta-heuristic optimisation algorithm-based capacity planning models applied to long-term MG capacity planning remain underutilised. In this context, only 9 (21%) of the 42 reviewed papers employ meta-heuristics to optimise a solution to the given energy planning optimisation problems, all of which are well-established ones, namely: genetic algorithm (GA) [51], particle swarm optimisation (PSO) [52], artificial bee colony (ABC) [53], and non-dominated sorting genetic algorithm-II (NSGA-II) [54]. Accordingly, the efficiency of an increasing number of state-of-the-art meta-heuristics has not yet been systematically evaluated in the MG investment planning literature. The need to continuously compare the accuracy of innovative new optimisers is mainly driven by the possibility for multiple optima when using meta-heuristics – making the efficiency testing of state-of-the-art meta-heuristics in strategic MG planning applications a continuous area of research. The research questions following from this gap are: (1) to which extent state-of-the-art meta-heuristics outperform well-established ones, and (2) whether the expected solution quality improvements provided by state-of-the-art meta-heuristics are statistically robust when applied to different MG configurations with different climatic, loading, and wholesale

electricity price conditions, with the answers to these questions implying potentially significant consequences for MG capacity planning design.

***RG2. Poor understanding of the incentive-price elasticity of customer-supplied DR capacity across different sectors and the associated strategic utility-aggregator-customer interactions:*** As Table SM1.1 shows, there is a growing body of literature lending support to the integration of DSM frameworks into the design phase of RSESs. However, as far as can be ascertained, no single study has evaluated the attitude of neither end-users, nor aggregators, nor electricity providers in relation to adopting these practices during the optimal design and planning processes of RSESs. Accordingly, oversimplified assumptions have commonly been made in the literature regarding the available capacity of responsive loads, which have substantially reduced the accuracy of associated responsive load capacity projections. That is, many hypotheses commonly made in the literature regarding the expected degree of end-users' participation in DR schemes are not well-grounded. Also, the table demonstrates that more than half of the existing sectoral DSM approaches during the MG planning phases (17 out of 30 studies that explicitly specify the employed DR segments) are tailored to the residential sector, while around one-third of existing DR solutions (12 out of the total of 42 eligible studies for review) do not account for the load type-dependent DR procurement factor. It is of paramount importance for the utility to understand how the willingness of customer-supplied DR capacity differs across different end-use categories – especially in the face of new sources of electricity demand, such as electrified heating and mobility. To aid the associated asset-allocation decision-making procedure, a long-term, DR-integrated MG investment planning approach needs to model the participation of aggregator-activated end-consumers in DSM mechanisms in a systematic, robust, transparent, equitable, market-driven approach, whilst accounting for the incentive-price elasticity of customer-supplied DR capacity [55] across different sectors. This necessarily entails capturing the dynamic nature of bidding strategies and strategic interactions among instrumentally rational economic agents involved in the dispatch and delivery of DR resources across different end-use segments in an aggregator-mediated DR market. More specifically, the sectoral DR procurement approach needs to

determine the equilibrium conditions in double-sided DSM market mechanisms, whilst adequately accommodating different end-users' preferences, willingness-to-participate, and elasticities of DR capacity provision – which could be derived from their energy service needs and the relative values they place on them. The above-mentioned two-sided (platform) demand-side flexibility markets normally start by offering financial incentives to DRAs. The DRAs then they take a percentage of the utility-offered incentive as compensation, passing the rest on to their customers in return for load reductions, where the incentive prices and customer participation rates are determined by the market principle of seeking to maximise profit (or utility). Accordingly, more work is needed to evaluate the effect of different levels of discomfort experienced by different customer classes on the economic feasibility of renewable energy projects as the characterisation of aggregator-mediated customer comfort constraints during the planning phases of RSESs is less well explored.

***RG3. Lack of comprehensive, high-level uncertainty-aware approaches:*** As Table SM1.1 shows, assuming non-perfect long-term input data forecasts – or, put differently, accounting for the uncertainty associated with input data – is becoming common practice in the long-term MG investment planning literature. However, as far as can be ascertained, the uncertainty associated with the power output from the solar PV plant has been characterised based solely on the variability of solar irradiance. However, to yield more complete representations of the uncertainty inherent in the PV plant's output power, an energy planning model needs to handle both the forecast uncertainties of solar irradiance and ambient temperature. Furthermore, with micro-hydro power plants present in the candidate technology pool of only 1 of the 42 reviewed papers, previous work has failed to address the uncertainty associated with river streamflow forecasts. Moreover, to ensure computational tractability, the existing meta-heuristic-based, uncertainty-aware, DR-integrated MG planning approaches have been limited to the simultaneous quantification of four sources of parametric (input data) uncertainty, with the forecast uncertainty of wholesale electricity prices addressed in only 9 (24%) of the 38 reviewed articles that study grid-connected MG architectures. This is attributable to the fact that adding a data-driven scenario-led stochastic dimension – as the

standard method for forecast uncertainty quantification – to the meta-heuristic-based MG capacity optimisation problem potentially makes it computationally intractable. The reason lies in the need to solve the problem for all possible combinations of data forecasts to represent a multi-variate scenario tree, with the nodes visited by each path (scenario) corresponding to values assumed for uncertain variables in the model [46]. Hence, a research question arises how more advanced stochastic energy planning models can be designed, which utilise state-of-the-art scenario reduction algorithms [56] to accommodate a multitude of parametric uncertainties without significantly impairing the associated solution quality, whilst additionally dealing with different uncertainty budgets, with the answer to this question having important financial implications for high-level uncertainty-aware energy planning processes.

***RG4. Underrepresented usage of joint operational and investment planning optimisation methods:*** While practically all the long-term energy planning optimisation models reviewed consider the life-cycle cost as a decision criterion, short-term energy scheduling optimisation objectives optimised simultaneously to the system design are not well-explored. The literature on the optimal sizing of RSESs has principally relied on rule-based, hourly-basis operational scheduling strategies to solve the energy balance problem for the first year of the operation of the system (a typical 8,760-h annual operational analysis with hourly increments), with no short-term scheduling strategy or foresight to the load demand, local generation, and electricity prices over the next time-steps of the system operation. However, a recent, growing body of literature has recognised and documented the increasing importance of the co-optimisation of investment planning and energy scheduling problems. More specifically, there exist 15 instances in the relevant reviewed literature where the optimal resource portfolio and optimal dispatch schedules are concurrently determined at an hourly time fidelity. However, as far as can be ascertained, no scholarly attention has been given to formulating an optimal stochastic, DR-aware MG design problem where a dynamic optimal dispatch strategy over a moving 24-h horizon is nested within. The reason lies in the time-consuming nature of the meta-heuristic-based solution algorithms, often making them intractable to include look-ahead scheduling provisions over a moving

daily horizon – that need to be repeated for each of the hundreds of their search agents. This has led to a systematic underestimation of the investment profitability gains from 100%-renewable MG systems given the lack of strategic foresight in business-as-usual optimal design methods – that do not solve for the optimal schedules to optimally dispatch energy storage technologies, DR resources, and energy trading with the utility grid with respect to the upcoming system conditions on a day-ahead basis. Consequently, important interactions between energy management parameters, such as wholesale rates, charging and discharging rates, and weather profiles, are neglected by the business-as-usual approaches with long-term implications in terms of the overall system cost, efficiency, reliability, and resilience. Hence, a research question arises how an efficient, computationally-tractable daily MG dispatch optimisation framework can be designed so that it can be integrated into meta-heuristic-based MG sizing approaches without incurring prohibitive computational costs.

***RG5. Paucity of 100%-renewable MG systems, especially in off-grid configurations:*** As Table SM1.1 shows, most reviewed papers have explored the potential pathways for wind power to cost-optimally contribute to the future energy needs of urban, rural, and remote communities. More specifically, wind energy is present in 29 (69%) of the portfolios of generation assets addressed in the relevant body of literature. As one would expect, solar PV has received the second most scholarly attention, which is considered in 27 (64%) of the strategic energy planning studies reviewed. However, other promising renewable energy generation technologies, particularly micro-hydro and biopower plants, which are respectively present in the power generation mix of only 1 and 2 of the papers reviewed, have not been frequently studied. Moreover, the vast majority (38, or 90%) of the reviewed papers have proposed grid-connected energy system topologies. This indicates poor knowledge on how to accommodate the specific challenges of deploying uncertainty-adjusted off-grid RSESs in the presence of DSM solutions. In addition, the review of the mainstream literature indicates an over-reliance on non-renewable energy sources (natural gas, coal, diesel, gasoline, oil, and nuclear), which are collectively present in 22 (52%) of the reviewed papers. The research question following from the above-mentioned gaps is how effective energy

planning models can be developed that are able to (i) handle high degrees of dimensionality due to the presence of a diversified array of (only) renewable technologies in the candidate pool (decision variables), (ii) limit the use of biomass resources to a sustainable level by imposing innovative new constraint terms, (iii) produce cost-optimal trade-offs between the levels of DR and storage allocation – especially for grid-connected installations, and (iv) deal with the more pronounced impact of the variability in generation sources on the adequacy costs of stand-alone MGs than the counterpart grid-tied systems.

***RG6. Negligence of the operational suitability of various energy storage technologies over specific timescales:*** As Table SM1.1 shows, only 25 (62%) of the 42 relevant reviewed papers have attempted to integrate energy storage systems, as sources of flexibility, into the given energy system architectures. This is presumably in large part because of the presence of DR interventions in the associated integrated resource portfolios, which are conceivably found to be more cost-effective flexibility resources in the associated prior feasibility and business case analyses. Another potential contributing factor to the trend of using storage-less test-case systems in the relevant reviewed literature is the widespread connection to the utility grid. Also, the reviewed renewable energy system configurations are solely dominated by battery energy storage systems (BESSs). That is, records investigating the integration of other energy storage media – either alone or in conjunction with BESSs – into RSESs are minuscule (n = 5). That is, hybrid energy storage systems that integrate two or more energy storage technologies with complementary characteristics have received little scholarly attention. Importantly, such hybrid storage systems provide a platform to reduce costs and energy curtailment, improve system efficiency, minimise the overall storage capacity, and prolong system lifetime by optimally operating each technology across the timescale it is specifically designed for – in accordance with the duration of energy storage capacity per unit of power capacity [57]. Furthermore, different energy system scales warrant different forms of energy storage hybridisation. Accordingly, relevant research questions that arise are (i) what the energy storage device mix for seasonal, inter- and intra-day, and transient load levelling exercises is in terms of technology and how the overall energy storage

system can be optimally scheduled, and (ii) how optimal trade-offs between importing electricity from the main grid (where appropriate), eliciting DR resources, and investing in various energy storage systems can be produced for community-scale, sector-coupled MG development projects, with the answer to these questions additionally contributing to address the existing ill-diversified portfolio of technologies in community energy systems.

***RG7. Limited procurement of V2G services as sources of system-balancing flexibility to manage supply-demand mismatches:*** Despite the fact that their significant advantages in terms of both peak shaving and electricity bill saving have been demonstrated in an increasing number business case analyses [58], V2G interventions – which can be treated as a demand-side flexibility resource – are found to be almost non-existent in the mainstream literature on the DR-centred investment planning of RSESs under uncertainty. Notably, no stochastic energy planning optimisation method was identified, which measures the effect size of the widespread adoption of V2G systems and the associated additional flexibility provided by V2G fleets on the economics and efficiency of sector-coupled community energy systems by reducing the need for investment in carbon-intensive peaking generation and/or capital-intensive storage capacity. Furthermore, energy planning research on V2G interventions has almost exclusively focused on battery EVs due to the less complicated technical processes involved and the fact that the fuel cell EV (FCEV) market share has remained relatively stagnant at less than 0.2% of total world sales since the year 2015 [59]. That is, a comprehensive, high-level analysis of the implications of emerging FCEV in V2G operation (FCEV2G) interventions is absent from the energy planning optimisation literature. Accordingly, specific research questions that arise are (i) how V2G resources, in general, can be adequately incentivised and V2G-addressable energy management frameworks can be designed in the context of the wider efforts to provide a ‘level playing field’ for all DR resources that offer flexibility services, and (ii) to which extent the heuristic integration of FCEV2G services, more specifically, influences the system-level dispatch and delivery of sectoral DR resources and, in turn, the sizing of MG infrastructure, where the integrated DSM market design framework

tailored to the system-wide interruptible flexibility resources is settled by hourly-basis uniform price (non-discriminatory) DR procurement auctions.

## 1.5. Aim and objectives

The systematic review and associated discussion lay the foundation for positioning this research within the identified gaps in the relevant reviewed literature. Accordingly, the specific aim of this research is to develop a novel, meta-heuristic-based, aggregator-mediated sectoral DR-integrated, V2G-addressable, uncertainty-aware, highly dimensional long-term equipment capacity planning and day-ahead energy scheduling co-optimisation model tailored towards sector-coupled, community-scale, multi-energy-storage-technology, 100%-renewable and -reliable energy systems. To this end, four core research objectives support the attainment of the overall research aim of the thesis. The planning models that address each of the research objectives are designed to build upon each other. Accordingly, each original objective and the associated subset of the key contributions of the thesis are addressed in a separate chapter, except for the objectives and the associated contributions that are highly inter-related. Table 1.1 summarises the overall sequential approach of the research, listing the key contributions of the research, which are put forward to achieve the four primary research objectives. In this context, primary research objectives 1 to 4 and the associated contributions are addressed in Chapters 2 to 4, namely: Objective 1 in Chapter 2, Objective 2 in Chapter 3, and Objectives 3 and 4 in Chapter 4.

Table 1.1: Increasing methodological complexity of MG equipment capacity planning models in this thesis.

| Primary research objective (PRO) | Contributions | Corres-ponding research gap |
|---|---|---|
| ***PRO1. Formulating a robust meta-heuristic-based, highly dimensional MG equipment capacity planning optimisation model tailored towards community-scale, sector-coupled, multi-energy-storage-technology, 100%-renewable and -reliable energy projects and identifying the superior meta-heuristic in MG sizing applications*** | • Developing a descriptive statistics-based comparative meta-heuristic performance analysis scheme for MG capacity planning applications that adequately accounts for varying efficiencies of meta-heuristics when applied to structurally different MG systems, as well as their initialisation-directed stochasticity in different simulation trials.<br>• Proposing a first-order, passive, low-pass energy filter-based operational planning algorithm for efficient scheduling of multiple energy storage technologies integrated into grid-connected and isolated MG systems.<br>• Devising an efficient energy management strategy for the coordinated integration of light-duty fuel cell electric commuter vehicles, as well as medium-duty fuel cell electric vessels, heavy-duty tractors, and heavy-freight trucks. | RG1 |
| ***PRO2. Formalising a sectoral aggregator-mediated, EV-charging-load-addressable, market-driven interruptible DR scheduling framework to give a realistic grounding to research on distributed DSM planning and integrating it into the proposed MG sizing model*** | • Devising a bi-level Stackelberg, non-cooperative game-theoretic DSM plan to characterise the strategic interactions of the MG operator (utility), intermediary sectoral DRAs, and end-customers in day-ahead, incentive-based DR programmes in a robust, equitable, transparent, market-driven manner.<br>• Developing an iterative, privacy-preserving distributed algorithm able to handle non-linearities in actors' payoff functions to determine the unique, pure-strategy Nash equilibrium of the DR dispatch game, whilst capturing the price elasticity of DR supply across different load segments to improve the forecast quality of load type-dependent DR participation.<br>• Designing a stochastic load disaggregation technique to break down the forecasted total sectoral electricity consumption into any individual number of end-users, whilst accounting for the diverse sector-wide customer behaviours and strategies, as well as the corresponding sectoral aggregator payoff profiles. | RG2 |
| ***PRO3. Large-scale, data-driven, scenario-led, multi-dimensional quantification of various problem-inherent parametric*** | • Proposing a large-scale Monte Carlo simulation (MCS)-based stochastic framework to simultaneously characterise a relatively large number of input data uncertainties – power outputs from various non-dispatchable generation | RG3 |

| | | |
|---|---|---|
| ***uncertainties based on the discretisation of the corresponding probability distribution functions (PDFs) and developing different energy planning decisions in accordance with different energy uncertainty budgets*** | technologies, load power demand, and wholesale electricity prices.<br>• Applying a MILP-based scenario clustering technique that yields a statistically representative subset of the original set of multi-dimensional uncertainty scenarios to reduce running times, while retaining the solution quality (optimality) within an acceptable limit.<br>• Characterising the uncertainties in ambient temperature and river streamflow forecasts by adequately deriving the PDFs that best fit the corresponding historical datasets, which respectively influence the estimated power outputs from solar PV and micro-hydro power generation plants. | |
| ***PRO4. Coordinated, system-level hybrid-energy-storage-technology MG design and dispatch co-optimisation, whilst accounting for the total incentive-responsive V2G resource capacity in the integrated resource plan, as well as various arbitrage opportunities*** | • Introducing a linear programming-based, arbitrage-aware, dynamic, look-ahead, predictive dispatch strategy for the optimal scheduling of MG systems – charging/discharging of energy storage systems and energy exchanges with the main power grid – over a moving 24-h dispatch horizon.<br>• Nesting the developed forward-looking operational planning problem – formulated to optimally respond to the dynamic nature of system conditions over a moving one-day period – within the proposed meta-heuristic-based, DR-integrated, stochastic MG sizing model to jointly optimise the design and dispatch of MG systems. | RG4 |

Also, Table 1.2 provides a mapping of case studies against the secondary objectives of the thesis – which are directly informed by the gaps in energy planning research on the structural complexity of the existing configurations of RSESs – as well as the set of specific tasks completed to achieve the secondary objectives. Note that these secondary objectives are achieved by means of conceptualising 'first-of-their-kind' on- and off-grid MG systems tailored towards sector-coupled community-scale projects, which are validated to be technically feasible and financially viable through numerical simulations. To this end, four grid-connected and stand-alone 100%-renewable MG systems were specifically conceptualised for the following cases in New Zealand: (1) the community of 400 permanent inhabitants on Stewart Island, (2) a rural community of about 350 people near Feilding, (3) the eight-lot Totarabank Subdivision located in the Wairarapa District, and (4) a 1,000-strong community in Ohakune that swells to 8,000 people (on average) during skiing season. Test-case MG systems 1 to 3 are presented in

Chapter 2, whereas test-case MG system 4 is presented in Chapter 3. Given that the load demand in test-case 4 is subject to high degrees of seasonality and sectoral diversity – and, therefore, represents the most numerically challenging case study – as well as for practical reasons, it solely forms the basis for all the model applications and methodological analyses carried out in Chapters 3 and 4.

Table 1.2: Secondary research questions pertaining to the configuration of test-case MG systems conceptualised in this thesis.

| Secondary research objective (SRO) | Specific tasks | Corres-ponding research gap |
|---|---|---|
| ***SRO1. Improving the dispatchability of future RSESs using more diversified portfolios of variable generation technologies with complementary characteristics (particularly, solar PV, wind, and run-of-the-river micro-hydro) together with a sustainable share of dispatchable RESs (particularly, biomass resources)*** | • Investigating the temporal complementary characteristics of variable renewables – solar, wind, and hydro resources – on both seasonal and daily bases, which impact their optimal combination in the corresponding generation mix.<br>• Optimal system integration of different bioenergy generation technologies, namely: (i) biomass gasifier-generator system, and (ii) biopower plants, comprising anaerobic digestion reactors, steam methane reformers, air separation units, and internal combustion engines.<br>• Optimal system integration of waste-to-energy (WtE) plants, wherein the non-organic fraction of municipal solid waste (MSW) is combusted to generate electricity.* | RG5 |
| ***SRO2. Optimal hybridisation of different energy storage technologies in compliance with the timescale relevant to the technical capabilities of each technology, particularly the duration of energy storage capacity per unit of power capacity*** | • Conceptualising different hybrid energy storage systems and integrating them into the test-case MG systems. Specifically, the explored hybrid energy storage systems in the thesis are: (i) hybrid hydrogen storage/vanadium redox flow batteries/super-capacitors (SCs), and (ii) hybrid hydrogen storage/SCs.<br>• Studying the impact of producing optimal trade-offs between importing electricity, discharging onsite energy storage media, and leveraging incentivised DR flexibility resources for the hours of the next day for which a net energy deficit is predicted in the presence of hybrid energy storage systems. | RG6 |
| ***SRO3. Investigating the potential of V2G technologies and FCEV charging/discharging coordination through DSM mechanisms in*** | • Designing specific hydrogen refuelling stations, as well as energy management strategies, for hydrogen fuel cell-powered light-duty commuter vehicles, medium-duty ferries, heavy-duty tractors, and heavy-freight trucks able to pump suitably pressurised hydrogen into a vehicle's or vessel's fuel tank. | RG7 |

| | |
|---|---|
| ***driving economic sustainability improvement for renewable energy development projects*** | • Devoting a specific DRA to activate the participation of a pool of FCEVs (of heterogeneous elasticity to supply DR capacity) in local flexibility markets, enabling them to reach the sufficient scale required for selling interruptible services to the system operator(s).<br>• Estimating the elasticity of DR supply capacity of FCEVs based on existing data for battery EVs, given the lack of relevant previous empirical studies on the DR potential of FCEVs. |

[*] While classifying bioenergy production and waste incineration practices as "renewable" is a controversial idea, they are assumed as renewable sources of energy for the purpose of this study, a sub-objective of which is to satisfy nearly all the energy needs of rural and remote communities – electricity, space heating, hot water, and transportation fuel of remote communities – whilst additionally providing a practical solution to manage their waste, in a cost-optimal and self-sufficient way.

Moreover, Table 1.3 maps each of the primary and secondary research objectives, which are directly defined by the identified knowledge gaps and the associated research questions, to the published journal articles, as well as the relevant thesis chapter.

Table 1.3: Mapping of journal publications, thesis chapters, and research objectives addressed.

| Thesis chapter | Journal article | Research objective |
|---|---|---|
| **Chapter 2** | • **S. Mohseni**, A.C. Brent, and D. Burmester, "A comparison of metaheuristics for the optimal capacity planning of an isolated, battery-less, hydrogen-based micro-grid," *Applied Energy*, vol. 259, p. 114224, 2020.<br>• **S. Mohseni** and A.C. Brent, "Economic viability assessment of sustainable hydrogen production, storage, and utilisation technologies integrated into on- and off-grid micro-grids: A performance comparison of different meta-heuristics," *International Journal of Hydrogen Energy*, vol. 45, no. 59, pp. 34412–34436, 2020.<br>• **S. Mohseni**, A.C. Brent, and D. Burmester, "A demand response-centred approach to the long-term equipment capacity planning of grid-independent micro-grids optimized by the moth-flame optimization algorithm," *Energy Conversion and Management*, vol. 200, p. 112105, 2019. | PRO1, SRO1, SRO2 |
| **Chapter 3** | • **S. Mohseni**, A.C. Brent, S. Kelly, W. Browne, and D. Burmester, "Strategic | PRO2, SRO1, SRO2, SRO3 |

| | | |
|---|---|---|
| | design optimisation of multi-energy-storage-technology micro-grids considering a two-stage game-theoretic market for demand response aggregation," *Applied Energy*, vol. 287, p. 116563, 2021.<br>• **S. Mohseni**, A.C. Brent, S. Kelly, W. Browne, and D. Burmester, "Modelling utility-aggregator-customer interactions in interruptible load programmes using non-cooperative game theory," *International Journal of Electrical Power and Energy Systems*, vol. 133, p. 107183, 2021. | |
| Chapter 4 | • **S. Mohseni**, A.C. Brent, D. Burmester, and W. Browne, "Lévy-flight moth-flame optimisation algorithm-based micro-grid equipment sizing: An integrated investment and operational planning approach," *Energy and AI*, vol. 3, p. 100047, 2021. | PRO3, PRO4 |

It is noteworthy that in addition to the six published journal papers, which are featured in this thesis, two further journal articles were written during this PhD (see the '*Publications*' section above). The papers, published in the journal *Energies*, have not been included in this thesis as they do not form the core of the work and do not properly fit into the overall narrative of the thesis.

## 1.6. Research approach

The research can be classified as a 'mathematical model-building' study, following the classification proposed by Mouton [60]. Mathematical models are tools for approximating the solution of problems arising from human activities – applied and social sciences, engineering, law, policy, economics, and so forth. They are derived from the logical foundations of certain areas of mathematics as a simplified representation or abstraction of reality [61], [62]. More specifically, mathematical modelling refers to the exercise of translating the beliefs about how any real-world system of interest functions, as well as how the associated sub-systems interact, with the following objectives [63]: (i) developing scientific understanding by expressing existing knowledge of a system quantitatively, (ii) evaluating the robustness of the system to variations in the settings of the underlying parameters, and (iii) assisting the decision-making processes including tactical decisions by managers/operators and strategic decisions by planners. The typical applications of mathematical model-building-oriented research are theoretical and conceptual frameworks aimed at refining existing theories [60].

Furthermore, in view of the objectives of this study, a constructivist philosophical perspective [64] is embraced throughout the research effort, and a primarily quantitative research strategy is followed. Moreover, given the nature of the problem statement and the research aim and objectives, the research can be squarely classified under the categories of (renewable energy) engineering and social economics – and integrates the two disciplines. Quantitative research efforts in engineering and social economics are often categorised in terms of the underlying reasoning approaches, namely: (i) inductive (from data to theory), and (ii) deductive (from theory to data). In this context, inductive reasoning begins with observations that are specific and proceeds to a generalised conclusion that is likely, but not certain, whereas deductive reasoning starts with the assertion of a general rule and proceeds to a guaranteed specific conclusion. That is, inductive reasoning moves from the specific level of focus to the general, while deductive reasoning moves from the general rule to the specific application [65]. In this setting, inductive approaches to quantitative research often deal with exploratory factor analysis, where a set of statistical techniques are applied to the analysis of assessment-generated data to identify the underlying theoretical constructs of the phenomena of interest, whereas deductive approaches are often hypothesis-driven, which involve a test of the validity and significance of the null hypothesis. Accordingly, arguments based on experience or observation are best expressed inductively, while arguments based on laws, rules, or other widely accepted principles are best expressed deductively [66].

In this light, this study adopts a combination of the above-mentioned two main logics of reasoning, namely: (i) a deductive, theory-testing approach (theory *from* the case), and (ii) an inductive, theory-building approach (theory *for* the case) [67]. A central part of the research effort is inductive in that it carries out a statistical quantitative comparative analysis of the efficiency of a wide array of well-established and state-of-the-art meta-heuristic optimisation algorithms in MG equipment capacity planning applications based on several case studies with different system configurations, as well as climatic, loading, and wholesale electricity price conditions, which provides a robust foundation for the other methodological contributions of the research to build upon. Accordingly, using the

superior meta-heuristic for optimal MG designing and asset allocation, identified from comprehensive statistical multi-case-study analyses, the deductive research strategy involves developing adequate conceptual frameworks for (i) characterising utility-aggregator-customer interactions in interruptible load DR programmes using non-cooperative game theory [68] and Stackelberg duopoly [69], (ii) adding a computationally tractable probabilistic dimension to simultaneously quantify multiple sources of forecast uncertainty, and (iii) developing an intelligent day-ahead scheduling optimisation algorithm to be nested within the proposed meta-heuristic-based optimal MG sizing problem.

In addition to the inductive and deductive reasoning approaches, the employed research design is founded on three complementary research approaches, namely: congruence analysis [70], theory-building through conceptual frameworks [71], and triangulation [72]. More specifically, the method of congruence analysis is used to verify the validity of the developed theoretical MG sizing approach. To this end, appropriate case studies yield statistically representative quantitative evidence for the explanatory significance of applicability of the devised theoretical approach, compared to another approach or approaches. Put differently, the congruence analysis in this thesis focuses on drawing conclusions from the congruence of observations from different case studies. The congruence analysis method, additionally, develops an understanding of the dynamics of the cases being studied to ascertain the relevance and strength of the theoretical MG sizing approach. In this light, two cycles of congruence analysis are conducted in this research effort. The first cycle addresses determining the superior meta-heuristic by evaluating the comparative efficiencies of the selected meta-heuristics in optimal MG sizing applications, which entails case studies 1 to 3 mentioned above. Moreover, the triangulation technique, which refers to the idea of utilising multiple data sources to enhance the credibility of generalisations [73], is adopted by optimising each of the conceptualised MG systems for distinct climatic, loading, and wholesale electricity price conditions. The second cycle of congruence analysis involves demonstrating the validity of the propositions put forward on the efficacy of integrating (i) behaviourally-founded aggregator-activated interruptible DR strategies, (ii) large-scale, data-driven, scenario-led, multi-dimensional stochastic

uncertainty quantification, and (iii) analytically-produced optimal dispatch solutions over a moving time window into the energy planning processes of MG systems (sizing and operation co-optimisation). To this end, the "theory-building through conceptual frameworks" approach is used to explain the underlying social and technical phenomena based on observed relationships between the elements of a system from the application of the above-mentioned three specifically developed conceptual frameworks to case study 4 – where conceptual frameworks are developed in the form of integration strategies.

Furthermore, as defined by Meredith [71], the normal cycle of theory-building research is an iterative process between description, explanation, and testing, whilst additionally accommodating the development of relevant taxonomies, techniques, and frameworks. The process is illustrated in Fig. 1.9. The iterative procedure starts by describing reality through identifying associated phenomena, exploring events, and documenting behaviours. It proceeds by producing the required conceptual or descriptive techniques, which are then extended into analytical frameworks that serve the purpose of explaining the behaviours and/or predicting the events. Finally, the explanations and propositions are tested for validity to ultimately develop the theory.

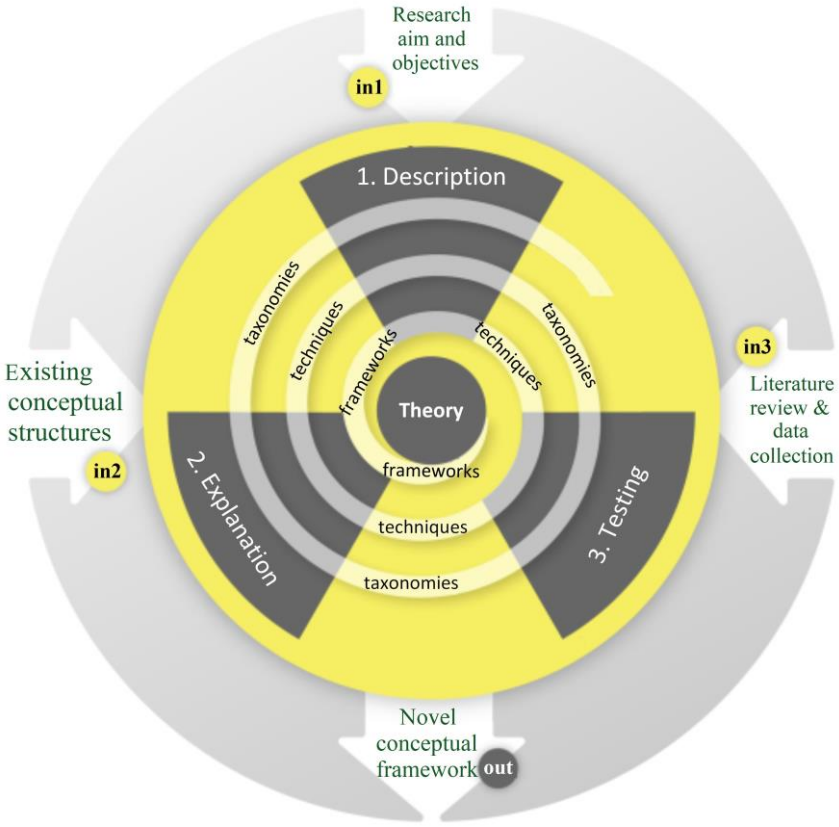


Figure 1.9: Illustration of the normal cycle of theory-building research (adapted from [71], [74]).

Collectively, the theoretical meta-heuristic-based optimal MG sizing approach and the underlying conceptual frameworks mentioned above aim to develop a new engineering economics model tailored to the long-term, strategic, stochastic, DR-integrated, community-scale, sector-coupled energy planning. Fig. 1.10 summarises the research approach and maps each research gap and objective against the inductive and deductive reasoning approaches.

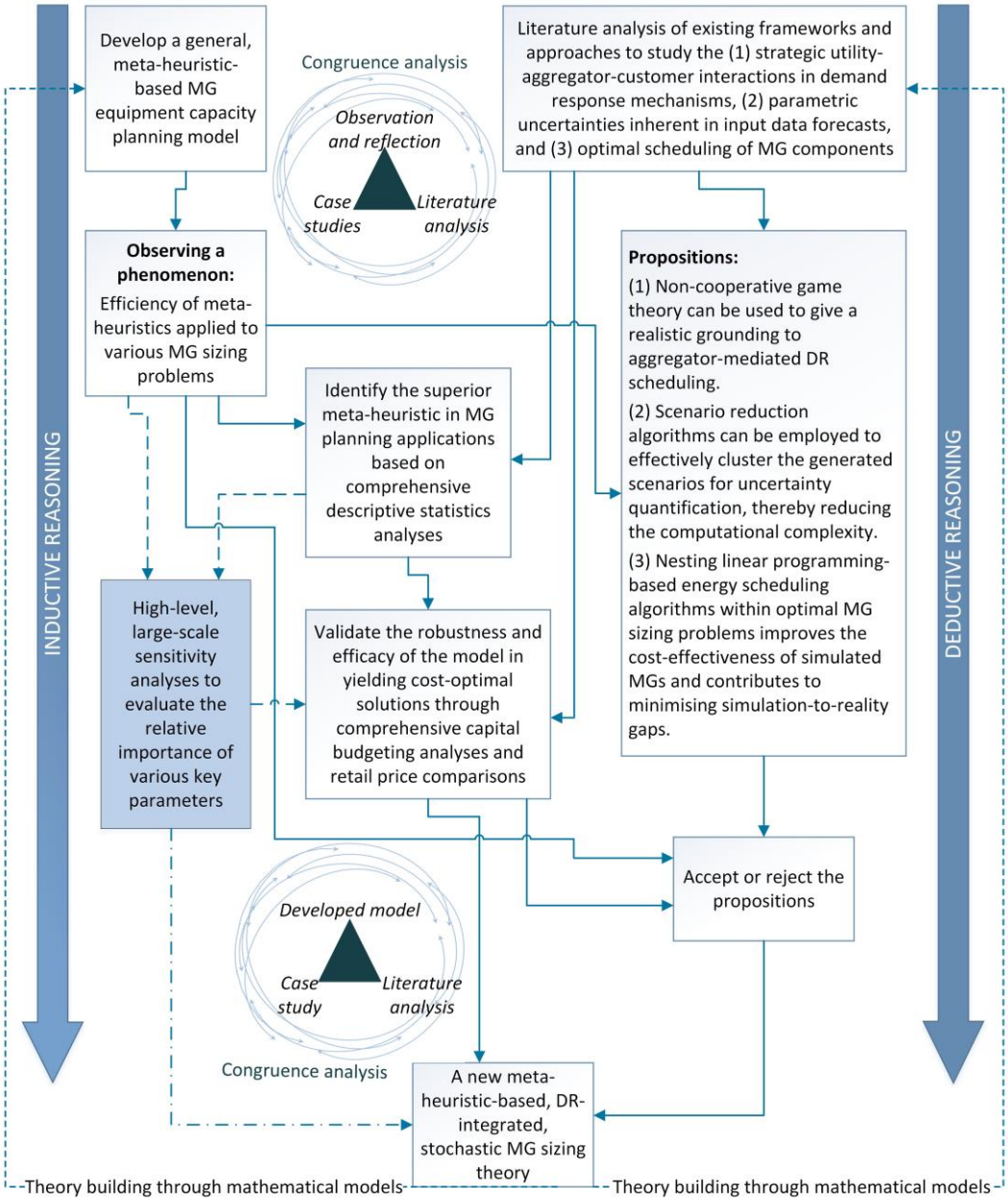


Figure 1.10: Summary of the research approach designed to address literature gaps and achieve research objectives.

## 1.7. Thesis structure

The research of the PhD project can be conceptualised as comprising four parts. Part I (Chapter 1) has defined and contextualised the study, presented a systematic review and meta-analysis of the literature on the larger DR-integrated energy planning optimisation under parametric uncertainties, identified the wider trends and the aspects for MG system design and operation modelling improvement the

thesis focuses on (research gaps and questions), the primary and secondary objectives of the research, and the set of specific original contributions and tasks, which need to be completed to achieve the objectives. Part II (Chapter 2) formulates the general structure of the MG equipment capacity planning problem and the associated meta-heuristic-based solution approach, whilst additionally presenting comprehensive, multi-case-study statistical analyses of the performances of 20 meta-heuristic optimisation algorithms, including both well-established and state-of-the-art single and hybrid techniques, which have shown promising results in preliminary studies involving a total of 226 meta-heuristics. Part III (Chapters 3 and 4) seek to contribute to the trends of broadening the scope and level of analysis of the optimal MG sizing problem to create novel, relevant, and encompassing energy infrastructure planning insights into the role of high-level DR characterisation, vigorous uncertainty treatment, and detailed operational planning in producing accurate representations of real-world scenarios. Finally, the research is concluded and recommendations for further work are provided in Part IV (Chapter 5). The schematic diagram in Fig. 1.11 shows the chapter layout and highlights how the chapters link with each other.

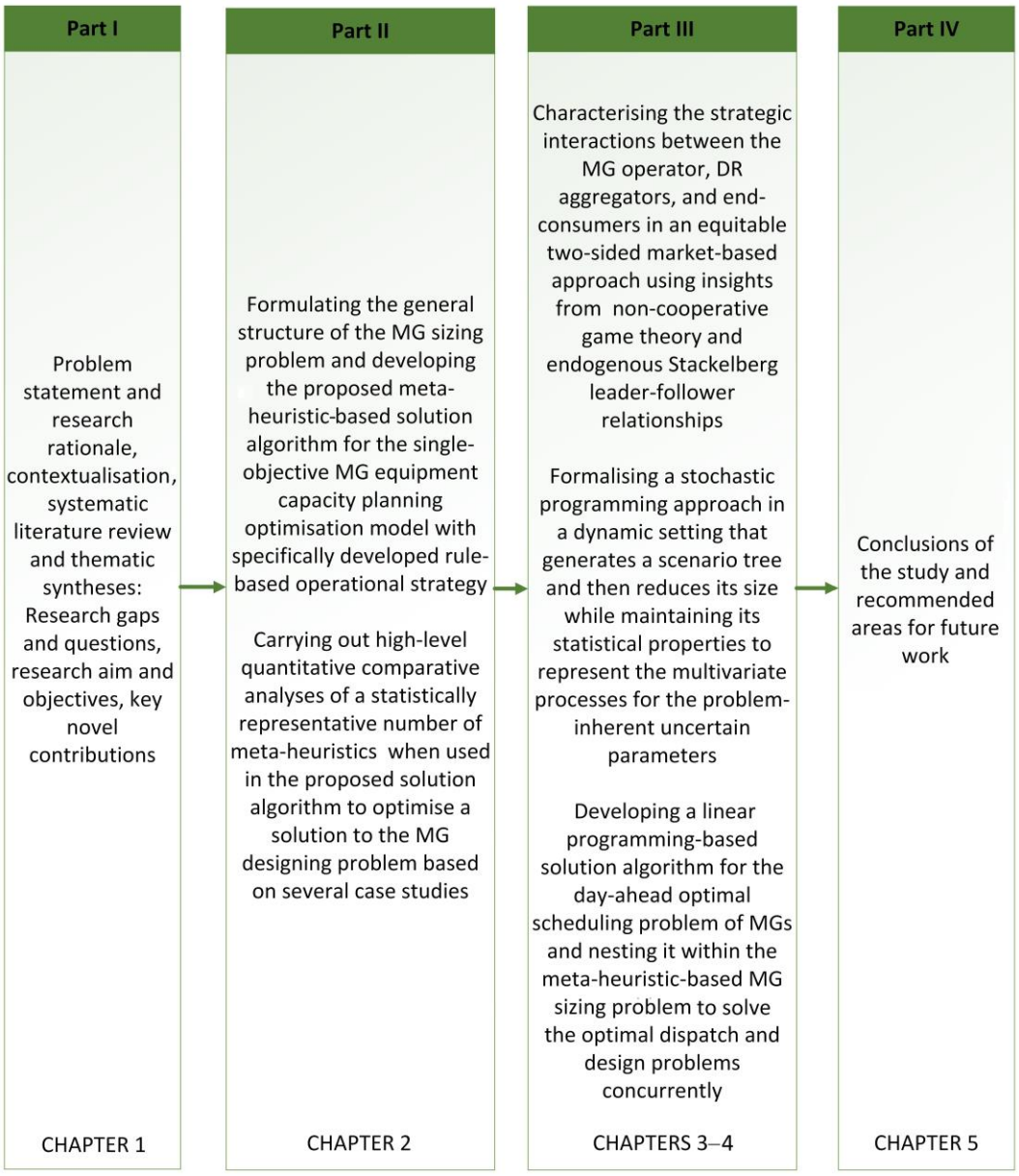


Figure 1.11: Schematic chapter layout and research flow.

## 1.8. Chapter summary

This chapter has provided the background to the research, introduced the theoretical foundations of deploying grid-connected and isolated MG systems, and formally defined the scope and delimitations of this study. Also, a systematic review of the wider DR-integrated, uncertainty-aware strategic MG planning optimisation literature is used to identify relevant methodological and content gaps and associated research questions, which directly define the research objectives and the key original contributions of the thesis. In particular, to develop a deeper

understanding of the optimal designs and dispatch strategies within the smart grid paradigm, this thesis focuses on promoting the introduction of the following previously neglected factors into the standard long-term meta-heuristic-based, stochastic energy planning optimisation methods in the presence of DR resources, namely: (1) identifying and making effective use of state-of-the-art meta-heuristic optimisation algorithms, (2) accounting for the elasticity of supply of DR capacity across various customer classes and the associated inter-dependent effects on the equilibrium conditions in local DSM markets, (3) providing in-depth, accurate, and robust decision-making support for energy planning under various uncertainty budgets, and (4) implementing multi-time-step, look-ahead, optimisation-based, FCEV2G-addrassable economic dispatch provisions during the investment planning phases, whilst leveraging the complementary characteristics of various energy storage devices, as well as different renewable energy generation technologies, necessary to effectively accommodate the variability of non-dispatchable renewables – a prerequisite for integrating significant volumes of DERs into the grid.

This contextualisation has supported the rationale for the investigation into the disconnection between the bodies of literature on the meta-heuristic-based optimal designing and equipment capacity planning of MG systems (Chapter 2), modelling utility-aggregator-customer interactions using tools borrowed from non-cooperative game theory and Stackelberg competition in sectoral aggregator-mediated interruptible DR programmes (Chapter 3), broadening the spectrum of the most salient forecast uncertainties associated with the operation of highly renewable energy systems, as well as considering the optimal dispatch of the MG components over a moving 24-h dispatch horizon simultaneously to the annual operation-based system design (Chapter 4) – with the overall aim of developing useful insights (from a theoretical, methodological, and practical perspective) regarding more integrated and holistic approaches to long-term energy planning that are realistic and appropriate.

More specifically, the following propositions are put forward: (1) carrying out rigorous statistical analyses to evaluate the comparative performances of meta-heuristics based on different tests cases in MG planning applications is able to

reveal the superior algorithm, (2) integrating behaviourally characterised, aggregator-activated responsive loads into the utilities' resource plans unlocks substantial programme budget savings, (3) employing state-of-the-art heuristic scenario reduction algorithms enables the simultaneous quantification of a relatively large number of uncertainty factors coupled with operational dynamics of MG systems with negligible impact on solution quality, and (4) coordinating an optimal MG sizing problem with a nested optimal dispatch strategy produces globally optimum solutions – the four potential generalisations that collectively contribute towards minimising simulation-to-reality gaps associated with long-term energy planning models tailored to 100%-renewable and -reliable, sector-coupled, community MG systems. Finally, the research approach has been outlined and the thesis structure has been presented.

# Chapter 2: Multi-Case-Study-Oriented Comparative Performance Analysis of Meta-Heuristics for Micro-Grid Equipment Capacity Planning Optimisation[1]

In accordance with the research aim highlighted in Chapter 1, this chapter begins the process of developing a novel, meta-heuristic-based, aggregator-mediated sectoral DR-integrated, V2G-addressable, uncertainty-aware, high-dimensional long-term equipment capacity planning and day-ahead energy scheduling co-optimisation model tailored towards sector-coupled, community-scale, multi-energy-storage-technology, 100%-renewable and -reliable energy systems with high degrees of energy security, resilience, and self-sufficiency. To this end, it introduces the basic structure of the proposed robust, meta-heuristic-based MG equipment capacity planning optimisation model, which excludes the features of (i) game-theoretic, market-based, sectoral aggregator-mediated, EV-charging-load-addressable DR integration, (ii) holistic, multi-dimensional uncertainty quantification, and (iii) optimisation-based forward-looking energy dispatch; addressed in Chapters 3 and 4. Accordingly, this chapter specifically focuses on addressing research gaps 1 (*narrow focus on state-of-the-art meta-heuristics*), 5 (*negligence of the operational suitability of various energy storage technologies*

[1] This chapter draws heavily (occasionally verbatim) on the following journal papers:

• **S. Mohseni**, A.C. Brent, and D. Burmester, "A comparison of metaheuristics for the optimal capacity planning of an isolated, battery-less, hydrogen-based micro-grid," *Applied Energy*, vol. 259, p. 114224, 2020.

• **S. Mohseni** and A.C. Brent, "Economic viability assessment of sustainable hydrogen production, storage, and utilisation technologies integrated into on- and off-grid micro-grids: A performance comparison of different meta-heuristics," *International Journal of Hydrogen Energy*, vol. 45, no. 59, pp. 34412–34436, 2020.

• **S. Mohseni**, A.C. Brent, and D. Burmester, "A demand response-centred approach to the long-term equipment capacity planning of grid-independent micro-grids optimized by the moth-flame optimization algorithm," *Energy Conversion and Management*, vol. 200, p. 112105, 2019.

*over specific timescales*), and 6 (*paucity of 100%-renewable MG systems, especially in off-grid configurations*).

In this context, the chapter aims to address the following research questions: (1) to which extent state-of-the-art meta-heuristics are able to outperform well-established ones when applied to MG test cases across a continuum of community scales from multi-family village communities to semi-urban communities of more than 1,000 people; (2) whether the expected solution quality improvements provided by state-of-the-art meta-heuristics are statistically robust when applied to different community MG configurations with different climatic, loading, and wholesale electricity price conditions; (3) how effective energy planning models can be developed that are able to (i) handle high degrees of dimensionality due to the presence of a diversified array of renewable and storage technologies (as decision variables) with complementary characteristics in pursuit of improved dispatchability, (ii) limit the use of biomass resources (for potential bioenergy generation technologies) to a sustainable level by imposing innovative new constraint terms, (iii) optimally integrate WtE plants under guaranteed waste stream assumptions, and (iv) deal with the more pronounced impact of the variability in generation sources on increasing the associated adequacy costs in stand-alone MGs than the counterpart grid-tied systems; as well as (4) what the optimal energy storage device mix for seasonal, inter- and intra-day, and transient load levelling exercises is in terms of temporally complementary technologies and how the overall energy storage system can be optimally scheduled – with the answers to these questions implying potentially significant financial and technical consequences and implications for sector-coupled, community-scale MG capacity planning designs.

The application of the basic version of the proposed integrative energy planning optimisation model to a typical solar PV/WT/battery MG, as well as two more structurally complex, grid-connected and isolated hydrogen-based test-case MG systems – that supply electrical (including space and water heating) and transportation hydrogen fuel loads – demonstrates the effectiveness and robustness of the model in yielding optimal MG planning solutions. The hydrogen-based cases, additionally, demonstrate the promise of fuel-cell-based green hydrogen economy for stationary applications, especially vis-à-vis the transportation sector, whilst

additionally providing a practical solution to manage the agricultural and municipal solid waste of remote, island, rural, peripheral, and semi-urban communities, in a cost-optimal and self-sufficient way that promotes energy democracy and independence – which directly contributes to the sustainable waste management, transport, and agriculture efforts in conjunction with sustainable energy provision.

## 2.1. Introduction

Over the last three decades, research in artificial intelligence (AI) has developed a wide variety of techniques and approaches that can be either adapted or utilised directly to solve complex problems in the energy sector – energy system investment planning, operational scheduling, as well as dynamic stability and control regulation – which are classified as analytically intractable without several (often strong) simplifying assumptions [75]–[77]. Nature-inspired meta-heuristic optimisation is a sub-discipline of AI that seeks to determine the globally optimum solutions to NP-hard problems [78]. Also, the optimal MG designing problem identifies the least-cost combination of the sizes of the components of the system over a decades-long – often spanning 20–30 years – investment planning horizon to meet the projected demand for energy subject to a set of operational and planning constraints [13], [79], [80]. It is a complex combinational optimisation problem with a non-smooth, nonlinear, non-convex, non-differentiable (with Lipschitz gradients), mixed-discrete-continuous, high-dimensional objective function subject to a variety of interconnected constraints. Accordingly, it has been classified as an NP-hard problem [36], [81].

In this light, although formulating the economic MG energy planning optimisation problem such that it is amenable to exact mathematical solution algorithms considerably alleviates the computational burden, it substantially increases the risk of sub-optimality – or, in other words, it can result in a loss of solution fidelity [21]. Associated developed simplified solution approaches, based on mathematical optimisation methods, have included various decomposition techniques, linear programming (LP), mixed-integer programming (MIP), mixed-integer linear programming (MILP), mixed-integer nonlinear programming (MINLP), and dynamic programming, of which the MILP is the most popular

approach. However, given that the optimal MG asset allocation is an off-line, one-time process, it can be argued that computational complexity should not be the primary concern from an optimisation point of view, provided that optimising a solution to the problem is not computationally intractable. Accordingly, a recent, emerging strand of the long-term MG investment planning optimisation literature has proposed using AI-based meta-heuristic optimisation algorithms as an alternative to classical mathematical optimisation methods. The long-term strategic MG energy planning optimisation literature has convincingly demonstrated that meta-heuristic optimisation algorithms can be effectively used to optimise an efficient solution to the MG infrastructure sizing problem [82]–[86].

Consequently, this has brought to light the importance of evaluating the efficiency of newly developed meta-heuristics using a trial-and-error mechanism, in pursuit of finding an algorithm, which reasonably improves the associated solution quality compared to the well-established meta-heuristics. For instance, Sharma et al. [87] have demonstrated the superiority of the grey wolf optimiser (GWO) over several well-established meta-heuristics, including the particle swarm optimisation (PSO) and the genetic algorithm (GA) in MG sizing applications. In another instance, Maleki and Pourfayaz [88] have shown the outperformance of the harmony search algorithm (HSA) over the simulated annealing (SA) algorithm when applied to the optimal sizing problem of a solar PV/wind/diesel MG system. Also, Singh et al. [89] have designed a cost-effective solar PV/wind/biomass MG using the artificial bee colony (ABC) algorithm and validated its superior performance over the classic PSO algorithm. Furthermore, Fetanat and Khorasaninenejad [90] have shown the superiority of the ant colony optimisation (ACO) algorithm to the GA in solving the size optimisation problem of a grid-independent solar PV/wind MG system. Kefayat et al. [91] go further and demonstrate the superiority of the hybrid ABC-ACO (HABC-ACO) algorithm for the probabilistic sizing of DERs within an active distribution network over the standard ABC and ACO algorithms. Bukar et al. [92] have, additionally, shown the superior performance of the grasshopper optimisation algorithm (GOA) to the cuckoo search algorithm (CSA) and the original PSO algorithm in optimising the long-term investment planning problem of a stand-alone solar

PV/wind/battery/diesel MG system. Moreover, Tolba et al. [93] have shown the higher efficiency of the salp swarm algorithm (SSA) in nearing the global optima in renewable energy system optimal design problems as compared to the PSO, the GOA, and the gravitational search algorithm (GSA). In addition, Ali et al. [94] have analysed the performance of the ant lion optimiser (ALO) algorithm for the optimal allocation of distributed renewable technologies in a distribution grid. Specifically, they have highlighted that the ALO excels the PSO, the GA, the Big Bang-Big Crunch (BB-BC), and the CSA approaches within the optimal DER allocation context.

The above review of the achievements in demonstrating the superiority of state-of-the-art meta-heuristics to well-established ones in the MG equipment capacity planning literature identifies the lack of a comprehensive comparative analysis among a wide variety of meta-heuristic algorithms. Put differently, most of the existing studies have been limited to the comparison of the results obtained by applying a single newly developed algorithm with those of some of the well-established meta-heuristics as benchmark algorithms. That is, less scholarly attention has been given to evaluating the efficiencies of a broad range of state-of-the-art meta-heuristics against each other and well-established algorithms alike. More specifically, the so-called '*no-free-lunch*' (NFL) theorem [95], which postulates that there cannot exist a meta-heuristic that is unequivocally the best for solving all types of NP-hard optimisation problems, necessitates the continuous efficiency testing of state-of-the-art meta-heuristics for MG sizing applications. On the other hand, from the MG structure point of view, most studies have tended to focus on battery energy storage systems (BESSs) to back up the variable renewable energy supplies. However, BESSs are not suitable for seasonal energy storage due to their high self-discharge rates, especially if they are placed under high stress [96]. They are also incapable of tracking the transient variability of RESs and loads.

In response, this chapter formulates a robust meta-heuristic-based, high-dimensional MG equipment capacity planning optimisation model tailored towards community-scale, sector-coupled, multi-energy-storage-technology, 100%-renewable and -reliable energy projects towards identifying the superior meta-

heuristic in MG sizing applications. To this end, it makes the following novel contributions:

- Developing a systematic descriptive statistics-based comparative meta-heuristic performance analysis scheme for MG capacity planning optimisation applications that adequately account for varying efficiencies of meta-heuristics when applied to structurally different MG systems of different sizes and input time-series data, as well as the associated initialisation-directed stochasticity in different simulation trials.

- Proposing a first-order passive low-pass energy filter-based operational planning algorithm for the efficient scheduling of multiple energy storage technologies integrated into grid-connected and isolated MG systems. The filter enables leveraging the potential of stationary power-to-gas (PtG) technologies for long-term energy storage applications and SC modules for ultra-short-term applications.

- Devising an efficient energy management strategy for the coordinated integration of hydrogen fuel cell-powered transportation fleets, namely medium-duty fuel cell electric vessels, heavy-duty tractors, and heavy-freight trucks.

## 2.2. Selection of meta-heuristics

Twenty meta-heuristic optimisation algorithms were selected based on comprehensive preliminary efficiency testing in simplified MG designing simulations involving a total of 226 meta-heuristics including both well-established and state-of-the-art single and hybrid algorithms. The selected meta-heuristics, which have shown promising results in preliminary studies, are: the PSO [52], the GA [51], the hybrid GA-PSO (HGA-PSO) [97], the ABC [53], the ACO [98], the HABC-ACO [99], the ALO [100], the improved harmony search algorithm (IHSA) [101], the BB-BC [102], the moth-flame optimisation algorithm (MFOA) [103], the sine-cosine algorithm (SCA) [104], the multi-verse optimiser (MVO) [105], the water evaporation optimisation (WEO) [106], the GWO [107], the CSA [108], the

SSA [109], the GOA [110], the dragonfly algorithm (DA) [111], the bat algorithm (BA) [112], and the firefly algorithm (FA) [113]. Table 2.1 highlights the advantages and disadvantages of the aforementioned algorithms. Furthermore, an overview of the evaluated meta-heuristics in this study can be found in the relevant original references.

Table 2.1: Strengths and weaknesses of the investigated meta-heuristics within the context of this study.

| Algorithm | Strength(s) | Weakness(es) | Reference |
|---|---|---|---|
| PSO | • Fast convergence speed<br>• Robustness to the choice of parameters | • Premature convergence | [52] |
| GA | • Exchange of information between the population to create new individuals | • Highly susceptible to the choice of the values of the operators | [51] |
| HGA-PSO | • Promoted diversity in the generation of new individuals<br>• Improved exploration of the search space | • Slow convergence rate | [97] |
| ABC | • Highly efficient in solving high-dimensional problems | • Computationally demanding | [53] |
| ACO | • High exploration power due to conducting parallel searches | • Changes in the parametric probability distribution used to generate candidate solutions throughout the iterations<br>• Poor performance when applied to continuous optimisation problems | [98] |
| HABC-ACO | • Enhanced efficiency in solving continuous optimisation problems | • Excessive number of the required function calls | [99] |
| ALO | • Few parameters to tune | • Highly sensitive to the choice of control parameters | [100] |
| IHSA | • Fair balance between the exploration and exploitation phases | • The need to fine-tune the parameters in different applications | [101] |
| BB-BC | • Easy implementation | • No trade-off between the exploration and exploitation potentials | [102] |
| MFOA | • Well-balanced exploration and exploitation abilities | • Highly vulnerable to changes in the values of the parameters | [103] |
| SCA | • Guaranteed convergence to the near-optima solution | • Computationally expensive | [104] |

| | | | |
|---|---|---|---|
| MVO | • Proven ability to avoid getting stuck in local optima | • Computationally intractable in some applications | [105] |
| WEO | • Low computational cost | • Stagnation in local optima | [106] |
| GWO | • Dynamic adjustment of control parameters | • High computational complexity | [107] |
| CSA | • Computationally-efficient | • Poor exploitation power | [108] |
| SSA | • Easy implementation stemming from its simple concept | • Poor local search ability | [109] |
| GOA | • The need to adjust only a few parameters | • Excessive computational overheads | [110] |
| DA | • Highly efficient in solving continuous problems | • Overflowing the allowed search space limits as a result of its relatively long step lengths | [111] |
| BA | • Providing quick convergence at initial stages by automatically switching from the exploration to the exploitation phase | • Rigorous theoretical foundation | [112] |
| FA | • Efficient in solving multi-modal optimisation problems | • Memory-less nature | [113] |

## 2.3. Test-case community micro-grid systems

This section describes the configuration and power flow of three structurally different MG systems, which are used for the comprehensive, descriptive statistics-based, multi-case-study efficiency comparison of the selected meta-heuristics in MG equipment capacity planning optimisation applications across a continuum of community scales – from multi-family village communities to semi-urban communities. Furthermore, the conceptualised MGs effectively shed new light on how to improve the dispatchability of future 100%-renewable MG systems by leveraging more diversified portfolios of variable renewable generation technologies with temporal complementary characteristics (particularly, solar PV, wind, and run-of-the-river micro-hydro) on both seasonal and daily bases, together with a sustainable share of dispatchable RESs (particularly, biomass resources) and optimally allocated (hybrid) energy storage systems.

Two of the community MGs, additionally, hybridise the hydrogen-based energy storage systems and SC modules for the first time in the literature to

effectively utilise the high power/energy density of SC bank/hydrogen storage, thereby providing a platform to reduce costs and energy curtailment, improve system efficiency, minimise the overall storage capacity, and prolong hybrid storage system lifetime by optimally operating each technology across the timescale it is specifically designed for. These two on- and off-grid MGs also offer the opportunity to effectively manage the agricultural and municipal solid waste of medium-scale rural and island communities (with a population of 100–1,000 people) in a self-sufficient way. The third MG system is conceptualised for smaller-scale grid-connected eco-village communities (with a population of up to 100 people) and, therefore, does not incorporate any waste management facilities. It also uses a single battery bank as a backup system given the technical and financial infeasibility of using green hydrogen-based energy storage solutions at current costs and efficiencies for supporting small-scale RSESs with the existing technologies. The exclusion of the SC bank in the battery-backed MG system can also be explained by the availability of the utility grid that is sufficient for providing primary frequency response and voltage sag mitigation in an economically viable manner given the smaller size of the system. Moreover, the two MG systems tailored to medium-scale communities are set to serve all the energy needs of the relevant communities, including electricity for transport and heat, whereas the smaller-scale MG does not aim to address e-mobility power loads.

As the above discussion suggests, the three MG systems provide diverse technological, topological, and loading bases for an in-depth, robust, comprehensive, descriptive statistics-oriented comparison of the efficiencies of the selected meta-heuristics. They, additionally, provide a platform to achieve primary research objective 1. It is also noteworthy that, for the purposes of this study, the leading brands of equipment in the Australian and New Zealand renewable energy asset markets were chosen based on the author's judgement of both prevalence and viability. The following sections mathematically model the systems' equipment.

### 2.3.1. Micro-grid 1

The first DC-coupled, grid-independent, hydrogen-based MG system, depicted in Fig. 2.1 seeks to meet the energy needs of remote island communities, whilst

additionally providing a practical solution to manage their waste. It utilises WTs for non-dispatchable renewable power generation and includes a hybrid energy storage system consisting of SCs and a hydrogen-based energy storage system. A reactor-reformer system, as well as a WtE plant, also contribute to the dispatchability of the overall energy mix, whilst also serving the purposes of waste management. Moreover, the system is equipped with a hydrogen refuelling station, which provides the fuel needed for hydrogen fuel cell-powered vessels.

In this layout, the MSW is separated by a one-way sorting and separation system, which involves two categories of MSW, namely: organics, and non-organics. The organic fraction of the MSW, together with the agricultural biomass, is fed to the reactor-reformer system to produce hydrogen via methanation and steam reforming processes. The hydrogen produced by the reformer is then stored in a hydrogen tank. The non-organic fraction of the MSW is incinerated in the WtE plant to generate electricity.

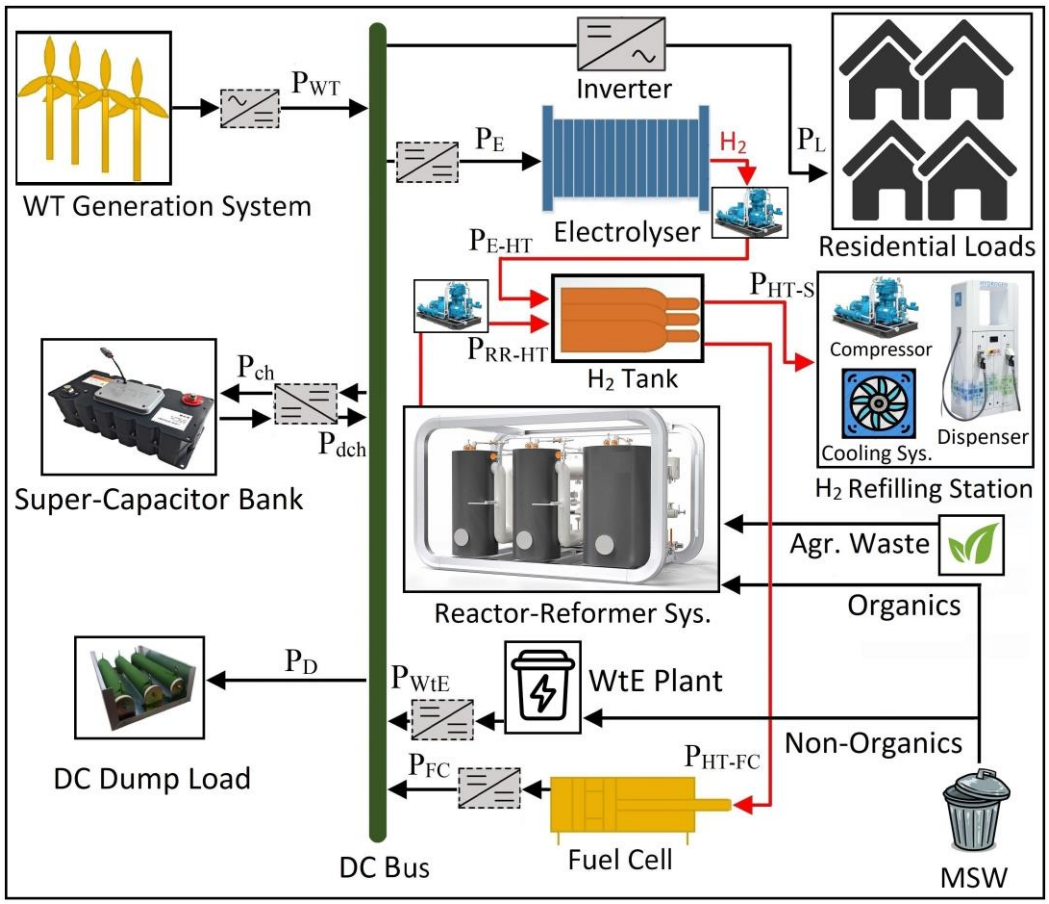


Figure 2.1: Schematic diagram and power flow of MG system 1.

The mathematical models of the components of the test-case MG system 1 are expressed in the following section, together with rule-based strategies on the operation of the network.

#### 2.3.1.1. Wind turbines

The Fuhrländer FL30 WT, the output power-wind speed (at the hub height) characteristic curve of which is shown in Fig. 2.2, is considered in this system. The WT has a rated power of 30 kW AC and a hub altitude of 27 m [114]. The wind plant's output power at each time-step, $P_{WT}(t)$ [kW], can be obtained by multiplying the optimal quantity of the WTs, $N_{WT}(t)$, by each turbine's output power estimated from the power curve presented in Fig. 2.2.

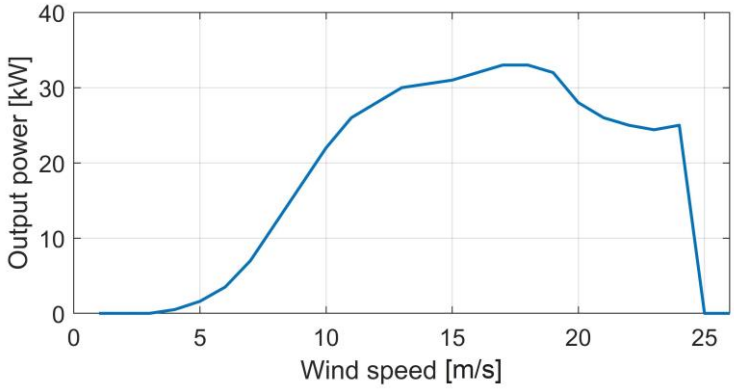


Figure 2.2: Characteristic curve of the FL30 WT (adapted from [114]).

To normalise the wind speed profile, measured at the height of $h_{ref}$, to the hub height of the WT under study, $h$, the following equation can be used [115]:

$$V_h = V_{ref} \times \left(\frac{h}{h_{ref}}\right)^{\gamma}, \tag{2.1}$$

where $V_{ref}$ represents the reference speed recorded at the height of $h_{ref}$ and $\gamma$ is a number in the range [0.1, 0.25] that reflects the status of the terrain on which the turbine is planned for installation. The value of this parameter is 0.25 for all the non-flat, tree-covered land areas considered in this study as case study sites.

#### 2.3.1.2. Waste-to-energy plant

The output power of the considered generic WtE plant at time step $t$ can be calculated by the following equation [116]:

$$P_{WtE}\,(t) = HHV_{NOW} \times \eta_{WtE} \times M_{NOW}(t), \tag{2.2}$$

where $\eta_{WtE}$ is the efficiency of the WtE plant (18%), $HHV_{NOW}$ stands for the higher heating value of the non-organic fraction of the MSW (35.7 MJ/kg), $M_{NOW}(t)$ is the amount of non-organics fed to the WtE plant at time step $t$, and $\Delta t$ is the length of each time step (1 h).

#### 2.3.1.3. Hybrid energy storage system

A hybrid energy storage system consisting of an SC bank and a hydrogen-based system – comprising an electrolyser, a hydrogen tank, and a fuel cell – is considered to support the system in the face of the variability in WTs' output power and energy demand. To this end, this study expands on the idea proposed by Xu et al. [117] that low-pass energy filters can be effectively used to calculate the share of each energy storage medium in supplying load power demand in multi-energy-storage MG systems. Accordingly, the power mismatch signal is first broken down into the low- and high-frequency components using a first-order passive low-pass filter with a transfer function given in Equation 2.3.

$$H(s) = \frac{K\omega_0^2}{s^2 + (\omega_0/Q)s + \omega_0^2}, \tag{2.3}$$

where $\omega_0$ denotes the cut-off frequency ($3.9545 \times 10^{-4}$ Hz), $K$ represents the DC gain (1.586), and $Q = 1/2\xi$ identifies the filter quality with $\xi$ indicating the damping factor (0.707).

By applying the filter, the low-frequency component of the shortage/excess power (addressed by the hydrogen storage system) at time-step $t$ can be obtained as follows:

$$\frac{P_{ex/sh}^{L}}{P_{ex/sh}} = \frac{\omega_n^2}{(\frac{1-z^{-1}}{\Delta t})^2 + \frac{\omega_n}{Q}\frac{1-z^{-1}}{\Delta t} + \omega_n^2}, \tag{2.4}$$

$$P_{ex/sh}^{L}(t) = \frac{\omega_n^2 \Delta t^2 P_{ex/sh}(t) + \left(2 + \frac{\omega_n \Delta t}{Q}\right) P_{ex/sh}^{L}(t-1) - P_{ex/sh}^{L}(t-2)}{1 + \frac{\omega_n \Delta t}{Q} + \omega_n^2 \Delta t^2}, \tag{2.5}$$

where the value of $P_{ex/sh}^{L}$ in the first two time-steps is assumed to be equal to the corresponding value of $P_{ex/sh}$. That is, $P_{ex/sh}^{L}(1) = P_{ex/sh}(1)$ and $P_{ex/sh}^{L}(2) = P_{ex/sh}(2)$.

The high-frequency component of the excess/shortage signal, which is directed to the SC bank, can accordingly be obtained as:

$$P_{ex/sh}^{H}(t) = P_{ex/sh}(t) - P_{ex/sh}^{L}(t). \tag{2.6}$$

As illustrated above, the low-frequency signal is directed to the hydrogen system, while the high-frequency signal is transferred to the SC system. The technical rationale underlying this power allocation approach is the longer cycle life, higher round-trip efficiency, and more rapid response capability of SCs to balance out generation-demand mismatches than the hydrogen system. That is, the shortest and longest periods of surplus or shortage of electricity are addressed using the SC bank and hydrogen system, respectively.[2]

Fig. 2.3 illustrates the concept of the energy filter for application to the decomposition of excess/shortage power signals addressed by the hybrid energy storage system consisting of a SC bank and a hydrogen-based storage.

[2] Note that the backup power allocation strategy employed in this study is tailored towards long-term capacity planning, at which stage long-term forecasted (projected) data are available. A forward-looking predictive modelling approach (using a critic network, for example) is indispensable for the real-time operation phase.

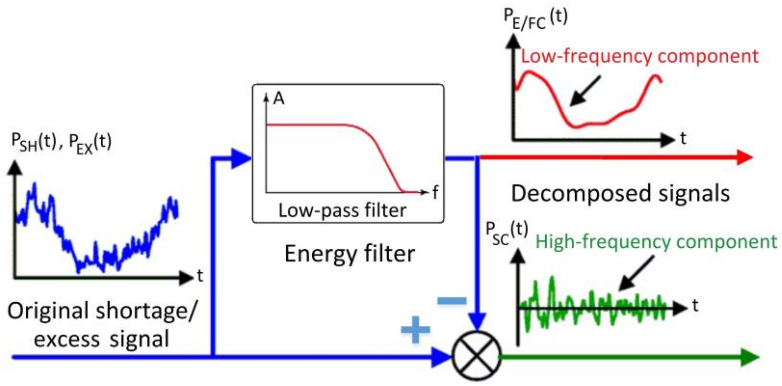


Figure 2.3: Illustration of the energy filter concept's application to the SC/hydrogen hybrid energy storage system.

#### 2.3.1.3.1. Super-capacitors

Eaton's 48-V, 166-F XLR-48R6167-R SC modules [118], which are of the type electrochemical double-layer capacitor (EDLC), are used to address ultra-short-term non-dispatchable renewable power and load demand mismatches – and improve the MG's dynamic response and overall efficiency. Using the $Work\ (W) = \frac{1}{2}\ Capacitance\ (C) \times Voltage\ (V)^2$ formula, the maximum amount of energy that could be stored within each SC module equals ~0.054 kWh. The SC bank's energy content at each hour of the MG operation can be calculated as follows:

$$E_{SC}(t) = E_{SC}(t-1) + (P_{ch,HF} - (\frac{P_{dch,HF}}{\eta_{SC}})) \times \Delta t, \tag{2.7}$$

where $\eta_{SC}$ represents the SC bank's round-trip efficiency (97%), while $P_{ch,HF}$ and $P_{dch,HF}$ are the high-frequency components of the filtered charging and discharging signals, respectively.

The energy content of the SC bank is constrained using Equation 2.8.

$$E_{SC,min} \leq E_{SC}(t) \leq E_{SC,max}, \tag{2.8}$$

where $E_{SC,min}$ and $E_{SC,max}$ are the minimum and maximum allowable storage capacities of the SC bank that are determined as follows [119]:

$$E_{SC,min} = (0.5 \times N_{SC} \times V_{SC,min}^2)/(3.6 \times 10^6), \quad (2.9)$$

$$E_{SC,max} = (0.5 \times N_{SC} \times V_{SC,max}^2)/(3.6 \times 10^6), \quad (2.10)$$

where $N_{SC}$ is the optimal number of SC modules in the bank; $V_{SC,min}$ (15 V) and $V_{SC,max}$ (48 V) are the minimum and maximum allowable voltage levels of the SC modules, respectively; with the numerical value of $3.6\times10^6$ converting the unit of measurement from J to kWh.

#### 2.3.1.3.2. Hydrogen-based energy storage system

The hydrogen-based energy storage system consists of polymer electrolyte membrane (PEM) electrolyser stacks, an intermediate-pressure compressor, a medium-pressure (20 bar) hydrogen reservoir, and stationary PEM fuel cell stacks. The H-TEC Systems' S 30/50 5-kW electrolyser stacks [120], a generic hydrogen compressor, a generic reservoir, and the Ballard's FCgen-1020ACS 3.3-kW stationary PEM fuel cell stacks have been utilised in this scheme [121].

The PEM electrolyser dissociates water molecules into oxygen and hydrogen atoms in the gas phase. The hydrogen power directed from the electrolyser outlet to the reservoir at time-step $t$ can be obtained as follows:

$$P_{E-HT}(t) = P_E(t) \times \eta_E, \quad (2.11)$$

where $P_E$ is the electrolyser's consumed power, which is controlled by the low-frequency component of the filtered charging signal, while $\eta_E$ denotes the electrolyser's efficiency (75%). An intermediate-pressure compressor, shown in Fig. 2.1, is utilised to compress the hydrogen produced by the electrolyser at around 1.2 bar pressure to around 20 bar in order to reduce the volume it occupies.

The other hydrogen production component in this layout is a united anaerobic reactor-reformer system that converts the organic fraction of the MSW, as well as the agricultural residues, into hydrogen, which is also pressurised by an intermediate-pressure compressor before being reserved in the tank. However, the

size of the reactor-reformer system is not directly linked to the parameters of the energy filter and, consequently, is treated independently.

The level of hydrogen energy stored in the tank at each time step can be calculated by the following equation:

$$E_{HT}(t) = E_{HT}(t-1) + \left(P_{E-HT}(t) + P_{RR-HT}(t) - \frac{(P_{HT-FC}(t) + P_{HT-S}(t))}{\eta_{tank}}\right) \times \Delta t, \quad (2.12)$$

where $P_{RR-HT}(t)$ is the delivered hydrogen power from the reactor-reformer system to the hydrogen tank at time-step $t$; $P_{HT-FC}(t)$ is the delivered hydrogen power from the storage tank to the fuel cell at time step $t$; $P_{HT-S}(t)$ is the delivered hydrogen power from the hydrogen reservoir to the refilling station at time step $t$; and $\eta_{tank}$ is the round-trip efficiency of the tank (95%).

Accordingly, the mass of stored hydrogen at each time step can be calculated as follows [122]:

$$m_{HT}(t) = \frac{E_{HT}(t)}{HHV_{H_2}}, \quad (2.13)$$

where $HHV_{H_2}$ is the higher heating value of hydrogen (39.7 kWh/kg).

The constraints imposed by Equation 2.14 ensure that the energy stored in the tank cannot exceed its nominal capacity and some fraction of the hydrogen energy cannot be released due to the concerns associated with the pressure drop.

$$E_{HT,min} \leq E_{HT}(t) \leq E_{HT,max}, \quad (2.14)$$

where $E_{HT,min}$ and $E_{HT,max}$ are the minimum and maximum allowable storage capacities of the reservoir, respectively. To avoid severe pressure drops in the hydrogen tank, complete releases of hydrogen are prevented by enforcing the hydrogen energy in store not to fall short of 5% of the optimised capacity of the tank ($E_{HT,min}$ = 5%). Also, to ensure that the design pressure of the tank is not

exceeded, the upper limit on the energy content of the tank is set as 95% of its optimum capacity [123].

The electric power output from the high-energy-density fuel cell unit at time-step $t$, which is controlled by the low-frequency component of the filtered discharging signal, can be obtained using Equation 2.15.

$$P_{FC}(t) = P_{HT-FC}(t) \times \eta_{FC}, \tag{2.15}$$

where $P_{HT-FC}$ represents the fuel cell's consumed hydrogen power and $\eta_{FC}$ denotes its electrical efficiency (40%), which is defined as the ratio between the electricity generated and the hydrogen consumed.

#### 2.3.1.3.2.1. Reactor-reformer system

The output hydrogen power of the generic united anaerobic reactor-reformer system, conceptualised originally by Hakimi and Moghaddas-Tafreshi [122], which has a waste-to-hydrogen efficiency of 4.54%, can be calculated by:

$$P_{RR-HT}(t) = 0.0454 \times HHV_{H_2} \times M_{OW-B}(t), \tag{2.16}$$

where $M_{OW-B}(t)$ is the aggregate amount of organic MSW and agricultural waste fed to the reactor-reformer unit at time step $t$.

### 2.3.1.4. Hydrogen refuelling station

The considered hydrogen refilling station in this study, is mainly composed of a high-pressure compressor (20 to 350 bar), a refrigeration unit, and a dispenser to a buffer storage, a cryogenic pump, a vaporiser, as well as multiple dispensers to deliver gaseous hydrogen fuel to the hydrogen fuel cell-powered vessels via nozzles [124]. Accordingly, vessels are assumed to be refuelled on a first-come/first-served basis using the multi-server Erlang-C queuing model [125], where C identifies the optimal number of dispensers. The total hydrogen power output of the station (kg-$H_2$/h) is considered in this study as a decision variable to detemine the optimal capacity of the station. The hydrogen refilling station conceptualised in this study is inspired by the schemes proposed in [126]–[129] and has an overall efficiency

($\eta_S$) of 95%. To this end, the Pure Energy Centre's customised hydrogen refilling station [130] is considered for integration into the proposed MG.

#### 2.3.1.4.1. Hydrogen fuel cell-powered vessels

Since MG system 1 is particularly designed for remote, island communities, hydrogen fuel cell-powered passenger ferries are integrated into the system through utilising the dedicated hydrogen station. To this end, the Hydrogenesis Passenger Ferry is selected as the eco-friendly, hydrogen fuel cell-powered boat. The ferry is powered by four 12 kW fuel cells that operate at a voltage of 48 V. Also, the 14-seater ferry is equipped with a purpose-built tank, which stores hydrogen at the pressure of 350 bar [131].

### 2.3.1.5. Inverter

The generic DC/AC inverter that ties the residential electrical loads to the MG's network is modelled by its efficiency, $\eta_I$, meaning that the actual load that must be satisfied at each time-step is ($1/\eta_I$)-times the imposed load on the MG. An efficiency of 95% is considered in this analysis for the loads' inverter.

### 2.3.1.6. Operational strategy

A rule-based, hourly-basis, cycle-charging operational strategy is adopted in this study for the dispatch of energy within the MG system. In the devised energy scheduling plan, (1) energy storage devices and vessels are charged/refilled using only the surplus non-dispatchable renewable power and reactor-reformer generations, (2) the mismatches between the non-dispatchable renewable power generation and electrical loads are partitioned into the high- and low-frequency components and then stored/supplied within/using the SC bank and the hydrogen tank/fuel cell, respectively. Put differently, when the hydrogen tank/SC bank is fully charged or the amount of low-/high-frequency component of the excess power is greater than the capacity of the electrolyser/hydrogen tank/fuel cell/SC bank, then the surplus power is dumped through a DC dump load. On the other hand, when the energy storage system is not able to compensate the power shortfall, a load-

shedding scheme ensures the stability of the system, which increases the unreliability of power supply.

### 2.3.2. Micro-grid 2

The second test-case system, schematically diagrammed in Fig. 2.4, is a grid-connected, DC-coupled MG, conceptually proposed to improve the energy self-sufficiency of rural communities that currently have access to the main grid – and, thereby, enhance their resilience to the upstream network outages – whilst simultaneously reducing the cost of energy. It also provides a platform to manage the rural communities' agricultural and municipal solid waste. In terms of DER mix, it is more diverse than MG 1, and integrates three non-dispatchable resources, namely: wind, solar PV, and run-of-the-river micro-hydro power plants.

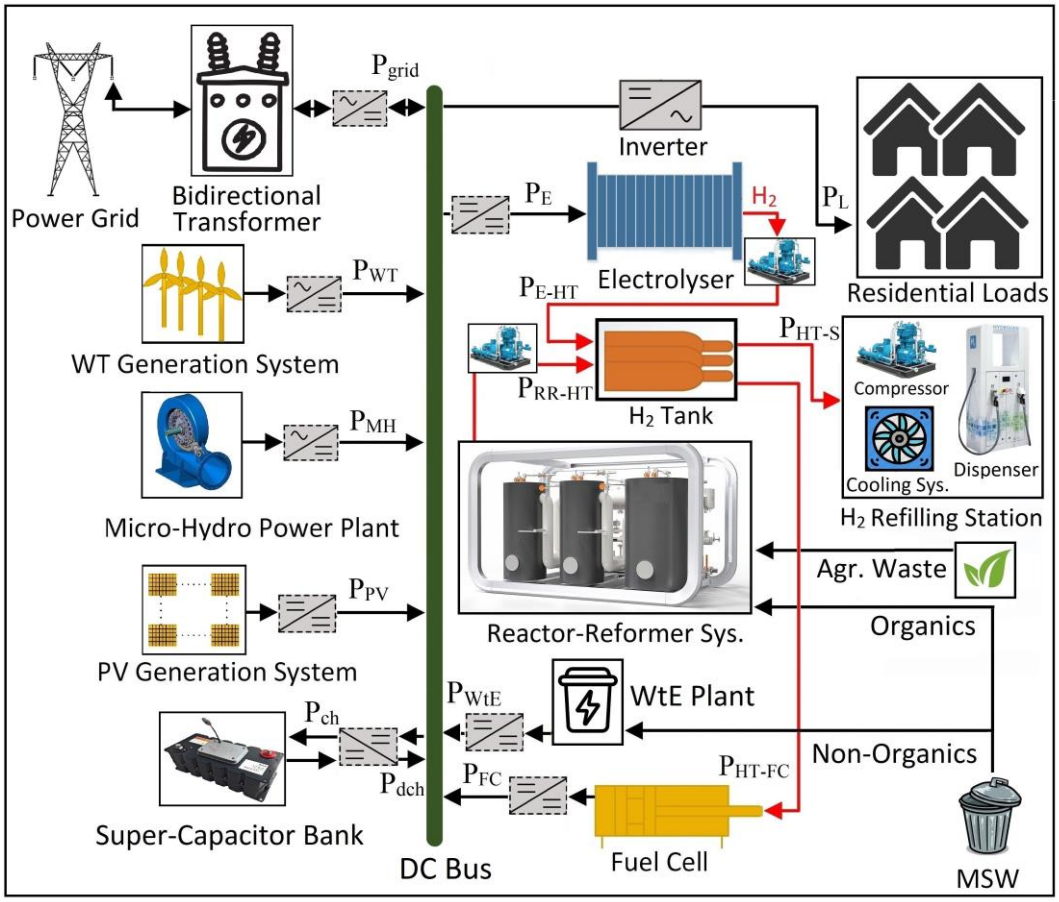


Figure 2.4: Schematic diagram and power flow of MG system 2.

The mathematical models of the hybrid SC/hydrogen energy storage system, the reactor-reformer system, the WtE plant, the residential loads' inverter, and the hydrogen refuelling station are the same as those presented for MG 1. The mathematical models of the upstream utility grid, as well as the wind, solar PV, and micro-hydro power plants, are expressed in the following sections.

#### 2.3.2.1. Utility grid

The MG system is connected to the upstream electricity network through a dedicated bidirectional MV/LV transformer, the optimal capacity of which is under investigation. The cost incurred by purchasing electricity from the utility grid at each time-step can be represented by Equation 2.17, while the income generated by the MG's electricity exports is obtained from Equation 2.18 [132].

$$cost_{im}(t) = \pi_{im}(t) \times P_{im}(t) \times \Delta t, \tag{2.17}$$

$$income_{ex}(t) = \pi_{ex} \times P_{ex}(t) \times \Delta t, \tag{2.18}$$

where $\pi_{im}(t)$ represents the (time-varying) wholesale electricity market price at time-step $t$ [$/kWh], $\pi_{ex}$ is the utility grid's single-tier (flat) buy-back rate (NZ$0.08/kWh), $P_{im}(t)$ is the amount of power imported from the utility grid at time-step $t$, $P_{ex}(t)$ is the amount of power exported to the main grid at time-step $t$, and $\Delta t$ represents the length of each time-step (1 h).

The power exchange with the main grid is planned to adhere to the following constraints:

$$P_{im}(t)/\eta_T \leq N_T, \tag{2.19}$$

$$P_{ex}(t)/\eta_T \leq N_T, \tag{2.20}$$

where $\eta_T$ denotes the transformer's efficiency (93%) and $N_T$ represents the rated active power capacity of the transformer, which is to be optimised.

The generic solid-state transformer, designed by Qin and Kimball [133], which utilises four-quadrant switch cells to allow bidirectional power flow and

controls the power via a phase shift mechanism between two active H-bridges, is considered in this study. The size of the transformer is characterised by the apparent power [kVA] and, as a simplifying assumption, the power factor is assumed to be fixed at 0.95.

#### 2.3.2.2. Wind turbines

The WT generation system in this scheme consists of Fuhrländer FL30 and FL100 WTs. The manufacturer-provided characteristic curve of the FL100 WT is shown in Fig. 2.5. The WT has a rated power of 100 kW AC and a hub altitude of 38 m [114]. The lower-rated FL30 WTs are, additionally, considered in MG system 2 to fine-tune the overall wind power generation capacity necessary to minimise the total curtailed power. Furthermore, Equation 2.1 is used to normalise the wind speed profile to the hub height of the selected WTs.

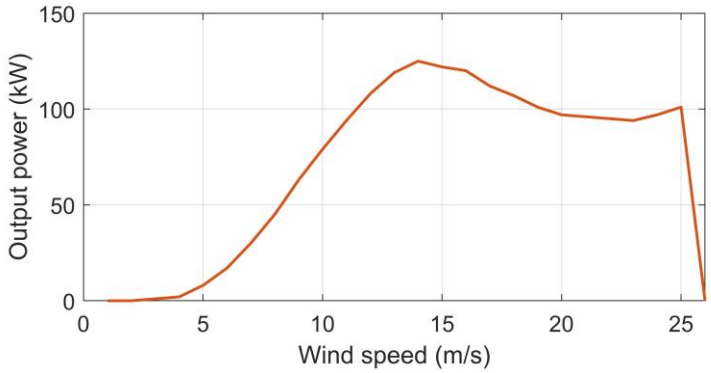


Figure 2.5: Characteristic curve of the FL100 WT (adapted from [114]).

#### 2.3.2.3. Solar photovoltaic plant

Canadian Solar's CS6K-280P polycrystalline PV modules [134], which have a nominal power of 280 W are employed in this study for PV power generation. The power output from the PV plant at each time-step, $P_{PV}(t)$ [kW], can be estimated as follows [135]:

$$T_m(t) = T_a(t) + I_G(t) \times \frac{NMOT - 20}{0.8}, \tag{2.21}$$

$$P_{PV}(t) = N_{PV} \times P_{PV,r} \times \eta_{PV,DC/DC} \times DF \times \frac{I_G(t)}{I_{STC}} \times \left(1 - \frac{K_p}{100} \times (T_m(t) - T_{STC})\right), \quad (2.22)$$

where $N_{PV}$ is the optimum quantity of the modules; $P_{PV,r}$ is the rated capacity of the modules under the standard test conditions (STC), which equals 0.28 kW; $\eta_{PV,DC/DC}$ is the PV plant's DC/DC converter efficiency (95%); $K_p$ is the temperature coefficient of the module (–0.40 %/°C); $T_m$, $T_a$, and $T_{STC}$ (25 °C) respectively represent the PV module temperature, ambient temperature, and the module temperature at the STC; $I_G$ and $I_{STC}$ (1 kW/m$^2$) respectively denote the global solar irradiance on the horizontal surface and the solar irradiance at the STC; while $NMOT$ (43 °C) and $DF$ (85%) respectively stand for the nominal module operating temperature and derating factor. The tilt angle is assumed as 30° and the Meteonorm software [136] is used to normalise the values of $I_G$ to the associated tilt angle. Also, the numeric values 20 and 0.8 respectively represent the ambient temperature [°C] and solar irradiance [kW/m$^2$] at which the $NMOT$ is defined.

#### 2.3.2.4. Micro-hydro plant

Suneco Hydro's XJ50-100SCTF6-Z 100-kW micro-hydro turbines are selected for integration into the run-of-the-river plant as part of the MG system [137]. The power output from the plant at each time-step [kW] can be estimated from Equation 2.23 [138].

$$P_{MH}(t) = \frac{N_{MH} \times \eta_{MH,AC/DC} \times \eta_{MH} \times \rho \times g \times h_g \times F(t)}{1000}, \quad (2.23)$$

where $N_{MH}$ denotes the optimum quantity of turbines, $\eta_{MH}$ is the total efficiency of the plant (including the turbine, generator, and water wheel efficiencies), which equals 78%, $\eta_{MH,AC/DC}$ is the efficiency of the plant's AC/DC converter (95%), $\rho$ represents the density of water (1000 kg/m$^3$), $g$ is the acceleration due to gravity (9.81 m/s$^2$), $h_g$ is the gross head (which is defined as the difference between the

head race and tail race levels when water is not flowing), which is fixed at 10 m, $F(t)$ is the flow rate at time-step $t$ [$m^3$/s], while the numeric value of 1000 converts the unit of measurement from Wh to kWh.

#### 2.3.2.5. Hydrogen fuel-cell powered trucks and tractors

Since the second MG system is specifically conceptualised for rural agricultural communities, hydrogen fuel cell-powered trucks and tractors are considered as hydrogen loads. Accordingly, Hyundai's heavy-freight Xcient fuel cell-electric trucks and heavy-duty New Holland's NH2 fuel cell-electric tractors are respectively considered as hydrogen fuel cell-powered vehicles that utilise the station. The considered trucks and tractors respectively hold 32.86 and 8.2 kg of gaseous hydrogen in their type IV carbon composite-based tanks at a pressure of 350 bar [139], [140].

#### 2.3.2.6. Operational strategy

Similar to the first test-case MG system's operational strategy (Section 2.3.1.6), a rule-based, hourly-basis, Greedy, cycle-charging operational dispatch strategy[3] is employed to operate the second MG. The only difference is that when the hybrid energy storage system is not able to supply/absorb the shortfall/excess of total non-dispatchable energy (sum of the power outputs from the wind, solar PV, and micro-hydro power plants), the upstream grid takes the responsibility to inject/withdraw the shortage/surplus energy, instead of load shedding/energy spillage. Nevertheless, if the associated energy shortage/surplus violates the constraints in Equations 2.19 and 2.20, still, load-shedding/energy spillage will be necessary.

### 2.3.3. Micro-grid 3

The third battery-backed, grid-tied, DC-coupled MG system, shown in Fig. 2.6, is less structurally complex than MG systems 1 and 2. It is tailored to small-scale, multi-family, grid-connected eco-villages. It provides four main benefits, namely:

[3] Under the Greedy, cycle-charging energy scheduling approach tailored to grid-connected systems, any excess local renewable power generation is used to charge the dedicated energy storage system before being exported, whereas any onsite resource deficiency is met by releasing the energy in store before purchasing from the wholesale market [286].

(i) improving the resilience of small communities against planned and unplanned grid outages, as well as low-probability, catastrophic events onsite, (ii) lowering energy costs and reducing energy hardship and poverty, (iii) increasing the self-sufficiency of eco-village communities with respect to energy procurement, as well as (iv) reducing environmental impacts of power generation. As Fig. 2.6 shows, the system is equipped with solar PV panels, WTs, and a lithium-ion (Li-ion) battery bank.

The mathematical models of the solar PV plant, the utility grid, and the residential loads' bi-directional inverter remain the same as those presented for MG systems 1 and 2. However, unlike MG 2, the capacity of the bi-directional transformer at the point of common coupling (PCC) is assumed to be known and equals the size of the existing installed transformer at the grid-connected site of interest. This can be explained by the fact that the third MG architecture is designed for smaller communities and, therefore, no significant profit margins are expected from temporal energy arbitrage, especially given that it is not suitable for integrating long-duration hydrogen-based energy storage systems. In addition, the transformer's efficiency for power exchanges with the AC grid was assumed to be 93%.

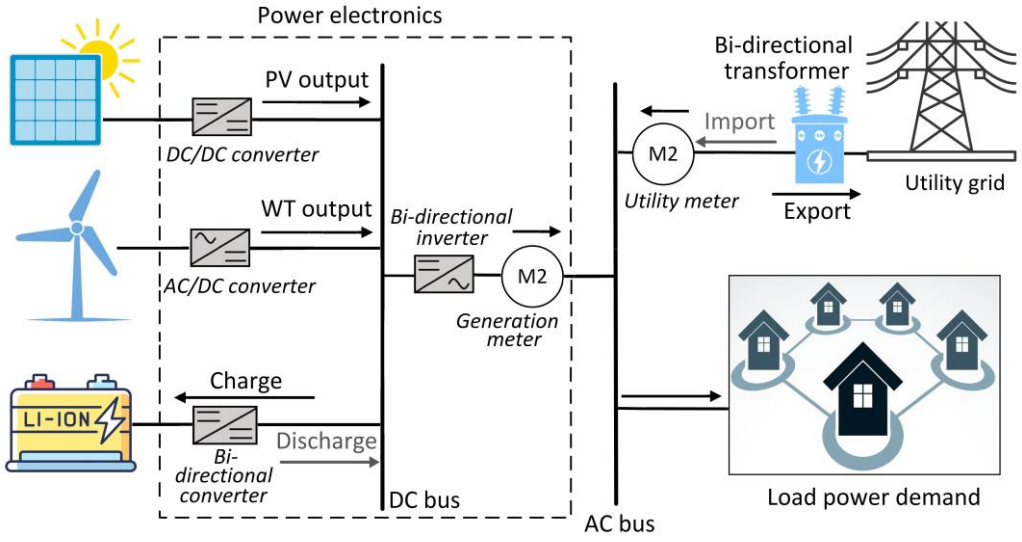


Figure 2.6: Schematic diagram and power flow of MG system 3.

The other two main components of the system – WTs and the Li-ion battery bank – are modelled in the following sections.

#### 2.3.3.1. Wind turbines

Unlike test-case MG systems 1 and 2, where WTs are modelled using the associated manufacturer-provided characteristic power-wind speed curves, a generic mathematical formulation is used for modelling WTs in MG 3. The reason lies in the lack of manufacturer-provided power curve for the selected small-scale WT product model – which is expected to be suitable for this case – in the relevant online databases. The power output from each WT is given by [141]:

$$P_{WT}(t) = \begin{cases} 0 & if\ v(t) \le v_{ci}\ or\ v(t) \ge v_{co}, \\ A & if\ v_{ci} < v(t) \le v_r, \\ P_{WT,r} & if\ v_r < v(t) < v_{co}, \end{cases} \quad (2.24)$$

$$A = \frac{P_{WT,r}}{v_r^3 - v_{ci}^3} v^3(t) - \frac{v_{ci}^3}{v_r^3 - v_{ci}^3} P_{WT,r}, \quad (2.25)$$

where $v(t)$ denotes wind speed at time-step $t$, $v_{ci}$ is the WT's cut-in wind speed (2.7 m/s), $v_r$ is the WT's rated wind speed (11 m/s), $v_{co}$ is the WT's cut-out wind speed (25 m/s), and $P_{WT,r}$ is the selected turbine's (AWS HC Wind Turbine) rated power (5 kW) [142]. Also, Equation 2.1 is used to normalise the wind speed profile to the hub height of the selected WT.

#### 2.3.3.2. Battery bank

A generic stationary, behind-the-meter, graphite-$LiFePO_4$ (lithium iron phosphate)-based Li-ion battery bank is considered for integration into MG 3. The battery bank's energy content at each hour of the MG operation can be calculated as follows:

$$E_B(t) = E_B(t-1).(1 - \sigma_B.\Delta t) + \eta_{ch,B}.P_{ch,B}(t).\Delta t - \frac{P_{dch.B}(t).\Delta t}{\eta_{dch,B}} \quad \forall t, \quad (2.26)$$

where $\eta_{ch,B}$ and $\eta_{dch,B}$ respectively denote the battery charging and discharging efficiencies (92%); $\sigma_B$ is the battery self-discharge rate (0.3%/day); and $\Delta t$ is the length of each time-step (1 hour).

The energy content of the battery bank is constrained using Equation 2.27.

$$E_{B,min} \leq E_B(t) \leq E_{B,max}, \tag{2.27}$$

where $E_{B,min}$ and $E_{B,max}$ are the minimum and maximum allowable storage capacities of the battery bank. The minimum allowable energy in store is controlled by the battery bank's maximum permissible energy content, as well as depth of discharge (DOD), which can be described by Equation 2.28. The maximum allowable DOD of the battery bank is considered as 85% in this analysis [143]. Also, the maximum allowable energy in store equals the optimal size of the battery bank.

$$E_{B,min} = \frac{100 - DOD}{100} \times E_{B,max}. \tag{2.28}$$

Furthermore, the battery storage power constraints in Equations 2.29 and 2.30 ensure that the charging and discharging rates of the battery bank are in the associated allowable ranges.

$$0 \leq P_{ch,B} \leq P_{ch,B}^{max}, \tag{2.29}$$

$$0 \leq P_{dch,B} \leq P_{dch,B}^{max}, \tag{2.30}$$

where $P_{ch,B}^{max}$ and $P_{dch,B}^{max}$ denote the charge and discharge power capacities, which are fixed at 0.5 kW per kWh of storage capacity (cycled at a C/2 rate), meaning that the battery bank can be fully charged or discharged within two hours.

#### 2.3.3.3. Operational strategy

A rule-based, hourly-basis, Greedy, cycle-charging operational dispatch strategy similar to that of MG 2 is employed to schedule the operation of the MG system. Likewise to the second MG's operational strategy, the absorbing/supplying of the excess/shortage of the total non-dispatchable renewable power by the storage system is prioritised above trading energy with the utility grid.

### 2.3.4. Assumptions

The following assumptions are made for the relevant test-case MG systems:

1. For all three test-case MG systems, there are existing overhead power distribution lines and the conceptualised MGs are not supposed to be first-access systems.

2. For grid-tied cases, the power factor – defined as active power in kW divided by apparent power in kVA – is assumed to be constant and equal to 0.95.

3. The hydrogen distribution networks in test-cases 1 and 2 are not expected to be large, as the electrolysis and hydrogen reservoir facilities could be placed in the vicinity of the hydrogen station and inverters, or vice versa.

4. The optimal sizing of the hydrogen station is carried out from a high-level perspective in the optimal planning phase, while the optimised capacity of the overall hydrogen refuelling infrastructure could be distributed among several optimally-sited stations during the implementation phase of the associated MG systems (MGs 1 and 2), which might entail building hydrogen distribution networks.

5. Except for the solar PV panels (where relevant), the effects of degradation on the lifetime and efficiency of the equipment are neglected.

6. The optimal sizes of the power conversion devices serving as interfaces between the MG components and the associated common DC buses are dependent on the optimal sizes of the corresponding energy generation/storage components. That is, out of the power electronics devices, only the size of the multi-mode (hybrid) system inverter is determined independently.

7. Conversions from AC to DC, from DC to AC, and from DC to DC, were assumed to have efficiencies of 95% for each direction.

8. The costs of power electronics devices, as well as the costs and efficiencies of the intermediate- and high-pressure hydrogen compressors, are included in the relevant MG components.

9. For simplicity, the wind fields were assumed to be horizontally uniform at each height.

10. The efficiencies of the renewable energy generation technologies are in accordance with their respective nameplate capacities.

11. All the potentially valuable RESs at the considered case study sites are accommodated in the modelled MG systems and, in this way, implicit prior techno-economic feasibility assessments of green energy resources are carried out – the optimisation protocol is able to reject the adoption of any of the sources by optimising its size to zero.

### 2.3.5. Cycle counting algorithm

In order to systematically count the heterogenous cycles of the battery and SC banks in the simulated MG systems, the three-point rainflow-cycle-counting algorithm is employed in this study [144]. The algorithm is able to translate a spectrum of varying states-of-charge into a set of discrete full- and half-change (charge/discharge) cycles as a function of cycle amplitude. To this end, first, the state-of-charge (SOC) profile is converted into a series of minima and maxima (known as reversals), where the delta SOC changes sign. The cycles are counted by using a moving reference point of the series, $Z$, as well as a moving ordered three-point subset with the following features [144]:

- The first and second points are collectively denoted by $Y$.

- The second and third points are collectively denoted by $X$.

- The sets of ordered pairs $X$ and $Y$ are sorted chronologically, but are not necessarily consecutive points in the SOC profile.

- The range of $X$, denoted by $r(X)$, is defined as the absolute difference of the amplitudes of the first and second points. The definition of $r(Y)$ is analogous.

In this context, Fig. 2.7 illustrates the process flow of the three-point rainflow-cycle-counting algorithm [145].

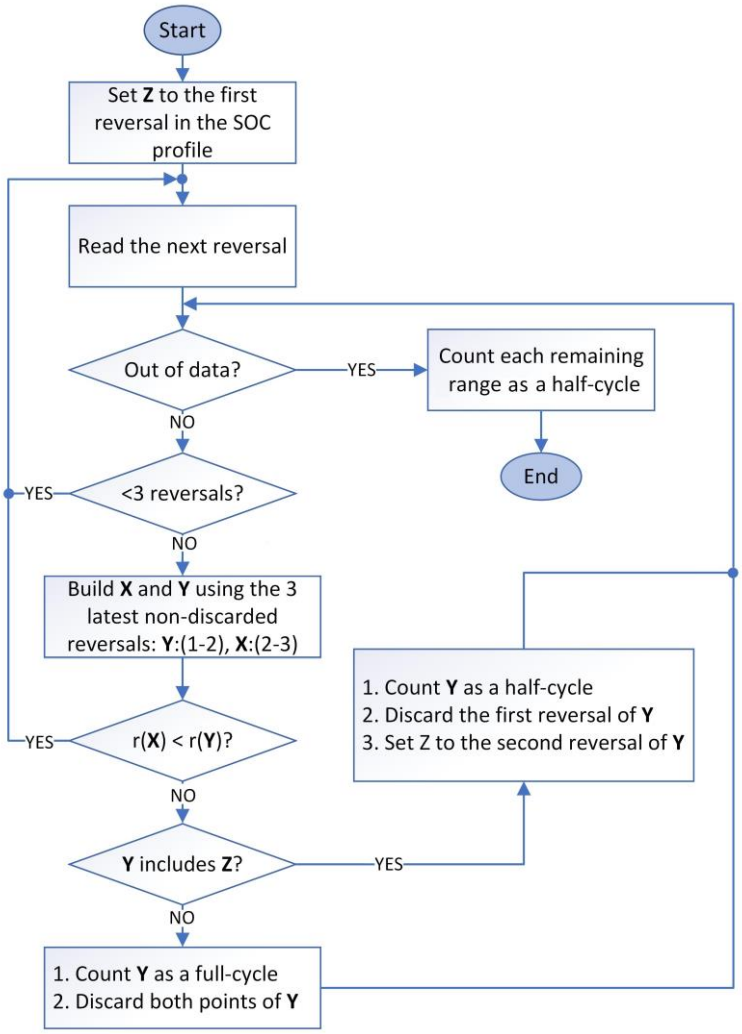


Figure 2.7: Illustration of the three-point rainflow-cycle-counting algorithm (adapted from [145]).

In addition, Fig. 2.8 illustrates the application of the rainflow-cycle-counting algorithm to a typical representative SOC profile [146]. In the figure, the full-cycles are represented by the planes enclosed by the mustard yellow triangles, whereas the half-cycles are represented by the planes enclosed by the triangles diagonally shaded in light blue. As the figure shows, the representative SOC profile contains three full-cycles – the triangular regions B-A′-B′, J-K′-J′, and I-F-I′ – and four half-cycles – the triangular regions C-D-C′, G-H-G′, L-M-L′, and N-O-N′.

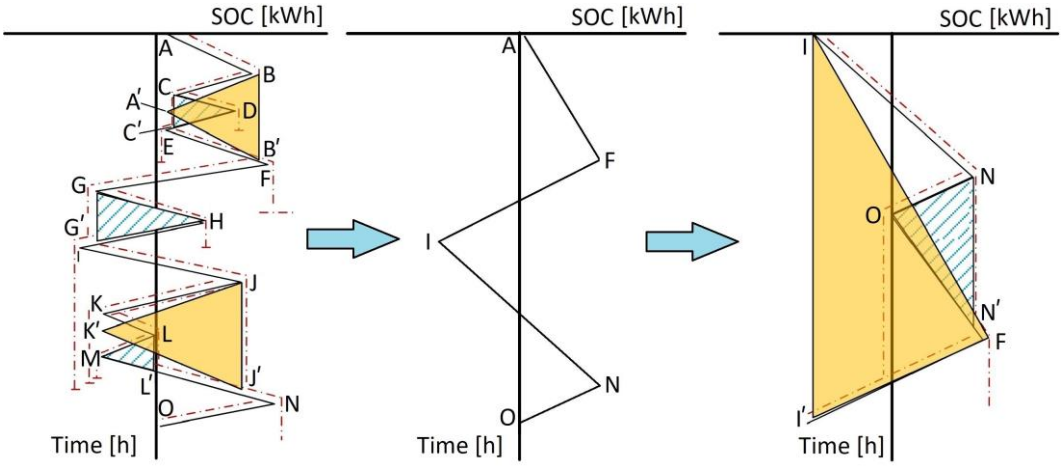


Figure 2.8: Illustrative application of the three-point rainflow-cycle-counting algorithm to a typical representative SOC profile (adapted from [146]).

In this study, the MATLAB's built-in '*rainflow*' function [145] is used to estimate the battery and SC cycle counts as part of calculating the application-specific expected cycle lives of the battery and SC banks.

### 2.3.6. Data: Selected product models

The techno-economic specifications of the MG equipment, namely the capital, replacement, and operation and maintenance (O&M) costs, as well as the expected service life and efficiency of the equipment are summarised in Table 2.2. Note that, throughout this thesis, all monetary values are expressed in 2019 NZ$. Where required, foreign currencies were converted into NZ$ at the yearly average currency exchange rates in 2019.

Table 2.2: Data values and sources for techno-economic specifications of the components of test-case MGs 1–3.

| Component | Manufacturer part number | Nameplate rating | Capital cost* | | Replacement cost† | Operation and maintenance cost† | Expected service life | Nominal efficiency | | Source |
|---|---|---|---|---|---|---|---|---|---|---|
| | | | Per unit | Per standard unit of generation /storage/ conversion capacity | | | | Notation | Value [%] | |
| PV module | CS6K-280P | 280 W | $437/unit | $1.6k/kW | $350/unit | $1.9/unit/year | 20 years | $\eta_{PV}$ | 17.11 | [134] |
| Wind turbine | Fuhrländer FL30 | 30 kW | $43k/unit | $1.4k/kW | $35k/unit | $573/unit/year | 20 years | N/A‡ | N/A‡ | [114] |
| | Fuhrländer FL100 | 100 kW | $140k/unit | $1.4k/kW | $110k/unit | $1.4k/unit/year | 20 years | N/A‡ | N/A‡ | [114] |
| | AWS HCM | 5 kW | $6.5k/unit | $1.3k/kW | $6.1k/unit | $28/unit/year | 20 years | N/A‡ | N/A‡ | [142] |
| Micro-hydro turbine | XJ50-100SCTF6-Z | 100 kW | $56k/unit | $560/kW | $50k/unit | $500/unit/year | 20 years | $\eta_{MH}$ | 78 | [137] |
| Transformer | Generic | – | – | $165/kVA | $55/kVA | $2/kVA/year | 30 years | $\eta_{T}$ | 93 | [133], [147] |
| Inverter | Generic | – | – | $1,200/kW | $1,200/kW | $3.9/kW/year | 15 years | $\eta_{I}$ | 95 | [148] |
| Super-capacitor module | XLR-48R6167-R | 166 F, 48 V ≡ 0.054 kWh | $1.3k/unit | $24k/kWh | $1.3k/unit | $3.3/unit/year | 1m cycles or 20 years | $\eta_{SC}$ | 97§ | [118] |
| Battery pack | Generic Li-ion | – | – | $885/kWh | $417/kWh | $2.1/kWh/year | 12k cycles or 15 years | $\eta_{B}$ | 92¶ | [149] |

| | | | | | | | | | | |
|---|---|---|---|---|---|---|---|---|---|---|
| Electrolyser stack | H-TEC S 30/50 | 5 kW | $6k/unit | $1.2k/kW | $5.5k/unit | $20/unit/year | 20 years | $\eta_E$ | 75 | [120] |
| Hydrogen tank | Generic | – | – | $500/kg | $500/kg | $1/kg/year | 20 years | $\eta_{HT}$ | 95[§] | [150] |
| Fuel cell stack | FCgen-1020ACS | 3.3 kW | $5k/unit | $1.5k/kW | $4k/unit | $0.02/unit/hour | 10k hours | $\eta_{FC}$ | 40 | [121] |
| Waste-to-energy plant | Generic | – | – | $9.6k/kW | $7.3k/kW | $210/kW/year | 10 years | $\eta_{WtE}$ | 18 | [116] |
| Reactor-reformer system | Generic | – | – | $34.5k/(kg-$H_2$/h) | $13.2k/(kg-$H_2$/h) | $910/(kg-$H_2$/h)/year | 20 years | $\eta_{RR}$ | 4.54 | [122] |
| Hydrogen station – refuelling unit | Generic (Pure Energy Centre) | – | – | $10k/(kg-$H_2$/h) | $5k/(kg-$H_2$/h) | $350/(kg-$H_2$/h)/year | 20 years | $\eta_S$ | 95 | [124], [130], [151] |

[*] All the reported capital costs represent the actual cost of buying the selected components in the Australian and New Zealand renewable energy asset markets as of October 2019.

[†] All the replacement and O&M costs were calibrated in accordance with the component-specific ratios of capital to replacement and O&M costs reported in [150], [152]–[156].

[‡] Not applicable as the WT efficiency is reflected in the associated power curves shown in Figs. 2.2 and 2.5, as well as the formulas in Equations 2.24 and 2.25.

[§] Round-trip efficiency.

[¶] Charge/discharge efficiency.

## 2.4. Methodology

The following sections lay out the structure of the proposed meta-heuristic-based long-term MG investment planning and capacity optimisation model.

### 2.4.1. Objective functions

The objective is to minimise the whole-life cost of the project, which consists of the lifetime costs of the components and the total cost of trading electricity with the utility grid (i.e., net electricity imports) over the MG life-cycle in present value, as follows:

$$\min WLC_{MG} = \sum_{c \in C} NPC_c + NPC_{tr,net} + p, \tag{2.31}$$

where $NPC_c$ denotes the net present cost of the candidate technology $c$ that is included in the model for consideration, $NPC_{tr,net}$ is the cost of total net energy purchased from the upstream grid in present value, while $p$ penalises the solutions that violate any of the imposed constraints.

The sets of candidate technologies for MG systems 1–3 are as follows:

$C_{MG1} = \{WT_{FL30}, WtE, E, HT, FC, RR, SC, S, I\}$,

$C_{MG2} = \{PV, WT_{FL30}, WT_{FL100}, MH, WtE, T, E, HT, FC, RR, SC, S, I\}$,

$C_{MG3} = \{WT_{AWS-HCM}, PV, B, T, I\}$,

where $WT_{FL30}$, $WT_{FL100}$, $WT_{AWS-HCM}$, $PV$, $MH$, $WtE$, $E$, $HT$, $FC$, $RR$, $SC$, $S$, $I$, $T$, and $B$ respectively denote FL30 wind turbines, FL100 wind turbines, AWS-HCM wind turbines, solar PV panels, micro-hydro turbines, the WtE plant, the electrolyser unit, the hydrogen tank, the fuel cell, the anaerobic reactor-reformer system, SC modules, the hydrogen refuelling station, the loads' inverter, the transformer, and battery packs. Also, for a non-grid-connected MG system, $NPC_{tr,net} = 0$.

The net present cost (NPC) of a component in the context of MG designing and capacity planning refers to the present value of all the costs associated with its new installation, replacement, as well as O&M over the life-cycle of the project. The term "present value" in this context describes costs that have been discounted back to the baseline year, which accounts for the growth of inflation and the rise of interest rates. Mathematically, the NPC of a component can be expressed by the following equation [122], [157]:

$$NPC_c = N_c \times \left( CC + RC \times SPPW + \frac{O\&M}{CRF(ir, PL)} - SV \right), \tag{2.32}$$

where $N_c$ denotes the optimal capacity/quantity of component $c$; $CC$ and $RC$ respectively represent the capital cost and replacement cost of the component; $SPPW$ stands for the single-payment present-worth factor, which is defined in Equation 2.33 [122];[4] $O\&M$ indicates the operation and maintenance cost of the component; $CRF$ stands for the capital recovery factor that is a function of the real interest rate, $ir$ (2.45% [158]),[5] and the expected service life of the project, $PL$ (20 years), as expressed in Equation 2.35 [122];[6] and $SV$ is the salvage value of the component, which is expressed in Equation 2.36 [159].[7] Any additional residual value, other than what is reflected in the equipment salvage value, is assumed to be counterbalanced by the costs associated with the equipment recycling or disposal.

$$SPPW = \sum_{n=1}^{N} \frac{1}{(1 + ir)^{CL \times n}}, \tag{2.33}$$

where $CL$ denotes the component lifetime and $N$ can be determined by the following equation:

[4] The single-payment present-worth factor calculates the unknown present value of a lump sum payment needed that returns a known future value given the interest rate.

[5] The real interest rate was projected by taking the mean of the historical records in New Zealand over a 10-year period, between 2010 and 2019.

[6] The capital recovery factor is used to calculate the present value of a series of equal annual cash flows as a ratio of a constant annuity to the present value of receiving that annuity.

[7] The salvage value, alternatively referred to as resale value, scrap value, and residual value, is the estimated value that is expected at the end of the useful life of a MG asset, which is used to calculate the asset's depreciation expense.

$$N = \begin{cases} \left\lfloor \frac{PL}{CL} \right\rfloor - 1 & if\ PL\ mod\ CL = 0, \\ \left\lfloor \frac{PL}{CL} \right\rfloor & otherwise, \end{cases} \tag{2.34}$$

$$CRF(ir, PL) = \frac{ir(1+ir)^{PL}}{(1+ir)^{PL}-1}, \tag{2.35}$$

$$SV = RC \times \frac{CL - \left(PL - CL \times \left\lfloor \frac{PL}{CL} \right\rfloor\right)}{CL}. \tag{2.36}$$

In addition, to adjust the energy exchange cost components for the real interest rate, the NPC of the net energy purchased from the utility grid over the MG life-cycle can be obtained as [160]:

$$NPC_{tr,net} = \sum_{n=1}^{PL} \frac{C_{tr,n}}{(1+ir)^n}, \tag{2.37}$$

where $C_{tr,n}$ denotes the total cost associated with the total net energy purchased from the grid in year $n$ of the MG operation, which can be obtained from Equation 2.38.

$$C_{tr,n} = \sum_{t=1}^{T} (\pi_{im,n}(t) \times P_{im,n}(t) - \pi_{ex,n} \times P_{ex,n}(t)) \times \Delta t, \tag{2.38}$$

where $T = \{1, 2, \dots, 8{,}760\}$ is the set of time-steps of the hourly-basis, year-long operation of the MG system.

Furthermore, for the components, the service lives of which are characterised by operating hours, rather than the expected years of reliable operation, the following equation is used to convert the associated hourly-basis operational life into the equivalent years of lifetime [161]:

$$CL = \frac{CL_h}{N_h}, \tag{2.39}$$

where $CL_h$ denotes the service life of the component given in terms of operational hours and $N_h$ represents the number of hours it is expected to operate over a one-year period, which is determined in the course of the optimisation process.

Moreover, the expected service lives of the battery and SC banks are specified by the expected number of charging/discharging cycles they can provide and their float lives. Accordingly, the following equation is used to calculate the battery and SC storage banks' service lives considering both the associated cyclic and calendar lives [162].

$$SL = \min\left(L_f, \frac{N_S.TC_S}{AC_S}\right), \tag{2.40}$$

where $N_S$ is the optimal quantity of the battery packs or SC modules in the relevant storage bank, $L_f$ is the associated storage device's float life [years], $TC_S$ is the expected number of cycles of a single storage module/pack (total lifetime number of cycles), and $AC_S$ is a single storage module's/pack's number of annual full-equivalent cycles (the number of full-equivalent cycles over a year-long operation).

### 2.4.2. Constraints

The objective function in Equation 2.31 is subject to two sets of constraints at the operational scheduling and investment planning levels.

#### 2.4.2.1. Operational-level constraints

The operational-level constraints incorporate system-wide power balance (Equations 2.41–2.43 for MGs 1–3, respectively); non-strictly positive minimum and maximum capacity bounds placed on the operating points of the energy generation and conversion assets (Equation 2.44); as well as lower and upper limits on the allowable energy in store and charge/discharge power capacity of the storage (Equations 2.8–2.10, 2.14, and 2.27–2.30). The upper bounds represent the optimal sizes of the associated components. The lower bounds are fixed at zero for the associated generation and conversion infrastructure, and controlled by the corresponding upper bounds for storage media as indicated in the relevant sections. Moreover, two separate constraints enforce the product of the hourly battery/SC

charging and discharging powers, as well as the hourly imported and exported powers to be equal to zero, as behind-the-meter batteries/SC cannot be operated to simultaneously charge and discharge (Equation 2.45), and the transformer at the PCC cannot be operated to concurrently import and export electricity (Equation 2.46).

$$P_{WT_{FL30}}(t) + P_{WtE}(t) + P_{dch,HF}(t) + P_{FC}(t) + P_{RR-HT}(t) + \frac{Q_L(t)}{\eta_I} + \frac{Q_S(t)}{\eta_S} = P_{ch,HF}(t) + P_E(t) + \frac{P_L(t)}{\eta_I} + \frac{P_S(t)}{\eta_S} + P_D(t) \quad \forall t, \tag{2.41}$$

$$P_{PV}(t) + P_{WT_{FL30}}(t) + P_{WT_{FL100}}(t) + P_{WtE}(t) + P_{MH}(t) + P_{dch,HF}(t) + P_{FC}(t) + P_{im}(t) + P_{RR-HT}(t) + \frac{Q_L(t)}{\eta_I} + \frac{Q_S(t)}{\eta_S} = P_{ch,HF}(t) + P_E(t) + P_{ex}(t) + \frac{P_L(t)}{\eta_I} + \frac{P_S(t)}{\eta_S} \quad \forall t, \tag{2.42}$$

$$P_{WT_{AWS-HCM}}(t) + P_{PV}(t) + P_{dch,B}(t) + P_{im}(t) + \frac{Q_L(t)}{\eta_I} = P_{ch,B}(t) + P_{ex}(t) + \frac{P_L(t)}{\eta_I} + \frac{P_S(t)}{\eta_S} \quad \forall t, \tag{2.43}$$

$$P_{gen/conv}^{min} \leq P_{gen/conv}(t) \leq P_{gen/conv}^{max} \quad \forall t, \tag{2.44}$$

$$P_{ch,B/SC}(t) \times P_{dch,B/SC}(t) = 0 \quad \forall t, \tag{2.45}$$

$$P_{im}(t) \times P_{ex}(t) = 0 \quad \forall t, \tag{2.46}$$

where $P_D(t)$ is the power consumed by the dump load at time-step $t$, while $Q_L(t)$ and $Q_S(t)$ respectively represent the unmet electrical and hydrogen demands at time-step $t$, which are used in the loss of power supply probability (LPSP) reliability index calculations described in the next section.

Additionally, the grid-connected MGs' transactions of energy with the upstream power network (grid power imports/exports) are constrained by Equations

2.19 and 2.20 to adhere to the optimal size of the transformer connecting the MG system to the upstream grid at the PCC.

#### 2.4.2.2. Planning-level constraints

Several constraints need to be relaxed at the investment planning level, which are presented in the following sections.

##### 2.4.2.2.1. Reliability

A maximum allowed unreliability constraint measured by the LPSP index (Equation 2.47) is considered [163], which is set to 0, i.e. load always satisfied.

$$LPSP_e \leq LPSP_e^{max}. \tag{2.47}$$

The LPSP is an indicator of the unreliability of power supply, which is defined as the sum of the shortages of power generation capacity divided by the total power demand on the system over the operation analysis period, which can be expressed as follows [163]:

$$LPSP = \frac{\sum_{t=1}^{T}(LPS(t) \times \Delta t)}{\sum_{t=1}^{T}(P_L(t) \times \Delta t)}, \tag{2.48}$$

where $LPS(t)$ is the loss of power supply at time-step $t$ when demand outstrips supply, as defined in Equation 2.49, $P_L(t)$ is the load power demand at time-step $t$, $\Delta t$ is the duration of each time-step, and $T$ is the length of the operating horizon.

$$LPS(t) = \begin{cases} P_L(t) - P_{sup}(t) & if\ P_L(t) > P_{sup}(t), \\ 0 & otherwise, \end{cases} \tag{2.49}$$

where $P_{sup}(t)$ denotes the total power supplied by the onsite DERs (i.e., the internal generation and storage equipment) at time-step $t$ of the system operation over the operating horizon $T$.

In the grid-connected renewable energy system context, $P_{sup}$ includes the power imported from the upstream grid in addition to the power generated by the onsite DERs. It is noteworthy that in the context of long-term renewable energy

system investment planning, $T$ is commonly set to 8,760 hours (i.e., a typical one-year simulation study) and the duration of each time-step is taken equal to 1 hour.

Similarly, where appropriate, a separate maximum allowed LPSP reliability constraint (Equation 2.50) ensures the 100% reliability of hydrogen supply over the expected 20-year lifespan of the MG system.

$$LPSP_{H_2} \leq LPSP_{H_2}^{max}. \tag{2.50}$$

#### 2.4.2.2.2. Self-sufficiency

A minimum allowed self-sufficiency ratio (SSR) constraint, measured as the percentage of demand served by local DERs over the one-year operation of the system (Equation 2.51) [164], ensures that the designed system is highly self-sufficient. The minimum allowable SSR is set to 80% in this study.

$$SSR \geq SSR^{min}. \tag{2.51}$$

Mathematically, the SSR can be defined as:

$$SSR = \frac{\sum_{t=1}^{T} P_L(t) - P_{im}(t)}{\sum_{t=1}^{T} P_L(t)}. \tag{2.52}$$

Accordingly, for an off-grid system, the resulting SSR equals 100%. Note that since the hydrogen loads are always met by internally generated (excess) renewable power, the definition of SSR excludes the load demand of the hydrogen station for MGs 1 and 2.

#### 2.4.2.2.3. Resilience

The capacity planning optimisation is enforced to meet two energy resilience constraints, namely the minimum autonomy hour of the overall energy storage system and the minimum grid outage survivability (where appropriate), which are respectively defined as the ratio of the overall storage size to the mean total annual load demand and the ratio of the overall storage size to the mean total annual net load demand (load minus local generation), as follows [165]:

$$AH_S \geq AH_S^{min}, \tag{2.53}$$

$$AH_S = \frac{OSC}{\left(\sum_{t=1}^{T} P_L(t)\right)/T}, \tag{2.54}$$

$$GOS_{MG} \geq GOS_{MG}^{min}, \tag{2.55}$$

$$GOS_{MG} = \frac{OCS}{\left(\sum_{t=1}^{T} P_L(t) - P_{RES}(t)\right)/T}, \tag{2.56}$$

where $OSC$ is the overall storage capacity of the MG system in the optimum solution set, $P_{RES}(t)$ is the total power output from the onsite renewable energy technologies at time-step $t$, while $AH_S^{min}$ and $GOS_{MG}^{min}$ respectively denote the minimum allowed (storage) autonomy hour and grid outage survivability of the system, which are assumed as 8 and 12 hours, respectively.

More specifically, the grid outage survivability characterises the MG resilience to outages on the grid, while the autonomy hour represents more severe events that disrupt access to the grid and the electricity generated from onsite renewable resources. Furthermore, the exclusion of hydrogen demand in the definition of the grid outage survivability indicator follows a similar logic to that of the energy self-sufficiency indicator, whereas it can be explained by the low priority of serving the hydrogen-refuelling loads for the autonomy hour indicator.

#### 2.4.2.2.4. Initial and terminal constraints

The MG planning optimisation problem is additionally subject to a set of initial and terminal constraints necessary for an adequate analysis. To ensure an economic serving of the peaks occurring early in the 8,760-h scheduling period, the storage media are set to be half-full-charged in the first iteration, as:

$$E_S(0) = 0.5 \times E_{S,opt}, \tag{2.57}$$

where $E_{S,opt}$ is the optimal capacity of the storage media determined over the course of simulations.

Also, for a balanced analysis, the storage devices' energy contents at the end of the year-long operational analysis period are constrained to be equal or exceed their initial states of charge, as:

$$E_S\,(T) \geq E_S\,(0). \tag{2.58}$$

#### 2.4.2.2.5. Decision variable limits

Specific upper bounds are set for the maximum values the non-negative design variables can take, as represented in Equation 2.59. These bounds are adjusted commensurate with the practical feasibility of implementing the conceptualised MG systems in the considered areas. For example, land limitations, characteristics of the catchment sites (for potential micro-hydro power plants), available biomass as a feedstock, and acceptable emissions limits (from potential WtE plants) could constrain the feasible solution space.

$$N_c \leq N_c^{max} \quad \forall c, \tag{2.59}$$

where subscript $c \in C$ indicates the MG component, the optimal size of which is under investigation, while the superscript $max$ denotes the maximum value of the optimum quantity/capacity of the component ($N_c$).[8]

### 2.4.3. Overview of the proposed model

An overview of the proposed general modelling framework – to optimally design on- and off-grid MGs – is shown in Fig. 2.9. As the figure shows, the solution algorithm takes all input data and applies the developed rule-based, hourly-basis operational scheduling strategy, while taking an iterative approach to optimise the discounted MG investment cost using meta-heuristics, which determines the respective size of the equipment. All the investigated meta-heuristic algorithms, which are embedded within the solution approach, start by creating a matrix of random search agents that evolve towards the globally optimum point in the design space based on the associated returned values of the objective function. This process

[8] The maximum permissible values of the design variables account for the rated powers of the corresponding components.

continues according to the particular rules and operators of each meta-heuristic until the stopping criterion – the maximum number of iterations – is satisfied. Finally, the best individual's fitness value (i.e., the return value of the objective function) in the last iteration of the algorithm is reported as the optimal value of the objective function over the feasible region of the optimisation problem as defined by the relevant operational- and planning-level constraints. For a detailed description of the rules and operators of the selected meta-heuristic algorithms, as well as a detailed guide on the optimal adjustment of their control parameters, the reader is referred to the relevant references provided for the algorithms.

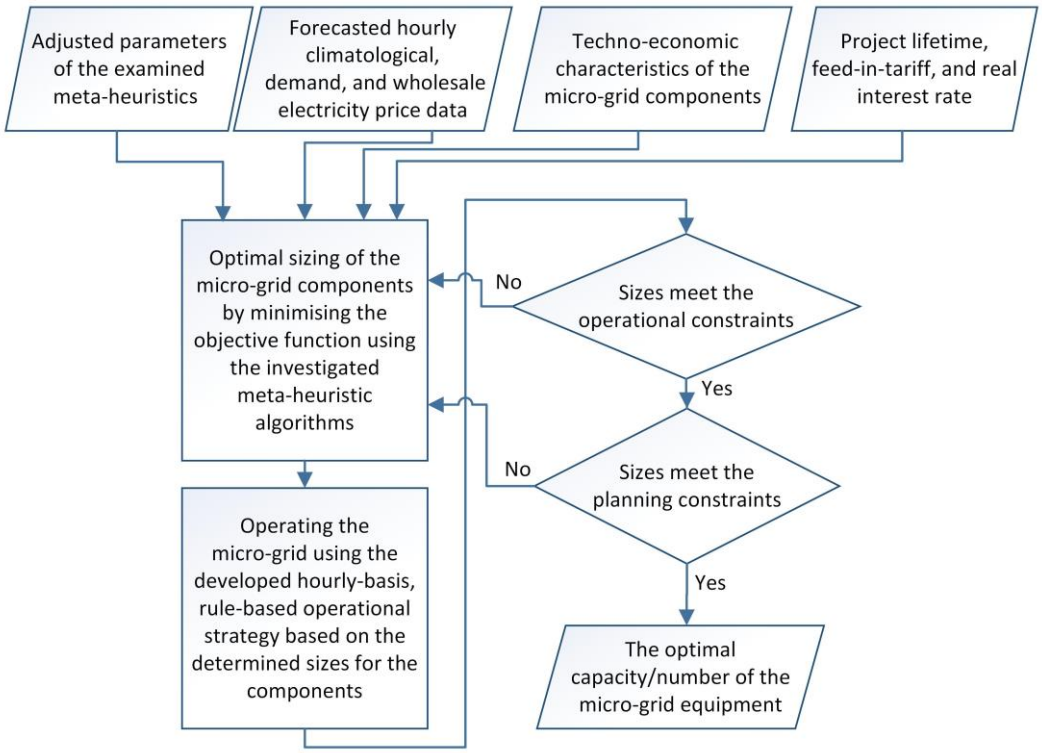


Figure 2.9: Flowchart of the proposed meta-heuristic-based MG capacity planning optimisation model.

## 2.5. Case studies

In order to evaluate the financial viability of the conceptualised community-scale sector-coupled MG designs in real-world applications, as well as to investigate the efficiency of the selected meta-heuristics, three case studies were analysed utilising the developed methodology in Section 2.4. The proposed MG systems 1–3 were

respectively considered to supply reliable, clean, affordable, self-sufficient, resilient electricity (including the electrified heating and transportation sectors' energy demands) and green hydrogen fuel to the following three island, rural, and village communities in New Zealand over a 20-year period, namely: (1) the community of 400 permanent inhabitants on Stewart Island (latitude 46.9973°S, longitude 167.8372°E), (2) a rural community of about 350 people near Feilding (latitude 40.2253°S, longitude 175.5675°E), and (3) the eight-lot Totarabank Subdivision located in the Wairarapa District (latitude 41.0178°S, longitude 175.6667°E). The locations of these case study sites are shown in Fig. 2.10 on the New Zealand's National Grid map [166]. In the figure, the filled blue and silvery circles respectively indicate the main load and generation centres; while the grey, mustard yellow, and blue lines respectively indicate the 350, 220, and 110 kV transmission lines. Also, Fig. 2.11 shows a satellite photograph of the Totarabank Subdivision with lots overlaid. Additionally, the Totarabank site has an existing installed transformer capacity of 50 kVA.

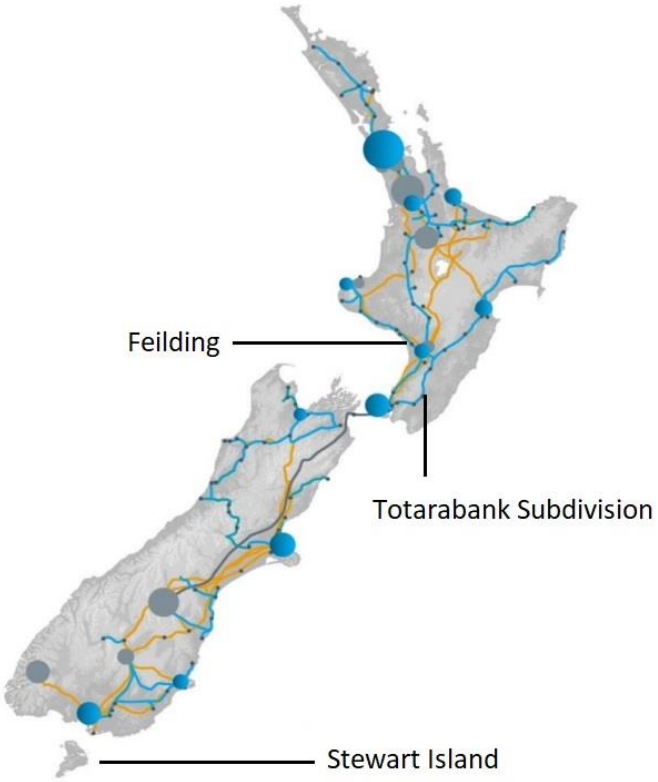


Figure 2.10: Locations of the considered case study sites on the New Zealand's National Grid map [166].


Figure 2.11: Satellite photograph of the Totarabank Subdivision with lots overlaid (image courtesy of Google Earth).

### 2.5.1. Meteorological data

This section provides the forecasted meteorological data relevant to the renewable energy technologies considered in the conceptual MG systems. To forecast the meteorological input data, the New Zealand's National Institute of Water and Atmospheric Research (NIWA) CLiFlo database [167] was used to retrieve historical records of the average wind speed, solar irradiance, ambient temperature, and river streamflow over a 20-year period, between 2000 and 2019 in hourly intervals.

The heat map-like plots in Fig. 2.12 show the monthly mean daily (24-h) wind speed profiles at the three case study sites considered. Since the wind speed data were measured at the height of 10 m, they were normalised to the selected WTs' hub heights using Equation 2.1. The contour plots in Fig. 2.13 display the monthly averaged daily solar irradiance profiles at case study sites 2 and 3. The monthly mean minimum and maximum daily temperatures at case study sites 2 and 3 are also shown in Fig. 2.14. The monthly mean streamflow profile for the Rangitikei River, which is situated at case study site 2, is plotted in Fig. 2.15. The forecasted monthly mean available biomass resources at sites 1 and 2, incorporating both the

agricultural biomass and the organic fraction of the MSW, are shown in Fig. 2.16. Furthermore, the organic and non-organic fractions of the MSW are estimated under the assumption that each individual in the population produces 600 g of wet waste and 2 kg of dry waste per day [122]. The aggregated bio-waste is fed to the reactor-reformer system on a constant basis throughout the day, creating a uniform hydrogen production output profile – and, therefore, can be treated as negative load. Note that all the figures depict New Zealand time for the relevant month. It is also noteworthy that all the simulations are carried out with an hourly resolution. However, the monthly mean daily profiles of input data are shown in Figs. 2.12–2.16 to better visualise the associated characteristic time trends.

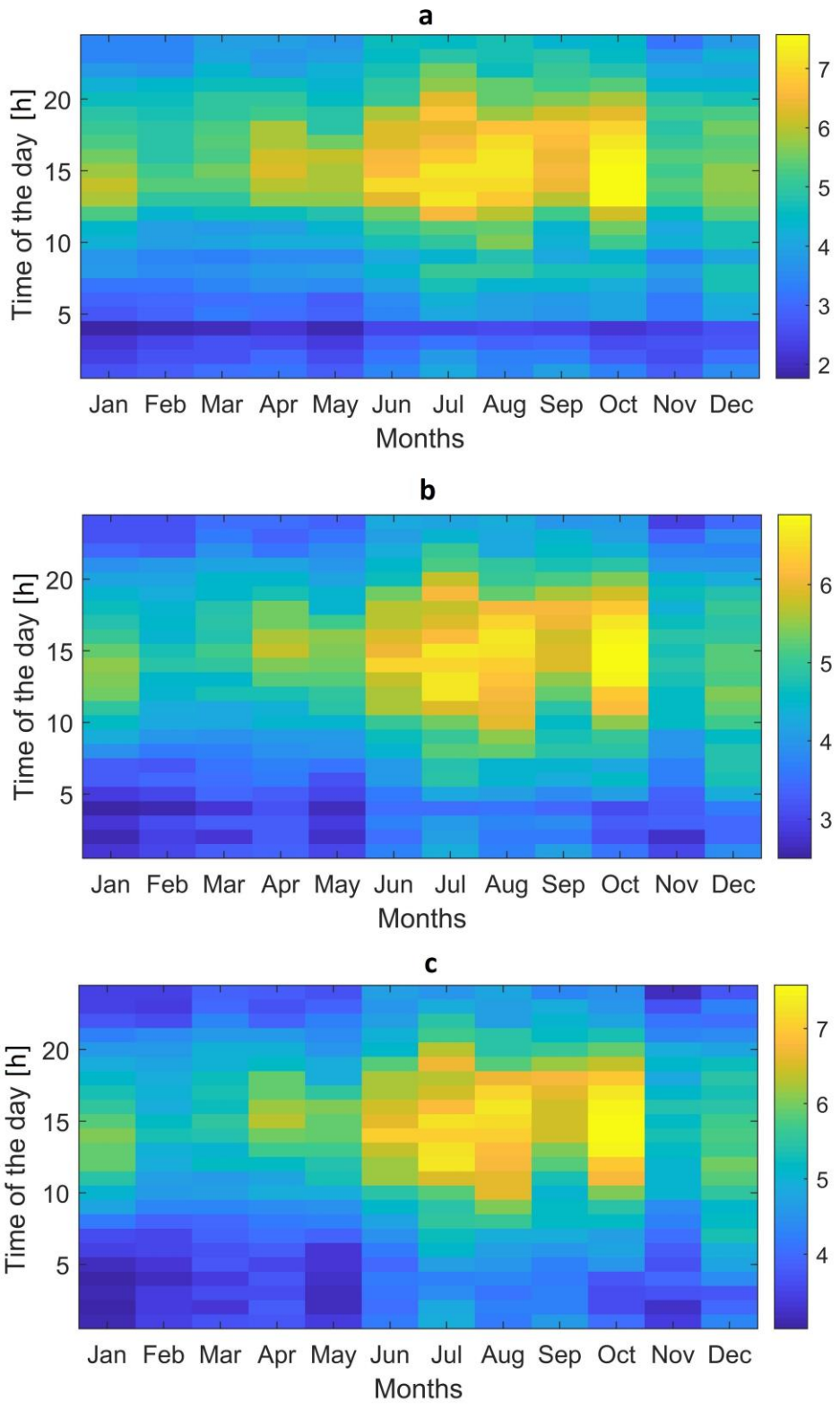


Figure 2.12: Monthly mean daily wind speed profile [m/s] at: (a) Stewart Island; (b) Feilding Valley; and (c) Totarabank Subdivision.

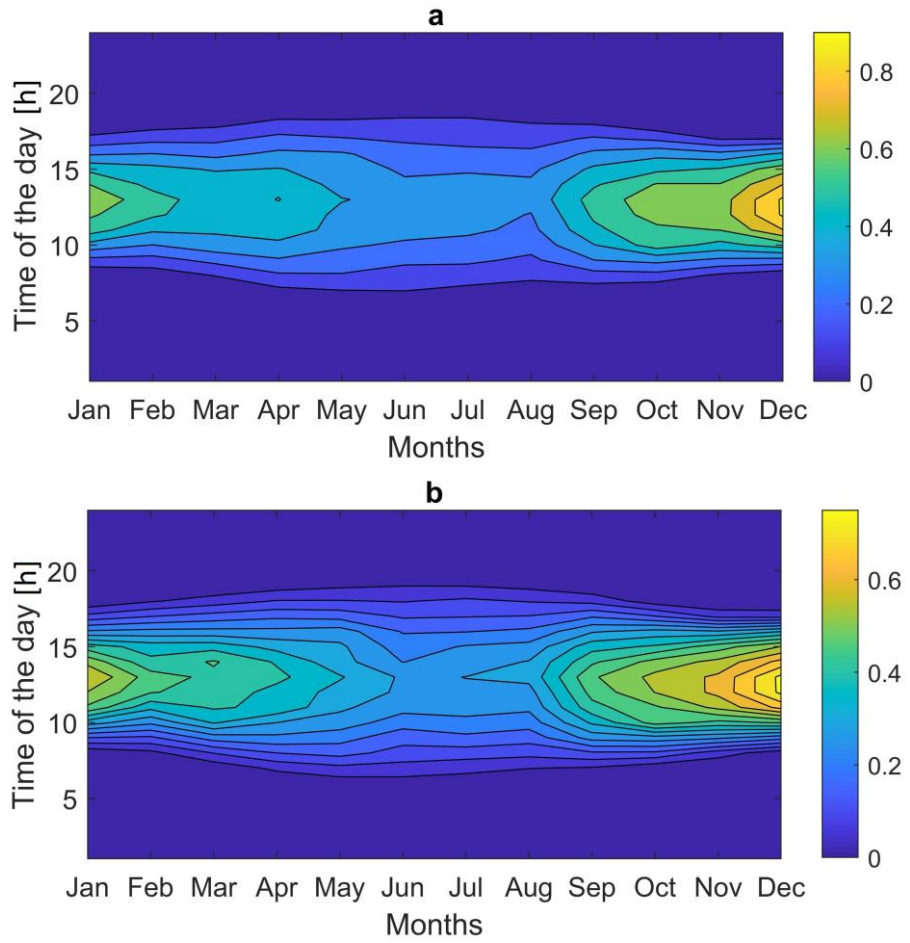


Figure 2.13: Monthly mean daily solar irradiance profile [kW/m$^2$] at: (a) Feilding Valley; and (b) Totarabank Subdivision.

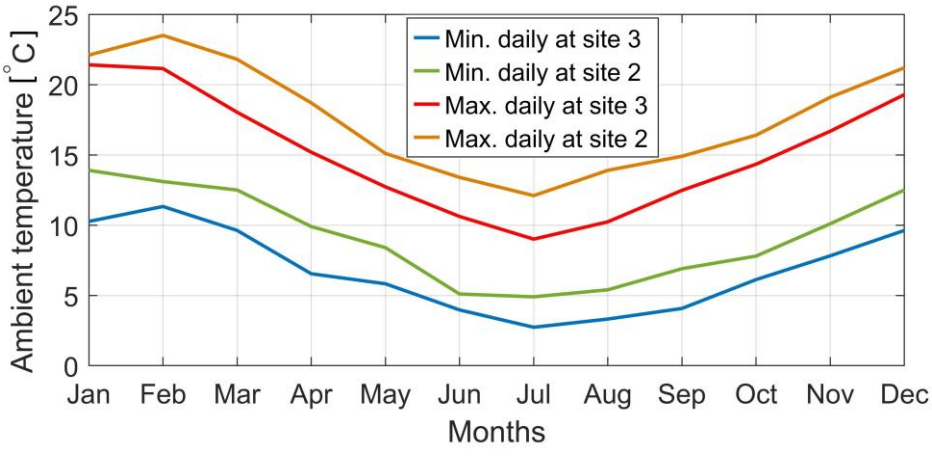


Figure 2.14: Monthly mean minimum and maximum daily air temperature profiles [°C] at: (a) Feilding Valley; and (b) Totarabank Subdivision.

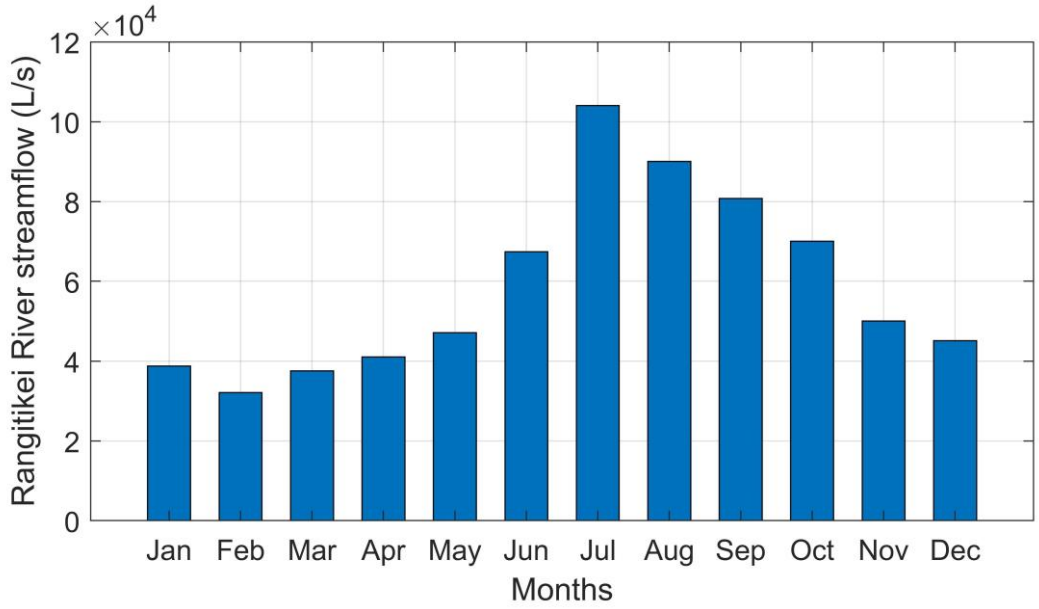


Figure 2.15: Monthly mean streamflow profile [L/s] for the Rangitikei River.

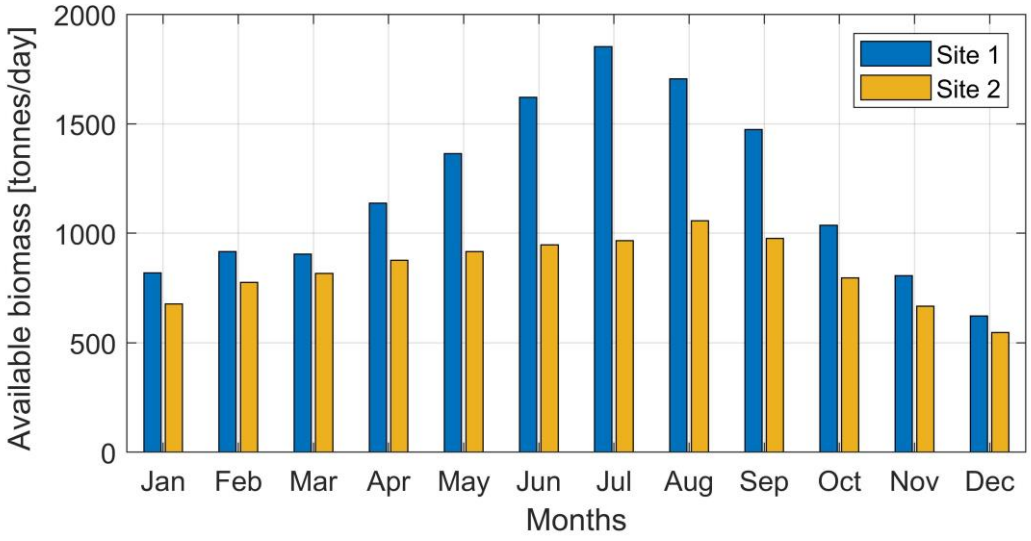


Figure 2.16: Monthly mean profiles for available biomass [tonnes/day] at: (a) Stewart Island; and (b) Feilding Valley.

### 2.5.2. Load demand data

The forecasted one-year monthly averaged daily profiles for the hourly residential electrical loads on the conceptualised MG systems for implementation at the case study sites are shown in 3D plots in Fig. 2.17. The power load profiles were synthesised based on the New Zealand GREEN grid study's estimates of the future

household electricity demand profiles in accordance with the site's population and household size distribution [168]. As the associated power load profiles in Fig. 2.17 suggest, low-grade heat uses are electricity-dominated, implying that load peaks occur on long dark cold winter nights. More specifically, it is assumed that low-temperature heat is the main source of household electrical energy use. Collectively, it amounts to 46% of the total electricity use, of which 27% is used for space heating and 19% is used for water heating. Also, residential appliances account for 54% of the total household electricity use, with the breakdown as follows: plug-load appliances (19%); refrigeration (15%); lighting (12%); and range (8%). Note that the above percentage points represent the associated total annual electricity uses, which are to a great degree subject to seasonality.

Also, the typical daily hydrogen load profiles for the modelled MG systems 1 and 2, which primarily aim to provide a sustainable solution to decarbonising the relevant transport sectors, are depicted in Fig. 2.18. In deriving the typical daily hydrogen load profiles – hydrogen power required by the stations at sites 1 and 2 to serve the medium-duty hydrogen fuel cell-powered electric vessels, heavy-duty tractors, and heavy-freight trucks – the following assumptions were made:

1. Five hydrogen fuel cell-powered Hydrogenesis passenger ferries are integrated into system 1. These 14-seater ferries are used to transport passengers between Stewart Island and the Bluff, Southland, New Zealand.

2. Five New Holland's NH2 fuel cell-powered tractors, as well as five Hyundai Xcient fuel cell-powered trucks, are integrated into system 2.

3. The vessels/vehicles are refuelled during the early morning hours (between 0 and 5 a.m.), which represent light residential load hours, to fill up the valley in the overall daily energy demand profiles of the corresponding MG systems. Accordingly, the associated hydrogen fuel cell-powered vehicles/vessels effectively contribute to flattening the overall profiles of energy demand.

4. When fully refuelled, the hydrogen tanks of the ferries, trucks, and tractors carry sufficient fuel to last them through 4, 3, and 6 days of ordinary

operations, respectively. Subject to this assumption, the hydrogen demands of the ferries and vehicles are distributed throughout the days to flatten the peaks in the associated hydrogen load patterns.

5. The vessels/vehicles are assumed to be refuelled on a first-come/first-served basis using the multi-server Erlang-C queuing model [125], where C identifies the optimal number of dispensers.

Accordingly, as Fig. 2.18 shows, constant hydrogen loads of 5.18 kg-$H_2$/h and 11.76 kg-$H_2$/h are respectively imposed on MG systems 1 and 2 everyday between 0 and 5 a.m.

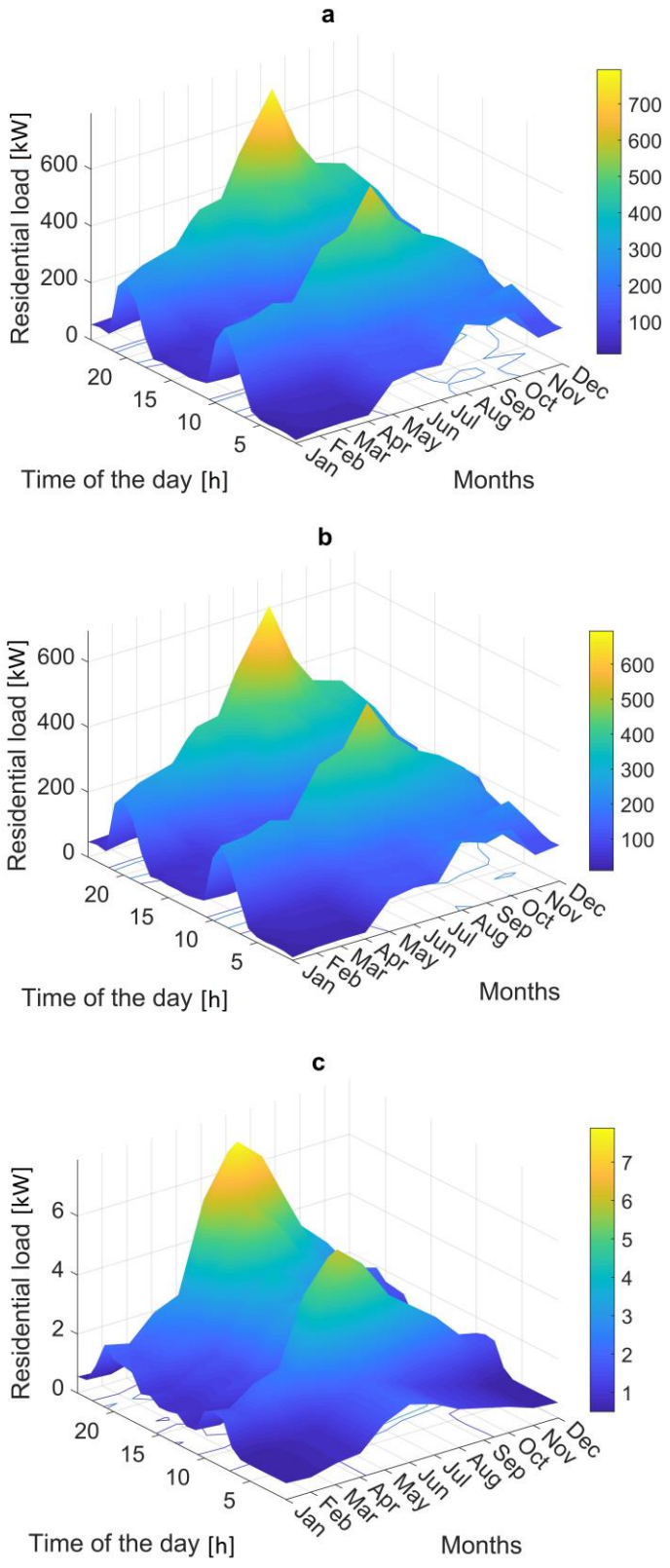


Figure 2.17: Forecasted monthly mean daily residential electrical load power profiles on the proposed MGs for: (a) Stewart Island; (b) Feilding Valley; and (c) Totarabank Subdivision.

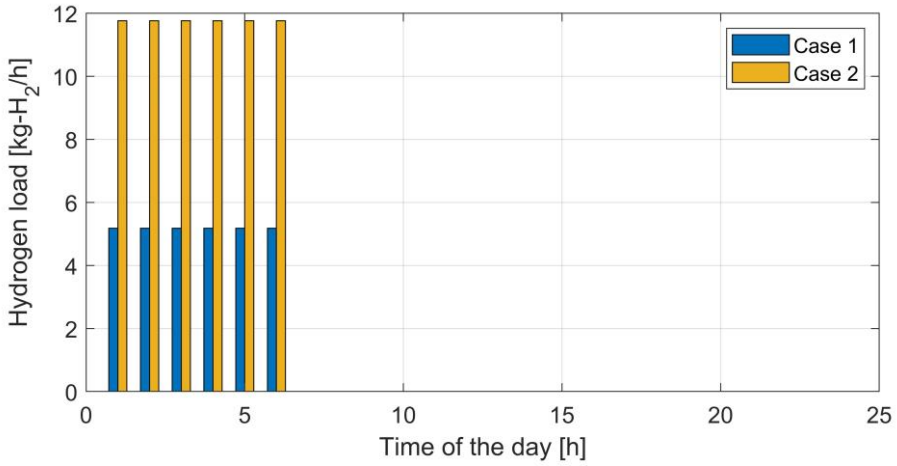


Figure 2.18: Typical daily hydrogen load profiles on the relevant MGs following the devised energy management strategies to integrate hydrogen vehicles/vessels.

### 2.5.3. Wholesale electricity price data

Given the assumption that the grid-connected MGs – populated for the cases of Feilding Valley and Totarabank – import electricity from the utility network that is purchased at time-varying wholesale prices, the per-unit cost of electrical energy imports had to be forecasted for a representative one-year period at an hourly resolution. To this end, first, the 10-year (2010 to 2019) historical locational marginal price data for the central North Island were retrieved from the New Zealand's electricity market datasets recorded at half-hourly intervals (as provided by the New Zealand Electricity Authority [169]) and converted to hourly values. Then, as a means to improve the accuracy of forecasts, the hourly-basis, year-round data streams were weighted (from 1 to 10, respectively) to account for unequal probabilities of the realisation of the data streams – the more recent the wholesale electricity price data stream, the higher its recurrence probability. The underlying rationale for using several independent wholesale electricity price time-series data streams with unequal weights is to add a stochastic dimension to the forecasts made.

The forecasted hourly-basis, year-long wholesale electricity price input data stream, $\pi_{im}(t)$, obtained using the weighted average method, is shown as a monthly averaged daily profile in Fig. 2.19 [169]. In the context of New Zealand's hydro-dominated power system, spot electricity prices are typically (though not necessarily) higher during the drier summer months when hydro lakes (storage) and

inflows are below average and the backup role is primarily fulfilled by more expensive natural gas-fired and coal power plants.

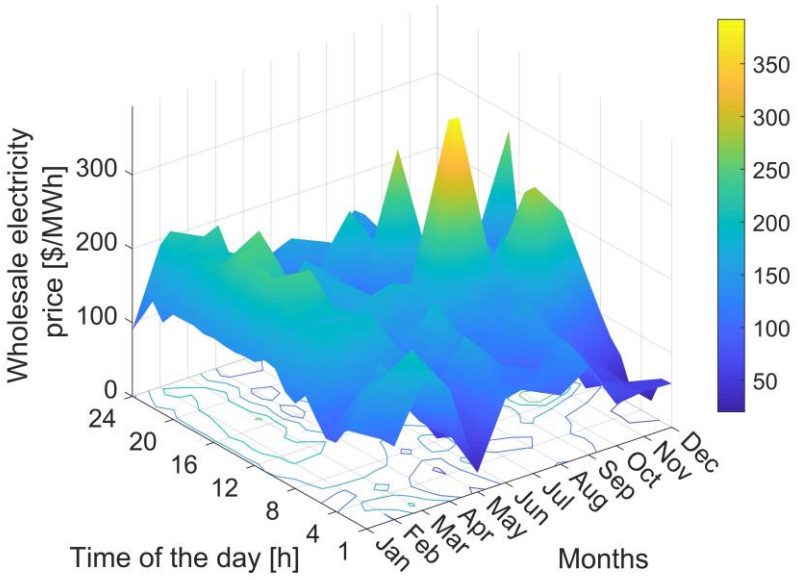


Figure 2.19: Forecasted monthly mean 24-h profile for the wholesale power price.

## 2.6. Simulation results and discussion

The results associated with the application of the developed model to the test cases are presented and discussed in this section. The section begins by providing a comprehensive multi-case-study-oriented, descriptive statistics-based performance comparison of the selected meta-heuristics embedded within the specifically developed solution algorithm applied to the sector-coupled community MG capacity planning optimisation problem (Section 2.6.1). In addition to the solution quality, the comparative meta-heuristic efficiency evaluation involves a comparison of the more effective optimisers in terms of convergence rate. The section then proceeds to focus explicitly on the systems optimised by the proposed model with case-study-specific energy balance analyses (Section 2.6.2), discounted cash flow analyses (Section 2.6.3), as well as capital budgeting and financial appraisal analyses including comparisons of optimised energy costs with retail energy tariffs (Section 2.6.4). All the numerical simulations in this thesis were carried out by coding the proposed model using the MATLAB software (version 9.5, R2018b) [170] running on a desktop computer (on the 64-bit Windows 10

platform) with an Intel® Core™ i7-8700 @ 3.20 GHz processor and 16 GB of RAM.

### 2.6.1. Systematic performance comparison of the selected meta-heuristics

To adequately rank the performance of the selected algorithms, a systematic descriptive statistics-based framework is developed in this study, which compares the algorithms' efficiencies considering their effectiveness in solving the three test-case MG investment planning and capacity optimisation problems defined. The proposed comparison framework employs the following four metrics: the best-case results ($Best$), the worst-case results ($Worst$), the mean results ($Mean$), and the median results ($Median$) of the MG whole-life cycle costs, obtained over 30 independent simulation runs (trials) for each MG instance – necessary to reach the statistical precision required for the efficiency comparison of meta-heuristics given their approximate nature [83]. The $Best$, $Worst$, and $Mean$ indicators reflect the accuracy of the algorithm, while the $Median$ indicator reveals its precision (i.e. the number of hits to the optimiser-specific globally optimum solution throughout 30 simulation runs). Also, in order to ensure a fair comparison, the maximum number of iterations, as well as the number of dedicated search agents (population size), are assumed to be the same for all the investigated algorithms, and equal to 300 and 50, respectively. The values were set based on the findings of Khan and Singh [83] on the appropriate values of the aforementioned parameters that ensure the convergence of a broad spectrum of meta-heuristics – including both well-established and state-of-the-art algorithms – in the context of MG design optimisation and asset capacity allocation. Other more specific control parameters of the evaluated algorithms are adjusted according to the values recommended by their developers.

The proposed comparison framework does not include any indicators to evaluate the convergence speed of the algorithms. The reason lies in the fact that the MG systems are usually planned for a projected 20- to 30-year period, making the computational cost a less substantial metric for the comparative evaluation of different optimisers, unless they are associated with intractable computational complexities, which has not been the case for the investigated algorithms. That is,

computational complexity was not factored into the comparative analyses because none of the algorithms reached the physical limits to how much computation can be executed during the planning phase of the studied MGs in real-world settings.

To determine the rank order of the meta-heuristics under analysis, the calculated indicators for each MG instance are first averaged ($Avg.1$). The meta-heuristics are then scored locally, based on the $Avg.1$ criterion obtained for each MG system. The mean values of the scores obtained for different optimisers under different testing conditions – when applied to different MG topologies in terms of both the grid connection layout and constituent DERs with different loading, meteorological, and wholesale electricity price conditions – are then calculated. These mean values ($Avg.2$) eventually determine the final rank order of the analysed meta-heuristic optimisation algorithms. Accordingly, Table 2.3 summarises the associated descriptive statistics and ranks the performance of the investigated meta-heuristics. The following notes are made to provide a better interpretation of the results presented in Table 2.3:

1. When the $Mean$ is lower than the $Median$, the distribution of the results obtained over 30 trials is called left-skewed (which appears as a right-leaning curve), meaning that the stability of the optimiser against different initial random solutions is low. Contrariwise, in the cases that the $Mean$ is higher than the $Median$, the distribution of the results is skewed to the right and the optimiser is highly robust against the variations in initial guess.

2. The scoring procedure presented in Table 2.3 eliminates the need to allocate any weights to the $Avg.1$ criterion in order to obtain the values of the $Avg.2$ criterion. More specifically, it leads to considering the same weight for all the identified performances of the algorithms on different test systems.

3. The NPC is the negative of the net present value; that is, a negative total NPC indicates that the expected revenues generated by the project exceed the total expected costs.

The summary statistics for the comparative efficiency of the examined meta-heuristics are revealing in the following ways:

1. It is not implausible that dissimilar evaluations arise when meta-heuristics are applied to a certain MG planning problem in different runs, or when they are applied to different MG planning problems. Therefore, the meta-heuristics' efficiencies need to be compared based on their performance on different test cases in different runs, whilst also taking a statistical approach to avoid incomplete, and ultimately mistaken comparative conclusions.

2. By comparing the results obtained by the GA, the PSO, the HGA-PSO, as well as the ABC, the ACO, and the HABC-ACO, it can be inferred that the hybrid version of two single algorithms generally outperforms any of them alone. Moreover, the HGA-PSO, the GA, and the PSO are ranked $2^{nd}$ to $4^{th}$, respectively, which explains their popularity in the mainstream MG capacity planning optimisation literature.

3. The MFOA, which is a recently developed meta-heuristic, outperforms all the other examined algorithms, albeit by a small margin, not only in terms of the overall performance measure, but also in terms of all the individual indicators. That is, while the examined meta-heuristics have yielded somewhat different rankings across different test cases and indicators, the MFOA has consistently ranked first in terms of all the individual indicators in all the test cases. This statistically robust evidence indicates that the MFOA is an ideal choice for meta-heuristic-based MG capacity planning optimisation. The outperformance of the MFOA can be attributed to its unique search process that uses two types of search agents – moths and flames – which enables it to improve the trade-off between the exploration and exploitation phases by conducting more effective long-range jumps around the global search space and an efficient local search near the global optima.

4. Based on the numerical tests undertaken in this study, the relative error in approximating the global optima – by comparing the $Best$ indices of the MFOA, which has shown the greatest performance, and the DA, which has shown the weakest performance – could be as high as 4.0%, 4.5%, and 2.5% respectively from the three target systems, equating to life-cycle cost

savings of $252,922, $346,180, and $1,254, respectively. That is, failure to employ a fitting optimisation algorithm, while optimally designing a MG system using meta-heuristics, could potentially result in an overestimation of its lifetime cost by up to 4.5%. However, these figures may not imply significant savings from a practical point of view, which is due to the relatively small scale of the case studies. That is, the outperformance of the MFOA over the investigated meta-heuristics is expected to be more substantial when applied to more structurally complex MGs of larger scales.

5. According to the $Avg.2$ criterion, the following overall efficiency ranking can be produced for the selected meta-heuristics within the context of optimal MG sizing: the MFOA < the HGA-PSO < the GA < the PSO < the HABC-ACO < the ABC < the ACO < the IHSA < the MVO < the GWO < the BA < the BB-BC < the CSA < the FA < the ALO < the WEO < the SCA < the GOA < the SSA < the DA.

6. The average root-mean-square error of the population of the MG whole-life costs returned by the proposed MFOA-optimised model over the 30 trials across the three test cases with respect to its corresponding best performances was found to be negligibly low (~0.4%). This indicates the robustness of the proposed MFOA-based model to the random population initialisation process, which, in turn, suggests the adequacy of a single run of the algorithm.

Table 2.3: Statistical, multi-test-case-oriented performance comparison of the selected meta-heuristics in minimising the whole-life costs of the test-case MGs for the case study sites [$].

| Alg. | Sys. | *Best* | *Worst* | *Mean* | *Median* | *Avg.*1 | Score | *Avg.*2 | Rank |
|---|---|---|---|---|---|---|---|---|---|
| PSO | MG 1 | 6,381,048 | 6,381,982 | 6,381,554 | 6,381,048 | 6,381,408 | 4 | 3.67 | 4 |
| | MG 2 | 7,344,083 | 7,355,001 | 7,346,527 | 7,344,083 | 7,347,424 | 3 | | |
| | MG 3 | –50,720 | –50,528 | –50,626 | –50,584 | –50,615 | 4 | | |
| GA | MG 1 | 6,379,004 | 6,381,746 | 6,380,531 | 6,379,004 | 6,380,071 | 3 | 3.33 | 3 |
| | MG 2 | 7,344,448 | 7,359,452 | 7,347,387 | 7,344,448 | 7,348,934 | 4 | | |
| | MG 3 | –50,723 | –50,529 | –50,629 | –50,595 | –50,619 | 3 | | |
| HGA-PSO | MG 1 | 6,372,109 | 6,376,111 | 6,374,557 | 6,372,109 | 6,373,722 | 2 | 2 | 2 |
| | MG 2 | 7,343,540 | 7,354,659 | 7,347,245 | 7,343,540 | 7,347,246 | 2 | | |
| | MG 3 | –50,723 | –50,529 | –50,635 | –50,601 | –50,622 | 2 | | |
| ABC | MG 1 | 6,383,870 | 6,401,540 | 6,389,321 | 6,383,870 | 6,389,650 | 6 | 6.33 | 6 |
| | MG 2 | 7,350,114 | 7,386,327 | 7,361,542 | 7,350,114 | 7,362,002 | 7 | | |
| | MG 3 | –50,716 | –50,522 | –50,622 | –50,576 | –50,609 | 6 | | |
| ACO | MG 1 | 6,382,219 | 6,403,274 | 6,391,374 | 6,382,219 | 6,389,772 | 7 | 6.67 | 7 |
| | MG 2 | 7,353,607 | 7,371,258 | 7,360,618 | 7,353,607 | 7,359,773 | 6 | | |
| | MG 3 | –50,715 | –50,521 | –50,618 | –50,574 | –50,607 | 7 | | |
| HABC-ACO | MG 1 | 6,383,955 | 6,384,741 | 6,384,005 | 6,383,955 | 6,384,166 | 5 | 5 | 5 |
| | MG 2 | 7,348,927 | 7,355,668 | 7,350,493 | 7,348,927 | 7,351,004 | 5 | | |
| | MG 3 | –50,718 | –50,525 | –50,622 | –50,584 | –50,611 | 5 | | |
| ALO | MG 1 | 6,386,072 | 6,415,984 | 6,396,482 | 6,389,974 | 6,397,128 | 13 | 15 | 15 |
| | MG 2 | 7,675,981 | 7,913,542 | 7,792,110 | 7,794,115 | 7,793,937 | 19 | | |
| | MG 3 | –50,697 | –50,516 | –50,584 | –50,516 | –50,578 | 13 | | |
| IHSA | MG 1 | 6,386,106 | 6,406,002 | 6,391,571 | 6,390,143 | 6,393,456 | 10 | 8.67 | 8 |
| | MG 2 | 7,350,974 | 7,379,651 | 7,363,444 | 7,360,457 | 7,363,632 | 8 | | |
| | MG 3 | –50,715 | –50,521 | –50,616 | –50,573 | –50,606 | 8 | | |
| BB-BC | MG 1 | 6,391,570 | 6,416,098 | 6,397,021 | 6,391,987 | 6,399,169 | 15 | 12.67 | 12 |
| | MG 2 | 7,354,027 | 7,391,610 | 7,364,771 | 7,354,027 | 7,366,109 | 9 | | |
| | MG 3 | –50,692 | –50,514 | –50,586 | –50,514 | –50,577 | 14 | | |
| MFOA | MG 1 | **6,142,109** | 6,144,576 | 6,143,850 | 6,142,109 | 6,143,159 | 1 | 1 | 1 |
| | MG 2 | **7,330,037** | 7,339,874 | 7,333,547 | 7,330,037 | 7,333,374 | 1 | | |
| | MG 3 | –**51,597** | –51,116 | –51,370 | –51,472 | –51,389 | 1 | | |

| | | | | | | | | | |
|---|---|---|---|---|---|---|---|---|---|
| | MG 1 | 6,392,449 | 6,418,995 | 6,401,825 | 6,393,736 | 6,401,751 | 17 | | |
| SCA | MG 2 | 7,361,540 | 7,402,329 | 7,383,669 | 7,389,495 | 7,384,258 | 12 | 15.66 | 17 |
| | MG 3 | –50,685 | –50,498 | –50,588 | –50,498 | –50,567 | 18 | | |
| | MG 1 | 6,383,775 | 6,406,108 | 6,388,937 | 6,383,775 | 6,390,649 | 9 | | |
| MVO | MG 2 | 7,360,297 | 7,400,103 | 7,373,639 | 7,388,436 | 7,380,619 | 10 | 9.33 | 9 |
| | MG 3 | –50,704 | –50,521 | –50,616 | –50,571 | –50,603 | 9 | | |
| | MG 1 | 6,386,254 | 6,416,024 | 6,396,552 | 6,391,309 | 6,397,534 | 14 | | |
| WEO | MG 2 | 7,361,990 | 7,402,773 | 7,383,990 | 7,390,061 | 7,384,704 | 13 | 15.33 | 16 |
| | MG 3 | –50,687 | –50,489 | –50,585 | –50,489 | –50,563 | 19 | | |
| | MG 1 | 6,384,002 | 6,404,870 | 6,386,654 | 6,385,192 | 6,390,180 | 8 | | |
| GWO | MG 2 | 7,362,555 | 7,409,351 | 7,386,473 | 7,392,652 | 7,387,758 | 14 | 10.66 | 10 |
| | MG 3 | –50,703 | –50,516 | –50,610 | –50,567 | –50,599 | 10 | | |
| | MG 1 | 6,392,004 | 6,419,259 | 6,397,508 | 6,392,966 | 6,400,434 | 16 | | |
| CSA | MG 2 | 7,361,478 | 7,401,691 | 7,389,006 | 7,379,309 | 7,382,871 | 11 | 13 | 13 |
| | MG 3 | –50,700 | –50,515 | –50,596 | –50,515 | –50,582 | 12 | | |
| | MG 1 | 6,393,406 | 6,419,889 | 6,403,574 | 6,396,555 | 6,403,356 | 19 | | |
| SSA | MG 2 | 7,675,505 | 7,912,888 | 7,693,343 | 7,790,128 | 7,767,966 | 18 | 18 | 19 |
| | MG 3 | –50,681 | –50,504 | –50,588 | –50,504 | –50,569 | 17 | | |
| | MG 1 | 6,392,907 | 6,419,962 | 6,401,939 | 6,395,680 | 6,402,622 | 18 | | |
| GOA | MG 2 | 7,674,547 | 7,911,748 | 7,689,900 | 7,758,609 | 7,758,701 | 17 | 17 | 18 |
| | MG 3 | –50,688 | –50,506 | –50,589 | –50,506 | –50,572 | 16 | | |
| | MG 1 | 6,395,031 | 6,501,430 | 6,452,684 | 6,472,200 | 6,455,336 | 20 | | |
| DA | MG 2 | 7,676,217 | 8,010,872 | 8,000,909 | 8,006,537 | 7,923,634 | 20 | 20 | 20 |
| | MG 3 | –50,343 | –50,332 | –50,336 | –50,332 | –50,336 | 20 | | |
| | MG 1 | 6,385,662 | 6,419,205 | 6,393,101 | 6,385,662 | 6,395,908 | 11 | | |
| BA | MG 2 | 7,362,751 | 7,409,399 | 7,386,982 | 7,399,505 | 7,389,659 | 15 | 12.33 | 11 |
| | MG 3 | –50,701 | –50,516 | –50,609 | –50,560 | –50,596 | 11 | | |
| | MG 1 | 6,384,584 | 6,421,009 | 6,394,741 | 6,384,584 | 6,396,230 | 12 | | |
| FA | MG 2 | 7,364,802 | 7,411,350 | 7,399,008 | 7,391,540 | 7,391,675 | 16 | 14.33 | 14 |
| | MG 3 | –50,695 | –50,510 | –50,590 | –50,510 | –50,576 | 15 | | |

Bold indicates the least-cost MG whole-life cost solution obtained across the examined meta-heuristics over 30 independent simulation runs.

Table arrays highlighted in grey indicate the results of the meta-heuristics with the best and worst overall performances.

Moreover, Table 2.4 provides a breakdown of the optimal combination of the decision variables optimised by the MFOA in its best performance trial. Note that, given the statistical insignificance of the equipment sizing results optimised by the studied meta-heuristics in that no salient differences in terms of the overall MG topology were observed – in light of the single cost-minimisation objective considered – as well as for reasons of space and tractability, it was decided to limit the equipment capacity analyses to the results obtained in the best run of the MFOA for the associated total discounted system costs (total net present values) bolded in Table 2.3. It should also be noted that, for the components, the optimum capacities (and not quantities) of which are under question (i.e., continuous variables), the optimum sizes are rounded up to the nearest integer, except for the reactor-reformer and hydrogen station, the optimum capacities of which are rounded up to the second decimal place due to comparatively higher per-unit costs.

Table 2.4: Breakdown of the optimal equipment-related costs yielded by the best run of MFOA out of 30 runs for test-case MG systems 1–3.

| Component | Product model | MG 1 | MG 2 | MG 3 |
|---|---|---|---|---|
| PV panels [no.] | CS6K-280P | – | 654 | 63 |
| Wind turbines [no.] | Fuhrländer FL30 | 36 | 2 | – |
| | Fuhrländer FL100 | – | 3 | – |
| | AWS HCM | – | – | 6 |
| Micro-hydro turbines [no.] | XJ50-100SCTF6-Z | – | 9 | – |
| Transformer [kVA] | Generic | – | 391 | 50* |
| Inverter [kW] | Generic | 794 | 662 | 9 |
| Super-capacitor modules [no.] | XLR-48R6167-R | 498 | 429 | – |
| Battery packs [kWh] | Generic Li-ion | – | – | 41 |
| Electrolyser stacks [no.] | H-TEC S 30/50 | 281 | 251 | – |
| Hydrogen tank [kg] | Generic | 901 | 730 | – |
| Fuel cell stacks [no.] | FCgen-1020ACS | 148 | 113 | – |

| | | | | |
|---|---|---|---|---|
| Waste-to-energy plant [kW] | Generic | 13 | 9 | – |
| Reactor-reformer system [kg-$H_2$/h] | Generic | 2.49 | 1.56 | – |
| Hydrogen station – refuelling unit [kg-$H_2$/h] | Generic (Pure Energy Centre) | 3.20 | 6.79 | – |

* Existing installed capacity.

Also, as an indication of the above-mentioned topological insignificance of the results obtained by different meta-heuristics, Table 2.5 provides a breakdown of the optimal combination of the decision variables of MG 3 optimised by the top 8 meta-heuristics in their best runs. The table is revealing in several important ways:

1. Intriguingly, the MFOA, the GA, the PSO, and the HGA-PSO agree on the optimal combination of the sizes of the solar PV and WT generation systems. That is, the difference in the efficiency of these algorithms arises from a difference in the optimised sizes of the battery bank and the multi-mode inverter, which consequently alter the energy trading capacity of the MG with the utility grid. More specifically, in all of these cases, the obtained reductions in the total net electricity exchange costs were not sufficient to offset the increased costs associated with the respective increased sizes of the battery and inverter. Further analyses revealed that the reductions in the total net electricity exchange costs – the sum of the hourly grid import costs minus the hourly grid export revenues over the project life-cycle – are, in large part, attributable to the reductions in grid import costs, rather than the increases in grid export revenues. This observation can be explained by the unaltered sizes of the distributed generation technologies; the larger battery bank capacity allows storing extra energy for later use, which can be translated into less imports during higher-priced peak periods.

2. Interestingly, the GA, the PSO, and the HGA-PSO yield exactly the same set of cost-optimal sizes for the technologies considered in the candidate pool; the difference in the MG life-cycle costs estimated by these algorithms is solely associated with the expected total net energy purchased from the grid with direct influence on the total net electricity exchange costs. Similar

observations held true for the ABC, the HABC-ACO, and the IHSA algorithms. It is also worth noting that no meta-heuristic yielded a battery-less MG configuration in the optimised mix of technologies.

3. All the examined meta-heuristic optimisation algorithms agree that the optimal total renewable energy generation capacity is equal to the active power rating of the existing installed transformer at the site. However, four different combinations of the sizes of the solar PV and WT plants (with different battery storage and inverter capacities) were observed across the best solutions returned by the best-performing subset of the selected meta-heuristic optimisers. The more the combinations of the sizes of the two generation technologies deviate from the point with 17.6 kW solar PV and 30 kW WT, the worse the MG whole-life cost solution.

Table 2.5: Optimal combination of the third MG investment planning decision variables obtained using a best-performing subset of investigated meta-heuristics in their best runs.

| Algorithm | PV size [kW] | WT size [kW] | Battery size [kWh] | Inverter size [kW] | Total net electricity exchange costs [$] |
|---|---|---|---|---|---|
| MFOA | **17.6** | **30** | **41** | **9** | **−173,825** |
| HGA-PSO | 17.6 | 30 | 48 | 12 | −187,919 |
| GA | 17.6 | 30 | 48 | 12 | −187,919 |
| PSO | 17.6 | 30 | 48 | 12 | −187,918 |
| ACO | 12.6 | 35 | 50 | 15 | −198,202 |
| ABC | 7.6 | 40 | 51 | 15 | −201,720 |
| HABC-ACO | 7.6 | 40 | 51 | 15 | −201,719 |
| IHSA | 7.6 | 40 | 51 | 15 | −201,719 |

Bold indicates the least-cost mix of the decision variables obtained across the examined meta-heuristics over 30 independent simulation runs.

Furthermore, Fig. 2.20 displays the comparative convergence curves of the best-performing subset of the selected optimisation algorithms in their best performance trials in terms of nearing the global optima. For reasons of brevity and tractability, the figure only depicts the convergence process of the top 8 algorithms when applied to MG 1, as shown in Table 2.3, in their best runs. As can be seen

from the figure, the PSO has the fastest convergence rate among all the applied algorithms and approximates the global optimal solution in a comparatively few iterations. The figure also reveals that (1) the GA has a very similar convergence trend to that of the PSO in the initial iterations, but it converges relatively slower than the PSO, (2) the convergence speed of the HGA-PSO is competitive with that of the GA, (3) the MFOA shows a strong capability of searching the design space in the last iterations, when the other algorithms have got stuck into local optimum points, which underlines its strong exploitation capability – the procedure aiming at better approximating the global optima by searching around the achieved solutions in the all-around exploration phase – defeating the HGA-PSO in the 232$^{nd}$ iteration, and (4) not only have the ABC, the ACO, the HABC-ACO, and the IHSA trapped into the local optima solutions prematurely and failed to near the global optima, but they also are associated with slow convergence behaviour. The figure, additionally, demonstrates the adequacy of the selected values for the stopping criteria – the maximum number of iterations and population size.

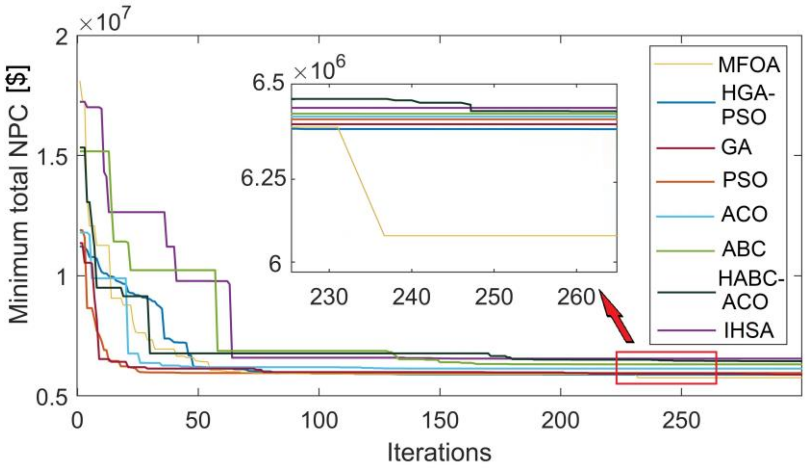


Figure 2.20: Convergence patterns of the top 8 algorithms applied to MG 1 in their best performance trials.

As its superiority to the other meta-heuristics studied is shown to be statistically robust and valid, the modelling results presented hereinafter are based on the best-performing trial of the MFOA (with the corresponding whole-life cost highlighted in bold in Table 2.3).

### 2.6.2. Energy balance analysis

This section presents annually and monthly resolved energy balance analyses of the conceptualised MG systems, which include an overview of the balance of energy generation/imports and consumption/exports/dissipation, on two different temporal scales. All the analyses were made based on the least-cost energy mix solution estimated by the best run of the proposed MFOA-based solution approach. The resulting values are based on a one-year operational period with hourly intervals under the reliability, self-sufficiency, autonomy hour, and grid outage survivability constraints of $LPSP^{max}$ = 0, $SSR^{min}$ = 80%, $AH_S^{min}$ = 8, and $GOS_{MG}^{min}$ = 12, respectively.[9]

#### 2.6.2.1. MG system 1

The results of the overall energy flow analysis of MG 1 for the generation and consumption components are summarised in Fig. 2.21 in terms of their percentage contribution to the total generation and consumption of energy. Note that only the primary sources of energy generation within the MG are incorporated in the energy flow analysis and the analysis of energy consumption within the system is not sub-categorised to detail the specific end-uses of the customers. Also, the positive values indicate the generation of energy, while the negative values represent energy consumption. Moreover, the total system losses include the energy losses associated with the non-ideal performances of the system components, which are characterised by their efficiencies, as well as spilled energy in the dump load as a result of reaching the energy storage upper limits.

The results presented in Fig. 2.21 provide an annual energy balance outlook for MG system 1. As the figure shows, wind is the main source of energy generation in the system, which makes up 93.4% of the total energy supply, which is followed by energy generation by the WtE plant (5%) and the integrated anaerobic reactor-

[9] Note that given the considered 100% energy dispatch reliability constraint in all cases, the total energy supplied by the onsite DERs is equal to the sum of the total energy demand on the system, the total net energy exported to the upstream grid (where relevant), the total excess energy curtailed, the total net energy storage charging power, and the total power loss due to conversion – on any given time scale.

reformer system (1.6%). On the consumption side, as expected, power loads are the main component of energy use, which account for nearly 48% of the total energy consumption within the MG system. The other load demand component, namely the hydrogen demand of the station, occupies about 18% of the whole MG energy consumption, which is followed by the total system losses. The aggregate losses take up around 34% of the total energy consumption. The total system losses consist of the energy circulated in the DC dump load as spilled energy (5%), as well as the losses in the power electronics devices (11%), the hydrogen-based energy storage system (10%), the WtE plant (4%), the SC bank (2%), the hydrogen station (1%), and the reactor-reformer system (1%).

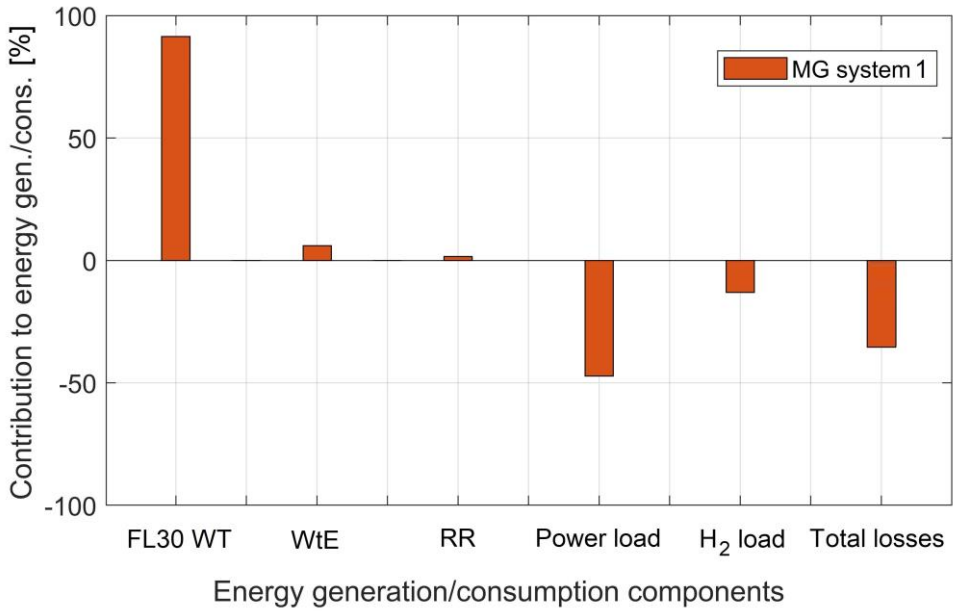


Figure 2.21: Breakdown of the generated/consumed energy within the conceptualised MG 1.

### 2.6.2.2. MG system 2

The results of the energy flow analysis on the generation side of MG 2 are presented in Fig. 2.22. It can be seen from the donut chart that approximately 27% of the total energy generated within the MG is contributed by WTs, of which the FL100 WTs have had a share of around 78%, with the FL30 WTs generating about 22% of the wind power generation within the MG. Also, the figure shows that the year-round energy production from micro-hydro turbines, solar PV panels, and energy from

waste technologies (the WtE and reactor-reformer digestion plants) have taken up around 56%, 13%, and 4% of the total energy generated within the MG, respectively.

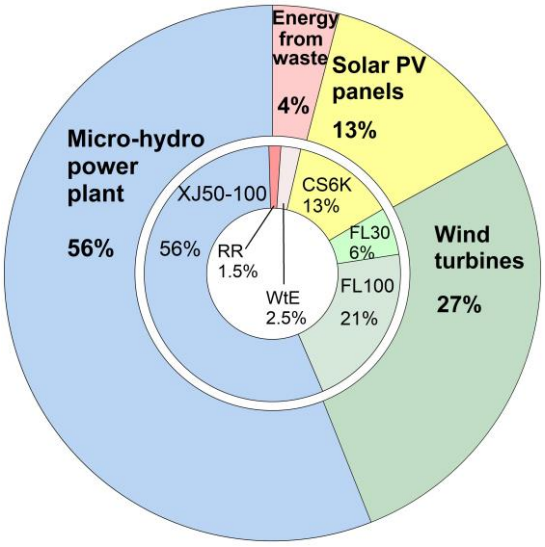


Figure 2.22: Contribution of renewable energy generation technologies to the total energy production in MG 2.

On the other hand, Fig. 2.23 shows the contribution of various energy consumption elements to the total energy consumption within the MG. As shown in the donut chart in Fig. 2.23, at the first stage, the amount of consumed energy can be classified into useful and lost energy. Accordingly, approximately 68% of the total renewable power generated within the MG is used for supplying the electrical and hydrogen loads, while 32% of the generated power is wasted due to the non-ideal characteristics of the components – characterised by the associated power/energy conversion efficiency ratings. The useful power can then be further classified into the electrical power consumed by residential loads and hydrogen power delivered to the station to refuel the hydrogen fuel cell-powered vehicles. The former contributes to approximately 91% of the total energy provided, while the latter is only responsible for circa 9% of the total useful energy consumption within the MG system.

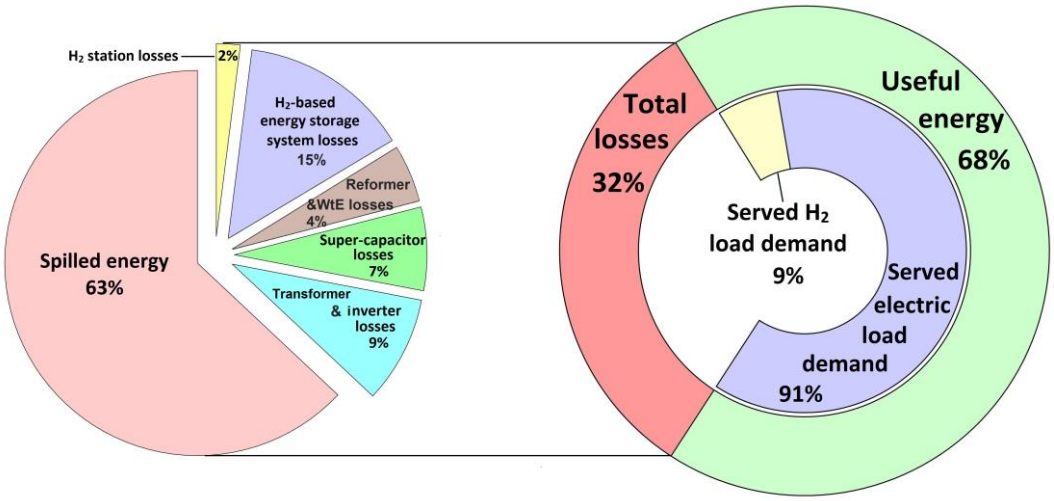


Figure 2.23: Contribution of different energy consumption components to the overall energy consumption in MG 2.

Moreover, as it can be seen in the pie chart in Fig. 2.23, around 63% of the total lost energy is dumped as excess energy by circulating through the DC dump load (due to the lack of demand and/or storage capacity in the determined optimal solution set for the sizes of the components and/or lack of transformer capacity for energy exports), while around 15%, 9%, 7%, 4%, and 2% of the lost energy are respectively used to cater for the losses of hydrogen-based energy storage system (including the electrolyser, the hydrogen reservoir, and the fuel cell), the transformer and power electronics devices, SCs, energy from waste technologies (the WtE and reactor-reformer plants), and the hydrogen station. In addition, the energy flow analysis implies that the optimal planning and designing of the conceptualised MG has led to the diversification of the potential RESs through an optimal quota allocation for the solar PV, wind, hydro, and bio resources; exploiting their complementary characteristics for power generation in short- and long-term horizons, thereby effectively ensuring the long-run security and resilience of energy supply.

### 2.6.2.3. MG system 3

Fig. 2.24 summarises the monthly energy generation/imports and consumption/exports/dissipation for MG system 3 operated over a representative year.

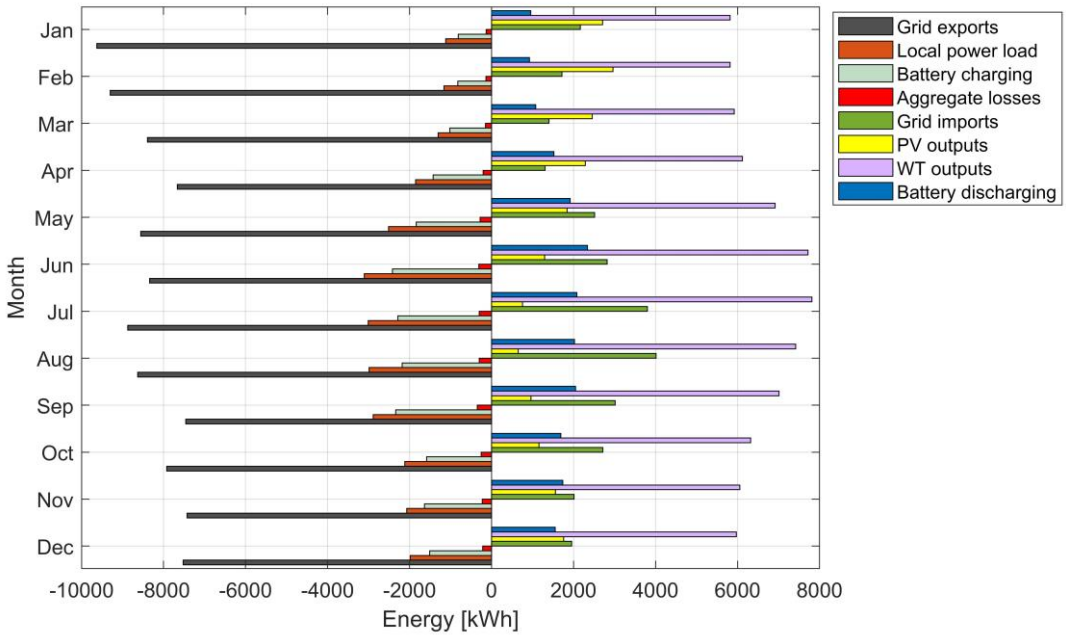


Figure 2.24: Monthly energy balance analysis of MG 3 over the baseline operating year. A positive (negative) value represents the inflow (outflow) of energy to (from) the busbars of the system.

As Fig. 2.24 shows, the ratio of monthly resolved solar PV-to-wind generation undergoes statistically significant changes throughout the year. Specifically, the ratio is highest during the summer period between December and February (at around 42%, on average) and lowest during the winter period between June and August (at around 18%, on average). The yearly breakdown of the onsite renewable power generation indicates around 20,382 kWh (~21%) of solar PV energy generation and 78,891 kWh (~79%) of wind energy generation per year, on average. The SSR of the optimal system was found to be 80% (i.e., the minimum allowed value), which indicates that 20% of the total yearly load demand on the MG is met through imports.

On the other hand, as planned, a substantial fraction of the year-round electricity generated by renewables (~71%) is sold back to the grid as ‘net excess generation’, followed by the local energy consumption (~23%). The remainder of the year-round renewable energy generation, totalling 5,957 kWh (~6%), is lost during the power and energy conversion processes, with the breakdown of the

contributors as follows: transformer, ~48%; hybrid inverter, ~33%; and the battery bank, ~19%.

Additionally, Fig. 2.24 gives further credence to the hypothesis that the battery bank contributes significantly to system cost reduction and efficiency improvement. Notably, further analyses identified that a significant ~76% of the total annual load demand is managed by the battery bank – as measured by the yearly average ratio of battery discharging power to power loads. As it can be inferred from a comparison of the actual battery capacity used over different seasons in Fig. 2.24, much of the battery bank-integrated system's success is due to its ability to flatten the net demand in the peak winter season, leading to a full (available) resource adequacy credit by protecting the MG from higher wholesale market prices. Moreover, it is interesting to note that unlike MG systems 1 and 2, the total amount of curtailed energy equals zero, which can be explained by the relatively large capacity of the existing installed transformer capacity at Totarabank – the size of which has not formed part of the MG capacity planning optimisation process and is treated exogenous to the model.

### 2.6.3. Breakdown of the whole-life system costs

This section presents a breakdown of the total NPCs of the simulated MG systems specifically parametrised for the considered cases. As stated earlier, the cash flow analyses are in accordance with the best performance trial of the MFOA. Also, all the values refer to an expected operational service life of 20 years.

#### 2.6.3.1. MG system 1

The optimised whole-life cost of implementing the conceptual MG 1 on Stewart Island – subject to meeting the reliability, self-sufficiency, and resilience constraints for electricity and hydrogen supply during its lifespan – is estimated to be $6,142,109, as highlighted in Table 2.3. The bar chart in Fig. 2.25 shows a breakdown of the total NPC of MG 1 optimised for the case of Stewart Island. Put differently, the figure depicts the contribution of the NPCs of the relevant components to the whole-life cost of the MG system for the best combination of the component sizes yielded by the MFOA over 30 trials. As can be seen in the figure,

the collective NPC of the hydrogen-based energy storage system's components – electrolyser, fuel cell, and hydrogen tank – constitutes the largest cost component, which is followed by the NPC of the wind power generation system. More specifically, the NPC of the hydrogen-based energy storage system as the dominant cost factor for installing the proposed MG system, accounts for around 45% of the total NPC of the MG system, of which 47%, 42%, and 11% are respectively attributable to the electrolyser, fuel cell, and hydrogen tank.

The other major cost component, namely the FL30 WTs, accounts for approximately 23% of the total NPC of the MG system, of which the underlying capital cost occupies about 79%. Also, the NPC of the load inverters takes up approximately 14% of the MG whole-life cost, which is followed by the NPCs of the SC bank (8%), the WtE plant (7%), the reactor-reformer system (2%), and the hydrogen refuelling station (1%). Note that the salvage values of the components are reflected in the associated replacement costs when calculating the above percentage contributions. It is also noteworthy that the fuel cell unit's replacement cost is greater than its capital cost as it is replaced two times over the lifespan of the MG system; specifically, in Years 8.31 and 16.62 over the 20-year life-cycle of the MG system.

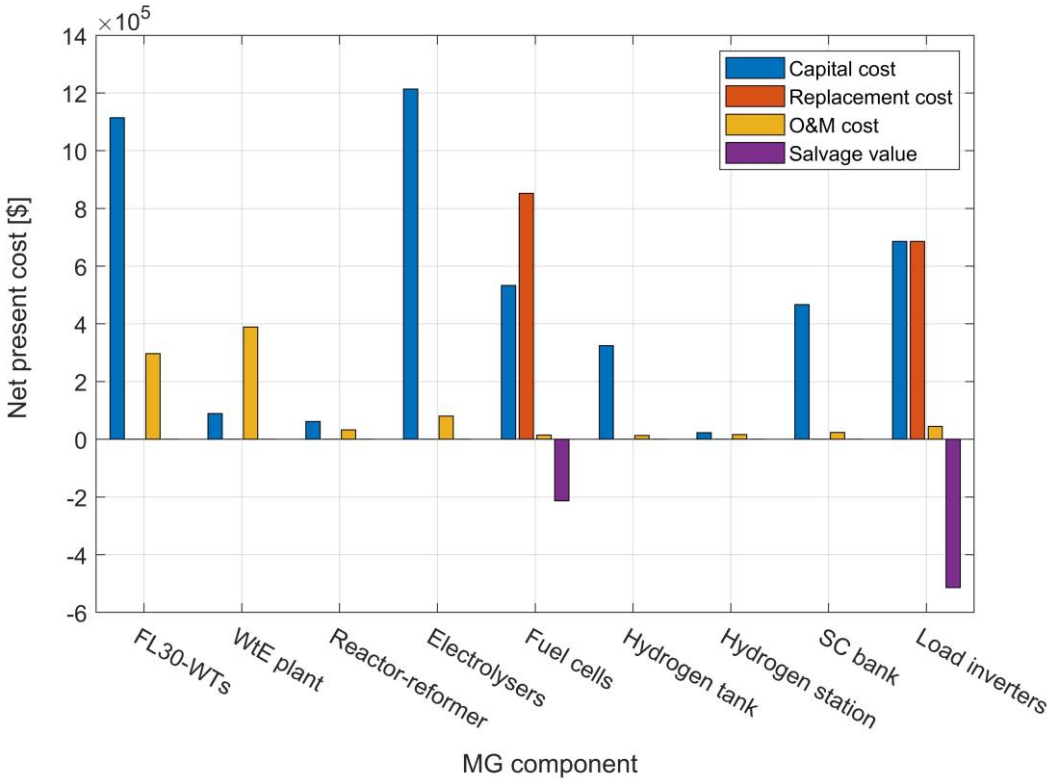


Figure 2.25: Cash flow breakdown by MG 1 components and cost categories.

### 2.6.3.2. MG system 2

As highlighted in Table 2.3, the estimated whole-life cost of MG 2 is optimised to be $7,330,037. The capital, replacement, and O&M costs of the MG respectively account for approximately 68%, 29%, and 3% of the total equipment-related NPC of the project adjusted for the total salvage value – in the associated replacement cost elements. Furthermore, the total salvage value of the investment proposal at the end of the 20$^{th}$ year – stemming from the difference between the project lifetime and lifetimes of multi-mode (load) inverters, the transformer, and the fuel cell unit – is calculated to be $1,052,214. The donut chart in Fig. 2.26 breaks down the equipment-related total NPC of the system by MG components. As illustrated in the figure, the contribution of the NPCs of the optimally sized components to the total equipment-related NPC of the system is as follows: PV panels, 5%; FL30 WTs, 2%; FL100 WTs, 8%; micro-hydro turbines, 10%; the bi-directional transformer, 1%; the hybrid inverter, 16%; SC modules, 9%; electrolyser stacks,

25%; the hydrogen reservoir, 6%; fuel cell stacks, 12%; the WtE plant, 3%; the reactor-reformer system, 1%; and the hydrogen refuelling station, 2%.

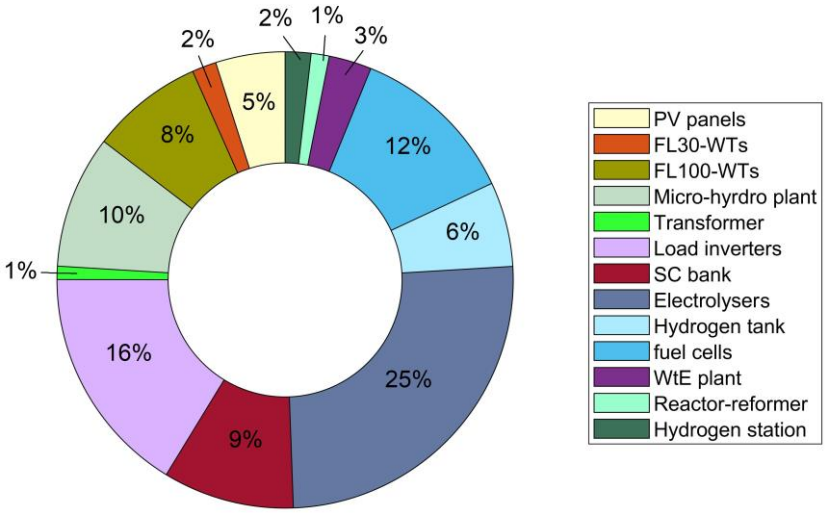


Figure 2.26: Breakdown of the best equipment-related whole-life cost of MG 2 obtained using the MFOA out of 30 runs by components.

Accordingly, the electrolyser, which plays a critical role in the conceptualised system by producing hydrogen for refuelling the hydrogen fuel cell-powered vehicles and backing up the intermittent renewable generation in the long run, has occupied the largest share of the total equipment-related NPC of the system. By analysing the correlations between the determined sizes for the hydrogen-based energy storage system's components, the solution algorithm's decision in utilising the available non-dispatchable renewable power during early morning hours to refuel the vehicles (and not to use the hydrogen stored in the tank for refilling purposes) has been identified as one of the responsible factors for the higher capacity of the electrolyser – when proportionally compared to the sizes of the reservoir and fuel cell in MG 1. The relevant observation supporting the above argument is that the input flow of the hydrogen reservoir (as the sum of the electrolyser and reactor-reformer outputs) is found to be equal to its outflow to the station plus its charging flow during early morning hours – between 0 and 5 a.m.

There also exists another contributing factor to the relatively disproportionate optimal capacities of the hydrogen energy storage system's components with respect to MG 1. Specifically, given the presence of a wider array of non-

dispatchable renewables with greater complementary diurnal production profiles than seasonal complementarity in case 2, the solution algorithm has decided that seasonal energy storage using hydrogen storage infrastructure with a relatively high-capacity electrolyser that produces large volumes of hydrogen in the low demand season but is less frequently used during the high demand season is a better option than (i) buying electricity from the upstream grid to meet the seasonal peaks in electricity demand, and (ii) oversizing the electricity generation components and selling the excess power to the grid during the light-load time-periods, particularly in summer. The usage of a significant capacity of the hydrogen system for seasonal storage functional roles further explains the longer life expectancy of the fuel cell stacks in case 2 (14.66 years) than case 1 (8.31 years) – due to the lower number of hours of operation.

Also, Fig. 2.27 displays the NPCs of the system equipment broken down into the underlying cost elements, which provides a platform for a more detailed cash flow analysis of the conceptualised MG system for the considered case study site. As detailed in the figure, all the components incur O&M costs, whereas only the fuel cell unit, the transformer, and inverters incur replacement costs. While the replacement time for the inverters and transformer is decided according to the associated calendar life, which is assumed to be known (as *a priori* information), the fuel cell's replacement time is estimated by its service hours. Also, given that the operational life of the WtE plant is assumed to be 10 years, it returns no salvage value at the end of the project lifetime following one replacement (20 years).

Furthermore, the salvage values of the transformer and hybrid inverters, which are respectively associated with useful lifespans of 30 and 15 years, are accordingly calculated and factored into the analysis. Moreover, a specific analysis of the cash flow has revealed that the fuel cell unit is replaced in Year 14.66 of the MG service life, and returns around 63% of its expected replacement cost at the end of the project lifetime. In addition, the power exchange-related cost component of the total NPC of the MG system is found to be −$311,321 over its cycle life, which can be translated into an average discounted yearly net income of $15,566 from exchanging electricity with the utility grid. Note that the net income in this context

refers to the MG's income from exporting excess non-dispatchable renewable power to the grid minus the costs of importing electricity from the grid to address onsite power shortfalls.

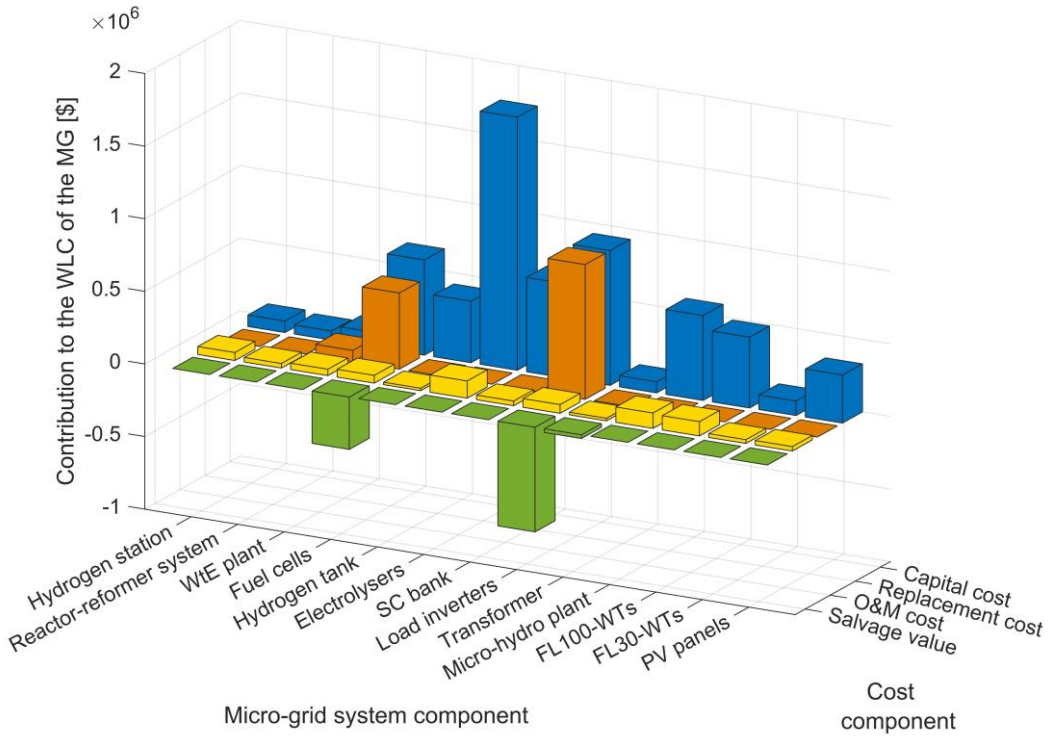


Figure 2.27: Cash flow breakdown of the NPCs of the second MG's components.

### 2.6.3.3. MG system 3

The optimal total NPC of MG system 3 populated for the case of Totarabank is found to be −$50,332, which is composed of the equipment-related and power exchange-related cost components. They are found to be $123,012 and −$173,344, respectively. That is, energy trading with the grid is highly profitable, making an estimated $2,517 of yearly discounted average net income. Note that the net income is derived, in large part, from selling the excess wind power, as the WT generation system capacity is optimised to be significantly larger than what is required to cost-effectively meet the local demand. This can be justified by the calculated payback period of the turbines (approximately 6.5 years), which is considerably lower than their expected lifetimes (20 years) when used solely for grid export purposes.

The equipment-related financial factor can be further broken down into the following subcomponents: total capital cost, $109,172; total replacement cost, $28,875; total O&M cost, $6,621; and total salvage value, −$21,656. Fig. 2.28 provides a further breakdown of the third MG's total net present worth by the underlying equipment-related financial subcomponents. As it can be seen from the figure, the PV generation system, WTs, battery packs, and inverters comprise about 18%, 34%, 34%, and 14% of the total equipment-related NPC of the MG system, respectively.

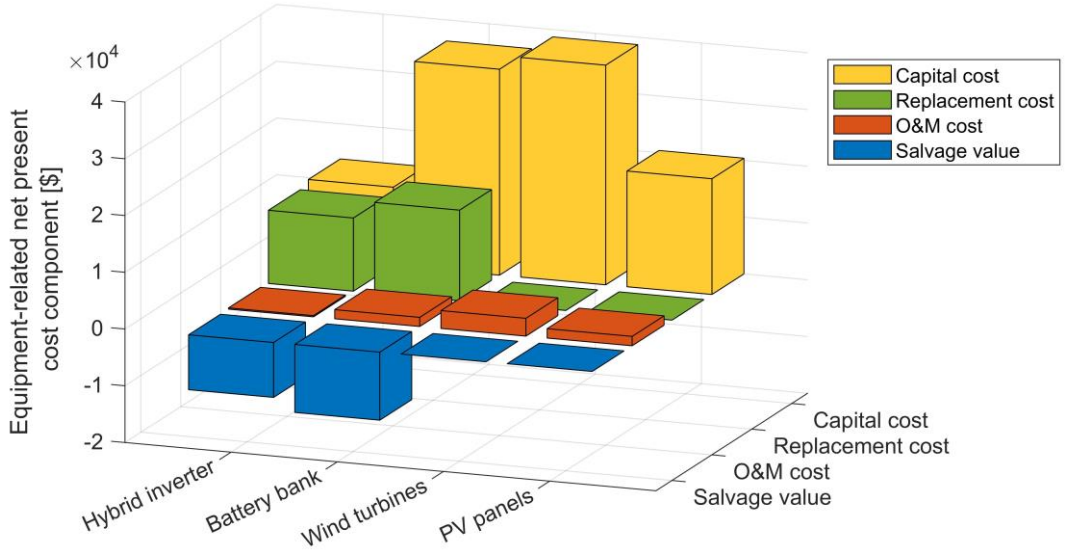


Figure 2.28: Breakdown of the third MG's lifetime cost by the equipment-related cost subcomponents.

### 2.6.4. Capital budgeting

This section aims to aid the associated capital planning decision-making processes by providing comprehensive cost-benefit analyses using four key financial appraisal metrics tailored to measuring the profitability of investment proposals in the long-term, strategic MG planning context, namely: the levelised cost of energy (LCOE), the discounted payback period (DPP), the modified internal rate of return (MIRR), and the discounted profitability index (DPI).

### 2.6.4.1. Levelised cost of energy

The LCOE of a MG system is defined as the discounted total lifetime costs it incurs divided by its discounted total lifetime (useful) energy outputs – supplies to the customers and grid exports (where appropriate). That is, the LCOE, in the MG context, represents the average revenue per unit of useful energy (in the forms of electricity and hydrogen, in this study) generated during the system life cycle that would be required to recoup the lifetime costs of the system [171]. Accordingly, the LCOE [$/kWh] of the MG systems under study, which are planned to serve the local demand with 100% reliability over their cycle lives, can be mathematically formulated as follows [172]:

$$LCOE = \frac{WLC_{MG}}{\sum_{n=1}^{PL} \frac{(\sum_{t=1}^{8760} P_L(t) + \sum_{t=1}^{8760} P_S(t) + \sum_{t=1}^{8760} P_{ex}(t))\,\Delta t}{(1+ir)^n}}, \quad (2.60)$$

where $PL$ represents the project lifetime (20 years), $ir$ denotes the real interest rate per annum (2.45%), the terms $\sum_{t=1}^{8760} P_L(t)$ and $\sum_{t=1}^{8760} P_S(t)$ respectively denote the total annual electric and hydrogen power demands on the MG,[10] and $\sum_{t=1}^{8760} P_{ex}(t)$ represents the total annual grid exports (where relevant), which are discounted to reflect the net present value of future energy flows.

For a better comprehension of the system's LCOE, it needs to be divided into the levelised cost of electric energy (LCOEE) and levelised cost of hydrogen (LCOH) for the cases that incorporate hydrogen demand. To this end, in view of the intertwined structure of MG systems 1 and 2 that serve the electric and hydrogen load demands, it is necessary to re-optimise the systems, while assuming that only the costs associated with delivering a particular energy service over the MG's duty cycle – electricity or hydrogen – are factored in and the demand for the other type of energy (electricity or hydrogen) is entirely withdrawn from the system. Put differently, the LCOE needs to be segregated into the levelised costs of electricity and hydrogen production, leveraging the fact that the costs associated with the

[10] Note that given the considered 100% energy dispatch reliability constraint, the total energy supplied by the MG (including imported power) equals the total energy demand on the system.

components that fulfil no functions in supplying each energy form (for example, the hydrogen station plays no functional role in supplying the electricity) should not be included in the associated levelised cost formulation. Accordingly, the following objective functions are derived by adapting the original objective function in Equation 2.31 for cases 1 and 2:

$$\min WLC_e^{MG1} = \sum\nolimits_{c \in C_{MG1}} NPC_c + p, \tag{2.61}$$

$$\min WLC_{H_2}^{MG1} = \sum\nolimits_{h \in H_{MG1}} NPC_{H_2} + p, \tag{2.62}$$

$$\min WLC_e^{MG2} = \sum\nolimits_{c \in C_{MG2}} NPC_c + NPC_{tr,net} + p, \tag{2.63}$$

$$\min WLC_{H_2}^{MG2} = \sum\nolimits_{h \in H_{MG2}} NPC_{H_2} + p, \tag{2.64}$$

where $WLC_e$ and $WLC_{H_2}$ respectively represent the whole-life costs of the re-structured MGs to specifically address the electricity and hydrogen demands, while the following sets represent the components that play a role in meeting the electrical and hydrogen load demands in the relevant MG systems:

$C_{MG1} = \{WT_{FL30}, WtE, E, HT, FC, RR, SC, I\}$,

$H_{MG1} = \{WT_{FL30}, E, HT, RR, S\}$,

$C_{MG2} = \{PV, WT_{FL30}, WT_{FL100}, MH, WtE, T, E, HT, FC, RR, SC, I\}$,

$H_{MG2} = \{PV, WT_{FL30}, WT_{FL100}, MH, E, HT, RR, S\}$.

Two points are noteworthy on Equations 2.61–2.64. Firstly, the 'electricity-only' scenarios represented by Equations 2.61 and 2.63 differ from the associated base-case objective function in Equation 2.31 only in that they exclude the costs associated with the hydrogen refuelling infrastructure, as well as hydrogen loads. Secondly, as defined in Equations 2.62 and 2.64, the hydrogen demand of the station is satisfied through onsite non-dispatchable renewable energy generation technologies and reactor-reformer outputs. More specifically, neither the energy

stored in the SC bank, nor the imported energy from the main grid (in the second case), nor the fuel cell and WtE generations were considered as a resource to serve the hydrogen loads. All the other assumptions and procedures remain the same as those in the base-case scenario.

Accordingly, the LCOEE and LCOH of the MG systems can be obtained as follows:

$$LCOEE = \frac{WLC_e}{\sum_{n=1}^{PL} \frac{(\sum_{t=1}^{8760} P_L(t) + \sum_{t=1}^{8760} P_{ex}(t))\,\Delta t}{(1+ir)^n}}, \tag{2.65}$$

$$LCOH = \frac{WLC_{H_2}}{\sum_{n=1}^{PL} \frac{(\sum_{t=1}^{8760} P_S(t))\,\Delta t}{(1+ir)^n}}. \tag{2.66}$$

### 2.6.4.2. Discounted payback period

The DPP criterion combines the classic payback period technique with the discounted cash flow analysis (utilised in the NPC method) to calculate the break-even point, after which an investment plan is projected to achieve profitability, whilst adjusting for the real discount rate [173]. The criterion can be adapted for application in the field of MG designing and strategic long-term investment planning as follows:

$$\sum_{t=0}^{DPP} S(1+ir)^{-t} - WLC_{MG} = 0, \tag{2.67}$$

where $S$ is the total annual income created by providing energy services to the consumers of the MG, as well as from selling electricity to the upstream power grid (where applicable).

### 2.6.4.3. Modified internal rate of return

While the classic internal rate of return (IRR)[11] indicator is widely adopted in the MG planning literature to measure the profitability of a project, it has a fundamental shortcoming: it (impractically) assumes the reinvestment to take place at the IRR, which could lead to overly optimistic projections and, consequently, capital budgeting mistakes. Furthermore, the IRR indicator is not applicable to projects where the intermediate cash flows are not planned for reinvestment. However, the MIRR provides project managers with direct control over the assumed reinvestment rate from future cash flows. In this light, the MIRR can be adapted for application in the context of MG planning as follows [174]:

$$MIRR = \sqrt[PL-1]{\frac{\sum_{n=1}^{PL} R(n) \times (1+RR)^{PL-n}}{\left|\sum_{n=1}^{PL} \frac{WLC_{ann}(n)}{(1+ir)^{n-1}}\right|}} - 1, \tag{2.68}$$

where $R(n)$ is the total revenue generated by providing energy services and power exports (cash inflows) in year $n$; $WLC_{ann}(n)$ denotes the annualised $WLC_{MG}$, which can be calculated by multiplying the whole-life cost of the system by the relevant capital recovery factor (see Equation 2.35); and $RR$ represents the reinvestment rate, which is assumed to be 0% in this study.

### 2.6.4.4. Discounted profitability index

The profitability index (PI), alternatively referred to as value investment ratio or profit investment ratio, measures the present value of future cash flows relative to the capital investment, or put differently, the present value of the total investment expenditure of a business plan across its lifetime to the associated initial costs – the ratio of payoff to the investment of a project. The DPI is a modified variant of the PI, which factors in the time value of money. Accordingly, the DPI of the modelled MG systems can be determined by the following equation [175]:

[11] The IRR is defined as the discount rate which makes the total NPC of an investment scheme equal to zero; thereby, leading the investment to break even before it starts creating any revenues.

$$DPI = \frac{\left| PV(TRC + TO\&M - TSV) + NPC_{tr,net} \right|}{TCC}, \tag{2.69}$$

where $TCC$ denotes the total capital cost of the MG assets; $TRC$, $TO\&M$, and $TSV$ respectively represent the total discounted replacement cost, O&M cost, and salvage value of the energy infrastructure; $NPC_{tr,net}$ identifies the total net present cost associated with trading with the utility grid over the MG lifetime (where appropriate); and $PV(\cdot)$ denotes the present value function.

Any DPI value lower than 1.0 is undesirable, as it indicates that the present value of the project is lower than the capital outlay. As the value of DPI increases above 1.0, the financial attractiveness of the proposed design does so as well.

#### 2.6.4.5. Resulting capital budgeting metrics

Table 2.6 lists the resulting values of the employed financial appraisal metrics to evaluate the profitability of the implementation of MG systems 1–3 at the considered case study sites. In calculating the associated capital budgeting metrics for the cost-optimal configurations of the conceptual MG systems 1–3 yielded for the corresponding case studies, the sources of cash inflow have included the power sold to the customers at flat rates of \$0.26/kWh,[12] \$0.21/kWh, and \$0.23/kWh, respectively, in compliance with the present average retail domestic electricity prices at the studied sites [176]. Also, where appropriate, hydrogen is sold to the refuelling station's customers at a flat rate of \$8.00/kg-$H_2$, which is far below the most recent estimated price of green hydrogen in New Zealand when produced locally on small-scale (\$13.91/kg-$H_2$), and is highly competitive with the estimated price of \$7.98/kg-$H_2$ for large-scale green hydrogen production schemes [177], [178]. Furthermore, for grid-connected cases, the power is exported back to the grid at a flat-rate feed-in-tariff set at \$0.08/kWh. On the other hand, power imports into the grid-connected systems (cases 2 and 3) are traded at the dynamic forecasts of wholesale electricity market prices shown in Fig. 2.19. It can be seen from Table

[12] At present, the power supply scheme on Stewart Island is entirely based on diesel generators operating in a centralised manner.

2.6 that the values of LCOEE and LCOH obtained for the devised energy systems are markedly below the corresponding present average retail prices of electricity and hydrogen in the relevant grid-tied and grid-independent areas in New Zealand. Not only do these findings verify the effectiveness of the proposed MG designing and capacity planning methodology, but they also provide direct, multi-variant evidence supporting the cost-effectiveness of implementing the studied MG development projects.

Table 2.6: Comparative summary of the capital budgeting analyses for the proposed and existing electricity supply systems at the studied sites.

| MG system | Capital budgeting metric | | | | | |
|---|---|---|---|---|---|---|
| | LCOE* | LCOEE | LCOH | DPP | MIRR | DPI |
| MG 1 | \$0.21/ kWh | \$0.18/ kWh | \$6.82/ (kg-$H_2$) | 9.03 years | 4.5% | 1.20 |
| MG 2 | \$0.14/ kWh | \$0.12/ kWh | \$6.17/ (kg-$H_2$) | 7.59 years | 7.2% | 1.91 |
| MG 3 | –\$0.02/ kWh | –\$0.02/ kWh | N/A | 3.95 years | 13.8% | 2.86 |

* Mathematically, the LCOE becomes negative when the present worth of the net cash flows in Years 1 and later of the project are more positive than the Year 0 cost is negative – or, put differently, when the projected total out-year benefits (generated from grid exports, local power sales, and equipment salvage value) are higher than the sum of the costs of initial investment, equipment replacement, system O&M, and grid imports.

For reasons of similarity and space, the detailed illustration of the DPP calculation is limited to cases 2 and 3. Based on the above premises, the value of parameter $S$ for system 2, which represents the total annual revenue created from selling energy to MG customers and grid exports, can be obtained from the following equation:

$$S\,[\$] = 0.21\left[\frac{\$}{kWh}\right] \times P_{L,TA}\,[kWh] + 0.08\left[\frac{\$}{kWh}\right] \times P_{ex,TA}\,[kWh] + 8.00\left[\frac{\$}{kg\ H_2}\right] \times P_{S,TA}\,[kg\ H_2], \tag{2.70}$$

where $P_{L,TA}$, $P_{ex,TA}$, and $P_{S,TA}$ respectively denote the total annual values of the supplied residential electrical loads [kWh], electrical energy exported back to the grid [kWh], and hydrogen delivered from the tank to the refuelling station [kg],

which are determined by the representative year-long operation of the MG. They are respectively found to be 3.70 GWh/year, 219.14 MWh/year, and 9.22 tonnes $H_2$/year – equivalent to 366.31 MWh/year. The graphical discounted break-even analysis of the proposed system for implementation at the second case study site on the basis of the 20-year revenue stream is presented in Fig. 2.29. As illustrated in the figure, the DPP of the project, if realised, would be 7.59 years. Furthermore, the discounted total net profit that could be gained over the planning horizon, through the sale of green electricity and hydrogen, is expected to be $8,134,808. It must be noted that the linearity of the cumulative total revenue curve is due to the simplifying assumption that load demand is constant and is not subject to growth over the expected lifetime of the project lifespan – and, hence, the grid exports. On the other hand, the nonlinearity of the cumulative total annualised cost curve is attributable to the O&M costs, as well as the costs associated with the replacement of the components. More specifically, to derive the cumulative total annualised cost curve, first, the total annualised capital cost of the MG system is calculated and then the discounted replacement (taking into account the corresponding salvage values) and O&M costs are added to the years they are incurred. Accordingly, the cumulative total annualised cost curve uncovers the relatively low contribution of the discounted O&M and replacement costs to the total NPC of the MG system relative to the capital cost of the system. Furthermore, the total annualised capital cost of the MG is calculated by multiplying the determined capital recovery factor (in the discounted cash flow analyses) by the total capital cost of the system, as suggested in [179]. In addition, the cumulative sum of the total annualised costs at the end of the investment horizon is equal to the best total NPC obtained by the MFOA out of 30 simulation runs, which was found to be $7,330,037.

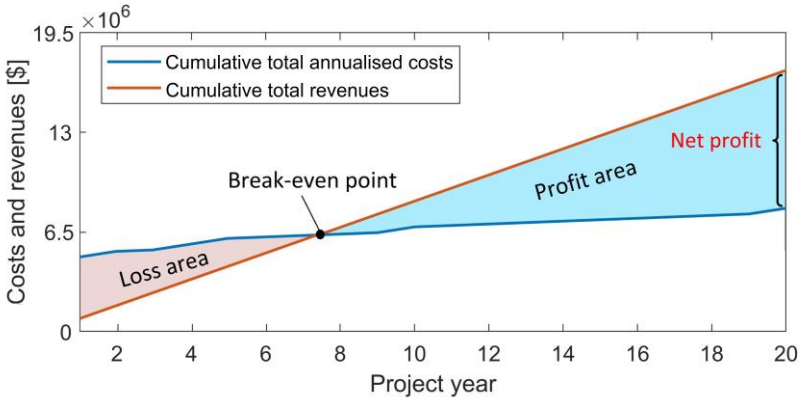


Figure 2.29: Discounted break-even analysis of project 2 over a 20-year operating life-cycle period.

Moreover, Fig. 2.30 provides an overview of the cumulative discounted cash flow analysis over the third MG's life cycle period. As the figure shows, a relatively significant capital outlay is expected, in addition to the battery and inverter replacement costs in Year 15 of the project, as well as annual O&M and grid import costs. The figure also indicates that the entire $123,012 investment, if realised, would be recouped within around 10 years.

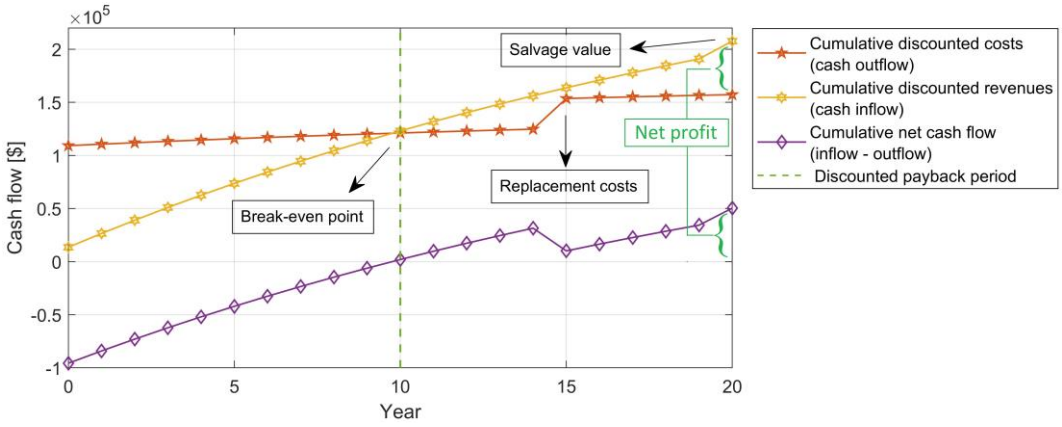


Figure 2.30: Discounted break-even analysis over the life-cycle of the third project.

Moreover, a comparison of the MIRR and DPI values of the three MG projects in Table 2.6 reveals that the exchange of energy with the upstream grid, along with the utilisation of solar and hydro (in the second case) resources, have significantly contributed to the profitability of the conceptualised systems for the

second and third cases. More specifically, the connection of the second and third MGs to the upstream network provides them with the opportunity to avoid curtailment of excess non-dispatchable generation and to import electricity during the non-coincident peak demand periods when wholesale prices are lower than the (additional) levelised cost of meeting peak demand by over-building of renewable generation and/or storage that would be utilised internally only during periods of highest onsite demand. In addition to the greater flexibility offered by treating the utility grid as a system resource to absorb otherwise-curtailed excess generation and as an additional resource for compensating power deficits, case study sites 2 and 3 are better endowed with solar PV and wind resources, which have complementary diurnal and seasonal production profiles – wind higher at night and in winter, solar PV higher in the daytime in summer. Another contributing factor to the greater economic feasibility of MG 2 than MG 1 – measured by the comparative net economic benefits – is the economies of scale. It should also be noted that the main reason underlying the achievement of a negative LOCE in the smallest test case (MG 3) is that it is currently equipped with an oversized transformer – which, specifically, has a high capacity of 50 kVA relative to the site's annual peak demand of 9.22 kW. This directly contributes to making an over-built renewable energy generation capacity solely for electricity exports as a profitable business plan, which, accordingly, results in a negative LCOE value.

Collectively, the in-depth capital budgeting analyses provide strong, multi-variant evidence supporting the proposition that not only are the renewable energy project proposals – that surpass retail grid parity – economically sustainable and financially profitable to undertake, but they can also be characterised as high-yield, low-risk investment opportunities due to their relatively short payback periods – which are able to ensure that stakeholders would yield a consistent profit stream. Additionally, implementing efficient wet biomass and municipal solid waste stream management programmes in cases 1 and 2, as well as laying the foundations for the integration of hydrogen fuel cell-powered tractors and trucks – that support the cost-effective and affordable movement towards the realisation of sustainable agriculture and waste management goals – and the system integration of hydrogen fuel cell-powered passenger ferries – that contribute to the sustainable

transportation goals – directly add to the collective efforts towards the sustainable socio-economic development of remote, island, rural, and peripheral communities. It should also be noted that the conceptualised MG systems meet the entire low-temperature heat demands of the studied communities without requiring any fossil-fuel imports. Most of all, given the projected useful lifetime of the MG systems (20 years), the circa 2% increase in domestic electricity prices in New Zealand per annum, the environmental benefits of the conceptualised 100%-renewable energy systems, as well as their substantial contribution to improving the reliability, resilience, self-sufficiency, stability, and quality of power supply in remote, village, and semi-urban communities, the economic viability of realising the proposed MGs for the considered case study sites is ensured.

## 2.7. Chapter summary

This chapter has introduced the general formulation of the proposed robust meta-heuristic-based, highly dimensional MG equipment capacity planning optimisation model tailored towards community-scale, sector-coupled, multi-energy-storage-technology, 100%-renewable and -reliable energy projects with high degrees of energy self-sufficiency (at least 80%) and resiliece (to planned and unplanned grid outages, as well as onsite low-probability, catastrophic events) – which directly contributes to the collective economy-wide deep decarbonisation efforts. To identify the most efficient (superior) meta-heuristic algorithm for utilisation in the formalised long-term strategic MG designing and capacity planning optimisation solution algorithm, a systematic descriptive statistics-based comparative meta-heuristic performance analysis scheme has been proposed that adequately accounts for varying efficiencies of meta-heuristics when applied to structurally different MG systems with different climatic, loading, and wholesale electricity price conditions, whilst accounting for the associated initialisation-directed stochasticity in different simulation trials. The long-term strategic multi-case-study-oriented comparative performance analyses of meta-heuristics for MG equipment capacity planning optimisation have been carried out considering a total of 20 meta-heuristics. The 20 algorithms have been selected from a pool of 226 meta-heuristics including both well-established and state-of-the-art single and hybrid techniques

based on comprehensive preliminary efficiency tests applied to simplified MG sizing problems.

Also, reinforcing RSESs with optimal energy storage solutions has been found as one of the most effective interventions to improve their overall efficiency through reduced cycling, resulting in lighter footprints, higher robustness and improved cost-effectiveness. In this context, this chapter has addressed the key design problem of multi-energy-storage-technology-integrated RSESs by yielding the optimal storage sizing solution that offers the best compromise between the total discounted costs incurred and the technical improvements from hybridising the storage technologies considered. To this end, a first-order passive low-pass energy filter-based operational planning algorithm has been proposed for efficient scheduling of multiple energy storage technologies integrated into grid-connected and isolated MG systems. The filter enables leveraging the potential of stationary PtG technologies for long-term energy storage applications and SC modules for ultra-short-term applications. Furthermore, an efficient energy management strategy has been devised for the coordinated integration of medium-duty fuel cell electric vessels, heavy-duty tractors, and heavy-freight trucks.

Moreover, the chapter has conceptualised two first-of-their-kind sector-coupled, multi-energy MG systems, as well as a typical solar PV/wind/battery MG system, tailored to grid-connected and isolated applications, which collectively offer the following opportunities: (1) improving the dispatchability of future RSESs using more diversified portfolios of variable generation technologies with complementary characteristics (particularly, solar PV, wind, and run-of-the-river micro-hydro) together with a sustainable share of dispatchable RESs (particularly, biomass resources), whilst simultaneously improving energy security; (2) optimal system integration of WtE plants, wherein the non-organic fraction of MSW is combusted to generate electricity; (3) optimal system integration of biomass gasifier-generator systems, which receive the organic fraction of MSW and wet biomass residues as input; and (4) hybridisation of different energy storage technologies in compliance with the timescale relevant to the technical capabilities of each technology, particularly the duration of energy storage capacity per unit of power capacity.

The modelling results of the previously unexplored numerical case examples of Stewart Island, Feilding Valley, and Totarabank Subdivision have generated a number of novel insights, as follows:

1. A statistically robust, representative, and significant body of evidence has been generated from test case simulations – which represent a continuum of community scales from multi-family village communities to semi-urban communities – supporting the proposition that the MFOA is an ideal choice for meta-heuristic-based community MG capacity planning optimisation. The global superiority of the MFOA can be attributed to its unique feature of systematically rebalancing exploration – the early stages of the optimisation process that mimics the long-range movement of individuals – for improved exploitation – the local search around promising regions – of the search space for potential solutions. The detailed descriptive statistics-based comparative performance analyses of the selected meta-heuristics have also validated the robustness of the findings on the outperformance of the MFOA to the other algorithms with respect to the variations in the MG configuration and structural complexity, as well as climatic, loading, and price conditions. It has also been shown that failure to employ an appropriate optimisation algorithm, while optimally designing a MG system using meta-heuristics, could potentially result in an overestimation of its lifetime cost by up to 4.5% – which could be substantially greater if comparisons were not restricted to the top 20 meta-heuristic identified from preliminary efficiency testing studies. However, from the comparative analyses, no differences have been observed in terms of the optimal configuration (architecture, structure, or topology) of the systems optimised by the selected 20 meta-heuristics – and all the further examined meta-heuristics have agreed in all cases on the presence or absence of the candidate technologies in the relevant optimum solution sets.

2. Intriguingly, it has been found that the average root-mean-square error of the population of the MG whole-life costs returned by the proposed MFOA-optimised model over the 30 trials across the three test cases with respect to its best performance is negligibly low (~0.4%). This indicates the robustness

of the proposed MFOA-based model to the random population initialisation process, which, in turn, suggests the adequacy of a single run of the algorithm.

3. Solving the MG sizing problem using meta-heuristics is computationally demanding as it involves determining the year-long, hourly-basis energy balance of the infrastructure portfolio selected by each of the hundreds of the meta-heuristic of interest's search agents. However, since the MG investment planning is a one-time optimisation exercise, the running time limits are exceptionally high within the renewable energy system optimisation context.

4. In terms of economic viability, comprehensive financial appraisal and discounted cash flow analyses have supported the proposition that it is not infeasible for the communities to have the financial means to be able to own the modelled systems outright, though they also can be readily financed through third-party ownership opportunities (such as power purchase and lease agreements) – as they represent attractive investment opportunities due to surpassing retail grid parity. The former business model guarantees significant savings on electricity bills of up to 108% (recall the negative LCOE obtained for case 3), whereas the latter is (at least) able to make an effective hedge against the energy price inflation and significantly improve the reliability, resilience, and adequacy reference margins of the communities at no extra cost – towards eradicating energy hardship and poverty in a sustainable manner. The results of high-level cost-benefit analyses, additionally, indicate that the proposed capital projects are economically feasible without any subsidies delivered as tax incentives – for example, renewable energy investment tax credits or production tax credits. More specifically, a comparison of the resulting levelised costs of electricity and hydrogen for the studied cases with the corresponding present retail tariffs has shown that, on average, the three project proposals are able to reduce electricity and hydrogen costs by as much as 61% (considering all three cases) and 56% (considering the first two hydrogen-based cases with a present hydrogen price of \$13.91/kg-$H_2$), respectively.

Furthermore, in-depth energy balance analyses have substantiated the feasibility and stability of the resulting optimal MG designs. In addition, detailed breakdowns of the whole-life costs of the conceptualised MG systems specifically optimised for the considered cases have corroborated the fact that energy storage represents a significant portion of the total discounted cost of community MG systems, especially for cases where seasonal load levelling using hydrogen storage infrastructure constitutes a better approach than seasonal peak imports and over-building of renewable generation – that would rarely be used internally during the off-peak season.

In conclusion, this chapter has demonstrated the technical feasibility and economic viability of deploying community-scale, sector-coupled on- and -off-grid MGs – that provide sustainable electricity and transportation fuel services to remote, island, rural, peripheral, and semi-urban communities – optimised by a novel MFOA-based MG sizing model that is able to (1) leverage the temporal complementary characteristics of variable renewables on both seasonal and daily bases and make effective use of a sustainable share of dispatchable renewables with implications on the optimal combination of the candidate technologies in the corresponding generation mix, (2) effectively integrate hybrid energy storage systems (specifically, hybrid hydrogen storage/SC bank) with complementary operational characteristics in terms of the timescale relevant to the technical capabilities of each technology, and (3) ascertain the technological competence and cost-competitiveness of utilising green hydrogen – produced by water electrolysis and gasification of biomass resources (the organic fraction of the MSW as well as the agricultural biomass residues) – as an energy vector in medium-scale community-scale MGs for niche applications – inter-seasonal energy storage to meet seasonal demand, and hydrogen mobility to decarbonise the transport sector. Accordingly, it can be concluded that the simulated systems are able to satisfy nearly all the energy needs of remote, island, rural, peripheral, and semi-urban communities – electricity, space heating, hot water, and transportation fuel – whilst additionally providing a practical solution to manage their agricultural and municipal solid waste, in a cost-optimal, reliable, affordable, sustainable, resilient, and self-sufficient way that promotes energy democracy and independence.

The following chapter seeks to improve the proposed MFOA-based MG sizing model by integrating a sectoral aggregator-mediated, EV-charging-load-addressable, market-driven, interruptible DR scheduling framework. The framework employs a specifically developed bi-level, Stackelberg, non-cooperative game-theoretic framework to accurately characterise the strategic interactions of the MG operator (utility), intermediary sectoral DRAs, and end-customers in day-ahead, incentive-based DR programmes in a robust, equitable, transparent, market-driven manner. This further improves the flexibility and cost-effectiveness of community MG systems in the face of new sources of electricity demand – particularly, heating and transport electrification. It also provides a platform to study the impact of producing optimal trade-offs between importing electricity, discharging onsite energy storage media, and leveraging incentivised DR flexibility resources for the hours of each day for which a net energy deficit is predicted in the presence of hybrid energy storage systems.

# Chapter 3: Game-Theoretic Sectoral Demand Response-Integrated Strategic Design Optimisation of Micro-Grids Considering a Platform-Mediated, Double-Sided Local Flexibility Market[1]

In accordance with primary research objective 1, the preceding chapter has formalised the basic structure of the proposed robust, meta-heuristic-based, highly dimensional MG equipment capacity planning optimisation model tailored towards community-scale, sector-coupled (electricity, low-temperature electrified heating, and e-mobility), multi-energy-storage-technology, 100%-renewable and -reliable energy projects, whilst additionally identifying the superior meta-heuristic in MG sizing applications based on comprehensive, comparative multi-case-study-oriented statistical efficiency tests following an inductive reasoning approach. Building on the general MG equipment capacity planning model put forward in Chapter 2, this chapter begins the process of improving the accuracy of long-term strategic MG development plans through the integration of fundamentally new modelling elements based on deductive reasoning.

To this end, this chapter mainly focuses on addressing primary research objective 2. Specifically, in addition to enabling the smaller customers across different classes to reap the full benefits of their demand flexibility potential in an equitable manner, as well as providing aggregators with a consistent revenue

[1] This chapter draws heavily (often verbatim) on the following journal papers:

• **S. Mohseni**, A.C. Brent, S. Kelly, W. Browne, and D. Burmester, "Strategic design optimisation of multi-energy-storage-technology micro-grids considering a two-stage game-theoretic market for demand response aggregation," *Applied Energy*, vol. 287, p. 116563, 2021.

• **S. Mohseni**, A.C. Brent, S. Kelly, W. Browne, and D. Burmester, "Modelling utility-aggregator-customer interactions in interruptible load programmes using non-cooperative game theory," *International Journal of Electrical Power and Energy Systems*, vol. 133, p. 107183, 2021.

stream, by applying insights from game theory to the study of small- to medium-scale interruptible DR provision and integrating the resulting framework into the design phases of MGs, this chapter seeks to unlock important long-term financial implications for MG operators in terms of sourcing costs. That is, the present chapter primarily aims to help MG operators better (less conservatively) project long-term load power demand in the presence of dispatchable loads, which results in narrowing the required system adequacy margins. In this context, in the long run, well-coordinated and well-forecasted DR programmes are hypothesised to reduce aggregate generation capacity requirements by shaving the peak load, whilst also allowing MG developers to: (1) build less new capital-intensive storage capacity, (2) defer or deter excessive costly investments in transmission and distribution network capacity expansions (which may then be significantly underutilised), (3) increase the penetration of non-dispatchable renewables, and (4) leverage cost-efficient frequency control and voltage control services.

In terms of secondary objectives, the chapter particularly aims to address secondary objective 3 (*investigating the potential of V2G technologies and FCEV charging/discharging coordination through DSM mechanisms in driving economic sustainability improvement for renewable energy development projects*), whilst additionally seeking to further verify the validity of the model in achieving secondary objectives 1 and 2 through comprehensive extreme scenario testing involving complex scenarios of hybrid storage and a previously unexplored bioenergy generation technology within the context of MG prior feasibly and business case analyses, namely biopower plants. Accordingly, the chapter, additionally, contributes to addressing secondary research objectives 1 and 2, namely: *improving the dispatchability of future RSESs using more diversified portfolios of variable generation technologies with complementary characteristics together with a sustainable share of dispatchable RESs*; and *the optimal hybridisation of different energy storage technologies in compliance with the timescale relevant to the technical capabilities of each technology*.

In this light, this chapter specifically focuses on addressing research gaps 2 (*poor understanding of the incentive-price elasticity of customer-supplied DR capacity across different sectors and the associated strategic utility-aggregator-*

*customer interactions*), 5 (*negligence of the operational suitability of various energy storage technologies over specific timescales*), 6 (*paucity of 100%-renewable MG systems*), and 7 (*limited procurement of V2G services as sources of system-balancing flexibility to manage supply-demand mismatches*).

The application of the modified, game-theoretic sectoral DR-integrated variant of the proposed energy planning optimisation model to an innovative new grid-tied, community-scale, sector-coupled MG integrating solar PV panels, WTs, and run-of-the-river micro-hydro (MH) power plants (as variable generation), a biomass power plant (as dispatchable generation), a hybrid energy storage solution incorporating a hydrogen-based energy storage system (electrolyser, hydrogen tank, fuel cell), a vanadium redox flow battery bank, and an EDLC SC bank, as well as a hydrogen refuelling station tailored to light-duty hydrogen fuel cell-powered personal passenger vehicles, demonstrates the utility and validity of the reformed MG sizing model in producing cost-minimal MG configuration results to meet sectorally disaggregated loads – and more specifically, cost-optimal trade-offs between the levels of DR dispatch, grid imports (for grid-connected installations), and internal DER allocation (including renewable generation and storage assets). The foregoing discussion also implies that the suggested MG configuration is novel as it constitutes the first community-scale energy system of any kind that delivers such a significant level of diversity in the associate portfolio of DERs, as well as targeted end-use sectors – residential, commercial, industrial, agricultural, and e-mobility.

In addition, the chapter provides statistical case study evidence to suggest the validity and effectiveness of integrating a behaviourally-founded, aggregator-mediated DR arrangement scheme into the base-case MG capacity planning model, which simultaneously implies the utility, robustness, and scalability of the general architecture of the original meta-heuristic-based MG sizing approach. Also, on a wider level, the larger-scale community MG case study findings (for the town of Ohakune, New Zealand, which has a permanent population of more than 1,000 people with around 7,000 seasonal ski tourists) add to the collective body of statistically valid evidence in Chapter 2 for smaller-scale community MG cases (cases 1 and 2 tailored to two rural communities with a population of several

hundred people) on the cost-effectiveness, reliability, and efficiency of transitioning to a green hydrogen economy (with hydrogen treated as an energy carrier/vector) where PEM fuel cells are used in stationary backup distributed generation and automotive (particularly, light-duty-vehicle, heavy transport, and agricultural machinery sectors) applications.

## 3.1. Introduction

Smart electrification with non-dispatchable renewables is set to play a pivotal role in accelerating the transition to the low-carbon economy [3]. However, non-dispatchable RESs are collectively plagued by unpredictability and variability of supply. This is especially problematic during daily peak times when demand is highest [180]. On the other hand, the increased electrification of end-uses – such as transport, space heating, and water heating – is a key contributor to rising these peaks, which results in the need for over-capacity of renewable supplies and/or (capital-intensive) storage devices, as well as additional transmission and distribution network capacity [181].

Accordingly, a key challenge in realising cost-effective electric power systems with high penetrations of non-dispatchable (variable) RESs is the temporal discrepancy between renewable power generation and peak power demand [86], [182]. Addressing this challenge in grid-connected RSESs requires an optimal trade-off between imported power demand from the upstream grid and reduced peak demand through DSM strategies for cost-optimal operation and investment [183]. In this light, utilising the flexibility potential of small- to medium-scale customers – as part of the goal of tapping all available sources of demand-side flexibility – is of utmost importance to reduce the cost of integrating high shares of renewables and the need to invest in network capacity reinforcement, especially under future scenarios of end-use sector coupling [184]. The associated DSM interventions enable consumers to proactively engage in electricity markets and benefit from DSM schemes designed and incentivised by utilities to curtail/interrupt or shift a proportion of electricity demand, and thereby flatten the overall load power profile – and improve the associated load factor.

While DR programmes have been in use to improve the energy efficiency of large-scale industrial and commercial consumers for years (for emergency periods when the utility cost of service exceeds a pre-defined threshold), the expansion of the concept to include less energy-dense demand sectors, namely the residential and agricultural sectors, as well as electrified transport, is enabled by recent advancements in ICTs, which have substantially contributed to the development of advanced metering infrastructure [185]. That is, the recent emergence of advanced control methods, founded on two-way communications for smart grid applications, has facilitated the coordination of small- to medium-scale DR resources – previously invisible to grid operators – through a new family of load-serving entities, called demand response aggregators (DRAs). The DRAs act as intermediaries between utilities and retail consumers and unlock the potential of retail demand-side flexibility resources by aggregating loads of the same class and packaging the total DR bids for submission in ancillary services markets [186]. Accordingly, the large-scale deployment of retail DSM services – which deliver competitive, efficient, and reliable interruptible DR services at scale – is recognised as one of the key enablers of the low-carbon economy [187].

In this context, it is commonly accepted that [188]: (1) open aggregator-mediated DSM marketplaces improve customer engagement due to the additional flexibility provided to the subscribers, while supporting the minimum expected utilities by end-consumers, and (2) wholesale electricity prices need to be valued as a primary means of signalling the worth of load reduction to the utility when developing load shifting and/or curtailment strategies.

In general, DR programmes can be classified into two main categories: price- and incentive-based. Price-based DR involves time-variant pricing schemes to reflect the value of electricity in different time periods. On the other hand, in incentive-based DR schemes, customers are offered incentive payments to reduce their energy use in case of grid reliability problems or high wholesale prices [189], [190]. The interruptible/curtailable services, which fall in the category of incentive-based programmes, are selected in this study for the modelling of aggregator-mediated DR events, which provide a platform for voluntary customer enrolments

and responses. That is, customers are given the discretion to select their level of participation in any DR event.

Additionally, DR programmes can be implemented over a broad range of timescales, from 15 minutes (real-time operation) to several years (system planning) ahead of schedule [190]. Among these timescales, day-ahead energy management is considered in this analysis for integration into MG life-cycle analyses as it has a considerable potential to benefit from market-based DR programmes. It also represents a unique scheduling horizon as it effectively captures the diurnal nature of energy demand and non-dispatchable renewable supplies.

### 3.1.1. Incorporating strategic interactions into demand response scheduling models

To reduce the gaps between modelled and real-world results for aggregator-mediated DR schemes, it is necessary to characterise the economic interactions between the utility, DRAs, and end-consumers. To this end, the simplifying assumptions commonly applied in designing aggregator-mediated DR programmes, which are not justified in many cases, need to be refined [191]. More specifically, a realistic grounding needs to be given to research on aggregator-mediated DR procurement to improve the quality and accuracy of the day-ahead DR supply capacity forecasts before integration into the MG business-case analyses. Accordingly, to be able to directly apply the aggregator-mediated DR frameworks to real-world problems, it is crucial to model the involved active economic agents – the utility, DRAs, and end-consumers – as rational, self-interested agents who make decentralised and utility-maximising decisions. Under this assumption, the problem of aggregator-mediated DR planning falls in the realm of algorithmic game theory [192] and, more particularly, algorithmic mechanism design [193]. Algorithmic mechanism design models the interaction of individuals using tools borrowed from game theory, where the institutions governing interactions are modelled as mechanisms, in strategic settings, where players act rationally [194]. The overall aim of algorithmic mechanism design within the context of this study

is to derive an economically stable allocation of DR resources, where a truthful preference report is the best strategy for every active economic agent involved.

On the other hand, market-driven incentive-based curtailable DR resources are often procured through "ascending bid" auctions where the incentive price is successively increased in rounds until the level of procured DR units minimises the system operational cost [195]. This characteristic can be represented by the Stackelberg leadership duopoly [69], which is a model of imperfect competition founded on sequential non-cooperative games [68], where the market leader moves first and then the followers move sequentially.[2] Accordingly, the aggregator-mediated DR procurement game can be modelled as a two-stage negative feedback game in which the utility and DRAs form a Stackelberg problem in the first stage, while the DRAs and end-consumers form another Stackelberg problem in the second stage (which assists the associated DRA decision-making process in deriving the aggregate sectoral DR capacity), both of which can be characterised as single-leader-multi-follower games. More specifically, the DRAs serve as the followers of the utility in the wholesale DSM market and are, at the same time, the leaders of the sector-specific retail DSM market, where end-consumers act as followers [196].

Several review studies have emphasised the important role that the characterisation of the strategic rationality of economic agents involved in the delivery of DR resources can play in making simulations more perceptually representative of real-world scenarios [45], [197], [198]. To this end, non-cooperative game theory [68] has been recognised as a standard analytical tool to understand the strategic economic behaviour of rational entities that interact through efficient and stable markets for the activation of smaller DR units – and make predictable and reproducible choices [199]. Notably, this strand of the energy planning literature expands the boundaries of non-cooperative game-theoretic DR markets and enables a more integrative approach to DSM planning. In particular, it seeks to address how to achieve economically stable and efficient divisions of the

[2] In game theory, a Stackelberg duopoly is a non-symmetric, strategic, sequential game with one party, or a group of parties, taking over the leading position and the other(s) acting as follower(s).

surplus created by incentivised load curtailments based on non-cooperative game theory in platform-mediated DR markets. In this context, the standard approach is to develop a two-stage (dual-loop) DR market design where the utility and DRAs compete in the top-level (wholesale) DSM market, while the DRAs and end-consumers compete in the bottom-level (retail) DSM market. Specifically, the utility offers load reduction incentive prices to the DRAs, who, in turn, offer a percentage of the utility-offered incentive rates to their end-consumers in the bottom-level (retail) DSM market (see Fig. 3.1). Notably, double-sided market designs for DR aggregation explore the conditions under which competitive market equilibrium is simultaneously reached at the upper utility level and the lower distribution network level. For instance, Yu and Hong [196] have formulated a two-loop Stackelberg, strategic game for an incentive-based, market-driven, aggregator-mediated scheduling of interruptible DR resources. Based on the numeric simulation results, the authors have confirmed the superiority of their proposed model in terms of reducing the hourly operational cost of a distribution grid by ~47%, as compared to the case where generation capacity deficits are addressed purely by onsite diesel generators. The authors have additionally applied their model to another test case including medium-scale industrial customers and reaffirmed their findings. Notably, they have shown the ability of their proposed model in reducing the hourly operational cost of a typical distribution network including medium-sized industrial customers by up to around 63%.

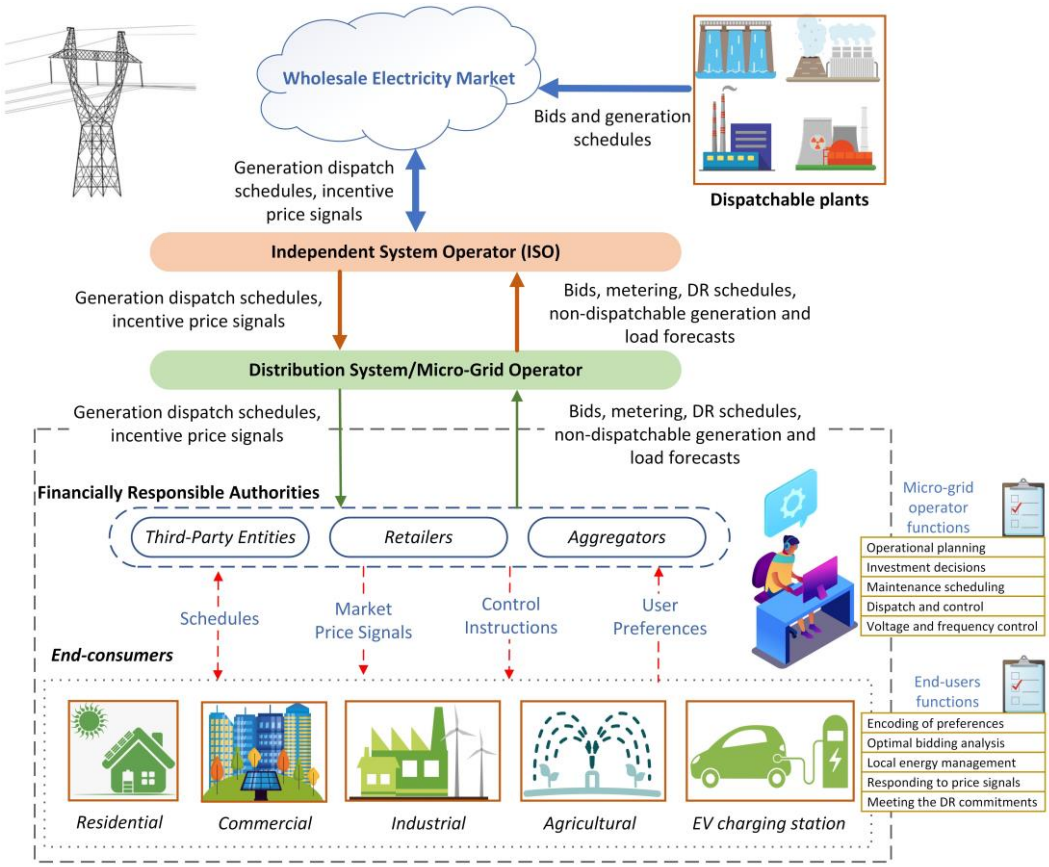


Figure 3.1: General architecture of platform-mediated, double-sided DSM markets with several customer segments involved under the end-use sector-coupling paradigm.

In another instance, Ren et al. [200] have proposed an optimal Stackelberg energy scheduling framework specifically tailored to the coordination of the interactions between the distribution network, EV aggregators (that combine the participating individual interruptible EV charging loads), and EV owners. The aggregator sells a joint capacity of smaller DR units to the utility, whilst accounting for the incentive price elasticity of aggregator-mediated DR capacity. The modelling framework accounts for the individual objectives of the three sets of the involved players, and is shown to be able to yield a participation rate of 99% in EV load management programmes. Şengör et al. [201] go further by characterising the uncertainties associated with the EV charging behaviours, while optimising the strategic bidding strategy of an aggregator participating in day-ahead and secondary control reserve markets. They have also demonstrated that their proposed iterative distributed algorithm to approximate the pure-strategy Nash equilibrium of the DR

dispatch problem has a relative error of less than 3% compared to counterpart analytically-derived solutions. Zhong et al. [202] have also put forward a coupon incentive-based DR scheme, where third-party load-serving entities participate in the wholesale DSM market and offer a flat incentive rate to the small-scale customers subscribed to them. Accordingly, they have proposed an algorithm to find the optimum coupon incentive price with respect to different wholesale market conditions. Also, Sobhani et al. [203] have modelled the interactions between several interconnected energy hubs – the operators of which essentially serve as DRAs – as a congestion game, whilst adhering to the associated coupling constraints. They have shown the existence and uniqueness of the pure-strategy Nash equilibrium of the developed non-cooperative game-theoretic model that is aware of the discomfort patterns of end-consumers, whilst additionally producing the numerical Nash equilibrium DR dispatch solution to the game using a specifically developed distributed algorithm for real-world applications. Specifically, they have highlighted the efficacy of the framework in reducing the daily peak-to-average ratio by ~9% on a representative winter day.

Furthermore, Feng et al. [204] have proposed a bi-level Stackelberg, non-cooperative game-theoretic model that is able to produce the Nash equilibrium of a transactive energy market where a set of independent DRAs compete to maximise their objective functions in the lower level. On the other hand, the upper level deals with updating a transactive incentive price signal sent to the DRAs in an iterative approach so as to cost-optimally meet the distribution system operator requirements, whilst maximising the social welfare with respect to the locational marginal price. Vuelvas et al. [205] have additionally analysed the incentive compatibility of aggregator-mediated incentive-based DSM schemes. To this end, the authors have formulated a two-stage stochastic programming problem for the strategic interactions between DRAs and end-consumers and solved it using ideas from game theory. Moreover, Gazafroudi et al. [206] have presented evidence of the effectiveness of an ‘agent-based’ non-cooperative game-theoretic approach to manage the smaller DR products, in terms of providing a sustainable platform for trading small- to medium-sized DR products under both individual rationality and collective rationality conditions in sequential games – which ensures the strategic

stability of the equilibrium solution. Also, Li et al. [207] employ a Stackelberg, non-cooperative game-theoretic framework to optimally dispatch energy hubs equipped with multi-energy DR resources, where demand-side flexibility capacities elicited from electrical and thermal loads are separately aggregated.

### 3.1.2. Long-term, demand response-integrated micro-grid infrastructure planning background

This section summarises the most rigorous studies carried out to date on the integration of demand-side resources (for the strategic planning of energy demand) into the long-term capacity optimisation models of RSESs, which helps situate this study in the context of the existing literature.

Recent studies have revealed that the consideration of DSM strategies in the optimum investment planning phase of RSESs for domestic applications can offer cost savings of about 15% to nearly 35% (depending on the participation rate of end-users in the DR programmes), whilst preserving consumer comfort standards [208]–[210]. That is, the proper integration of DR programmes into RSESs would result in a win-win-win situation – the third winner being the environment, as they will accelerate the transition to a low-carbon energy economy and a world (increasingly) run on green energy.

A reformed formulation of the MG equipment capacity-planning problem is required to make effective use of the economic opportunities offered by DSM processes to support decision-making in developing cost-effective RSESs [211]. A solution to the optimal DR-integrated MG design problem identifies the least-cost combination of the size of the components of the system over a decades-long – often spanning 20 to 30 years – investment planning horizon to meet the projected demand for energy, while leveraging the potential of responsive loads [212], [213].

Recent review studies have focused on discussing methods and trends for harvesting the potential of the demand-side flexibility to contribute significantly to energy affordability in energy networks with a high penetration of distributed renewables. Gelazanskas and Gamage [214], Haider et al. [215], Esther and Kumar [216], Wang et al. [197], Robert et al. [217], as well as, more recently, Jordehi [44]

have scrutinised various approaches to implementing DR arrangements, while optimally designing RSESs, with a particular focus on residential DR resources. Moreover, various types of DSM strategies have been incorporated in the formulation of the MG capacity-optimisation models. This implies that DR programmes are well-analysed for the investment planning of RSESs, a statement that has likewise been made in the context of different DSM business models in electricity markets [218], as well as for the optimal operational scheduling (energy management) of RSESs [197].

There have also been attempts to exploit other types of DR structures for the optimal capacity planning of RSESs. For instance, Kahrobaee et al. [219] have devised a PSO-based planning model for a smart home nano-grid that utilises the real-time pricing (RTP) scheme, which allows for leveraging the historical records of the price elasticity of demand for personalised dynamic pricing. In another instance, Yu et al. [220] have proposed a robust flexible-programming approach for the integration of renewables into a municipal energy system, which runs a critical peak pricing (CPP) rate structure. Moreover, Varasteh et al. [221] employ a hybrid direct load control-time-of-use (DLC-ToU) DR framework to drive down the whole-life cost of a grid-tied combined heat and power (CHP) MG system.

In addition, some studies have explored the potential of V2G technologies and EV charging/discharging coordination through DSM mechanisms in driving economic sustainability improvement for renewable energy development projects. For instance, Cardoso et al. [222] have proposed a DLC decision model for the aggregated energy scheduling of EVs and demonstrated its distinctive contribution to reducing the lifetime cost of a multiple energy carrier MG, while considering the uncertainty associated with the EV driving schedules. In another instance, Hosseinnia et al. [223] have provided further evidence of the utility and economic benefits of EV fleet trip level energy management and V2G connectivity in the context of sustainable energy system design and planning. Moghaddas-Tafreshi et al. [224] have also underlined the potential of optimal charging/discharging scheduling of plug-in hybrid EVs in improving the profitability of an energy hub and reaping cost-savings for vehicle owners, while addressing the uncertainty associated with the power consumption of vehicles during trips.

### 3.1.3. Demand response-integrated life-cycle planning of micro-grids: knowledge gaps and proposition

As the above literature review indicates, there is a growing body of literature lending support to the integration of DSM frameworks into the design phase of RSESs. However, as far as can be ascertained, no single study has evaluated the attitude of neither end-users nor electricity providers in relation to adopting these practices during the optimal designing and planning processes of RSESs. Accordingly, oversimplified assumptions have commonly been made in the literature on the available (releasable or practical) capacity of responsive loads, which have substantially reduced the accuracy of the associated energy demand and investment planning projections. That is, many hypotheses regarding the degree of end-users' participation in the DR schemes are not well-grounded. To aid the associated asset-allocation decision-making procedure, a long-term, DR-integrated MG investment planning approach needs to model the involvement of aggregator-mediated customers in DR programmes in a systematic, market-driven approach. Market-based aggregator-mediated flexibility procurement approaches ensure that system-level dispatch of DR capacity is aware of the value of flexibility to all actors. To this end, the market-driven approach needs to capture the dynamic nature of strategic interactions between instrumentally rational, utility-maximising active economic agents in an aggregator-mediated DSM market. More specifically, the approach needs to identify the reaction and commitment of different classes of customers mediated by third-party DRAs, when exposed to variations in the economic incentives for load curtailment/shifting.

In addition, the interruptible load DRAs round up parcels of distributed sectoral interruptible loads to enable them to reach the sufficient scale required for selling flexibility services to the system operator(s) [17], [225]. In this context, more work is needed to evaluate the effect of different levels of discomfort experienced by different customer classes on the economic feasibility of renewable energy projects as the characterisation of aggregator-mediated customer comfort constraints during the planning phases of RSESs is less well explored. To assist decision-makers in designing cost-optimal sustainable energy systems consistent with the expectations of their customers, it is critically important to devise accurate

models aimed at reflecting user values and preferences (which furnish the basis for service flexibility) during the design phase of MG projects. This brings to light the need for an investment decision-making framework that accommodates end-consumers' perceptions and preferences with respect to incentivised load interruption (which could be derived from their energy service needs and the relative values they place on them) within the long-term MG capital-investment plans.

As the above discussion indicates, the literature on the DR-integrated long-term energy planning optimisation, as well as the day-ahead, aggregator-mediated DR scheduling, has convincingly shown the significance of characterising the strategic, interactive rationality of the players involved in harnessing the flexibility potential of smaller customers using Stackelberg, non-cooperative games in general. Yet, despite this achievement, there are still some previously unexplored considerations, which need to be factored into the analysis of aggregator-mediated DR scheduling – to give a more realistic grounding to the research in this area. More specifically, three important aspects necessary to better reflect reality, while characterising the utility-aggregator-customer interactions, have not yet been addressed in the mainstream Stackelberg, non-cooperative game-theoretic DSM literature, namely:

1. *Lack of an optimal trade-off analysis from the utility's perspective between importing power and exploiting DR resources:* Although the potential benefits of characterising the strategic interactions between the utility (MG operator), DRAs, and end-consumers have been demonstrated in several instances, no study, as far as can be ascertained, has developed a systematic framework to facilitate the decision-making process for utilities to determine the best compromise between importing electricity and procuring load reductions. This raises the question to what extent producing such an optimal trade-off solution is able to reduce the operational cost of the utility, with the answer to this question implying potential consequences for renewable energy system design optimisation.

2. *Poor understanding of the incentive-price elasticity of customer-supplied DR capacity across different sectors:* While nearly all the reviewed studies consider the discomfort cost imposed on end-consumers due to load reduction as a decision criterion, elasticity of supply of DR capacity is seldom accounted for in the DSM planning models. It is of paramount importance for the utility to understand how the willingness of customer-supplied DR capacity differs across different end-use categories – especially in the face of new sources of electricity demand, such as the electrification of the transport sector. The research question following from this gap is how an effective model can be designed to limit the use of DR resources from each sector to an economically viable level.

3. *Insufficiency of the number of considered end-consumers to be a suitable representative of real-world practice:* Whilst considerable effort has been devoted to developing a range of non-cooperative game-theoretic, aggregator-mediated DR interventions to reduce or shift energy use, the number of small-sized customer samples cannot be considered representative of a real distribution system. More specifically, the set of end-consumers in previous studies on the aggregator-mediated DSM has never, as far as can be ascertained, comprised of more than a few customers. Hence, a research question arises as to how community-scale energy systems can benefit from such schemes. This is especially relevant when conducting pre-feasibility analyses of RSESs, where forecasts of the total load demand on the system are available, but there is no mechanism to allocate the total load to a certain number of end-consumers.

### 3.1.4. Objective

The main objective of the chapter is to demonstrate the potential of aggregator-mediated, incentive-based, market-driven DSM programmes tailored to small- to medium-scale end-consumers in improving the economic viability of community-scale MG systems. Accordingly, the chapter expands the boundaries of knowledge and understanding of the positive impacts of altering the energy consumption behaviour of different types of electrical loads – through effective incentive-based

DR programmes – on the cost-optimal design of MGs. Also, a secondary objective of the chapter is to corroborate the technological competence and cost-competitiveness of hybrid energy storage systems, as well as hydrogen as an energy vector in larger-scale community MGs (in addition to the evidence presented in Chapter 2) for niche applications – inter-seasonal energy storage to meet seasonal demand, and hydrogen mobility to decarbonise the transport sector.

More specifically, the chapter contributes to the trend of the conservation of energy through procuring DSM provisions for the strategic decision-making related to the optimal mix of DERs to be integrated into RSESs – which is discussed in the literature review in Section 3.1.2. It also distinctly contributes to the to the trend of broadening the DRA-mediated DSM problem to include the interactions between all the involved active economic agents in the system-level DR dispatch game – the utility, DRAs, and end-consumers – evident in the literature review. Accordingly, a novel long-term, comfort-preserving MG equipment capacity-planning decision-making framework is put forward that offers a new solution to address the literature gaps highlighted in Section 3.1.3. Notably, the following key contributions are made:

1. The strategic interactions between the MG operator (utility), intermediary sectoral monopoly (specifically defined) DRAs, and end-consumers are characterised using an equitable day-ahead market model for incentive-based DR aggregation in community-scale renewable energy projects in a robust, competitive, equitable, transparent, liquid market-driven manner using tools borrowed from non-cooperative game theory [68] and the endogenous Stackelberg leader-follower relationships [69]. The proposed sectoral aggregator-mediated, EV-charging-load-addressable, market-driven interruptible DR scheduling framework – that gives a realistic grounding to research on distributed DSM planning – is designed on the basis of interruptible DR programmes and accounts for the elasticity of customer-supplied DR capacity (load type-dependent DR procurement factor). The most salient distinction of the proposed platform-mediated dynamic DSM market model is the continual process of trading, with incentive prices unique to each transaction.

2. The proposed DSM market design is systematically integrated into a standard model of robust, long-term, meta-heuristic-based, high-dimensional equipment capacity planning optimisation of grid-connected MGs tailored towards community-scale, sector-coupled, multi-energy-storage-technology, 100%-renewable and -reliable projects to elucidate the contributions of more accurate DR resource projections in improving the economic viability of MG development projects.

3. A novel hydrogen-based MG system is conceptualised, which is the first to capture the potential of the FCEV2G technology in improving the dispatchability of 100%-renewable MG systems and, in turn, ensuring the economic sustainability of strategic MG investment planning decisions.

4. The application of the energy filter-based approach to scheduling energy storage infrastructure is expanded to multiple energy storage technologies, namely: hydrogen storage, vanadium redox flow batteries, and SCs. This provides a platform to more efficiently address the intermittency of renewables by economically dispatching different backup systems running at various temporal resolutions, namely: seasonal, inter- and intra-day, and transient.

Moreover, improving and expanding the existing Stackelberg, non-cooperative game-theoretic, aggregator-mediated DR scheduling models, so that they can be more readily applied to the real energy management problems posed by utility companies, DRAs, and end-consumers alike, is associated with several novel contributions. Specifically, the novel two-stage, day-ahead, market-driven, incentive-based, aggregator-mediated, Stackelberg, strategic game-theoretic DSM model, features the following key contributions, each addressing one of the three knowledge gaps identified in the previous section, namely:

1. The robust, bi-level Stackelberg, non-cooperative game-theoretic DSM planning decision support model, detailed above, is able to effectively assist the associated DR scheduling decision-making process for grid-tied RSESs in day-ahead, incentive-based DR programmes – by providing flexibility

services to the MG. Notably, by producing the optimal trade-offs between importing power and employing DR flexibility resources for the hours of the next day for which a net energy deficit is predicted, the model is able to derive important implications for the cost-optimal planning of RSESs.

2. The load type-specific price elasticity of DR supply is effectively captured in the model, enabling it to more accurately forecast the participation rate of different customer classes, namely: residential, commercial, industrial, agricultural, and FCEV-refuelling loads. To this end, in addition to demonstrating the existence and uniqueness of a closed-form solution to the derived game-theoretic DSM problem, an iterative distributed algorithm is developed to approximate the pure-strategy Nash equilibrium point with minimum information exchange, with the aim of preserving the private preferences of players. The iterative, privacy-preserving distributed algorithm is, additionally, able to handle non-linearities in actors' payoff functions and deal with the imperfect information about the exact form of payoff functions the players are seeking to optimise, while determining the unique, pure-strategy Nash equilibrium of the system-level DR dispatch game.

3. The model incorporates a specifically designed stochastic load disaggregation technique, which randomly breaks down the forecasted total sectoral electricity consumption into any specified number of end-users. This feature makes the model applicable to a wider range of settings, including greenfield pre-feasibility studies where no smart meter data are available. Accordingly, the application of the model to a large number of end-consumers spread across a distribution network is able to improve the understanding of diverse sector-wide customer behaviours based on a broader set of end-consumers' strategies, as well as the corresponding sectoral aggregator payoff profiles.

A schematic outline of the chapter, which illustrates the steps followed in this study and their interconnectedness, is laid out in Fig. 3.2.

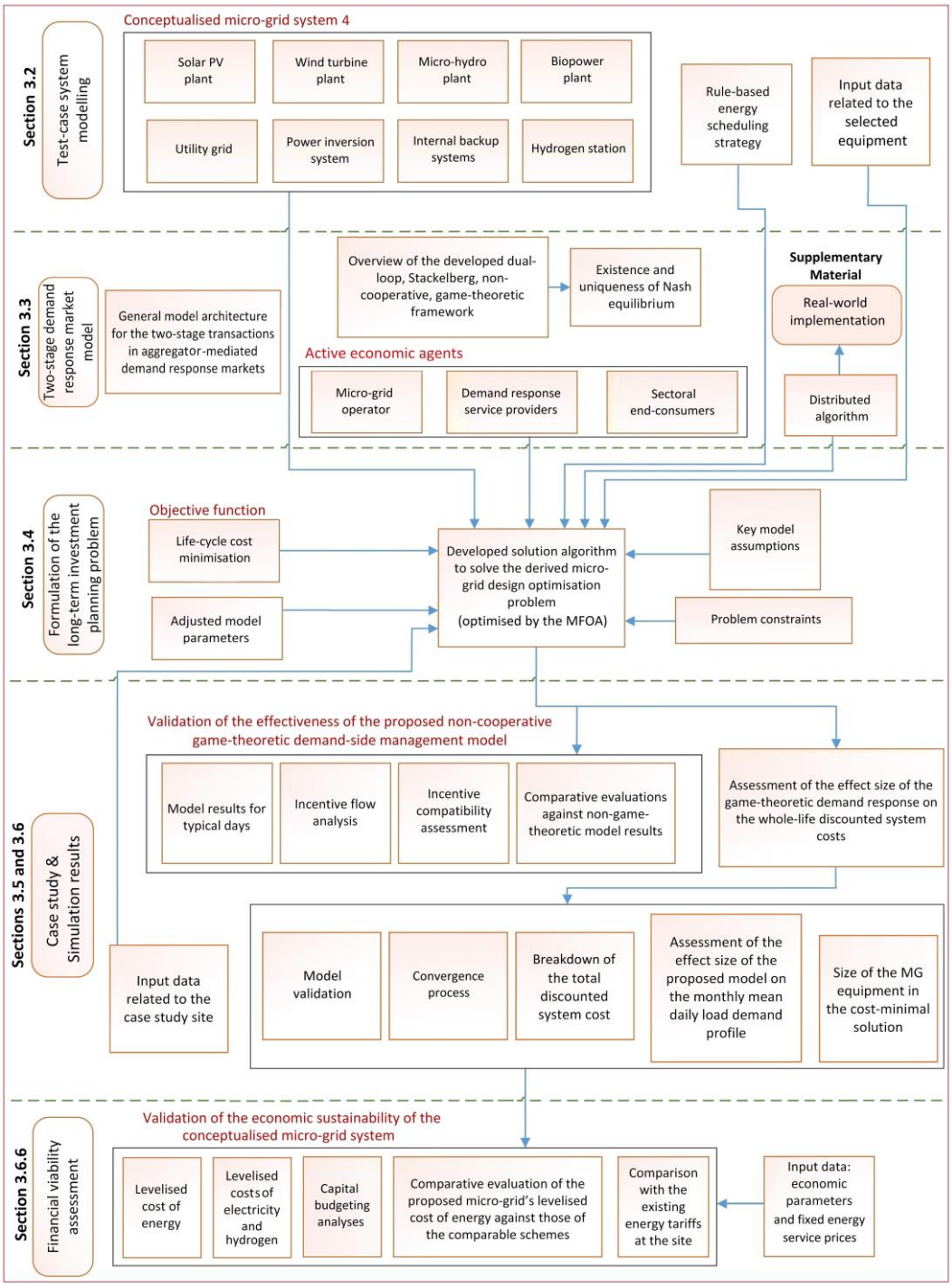


Figure 3.2: Overview of the chapter-wise modelling procedure for the game-theoretic, aggregator-mediated, market-driven integration of flexible demand resources into the long-term planning of MGs.

## 3.2. Test-case micro-grid system

This section conceptualises a grid-connected, DC-coupled, multiple energy carrier MG test-case system, the configuration and power flow of which is shown in Fig. 3.3. The system is used as a test case to evaluate the effectiveness of the proposed Stackelberg, non-cooperative game-theoretic, aggregator-mediated, incentive-driven, DSM market framework tailored towards distributed sectoral demand-side flexibility resources. It, additionally, measures the efficacy of integrating the above-mentioned double-sided, platform-mediated interruptible DR market into the standard model of robust, long-term, meta-heuristic-based, high-dimensional equipment capacity planning optimisation of grid-connected MGs tailored to community-scale, sector-coupled, multi-energy-storage-technology, 100%-renewable and -reliable projects introduced in Chapter 2. Technologically, the MG system (hereinafter denoted as MG 4) is envisioned to supply green power and transportation fuel to large-scale semi-urban communities (more than 1,000 people) residing in the vicinity of, or within relatively short distances from, the main power grid whose electrical consumptions are subject to high degrees of seasonality – due to the seasonality, for example, in tourist flows. Also, it serves five different categories of energy demand: (1) residential, (2) agricultural, (3) commercial, and (4) industrial load power demands, as well as (5) the demand for hydrogen (served through dedicated hydrogen refuelling infrastructure) from FCEVs. As stated above, the test-case MG system is used to verify the effectiveness of the proposed DR-integrated energy planning optimisation model.

Notably, MG 4 features the following salient properties: (i) leverages a diversified portfolio of variable renewable energy with complementary characteristics together with a sustainable share of agricultural and woody biomass resources, (ii) employs an advanced three-timescale hybrid energy storage system, and (iii) harnesses the potential of V2G technologies and FCEV charging/discharging coordination through DSM mechanisms – thereby, directly contributing to the achievement of secondary research objectives 1 to 3.

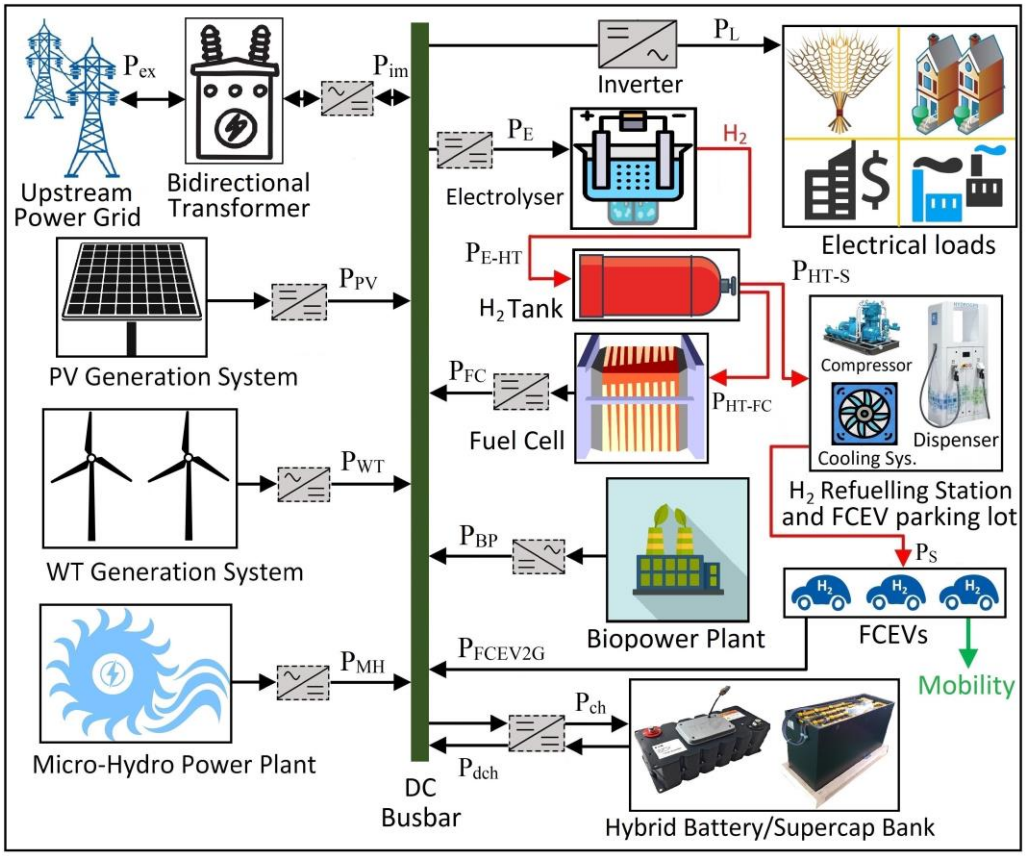


Figure 3.3: Schematic architecture and streams of energy of the DC-linked, grid-connected community MG system, feeding residential, commercial, industrial, agricultural, and FCEV-refuelling loads.

The proposed system is mainly driven by onsite renewable resources (namely, solar PV, WT, MH, and biomass power), and is equipped with three complementary energy storage media (namely, SCs, battery packs, and a hydrogen-based energy storage system). It also looks upon the main grid as the auxiliary storage system with the option for energy exports. The mathematical modelling of the utility grid, transformer, solar PV panels, MH turbines, SC modules, electrolyser and fuel cell stacks, hydrogen tank, and the hydrogen refuelling unit are the same as those presented for MGs 1–3 in Chapter 2. Also, similar to MGs 1 and 2, the WT generation plant is modelled by the selected WT's manufacturer-provided characteristic power-wind speed curve. The turbine ECO 48/750, which has a rated power of 750 kW, is considered for wind power generation in this study. The wind plant's output power at each time-step, $P_{WT}(t)$ [kW], can be obtained by multiplying the optimal quantity of the WTs, $N_{WT}$, by each turbine's output power

estimated from the power curve. Also, since the power curve of the WT is characterised for its hub height wind speed, Equation 2.1 is used to normalise the wind speed data measured at other heights to the turbine's hub height with the wind shear exponent fixed at 0.25. It is also noteworthy that, similar to MGs 1–3, the leading brands of equipment in the Australian and New Zealand renewable energy asset markets were chosen based on the author's judgement of both viability and prevalence. Furthermore, the costs and efficiencies of the power conversion apparatuses shown in the dashed boxes in Fig. 3.3, as well as the costs and efficiencies of the unshown intermediate-pressure hydrogen compressors (which compresses the electrolytic hydrogen), are included in the associated main components. The following sections mathematically formulate the rest of the components in the candidate pool, namely the biopower plant, loads' hybrid inverters, battery bank, and the FCEV2G unit, before presenting a rule-based expert system specifically devised for the operational scheduling of the system – that models the energy management relationships between the candidate components.

### 3.2.1. Biomass plant

The integrated biomass gasifier-generator system PP30 Cogen-CS manufactured by All Power Labs [226] is utilised in this study. The plant, the flow diagram of which is shown in Fig. 3.4, is a commercially available, off-the-shelf component with an electrical rated power of 25 kW. The system uses the pyrolysis process to produce syngas, which is then combusted for power generation. Since long-term biomass feedstock availability in an area could be projected with a high degree of certainty, the biopower plant contributes, to a certain extent, to the dispatchability of the conceptualised MG system. Indeed, the plant is sought to replace the commonly-used small-scale diesel generators in conventional hybrid renewable energy systems. Importantly, on a life-cycle basis, a biopower plant emits ~70% less emissions than diesel generators [227]. The power output from the biomass plant at each time-step [kW] can be calculated from Equation 3.1 [89].[3]

[3] Note that, given the associated equations for estimating the power outputs from micro-hydro and biopower plants, the rated powers of micro-hydro turbines and biopower units of the associated plants are incorporated into the model and the decision-making process in an indirect manner using the power rating-dependent parameters – the gross head in the case of micro-hydro turbines, and the

$$P_{BP}(t) = M_{BP}(t) \times CV \times \eta_{BP} \times \eta_{BP,AC/DC}, \tag{3.1}$$

where $M_{BP}(t)$ denotes the feedstock mass consumption rate at time-step $t$ [kg/h], $CV$ stands for the gross calorific value of the biomass feedstock (5.07 kWh/kg), $\eta_{BP}$ is the overall bio-electricity generation efficiency of the system (23%), and $\eta_{BP,AC/DC}$ is the efficiency of the plant's AC/DC converter (95%).

Furthermore, the system is characterised by the following emission factors [228]: 1.53 kg-$CO_2$, 11.3 g-CO, 8.7 g-$CH_4$, 2.4 g-NOx, and 0.01 g-soot per kg of feedstock consumed. Accordingly, the social cost of the above-mentioned emissions needs to be factored into the decision-making process – for an eco-design of the MG system. However, given the substantially higher rate of $CO_2$ emissions as compared to other emission factors, coupled with the lack of a reliable estimate of the social cost of other emission factors, only the social cost of $CO_2$ is used to define a penalty term, whereby the size of the biopower plant is delimited to a sustainable level. The following equation can be used to calculate the life-cycle penalty imposed on the MG for $CO_2$ emissions:

$$cost_{em} = \frac{\xi_{CO_2}}{1000} \times E_{CO_2} \times \sum_{t=1}^{T} M_{BP}(t), \tag{3.2}$$

where $E_{CO_2}$ represents the $CO_2$ emission factor of the plant (1.53 kg-$CO_2$/kg-feedstock), and $\xi_{CO_2}$ [\$/t$CO_2$] denotes the social cost of $CO_2$ emissions used as a reference to account for life-cycle GHG impacts of the biopower plant in the model. A central value of \$42/t$CO_2$ is applied for the first 10-year planning horizon (covering the years 2020 to 2030), which rises to \$50/t$CO_2$ for the second half of the projected lifespan of the project in accordance with the Obama administration's central estimates [229].

maximum allowed biomass input in the case of biopower units. That is, the actual nameplate capacities of the constituent units of the plants are proxied by the above-mentioned parameters for the total power output estimation of the plants.

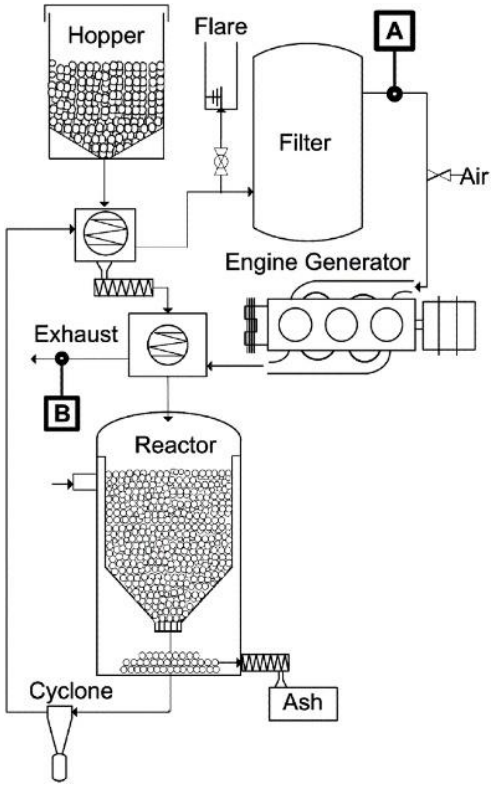


Figure 3.4: Schematic diagram of the considered integrated biomass gasifier-generator system. Source: [228].

### 3.2.2. Power conversion apparatuses

As shown in Fig. 3.3, the MG system is equipped with several converters to serve the purpose of coupling the equipment to a common DC busbar. Similar to MGs 1–3, all the converters except the one connecting the electrical loads to the MG's common busbar, are modelled through integrating their costs and efficiencies into the corresponding components' costs and efficiencies. However, for electrical loads, Leonics' GTP-519-S 900-kW, GTP-506 115-kW, and GTP-501 33-kW multi-mode inverters are separately modelled in this study [230]. The consideration of three inverter types with three widely varying rated capacities allows for leveraging economies of scale (as measured by rated capacity), whilst effectively fine-tuning the overall hybrid inverter capacity such that the overall unused capacity is minimised.

To calculate the size of the electrical loads' inverters, first, the following equation is used to determine the nominal power of the overall power inversion system:

$$N_I = \frac{P_{L,max}}{\eta_I}, \tag{3.3}$$

where $P_{L,max}$ represents the demanded annual peak electrical loads and $\eta_I$ identifies the power inversion equipment's efficiency (95%).

Then, $N_I$ is rounded up to the next integer and the number of each inverter model is identified by the following equations, which give priority to higher-rated inverters as they carry a lower per-unit cost:

$$N_{900} = \left\lfloor \frac{N_I}{C_{900}} \right\rfloor, \tag{3.4}$$

$$N_{115} = \left\lfloor \frac{N_I - (N_{900} C_{900})}{C_{115}} \right\rfloor, \tag{3.5}$$

$$N_{33} = \left\lceil \frac{N_I - (N_{900} C_{900}) - (N_{115} C_{115})}{C_{33}} \right\rceil, \tag{3.6}$$

where $N_{900}$, $N_{115}$, and $N_{33}$ respectively denote the quantity of the 900-kW, 115-kW, and 33-kW inverters, while $C_{900}$, $C_{115}$, and $C_{33}$ indicate their respective rated capacities, with $\lfloor \cdot \rfloor$ and $\lceil \cdot \rceil$ respectively denoting floor and ceiling functions.

In this way, planning decisions made on the capacity of the hybrid power conversion system are independent of the other MG equipment, the optimum size of which is under investigation.

### 3.2.3. Internal backup energy storage

The proposed system leverages the temporal characteristics of various DERs providing backup power, or energy storage. Notably, it uses SCs, batteries, and a hydrogen-based energy storage system respectively as ultra-short-term, short- to mid-term, and long-term storage technologies, which respectively serve the purpose of addressing transient, intra- and inter-day, and seasonal variations in net load

power demand [231]. Such a hybridisation of different technologies leads to a worthwhile trade-off between the specific power and specific capacity (energy) of the overall storage system, which consequently reduces the costs associated with the so-called '*load levelling*' operations. Notably, the battery bank in the proposed hybrid energy storage system bridges the gap between the high specific power of SCs and the high specific energy of the hydrogen-based storage system – owing to the intermediary levels of both its specific power and energy.

The allocation of non-dispatchable renewable excess/shortage power to the storage technologies is conducted using an advanced variant of the energy filter-based decomposition technique presented in Section 2.3.1.3, which uses two consecutive low-pass filters. To this end, the first filter breaks down the internal power mismatch signal into low- and high-frequency components. The low-frequency signal is directed to the hydrogen system (including the electrolyser, hydrogen tank, and the fuel cell), while the high-frequency signal is transferred to the hybrid battery-SC system. Subsequently, another low-pass filter with a greater cut-off frequency identifies the contribution of the battery and SC banks in serving loads. These cut-off frequencies are optimised by making effective use of a logarithmic transformation commensurate with the related timescales mentioned above, whilst leveraging the "roll-off" concept [232]. Accordingly, the optimal cut-off frequencies of the first and second filters were respectively determined to be $3.1970\times10^{-5}$ Hz and $8.3331\times10^{-4}$ Hz. Expectedly, the second filter's cut-off frequency is greater than that of the first one, as it is geared towards decomposing renewable excess/shortage signals on a finer timescale. Other relevant parameter settings, namely the DC gain and damping factors of the filters, remain the same as those selected for MGs 1 and 2.

#### 3.2.3.1. Battery bank

CellCube's vanadium redox flow-based battery bank [233], which is a "real" green battery type is used in the conceptualised MG, the main advantages of which over commonly-used lead-acid and Li-ion batteries include: (1) negligible self-discharge rate (< 1% per year), (2) longer lifetime (20 years), (3) 100% depth of discharge capable, (4) practically unlimited cycling with approximately no degradation over

time, and (5) much less potential for toxicity at its end-of-life phase. Likewise to the inverter system, three different battery product models are selected and the same procedure is followed to apportion the total optimal size of the battery bank to different model types, following the same logic. Yet, note that unlike the overall capacity of the electrical loads' inverter, which is considered as an exogenous variable in the model (that does not form part of the optimal equipment capacity-planning process), the overall capacity of the battery bank is one of the problem's equipment-related decision variables.

The battery product models are: FB 10-100 (100 kWh), FB 200-400 (400 kWh), and FB 400-1600 (1600 kWh). The battery bank's energy content at each hour can be obtained as follows:

$$E_B(t) = E_B(t-1) + \left( P_{ch,LF2} - \left( \frac{P_{dch,LF2}}{\eta_B} \right) \right) \times \Delta t, \tag{3.7}$$

where $\eta_B$ is the battery bank's round-trip efficiency (80%), while $P_{ch,LF2}$ and $P_{dch,LF2}$ denote the low-frequency components of the outputs of the second-stage-filtered charging and discharging signals, respectively.

The energy content of the battery bank is constrained using Equation 2.27, while Equations 2.29 and 2.30 ensure that the charging and discharging rates of the battery bank are in the corresponding allowable ranges. The charge and discharge power capacities are also fixed at 0.5 kW per kWh of storage capacity (cycled at a C/2 rate), meaning that the battery bank can be fully charged or discharged in two hours.

Furthermore, the three-point rainflow cycle algorithm, presented in Section 2.3.5, is employed to count the number of cycles of the battery packs and SC modules.

### 3.2.4. Fuel cell electric vehicle refuelling station

In addition to the hydrogen refuelling unit, presented in Section 2.3.1.4, the station in this MG system, is equipped with a FCEV2G system, which is mathematically modelled in the next section.

#### 3.2.4.1. Fuel cell electric vehicles in vehicle-to-grid operation

While the FCEVs are parked in the station, they could be left plugged in through dedicated equipment and make effective use of their flexibility potential to help provide peak power supplies economically – as long as it does not interfere with their owners' requested level-of-hydrogen at the pre-defined departure times. To provide a platform for harnessing the V2G capabilities of the FCEVs, the FCEV2G setup designed in [234] is used in this study. The setup enables the conversion of the DC power of the vehicle's fuel cell engine into AC that can be directed to the input port of the electrical loads' inverter after frequency synchronisation, with an overall efficiency of $\eta_{FCEV2G}$ (44%). Accordingly, modulation of the power output from each FCEV, the owner of which aspires to participate in the V2G operations, can be made from 0 to 8.5 kW DC – in compliance with the nominal capacity of Rasa's built-in fuel cell. This means that the costs arising from payments made to FCEV owners to provide V2G power at each time-step – under a feed-in-tariff style programme – can be calculated by the following equation:

$$cost_{FCEV2G}(t) = \pi_{FCEV2G} \times \eta_{FCEV2G} \times P_{FCEV2G}(t) \times \Delta t, \tag{3.8}$$

where $\pi_{FCEV2G}$ represents the per-unit premium tariff rate for V2G power [$/kWh] and $P_{FCEV2G}(t)$ denotes the amount of V2G power used for operational scheduling at time-step $t$.

In this context, the FCEV refuelling station's optimal capacity for V2G operations, $N_{FCEV2G}$ [kW], needs to be determined, as a simultaneous decision variable alongside its optimal refuelling capacity, $N_S$ [kg-$H_2$/h].

For the sake of simplification, it was assumed that at each time-step of the MG operation, the maximum amount of available V2G power that can be provided

by the station at each time-step, $P_{FCEV2G}^{max}(t)$, equals 25% of the load reduction potential of the station at that time-step.

#### 3.2.4.2. Selected fuel cell electric vehicles

The light-duty FCEVs are selected to be of the model Riversimple Rasa. Rasa is a two-seater vehicle, which is propelled by an 8.5-kW fuel cell running on 1.5 kg of hydrogen compressed to 350 bar – and not the 700-bar industry majors use nowadays – with a driving range of up to 300 miles and a top speed of 96 km/h [235], [236]. Not only has running on 350-bar hydrogen led to reduced energy use, but it also has permitted much cheaper refuelling stations to be realised. The FCEVs are meant to be used for home-to-work commuting and other small inner-city trips.

### 3.2.5. Operational strategy

Similar to MGs 1–3, a rule-based, hourly-basis, cycle-charging operational strategy is adopted in this study for the dispatch of energy within the MG system, which is illustrated by the flowchart in Fig. 3.5. The following specific rules are defined in the devised energy scheduling plan:

1. Energy storage devices and FCEVs are charged/refilled using only the surplus non-dispatchable renewable power.

2. Mismatches in non-dispatchable renewable power and electrical loads are partitioned into the ultra-high, high, and low-frequency components and then stored/supplied within/using the SC bank, battery bank, and the hydrogen tank/fuel cell, respectively.

3. The dispatchable biopower plant can only be operated during the time-slots stamped as peak hours to partially or wholly offset the lack of sufficient fuel cell power.[4]

[4] This assumption can be explained by the relatively long cold start-up time of the biopower plant (i.e., ~10–15 minutes) and the inefficiency of leaving the biopower plant on standby at all times.

4. The upstream grid serves as the ultimate guarantor of the perfect satisfaction of the electric load demand.

5. All the components are bounded to adhere to their corresponding operating power/energy storage capacity limits.

6. The FCEV2G capability is considered as a resource to compensate for at least part of the electricity left unserved by the fuel cell and the biopower plant, or the shortage of battery and SC capacity to meet the load power demand. To this end, morning and evening peak demands were assumed to occur between the hours of 6 a.m. to 10 a.m. and 5 p.m. to 10 p.m., respectively – in compliance with historical records of electricity consumption in New Zealand.

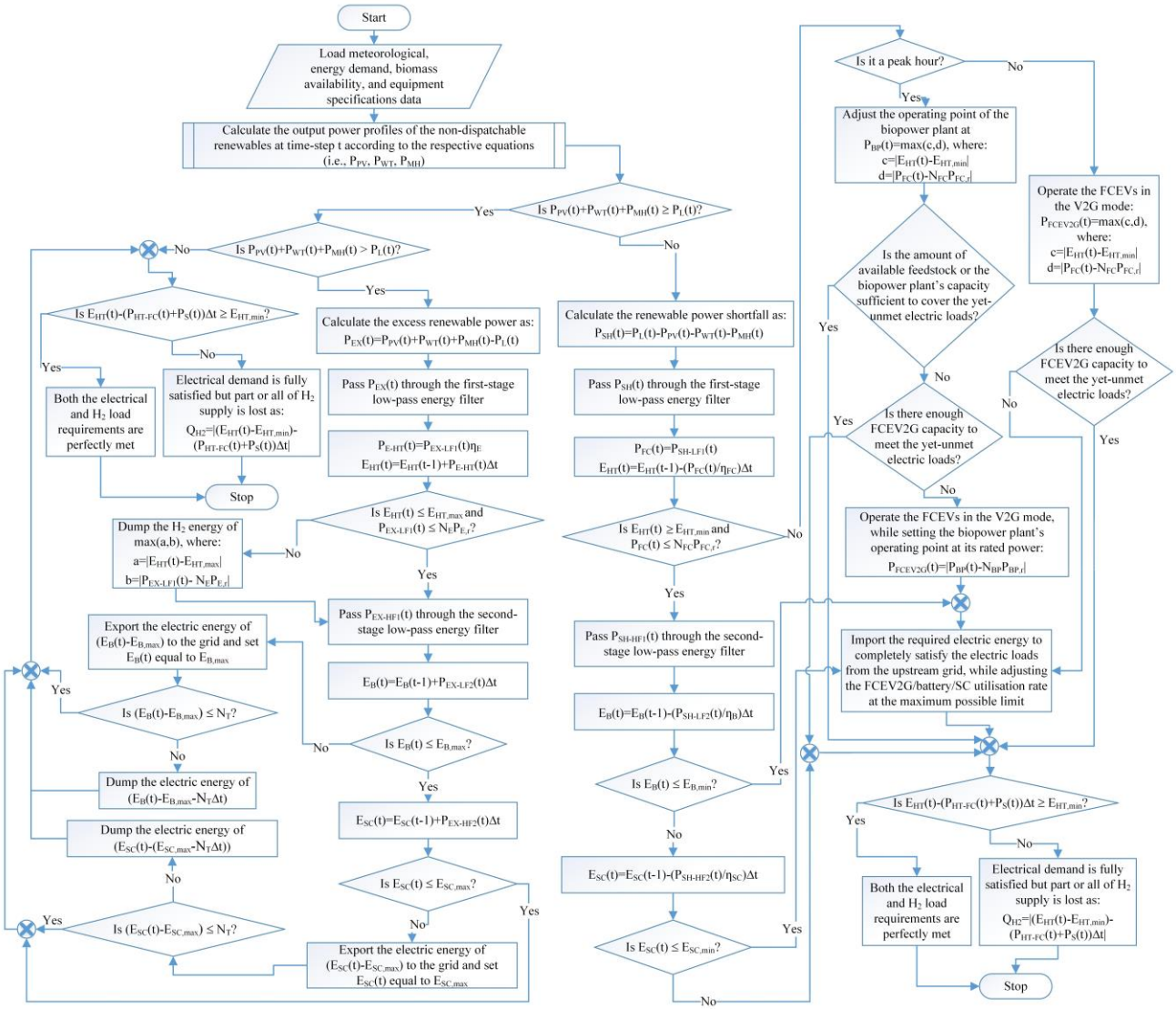


Figure 3.5: Flowchart of the MG's energy management scheme, consisting of a set of pre-defined control logics.

It is also noteworthy that, similar to MGs 1–3, the design of MG 4 is limited by a set of key assumptions made underlying the conceptualisation of MG models and carrying out the associated life-cycle analyses, listed in Section 2.3.4. Moreover, except for the optimal capacity of the hydrogen refuelling station, which needs to be rounded up to the second decimal place, continuous decision variables, which represent the optimal size of the generic components – the hydrogen tank [kg], the FCEV2G setup as part of the station [kW], and the transformer [kVA] – as well as the optimal capacity of the overall battery bank [kWh] and inverter [kW] (which consist of three different product models), are to be rounded up to the nearest integer. This is because the capacity of the hydrogen refilling station is measured in a comparatively large unit, namely: kg-$H_2$/h.

### 3.2.6. Data: Selected product models

The same equipment product models of PV panels, MH turbines, transformer, SC modules, electrolyser and fuel cell stacks, hydrogen tank, and hydrogen refuelling unit, as those listed in Table 2.2 for MG systems 1–3, are used for MG system 4. The techno-economic specifications of the other MG components, namely the capital, replacement, and O&M costs, as well as the life-cycle expectancy and efficiency of the WTs, biopower plant, power loads' inverters, battery packs, and the FCEV2G unit of the hydrogen station are summarised in Table 3.1.

The rationale underlying the choice of a different WT product model with a larger nameplate capacity was leveraging the associated lower per-unit costs, given the considerably greater size of MG 4 than MGs 1–3. As stated above, MG 4 is exclusively envisioned to supply reliable, clean, affordable, self-sufficient electricity (including the electrified heating and transportation sectors' energy demands) to agricultural towns (with a permanent population of more than 1,000 people) with highly seasonal demands, whereas MGs 1–3 are specifically conceptualised for smaller island, rural, and village communities (with a population of several hundred people), respectively. Also, recall that the rationale behind using inverters/battery modules of different nameplate capacities in the larger-scale MG 4 is to minimise the overhead and unused capacity, whilst additionally capturing the cost-effectiveness of higher-capacity inverters/battery modules. In the course of

allocating the calculated overall capacity of the loads' inverter and the optimised total capacity of the battery bank to different product model options, the optimal quantity of the product model with the smallest capacity is to be rounded up to the nearest integer, whereas the optimal quantities of the other product models are to be rounded down to the corresponding nearest integers using the ceiling and floor functions, respectively (refer to Equations 3.4–3.6). Furthermore, recall that, throughout this thesis, all monetary values are expressed in 2019 NZ$. Moreover, where appropriate, foreign currencies were converted to NZ$ at the yearly average currency exchange rates in 2019.

Table 3.1: Data values and sources for techno-economic specifications of the components of test-case MG system 4.

| Component | Manufacturer part number | Nameplate rating | Capital cost* | | Replacement cost† | Operation and maintenance cost† | Expected service life | Nominal efficiency | | Source |
|---|---|---|---|---|---|---|---|---|---|---|
| | | | Per unit | Per kW or kWh | | | | Notation | Value [%] | |
| Wind turbine | ECO 48/750 | 750 kW | $1.096m/unit | $1.46k/kW | $822k/unit | $21k/unit/year | 20 years | N/A‡ | N/A‡ | [237] |
| Biopower unit§ | PP30 Cogen-CS | 25 kW | $32k/unit | $1.28k/kW | $23k/unit | $0.01/unit/hour | 10k hours | $\eta_{BP}$ | 23 | [226] |
| Inverter | GTP-501 | 33 kW | $12k/unit | $364/kW | $12k/unit | $85/unit/year | 15 years | $\eta_I$ | 95 | [230] |
| | GTP-506 | 115 kW | $38k/unit | $330/kW | $38k/unit | $250/unit/year | | | | |
| | GTP-519-S | 900 kW | $270k/unit | $300/kW | $270k/unit | $1.9k/unit/year | | | | |
| Battery pack | FB 10-100 | 100 kWh | $110k/unit | $1.1k/kWh | $110k/unit | $220/unit/year | 20 years with unlimited cycles | $\eta_B$ | 80¶ | [152], [233] |
| | FB 200-400 | 400 kWh | $400k/unit | $1k/kWh | $400k/unit | $840/unit/year | | | | |
| | FB 400-1600 | 1600 kWh | $1.442m/unit | $901/kWh | $1.442m/unit | $4k/unit/year | | | | |
| Hydrogen station – FCEV2G unit | Generic, TU Delft# | – | – | $155/kW | $95/kW | $3.2/kW/year | 20 years | $\eta_{FCEV2G}$ | 44** | [238]–[241] |

* All the reported capital costs represent the actual cost of buying the selected components in the Australian and New Zealand renewable energy asset markets as of October 2019.

† All the replacement and O&M costs were calibrated in accordance with the component-specific ratios of capital to replacement and O&M costs reported in [150], [152]–[156].

‡ Not applicable.

§ To effectively value the positive impact of the biopower plant on the internal dispatchability of the MG, the total discounted cost of pellet feedstock was considered to be an exogenous variable, which is determined outside the model based on the imposed emission credits (see Equation 3.2) with respect to the total discounted energy output of the plant (see Equation 3.1).

¶ Round-trip efficiency.

# In view of the assumption that the DC power provided by the FCEVs is fed into the electrical loads' inverter, the costs associated with the FCEV2G technology only include the costs of V2G electric vehicle supply equipment, as well as the costs of modifying the vehicles with a V2G DC outlet plug.

** The V2G infrastructure's efficiency in this study represents a tank-to-DC-bus efficiency (units converted based on the higher heating value of hydrogen).

## 3.3. Game-theoretic, market-driven, incentive-based demand response programme

The optimal scheduling of flexible demand-side resources can be classified as a multi-decision-maker problem, which is not amenable to business-as-usual (BAU), centralised, non-behaviour-aware treatments if the epistemic risk factors affecting the supply of DR services are to be characterised – to improve the reliability and validity of DSM business models.

### 3.3.1. Aggregator-mediated demand response procurement as a Stackelberg, non-cooperative game

The Stackelberg, strategic (non-cooperative) game concept [242] can provide a systematic framework to unveil the hidden relationships between the targeted incentive-driven load reductions and what would be achieved in practice provided that there are no penalties for non-compliance with the grid operator orders – in an attempt to make explicit the assumptions underlying the core concepts of the discipline. Non-cooperative game theory centres on the study of independent, rational decision-making in circumstances of strategic interaction (conflict) to achieve the Nash equilibrium [243]. That is, it furnishes the opportunity to analyse the DR arrangements based on ordinal information, rather than conventional cardinal information. Compared to the cardinal analysis, the ordinal analysis of a decision-making process is less subject to 'knowledge' uncertainty so long as the sequential order of the process remains unchanged [244]. The key components of an aggregator-mediated, incentive-based DSM programme include: (1) energy service providers (utilities), DRAs, and customers, (2) incentive plans, and (3) customer performance (participation rates). These components respectively correspond to the core elements of a non-cooperative game: (1) players, (2) strategies, and (3) expected payoffs from potential consequences, where the set of consequences reflects the outcome of every possible combination of available strategies of players. Such resemblances of the DSM planning and the associated strategic game are illustrated in Fig. 3.6.

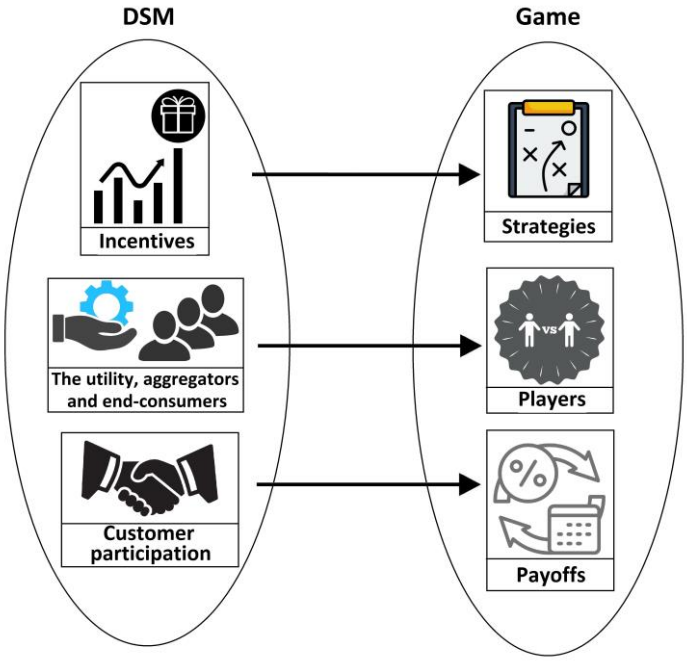


Figure 3.6: One-to-one correspondence of an incentive-driven DR programme's elements to the fundamentals of non-cooperative game theory.

As discussed in Section 3.1.1, the Stackelberg competition [245] is a leadership model in finance, in which the leader entity moves first and then the follower entities move in sequence. From a game theory perspective, the players of such a game compete on quantity, and therefore it falls under the category of non-cooperative games. The core assumptions behind the Stackelberg competition models are as follows [246]: (1) the leader is aware *ex-ante* that the followers notice its moves, and (2) the followers have perfect information about, and react rationally to, changes in strategies taken by the leader. Along the same line as the Stackelberg competition model, the incentive-based approaches of implementing DR programmes start by offering financial incentives to end-users in return for load reductions, where the incentive prices and customer participation rates are determined by the market mechanism of seeking to maximise profit (or utility). It is also noteworthy that it is proven that a Stackelberg, strategic game can be solved to obtain the Nash equilibrium, given every follower plays its best-response strategy to the leader's best action [247]. As the foregoing discussion indicates, the market-oriented, incentive-driven DR plans can be analysed through the framework of a Stackelberg, non-cooperative game via strategic market interactions.

### 3.3.2. Proposed Stackelberg, non-cooperative game framework to model interruptible demand response

The interruptible load programme is employed in this study as the DR service provision framework due to its unique advantage in providing a cost-effective means of improving the system's robustness against the variability inherent in weather patterns. In this light, the proposed game-theoretic DR scheduling structure serves as a forum to implement the day-ahead interruptible load programme. Building on the interruptible load programmes, the model is designed specifically to improve the accuracy of projections of the small- to medium-scale DR resource availability across different end-use sectors – residential, commercial, industrial, agricultural, and electrified transportation. More specifically, the required quantity of interruptible loads at each time-step of the system operation is procured by the system operator in a day-ahead reserves market using a specifically developed procurement system that co-optimises the imported power from the national grid and the utilised capacity of DR resources. The proposed market design provides a forum for these active economic agents to negotiate on how to mutually optimise their objective functions in non-cooperative (strategic) game settings under the Stackelberg competition. It also identifies the minimum operational MG costs based on hourly-priced DR products and the corresponding hourly wholesale power price. In this way, the model enables all the active entities within the MG to be involved in co-designing a business model for more independent, yet integrated, energy procurement decisions.

To this end, after introducing different players involved in the system-level DR dispatch game, this section mathematically models the proposed Stackelberg, strategic game framework to leverage the potential of flexible DR resources for the day-ahead operational scheduling of MGs, which promotes fair competition among different parties involved in the provision of DSM services. It then verifies the existence and uniqueness of an analytical solution to the developed game. Also, to preserve the privacy of players, an iterative distributed algorithm is presented to obtain the Nash equilibrium of the game before describing the sequence of operations carried out to implement the proposed game-theoretic distributed algorithm framework. The sequence of operations details the process of information

exchange between different entities involved in the game. Moreover, the proposed game-theoretic formulation of the incentive-based DSM plans in this study is specifically adapted for application to the day-ahead DR resource forecasting as part of the operational scheduling problem of MGs. As noted above, the proposed framework also leverages the potential advantages of integrating flexible load aggregators into the DR market – with the twin goals of achieving scale as well as improving market competitiveness and liquidity.

#### 3.3.2.1. Players of the game

As shown in Fig. 3.7, the game is played with three distinct sets of players, namely: the MG operator, responsive load aggregators, and different classes of end-consumers – residential, commercial, industrial, agricultural, and electrified transport. That is, it characterises the interactions between a MG operator, DRAs, and end-consumers. To this end, the model consistently treats these three sets of actors as rational, utility-maximising (self-interested), active economic agents. The MG operator is assumed to be an entity belonging to the utility providing electricity service to the considered case study area, which has full ownership of the MG assets and seeks to alleviate the load on the MG in predicted periods of peak energy use. As a principal element of the model, the day-ahead, hourly-basis forecasts of wholesale prices, load demand, and non-dispatchable renewable power generation capacity are assumed to be available based on the prior MG system state estimation studies. Responsive load aggregators act as intermediary agents between the utility and customers, as described in Section 3.1. Energy customers, which are placed at the lowest level of the proposed hierarchical architecture, modify their habitual energy consumption patterns to take the best advantage of the financial incentives offered by the aggregator they have subscribed to. An overview of the proposed game-theoretic framework to schedule the incentive-driven DR resources through market interactions is shown in Fig. 3.7. Note that all the players were assumed to be rational, risk-neutral, utility-maximising, and myopic.[5]

[5] Myopic behaviour means that players do not examine how their bids might influence the bids of other players in future iterations [192].

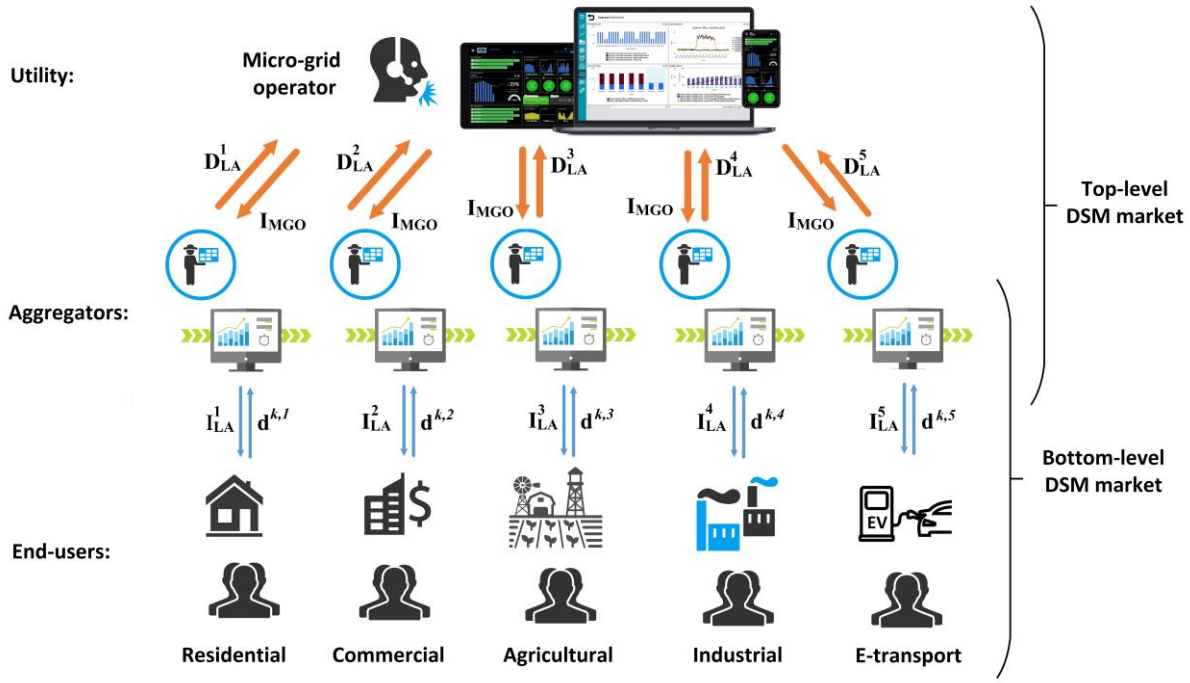


Figure 3.7: Overview of the developed Stackelberg, strategic game framework to model the market-driven, incentive-based, aggregator-mediated DR.

Also, Fig. 3.8 displays a schematic of the overall structure of the model with the sequence of incentive price/DR supply communications between the market participants overlaid.

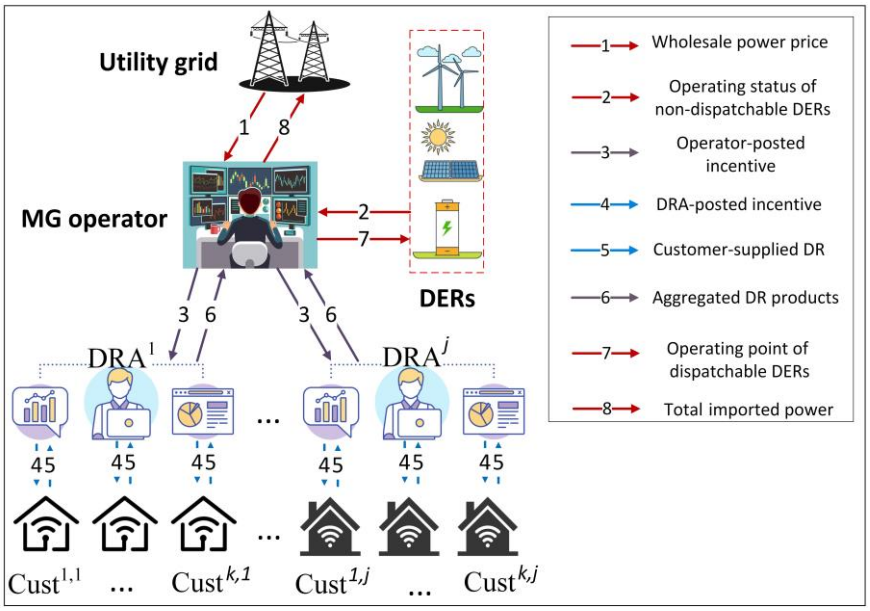


Figure 3.8: General architecture of the proposed two-stage, aggregator-mediated, incentive-based DSM market design.

As Fig. 3.8 shows, the market-based, aggregator-mediated DSM strategy is modelled as an interactive hierarchical decision-making process, which consists of two levels of leader-follower relationships, namely between the MG operator and the DRAs (wholesale DSM market), and between the DRAs and their customers (retail DSM market). Although the DSM market participants are hierarchically related with respect to the DR service, each has an independent viewpoint on the problem, which is modelled by specific objective functions in the following sections.

#### 3.3.2.1.1. Mathematical model of the utility

It is assumed that the conceptualised MG system, laid out in Section 3.2, runs on an energy-as-a-service (EaaS) business model, where not only does a third-party (private company) own the MG, but it also provides an overarching framework for energy management (through effective incentive arrangements reflective of wholesale market prices) tailored to the needs of the MG.

Specifically, on a 24-h day-ahead basis, the MG operator predicts the net energy deficit of the MG, which needs to be procured by a combination of imported power and customer-supplied DR units. In the face of an estimated internal power generation capacity deficit to meet the loads at the $t$-th time-step of operating the MG, $D_{def}(t)$, the MG operator attempts to balance out supply and demand by purchasing power from the upstream grid and/or offering financial incentives for load reduction. Accordingly, it sends an incentive payment signal to the aggregators to induce lower energy use at times of high wholesale power prices, when the total power output from the internal renewable power generation technologies is low, or during periods when reserve shortfalls arise. Equation 3.9 expresses the objective function (the hourly-basis operational cost of offsetting power deficit) of the MG operator, which needs to be minimised for each critical hour of the next day ($t \in P_d \subset T = \{1, 2, \dots, 8760\}$) while adhering to the constraints in Equations 3.10–3.12.

$$\min OC_{MG}(t) = cost_{im}(t) + I_{MGO}(t).\sum_{j\in J} D_{LA}^{j}(t) \ \ \forall t, \tag{3.9}$$

$$I_{MGO}^{min} \le I_{MGO}(t) \le I_{MGO}^{max} \ \ \forall t, \tag{3.10}$$

$$D_{def}(t) = P_{im}(t) + \sum_{j\in J} D_{LA}^{j}(t) \ \ \forall t, \tag{3.11}$$

$$cost_{im}(t) = \pi_{im}(t).P_{im}(t) \ \ \forall t, \tag{3.12}$$

where $OC_{MG}$ is the MG's operational cost defined based on the cost of the imported power from the national grid, $cost_{im}$, and the total incentive payments for load reduction; $I_{MGO}(t)$ represents the rate of incentive payment for load reduction offered by the utility at time-step $t$ of the day-ahead MG scheduling (i.e., the MG operator-posted incentive price signal to the wholesale DSM market); $I_{MGO}^{min}$ and $I_{MGO}^{max}$ respectively represent the lower and upper bounds of $I_{MGO}$; $D_{def}$ denotes the net energy deficit of the system; $D_{LA}^{j}$ is the total load reduction contributed by the $j$-th aggregator (DRA $j \in J$), which is a member of the set of aggregators containing $|J|$ members; $\pi_{im}$ is the wholesale power price; and $P_{im}$ denotes the imported power.

#### 3.3.2.1.2. Mathematical model of the aggregators

As mentioned earlier, responsive load aggregation agents join the flexible demand resources of the same type to make them tractable in the capacity market and enable them to become price-makers (by actively participating in the price-setting process) – and do not remain as price-takers. The DRAs serve as a go-between, interfacing with the smaller DR providers and the broader MG system operator so as to maintain the visibility of the small-scale DR products. More specifically, third-party aggregators enlist end-consumers of the same load segment and give them enough scale to take part in interruptible load programmes. The independence of the DRAs is fully preserved in the proposed model as they are precluded from ownership of any energy infrastructure. To this end, they take a percentage of the MG operator-offered incentive as compensation, passing the rest on to their

customers. In this context, each aggregator aims to maximise its net profit (to be gained from procuring aggregated DR products) by paying least possible, financially stable incentives to its subscribers than what it receives from the utility, which is expressed by Equation 3.13 subject to Equations 3.14 and 3.15.

$$\max Pr_{LA}^{j}(t) = \left(I_{MGO}(t) - I_{LA}^{j}(t)\right).D_{LA}^{j}(t) \quad \forall j,t, \tag{3.13}$$

$$I_{LA}^{j,min} \leq I_{LA}^{j}(t) \leq I_{LA}^{j,max} \quad \forall j,t, \tag{3.14}$$

$$D_{LA}^{j}(t) = \sum_{k \in N_J} d^{k,j}(t) \quad \forall j,t, \tag{3.15}$$

where $I_{LA}^{j}$ is the incentive payment offered by the $j$-th aggregator (i.e., the incentive rate posted by the $j$-th aggregator to the retail DSM market), $d^{k,j}$ is the capacity of load reduction (as DR product) supplied by the $k$-th customer serviced by the $j$-th aggregator, $N_J$ represents the set of customers who have subscribed to the $j$-th aggregator, which is a proper subset of the set of all the customers within the MG system's service (operational) territory, $K$, while $I_{LA}^{j,min}$ and $I_{LA}^{j,max}$ denote the lower and upper bounds of the incentive rates offered by the $j$-th aggregator, respectively.

#### 3.3.2.1.3. Mathematical model of the customers

End-consumers, who are activated by third-party DRAs, have the opportunity to take full advantage of their flexibility potential, whilst adhering to a set of discomfort cost constraints. Accordingly, the main goal of the end-users of the MG system who opt to participate in the interruptible load programme is to maximise their utility on the financial incentives offered by their corresponding aggregators to determine the optimum supply of their DR resources with respect to the DRA-offered incentive prices, whilst simultaneously keeping their comfort levels above certain thresholds, which is expressed by Equation 3.16 subject to Equations 3.17 and 3.18.

$$\max U^{k,j}(t) = d^{k,j}(t).I_{LA}^{j}(t) - dis^{k,j}(t) \quad \forall k,t, \tag{3.16}$$

$$0 \leq d^{k,j}(t) \leq d_{ncr}^{k,j}(t) \ \ \forall k, t, \tag{3.17}$$

$$d_{full}^{k,j}(t) = d_{cr}^{k,j}(t) + d_{ncr}^{k,j}(t) \ \ \forall k, t, \tag{3.18}$$

where the term $(d^{k,j}(t).\, I_{LA}^{j}(t))$ indicates the amount of financial incentive received by the $k$-th customer of the $j$-th aggregator in return for experiencing the discomfort (inconvenience) level to the value of $dis^{k,j}$ associated with load reductions (as a measure of the value of electricity), which is translated into cost by Equation 3.19 [248], [249];[6] $d_{full}^{k,j}$ and $d_{ncr}^{k,j}$ respectively denote the original (full) load and the non-critical (dispatchable) portion of the original load (which can be interrupted by making effective incentive payments to customers for curtailing load) demanded by customer $k$ of aggregator $j$; while $d_{cr}^{k,j}$ represents the critical portion of the original load demand, which cannot be interrupted under any circumstances as any shedding of which results in impaired reliability.

In this study, the administrative customer baselines are used to measure the amounts of load reduction, which are represented by $d^{k,j}$ in the model.

$$dis^{k,j}(t) = c_1^{k,j}.\,(d^{k,j}(t))^2 + c_2^{k,j}.\,(1 - \delta_j).\, d^{k,j}(t) \ \ \forall k, t, \tag{3.19}$$

where $c_1^{k,j}$ and $c_2^{k,j}$ are customer-specific (individual-level), positive coefficients specified by end-consumers, which characterise their sensitivity to load reductions and reflect the customers' attitude with regard to load interruption as a function of financial incentive offers, while $0 \leq \delta_j \leq 1$ is a load type-dependent factor (sector-level elasticity) associated with customer-supplied DR capacity, which represents the willingness of different categories of customers in contributing to load reduction (heterogeneous willingness of end-users to participate in interruptible DR activities) with values in the range [0, 1], as stated above.

As constrained by Equation 3.20, the discomfort cost to end-users is enforced to lie within a certain range to always meet the customers' expectations.

[6] The customer discomfort cost function can be viewed as the second-order best-fit equation to individual-level, user-specified data points representing ordered pairs of DR capacity supply and the associated discomfort cost incurred.

$$dis^{k,j,min} \leq dis^{k,j}(t) \leq dis^{k,j,max} \ \forall k,t, \tag{3.20}$$

where $dis^{k,j,min}$ and $dis^{k,j,max}$ represent the minimum and maximum allowable limits of customer-specific discomfort cost experienced by each participant in the DR events, respectively.

Furthermore, as could be expected, the greater the values of $c_1^{k,j}$ and $c_2^{k,j}$, the greater the discomfort cost of load interruption (for non-participating customers, who are totally indifferent to the level of incentive payment, $c_1^{k,j}, c_2^{k,j} \to \infty$), while the greater the value of $\delta_j$, the greater the willingness of the customer of type $j$ to participate in the load reduction programmes. For the most willing customers to enrol in the DSM programmes, $\delta_j \to 1$, whereas for the least willing customers (a hypothetical completely inelastic customer category), $\delta_j \to 0$.

Furthermore, incorporating the term $(-c_2^{k,j}\delta_j d^{k,j}(t))$ in Equation 3.19 ensures that the market equilibrium of the two-stage aggregator-mediated DSM game is aware of the marginal values the end-users across different sectors place on an uninterrupted power supply – that is, the value to consumers of the last (incremental) unit of DR capacity supply. It should be noted that this analysis does not account for the impact of supply elasticity of inframarginal sectoral DR capacity on DSM market-clearing prices.

#### 3.3.2.1.3.1. Stochastic load disaggregation

It is assumed that the total energy use forecasts are available for each energy consumption sector, which contains a certain number of end-users, over a 24-h day-ahead timeframe. However, the individual end-consumers' hourly demand data are not available and need to be estimated by disaggregating the total sector-wise energy consumption data over each hour of the system's operation. To this end, a stochastic algorithm is employed to determine the load share of each energy customer over each hour of the day-ahead energy consumption data stream. The stochastic algorithm is built on seven parameters, namely: the load-type dependent estimates of the DR supply elasticity, $\delta_j$; the customer-specific willingness to

supply DR capacity, characterised by $c_1^{k,j}$ and $c_2^{k,j}$; the full load demanded by each customer, $d_{full}^{k,j}$, and its and non-critical portion, $d_{ncr}^{k,j}$; the maximum participation rate of different consumer categories in the incentive-directed DR programmes, $Par_{max}^{j}$; as well as the number of customers in each load type cluster (i.e., the number of customers signed up with each aggregator for load curtailment services and opt to supply their DR flexibility products), $N_{cust}^{j} = |N_J|$. More specifically, the stochastic algorithm generates $j$ random $N_{cust}^{j}$-element vectors of reduced load values, $\left[d^{1,j}, d^{2,j}, \dots, d^{N_{cust}^{j},j}\right]$, each with a fixed sum determined by the share of load category $j$ in the total load reduction, which is controlled by $\delta_j$, while adhering to the constraint in Equation 3.21 [250]. Also, it is noteworthy that the parameter $Par_{max}^{j}$ in the algorithm serves the purpose of defining the upper limit of $d_{ncr}^{k,j}$, as expressed in Equation 3.22. Furthermore, the randomly selected $c_1^{k,j}$ and $c_2^{k,j}$ values characterise the DR supply decisions of individual end-consumers with respect to the aggregator-offered incentive rates in the algorithm.

$$\underline{d_{ncr}^{k,j}} \leq d^{k,j}(t) \leq \overline{d_{ncr}^{k,j}} \quad \forall k, t, \tag{3.21}$$

$$d_{ncr}^{k,j}(t) \leq Par_{max}^{j} \times d_{full}^{k,j}(t) \quad \forall k, t, \tag{3.22}$$

where $\underline{d_{ncr}^{k,j}}$ and $\overline{d_{ncr}^{k,j}}$ respectively denote the lower and upper bounds of the non-critical portion of the customer-specific loads subscribed to the $j$-th aggregator.

Fig. 3.9 shows a flowchart of the employed stochastic algorithm to synthetically disaggregate the total load reduction capacity procured by the proposed incentive-based DR programme into individual end-users who subscribe to the programme. First, the values of sectoral elasticities of customer-supplied DR capacities, $\delta_j$, sector-specific maximum participation rates, $Par_{max}^{j}$, the number of customers in each load category, $N_{cust}^{j}$, sector-wide lower bounds of the non-critical portions of full load demands (available load interruption capacities of end-users), $\underline{d_{ncr}^{k,j}}$, the DRA-offered incentive price for load reduction, $I_{LA}^{j}$, the forecasted share of each load category in the total load demand, the expected total sectoral load

interruptions, as well as the sectoral ranges of discomfort factors and full loads, are loaded as input data.

For each load category, the algorithm then synthesises $N_{cust}^{j}$-element vectors of full load by normalising the uniformly-distributed pseudo-random numbers generated in the interval (0, 1) using the MATLAB '*rand*' function – which represent the original (non-reduced) loads of sector-wide customers – to fall within the pre-defined allowable range before scaling them so that their sum is equal to the total sectoral load demand forecasted. As the figure shows, if the associated condition is not met, the process of random full load generation for the sectoral customers is iterated until no synthesised load is outside the pre-defined range.

After recording the synthesised full loads across all sectors, customer-specific discomfort factors are randomly generated and normalised to lie within the pre-specified ranges. Then, based on the generated discomfort factors, best-strategy load reductions of the participating end-users of each sector are derived. The calculated interruptible loads are then normalised to fit the customer-type-specific allowable range, and also scaled so that their sum is equal to the total sectoral DR capacity procurement expected. At this stage, if the condition that, all the curtailable loads synthesised should lie within the allowable sectoral range, is not satisfied, the process of random interruptible load synthesis is repeated from the random customer-specific discomfort factor generation block.

Also, given that the synthesised values of load reduction are first normalised to lie within the corresponding allowable range and then scaled to satisfy the expected total sectoral load curtailment, there exists the possibility that the discomfort factors that correspond to the corrected customer-supplied interruptible loads do not lie within the allowable range. Accordingly, another condition block checks if the aforementioned expression is false and, in that case, executes the random load reduction-related statements repeatedly until the specified condition result will be true.

As one would expect, the stochastic algorithm's probability of acceptance decreases as the dimensionality of the problem increases. This leads to either very

long running times (due to the need for many iterations) or computational intractability of the overall simulation process for ultra-high-dimensional problems, which necessitate the use of heuristic and meta-heuristic optimisation-based algorithms – for the disaggregation of the total load forecasted, as well as the expected curtailable portion of it, into individual end-consumers across different sectors. However, given the relatively small scale of the case study considered in this research (and hence, the relatively small number of sectoral end-consumers), the stochastic algorithm was able to yield the disaggregated load reductions with a standard desktop computer in a few seconds of computational time.

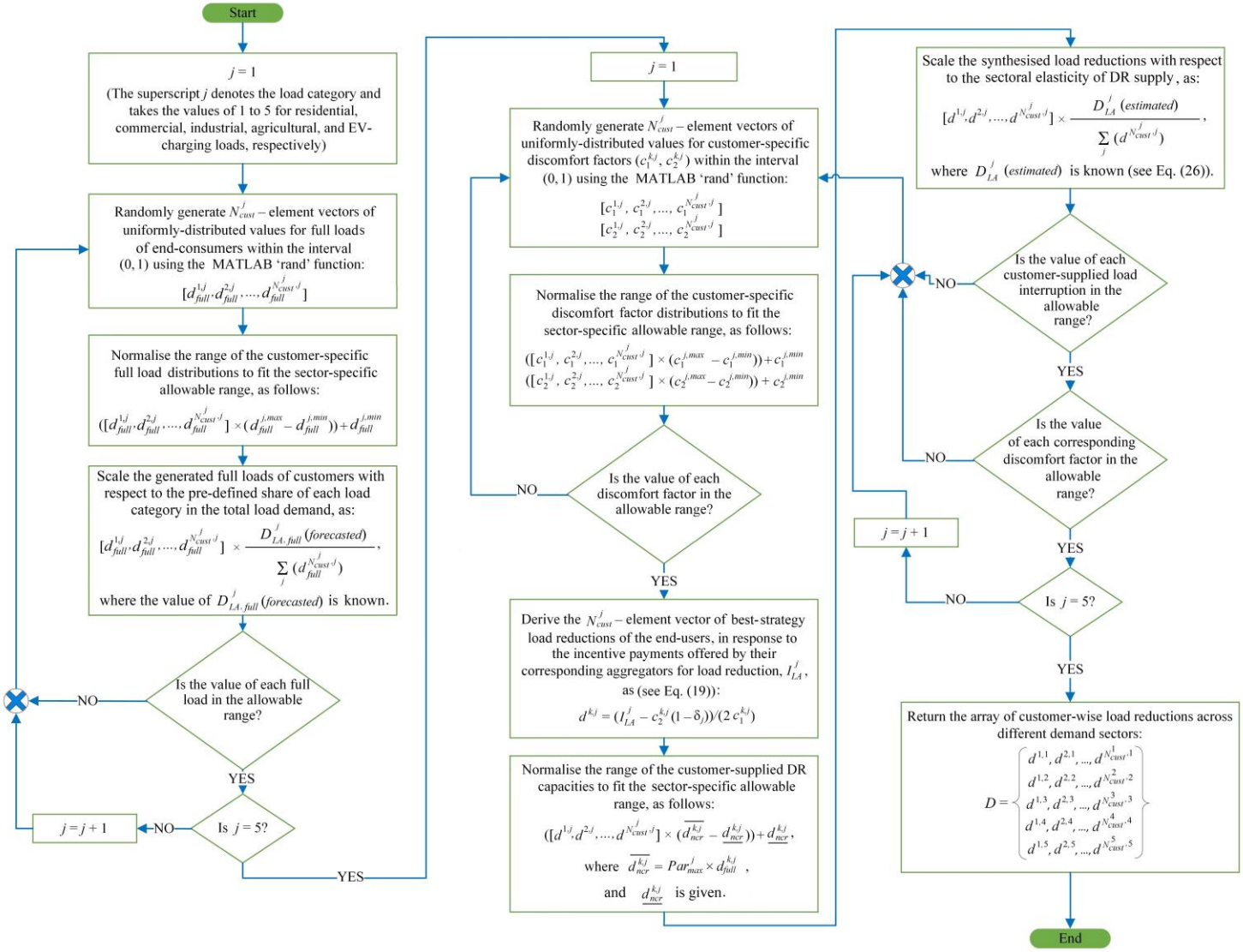


Figure 3.9: Flowchart of the stochastic total customer-supplied DR capacity disaggregation algorithm.

It should be noted that the stochastic algorithm is implemented for each hour of the next day for which a net energy deficit is predicted and is embedded within the main distributed algorithm (Algorithm 3.1) developed to determine the unique, pure-strategy Nash equilibrium of the day-ahead, non-cooperative DR dispatch game (see Section 3.3.2.3). It is also noteworthy that the employed disaggregation mechanism is not required for model implementation in real-world practice (during the operational phases), as it is used only as a means to synthetically generate individual-level energy demand and DR supply capacity.

#### 3.3.2.2. Mathematical formulation of the game

This section presents the mathematical formulation of the two-stage, aggregator-mediated, incentive-based DSM market model specifically developed for a systematic integration into the standard, robust, long-term, meta-heuristic-based, high-dimensional equipment capacity planning optimisation of grid-connected MGs tailored towards community-scale, sector-coupled, multi-energy-storage-technology, 100%-renewable and -reliable projects.

As shown in Fig. 3.10, the proposed dual-loop framework, which establishes a two-level strategic, day-ahead DSM market game for decision-making regarding the optimal dispatch of flexible DR resources is driven by two separate types of financial incentive offers: (1) those provided by the utility (MG operator) at the top (wholesale) level, and (2) those proposed by load aggregators at the bottom (retail or downstream) level. The operator-provided incentive rates directly impact the aggregate load reduction provided by the aggregation agents and, by the same token, the aggregator-provided incentive rates have a direct influence on the participation rate of end-users in the interruptible load management programme. Looking from the inside out, the financial incentives offered by the utility/aggregators evolve with reference to the aggregators'/customers' responses to different levels of the offered incentive rates – and, in this sense, the devised framework is an intertwined system with a negative feedback loop. The DRAs in the proposed dual-loop, Stackelberg, strategic game-theoretic model, represented in Fig. 3.10, fulfil a twofold purpose: they act as the followers of the utility in the

top-level loop, whilst, at the same time, leading the bottom-level loop, where end-users serve as final followers.

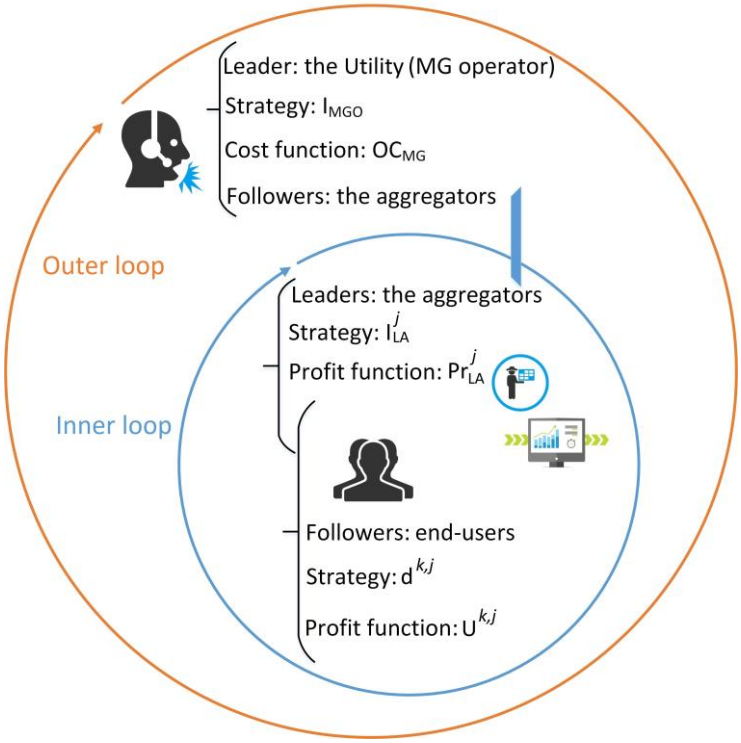


Figure 3.10: Two-loop structure of the proposed Stackelberg, strategic game-theoretic DR management framework.

For the dual-loop, Stackelberg, strategic game-theoretic DR provision framework modelled above, a finite set of best strategies $(I_{MGO}^{*}, I_{LA}^{*}, D^{*})$ establishes the pure-strategy Nash equilibrium of the game, if, and only if, the following inequality constraints are relaxed:

$$OC_{MG}(I_{MGO}^{*}, I_{LA}^{*}, D^{*}) \leq OC_{MG}(I_{MGO}, I_{LA}^{*}, D^{*}), \tag{3.23}$$

$$Pr_{LA}^{j}\left(I_{MGO}^{*}, I_{LA}^{j,*}, D_{LA}^{j,*}\right) \geq Pr_{LA}^{j}\left(I_{MGO}^{*}, I_{LA}^{j}, D_{LA}^{j,*}\right) \quad \forall j, \tag{3.24}$$

$$U^{k,j}\left(d^{k,j,*}, I_{LA}^{j,*}\right) \geq U^{k,j}\left(d^{k,j}, d^{-k,j,*}, I_{LA}^{j,*}\right) \quad \forall k, \tag{3.25}$$

where $I_{LA}^{*} = \{I_{LA}^{1,*}, I_{LA}^{2,*}, I_{LA}^{3,*}, I_{LA}^{4,*}, I_{LA}^{5,*}\}$ represents the union of pure strategies taken by all aggregators; $D^{*} = \{d_1^{*}, d_2^{*}, \dots, d_K^{*}\}$ denotes the union of pure strategies taken by the customers subscribed to each aggregator $j \in J$, where $K$ is the number of all the

customers of the MG; $d^{k,j,*}$ represents the pure strategy taken by the $k$-th customer subscribed to the $j$-th aggregator; $d^{-k,j,*} = \{d^{1,j,*}, d^{2,j,*}, \dots, d^{k-1,j,*}, d^{k+1,j,*}, \dots, d^{N_j,j,*}\}$ denotes the set of pure strategies of all the customers of the $j$-th aggregator except its $k$-th customer; while $D_{LA}^{j,*} = \{d^{k,j,*}, d^{-k,j,*}\}$ identifies the pure strategies of all the customers signed up to the $j$-th aggregator.

The constraints in Equations 3.23–3.25 ensure that at the pure-strategy Nash equilibrium of the game, neither the MG's operational cost, nor the aggregators' profits, nor the customers' utilities can be further improved by taking a different strategy. As the next section demonstrates, the developed dual-loop, Stackelberg, strategic game has a unique, pure-strategy Nash equilibrium solution, at which no player can improve its payoff without reducing the payoff to at least one other player.

#### 3.3.2.2.1. Existence and uniqueness of the Nash equilibrium

In view of the hierarchical structure of the proposed game-theoretic model for the provision of DR resources, backward induction can be utilised to identify the Nash equilibrium point. To this end, first, the best-response strategies of the end-users to the aggregator-provided incentive prices have to be determined as part of the inner loop of the game. The second step is to determine the aggregators' best strategies, while the last step is to examine the existence of the best strategy for the MG operator in the outer loop of the game, laid out in Fig. 3.10. The following theorem provides the necessary and sufficient conditions for the existence and uniqueness of a Nash equilibrium point for the devised game-theoretic model.

**Theorem 1.** *There exists a unique, pure-strategy Nash equilibrium solution to the devised dual-loop, Stackelberg, non-cooperative game-theoretic framework for implementing the proposed customer utility-preserving, system state-aware, incentive-based load demand interruption programme, at which no player can obtain a higher level of payoff by deviating from its best strategy.*

**Proof.**

(1) Determine the best strategies of the end-users, $d^{k,j,*}$, in response to the incentive payments offered by their corresponding aggregators for load reduction, $I_{LA}^{j}$, by taking the first-order derivative of $U^{k,j}$, given in Equation 3.16, with respect to the amount of load reductions they provide, and then setting them equal to zero, as follows:

$$\frac{\partial U^{k,j}}{\partial d^{k,j}} = I_{LA}^{j} - \left(2c_1^{k,j}.\, d^{k,j} + c_2^{k,j}.\left(1-\delta_j\right)\right) = 0, \tag{3.26}$$

$$d^{k,j,*} = \frac{I_{LA}^{j} - c_2^{k,j}.\,(1-\delta_j)}{2c_1^{k,j}}. \tag{3.27}$$

Then, the second-order derivative of $U^{k,j}$, given in Equation 3.16, with respect to the customer-supplied DR capacity can be obtained as:

$$\frac{\partial^2 U^{k,j}}{\partial (d^{k,j})^2} = -2c_1^{k,j} < 0. \tag{3.28}$$

Given the positive value of $c_1^{k,j}$, the second-order derivative of $U^{k,j}$ is strictly negative, which implies that $U^{k,j}$ is strictly concave over the feasible region of $d^{k,j}$. Hence, the best-response strategies of the end-users, derived in Equation 3.27, are guaranteed to return the unique, globally-optimum solutions.

(2) Identify the best strategies of the aggregators, $I_{LA}^{j,*}$, using the backward induction approach by substituting the best strategies of the end-users, given in Equation 3.27, into Equation 3.13, as follows:

$$\begin{aligned} Pr_{LA}^{j} &= \left(I_{MGO} - I_{LA}^{j}\right).\sum_{k\in N_J}\frac{I_{LA}^{j} - c_2^{k,j}.\left(1-\delta_j\right)}{2c_1^{k,j}} = -\left(I_{LA}^{j}\right)^2.\sum_{k\in N_J}\frac{1}{2c_1^{k,j}} \\ &+ I_{LA}^{j}.\left(\sum_{k\in N_J}\frac{c_2^{k,j}.\left(1-\delta_j\right)}{2c_1^{k,j}} + \sum_{k\in N_J}\frac{I_{MGO}}{2c_1^{k,j}}\right) + I_{MGO}.\sum_{k\in N_J}\frac{-c_2^{k,j}.\left(1-\delta_j\right)}{2c_1^{k,j}}. \end{aligned} \tag{3.29}$$

Taking the first-order derivate of the re-written $Pr_{LA}^{j}$, given in Equation 3.29, with respect to the amount of financial incentives offered by the aggregators and then setting it equal to zero, the best strategies of the aggregators can be obtained as:

$$\frac{\partial Pr_{LA}^{j}}{\partial I_{LA}^{j}} = -I_{LA}^{j} \sum_{k\in N_J} \frac{1}{c_1^{k,j}} + \left(\sum_{k\in N_J} \frac{c_2^{k,j}.\left(1-\delta_j\right)}{2c_1^{k,j}} + \sum_{k\in N_J} \frac{I_{MGO}}{2c_1^{k,j}}\right) = 0, \tag{3.30}$$

$$\begin{aligned} I_{LA}^{j,*} &= \frac{\left(\sum_{k\in N_J} \frac{c_2^{k,j}.\left(1-\delta_j\right)}{2c_1^{k,j}} + \sum_{k\in N_J} \frac{I_{MGO}}{2c_1^{k,j}}\right)}{\sum_{k\in N_J} \frac{1}{c_1^{k,j}}} \\ &= \frac{1}{2}\sum_{k\in N_J} c_2^{k,j}.\left(1-\delta_j\right) + \frac{1}{2} I_{MGO}. \end{aligned} \tag{3.31}$$

It is noteworthy that the aggregators' best strategies, derived in Equation 3.31, are reflective of the associated sectoral elasticity of customer-supplied DR capacities, whilst additionally relying on the utility's best strategy – a mechanism consistent with the fundamental purposes of the aggregators.

Furthermore, the second-order derivative of $Pr_{LA}^{j}$, re-written in Equation 3.29, with respect to the aggregator-offered incentive payments can be obtained as:

$$\frac{\partial^2 Pr_{LA}^{j}}{\partial (I_{LA}^{j})^2} = -\sum_{k\in N_J} \frac{1}{c_1^{k,j}} < 0. \tag{3.32}$$

Given the positive value of $c_1^{k,j}$, the second-order derivative of $Pr_{LA}^{j}$ is strictly negative, which implies that $Pr_{LA}^{j}$ is strictly concave over the feasible region of $I_{LA}^{j}$; therefore, the best strategies of the aggregators, given in Equation 3.31, are guaranteed to yield the globally-optimum solutions.

(3) Verify the existence and uniqueness of the MG operator's best strategy by the following steps:

Substituting the best strategies of the aggregators, given in Equation 3.31, into the best-response strategies of the customers, provided in Equation 3.27, yields:

$$d^{k,j,*} = \frac{(\frac{1}{2}\sum_{k\in N_J} c_2^{k,j}.\left(1-\delta_j\right) + \frac{1}{2}I_{MGO}) - c_2^{k,j}.(1-\delta_j)}{2c_1^{k,j}}$$
$$= (\frac{1}{4c_1^{k,j}}.\sum_{k\in N_J} c_2^{k,j}.\left(1-\delta_j\right)) + \frac{1}{4c_1^{k,j}}.I_{MGO} - \frac{c_2^{k,j}.\left(1-\delta_j\right)}{2c_1^{k,j}}. \quad (3.33)$$

Accordingly, the aggregated load reduction of each aggregator can be calculated as:

$$D_{LA}^{j,*} = \sum_{k\in N_J} d^{k,j,*}\,(\frac{I_{MGO}}{4}.\sum_{k\in N_J}\frac{1}{c_1^{k,j}}) + (\frac{1}{4}\sum_{k\in N_J}\frac{c_2^{k,j}.\left(1-\delta_j\right)}{c_1^{k,j}})$$
$$-\frac{1}{2}\sum_{k\in N_J}\frac{c_2^{k,j}.\left(1-\delta_j\right)}{c_1^{k,j}} = \frac{I_{MGO}}{4}.\sum_{k\in N_J}\frac{1}{c_1^{k,j}} - \frac{1}{4}\sum_{k\in N_J}\frac{c_2^{k,j}.\left(1-\delta_j\right)}{c_1^{k,j}}. \quad (3.34)$$

Then, the total amount of load reduction provided by all the aggregators can be expressed as:

$$\sum_{j\in J} D_{LA}^{j,*} = \sum_{j\in J}\sum_{k\in N_J} d^{k,j,*} = \frac{I_{MGO}}{4}.\sum_{j\in J}\sum_{k\in N_J}\frac{1}{c_1^{k,j}} - \frac{1}{4}\sum_{j\in J}\sum_{k\in N_J}\frac{c_2^{k,j}.\left(1-\delta_j\right)}{c_1^{k,j}}. \quad (3.35)$$

For the sake of simplicity, let $\alpha = \sum_{j\in J}\sum_{k\in N_J}\frac{1}{c_1^{k,j}} > 0$ and $\beta = \sum_{j\in J}\sum_{k\in N_J}\frac{-c_2^{k,j}.(1-\delta_j)}{c_1^{k,j}} > 0$. Accordingly, Equation 3.35 can be simplified to the following equation:

$$\sum_{j\in J} D_{LA}^{j,*} = \frac{I_{MGO}}{4}.\alpha + \frac{1}{4}\beta. \quad (3.36)$$

Substituting Equations 3.11, 3.12, and 3.36 into the operational cost imposed on the utility to meet the onsite power generation capacity deficit, presented in Equation 3.9, gives:

$$\begin{aligned} OC_{MG} &= \pi_{im}.P_{im} + I_{MGO}.\left(\frac{I_{MGO}}{4}.\alpha + \frac{1}{4}\beta\right) \\ &= \pi_{im}.\left(D_{def} - (\sum_{j\in J} D_{LA}^{j,*})\right) + \frac{\alpha}{4}.{I_{MGO}}^2 + \frac{\beta}{4}.I_{MGO} \\ &= \pi_{im}.\left(D_{def} - \left(\frac{I_{MGO}}{4}.\alpha + \frac{1}{4}\beta\right)\right) + \frac{\alpha}{4}.{I_{MGO}}^2 + \frac{\beta}{4}.I_{MGO} \\ &= \frac{\alpha}{4}.{I_{MGO}}^2 + \left(\frac{\beta - \pi_{im}.\alpha}{4}\right).I_{MGO} + \pi_{im}.D_{def} - \frac{\pi_{im}.\beta}{4}. \end{aligned} \tag{3.37}$$

The first- and second-order derivatives of the re-formulated operational cost of meeting the onsite power generation capacity deficit with respect to the utility-offered financial incentives can be obtained as follows:

$$\frac{\partial OC_{MG}}{\partial I_{MGO}} = \frac{\alpha}{2}.I_{MGO} + \left(\frac{\beta - \pi_{im}.\alpha}{4}\right), \tag{3.38}$$

$$\frac{\partial^2 OC_{MG}}{\partial (I_{MGO})^2} = \frac{\alpha}{2} > 0. \tag{3.39}$$

Given the positive value of the second-order derivative of $OC_{MG}$, it can be deduced that it is a strictly convex function of $I_{MGO}$. Setting the first-order derivative of the reformulated $OC_{MG}$, given in Equation 3.38, equal to zero, the globally-optimum and, at the same time, the unique best strategy of the MG operator can be determined as follows:

$$I_{MGO}^{*} = \frac{\pi_{im}.\alpha - \beta}{2\alpha}. \tag{3.40}$$

When the MG operator's pure strategy is identified, it can be substituted into Equation 3.31 to find the pure strategies of the aggregators. Consequently, the best-response strategy of each end-user can be calculated by substituting the unique, globally-optimum incentive rate offered by the aggregator it is enrolled with, expressed in Equation 3.31, into Equation 3.27. Finally, the vector of the identified best strategies $(I_{MGO}^{*}, I_{LA}^{j,*}, d^{k,j,*})$ represents the pure-strategy Nash equilibrium of

the devised dual-loop, Stackelberg, strategic game and, thus, the proof of Theorem 1 is complete. □

### 3.3.2.3. Distributed algorithm

The pure-strategy Nash equilibrium of the dual-loop, Stackelberg, non-cooperative game tailored to the two-stage, aggregator-mediated, incentive-based DSM market model, derived analytically in the previous section, is subject to privacy concerns; the derived backward induction-based optimal solution finds the pure strategy of the MG operator assuming that the utility has perfect information about the game. However, this is not a commonplace, accepted practice. Not only might this result in destructive strategies from the utility that subvert, rather than uphold, the social welfare, it would also put the privacy of customers at risk. To address these shortcomings, an iterative distributed algorithm is derived in this section to iteratively approximate the pure-strategy Nash equilibrium solution to the devised game by dynamically updating the MG operator-offered incentive price. Nevertheless, for the sake of simplification, it is still assumed that aggregators are trusted agents of customers playing on the same side of the line at the top level (outer loop) of the proposed dual-loop game, shown in Fig. 3.10. The main advantages of the iterative distributed algorithm over closed-form solutions are: (i) revealing only necessary information about the customers' incentive-directed load interruption decisions (driven by the customers' marginal utilities of supplying DR capacities) while preserving privacy, and (ii) handling high-degree non-linearities often present in the players' payoff functions without the need for making several simplifying assumptions that potentially impair the solution quality.

Accordingly, the distributed algorithm, derived in Algorithm 3.1, serves as the ultimate framework to obtain the Nash equilibrium solution set of the game, which identifies the best-response strategies of the DRAs and end-consumers. It, more specifically, serves as an effective forum to quantify the optimal trade-off between the imported power and dispatched load reduction during the critical hours of MG operation in terms of onsite resource adequacy. The superscript "*" in the algorithm denotes the global optimality. The fundamental principle of the algorithm is to iteratively update the amount of incentive price offered by the utility (MG

operator-posted incentive price) – as the wholesale-market-maker – from $I_{MGO}^{min}$ to $I_{MGO}^{max}$ with an increment size of $i_{MGO}$, and then determine the optimal incentive price offered by each aggregator and the participation rate (i.e., load demand reduction) of the customers enrolled with each aggregator using a distributed variant of the proposed analytical framework in the previous section. This provides a platform to determine the hourly operational cost of the MG as a function of the wholesale power price and contributed load reductions. To this end, the model is solved repeatedly for different values of the MG operator-offered incentive prices until no further improvement (reduction) in the MG operational cost occurs (terminating condition). More specifically, for each utility-offered incentive rate, the aggregators, first, send the incentive rate signals (the analytically-derived optimal values of which can be calculated according to Equation 3.31) to their customers; the customers then determine their best-response strategies (the analytically-derived optimal values of which can be determined using Equation 3.27) and submit their optimal load reductions to their corresponding aggregators; and finally, the flexible load aggregation agents accumulate the reduced demands (the analytically-derived optimal values of which can be obtained using Equation 3.36) and transmit them to the MG utility. At this point, the utility calculates the operational cost of addressing power deficiencies using Equation 3.9 and keeps a log of the results $(I_{MGO}^{*}, OC_{MG}^{*})$ in case it leads to a lower operational cost as compared to the last minimum value of $OC_{MG}$ recorded. For each predicted critical peak time-step of the day-ahead operation of the MG, the distributed algorithm is run iteratively until the constraints contained in Equations 3.23–3.25 are all relaxed and the termination condition of the algorithm is met, implying that the unique, pure-strategy Nash equilibrium of the game is found. Such decentralisation of the decision-making platform ensures that all the economic actors have some clout in the game.

Note that as proved in the previous section, $OC_{MG}$ is strictly convex with respect to $I_{MGO}$; hence, search space enumeration is guaranteed to find the optimum incentive price to be offered by the utility to the aggregators, $I_{MGO}^{*}$, and, accordingly, Algorithm 3.1 is guaranteed to converge to the unique, pure-strategy Nash equilibrium solution set of the devised game $(I_{MGO}^{*}, I_{LA}^{j,*}, d^{k,j,*})$.

**Algorithm 3.1:** Proposed distributed algorithm to produce the unique, pure-strategy Nash equilibrium of the developed game (optimal day-ahead trade-offs between imported power and utilised DR resources during the critical peak hours of MG operation).

---

1: The MG operator initialises $I^*_{MGO} = 0$ and $OC^*_{MG} = cost_{im}(D_{def})$

2: **for** the utility-posted incentive rate of $I_{MGO}$ ranging from $I^{min}_{MGO}$ to $I^{max}_{MGO}$ at steps of $i_{MGO}$ **do**

3: Broadcast the incentive price signal $I_{MGO}$ to all the flexible load aggregators by submitting it to the wholesale DSM market

4: **for** each aggregator $j \in J$ run the retail market and **do**

5: Calculate the best-strategy incentive rate to be offered to the end-users, $I^{j,*}_{LA}$ (using Equation 3.31) – by setting the first-order derivative of the DRA's profit function in Equation 3.13 equal to zero, in which $d^{k,j}$ is substituted with the best-response strategy of the corresponding customers derived by setting the first-order derivative of their utility functions in Equation 3.16 equal to zero

6: Send the calculated incentive price signal $I^{j,*}_{LA}$ to the customers registered to participate in the load reduction programme

7: **for** each registered customer $k \in N_J$ **do**

8: Derive the best-response strategy of the customer to the financial incentive rate offered by the aggregator it is enrolled with, $d^{k,j,*}$ (using Equation 3.27) – by setting the first-order derivative of its utility function given in Equation 3.16 equal to zero

9: Calculate the best-response load reduction with respect to the financial incentive offered by the DRA it has subscribed to, using the customer-specific best-response strategy derived

10: Send the best-response strategy of each registered customer (the amount of load curtailment contributed by the customer) back to the corresponding aggregator

11: **end for**

12: Aggregate the curtailable load resources (load reductions) supplied by the end-users (using Equation 3.36)

13: Transmit the identified optimum value of the aggregated load reduction capacity procured by the DRA back to the MG operator

14: **end for**

15: Update the hourly operational cost of the MG to balance out the power deficit as:

$$OC_{MG} = \pi_{im}.P_{im}\left(D_{def} - \sum_{j\in J} D^j_{LA}\right) + I_{MGO}.\sum_{j\in J} D^j_{LA}$$

16: **if** $(OC_{MG} < OC^*_{MG})$ **then**

17: Update the optimal values of the MG operator-offered incentive price and the operational cost of the MG as: $I^*_{MGO} = I_{MGO}$ and $OC^*_{MG} = OC_{MG}$

18: **end if**

19: **end for**

20: Return the set of $(I^*_{MGO}, I^{j,*}_{LA}, d^{k,j,*})$ as the unique, globally-optimum, pure-strategy Nash equilibrium solution to the game for each hour of the coming day

---

### 3.3.2.4. Sequence of operations

Fig. 3.11 presents a general sequence diagram of the proposed dual-loop, market-driven, incentive-based, aggregator mediated DR scheduling framework that uses the developed privacy-preserving distributed algorithm to yield the pure-strategy Nash equilibrium of the game. Additionally, the application-driven sequence diagram of Algorithm 3.1, shown in Fig. 3.12, helps better understand the sequence of actions and reactions required to execute the proposed interruptible DR market design for the conceptualised MG 4, laid out in Section 3.2. As the figure shows, first, the MG system operator requests the forecasted total power output from renewable power generation assets from the MG asset manager for each hour of the next day. Accordingly, the day-ahead state estimates of non-controllable renewables and dispatchable renewable energy reserves (namely, biomass resources) are communicated from one utility-owned entity, the MG asset manager, to another utility-owned entity, the MG operator. After receiving a response to its enquiry regarding the availability of biomass resources from the MG asset manager and commanding the operational point of the biopower plant (in accordance with the feedstock availability and size of the plant), the MG operator sends financial incentive signals to the DRAs and asks about the amount of available interruptible loads at each hour of the upcoming day in a privacy-preserving manner. To this end, the two-stage iterative Stackelberg incentive pricing game is run in accordance with Algorithm 3.1, which enables decentralised decision-making. Recall that the MG operator calls a DR event and sends the incentive price signals to the aggregators for the time-steps at which a net energy deficit is predicted. Yet, a vigorous discussion on the communications technologies and systems required for the real-world implementation of the proposed coordinated, sectoral aggregator-mediated, system-level interruptible (incentive-responsive) DR dispatch game in a transparent, robust, equitable, two-sided market platform (with a particular focus on the implementation within a New Zealand context) is needed for real-world developments.

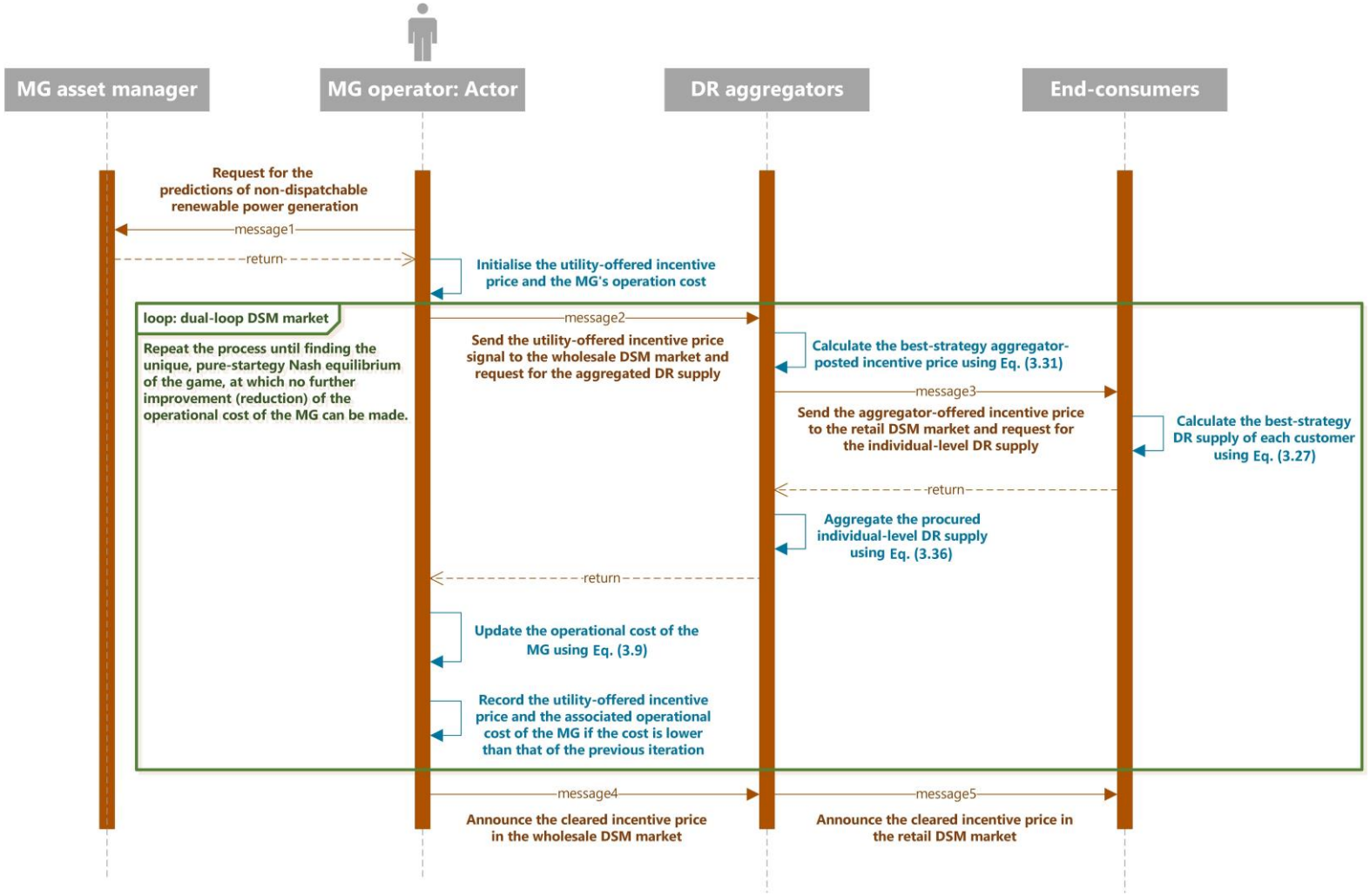


Figure 3.11: Sequence diagram of the suggested distributed algorithm to solve the non-cooperative game of utility-aggregator-customer interactions in the delivery of smaller interruptible DR products.

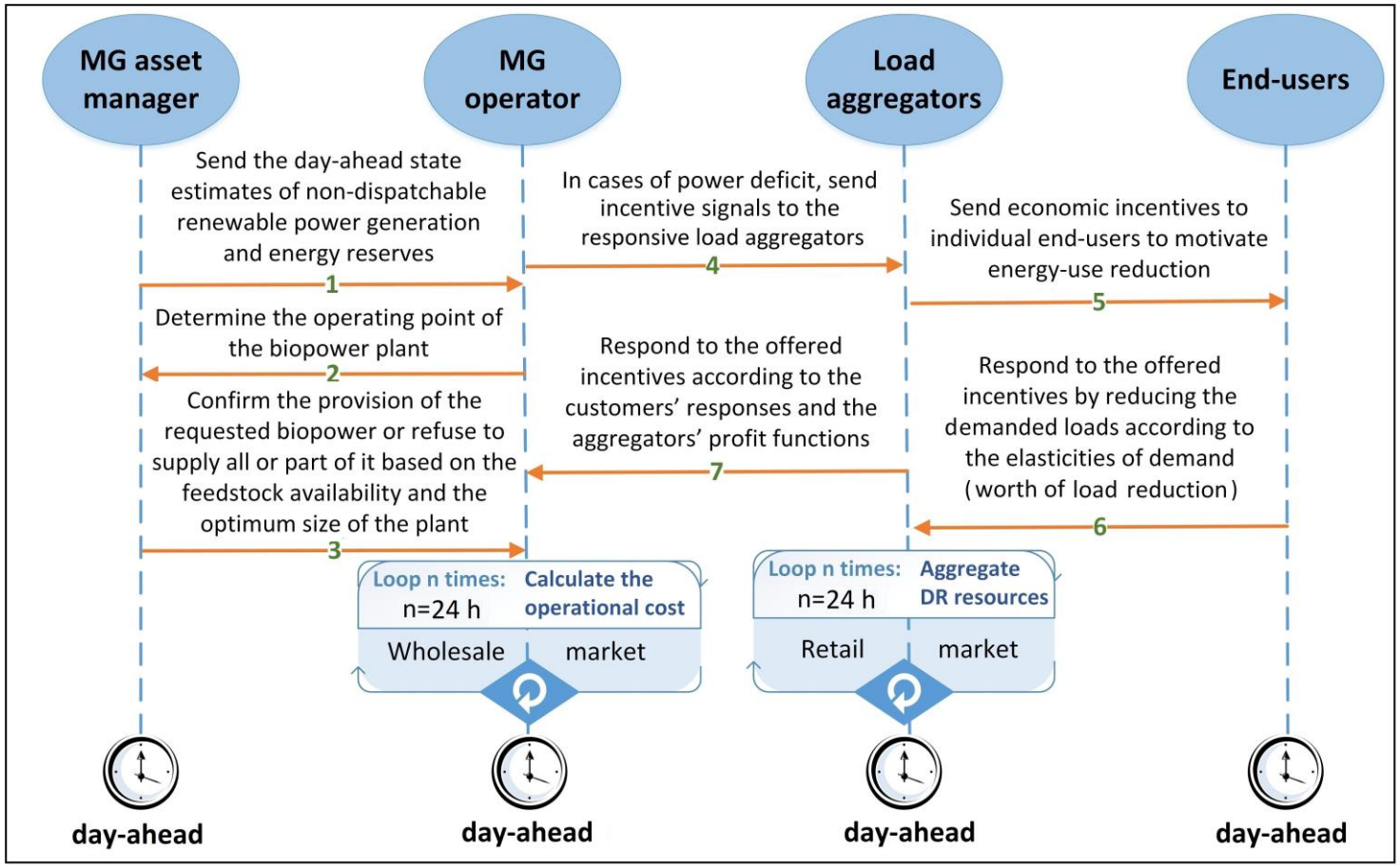


Figure 3.12: Sequence diagram of implementing the proposed DSM model in the context of the conceptualised MG system.

As Figs. 3.11 and 3.12 show, the MG operator sends a signal to the DRAs, which announces a DR event and triggers the proposed dual-loop DSM market framework to optimally schedule the power imports and system-level dispatch of DR resources. The dual-loop DSM market design is then run iteratively at increasing values of the utility-offered incentive price for load reduction to produce an optimal trade-off between imported power and procured DR units. After determining the cost-optimal solution, the MG operator announces the cleared utility-offered incentive price to the DRAs who, in turn, announce the cleared DRA-offered incentive price to their customers. This process is repeated for each critical peak time-step of the next day. Specifically, the critical peak time-steps are considered to be the time-steps of MG operation for which a net energy deficit (positive net load) is predicted, based on the next day's total load and onsite renewable power generation forecasts.

As the above discussion suggests, the end-consumers and, in turn, the DRAs, only disclose the information that is really required by the MG operator to be able to find an optimal DR allocation. That is, the developed iterative auction protocol that clears the proposed game-theoretic DSM market design is able to reduce the amount of information exchanged – and all associated complexities – to the essential minimum, thus preserving the privacy of the players' valuations. Indeed, the suggested iterative auctions are modelled by considering the DRAs and end-consumers as "black-boxes" that are represented by oracles, where the MG operator and DRAs repeatedly query these oracles, respectively. These oracles are shown to be incentive-compatible in Section 3.6.3, meaning that the design of the market is consistent with the factors that motivate the DRAs and end-consumers to truthfully participate in the DSM market.

The proposed DR scheduling framework, the application-driven sequence diagram of which is shown in Fig. 3.12, forms part of the input to the hourly energy management strategy of the proposed equipment capacity-planning method, the flowchart of which is provided in Fig. 3.5. That is, the energy demand data input to the flowchart is aware of the interruptible demand resources – or, better put, both the power and hydrogen demand on the system are scaled-down (modified) through

running the proposed DR scheduling framework for the specific peak hours of each day of the representative year before being fed to the hourly operational scheduling strategy outlined in Fig. 3.5. The process continues by transmitting the aggregators' incentives for load reduction to their corresponding customers, and completes by clearing the DSM markets respectively at the local (retail) and wholesale levels. As mentioned above, this procedure is repeated for each hour of a representative hourly-basis, one-year operational timeframe. To this end, the year-long demand profiles are decomposed into daily profiles for use in the day-ahead DR management plan of the MG (see Fig. 3.12), the DR-adjusted values of which are then utilised in the course of the hourly-basis, year-long energy management of the system (see Fig. 3.5).

#### 3.3.2.5. Data: Adjusted game-theoretic DR scheduling model parameters

This section presents the input data supplied to the model. Table 3.2 presents the data values for the proposed Stackelberg, non-cooperative game-theoretic DSM model scalars, namely: the step size of the iterative distributed algorithm, as well as the minimum and maximum bounds for the utility- and aggregator-offered incentive prices and the inconveniences experienced by the end-users due to load reduction.

Table 3.2: Data values and the proposed game-theoretic DSM model scalars.

| Parameter | Value | Parameter | Value |
|---|---|---|---|
| $i_{MGO}$ | \$0.020/kWh | $I_{LA}^{j,max}$ | \$0.300/kWh |
| $I_{MGO}^{min}$ | \$0.020/kWh | $dis^{k,j,min}$ | \$0.001/kWh |
| $I_{MGO}^{max}$ | \$0.320/kWh | $dis^{k,j,max}$ | \$0.280/kWh |
| $I_{LA}^{j,min}$ | \$0.010/kWh | | |

## 3.4. Micro-grid capacity-optimisation model

This section presents the deterministically formulated life-cycle cost estimation model of the conceptualised MG system 4 before describing how the proposed Stackelberg, non-cooperative game-theoretic DR management scheme is integrated into the robust meta-heuristic-based, high-dimensional MG equipment capacity planning optimisation model tailored towards community-scale, sector-coupled,

multi-energy-storage-technology, 100%-renewable and -reliable energy projects – the general structure of which is derived in Chapter 2. Recall that a meta-heuristic-based solution approach is suggested in this study as the underlying MG capacity-planning problem is a nonlinear, non-convex, NP-hard decision problem at its core, and consequently, cannot be solved exactly without simplifications or by enumerating the entire search space explicitly or implicitly.

As comprehensively discussed in Chapter 2, the proposed meta-heuristic-based MG capacity-optimisation model consists of three key elements: (1) the net present cost (NPC) and net present value (NPV) methods utilised to formulate the total discounted system cost function, (2) the LPSP technique to quantify the reliability of the system in servicing the electrical and hydrogen load demands, and (3) a single-objective meta-heuristic optimisation algorithm to determine the globally optimum solution to the problem by minimising the life-cycle cost of the MG, whilst adhering to a set of technical, reliability, self-sufficiency, resilience, and systemic constraints governing the feasible search (design) space. Also, in accordance with the systematic, multi-case-study-oriented, descriptive statistics-driven comparative analyses of the efficiencies of a number of meta-heuristics (selected based on comprehensive preliminary efficiency testing), multi-variant evidence has been generated in Chapter 2 that lend statistically significant support to the superiority of the MFOA to the well-established meta-heuristics in the MG investment planning literature – for instance, the GA and the PSO – as well as to a wide variety of state-of-the-art meta-heuristics in terms of nearing the globally optimum solution. Therefore, the formulated deterministic long-term MG equipment capacity planning model parametrised for the case of the fourth MG is also solved using the MFOA. However, owing to the mixed-discrete-continuous structure of the formulated problem, the technique proposed by Chowdhury et al. [251] is employed to modify the original continuous MFOA to make it applicable to the problem at hand. Also, likewise to Chapter 2, the control parameters of the MFOA were adjusted as suggested by its developer [103], while the number of search agents, $N_{SA}$, and the maximum number of iterations, $Iter_{max}$, were set based on the findings of Khan and Singh [83], as discussed in Chapter 2.

### 3.4.1. Objective function

The static analysis of the expected future cash flows for the underlying project lays the basis for the mathematical formulation of the objective function. The derived whole-life cost of MG 4, based on the NPC and NPV calculations, which is to be minimised, can be expressed as follows:

$$\min WLC = \left(\sum_{c\in C} NPC_c\right) + NPC_I + NPV\left(\sum_{t=1}^{8760} OC_{MG}(t)\right) + NPV\left(\sum_{t=1}^{8760} cost_{em}(t)\right) + NPV\left(\sum_{t=1}^{8760} cost_{FCEV2G}(t)\right) - NPV\left(\sum_{t=1}^{8760} income_{ex}(t)\right) + pen_{const}. \quad (3.41)$$

In the whole-life cost function adapted for application of MG system 4 in Equation 3.41, $NPC_c$ represents the NPC of the components, the optimal size of which is under investigation and are indexed by $c \in C = \{PV, WT, MH, T, E, FC, HT, BP, B, SC, S, FCEV2G\}$; $NPC_I$ denotes the NPC incurred by the inverter; $OC_{MG}$ is the operational cost of the MG to serve the unmet loads by non-dispatchable renewables, either by paying incentives for load reduction or purchasing power from the upstream grid (Equation 2.17), as defined in Equation 3.9; $cost_{em}$ is the cost imposed on the system for buying emission credits on account of running the biopower plant, as given in Equation 3.2; $cost_{FCEV2G}$ denotes the cost resulting from the provision of FCEV2G services, as expressed in Equation 3.8; $income_{ex}$ is the income generated by selling the surplus power to the main grid, as expressed in Equation 2.18; while the term $pen_{const}$ enforces the solutions to meet the constraints set out in Section 3.4.2. In this context, similar to the analyses carried out for MG systems 1–3, the useful lifespan of the project (MG 4) was considered to be 20 years and the real interest rate was set to 2.45%.

### 3.4.2. Problem constraints

As discussed in Section 2.4.2, the objective function derived above is subject to two sets of constraints at the investment planning and operational scheduling levels. The

long-term strategic investment planning-related constraints are set similarly to those of MGs 1–3. That is, the LPSP reliability metric (Equations 2.47–2.50) is employed to characterise the system performance over its projected 20-year life span (using two separate LPSP indices to evaluate the reliability of electricity and hydrogen supply), a self-sufficiency ratio is considered to ensure a pre-determined level of energy independence with respect to the utility grid (Equations 2.51 and 2.52), grid outage survivability and autonomy hour indices (Equations 2.53–2.56) guarantee the resilience of the optimal design, whilst initial and terminal constraints on the energy in store ensure the adequacy of the multi-energy-storage-technology-integrated analyses by setting the state of energy reserves in the first and last operating hours to specific values (Equations 2.57 and 2.58). Also, specific upper bounds are imposed on the maximum values the non-negative equipment design variables can take (denoted by $\{N_c^{max}\}_{\forall c}$) in compliance with the practical feasibility of the energy development plan; for example, acceptable emissions limits (from the potential biopower plant). The upper bounds constrain the overall feasible solution space for the considered case (see Equation 2.59).[7]

On the other hand, the operational scheduling-level constraints incorporate system-wide power balance (Section 3.4.2.1); constraints related to the implementation of the proposed DR scheduling market design (Section 3.4.2.2); as well as lower and upper limits on the allowable energy in store and charge/discharge power capacity of the storage media and FCEV2G units (Section 3.4.2.3). Also, non-strictly positive minimum and maximum capacity bounds are placed on the operating points of the energy generation and conversion assets (Equation 2.44), while two separate constraints enforce the product of the hourly battery/SC charging and discharging power, as well as the product of the hourly imported and exported power to be equal to zero (Equations 2.45 and 2.46). Additionally, grid power imports/exports are enforced to lie within the allowable range defined by the optimal capacity of the bi-directional transformer at the PCC (Equations 2.19 and

[7] The maximum permissible values of the design variables are aware of the rated powers of the corresponding components.

2.20). Also, unless otherwise noted, all the associated constraint values remain the same as those selected for MGs 1–3.

Moreover, in the interest of preventing the performance degradation – and mitigating the energy losses – during the start-up and shut-down cycles of the electrolyser, fuel cell, and biopower plant, a specific constraint preserves the durability of their operation. To this end, when the electrolyser, fuel cell, and biopower plant are started up, they are constrained to continue to run for at least $t_{up}$ time-steps – as a minimum up-time constraint – at operating points equal to, or greater than, the initially adjusted operating points. Accordingly, the power outputs from the fuel cell and biopower plant are treated as negative loads in the course of the MG operation on the extra hours mentioned above, whilst also being allowed to take higher operating point values if needed.

### 3.4.2.1. System-wide power balance

According to Equation 3.42, at each time-step of the system operation, the sum of all the internally generated energy components, energy releases from the storage media and FCEV2G, energy imports from the main grid, and any unmet load must be equal to the sum of the total energy consumed within the MG (to serve the loads or to charge the energy storage devices) and any power sold to the upstream grid:

$$\begin{aligned} &P_{PV}(t) + P_{WT}(t) + P_{MH}(t) + P_{BP}(t) + P_{dch}(t) + P_{FC}(t) + P_{im}(t) \\ &+ P_{FCEV2G}(t) + \frac{Q_L(t)}{\eta_I} + \frac{Q_{H_2}(t)}{\eta_S} \\ &= P_{ch}(t) + P_E(t) + P_{ex}(t) + \frac{P_L(t)}{\eta_I} + \frac{P_S(t)}{\eta_S} \quad \forall t, \end{aligned} \tag{3.42}$$

where $Q_L(t)$ and $Q_{H_2}(t)$ respectively represent the unmet electrical and hydrogen demands at time-step $t$, which are used in the LPSP calculations.

### 3.4.2.2. Demand response scheduling

As mentioned previously, under equilibrium conditions of the proposed two-stage, aggregator-mediated, market-driven DR arrangement, the constraints in Equations

3.10–3.12, 3.14, 3.15, 3.17, 3.18, and 3.20 must be relaxed. It is also assumed that the FCEVs cannot be in refuelling and V2G provisioning modes at the same time.

### 3.4.2.3. Energy storage systems and FCEV2G units

The optimisation of the MG equipment capacity must additionally adhere to a set of constraints in terms of the allowable energy in store, as well as charge/discharge rate limits of the energy storage media and FCEVs at each time-step of the MG operation (bounding the state of charge/hydrogen of the storage systems and vehicles), which could be expressed mathematically in accordance with Equations 3.43–3.45:

$$E_{es,min} \leq E_{es}(t) \leq E_{es,max} \quad \forall t, es, \tag{3.43}$$

$$P_{es}^{ch,min} \leq P_{es}^{ch}(t) \leq P_{es}^{ch,max} \quad \forall t, es, \tag{3.44}$$

$$P_{es}^{dch,min} \leq P_{es}^{dch}(t) \leq P_{es}^{dch,max} \quad \forall t, es, \tag{3.45}$$

where $E_{es}(t)$ is the energy content of the energy storage technology $es \in ES = \{B, SC, HT, FCEV\}$ at time-step $t$; $E_{es,min}$ and $E_{es,max}$ respectively denote the minimum and maximum allowable energy contents of storage technology $es$; $P_{es}^{ch}(t)$ and $P_{es}^{dch}(t)$ respectively represent the charging and discharging rates of storage technology $es$ at time-step $t$; $P_{es}^{ch,max}$ and $P_{es}^{dch,max}$ are the maximum charging and discharging rates of storage technology $es$, respectively; and $P_{es}^{ch,min}$ and $P_{es}^{dch,min}$ are the minimum charging and discharging rates of storage technology $es$, respectively.

The maximum allowable energy contents of the battery bank, SC bank, and hydrogen tank are defined by their optimal capacities at each iteration of the optimisation process, whereas the maximum total energy content of the releasable hydrogen stored in the FCEVs' tanks ($\max(P_{FCEV2G}^{max}(t)\Delta t)$ where $t \in T$) is limited by the maximum (optimal) capacity of the FCEV2G setup (as part of the hydrogen station) in addition to the level of stored hydrogen in the vehicles' tanks at time-

step $t$. That is, the variables $E_{es,max}, es \in ES$ are treated as endogenous variables in the model. Also, the same principle holds for the variables $P_{es}^{ch,max}$ and $P_{es}^{dch,max}$.

Moreover, as stated in Chapter 2, to avoid severe pressure drops in the hydrogen tank, complete releases of hydrogen are prevented by enforcing $E_{HT,max}$ not to fall short of 5% of the optimised capacity of the tank. Also, to ensure that the design pressure of the tank is not exceeded, the upper limit on the energy content of the tank is set as 95% of its optimum capacity [123].

### 3.4.3. Data: Adjusted demand response-integrated micro-grid equipment capacity planning model parameters

Table 3.3 lists the chosen data values for the parameters used to build the proposed DR-integrated MG equipment capacity-planning model.

Table 3.3: Data values for the DR-integrated MG equipment capacity planning model parameters.

| Scalar | Value | Scalar | Value |
|---|---|---|---|
| $E_{es,max}$ | (endogenous variable) | $N_{PV}^{max}$ | 20,000 |
| $E_{es-\{HT\},min}$ | 0 kWh* | $N_{SA}$ | 50 |
| $E_{HT,min}$ | (endogenous variable) | $N_{S}^{max}$ | 100 kg-$H_2$/h |
| $Iter_{max}$ | 300 | $N_{SC}^{max}$ | 10,000 |
| $LPSP_{e}^{max}$ | 0% | $N_{T}^{max}$ | 8,000 kVA |
| $LPSP_{H_2}^{max}$ | 0% | $N_{WT}^{max}$ | 15 |
| $N_{B}^{max}$ | 20,000 kWh | $P_{es}^{ch,max}$ | (endogenous variable) |
| $N_{BP}^{max}$ | 50 | $P_{es}^{ch,min}$ | $\varepsilon$† kW |
| $N_{E}^{max}$ | 1,000 | $P_{es}^{dch,max}$ | (endogenous variable) |
| $N_{FC}^{max}$ | 2,000 | $P_{es}^{dch,min}$ | $\varepsilon$† kW |
| $N_{FCEV2G}^{max}$ | 5,000 kW | $pen_{const}$ | $(1/\varepsilon$†$)$ |
| $N_{HT}^{max}$ | 50,000 kg | $t_{up}$ | 3 h |
| $N_{MH}^{max}$ | 30 | | |

* Note that the depth of discharge capability of the vanadium redox flow battery is 100% and the total energy content of the FCEVs' tanks is assumed to be aware of the specific level of hydrogen expected (desired) by each FCEV owner at the scheduled departure time.

† The symbol $\varepsilon$ denotes a small positive infinitesimal quantity.

### 3.4.4. Overview of the proposed solution algorithm

The flowchart of the proposed MG equipment capacity-planning model, which integrates the proposed two-stage, aggregator-mediated market-driven DR model to realistically project the customer engagement in incentive-based DR programmes – based on an economically stable allocation of the profits generated from interruptible load programmes between the sole energy service provider, DSM aggregators, and end-users – is presented in Fig. 3.13. As can be seen from the figure, the solution algorithm integrates the proposed DR provision framework (the yellow block) and applies the developed rule-based hourly-basis operational scheduling strategy (the light coral block), while taking an iterative approach to optimise the total discounted MG investment cost function, which determines the respective size of the equipment (the blue blocks).

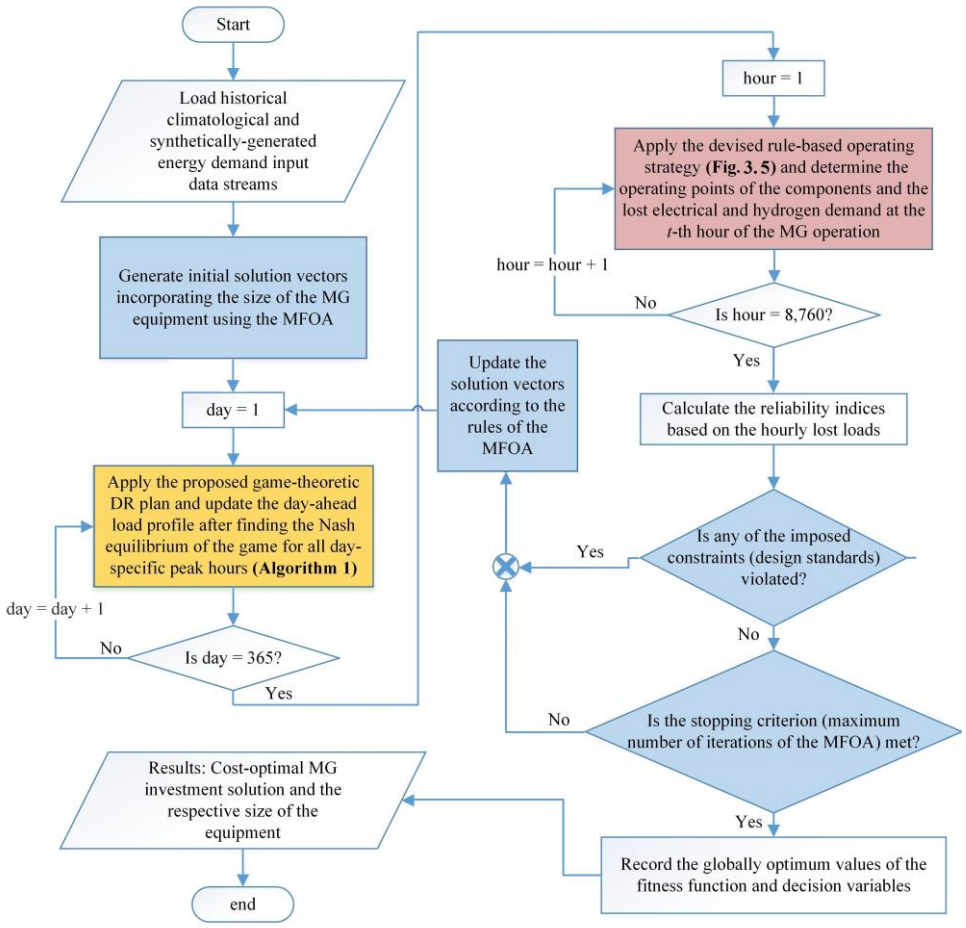


Figure 3.13: Flowchart of the proposed Stackelberg, non-cooperative game-theoretic DR-integrated approach for the optimal capacity planning of MGs.

Furthermore, the step-wise representation of the integrated simulation procedure to optimally design the conceptualised MG while managing the DR resources using the proposed DR scheduling approach is summarised in Fig. 3.14. Following the procurement and pre-processing of the input data, the model is built up in a multi-layered structure, which consists of (from bottom to top): (1) a rule-based hourly energy scheduling strategy, (2) a two-stage, aggregator-mediated, DSM market design to arrange the delivery of the DR resources on a day-ahead basis, (3) various constraints the objective function is subjected to, and (4) the derived fitness function representing the whole-life cost of the system, which is to be optimised using the MFOA.

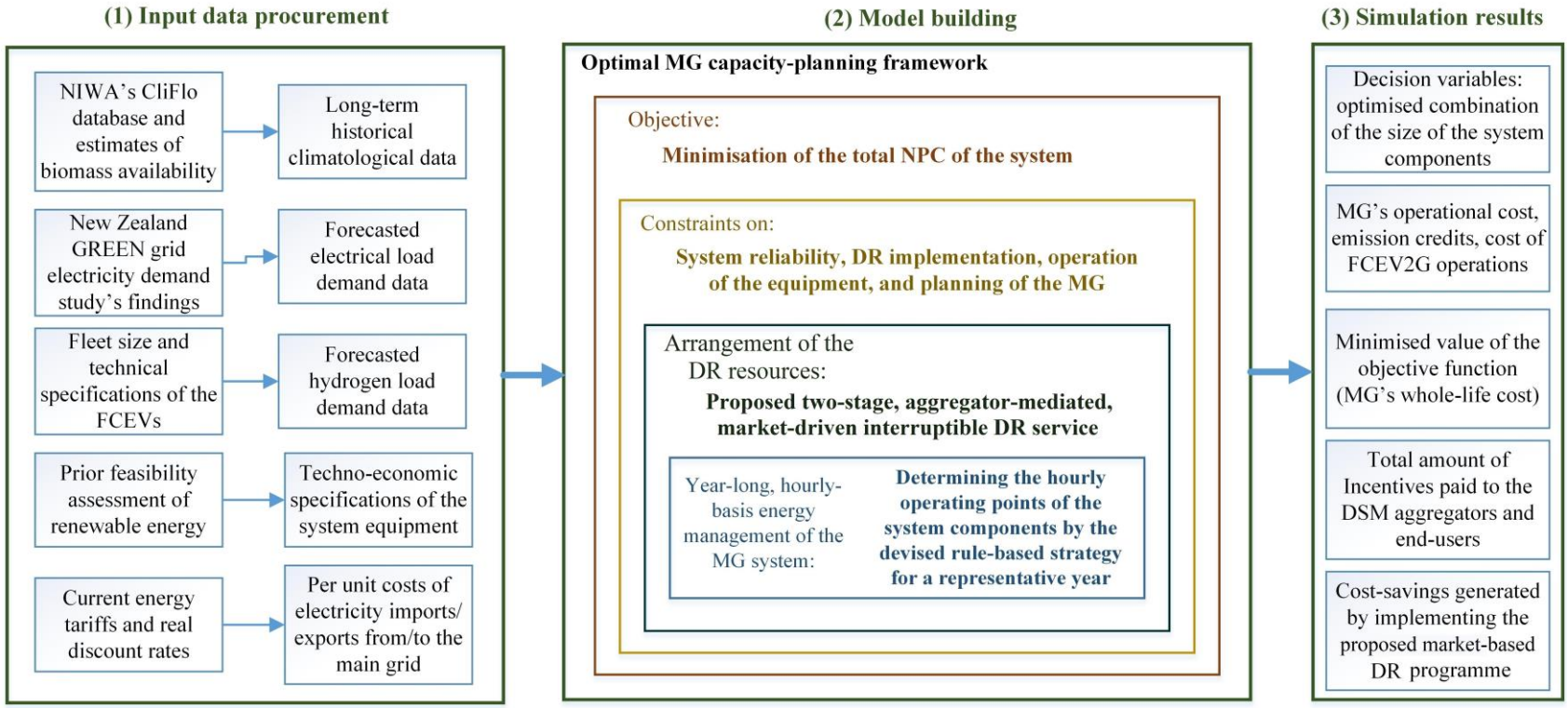


Figure 3.14: Diagrammatic representation of the step-wise procedure for implementing the proposed optimal MG planning framework.

## 3.5. Case study

To demonstrate the effectiveness of the proposed Stackelberg, non-cooperative game-theoretic approach to optimally dispatch distributed sectoral DR resources, as well as its utility in reducing MG development capital costs when integrated into business-case analyses, a case study is carried out for the town of Ohakune, in New Zealand (latitude 39.4180°S, longitude 175.3985°E). Located in the central part of the North Island of New Zealand, Ohakune is a gateway to the Turoa Ski Area and is known as the 'snow season' capital of the North Island. It is also known as the 'Carrot Capital' of the country. As of 2019, it has a permanent population of around 1,000 inhabitants, which swells to 7,000–10,000 people during the winter ski season [252]. As a result of this, and the fact that a substantial part of the electrical demand on its distribution network is for low-temperature heating purposes, the load power on the town's distribution network is subject to a considerable degree of seasonality. Presently, the electricity demand of the town is supplied through a distribution network, the power input to which is entirely supplied by the national grid. However, the residential community in the town has consistently suffered from excessive bills in the wintertime, which is induced by the capacity deficit of the transmission line/transformer connecting the local distribution network to the national grid due to congestion.

In response, the conceptualised MG 4 is a resilient energy system that can provide democratic energy independence, whilst protecting the natural environmental resources of the region. Furthermore, the town is rich in renewable energy resources, both dispatchable and non-dispatchable: it has vast and unexploited solar potential with a total average of about 1,400 kWh/$m^2$-year [167], large untapped resources of wind (with a yearly average wind speed of around 6 m/s at a height of 10 m [167]) and MH power from the Mangawhero River (which has a yearly average streamflow of 2.9 $m^3$/s [253]), as well as high levels of high-quality biomass (coming not only from discarded carrot crop, but also from indigenous forests in the form of foliage and woody biomass). It must be noted that there is no opportunity for pumped hydropower in the target site's energy mix due to its failure to meet the criteria in place as part of the New Zealand's National

Water Conservation Order 1988 to assure minimal environmental impact of storage on the overall river flow. Accordingly, the notional MG system 4 proposed in this study is populated to decarbonise the energy economy of the town of Ohakune [252].

### 3.5.1. Micro-grid business model

The grid-connected community MG system, which is set to reduce the cost of energy and provide more reliable energy from RESs, is assumed to be financed by the EaaS business model. The EaaS business model provides a flexible ownership platform, which allows end-consumers, utilities, and other financing partners to strategically collaborate and capitalise on the system [254]. However, it was decided to make a simplification of the single ownership structure, where a third party (an energy service company) – with enough experience, knowledge and financial resources – designs, builds, operates, owns, and maintains the renewables-based MG to serve different electrical load classes and charges a fee in exchange for its service. The energy tariffs are assumed to be fixed and not reflective of wholesale electricity prices. However, the end-consumers are offered financial incentives for reducing their energy use during the critical coincident peak time-steps – where the net load on the MG is positive and wholesale prices are high – in accordance with the proposed dual-loop aggregator-mediated DSM market design.

### 3.5.2. Meteorological input data

To forecast the climate-related input data, the NIWA National Climate Database (CliFlo) [167] was used and historical records (over a 20-year period, between 1999 and 2018) of the average solar irradiance, ambient temperature, wind speed, and the Mangawhero River's streamflow were collected in hourly (average) intervals. Since the wind speed data were measured at the height of 10 m, they were normalised to the selected WT's hub height using Equation 2.1. The forecasted hourly-basis, year-long climatic input data streams, are presented as monthly mean 24-h profiles in 3D plots in Fig. 3.15. Also, to forecast the profile of the available biomass over the year, it is assumed that around 15,000 tonnes of discarded carrots are available per year with peaks in late spring and fall, and 1,500 tonnes of forest biomass per month

are ready to be collected or harvested from the native forests. The forecasted monthly averaged profile for biomass availability is shown in Fig. 3.16, assuming that the amount of monthly available biomass is evenly distributed over the days of the months [255], [256].

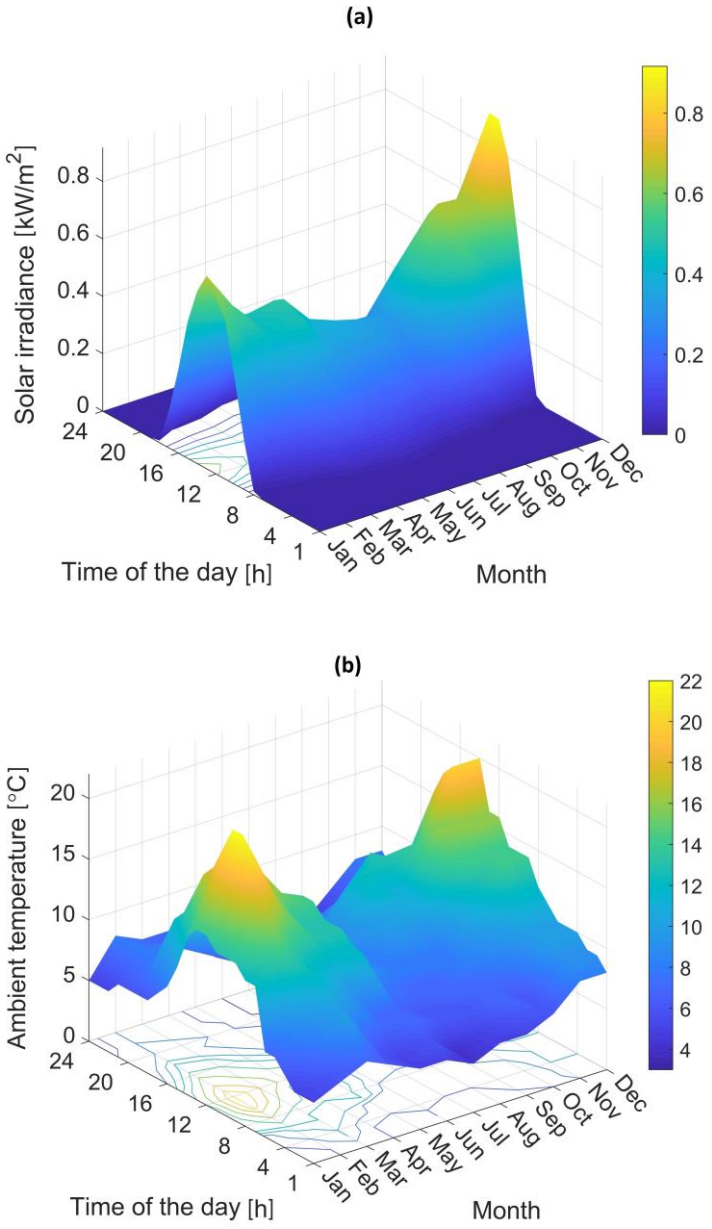

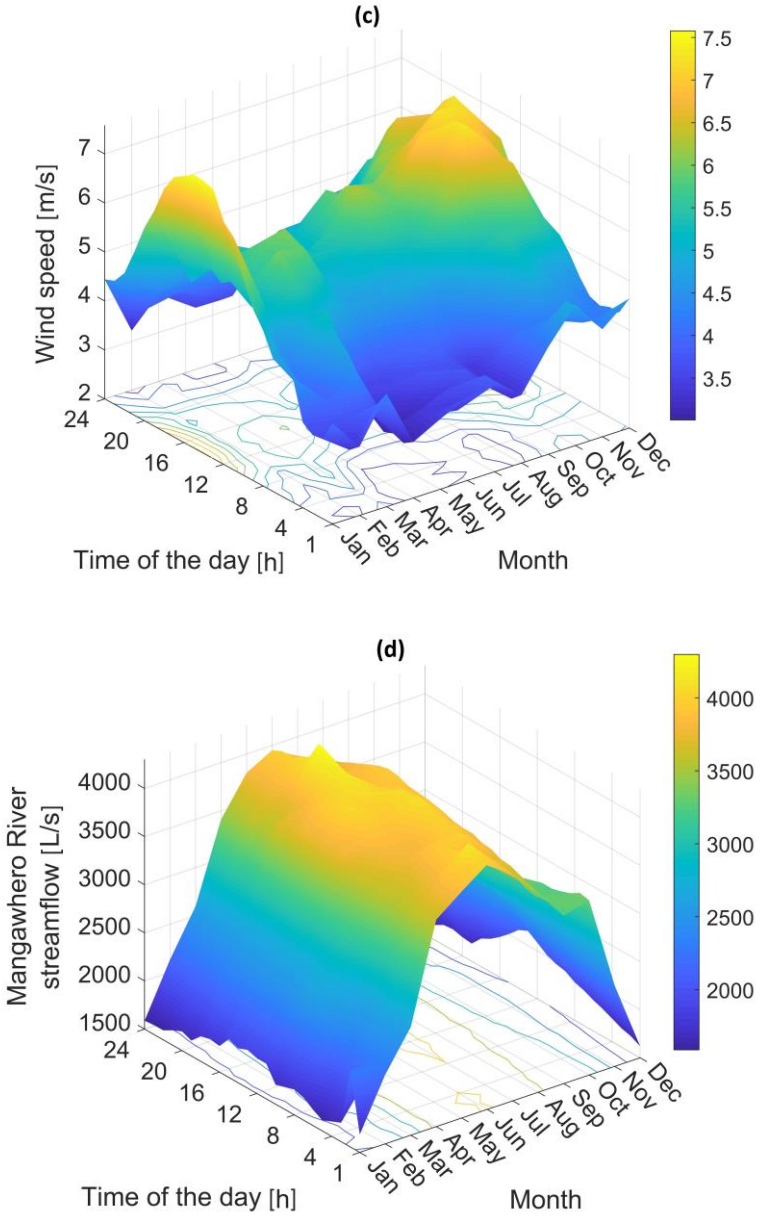


Figure 3.15: CliFlo-compliant forecasted meteorological input data (at an hourly resolution) for Ohakune, New Zealand: (a) solar irradiance; (b) ambient temperature; (c) wind speed; and (d) streamflow.

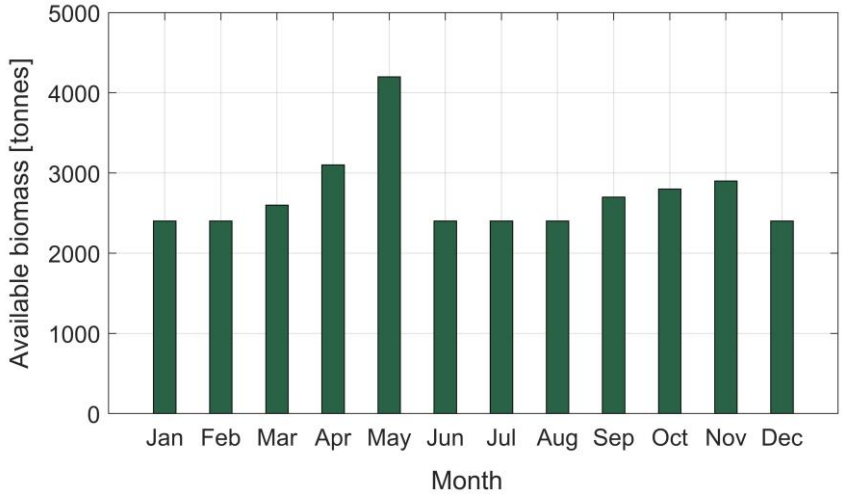


Figure 3.16: Monthly mean profile for the estimated total biomass available per month at the site: Ohakune, New Zealand.

#### 3.5.2.1. Extreme day non-dispatchable generation data

In Section 3.6 (*Simulation results and discussion*), before analysing the impact of the integration of the proposed DSM market design into the meta-heuristic-based MG sizing model, day-ahead energy management scenario testing is conducted for a representative day (24 h at hourly intervals) of the winter and summer seasons, where the one-day total energy consumption is assumed to be highest and lowest, respectively.[8]

Accordingly, any net energy deficits during normal grid-connected operations need to be addressed by an optimal combination of imported power and curtailed loads. Such an optimal trade-off solution at event-driven, system-wide critical peak time-steps (where supply-demand mismatches are present) can be produced by applying the proposed game-theoretic DR-integrated day-ahead MG energy management framework. The indicative day-ahead operational scheduling scenario testing analyses are carried out in accordance with the optimal size of non-dispatchable generation technologies yielded as the ultimate solution. That is, the optimum size of the MG equipment is assumed to be known from posterior game-

[8] For the purposes of this study, winter is defined between the 1st of June and the 31st of August, while summer is defined between the 1st of December and the 28th of February. Accordingly, as a simplifying assumption, leap days are not factored in.

theoretic sectoral DR-integrated strategic design optimisation analyses. Accordingly, this section presents power output profiles for the solar PV, WT, and MH generation systems, which are determined based on the associated forecasted meteorological data (hourly solar irradiance, ambient temperature, wind speed, and river streamflow) using the corresponding equations provided in Chapter 2 for solar PV and MH technologies, as well as the associated power curve for the WT technology.

Fig. 3.17 displays the forecasted power outputs from the onsite PV, WT, and MH power plants for the representative extreme days of the summer and winter seasons – on which the lowest and highest one-day total demands are expected to occur.

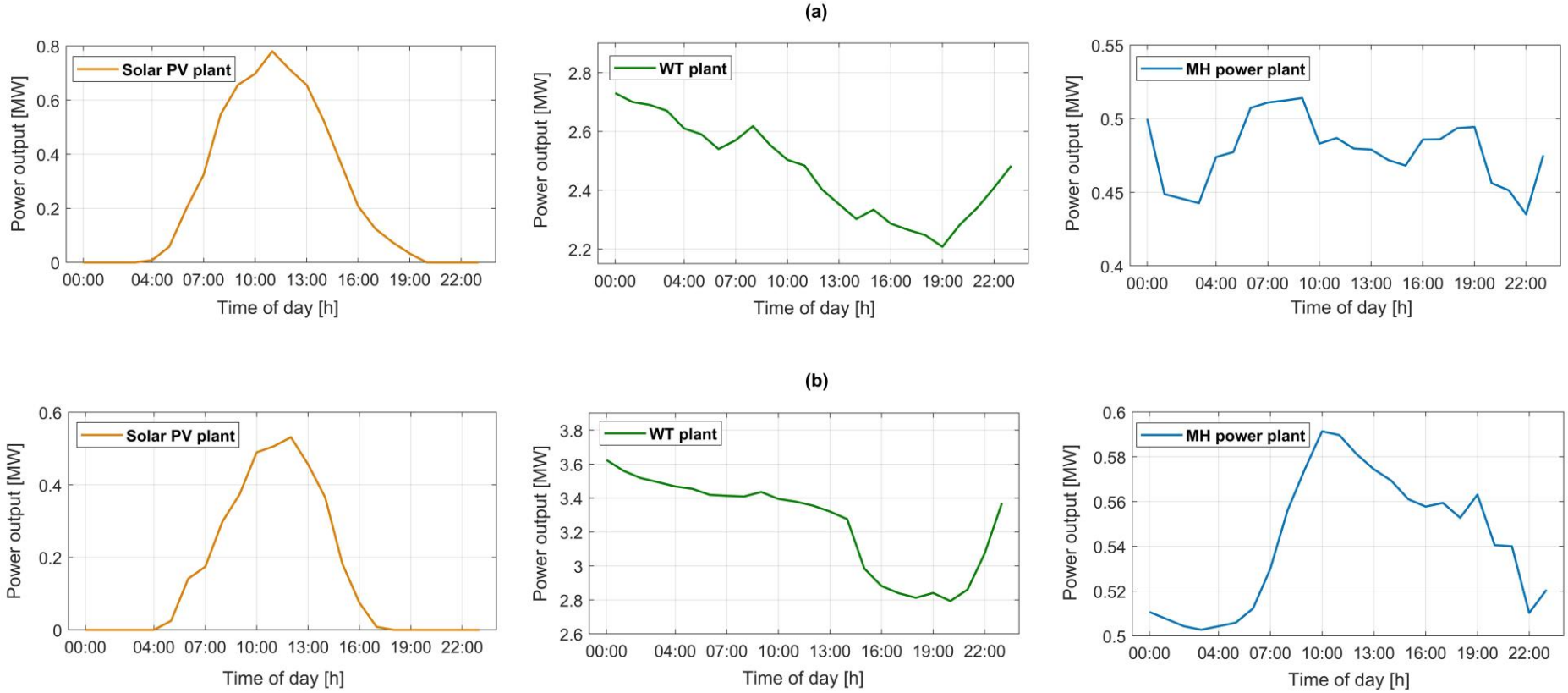


Figure 3.17: Power outputs from the PV, WT, and MH power plants for the representative day of: (a) summer; and (b) winter.

### 3.5.3. Load demand input data

To forecast the total sectoral loads on the MG (excluding the FCEV-refuelling demand), first, the mean yearly peak load demand was determined based on the historical demand data [257]. The forecasted total annual peak demand was then broken down by the residential, commercial, industrial, and agricultural sectors in accordance with the New Zealand's Ministry of Business, Innovation and Employment's (MBIE's) most recent energy statistics [258]. Then, the forecasted annual residential peak demand was used to derive year-long, hourly-basis residential load profiles based on the findings of the New Zealand GREEN grid household electricity demand study [168] on the power usage per person and household size distributions in New Zealand to shape the primary profile for electricity consumption based on the town's synthetically estimated population of permanent residents (in accordance with the above-mentioned share of residential loads in the total yearly peak load), fixed at 1,000 people, which was then adjusted for the electricity consumption of the assumed number of seasonal ski tourists (7,000 people) [259]. Also, the season-wise typical annual consumption patterns of electricity in Ohakune, derived from real demand profiles (from substations), were used to shape the year-long, hourly-basis load profiles of the commercial (including the Turoa Ski-Field), agricultural, and industrial sectors [257].

Also, in line with the goals of decarbonising the transport sector, a fleet of 180 light-duty personal passenger vehicles is planned for integration into the envisioned system through the coordinated use of the refuelling infrastructure. To derive the e-mobility load profile, the EU-funded Green eMotion project dataset [260] was used as a proxy for New Zealand uptake. Accordingly, the real-driving energy consumption of a typical A-segment, small-sized EV was considered to be 257 Wh/km, while accounting for the fact that the median winter energy consumption per km is higher than the median summer consumption by 40%. The scaled e-mobility energy consumption data were then put into a New Zealand context in accordance with the estimated total energy consumption and typical daily consumption pattern of a fleet of 45 Nissan Leafs monitored by the Flip the Fleet project in New Zealand [261]. Moreover, the amount of driving done per driver was assumed to be 29 km/day, in accordance with New Zealand's household travel

survey [262]. Also, considering a maximum waiting time of 10 minutes in the queuing theory, discussed in Section 3.5.3, and a refuelling time of 3 minutes for the empty tank of an FCEV, a hydrogen demand profile was shaped for the planned fleet of 180 vehicles. More specifically, the profile was generated stochastically by pseudo-randomly assigning the vehicles to different trip levels and assuming that they arrive at the station following an hour-specific normal distribution between the hours of 8 a.m. and 10 p.m. with stochastic levels of the stored hydrogen. Accordingly, vehicles are assumed to be refuelled on a first-come/first-served basis using the multi-server Erlang-C queuing model [125], where C identifies the optimal number of dispensers.

The forecasted one-year, hourly average load power demand on the system, which is represented as a monthly mean 24-h profile for greater clarity, is shown in a 3D plot in Fig. 3.18 (a). Also, the forecasted monthly mean 24-h profile for the hydrogen demand of the refuelling station – considering the seasonal variation in demands for transportation fuel as suggested in [263] – is shown in a 3D plot in Fig. 3.18 (b).

It is also noteworthy that energy demand projections are in line with the New Zealand government's aspirations of electrifying transport to help meet its target of net-zero GHG emissions by 2050, as well as the recent government-funded 'Warmer Kiwi Homes' programme offering up to 90% heat pump grants to low-income home owners. Specifically, the penetration levels of light-duty FCEVs and heat pumps were assumed to be 40% and 60%, respectively at the time of commitment. Accordingly, smart charging of FCEVs and control of heat pump demand is of utmost importance to smooth and manage the overall load during peak periods.

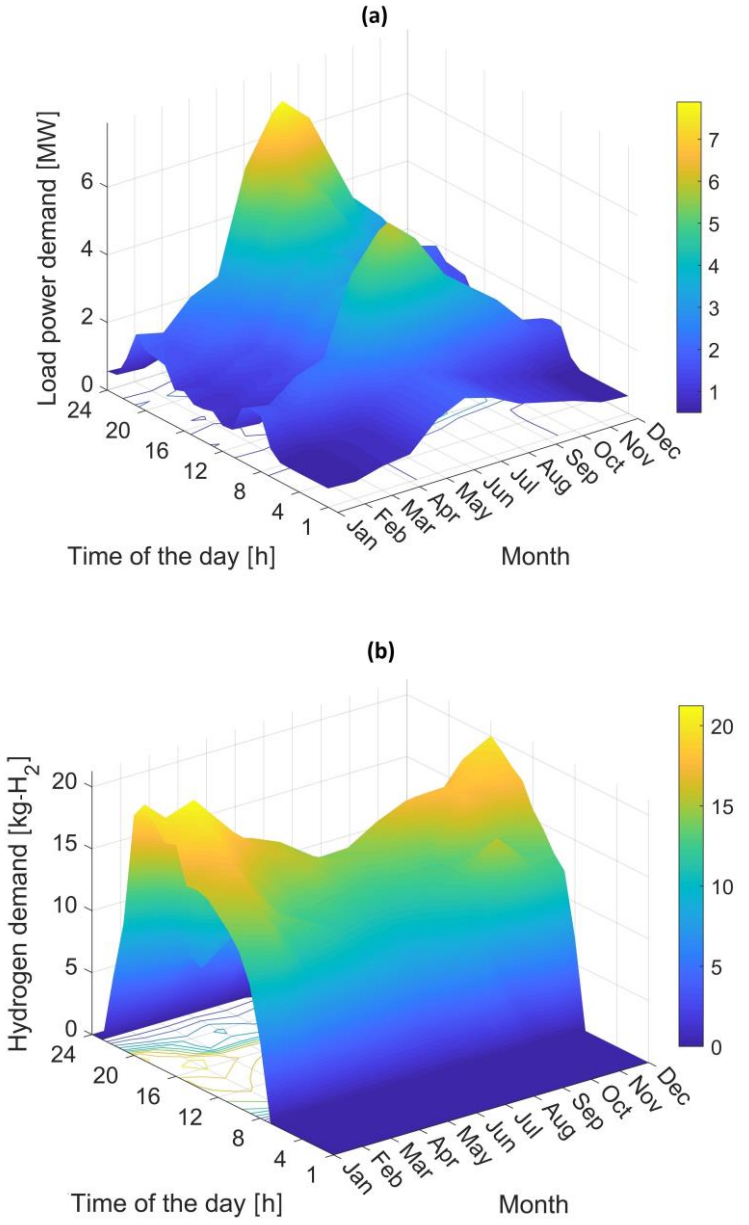


Figure 3.18: Forecasted monthly mean 24-h profiles for the energy demand of the town Ohakune: (a) load power demand; and (b) hydrogen demand.

### 3.5.3.1. Extreme day load demand data

It is assumed that the total sectoral demand forecasts are available for each hourly time-step of the above-mentioned extreme-day case examples in accordance with the year-long, hourly-basis load demand profile. Fig. 3.19 shows the hourly total sectoral load demand on the MG for the two representative extreme days of the summer and winter seasons. As illustrated above, the forecasted residential load

power profile for Ohakune is associated with a substantial growth in the demand for electricity during the wintertime as it covers the effect of seasonal variation in load demand due to the presence of skiers. That is, demand for electricity in the town of Ohakune peaks in winter with the highest daily electricity consumption occurring during the evening peak period [257].

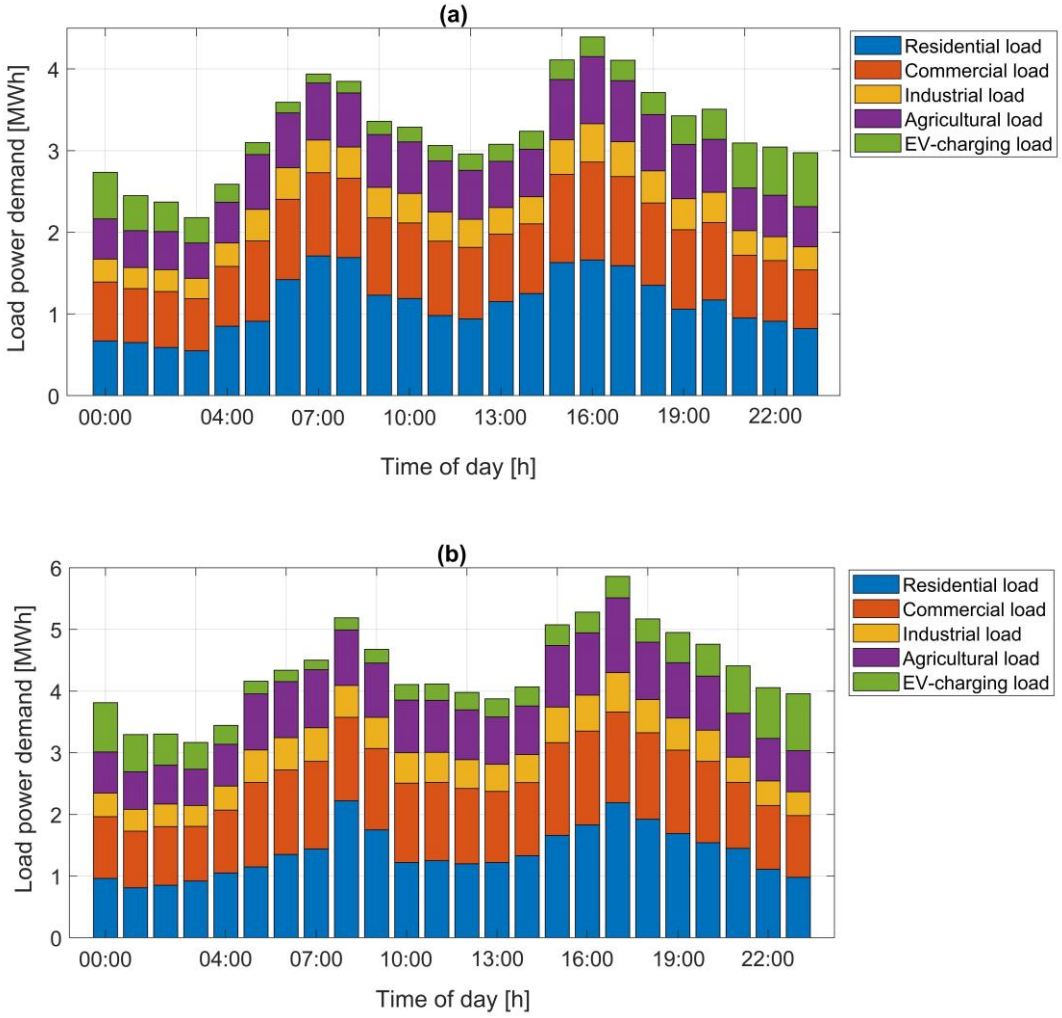


Figure 3.19: Forecasted hourly total sectoral load power demand on the Ohakune's distribution system for the representative day of: (a) summer; and (b) winter.

### 3.5.3.2. System-level demand response dispatch game data

This study is based on a synthesised district of 250 detached houses, a total of 65 small-to-medium commercial buildings and sites, a total of 10 medium-scale industrial facilities, a total of 55 large-scale irrigation systems, as well as a fleet of

180 FCEVs – in pursuit of transitioning the town's light vehicle fleet to low-emissions.[9] Accordingly, the forecasted sector-wise total load demands are disaggregated into individual customers. To this end, the DR capacity of the electrical loads are specifically parametrised by $\delta_j$, $c_1^{k,j}$, $c_2^{k,j}$, $d_{full}^{k,j}$, $d_{ncr}^{k,j}$, $Par_{max}^{j}$, and $N_{cust}^{j}$, while employing the disaggregation algorithm presented in Section 3.3.2.1.3.1.

Data values for load type-specific and individual-level load demand parameters mentioned above were not readily available and had to be estimated based on the corresponding information available. The values of $\delta_j$ for residential, commercial, industrial, and agricultural loads were set according to the mean of the corresponding values of lost load in a New Zealand context [264], while for the FCEV-refuelling loads, they were set based on the mean of the values of lost load for a fleet of plug-in EVs reported in [265]. The range of values the parameters $c_1^{k,j}$ and $c_2^{k,j}$ can take were chosen based on the values reported in [266], [267] for different load types, which were normalised to the load type-dependent DR procurement factors ($\delta_j$) in an inversely proportional manner. Furthermore, in view of the lack of reliable data for a New Zealand context, relevant data for 11 large U.S. utilities [268] were adopted to adjust the values of $Par_{max}^{j}$ for residential, commercial, industrial, and agricultural loads, while the value of this parameter was taken from [269] for FCEV-refuelling loads. Table 3.4 lists data values and sources for the proposed game-theoretic, two-stage, aggregator-mediated, incentive-based DR scheduling model parameters.

[9] For the sake of simplification, the entire FCEV-refuelling load demand is assumed to be served through the dedicated FCEV charging station.

Table 3.4: Data values and assumption sources for the DR capacity of different customer classes participating in the two-stage, aggregator-mediated, incentive-based DSM framework.

| Parameter | | Aggregator | | | | |
|---|---|---|---|---|---|---|
| | | **Residential** | **Commercial** | **Industrial** | **Agricultural** | **FCEV-refuelling** |
| $\delta_j^*$ | Value | 0.48 | 0.51 | 0.57 | 0.63 | 0.76 |
| | Source | [264] | [264] | [264] | [264] | [265] |
| $c_1^{k,j}$ [\$/kWh$^2$] | Range | [1.08×10$^{-3}$, 1.15×10$^{-3}$] | [1.04×10$^{-3}$, 1.07×10$^{-3}$] | [0.99×10$^{-3}$, 1.03×10$^{-3}$] | [0.95×10$^{-3}$, 0.98×10$^{-3}$] | [0.91×10$^{-3}$, 0.94×10$^{-3}$] |
| | Source$^\dagger$ | [266], [267] | [266], [267] | [266], [267] | [266], [267] | [266], [267] |
| $c_2^{k,j}$ [\$/kWh] | Range | [11.49×10$^{-3}$, 11.70×10$^{-3}$] | [11.31×10$^{-3}$, 11.48×10$^{-3}$] | [11.71×10$^{-3}$, 11.86×10$^{-3}$] | [11.25×10$^{-3}$, 11.30×10$^{-3}$] | [11.40×10$^{-3}$, 11.57×10$^{-3}$] |
| | Source$^\dagger$ | [266], [267] | [266], [267] | [266], [267] | [266], [267] | [266], [267] |
| $d_{full}^{k,j}$ [kWh] | Range | [8, 30] | [20, 100] | [100, 200] | [30, 65] | [5, 30] |
| | Source | (this study) | (this study) | (this study) | (this study) | (this study) |
| $d_{ncr}^{k,j}$ [kWh] | Range | [2.5, 16.5] | [5, 60] | [20, 84] | [10, 46.2] | [4, 25.5] |
| | Source | (this study) | (this study) | (this study) | (this study) | (this study) |
| $Par_{max}^{j}$ [%] | Value | 55 | 60 | 42 | 71 | 85 |
| | Source | [268] | [268] | [268] | [268] | [269] |
| $N_{cust}^{j}$ | Value(s) | 250 | 65 | 10 | 55 | {1, 2, …, 180}$^\ddagger$ |
| | Source | (this study) | (this study) | (this study) | (this study) | (this study) |

$^*$ The load type-dependent DR procurement factor (sectoral elasticity of customer-supplied DR capacity) for the residential, commercial, industrial, and agricultural loads (normalised to the range [0, 1]) were adjusted in proportion with the weighted average values of unserved energy for various durations of interruption in a New Zealand context [270], while this factor for the FCEV-refuelling load was adjusted based on the plug-in EVs' value of lost load reported in [265].

$^\dagger$ The range of values the discomfort tolerance coefficients of customers can take were arbitrarily selected. Yet, the chosen values were guided by those used in [266], [267] for the customer outage cost function coefficients for the relevant customer categories. Additionally, the range of sector-wide customer discomfort tolerance coefficients was normalised with respect to the corresponding load type-dependent DR procurement factor (in an inversely proportional manner).

$^\ddagger$ Since the number of FCEVs that utilise the station varies with the time of day, it was modelled as a range of possible scenarios; i.e., the number of vehicles.

### 3.5.4. Wholesale electricity price input data

Similar to Feilding and Totarabank, Ohakune is located in central North Island. Accordingly, the forecasted hourly-basis (hourly average), year-long wholesale electricity price input data stream, $\pi_{im}(t)$, obtained using the weighted average method, shown as a monthly averaged daily profile in Fig. 2.19, can be used for this case study as well.

#### 3.5.4.1. Extreme day wholesale electricity price data

Wholesale electricity market prices for the two representative extreme days are provided in Fig. 3.20. The figure presents the weighted average of the electricity price for each hour of the historical days on which the lowest and highest one-day total demands were recorded, during the timeframe of 2008 to 2019. To this end, historical nodal electricity price data at the Ohakune's grid exit point were retrieved from the New Zealand's electricity market database [169].

Note that although wholesale electricity prices are high during the morning peak hours of the representative days, higher levels of total power generation from onsite DERs – and, particularly, WTs – offset, to a considerable extent, the need to implement a DR programme during these hours. Also note that given that hydropower is the dominant source of power generation in New Zealand's energy mix, spot electricity prices are higher during the summer season in most regions of New Zealand, including Ohakune.[10]

[10] The reason for this is the more reliance on thermal electricity generation and natural gas- and coal-fired 'peaker' power plants during the dryer season.

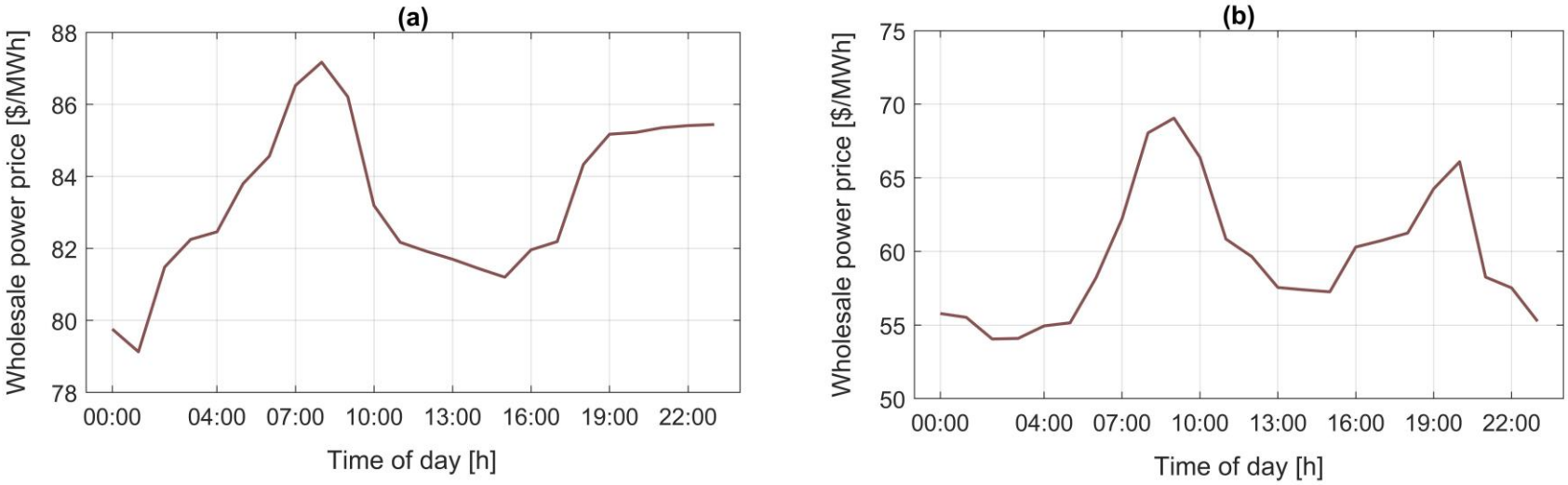


Figure 3.20: Forecasted nodal wholesale electricity price data at the Ohakune's grid exit point for the representative day of: (a) summer; and (b) winter.

## 3.6. Simulation results and discussion

To confirm the proposition put forward in Chapter 1 on the effectiveness of integrating the developed DR management framework into the standard meta-heuristic-based MG capacity planning approach, as well as the viability of the conceptual test-case MG system 4, laid out in Section 3.2, this section presents and discusses the results of the case study analysis conducted for the town of Ohakune, New Zealand. The section begins with in-depth extreme scenario testing-based impact analyses of the application of the proposed day-ahead DSM planning framework to MG 4 populated for the case of Ohakune. More specifically, to validate the feasibility and utility of the proposed dual-loop, Stackelberg, strategic game-theoretic DR scheduling framework in producing the best compromise between the imported power and utilised DR capacity on the day-ahead timeframe, two extreme scenarios are tested, with the representative extreme summer and winter days discussed in Section 3.5. Subsequently, the discomfort costs and revenues of end-consumers, the profits of DRAs, and the utility of the MG operator are presented and analysed for the two scenarios. Specifically, the efficacy of the proposed distributed algorithm to determine the unique, pure-strategy Nash equilibrium of the aggregator-mediated DSM game is verified in Section 3.6.1; the financial balance assessment of the devised game structure is conducted in Section 3.6.2; and the incentive compatibility[11] of the proposed DR scheduling design is demonstrated in Section 3.6.3.

The section proceeds by confirming the validity of the model through a direct descriptive statistics-based comparison of the extreme-case model results with those of a BAU, non-game-theoretic variant of the interruptible DR scheduling framework for a year-long operation of the MG system in Section 3.6.4. Then, the economic viability of integrating the developed DSM strategies into the long-term MG investment decision-making processes is benchmarked in Section 3.6.5 against two counterpart cases where: (1) the DSM market is cleared without employing

[11] Put simply, a mechanism is said to be incentive-compatible (truthfully implementable) in the context of mechanism design, if every player can attain the best outcome possible by behaving in accordance with their true preferences [192].

ideas from non-cooperative game theory for interactive decision-making regarding the practical capacity of DR resources, and (2) no provision is made to employ the responsive loads as a backup resource in the proposed MG system. Finally, in-depth economic viability analyses in Section 3.6.6 demonstrate the economic sustainability of the proposed renewable energy project.

### 3.6.1. Scenario analysis

As comprehensively discussed in Section 3.3, the proposed Stackelberg, non-cooperative game-theoretic DR scheduling framework is applied on a day-ahead basis and relies on the forecasts of non-dispatchable renewables, wholesale prices, and load demand, based on which financial incentives are posted to the wholesale DSM market by the MG operator for potential load reduction. Accordingly, to demonstrate the model behaviour, the process of procuring DR provisions is illustrated by two representative extreme-day scenarios for the summer and winter seasons, where the MG loading levels are lowest and highest, respectively. More specifically, the two days that represent the most intense peak and trough on the year-round, mean daily load profile (consisting of the mean of the load power demand forecasts for 24 equidistant times in the course of each continuous 24-hour period of the representative year), namely July 21$^{st}$ and February 14$^{th}$, were chosen for scenario analyses. Such seasonality of the load demand on the system can be explained by the New Zealand GREEN grid household electricity demand study [168], according to which low-temperature heat is the main (~46%) use of household energy in New Zealand, providing space heat (~27%) and water heat (~19%).

The convergence process of the proposed iterative distributed algorithm (described in Section 3.3.2.3) to the unique, pure-strategy Nash equilibrium of the devised dual-loop, platform DSM market game is depicted in Fig. 3.21 for the hours of the two representative extreme-case summer and winter days at which interruptible DR resources are called to be elicited. Also, the contribution of load power demand reduction and imported electricity from the main grid at the hours of these two extreme days at which there is a shortfall in onsite power generation capacity to meet the load on the MG is detailed in Fig. 3.22. The figure also shows

the sector-wise unreleased DR capacity to suggest the validity of the model results in terms of producing optimal trade-offs between importing electricity and harnessing the capacity of DR resources, whilst adhering to the quality of service desired by different customer classes. As can be seen in the figure, the highest daily rate of DR execution on the extreme-case summer and winter days is expected to occur at 5 p.m. and 6 p.m., respectively, which can be characterised as the "daily most critical peak hour". Moreover, to provide a more in-depth understanding of the iterative incentive coordination mechanism, a breakdown of the optimised operational cost of the MG at the most critical peak hour of each representative day – to offset the anticipated power supply deficit (refer to Equation 3.9) – into incentive payments and cost of purchasing power from the main grid against various rates of utility-provided financial incentives, is summarised in Fig. 3.23. Furthermore, a closed-form solution to the optimal incentive rate from the utility's perspective for the two daily most critical peak hours can be obtained using Equation 3.40. Accordingly, the analytically-calculated optimal incentive rates offered by the utility to the load aggregators at the considered hours are presented in Fig. 3.24.

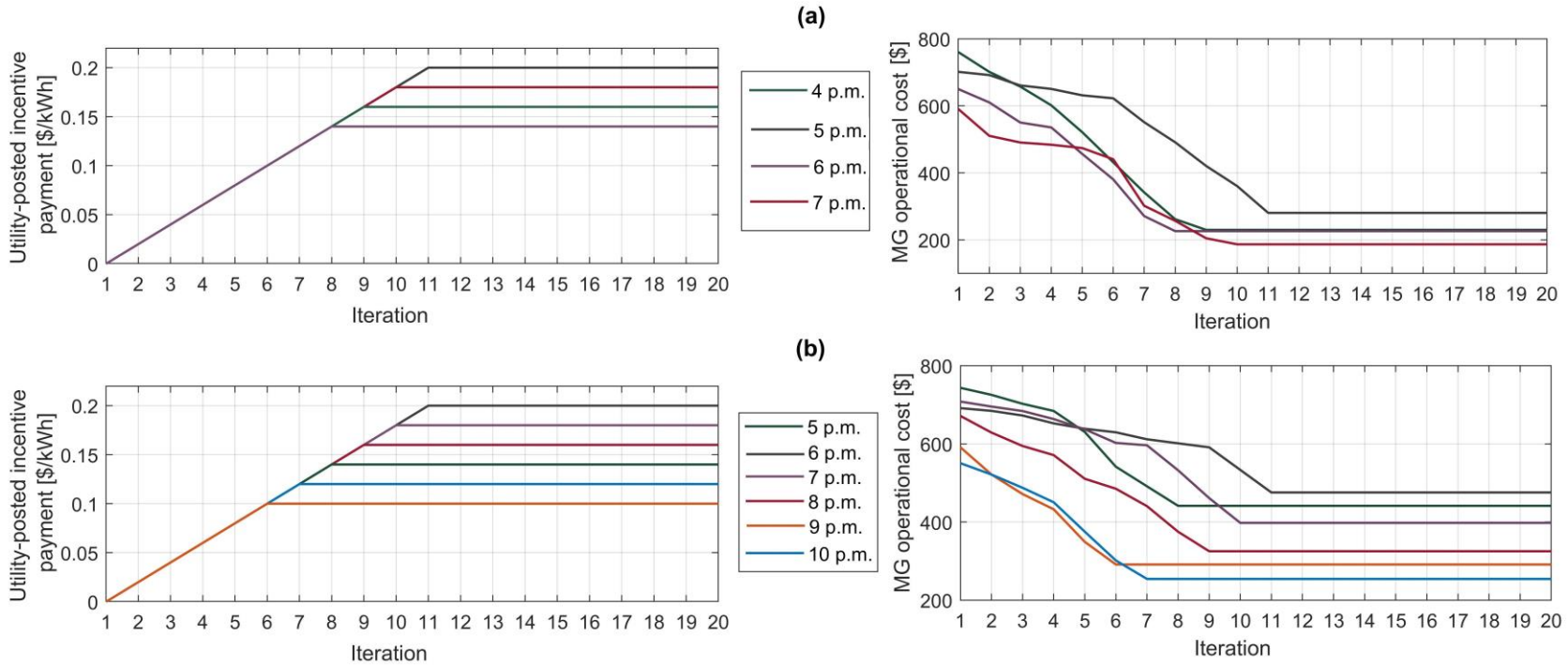


Figure 3.21: Convergence process of the distributed algorithm developed to determine the unique, pure-strategy Nash equilibrium of the proposed game-theoretic DR framework on the representative days: (a) summer day (February 14$^{th}$); and (b) winter day (July 21$^{st}$).

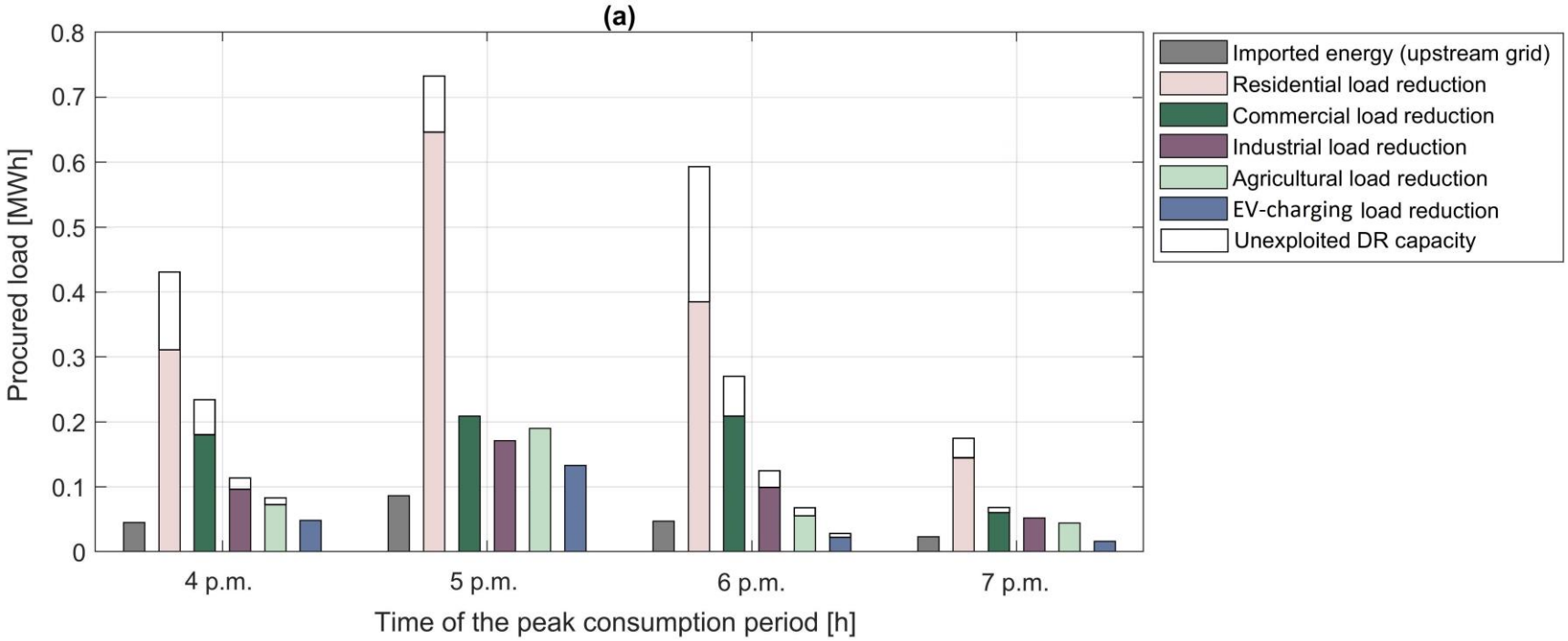
(a)
Procured load [MWh]
0.8
0.7
0.6
0.5
0.4
0.3
0.2
0.1
0
4 p.m.
5 p.m.
6 p.m.
7 p.m.
Time of the peak consumption period [h]
Imported energy (upstream grid)
Residential load reduction
Commercial load reduction
Industrial load reduction
Agricultural load reduction
EV-charging load reduction
Unexploited DR capacity

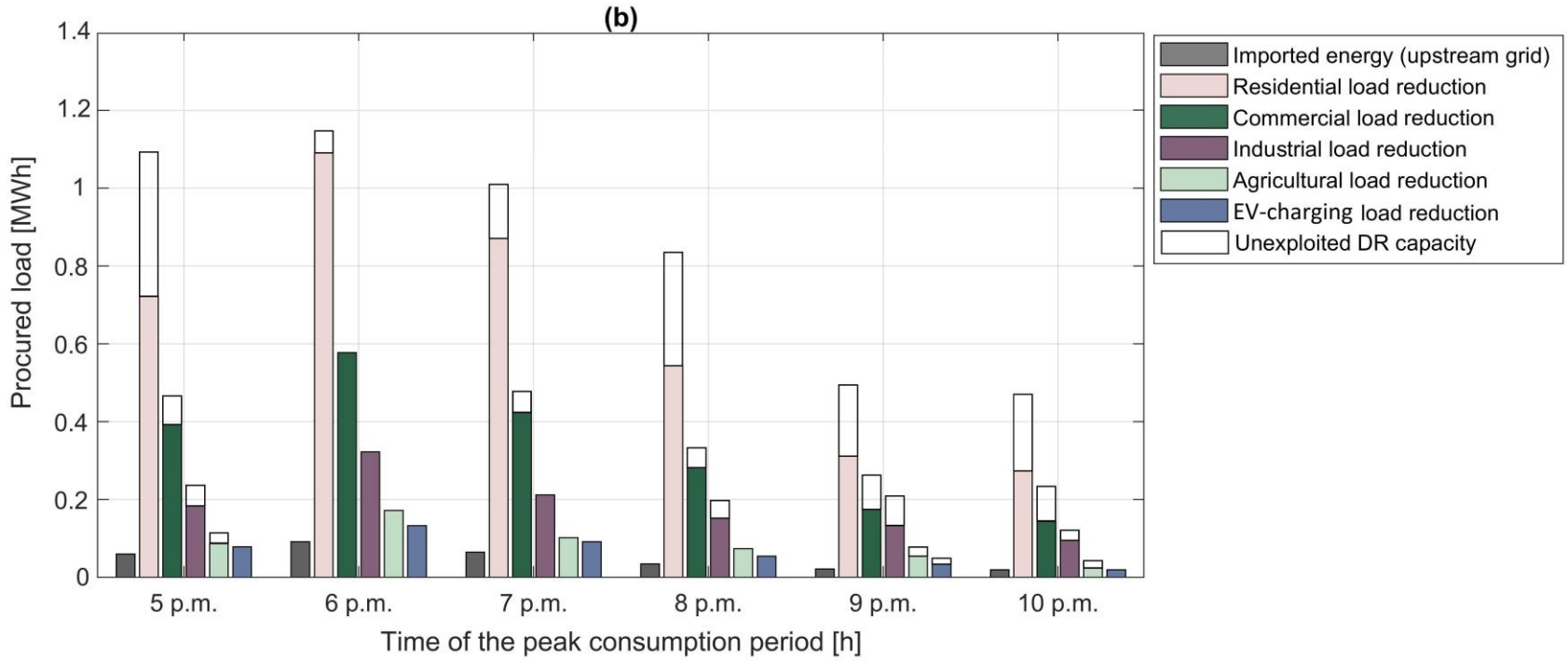


Figure 3.22: Breakdown of the contribution of demand reduction and imported electricity from the main grid in the face of onsite generation capacity deficits on the representative days: (a) summer day (February 14$^{th}$); and (b) winter day (July 21$^{st}$).

Note the change in scale in the dependent axes.

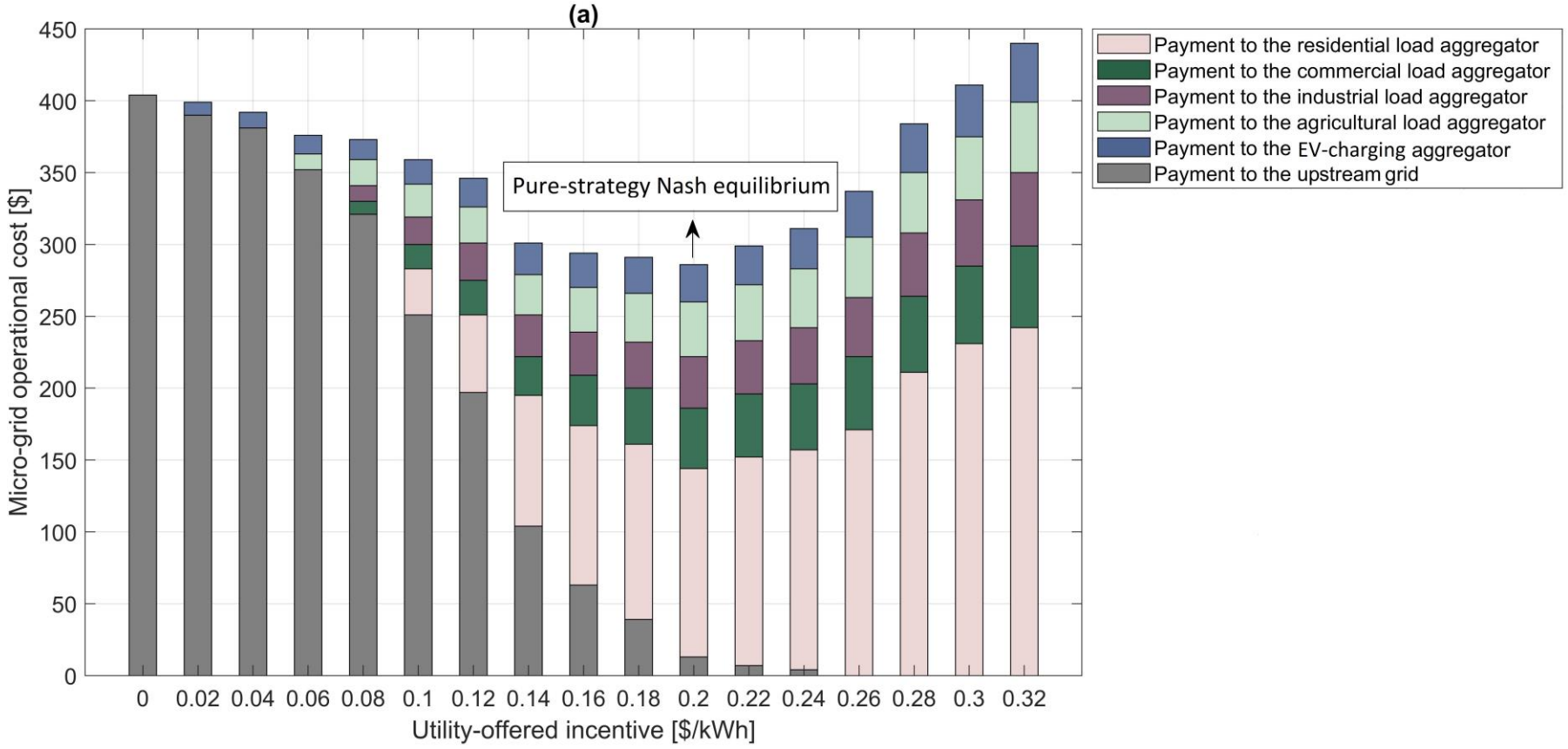
(a)
Micro-grid operational cost [$]
Utility-offered incentive [$/kWh]
Pure-strategy Nash equilibrium
Payment to the residential load aggregator
Payment to the commercial load aggregator
Payment to the industrial load aggregator
Payment to the agricultural load aggregator
Payment to the EV-charging aggregator
Payment to the upstream grid
0
50
100
150
200
250
300
350
400
450
0
0.02
0.04
0.06
0.08
0.1
0.12
0.14
0.16
0.18
0.2
0.22
0.24
0.26
0.28
0.3
0.32

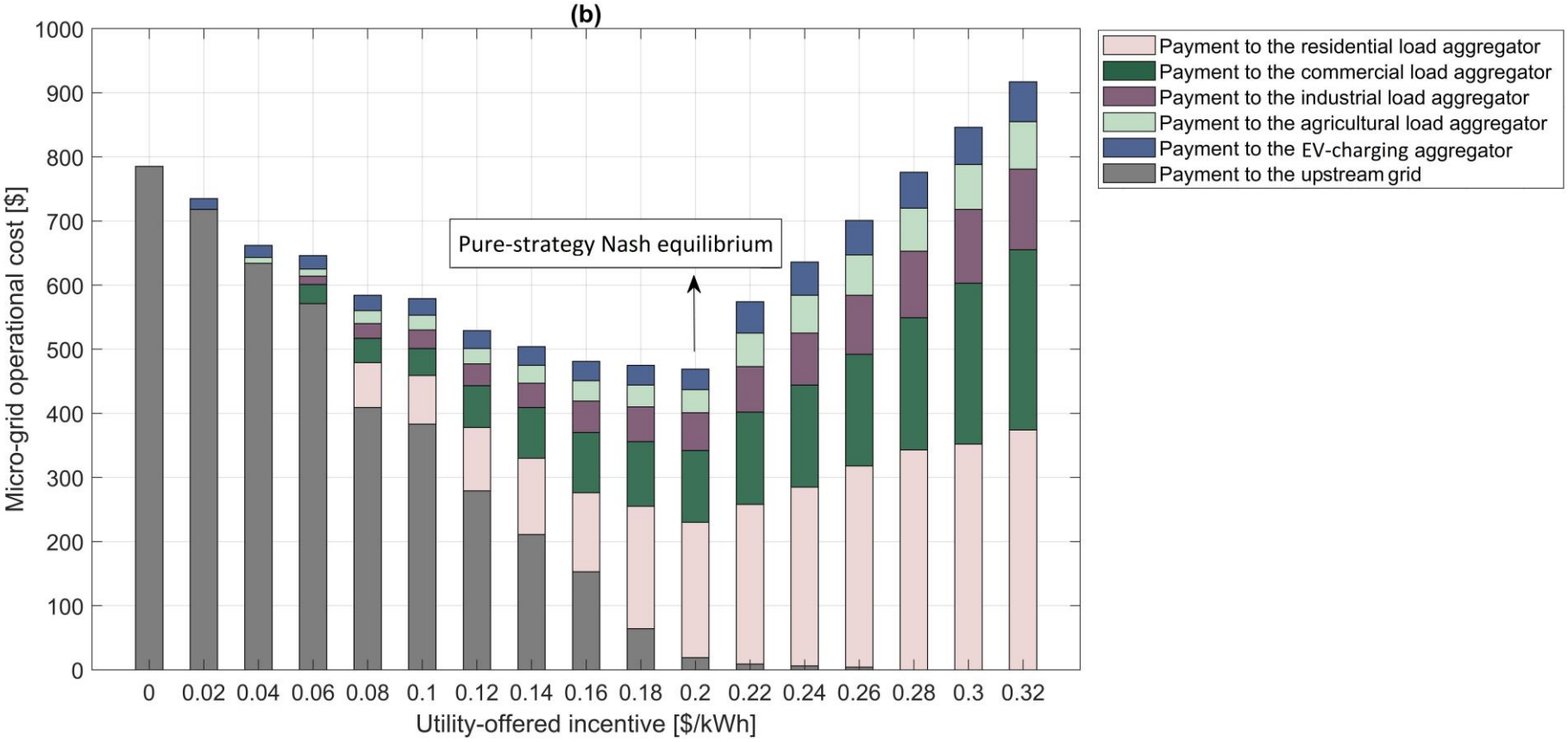


Figure 3.23: Breakdown of the minimised day-ahead operational cost of the MG with respect to different utility-posted incentive rates at the most critical peak hour of the representative days: (a) 5 p.m. summer day (February 14$^{th}$); and (b) 6 p.m. winter day (July 21$^{st}$). Note the change in scale in the dependent axes.

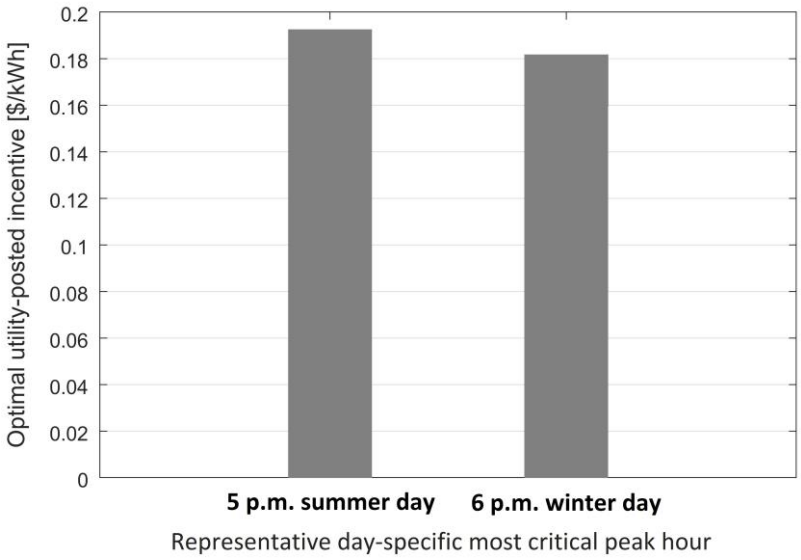


Figure 3.24: Closed-form solution to the optimal utility-posted incentive rate at the two representative daily most critical peak time-steps.

Several key implications can be derived from the results presented in Figs. 3.21–3.24:

1. The proposed dual-loop, Stackelberg, strategic game-theoretic framework can be viewed as a two-sided, zero-sum game with complete but imperfect information,[12] which delivers significant economic benefits to all the active economic agents involved in the game, namely: the utility, responsive load aggregators, and end-consumers. More specifically, the aggregate MG operational cost during the critical peak hours of the representative extreme-case summer and winter days is reduced to $911.66 (~66%) and $2,124.16 (~47%), from $2,692.25 and $4,039.30, respectively, compared to the case with no DR procurements; determined in the first iteration of the distributed algorithm (see Fig. 3.21).

2. The results presented in Fig. 3.23 indicate that there exists a knee point on the curve fitted to the hourly day-ahead operational costs of the system to

[12] This assumes that each player knows who the other players are and what their strategy sets are, but does not generally know the exact form of the objective functions they are trying to optimise – and thus how they will react in different situations. That is, there exists uncertainty in conjectures about possible errors in the choices of other players due to imperfect information.

address onsite generation capacity deficits. The more the solution deviates from this knee point (from either side), the worse the cost solution. However, a comparison of the impacts of the rightward and leftward deviations from the unique, pure-strategy Nash equilibrium of the game suggests that the overpayment to the aggregators has a more negative impact on the optimal trade-off cost solution than under-exploiting the DR resources. Also note that the above-mentioned knee point is driven by the total amount of DR resources available, as well as the overall discomfort characteristics of the customers.

3. A one-by-one comparison of the analytically-determined (closed-form), optimal utility-offered incentive prices with those obtained by the proposed distributed algorithm shows a discrepancy of less than \$0.02/kWh, which equals the step size used to update the utility-offered financial incentives ($i_{MGO}$). Not only does this corroborate the validity and usefulness of the distributed algorithm, but it also indicates that the precision of the proposed distributed algorithm is controlled primarily by the selected step size.

### 3.6.2. Incentive flow analysis

This section aims to provide details on the financial balance of the proposed incentive-directed, non-cooperative game-theoretic DR management framework through illustrative examples. To this end, the hours at which the highest levels of DR resources were elicited in the two extreme-day scenarios concerned, namely 5 p.m. summer day and 6 p.m. winter day, were selected for a comprehensive financial incentive flow analysis. Accordingly, Table 3.5 details the flow of financial incentives, from the utility to the aggregators and then to the end-consumers, together with their associated levels of expected utility, demand reduction, and discomfort cost. Note that all the information is extracted from the unique, pure-strategy Nash equilibrium obtained by the proposed distributed algorithm.

Table 3.5: Detailed results of the inflow and outflow of financial incentives for the two illustrative time-steps: 5 p.m. summer day (February 14th) and 6 p.m. winter day (July 21st).

| Player category | Variable | Energy-use sector* | Scenario | |
|---|---|---|---|---|
| | | | 5 p.m. summer day | 6 p.m. winter day |
| The utility | Total incentive payment of the utility to the aggregators [$] | – | 271.8 | 459.1 |
| | Total load reduction expected by the utility [kWh] | – | 1,358.8 | 2,295.7 |
| Demand response aggregators | Total incentive payment of the aggregator to its customers [$] | R | 55.6 | 88.5 |
| | | C | 16.6 | 42.7 |
| | | I | 15.5 | 18.7 |
| | | A | 14.1 | 11.3 |
| | | E | 8.9 | 7.7 |
| | Total profit gained by the aggregator [$] | R | 75.3 | 129.9 |
| | | C | 24.4 | 72.7 |
| | | I | 20.9 | 45.8 |
| | | A | 25.0 | 23.0 |
| | | E | 15.5 | 18.8 |
| | Total load reduction procured by the aggregator [kWh] | R | 654.5 | 1,092.0 |
| | | C | 205.0 | 577.1 |

| | | | | |
|---|---|---|---|---|
| | | I | 181.9 | 322.5 |
| | | A | 195.6 | 171.6 |
| | | E | 121.9 | 132.4 |
| End-consumers[†] | Total utility of the customers [$] | R | 26.7 | 42.6 |
| | | C | 8.5 | 21.7 |
| | | I | 8.2 | 9.9 |
| | | A | 8.9 | 7.1 |
| | | E | 6.8 | 6.0 |
| | Total discomfort cost of the customers [$] | R | 28.9 | 45.9 |
| | | C | 8.1 | 20.9 |
| | | I | 7.3 | 8.8 |
| | | A | 5.2 | 4.2 |
| | | E | 2.1 | 1.7 |

[*] The letters 'R', 'C', 'I', 'A', and 'E' respectively stand for 'Residential', 'Commercial, 'Industrial', 'Agricultural', and 'E-mobility'.

[†] Given the high number of customers considered in the case study (refer to Table 3.4), the reader is referred to Supplementary Material 2 (Tables SM2.1–SM2.5) for a detailed breakdown of the customers' individual incentive income, utility, discomfort cost, and contribution to load reduction.

In accordance with Table 3.5, the following observations can be made from the daily most critical peak time-step analyses:

1. According to the top-level transactions processed in the wholesale DSM market, the total incentives paid by the utility equals the sum of the financial incentives received by the aggregators.[13] Accordingly, the total load reduction expected by the utility equals the aggregated load reduction packages delivered by the associated aggregators.

2. Based on the bottom-level transactions made in the retail DSM market, the sum of the total utility of each category of end-consumers – generated by delivering their interruptible DR resources – and the associated total discomfort cost imposed on them, equals the total incentive payment made by their respective aggregator. Accordingly, the sum of load reductions contributed by each aggregator's customers equals the respective aggregator's contribution to the expected overall load reduction consistent with its commitment in the wholesale DSM market.

The observations discussed above collectively confirm the balance of incentive inflows and outflows over the considered time-steps from the perspective of all the players of the game.

Moreover, comparative analyses of the per-unit profits obtained by load aggregators – defined as a ratio of the total profit gained by each aggregator to the total load reduction it has procured at a given time-step [$/kWh] – by acting as energy brokers in the wholesale DSM market and, at the same time, leading the retail DSM market, indicate that the utility of a DRA is positively correlated with the overall willingness of its consumers to participate in the devised interruptible DR programme. The uniform (non-discriminatory) incentive price settlement

[13] Note that according to Equation 3.13, the amount of financial incentive received by each DRA equals the sum of the profit it earns by playing the role of DR broker and the total amount of financial incentives it pays to its participating customers.

design considered in the two-stage DSM market is the main underlying reason for this observation.

### 3.6.3. Incentive compatibility assessment

To verify that the proposed game-theoretic DSM approach is incentive-compatible (truthfully implementable) from the utility's perspective, the consequences of the aggregators' and end-consumers' deviations from their best strategies are explored in this section. To this end, the most critical peak hours of the representative days are studied. The profits gained by the aggregators are calculated with respect to various levels of financial incentives offered to their customers, which are shown in Fig. 3.25. Also, the results of the sensitivity analysis of the utility of a randomly-selected end-consumer, from each load category, to variations in its load reduction supply capacity, are shown in Fig. 3.26. The values of the representative customers' discomfort-related coefficients and DR capacities, as well as detailed results of the inflow and outflow of incentives for the two indicative time-steps, are highlighted in grey in the relevant tables in Supplementary Material 2 (Tables SM2.1–SM2.5).

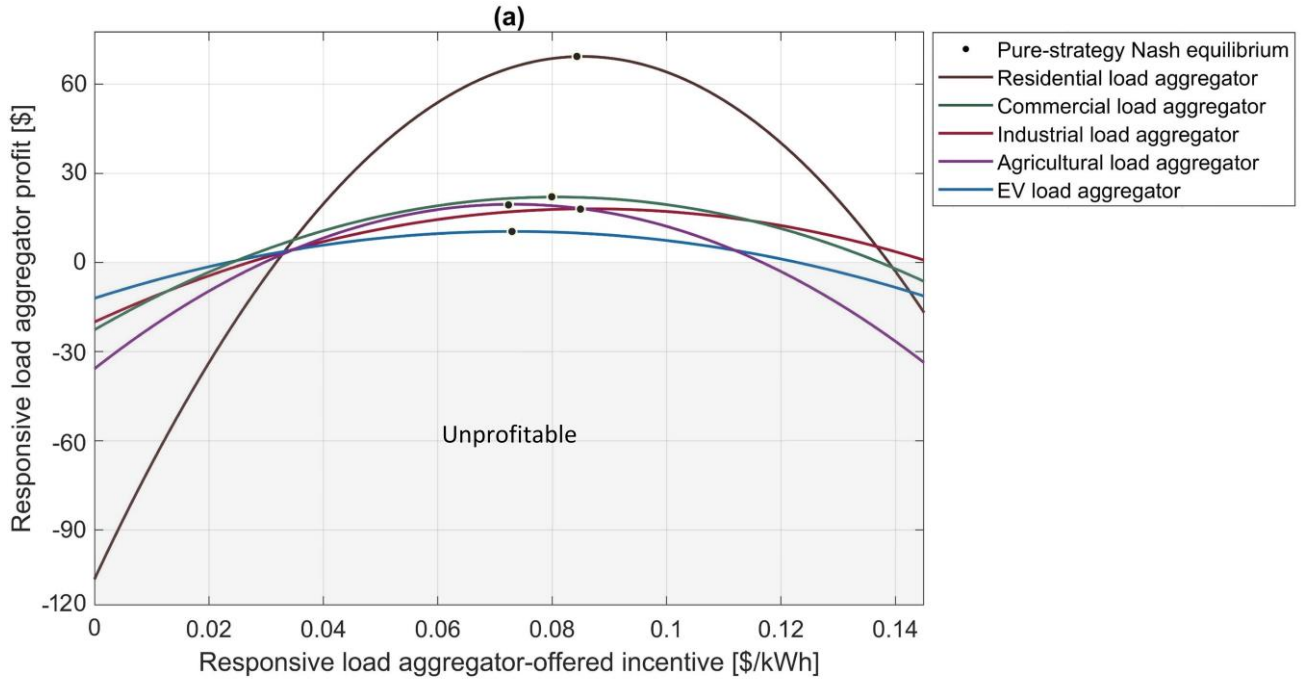
(a)
Responsive load aggregator profit [$]
Responsive load aggregator-offered incentive [$/kWh]
Unprofitable
Pure-strategy Nash equilibrium
Residential load aggregator
Commercial load aggregator
Industrial load aggregator
Agricultural load aggregator
EV load aggregator
60
30
0
-30
-60
-90
-120
0
0.02
0.04
0.06
0.08
0.1
0.12
0.14

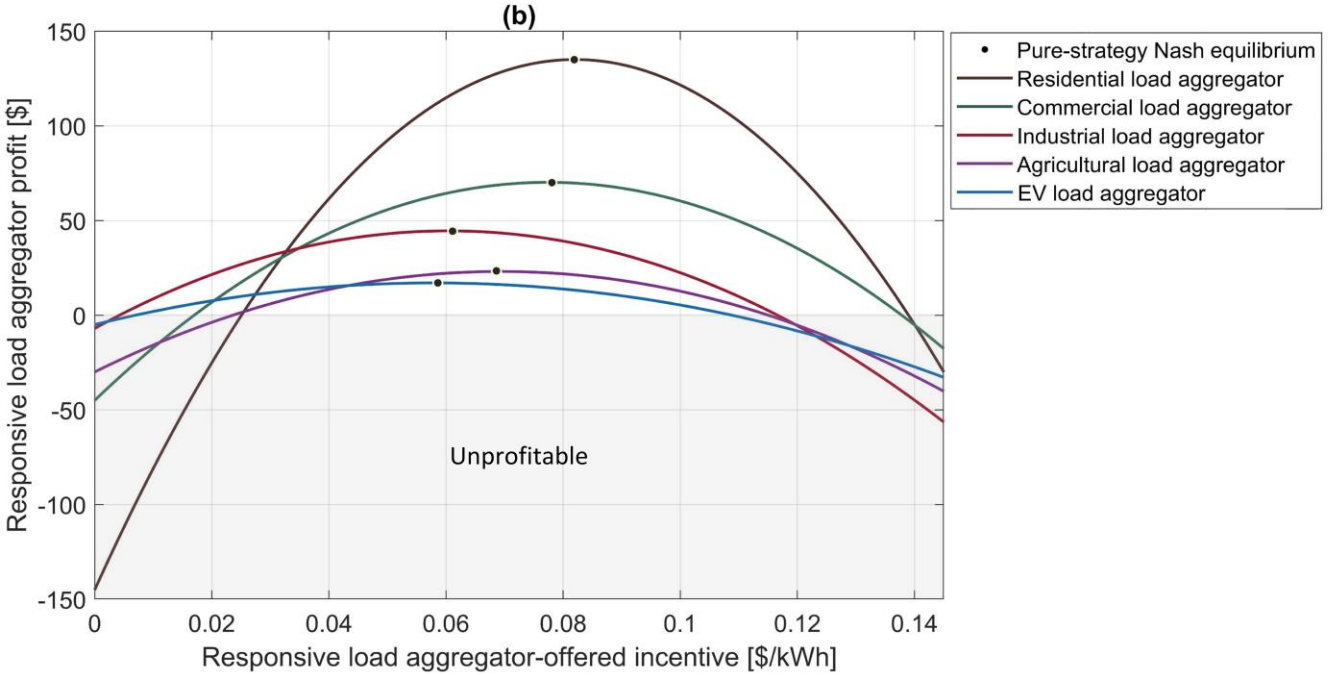


Figure 3.25: Sensitivity of the aggregators' profits to variations in their incentive payment rates offered to end-consumers at the most critical peak hour of the representative days:
(a) 5 p.m. summer day (February 14$^{th}$); and (b) 6 p.m. winter day (July 21$^{st}$).
Note the change in scale in the dependent axes.

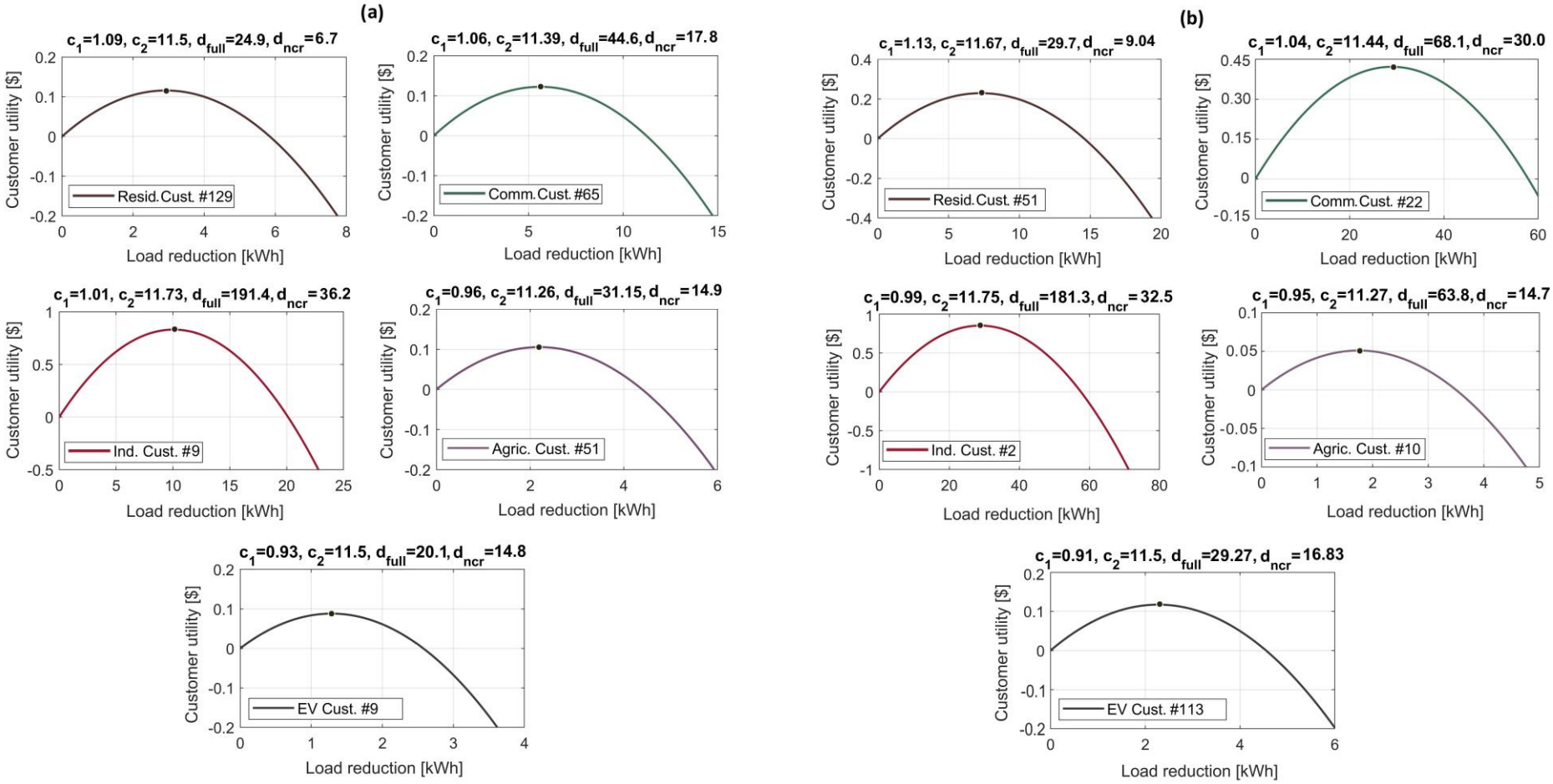


Figure 3.26: Sensitivity of the utility of a representative customer of each aggregator to variations in its load reduction supply capacity at the most critical peak hour of the representative days: (a) 5 p.m. summer day (February 14th); and (b) 6 p.m. winter day (July 21st). Note the change in scale in the dependent and independent axes.

As shown in Fig. 3.25, any deviation of the aggregators from their best-response strategies at the Nash equilibrium point leads to a reduction in their expected profits; thus, none of the aggregators have any useful deviations. It should be noted that each aggregator's profit can be expressed as a second-order polynomial function of the incentive rate it offers, by substituting the best-response strategies of its customers into its profit function (refer to Equation 3.29). The rationale behind this quadratic polynomial equation for an aggregator's profit is straightforward. For any utility-posted incentive rate, increasing the aggregator-offered incentive rate increases customer engagement, which improves the aggregator's expected profit. However, at a certain point – vertex of the associated parabola – this effect levels off and increasing the aggregator-offered incentive rate begins to show a reverse effect in which the gains from increased participation tends to drive the aggregator's expected profit down – where the aggregator's marginal revenue falls below its marginal cost – as a result of dealing with less-elastic customers and/or overcompensation of DR suppliers in the retail DSM market.

Also, the prime reason why the optimal aggregator-offered incentive rate varies across different customer classes is that the model accommodates detailed customisation for the sector- and customer-specific DR supply elasticities (refer to Table 3.4), which generally assumes that the supply of DR capacity is more responsive for FCEV-refuelling customers, as well as for industrial and agricultural customers, than for residential and commercial customers.

Furthermore, a comparison of the aggregators' profit profiles for the considered two extreme time-steps, from Fig. 3.25, reveals that each aggregator's best-response incentive price strategy also varies over the course of time. To illustrate, while the best-response strategies of the aggregators for the time-step 6 p.m. winter day, shown in Fig. 3.25 (b), seems to be in inverse proportion to the DR supply elasticity of the associated customer sectors, no specific trend can be discerned for the relationship between the best-response strategies of the aggregators and the sectoral DR supply elasticity for the time-step 5 p.m. summer day, depicted in Fig. 3.25 (a). The latter observation indicates the possibility of the involvement of additional factors in determining the aggregators' best strategies,

such as the stochasticity inherent in the employed load demand disaggregation algorithm and the randomness associated with the number of FCEVs that initiate a standard refuelling event at each time-step, or plug in and supply V2G capacities (and therefore, cannot be refuelled at the same time-step), which remain to be characterised. In addition, the difference in the profit levels of different aggregators can be principally explained by the share of each sector in the total energy demand and its respective DR supply capacity. In this light, a key insight from Fig. 3.25 is that while the aggregators' payoff varies as a function of the utility demand for DR capacity and the associated sector-wide share in the total energy consumption, the rank order of their profitability is subject to instability throughout time – excluding the residential and FCEV aggregators that most and least benefitted from economies of scale, respectively. Such instability results largely from the sector-specific seasonal and diurnal variations in load demand. Additionally, the aforementioned rank order instability can, in lesser part, be attributed to the same sources of uncertainty as those noted for the variability of each aggregator's optimal incentive rate. Moreover, as demonstrated in Fig. 3.26, no representative customer has an incentive to deviate from its best-response strategy, as it results in reducing the utility it derives from load reduction – compared to the optimal solution. Recall that the customer discomfort cost, the lower and upper bounds of which are adjusted, is a function of the reduced load by the customer (see Equation 3.19), whereby the maximum load reduction that can be procured by each customer is calculated.

As demonstrated above, in both cases, the proposed game-theoretic DR scheduling framework leads to truth-revealing and deviation-proof solutions – where there is no deviation by load aggregators or end-consumers. Moreover, the evidence from these analyses points towards the idea that the obtained optimal solution can be regarded as the fully-revealing rational expectations equilibrium of the game – where none of the game's players would change their actions even if they were aware of the outcomes of the game. It should also be emphasised that the sensitivity of the aggregators' profits to variations in their corresponding posted incentive rates, as well as the sensitivity of the customers' utilities to variations in their corresponding supplied load reductions, are mainly controlled by the adjusted values for the willingness of different load classes to engage in DR programmes.

### 3.6.4. Validation of the proposed demand-side management market

To validate the effectiveness of the proposed two-stage aggregator-mediated DSM market model, two instances of day-ahead energy management analysis are conducted for the aforementioned extreme-day cases and the obtained results are compared with those of the case where the aggregator-mediated interruptible/curtailable DR resources are scheduled in a BAU way. Accordingly, the non-market-driven (BAU) procurement of aggregator-activated interruptible/curtailable responsive loads excludes the ability to adaptively update the incentives offered by the MG operator, based on which the aggregators post their incentives to the retail DSM market, and subsequently the end-consumers select their participation rate in load reduction programmes. More specifically, in the BAU approach, the MG operator offers a fixed, day-specific incentive rate to the aggregators, who also offer fixed levels of incentive price to their customers – for load reduction during the pre-determined peak hours of electricity consumption. Subsequently, the end-users and aggregators respond to the aggregator-determined and MG operator-offered incentive rates, respectively. In this way, the retail and wholesale DSM markets are sequentially cleared for the day-specific incentives by stacking the customers' and aggregators' bids, low to high, and allocating demand reduction schedules to the customers and aggregators in the merit order irrespective of whether the power shortage is addressed with the best compromise between load reduction and imported electricity for each hourly period.

Expectedly, as there exists no mechanism to update the initial strategy of the MG operator, the efficiency of such a framework is particularly sensitive to the choice of the MG operator-offered incentive rate. Hence, the model response is determined for various day-specific MG operator-offered incentive rates. Accordingly, Table 3.6 summarises the results obtained by simulating the above-described BAU interruptible DR mechanism when applied to the DR provision problem at hand for the two extreme scenarios with the MG operator-offered incentive payment ranging from \$0.02/kWh to \$0.32/kWh in intervals of \$0.02/kWh. The table, furthermore, presents the results of the suggested market-driven interruptible DR model for the extreme days considered.

Table 3.6: Comparative analysis of the proposed and BAU realisations of the interruptible DR programme on the extreme days (over the critical peak hours): February 14th (summer day) and July 21st (winter day).

| **MG operator-offered incentive* ($I_{MGO}$) [$/kWh]** | | **Total daily incentive payment to the aggregators ($I^{p}_{MGO}(\sum_{p\in P_d}\sum_{j\in J} D^{j,p}_{LA})$) [$/d]** | | **Total daily incentive payment to the customers ($\sum_{p\in P_d}\sum_{j\in J} I^{j,p}_{LA} D^{j,p}_{LA}$) [$/d]** | | **Total daily load reduction procured by the customers ($\sum_{p\in P_d}\sum_{j\in J}\sum_{k\in N_J} d^{k,j,p}$) [kWh/d]** | | **Total daily cost of electricity imports ($\sum_{p\in P_d} cost^{p}_{im}$) [$/d]** | | **Total daily operational cost of the MG ($\sum_{p\in P_d} OC^{p}_{MG}$) [$/d]** | |
|---|---|---|---|---|---|---|---|---|---|---|---|
| **Feb. 14th** | **Jul. 21st** | **Feb. 14th** | **Jul. 21st** | **Feb. 14th** | **Jul. 21st** | **Feb. 14th** | **Jul. 21st** | **Feb. 14th** | **Jul. 21st** | **Feb. 14th** | **Jul. 21st** |
| ***Business-as-usual interruptible DR scheduling approach*** | | | | | | | | | | | |
| 0.02 | 0.02 | 10.5 | 43.3 | 3.9 | 15.6 | 525.0 | 2,165.0 | 870.8 | 1,997.7 | 881.3 | 2,041.0 |
| 0.04 | 0.04 | 22.5 | 102.1 | 9.2 | 41.9 | 562.5 | 2,552.5 | 863.2 | 1,916.1 | 885.7 | 2,018.2 |
| 0.06 | 0.06 | 44.8 | 162.8 | 18.8 | 70.0 | 746.7 | 2,713.3 | 824.3 | 1,882.4 | 869.1 | 2,045.2 |
| 0.08 | 0.08 | 81.7 | 390.4 | 35.9 | 171.8 | 1,021.3 | 4,880.0 | 766.6 | 1,427.4 | 848.3 | **1,817.8** |
| 0.1 | 0.1 | 180.9 | 528.5 | 83.2 | 232.5 | 1,809.0 | 5,285.0 | 601.2 | 1,342.3 | **782.1** | 1,870.8 |
| 0.12 | 0.12 | 217.1 | 634.2 | 91.8 | 310.8 | 1,809.0 | 5,285.0 | 601.2 | 1,342.3 | 818.3 | 1,976.5 |
| 0.14 | 0.14 | 264.7 | 787.8 | 105.9 | 409.7 | 1,890.7 | 5,627.1 | 584.1 | 1,270.5 | 848.8 | 2,058.3 |
| 0.16 | 0.16 | 302.5 | 900.3 | 115.8 | 459.2 | 1,890.7 | 5,627.1 | 584.1 | 1,270.5 | 886.6 | 2,170.8 |
| 0.18 | 0.18 | 377.3 | 1,013.7 | 188.7 | 547.4 | 2,096.1 | 5,631.7 | 540.9 | 1,269.5 | 918.2 | 2,283.2 |
| 0.2 | 0.2 | 421.5 | 1,341.0 | 219.2 | 643.7 | 2,107.5 | 6,705.0 | 538.5 | 1,044.1 | 960.0 | 2,385.1 |
| 0.22 | 0.22 | 486.0 | 1,611.0 | 233.3 | 757.2 | 2,209.1 | 7,322.7 | 517.3 | 914.4 | 1,003.3 | 2,525.4 |
| 0.24 | 0.24 | 551.8 | 2,093.1 | 253.8 | 879.1 | 2,299.2 | 8,721.3 | 498.3 | 620.7 | 1,050.1 | 2,713.8 |
| 0.26 | 0.26 | 708.6 | 2,593.3 | 311.8 | 959.5 | 2,725.4 | 9,974.2 | 408.9 | 357.6 | 1,117.5 | 2,950.9 |

| | | | | | | | | | | | |
|---|---|---|---|---|---|---|---|---|---|---|---|
| 0.28 | 0.28 | 1,040.2 | 2,906.8 | 436.9 | 1,133.6 | 3,714.9 | 10,381.4 | 201.2 | 272.1 | 1,241.4 | 3,178.9 |
| 0.3 | 0.3 | 1,401.8 | 3,503.2 | 560.7 | 1,191.1 | 4,672.7 | 11,677.3 | 0 | 0 | 1,401.8 | 3,503.2 |
| 0.32 | 0.32 | 1,495.2 | 3,736.7 | 586.2 | 1,195.7 | 4,672.7 | 11,677.3 | 0 | 0 | 1,495.2 | 3,736.7 |
| ***Proposed market-driven interruptible DR scheduling approach*** | | | | | | | | | | | |
| 0.17 | 0.15 | 566.3 | 1,327.8 | 230.7 | 488.6 | 3,253.8 | 8,155.2 | 50.8 | 76.9 | 617.1 | 1,404.7 |

Values in bold indicate the total daily operational cost of the MG in the best performance of the BAU interruptible DR management framework.

* Given the variability of the best-strategy incentive offered by the MG operator at different peak hours of the day in the proposed market-driven model, the mean daily value of the optimal incentive rate offered by the MG operator ($\overline{I_{MGO}^{p,*}}$) is presented for the proposed model.

The following observations can be made from a comparative analysis of the proposed model and BAU model results presented in Table 3.6:

1. The systematic updating of the MG operator-offered incentive for load reduction – for the time-steps at which the system is predicted to be under stress – using an aggregator-mediated, market-driven DSM market model, can play a pivotal role in unlocking the full potential of demand-side resources by finding the economically efficient DR allocation solutions. In other words, the lack of a systematic framework to enable the DR programme administrator to vary the rate of incentive payment to increase or decrease the supply of DR capacity, either results in an overpayment for access to the DR resources, or leads to the under-trading of the responsive loads. More specifically, the proposed model has outperformed the BAU model by at least ~21.1% (equating to a saving of $165) and ~22.7% (equating to a saving of $413.1) in terms of the daily operational cost (over the critical peak hours) of the MG ($\sum_{p\in P_d} OC_{MG}^{p}$) respectively for the February 14$^{th}$ and July 21$^{st}$ scenarios.

2. The BAU realisation of the interruptible DR programme has failed to harness the full potential of the demand-side flexibility resources available. The most crucial factor underpinning this underutilisation of the responsive loads in this model is the lack of interaction between the MG operator and responsive load aggregators, as well as between aggregators and end-consumers to dynamically update the incentives for load reduction at different times of the day. This is evident from Table 3.6, where increasing the MG operator-posted incentive rate from $0.1/kWh to $0.12/kWh, and also from $0.14/kWh to $0.16/kWh, has led to an increase in the total daily payment to the aggregators, despite no increase in the net load reduction in both the scenarios considered.

3. In contrast to the proposed model where the daily operational cost of the system strictly decreases as the MG operator-offered incentive rate increases up to a saturation point, the BAU model's response to variations

in the MG operator-offered incentive rate does not tend to follow a particular pattern. For example, increasing the MG operator-offered incentive rate from \$0.02/kWh to \$0.04/kWh in the case of July 21st has resulted in a reduction of the daily operational cost of the MG (over the critical peak hours) by ~1.1%, then increasing the incentive rate from \$0.04/kWh to \$0.06/kWh has increased the daily operational cost of the MG by ~1.3%, and then increasing the incentive rate from \$0.06/kWh to \$0.08/kWh has substantially driven down the daily operational cost of the MG system – to the globally optimal level (from the BAU model's perspective). Much of the reason for such an erratic behaviour of the BAU model lies in the fact that the participation of the aggregators depends on meeting certain threshold levels of profits. Put differently, increasing the rate of incentive payments leads to a worthless overpayment unless it triggers the participation of a further MG customer, provided that a lower incentive rate than the per-unit cost of electricity import is deemed sufficient by the customer. However, the interactive DSM market-clearing mechanism embedded in the proposed DSM market model – that is implemented using the proposed interactive value iteration solution approach (refer to Algorithm 3.1) – has addressed such a source of unreliability.

To evaluate the weather sensitivity of each model, the analysis is expanded to include all the days in which the interruptible DR programme is executed. Table 3.7 summarises the descriptive statistics for the DR scheduling variables during the hours of peak demand for which a net energy deficit is predicted. Note the change in temporal resolutions of the dependent variables compared to Table 3.6. Specifically, the results are presented for the morning peak (MP) and evening peak (EP) hours across the seasons to provide insight into the temporal distribution of utilising the DR resources.

Table 3.7: Summary statistics for the DR scheduling variables obtained for the year-round MG operation.

| Variable | | Spring | | Summer | | Autumn | | Winter | |
|---|---|---|---|---|---|---|---|---|---|
| | | MP | EP | MP | EP | MP | EP | MP | EP |
| MG operator-offered incentive [$/kWh] | Avg. | 0.159 | 0.202 | 0.140 | 0.168 | 0.120 | 0.097 | 0.128 | 0.183 |
| | Med. | 0.160 | 0.200 | 0.140 | 0.173 | 0.120 | 0.097 | 0.120 | 0.189 |
| | SD | 0.031 | 0.034 | 0.026 | 0.027 | 0.015 | 0.038 | 0.039 | 0.029 |
| | Obs. | 291 | 97 | 208 | 76 | 344 | 390 | 400 | 432 |
| Incentive payment to the aggregators [$/h] | Avg. | 49.004 | 111.484 | 26.866 | 62.378 | 48.504 | 63.166 | 77.043 | 147.260 |
| | Med. | 47.409 | 101.634 | 26.492 | 61.087 | 48.996 | 64.636 | 78.349 | 147.850 |
| | SD | 11.852 | 26.799 | 4.103 | 5.268 | 1.665 | 5.667 | 6.336 | 8.320 |
| | Obs. | 291 | 97 | 208 | 76 | 344 | 390 | 400 | 432 |
| Incentive payment to the customers [$/h] | Avg. | 20.092 | 51.281 | 12.105 | 29.448 | 22.627 | 28.039 | 30.510 | 67.382 |
| | Med. | 20.115 | 52.360 | 10.606 | 29.282 | 20.901 | 27.432 | 29.660 | 67.446 |
| | SD | 5.570 | 5.954 | 6.314 | 2.940 | 6.307 | 3.483 | 4.240 | 4.252 |
| | Obs. | 291 | 97 | 208 | 76 | 344 | 390 | 400 | 432 |
| Load reduction procured by the customers [kWh] | Avg. | 308.201 | 551.901 | 191.900 | 371.298 | 604.200 | 651.196 | 801.898 | 804.699 |
| | Med. | 311.051 | 553.074 | 192.312 | 371.649 | 603.094 | 651.628 | 804.004 | 805.741 |
| | SD | 9.814 | 11.053 | 5.593 | 11.579 | 6.587 | 11.687 | 9.678 | 6.922 |
| | Obs. | 291 | 97 | 208 | 76 | 344 | 390 | 400 | 432 |
| Cost of electricity imports [$/h] | Avg. | 8.611 | 15.237 | 3.985 | 7.907 | 5.531 | 8.402 | 9.004 | 17.516 |
| | Med. | 9.044 | 15.780 | 4.238 | 7.974 | 5.406 | 7.941 | 8.172 | 17.049 |
| | SD | 3.531 | 2.020 | 0.881 | 0.187 | 1.087 | 1.873 | 2.556 | 4.937 |
| | Obs. | 291 | 97 | 208 | 76 | 344 | 390 | 400 | 432 |
| Total operational cost of the MG [$/h] | Avg. | 57.615 | 126.721 | 30.851 | 70.285 | 54.035 | 71.568 | 86.047 | 164.776 |
| | Med. | 56.453 | 117.414 | 30.730 | 69.061 | 54.402 | 72.577 | 86.521 | 164.899 |
| | SD | 2.618 | 7.981 | 2.771 | 3.217 | 2.410 | 3.651 | 4.206 | 9.325 |
| | Obs. | 291 | 97 | 208 | 76 | 344 | 390 | 400 | 432 |

The table is revealing in the following important ways:

1. The DR events occur more frequently in autumn (734 times) and winter (832 times) than in spring (388 times) and summer (284 times). A comparison of the total number of DR event observations during the morning and evening peak periods across different seasons offers the following key insights: (i) two distinctive daily periods of positive net load demand – the total electric demand on the system minus local generation – can be identified for autumn and winter, while (ii) the net load demand in spring and summer is primarily characterised by one period, namely the MP period. This change in the capacity deficit pattern is mainly driven by weather conditions; the warmer months reduce the necessity of utilising electric space heating systems. Other seasonal covariates, including daylight saving and longer daylight hours in spring and summer, which lead to both lower lighting use and higher solar PV generation in the early evening, also contribute to this variation, albeit to a lesser degree.

2. Although the number of DR events that occurred during the MP period is lower than the corresponding EP period in the colder months, the average hourly load reduction procured is nearly the same for the morning and evening peak periods in autumn and winter. This implies that the profile of the net load demand has a shorter, sharper peak in the morning, but a longer, flatter peak in the evening in autumn and winter. This is not only due to the coincidence of the residential load with the start of the business day, but also the fact that non-dispatchable renewable power generation from wind and hydro resources is considerably less during the autumn and winter MP period than the corresponding EP period (see Fig. 3.15). Crucially, the proposed Stackelberg, non-cooperative game-theoretic DR scheduling model has yielded reductions in load demand of, on average, ~24% and ~22% respectively during the winter morning and evening peak periods. This equates to an average hourly energy reduction of ~802 kWh in the MP period and ~805 kWh in the EP period. In summer, this percentage

decreases to ~13% (192 kWh) in the MP period, and ~15% (371 kWh) in the EP period.

3. Defining the data skewness as (mean – median) / standard deviation, it can be shown that the skewness values of the 'cost of electricity imports' and the 'incentive payments made by the utility to the aggregators' datasets have opposite signs at all the eight quarterly time intervals. For example, the skewness values of the above-mentioned datasets for the winter MP period are 0.326 and −0.206, respectively. Accordingly, the mean of the former dataset is greater than its median (i.e., the dataset distribution is positively skewed), whereas the mean of the latter dataset is less than its median (i.e., negatively skewed). This suggests that the optimal trade-off between imported power and utilised DR capacity tends to follow an approximately consistent pattern during each period of peak electricity use. This finding further corroborates the robustness and validity of the proposed Stackelberg, non-cooperative game-theoretic DSM approach in producing the best compromise between the imported power and elicited DR capacity.

Moreover, Table 3.8 provides a statistical evaluation of the efficacy of the proposed market-based integration (MBI) of responsive loads using non-cooperative game theory as compared to the BAU model in the four seasons. Note that, for reasons of space, the modelling results are not broken down into the morning and evening peak periods.

Table 3.8: Comparative statistical analysis of the proposed and BAU-DR scheduling models.

| Variable | | Spring | | Summer | | Autumn | | Winter | |
|---|---|---|---|---|---|---|---|---|---|
| | | BAU* | MBI | BAU* | MBI | BAU* | MBI | BAU* | MBI |
| MG operator-offered incentive [$/kWh] | Avg. | 0.147 | 0.170 | 0.112 | 0.148 | 0.051 | 0.109 | 0.073 | 0.155 |
| | Med. | 0.152 | 0.159 | 0.108 | 0.146 | 0.045 | 0.110 | 0.074 | 0.156 |
| | SD | 0.017 | 0.033 | 0.017 | 0.029 | 0.025 | 0.031 | 0.030 | 0.028 |
| | Obs. | 388 | 388 | 284 | 284 | 734 | 734 | 832 | 832 |
| Incentive payment to the aggregators [$/h] | Avg. | 16.821 | 64.624 | 9.725 | 36.369 | 13.342 | 55.595 | 35.537 | 111.054 |
| | Med. | 16.874 | 55.729 | 9.777 | 29.113 | 12.242 | 51.287 | 33.964 | 87.232 |
| | SD | 1.670 | 31.920 | 0.863 | 5.482 | 4.387 | 8.279 | 5.125 | 35.922 |
| | Obs. | 388 | 388 | 284 | 284 | 734 | 734 | 832 | 832 |
| Incentive payment to the customers [$/h] | Avg. | 6.390 | 27.889 | 3.112 | 16.746 | 6.538 | 25.245 | 18.835 | 48.370 |
| | Med. | 6.454 | 23.463 | 3.223 | 13.639 | 6.458 | 25.131 | 17.657 | 36.607 |
| | SD | 0.574 | 14.624 | 0.279 | 9.624 | 1.837 | 5.914 | 10.386 | 18.948 |
| | Obs. | 388 | 388 | 284 | 284 | 734 | 734 | 832 | 832 |
| Load reduction procured by the customers [kWh] | Avg. | 104.263 | 369.126 | 80.929 | 239.908 | 240.608 | 629.171 | 465.260 | 803.352 |
| | Med. | 104.979 | 314.339 | 81.951 | 194.866 | 238.388 | 512.418 | 463.248 | 714.444 |
| | SD | 7.450 | 106.143 | 4.920 | 79.940 | 14.018 | 123.846 | 16.353 | 101.754 |
| | Obs. | 388 | 388 | 284 | 284 | 734 | 734 | 832 | 832 |
| Cost of electricity imports [$/h] | Avg. | 76.462 | 10.268 | 41.742 | 5.034 | 61.044 | 6.919 | 113.148 | 13.127 |
| | Med. | 76.845 | 10.633 | 42.059 | 5.074 | 31.421 | 6.948 | 55.583 | 13.392 |
| | SD | 1.902 | 4.274 | 2.314 | 0.148 | 6.255 | 2.935 | 5.206 | 3.129 |
| | Obs. | 388 | 388 | 284 | 284 | 734 | 734 | 832 | 832 |
| Total operational cost of the MG [$/h] | Avg. | 93.283 | 74.892 | 51.467 | 41.404 | 74.386 | 62.515 | 148.685 | 124.181 |
| | Med. | 93.836 | 58.145 | 52.657 | 33.028 | 72.784 | 57.739 | 146.465 | 94.166 |
| | SD | 1.766 | 30.248 | 3.311 | 17.753 | 7.011 | 9.224 | 7.104 | 40.021 |
| | Obs. | 388 | 388 | 284 | 284 | 734 | 734 | 832 | 832 |

* The BAU results represent the business-as-usual model's best performance out of different daily utility-offered incentives ranging from $0.02/kWh to $0.32/kWh in intervals of $0.02/kWh.

From Table 3.8, a number of key statistically valid evidence emerge to further support the superiority of the proposed game-theoretic DR scheduling model to the BAU interruptible programmes:

1. The proposed aggregator-mediated, market-based DR programme is able to unlock new sources of economic value that are inaccessible by the BAU-DR scheduling approach. This has resulted in a ~17% (equating to ~$39k) reduction in the operational cost of the MG in the baseline year. In large part, this is because the proposed model ensures a level playing field for all the DR providers and equitably allocates the benefits of third-party DR aggregation, whilst additionally providing a platform for the MG operator, DRAs, and end-consumers to mutually optimise their portfolios and determine the lowest operational costs.

2. A comparison of the seasonal performance of the proposed model and the BAU approach reveals that, on average, the DR resources are underutilised in autumn and winter, whilst additionally the DR providers are over-compensated in spring and summer in the BAU approach. More specifically, contrary to the obtained results from the proposed model, where the distributions of the 'incentive payments to the aggregators' and the 'cost of electricity imports' data are oppositely skewed, they have similar skewness patterns in the BAU approach. The BAU approach's results indicate that both of the above-mentioned distributions are skewed to the left (i.e., most of the observations lie to the right of the mean) in spring and summer, whereas they are both positively skewed (i.e., most of the observations lie to the left of the mean) in autumn and winter. A major explanation for these observations is the incapability of the BAU interruptible service approach to provide a targeted, non-prespecified incentive price signal that fluctuates hourly reflecting changes in the wholesale prices of electricity.

3. While the percentage of incentive payments to the customers to the incentive prices received by the aggregators remains nearly the same across the seasons in the proposed game-theoretic modelling results (within the range of approximately 43%−46%), it varies significantly from season to

season if the problem is solved in a BAU way. In particular, the BAU modelling results yield the highest utility margin for the customers (with the customers' share of the utility incentives of ~53%) during the winter months (June to August) when their use of electricity for heating contributes to high network loads. On the other hand, the per-unit profit of the DRAs is largest during the summer months (December to February) when there is no electric heating load to provide DR, which reduces the customers' share of revenues to as low as ~32%. This indicates the BAU approach's failure to provide a fair division of the utility-offered financial incentives between the DRAs and their corresponding customers, or more generally, an equitable allocation of net benefits (surpluses) – derived from the utilisation of DR flexibility resources – among all the participants – which results in the overall DR underperformance.

The evidence gained from the above observations indicates that DR liberalisation using the proposed marketplace, which supports free-market activities in a hybrid opt-in/opt-out economic regime – and assumes no market power, no externalities, and well-informed actors – delivers substantial efficiency gains, whilst protecting less well-off customers. Additionally, as an interesting insight arising from the collective observations, giving customers the power to choose their participation rates in the DR events (and whether or not to participate when faced with pricing incentives at all) has also shown to be able to generate collective social benefit to increased platform adoption by end-users, with positive implications on the robustness of the solution due to the participation of more players. The associate comparative results with the BAU approach have also highlighted the dynamics and patterns of social convergence into the uptake of incentive-based, game-theoretic DR programmes. Consequently, using consumer load response as an effective means of system control through modelling the normative behaviour of active economic agents based on non-cooperative game theory, is able to save money and resources, minimise environmental impacts, and help move towards a robust and equitable allocation of the costs and benefits of third-party DR procurement among the players. Moreover, game-theoretic DR management systems leave no room for free-riding actions of aggregators (resulting from under-payments to enrolled

customers). As these findings are shown to remain valid for the year-round operation of the system, their positive impact on the lifetime cost and cost-effectiveness of the conceptualised system is discussed in the next section.

### 3.6.5. Optimal equipment capacity-planning results

To evaluate the effectiveness of the proposed DR scheduling framework in reducing the whole-life cost of MGs, the equipment capacity-planning of the conceptualised MG was carried out under three cases: (1) taking a BAU (static) interruptible load approach to manage the smaller DR resources (as detailed in Section 3.6.4), (2) using the proposed market-based (dynamic) integration of the aggregator-mediated interruptible responsive loads (presented in Section 3.3), and (3) not implementing any DSM strategies. Tables 3.9 and 3.10 present the MG investment planning model results under the above-mentioned three cases, which are respectively denoted by 'BAU-DR', 'MBI-DR', and 'NO-DR'. Specifically, Table 3.9 details a breakdown of the optimised cost components included in the life-cycle analysis of the MG system (see Equation 3.41), while Table 3.10 provides the optimum size of the MG equipment, which are the main decision variables of the optimisation problem. Note that the optimisation model results are adjusted for the value of biomass feedstock. To this end, the total cost associated with the pelletisation of blended biomass feedstocks – agricultural and woody biomass – was considered to be $98/tonne of pellets [271], [272]. The case study site's natural endowment of forest biomass together with its temperate climate that is ideally suited to agricultural activities, narrows, to a considerable extent, the feedstock supply uncertainty bounds. This provides strong support for taking an exogenous approach to account for the biomass feedstock costs – in the post-optimisation phase.

It is also noteworthy that the results reported in the tables represent the best-case performance of the MFOA out of 30 independent trials. Moreover, to further demonstrate the adequacy of the maximum number of iterations, and the number of search agents considered, the convergence curves of the MFOA in its best and worst overall performances for each of the above-mentioned cases are shown in Fig. 3.27.

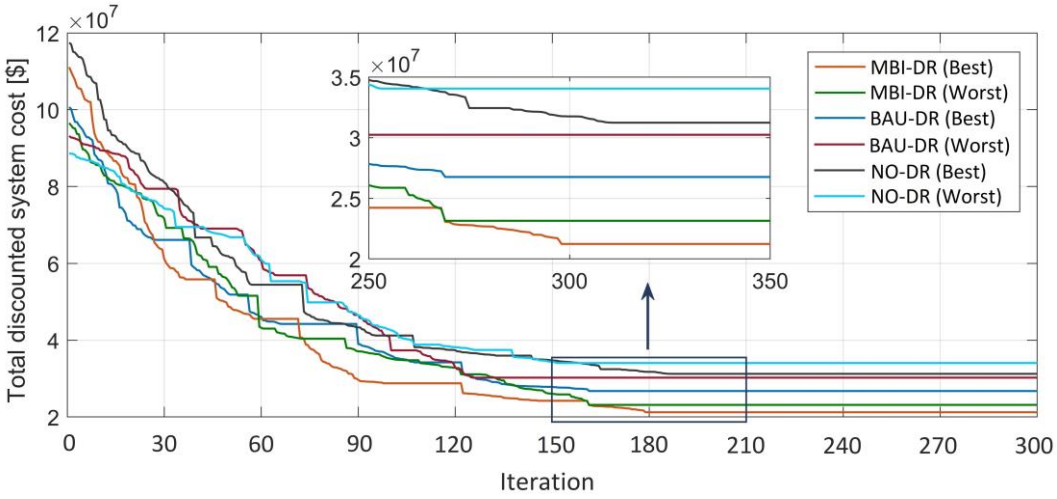


Figure 3.27: Convergence process of the MFOA in its best and worst runs throughout 30 simulation cases.

Table 3.9: Breakdown of the total discounted system cost under different DR provision strategies.

| Cost component | Cost subcomponent | Simulation case | | |
|---|---|---|---|---|
| | | **MBI-DR** | **BAU-DR** | **NO-DR** |
| Total discounted equipment-related costs $((\sum_{c\in C} \underset{20-yr}{NPC_c}) + \underset{20-yr}{NPC_I})$ [$] | | 18.25m | 21.88m | 25.62m |
| Total discounted MG operational costs $(\underset{20-yr}{NPV}(\sum_{t=1}^{8760} OC_{MG}(t)))$ | Total discounted incentive payment to the aggregators $(\underset{20-yr}{NPV}(\sum_{t=1}^{8760} I_{MGO}(t) \sum_{j\in J} D_{LA}^{j}(t)))$ [$] | 3.99m | 3.48m | – |
| | Total discounted cost of electricity imports $(\underset{20-yr}{NPV}(\sum_{t=1}^{8760} cost_{im}(t)))$ [$] | 0.46m | 2.76m | 7.46m |
| Total discounted FCEV2G electricity provision costs $(\underset{20-yr}{NPV}(\sum_{t=1}^{8760} \pi_{FCEV2G} P_{FCEV2G}(t)))$ [$] | | 0.42m | 0.49m | 0.50m |
| Total discounted operating costs of the biopower plant | Total discounted emission credits $(\underset{20-yr}{NPV}(\sum_{t=1}^{8760} cost_{em}(t)))$ [$] | 0.52m | 0.57m | 0.62m |
| | Total discounted biomass feedstock costs* $(\underset{20-yr}{NPV}(0.098\ [\$/kg] \times \sum_{t=1}^{8760} M_{BP}(t)\ [kg]))$ [$] | 0.49m | 0.54m | 0.58m |
| Total discounted income derived from electricity exports $(-\underset{20-yr}{NPV}(\sum_{t=1}^{8760} income_{ex}(t)))$ [$] | | −2.41m | −2.42m | −2.97m |
| Whole-life cost of the system ($WLC$) [$] | | 21.72m | 27.30m | 31.81m |

* The total cost of the biomass feedstock is not systematically affected by changes in the endogenous variables of the model in this study. That is, the total cost incurred by the biomass feedstock was calculated outside the optimisation model and the results were then corrected accordingly.

Table 3.10: Size of the MG equipment in the cost-minimal solution under different DR provision strategies.

| Component | | Simulation case | | |
|---|---|---|---|---|
| | | MBI-DR | BAU-DR | NO-DR |
| PV plant | $N_{PV}$ [no.] | 3,594 | 3,690 | 4,742 |
| | STDEC* [%] | 3.54 | 3.04 | 3.33 |
| Wind plant | $N_{WT}$ [no.] | 4 | 5 | 6 |
| | STDEC* [%] | 24.11 | 26.35 | 26.73 |
| Micro-hydro power plant | $N_{MH}$ [no.] | 6 | 6 | 6 |
| | STDEC* [%] | 1.91 | 1.59 | 1.36 |
| Biopower plant | $N_{BP}$ [no.] | 4 | 4 | 7 |
| | STDEC* [%] | 0.77 | 0.64 | 0.96 |
| Transformer | $N_T$ [kVA] | 310 | 320 | 329 |
| | STDEC* [%] | 0.11 | 0.10 | 0.08 |
| Hydrogen tank | $N_{HT}$ [kg] | 6,079 | 7,904 | 9,168 |
| | STDEC* [%] | 16.93 | 18.11 | 18.16 |
| Electrolyser | $N_E$ [no.] | 122 | 144 | 157 |
| | STDEC* [%] | 4.14 | 4.08 | 3.80 |
| Fuel cell | $N_{FC}$ [no.] | 238 | 378 | 440 |
| | STDEC* [%] | 6.75 | 8.58 | 8.66 |
| Battery bank | $N_{1600}$ [no.] | 2 | 2 | 2 |
| | $N_{400}$ [no.] | 0 | 1 | 2 |
| | $N_{100}$ [no.] | 2 | 0 | 3 |

| | | | | |
|---|---|---|---|---|
| | STDEC* [%] | 17.49 | 15.06 | 16.00 |
| Super-capacitor bank | $N_{SC}$ [no.] | 1,982 | 2,090 | 2,136 |
| | STDEC* [%] | 14.53 | 12.61 | 11.01 |
| FCEV2G setup | $N_{FCEV2G}$ [kW] | 504 | 573 | 608 |
| | STDEC* [%] | 0.57 | 0.53 | 0.49 |
| Hydrogen station | $N_S$ [kg-$H_2$/h] | 6.14 | 7.94 | 9.15 |
| | STDEC* [%] | 0.42 | 0.45 | 0.45 |
| Inverter | $N_{900}$ [no.] | 5 | 6 | 7 |
| | $N_{115}$ [no.] | 2 | 3 | 5 |
| | $N_{33}$ [no.] | 1 | 3 | 1 |
| | STDEC* [%] | 8.73 | 8.86 | 8.97 |

* STDEC stands for the share of the total discounted equipment-related costs, which can be expressed explicitly in mathematical terms as $((\sum_{c\in C} \underset{20-yr}{NPC_c}) + \underset{20-yr}{NPC_I})$.

The comparative results presented in Table 3.9 reveal that the proposed market-based modelling of the interruptible DSM processes in the planning phase of the conceptualised MG reduces the estimated whole-life cost of the system by at least 21% and up to a maximum of 32% (with an incentive resolution of \$0.02/kWh), as compared to the BAU interruptible DR-integrated and non-DR-integrated MG planning cases, respectively.

Furthermore, the results summarised in Tables 3.9 and 3.10 are indicative of the high efficiency of the proposed model of the aggregator-activated, responsive load-aware MG capacity design in the following ways:

1. While the total discounted equipment-related costs in the BAU case are higher by ~20% than the MBI case, the total discounted income derived from electricity exports has remained at nearly the same level. This is because the majority of this extra cost is spent on the backup power equipment, the energy output of which, according to the MG's hourly operational strategy in Fig. 3.5, cannot be sold to the main grid – for energy efficiency considerations. To examine the robustness of this assumption, a further unreported model was run in both the MBI and BAU simulation cases, where the backup power was allowed to be sold into the utility grid, while maintaining the rest of the model unchanged. A comparative analysis of the results of the two models for the investigated test case is presented in Table 3.11. The results show that the relative difference of the total discounted equipment-related costs in the MBI and BAU cases reduce to ~15%, from ~20% for the base-case model, when the sale of backup power into the grid is not prohibited. The key factor underpinning this change is that the unreported optimisation model that supports the sale of backup power to the main grid finds the opportunity to arbitrage intertemporal differences in wholesale prices and buy-back rates (though non-intelligently). The unreported model, therefore, increases the proportion of total nominal storage to generation capacity in the optimal equipment capacity configuration as compared to the base-case model. More specifically, the proportion of the share of the total backup components'

capacity to the share of the total primary generation components' capacity in the system's whole-life cost increases from 1.97 and 1.85 to 3.51 and 3.22 in the MBI and BAU model realisations, respectively, at relatively modest extra total equipment-related costs – ~9% and ~5%, respectively. This, however, increases the MG's total net income from the exchange of energy with the utility grid by ~76% and ~429%, respectively, in the aforementioned two cases. As a consequence, the MG's whole-life cost reduces by ~3% and ~5%, respectively, in the two cases mentioned above – but at the cost of higher total energy dissipated as a result of increased energy conversion processes due to non-intelligent arbitrage operations.

Table 3.11: Comparison of the proposed model's performance with and without the backup power trading strategy under the market-based and business-as-usual realisations.

| Cost component | Cost subcomponent | Modelling framework | | | |
|---|---|---|---|---|---|
| | | With backup power trading | | No backup power trading | |
| | | MBI-DR | BAU-DR | MBI-DR | BAU-DR |
| Total discounted equipment-related costs $((\sum_{c\in C} \underset{20-yr}{NPC_c}) + \underset{20-yr}{NPC_I})$ [$] | | 18.25m | 21.88m | 19.92m | 22.97m |
| Total discounted MG operational costs $(\underset{20-yr}{NPV}(\sum_{t=1}^{8760} OC_{MG}(t)))$ | Total discounted incentive payment to the aggregators $(\underset{20-yr}{NPV}(\sum_{t=1}^{8760} I_{MGO}(t) \sum_{j\in J} D_{LA}^{j}(t)))$ [$] | 3.99m | 3.48m | 3.51m | 2.95m |
| | Total discounted cost of electricity imports $(\underset{20-yr}{NPV}(\sum_{t=1}^{8760} cost_{im}(t)))$ [$] | 0.46m | 2.76m | 1.39m | 3.92m |
| Total discounted FCEV2G electricity provision costs $(\underset{20-yr}{NPV}(\sum_{t=1}^{8760} \pi_{FCEV2G} P_{FCEV2G}(t)))$ [$] | | 0.42m | 0.49m | 0.28m | 0.31m |
| Total discounted operating costs of the biopower plant | Total discounted emission credits $(\underset{20-yr}{NPV}(\sum_{t=1}^{8760} cost_{em}(t)))$ [$] | 0.52m | 0.57m | 0.37m | 0.44m |
| | Total discounted biomass feedstock costs $(\underset{20-yr}{NPV}(0.098\ [\$/kg] \times \sum_{t=1}^{8760} M_{BP}(t)\ [kg]))$ [$] | 0.49m | 0.54m | 0.35m | 0.42m |
| Total discounted income derived from electricity exports $(-\underset{20-yr}{NPV}(\sum_{t=1}^{8760} income_{ex}(t)))$ [$] | | −2.41m | −2.42m | −4.83m | −5.04m |
| Whole-life cost of the system ($WLC$) [$] | | 21.72m | 27.30m | 20.99m | 25.97m |

2. The total discounted income derived from electricity exports in the non-DR-integrated case is higher by ~23% in comparison with the base case, which is mainly due to the increased excess of renewable energy generation in low-demand periods. Note that the export of energy is seen merely as a means to avoid spillage of non-dispatchable renewable energy, and the low export tariff makes it irrational for the solution algorithm to optimise the capacity of the MG equipment for energy export purposes. It should not be overlooked, however, that energy export made a fair contribution to the cost-efficiency of the proposed MG system in all of the cases studied. It is also important to note that the solution algorithm, in the MBI case, has almost always avoided buying and storing electricity from the upstream grid at times of low demand; rather, the surplus renewable energy is sold to the grid at these times due to: (1) the higher level of feed-in-tariff than the system's LCOE at most of the off-peak times of the year, and (2) the fact that the battery and SC banks soon reach their maximum capacity limits when the MG system is lightly loaded. This is while the total discounted cost of electricity imports occupies ~10% and ~24% of the total discounted system costs in the BAU-DR-integrated and non-DR-integrated cases, respectively.

3. In all of the investigated cases, the optimised size of the electrolyser unit is considerably lower compared to those in established size combinations – of electrolyser to hydrogen reservoir to fuel cell – in the literature (see, for example, [126], [273], [274]). This statement also holds true for the comparison of the optimal combination of the sizes of the hydrogen-based energy storage system's components with those of the disparate optimal hydrogen storage equipment capacity combinations generated for MG systems 1 and 2 – for the cases of Stewart Island and Feilding Valley, respectively – in Chapter 2. This is due to the specific conditions of the present case study site (Ohakune), where load demand is subject to a high degree of seasonality. Accordingly, an electrolyser of lower capacity is sufficient for the purpose – since the hydrogen tank can be filled gradually during the low season, from October through June. That is also why the

optimum capacity of the electrolyser experienced the least changes among the backup power equipment in the three scenarios investigated.

4. As planned, the fuel cell generation using the stored hydrogen has accounted for seasonal load levelling. The optimal capacity of the fuel cell is more dramatically impacted by the proposed interruptible DR implementation as compared to the battery and SC banks. This observation implies that peak load shaving – fulfilled by utilising the responsive loads – has had a substantial role in smoothing out the seasonal variation in load demand, and, in turn, improving the load factor of the annual load power demand profile. In other words, much of the suggested DR scheduling strategy's positive impact on the cost-efficiency of the conceptualised MG is derived from its implementation in the winter high season. This also explains the marked increase in the size of the WT, hydrogen tank, fuel cell, and the electrical loads' inverter – as the main drivers of increasing the equipment-related costs – when the DR is implemented in a BAU manner, or, more significantly, when no DR scheduling process is implemented. To provide a clearer picture of the impact of the proposed DSM model on the load power demand data fed into the optimal capacity planning algorithm, the overall monthly mean 24-h electricity consumption profile for load power is presented in Fig. 3.28 for the simulation cases investigated. According to the figure, realising the proposed DSM model under the BAU and MBI cases shaves ~24% and ~38% off the maximum peak power demand compared to the NO-DR case, respectively. This, consequently, increases the load factor from 0.25 in the NO-DR case to 0.31 and 0.35 in the BAU and MBI simulation cases, respectively.

5. The relatively low share of biomass in the optimised energy resource mix, in spite of its vast potential in the studied site (see Fig. 3.16), is revealing in two ways, namely: (1) the solution algorithm has succeeded in restricting the bioenergy use to a sustainable level by imposing an emission penalty and, more importantly, (2) it gives credence to the idea that biomass resources need to be deployed in a way that contributes primarily to energy

security, rather than pure cost-optimality – in favour of a deep green approach to renewable energy system planning [275]. More specifically, the biopower plant in the conceptualised MG plays a critical role in improving the system's self-sufficiency, as it is the only dispatchable power generation unit in the system.

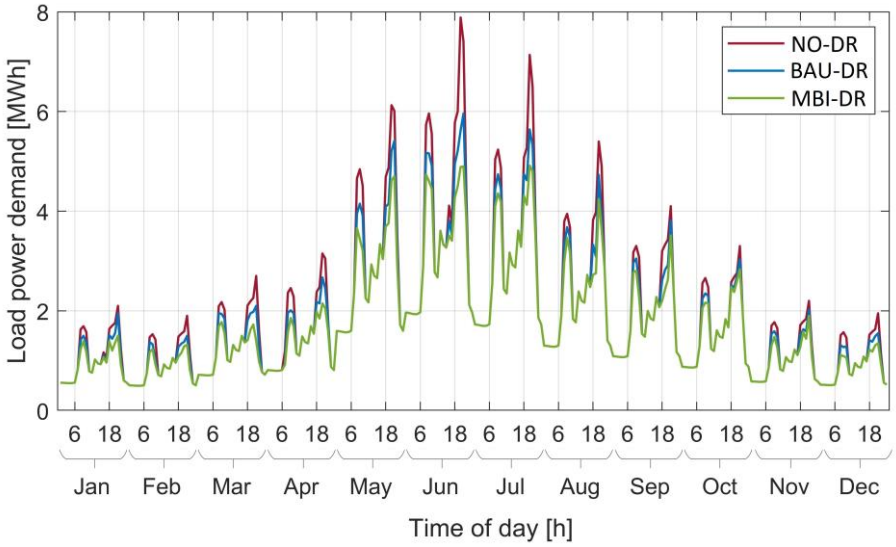


Figure 3.28: Comparison of the monthly mean daily profile for load power demand in different simulation cases.

### 3.6.6. Economic viability analyses

To demonstrate the financial sustainability of the long-term investment proposal on the optimally planned MG system, two rounds of economic viability analysis are carried out. The first round comprises financial appraisal using the set of capital budgeting indicators employed in Chapter 2 (see Section 2.6.4), namely: MIRR, DPP, DPI, and LCOE – with associate comparative analyses of the decomposed LCOE of the MG into levelised costs of electric energy (LCOEE) and hydrogen (LCOH) with the existing average retail domestic electricity and green hydrogen prices at the site. The second round involves comparative analyses of the resulting LCOE of the system with the LCOEs reported in the literature for the most similar projects – as benchmark studies. More specifically, the project was benchmarked against the studies in the literature that met the following four criteria: (1) a self-sufficiency ratio of at least 80% if the system is grid-connected, (2) powered by at

least 70%-renewable onsite energy sources, (3) tailored to the electrification of small- to medium-scale communities, and (4) conducted within the last 5 years.

However, given the lack of energy resilience criteria in the mainstream long-term energy planning optimisation literature to measure the system performance under 'low-frequency, high-impact' events, meeting the pre-determined levels of minimum autonomy hour and grid outage survivability ($AH_S^{min}$ = 8 h, and $GOS_{MG}^{min}$ = 12 h) by the proposed meta-heuristic-based MG sizing approach is treated as an added benefit – and is not factored into the comparative levelised cost analyses. Note that all the analyses in this section are undertaken for the case where distributed sectoral demand-side flexibility resources are scheduled using the proposed Stackelberg, non-cooperative game-theoretic, aggregator-mediated DSM market design under the simulation trial that has yielded the best overall results – where the whole-life cost of the MG is optimised to be $21.72m.

### 3.6.6.1. Capital budgeting

The mathematical formulations of the LCOE, DPP, MIRR, and DPI remain the same as those presented for MG systems 1–3 in Chapter 2 (see Sections 2.6.4.1–2.6.4.4, respectively). Also, the LCOE of the MG system is decomposed into the LCOEE and LCOH components following the same principles and assumptions set forth in Section 2.6.4.1. Accordingly, the following equations are derived for the objective functions (whole-life costs) associated with meeting the electricity and hydrogen loads on MG system 4 exclusively:

$$\begin{aligned}\min WLC_e \\ = \Big(\sum_{c\in C-\{S\}} NPC_c\Big) + NPC_I + NPV\left(\sum_{t=1}^{8760} OC_{MG}(t)\right) \\ + NPV\left(\sum_{t=1}^{8760} cost_{em}(t)\right) + NPV\left(\sum_{t=1}^{8760} cost_{FCEV2G}(t)\right) \\ - NPV\left(\sum_{t=1}^{8760} income_{ex}(t)\right) + pen_{const},\end{aligned} \tag{3.46}$$

$$\min WLC_{H_2} = \left(\sum_{h\in H} NPC_h\right) + NPV\left(\sum_{t=1}^{8760} OC_{MG}(t)\right) + NPV\left(\sum_{t=1}^{8760} cost_{em}(t)\right) + pen_{const}, \quad (3.47)$$

where $WLC_e$ and $WLC_{H_2}$ represent the whole-life costs of the re-structured MG 4 to exclusively address the electricity and hydrogen demands, respectively, and $H = C - \{T, FC, B, SC, FCEV2G\}$ represents the set of components that fulfil a functional role in meeting the hydrogen load demand.

It should also be pointed out that, given the absence of hydrogen loads in the 'electricity-only' scenario, the FCEV load aggregator is omitted from the list of DRAs, whereas it is the only responsive load aggregator in the 'hydrogen-only' scenario. All the other assumptions and procedures remain the same as those in the base-case, integrated scenario.

By solving Equation 2.60 for the case of MG 4, the LCOE of the simulated system is found to be \$0.11/kWh. Also, considering Equations 3.46 and 3.47 as objective functions, the LCOEE and LCOH of the more exclusive systems in the associated solution sets determined by the best performance trial of the MFOA – out of 30 trials – were found to be \$0.10/kWh and \$5.27/kg-$H_2$. The most recent yearly average retail price of domestic electricity is as high as \$0.22/kWh at the studied site [176]. Also, recall that the most recent estimates of green hydrogen in New Zealand for local, small-scale and large-scale production schemes are \$7.98/kg-$H_2$ and \$13.91/kg-$H_2$ respectively. A direct comparison of the obtained levelised costs of electricity and hydrogen from the estimated relevant cost-optimal solutions with the present average retail rates of domestic electricity and locally-produced, small-scale green hydrogen at the considered case study site, shows significant cost reductions of approximately 55% and 62%, respectively, per unit of electricity and hydrogen served.

Also, in calculating the other three financial appraisal metrics – MIRR, DPI, DPP – the sources of cash inflow were adjusted as follows (apart from any salvage

values of the components): (1) electricity is sold to the customers at a flat rate of \$0.22/kWh (in compliance with the existing average retail domestic electricity price), (2) hydrogen is sold to the refilling stations' customers at a flat rate of \$8.00/kg-$H_2$ (which is significantly lower than the most recent estimated price of small-scale, locally-produced green hydrogen in New Zealand and is approximately equal to the retail cost of large-scale green hydrogen production schemes, mentioned above), and (3) electricity is exported back to the grid at a flat-rate feed-in-tariff of \$0.08/kWh. The key financial strength (performance) indicators for the optimally planned MG development proposal (in accordance with the cost-minimal solution) were found to be as follow: MIRR = 10.08%, DPI = 2.66, and DPP = 7.04 years – that is, the investment is expected to reach the break-even point and move to a positive cash flow position after 7.04 years of service.

Accordingly, implementing the proposed MG system is expected to realise savings of up to 62% in the community's energy costs if financed as a community-owned renewable energy project. The project is also readily able to secure third-party investment due to surpassing retail grid parity to a substantial extent. The associated potential power purchase and lease agreements can benefit the community in terms of creating a hedge against the energy price inflation, whilst complementarily improving the reliability, resilience, and adequacy reference margins of the community. Moreover, a direct comparison of the optimal values of LCOEE and LCOH for MG 4 with those of MG 2 (see Table 2.6), as well as the associated values of the key capital budgeting metrics, reveals greater economic profitability of MG 4, despite the facts that both the cases are connected to the main grid, and are located relatively close to each other geographically with the same primary sources of renewable energy considered in the associated candidate pools. There are three reasons underlying the above observation, namely: (1) the scale of MG 4 is greater than MG 2 by a factor of more than 10 (measured based upon the relevant annual peak loads), which creates fundamental value through capitalising on economies of scale, (2) there exist specific seasonal loading conditions on the Ohakune network, which increases the size of the overall hydrogen-based energy storage system (measured based upon the size of the relevant hydrogen tank) by as much as ~727%, and (3) MG 4 is equipped with a BESS in the associated hybrid

energy storage system, which bridges the gap between the high specific power of SCs and the high specific energy of the hydrogen storage system. Note that the BESS was found to be economically inviable for integration into system 2 based on the associated prior feasibility simulations. This can be primarily explained by the insignificant intra-day variability of associated net load demand on test-case 2, making the BESS an uneconomical solution in the presence of a hybrid SC/hydrogen energy storage system.

The above cost-benefit analyses have substantiated the economic benefits of the proposed capital project. Yet, to further validate the financial viability of the investment proposal, the system's LCOE is benchmarked against the LCOE values reported for similar projects in the literature. As stated above, to select the benchmarking studies, four criteria were considered for the MG system: (1) having an energy self-sufficiency ratio – defined as the number of hours where energy demand can be met without support from the grid divided by the total hours in a year – of at least 80% in case of connectedness to the upstream grid, (2) having a renewable fraction of at least around 70%, (3) being tailored towards the electrification of small communities to avoid comparisons with schemes that benefitted from the economies of scale effects or, on the other hand, those designed for ultra-small-scale applications such as radio base stations, and (4) being conducted within the last 5 years to ensure the fairness of comparisons in view of the rapidly falling costs and growing maturity of renewable energy technologies. Accordingly, the proposed system's LCOE and renewable fraction are compared with those of the most similar, recent studies in the literature in Table SM3.1 in the Supplementary Material accompanying the main text (Supplementary Material 3).

As shown in Table SM3.1, the LCOE of the proposed MG is highly competitive with those of the best values reported in the recent literature for international community-scale, highly renewable electrification projects. Add to this the fact that a carbon-free, hydrogen-based, light-duty transportation fleet is integrated into the proposed MG, making it one of the first of its kind, and that the conceptual MG offers distinctive resilience benefits. This provides additional support for the economic sustainability of the conceptualised community energy

system. It should be emphasised, however, that the cost-efficiency of sustainable energy solutions depends, to a large extent, on the target site's renewable energy potential, and region-specific equipment costs, feed-in tariffs and wholesale prices (for grid-connected systems), as well as the context-constrained levels of energy supply interruption that can be tolerated – or deemed acceptable by the target community. It is also noteworthy that for reasons of simplicity, the heat generated by the PEM fuel cell and biopower plant units were entirely spilled in this study. Presumably, the profitability of the proposed system can be further improved by, for example, integrating a heat recovery system to convey waste heat from the fuel cell and biopower plant for space heating purposes [276]. This can also further relieve stresses on the proposed MG system during the heating season. Moreover, according to statistics from the International Energy Agency (IEA) in 2018 [277], green hydrogen production cost estimates range from NZ\$4.2/kg-$H_2$ to NZ\$10.5/kg-$H_2$ as of 2018, depending on whether the production is centralised or decentralised, as well as on the renewable energy and hydrogen production technologies employed, the case study site's potential for renewable energy, the target market segment, and the availability of installers, distributors, and original equipment manufacturers. Accordingly, the LCOH of the conceptualised MG system, i.e. NZ\$5.27/kg-$H_2$, sits reasonably close to the lower bound of the present estimates of the green hydrogen price, which provides further support for the financial viability of the proposed investment plan.

## 3.7. Chapter summary

This chapter has begun the process of improving the basic version of the robust, long-term, meta-heuristic-based, high-dimensional equipment capacity planning optimisation model tailored towards community-scale, sector-coupled, multi-energy-storage-technology, 100%-renewable and -reliable projects, presented in Chapter 2. To this end, it has demonstrated the potential of aggregator-mediated, incentive-based, market-driven DSM programmes tailored to small- to medium-scale end-consumers in improving the economic viability of community-scale, sector-coupled MG systems. Accordingly, a specifically developed platform-mediated, double-sided DSM market design, which characterises the strategic

interactions between the MG operator, monopoly DRAs, and end-consumers in interruptible DR programmes using insights from non-cooperative game theory and endogenous Stackelberg leader-follower relationships is integrated into the proposed meta-heuristic-based optimal MG sizing model. The game-theoretic, elasticity- and comfort-aware DSM market model tailored to grid-connected RSESs has successfully generalised the Stackelberg, non-cooperative game-theoretic, aggregator-mediated day-ahead DR planning problem in the following three areas:

1. The model has quantified the optimal trade-off between electricity importing costs and incentive payments made to the DRAs by incorporating the cost of electricity imports (as a function of the wholesale electricity price) and the cost of procuring incentivised DR flexibility products in the utility's operational cost (payoff) function.

2. The model has addressed the estimated elasticity of supply of DR capacity across different end-use sectors – residential, commercial, industrial, agricultural, and electrified transport – to improve the quality and accuracy of forecasts on the participation rate of different customer classes. This has enabled the model to identify the more cost-effective sectoral dispatchable loads (and hence, more profitable DRAs) in a uniform price settlement structure.

3. The model has included a large number of end-users in each sector, which has allowed the analysis of a broad spectrum of strategy profiles and the corresponding statistically representative payoffs across different end-use sectors. To this end, a stochastic total sectoral load disaggregation algorithm has been employed with real-world implications for the pre-feasibility and techno-economic assessment of grid-connected RSESs for greenfield sites.

Furthermore, the chapter has analytically demonstrated the existence and uniqueness of a pure-strategy Nash equilibrium for the formulated aggregator-mediated, Stackelberg, non-cooperative game-theoretic DSM problem. It has also developed a specific distributed algorithm to approximate the unique, pure-strategy Nash equilibrium solution to the system-level DR dispatch game based on the

endogenous Stackelberg leader-follower relationships. Importantly, the proposed iterative, privacy-preserving distributed algorithm uses an indirect way of sending information about the players' valuation, namely an iterative auction. Notably, on both the wholesale and retail levels, the DSM auction protocol has iteratively interacted with different DR service providers and end-consumers, eliciting minimum sufficient information about their preferences to determine the optimal allocation of DR units in the presence of grid power. This adaptive process has provided a platform to preserve the privacy of the DRAs and end-consumers. The distributed algorithm has also been statistically verified to perform well in converging to the approximate Nash equilibrium of the devised game, with the algorithm precision controlled by the iteration step length.

A number of novel insights have emerged from the indicative modelling results of the numerical test-case MG of the town of Ohakune for representative extreme days of the winter and summer seasons with the highest and lowest one-day total energy consumption (the minimum and maximum system demand days), respectively:

1. Producing the optimal trade-off between importing power and exploiting the flexibility potential of smaller interruptible DR resources for the critical peak hours of system operation – for which a net energy deficit is predicted – is able to reduce the daily system operational cost of a grid-tied MG system (over the critical peak hours) by ~66% (equating to a saving of $912) and ~47% (equating to a saving of $2,124) on representative extreme summer and winter days, respectively.

2. There is a saturation point for the use of DR resources, which varies with respect to the wholesale electricity price and sectoral supply elasticity of DR units. The more the optimal trade-off cost solution deviates from this saturation point, the worse the hourly operational cost solution. Specifically, overpayment for DR products more negatively affects the trade-off operational cost solution than the underutilisation of flexible DR resources.

3. Likewise to the optimal utility-offered incentive price, the best-response-strategy aggregator-posted incentive price is time-step-specific, which occurs at different prices across different aggregators. Specifically, the hourly rank order of the profitability of different aggregator classes varies mainly as a function of the share of each end-use sector in the total procured DR capacity, while the best-response aggregator-determined incentive rate varies with respect to the associated customer-specific (individual-level) discomfort cost parameters, as well as sectoral DR supply elasticities, which define the strategic behaviours of end-users and aggregators – in addition to the utility-posted incentive price in the wholesale DSM market.

Furthermore, the integration of the developed DSM market design into the proposed meta-heuristic-based MG capacity planning model has provided an effective framework for improving the accuracy of investment assessments made for DR-aided energy systems by increasing the quality of long-term forecasts of distributed sector-wide end-users' participation in incentive-directed DR programmes, whilst adopting the endogenous Stackelberg leader-follower relationships in two stages, namely: first, for interactions between the MG operator and responsive load aggregators, and second, for aggregator-customer exchanges. Accordingly, the modified MG investment planning model has successfully generalised the long-term, community-level renewable energy system design problem in the following five areas:

1. It has, for the first time in the literature on energy planning optimisation, produced optimal trade-offs between importing electricity, discharging onsite energy storage media, procuring FCEV2G provisions, dispatching controllable generation (biopower plants), and leveraging incentivised DR flexibility resources, especially during coincident peak time-steps where the total variable renewable energy supply falls short of demand.

2. It has guaranteed a level playing field for a variety of clean energy technologies – in the interest of energy diversification – where the use of biomass resources is limited to a sustainable level by imposing a new constraint term.

3. It has implemented the potential of cross-vector integration (in particular, power-to-gas technology) in conjunction with the value of FCEVs in V2G operations to improve the flexibility of energy systems with deep penetration of renewables.

4. It has allowed for a meta-heuristic solution algorithm based on the MFOA to find the cost-optimal mix of MG assets, whilst facilitating long-term decision-making on the delivery of aggregator-mediated incentive-responsive loads using a realistic example. The use of a case study has illustrated the application of the model in Ohakune, demonstrating that many of the challenges for integrating a 100%-renewable energy system can be surmounted.

5. The suggested solution algorithm has also shown to be efficient in nearing the formulated problem's globally optimum solution. In addition, a comparative analysis of the proposed market-driven and BAU realisations of the interruptible load programme has verified the validity of the proposed modelling framework as a decision support tool for utilities to make reliable forecasts about the engagement rate of different classes of end-consumers in DR programmes. This is particularly important when designing greenfield renewable energy systems, or as MGs are used to increase the penetration of responsive loads.

The numeric results obtained from the modified MG investment planning model's application to the test-case system of Ohakune have also revealed three novel insights, namely:

1. The use of the proposed two-stage DSM market design for the projection of flexible demand resources, which has shown to be incentive-compatible (truthfully implementable) and associated with a balanced financial incentive flow, brings higher-order information about MG operator-aggregators-customers interactions into the analysis, which can be leveraged towards improving the economic viability of renewable energy systems. Notably, as compared to the case where demand-side resources are

managed using a BAU interruptible load approach, the model results have indicated that a cost saving of at least 21% (equating to approximately $5.5m) can be generated for the simulated MG for Ohakune, while imposing approximately the same discomfort cost on end-users.

2. The large-scale supply of demand-side flexibility resources, enabled by DRAs, has the potential to significantly reduce the estimated life-cycle cost of sustainable energy systems. Specifically, the evidence from this study has demonstrated that assisting the conceptualised MG with incentive-driven, market-directed DSM processes reduces the total discounted system costs by a significant ~32% (equating to around $10m in this case study). In this light, a thorough analysis of the value of lost load to the target customers – in the interest of improving the accuracy of the forecasted willingness of the end-users to deliver their DR resources – is of paramount importance in the design phase of all-renewable MGs. This is especially true for the development of first-access energy systems in remote areas where the values of unserved energy are expected to be lower than those estimated for urban and industrial customers.

3. At present, Ohakune's electricity distribution network is plagued by congestion [257]. That is, The Lines Company, the owner and operator of the network, has announced multi-phase projects involving the upgrade of the Ohakune supply point by ~1.5 MVA over a 10-year period from 2019 to 2028 [278]. However, the conceptualised MG system's levelised costs of electricity and hydrogen – $0.10/kWh and $5.27/kg-$H_2$, respectively – indicate that the project proposal from this study can substantially reduce the energy tariffs at the considered site. This also implies that the developed DSM strategy can produce a steady revenue stream for the local community in addition to a resilient energy system that provides cost-effective energy independence.

The cost-minimal long-term MG designing results obtained using the MFOA out of 30 trials have also lent further credence to the insights gained in Chapter 2 on the adequacy of a single run of the MFOA in yielding in-depth, robust, and

accurate MG infrastructure planning and asset allocation decision-making support – in view of the relatively negligible percentage error of the associated best and worst simulation run results. Furthermore, the relevant convergence behaviours of the MFOA have further verified the adequacy of the selected values for the stopping criteria – the maximum number of iterations and population size.

In terms of the chapter's contribution to address the secondary objectives of the research, discussed in Chapter 1, the numerical simulation results have reaffirmed the technological competence and cost-competitiveness of hybrid energy storage systems, as well as using hydrogen as an energy vector in larger-scale community-scale MGs for niche applications – inter-seasonal energy storage to meet seasonal demand, and hydrogen mobility to decarbonise the transport sector. Furthermore, the proposed energy filter-based approach to scheduling hybrid energy storage systems has been effectively expanded to three energy storage technologies, namely: hydrogen storage, vanadium redox flow batteries, and SCs. This has provided a platform to more efficiently address the variability of renewables by economically dispatching different backup systems running at seasonal, inter- and intra-day, and transient temporal resolutions as necessitated by the specific diurnal and seasonal loading conditions of the test case of Ohakune. Also, the cost-efficiency of integrating a town-wide fleet of light-duty personal passenger hydrogen fuel-cell powered vehicles with FCEV2G capabilities is demonstrated using the suggested efficient and cohesive energy management strategy for the coordinated charging/discharging of vehicles, with direct implications for the activation of a pool of FCEVs (of heterogeneous elasticities to supply DR capacity) to participate in local flexibility markets, as well as estimating the associated overall elasticity of sector-specific DR supply capacity. Moreover, on a deeper level, the chapter has generated an additional layer of supporting observations – consistent with the findings of Chapter 2 yielded by the application of the basic MG sizing model to systems 1 to 3 – that substantiate the proposed meta-heuristic-based solution algorithm's efficacy in handling highly diversified portfolios of variable generation and energy storage technologies with corresponding temporally complementary characteristics, together with a sustainable share of dispatchable RESs (through optimal system integration of

different bioenergy generation technologies), in pursuit of improving the dispatchability of all-renewable MGs.

A comprehensive analysis of the economic viability of implementing the optimised MG configuration for the case of Ohakune has, additionally, supported the financial sustainability of the capital proposal. The economic viability analyses have incorporated (i) high-level financial appraisal evaluation metrics, (ii) comparative analyses of the returned levelised costs of electricity and hydrogen with the respective existing average retail prices, and (iii) benchmarking the resulting LCOE with those of the best values reported in the recent literature for international, community-scale, highly renewable electrification projects. The comprehensive financial sustainability analyses have highlighted that not only is the suggested renewable energy development project economically feasible without any government subsidies, loans, or tax breaks for renewable energy, it can also be viewed as a prime investment opportunity with a solid high return on low-risk, a robust revenue stream, and reasonably predictable, large yields. In addition, valuable insights have been gained into the significant impact of reaping synergies across the electricity, low-temperature heat, and transport sectors on the applicability and effectiveness of long-term energy planning optimisation models. Moreover, the study has shown that the conceptualised grid-tied MG system can pave the way toward achieving greater energy independence, energy democracy, and energy security in rural and semi-urban areas in a cost-effective, socially acceptable, and environmentally efficient way.

Based on the above premises, the modelled MG provides an evidence base to inform the energy sector and climate change policy, infrastructure providers, and the wider modelling community of the technical feasibility, social acceptability, and economic viability of leveraging the potential flexible synergies in the integration of energy networks for electricity, heating, and transport to realise economy-wide deep decarbonisation. Additionally, a discussion on the adaptability of the proposed two-stage aggregator-mediated, incentive-based, customer comfort-aware DR procurement marketplace to real-world scenarios within a New Zealand context has been planned with the key enabling smart grid technologies – advanced metering,

control, and communications infrastructure – as well as the associate communications protocols and standards to be detailed.

In conclusion, this chapter has demonstrated that improving renewable energy system investment planning approaches to accommodate the rational and strategic behaviour of relevant actors during the dispatch processes of demand-side resources based on non-cooperative game theory can reveal new, useful information that helps address epistemic uncertainty in the practical DR capacity of end-consumers, and consequently, the systematic uncertainty in the total discounted system costs arising from lack of knowledge endogenous to the incentive pricing behaviour of the DR platform. It has also revealed how significant the financial consequences during the MG planning phases are of a fair allocation of the overall benefits that accrue from activating smaller sources of DR among the market participants.

The following chapter goes further and expands the level of analysis by adding a computationally tractable probabilistic dimension to the proposed sectoral DR-integrated meta-heuristic-based MG configuration planning optimisation model formulated in the present chapter. The novel scenario reduction-oriented, high-dimensional, data-driven MCS-based uncertainty quantification layer added to the meta-heuristic-based, sectoral DR-aware MG energy planning optimisation model is able to produce different energy planning decisions in accordance with the uncertainty budget of interest for the realisation of the most salient model-inherent parametric uncertainties. It also seeks to provide a coordinated, system-level hybrid-energy-storage-technology MG design and dispatch co-optimisation framework under the most likely uncertainty characterisation scenario, whilst accounting for the total incentive-responsive V2G resource capacity in the integrated resource plan, as well as various arbitrage opportunities. To this end, it additionally nests a consecutive sequence of forward-looking, predictive, linear programming-based daily operational scheduling optimisation problems – tailored to the system-level dispatch of controllable DERs, FCEV2G resources, and grid energy trades – into the stochastic, DR-integrated, meta-heuristic-based MG designing and equipment capacity planning model, which replaces the associated heuristic, Greedy, fixed-controller, cycle-charging energy dispatch strategy.

# Chapter 4: Adding a Computationally Tractable Probabilistic Dimension to Micro-Grid Investment Planning and Operational Scheduling Co-Optimisation[1]

In accordance with Part III of the research, the preceding chapter has begun the process of developing a more integrative meta-heuristic-based energy planning optimisation approach in pursuit of reducing the adequacy and security reference margins of highly renewable, reliable, resilient, and self-sufficient sector-coupled community energy systems. To this end, by specifically addressing primary research objective 2, it has shown that the projections on the sectoral engagement in DR programmes used in the long-term capital infrastructure planning of sustainable energy systems are substantially prone to the biases and preferences of end-consumers, which need to be modelled explicitly by means of the sectoral elasticity of the customer supply of DR capacity under hybrid opt-in/opt-out methods of recruitment. Accordingly, it has developed an understanding of the impact of characterising sectoral end-consumer behavioural traits in long-term DSM schemes on renewable energy investment projections.

More specifically, the previous chapter has demonstrated that market-driven sectoral distributed flexibility procurement solutions processed in a non-discriminatory settlement format with an iterative first-price sealed-bid auction at both the wholesale and retail levels are able to maximise the associated social welfare, liquidity of customer-supplied DR capacity, fiscal transparency, as well as the overall robustness and stability of sectoral DR provision in the long run – necessary to improve the security and resilience of DR-integrated sustainable

[1] This chapter draws partly (occasionally verbatim) on the following journal paper:

• **S. Mohseni**, A.C. Brent, D. Burmester, and W. Browne, "Lévy-flight moth-flame optimisation algorithm-based micro-grid equipment sizing: An integrated investment and operational planning approach," *Energy and AI*, vol. 3, p. 100047, 2021.

energy systems of the future. It has also highlighted how renewable energy business models can benefit from having greater visibility over potentially dispatchable demand-side flexibility resources in the long run in light of the stable interactive strategies envisioned using game theory – and how that can drive the deployment of community-level clean energy projects.

While all the analyses in Chapters 2 and 3 were carried out from a deterministic perspective, it is common knowledge that modern community energy systems are subject to incremental sources of long- and short-term uncertainties, not only as a result of the increasing penetration and diversification of non-dispatchable distributed energy supplies, but also because of the emerging smart grid-enabled interventions, such as large-scale, aggregator-mediated DR activation. That is, energy demand is no longer the only source of forecast uncertainty and the correlated uncertainties of variable renewable energy generation, loads, and wholesale prices, particularly, complicate the accurate and efficient planning and operating processes of RSESs. This brings to light the importance of comprehensive, high-level comparative analyses of the implications and accuracy of deterministic scheduling and planning optimisation models of RSESs and the counterpart uncertainty-aware methods in the presence of large volumes of non-dispatchable renewables and distributed sources of demand-side flexibility. Accordingly, the renewable energy system modelling community has faced the inevitable trade-off of attempting to capture the complexity of reality vis-à-vis developing a manageable model that can be populated with high-quality data to deliver findings that better aid the associated decision-making processes.

On the other hand, considering the optimal dispatch strategy simultaneously to the system design using the specifically devised *fixed* energy management framework in the previous chapters has the potential to impair the economic viability of the system as a result of less predictability of the future operating states of the system. That is, rule-based, heuristic operational decisions, which lack any foresight of future system conditions and do not algorithmically seek out minimum operational costs, are prone to excessively oversizing the system (leading to increased cost) or undersizing the system (leading to poor reliability), which

respectively represent potentially over-conservative or inadequate MG planning decisions.

In this light, this chapter takes a probabilistic approach to capital investment planning of renewable energy systems by simultaneously quantifying uncertainties in climatological, power load demand, and wholesale electricity market price forecasts – which are found to be of fundamental importance to ensure the validity and reliability of the associated numerical simulation results – in conjunction with producing portfolio-level optimal dispatch decisions that ensure a non-degraded performance in a realistic implementation and yield a better match of the future operating states to reality. More specifically, in line with primary research objective 3, the chapter presents a large-scale, data-driven, scenario reduction-led, multi-dimensional approach for the quantification of various problem-inherent parametric uncertainties at a time – based on the discretisation of the corresponding probability distribution functions (PDFs) – necessary to develop stochastic energy planning decisions in accordance with different uncertainty budgets, whilst additionally characterising the uncertainties in ambient temperature and river streamflow forecasts for the first time in the literature.

Also, in line with primary research objective 4, the chapter presents an optimal operational planning optimisation formulation that determines the year-long optimal multi-component schedules over a moving one-day horizon, where dispatchable and non-dispatchable DERs, incentive-response loads, and V2G interventions are present in the system with the option to exchange energy with the wider utility grid. Nesting the proposed optimal dispatch strategy into the stochastic, DR-integrated, meta-heuristic-based MG sizing model, such that the optimal design and dispatch problems are decomposed into separate sub-problems, produces systematically coordinated investment planning (long-term) and operational scheduling (short-term) decisions that adequately value the operational benefits of arbitrage strategies – by charging the battery storage daily utilising low-cost energy during the system- and utility-grid-wide off-peak periods and discharging it during high-cost coincident peak periods. Considering the capacity planning of MG equipment jointly with its economic dispatch provides a platform

to improve the practical utility of uncertainty budget-constrained, probabilistic MG investment cost/benefit analyses that ensure globally optimum designs.

In this setting, the chapter aims to address research gaps 3 (*lack of comprehensive, high-level uncertainty-aware approaches*) and 4 (*underrepresented usage of joint operational and investment planning optimisation methods*) identified in Chapter 1. This forms part of the overall goal of the deductive reasoning-oriented part of the research (Part III) studied in Chapters 3 and 4, which seeks to address a number of unjustified simplifying assumptions commonly made during the planning phases of RSESs, which disconnect the proposed models from reality and obscure the real challenges of transferring simulation results into the real-world.

## 4.1. Introduction

As discussed in detail in Chapter 2, the standard meta-heuristic-based MG equipment capacity planning problem needs to conduct an hourly-basis, year-long energy balance analysis for promising candidate combinations of the components, which makes the problem computationally complex. Further compounding the computational intensity issue is that the associated energy dispatch problem deals with multiple stochastic input parameters, such as long-term forecasts of load demand, weather conditions, and wholesale electricity prices (in the case of grid-connected systems). Such sources of uncertainty can affect the energy balance analysis, propagating upward into the optimal sizing problem [279]. Accordingly, the uncertainties inherent in the mathematical models of RSESs make the associated decision-making processes of integrated resource operation, planning, and designing profoundly complex. Supporting the associated stochastic decision-making processes during the long-term investment planning and short-term operational scheduling of RSESs in the presence of distributed demand-side flexibility resources is of paramount importance in order to develop a deeper understanding of the optimal designs and dispatch strategies within the smart grid paradigm. Fig. 4.1 summarises a wide range of input parameters of the energy planning optimisation problem, which are associated with data uncertainty.

Notably, addressing the parametric uncertainty inherent in forecasted load demand, output power from weather-dependent sources, and electricity market prices – as the most salient sources of data uncertainty – has been found to be of prime importance to ensure the economic sustainability of renewable energy projects [280]. Importantly, if such sources of uncertainty are not hedged against (quantified and managed) effectively, the estimated size and total life-cycle costs of renewable energy systems' equipment – and consequently, the associated energy dispatch decisions – will not be realistic. That is, such inaccuracies in input data forecasts potentially significantly under- or over-estimate the associated lifetime costs and, therefore, increase the performance risk of sub-optimal operation, indicating that inferior energy resource portfolios and operational schedules incur additional costs associated with incompatible systems or re-engineering. More specifically, oversizing of non-dispatchable renewable power generation resources and energy storage devices induces excessive capital costs, while undersized systems might not be able to provide the desired economic, reliability, or environmental benefits [281]. For grid-connected systems, oversizing translates into uneconomical excess renewable power exports, whereas undersizing – which often entails a lack of aggregate energy reserves – means extremely expensive grid imports during periods of highest electricity prices, where local system-wide peak usage coincides with network congestion periods. Based on the studies carried out to date, a discrepancy of up to around 25% between deterministic and stochastic models proposed to optimally design and operate RSESs is expected [46], [282], [283].

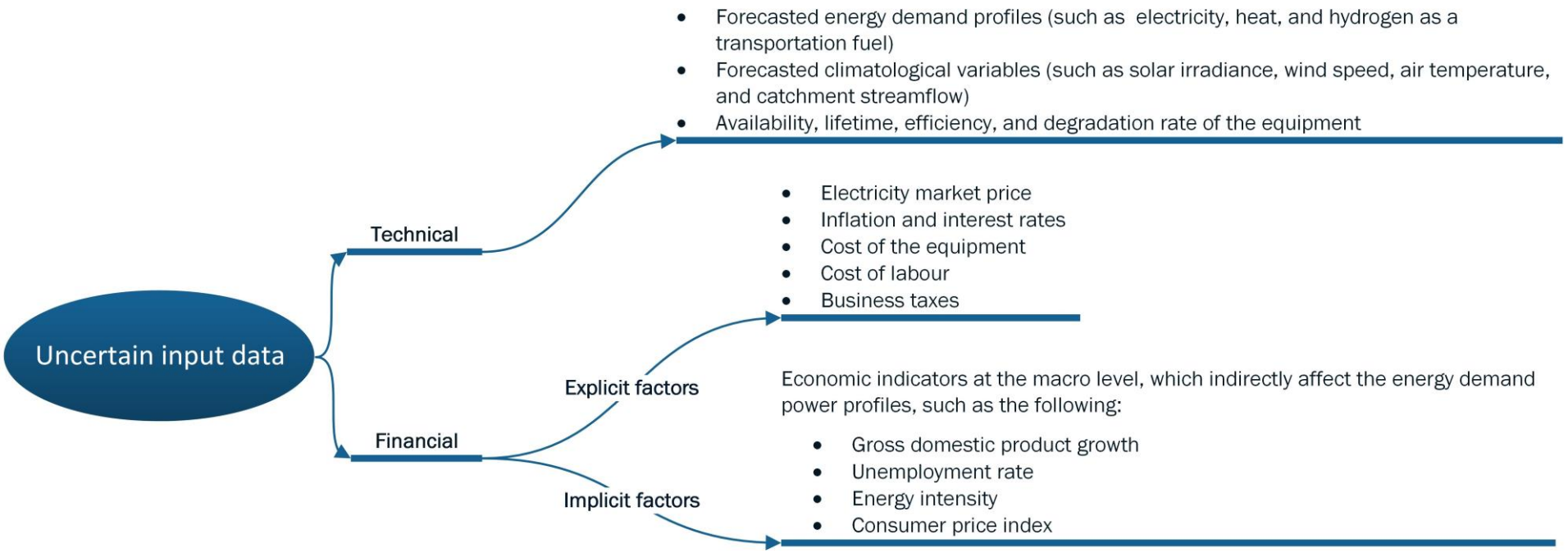


Figure 4.1: Classification of the sources of data uncertainty for the MG design and planning problem.

On the other hand, evaluating the operational performance of a particular MG design (the overall system configuration and the associated unit sizes) is integral to the associated probabilistic designing and planning processes. The associated operational performance analysis entails simulating the expected operating states of non-dispatchable (passive) generation technologies, while simultaneously modelling the components that can be centrally dispatched by system operators through dedicated controllers to balance out supply and demand. The complexity of the MG design and dispatch co-optimisation problem stems from the need to evaluate each design by producing the operational schedules for the MG at discretised time increments (commonly, one hour) over some time period (commonly, one year) to understand a given design's performance.

For conventional rule-based (heuristic or fixed) operational strategies used in the mainstream MG sizing approaches, this consists of producing fixed operational decisions, as directed by the associated pre-defined control logics per dispatchable unit – for example, to charge the storage when the net load is negative (excess power is present), and to discharge when the non-dispatchable RESs fall short of load demand, in an off-grid setting. However, the fixed-controller method (with pre-programmed rules) is not a formal 'optimal' approach as it does not algorithmically seek out minimum operational costs, nor does it have any foresight about the future system conditions in that the dispatch decision for each time-step is determined independently of the preceding or following time-steps. That is, generating the dispatch decision using the control logics for a given time-step only requires information from the previous time-step. Consequently, the fundamental goals of economic dispatch scheduling pursued during the operational phases are not fulfilled completely when using such simplified rule-based operational strategies, with the associated errors directly propagating into the design problem's outputs. More specifically, the (optimal) economic dispatch problem entails solving the dispatch of the controllable elements over multiple time-steps concurrently to achieve some optimal objective, such as minimum energy not supplied or minimum day-ahead operational cost. In this light, the computational efficiency and straightforwardness of using pre-specified heuristic operational rules come at the risk of sub-optimality [21].

This brings to light the importance of a coordinated, portfolio-level MG asset allocation and operational scheduling problem that simultaneously addresses the size optimisation and dispatch control strategy of the DERs in the candidate pool, whilst systematically characterising the most salient model-inherent parametric uncertainties. The key driver of the complexity of the underlying optimal dispatch problems is the need to generate scheduling decisions for many dispatchable units at a time for each time-step along an operational horizon, which potentially leads to a high-dimensional optimisation problem. As an indication, optimising a dispatch problem incorporating 10 controllable units over an hourly-basis, year-long time period results in 10 (units) × 8,760 (h) = 87,600 variables. Further complicating the associated integrated strategic resource planning problem, apart from the quantification of uncertainties discussed above, is the consideration of a connection to the wider network, as well as a decentralised system-level incentive-based DR dispatch, where DR is treated as a heterogeneous system resource. Additionally, the special case of utilising inherently computationally expensive meta-heuristics to optimise a solution to the design optimisation problem adds significant computational complexity.

As illustrated above, although using long horizons (for example, one year) during the dispatch optimisation theoretically improves the optimality of operational planning solutions, it is not computationally feasible, nor does it represent how a MG would be scheduled in real-world conditions with a non-fixed controller. Such a controller would be able to dynamically receive optimal dispatch decisions from a controller software that is generated from the controller model (dispatch optimisation model) running on a desktop computer on a day-ahead basis, for example. Accordingly, the whole-year dispatch time horizon widely used in the planning approaches with rule-based dispatch strategies need to be decomposed into a sequential series of smaller subsets (knowns as *decision horizons*) when using optimisation-based operational strategies. A decision horizon length of 24 hours indicates a real option given the 24-hour cycles that take place with loads, prices, and non-dispatchable generation. Additionally, it has been demonstrated in prior work that, when parametric uncertainties are quantified, longer time horizons have no advantage because the error in parameter forecasts compounds as the forecast

horizon lengthens [21]. Moreover, it is important for the optimisation-based operational strategy to be able to maximise potential profits from energy arbitrage using the storage systems (where applicable), especially in the presence of uncertainty – in pursuit of realistic and truly globally minimum total discounted system cost estimates incorporating well-balanced investment and operational cost components.

### 4.1.1. Literature review

In this light, a recent, growing body of literature has developed a range of 'uncertainty-aware' MG investment planning modelling frameworks [46], [284]. Accordingly, there are several review papers around the implications of multi-dimensional stochastic energy planning decision-making processes. For example, Mavromatidis et al. [46] have presented a review of different uncertainty treatment approaches in the optimal planning phase of RSESs. Zubo et al. [47] have focused on reviewing the literature on uncertainty-aware operation and planning of distribution grids with a high penetration of renewables. Moreover, Aien et al. [48] have classified different emerging methods employed to capture different sources of uncertainty associated with various levels of power system analysis.

Table SM4.1 in Supplementary Material 4 presents a summary of the most vigorous MG capacity planning optimisation approaches in the literature that have managed to accommodate at least one source of (forecast) data uncertainty (listed in chronological order of publication date). It also highlights the presence or absence of an optimisation-based operational scheduling modelling element within the existing probabilistic MG sizing methods (with or without benefitting from energy arbitrage services). The table, additionally, provides a platform to position this chapter within the identified knowledge gaps and previously neglected factors in the stochastic hybrid renewable energy system planning optimisation.

### 4.1.2. Identified mainstream approaches and knowledge gaps

The comprehensive thematic literature review in Table SM4.1 reveals a number of key research gaps within the mainstream uncertainty-aware renewable energy system capacity planning decision models, namely: (1) the potential intractability

of the existing stochastic approaches to simultaneously handle a broad spectrum of input data uncertainty; particularly, more than four sources of parametric uncertainty, (2) the absence of long-term energy planning optimisation decisions in accordance with different uncertainty budgets on the acceptable levels of uncertainty in design quantities of interest, defined by the allowable risk in not meeting a critical design constraint (particularly, reliability) and the allowable deviation in the total discounted system cost metric, and (3) the systematic negligence of the uncertainty coupled with ambient temperature in conjunction with the uncertainty in solar irradiance forecasts (for potential solar PV generation plant), as well as the lack of scholarly attention to the optimal system integration of micro-hydro resources, and thus, failure to characterise the uncertainty associated with river streamflow.

Most strikingly, quantification of the input data uncertainty, as far as can be ascertained, has often been limited to two or three uncertain parameters, with very few studies simultaneously addressing four sources of data uncertainty – most of which are analytically solved (as opposed to using meta-heuristics). That is, the maximum number of uncertainty factors accounted for at a time in the literature is as low as four, as far as can be ascertained. Furthermore, the *average* number of parametric uncertainties quantified concurrently has remained stagnant at around two, implying a relatively low overall level of data uncertainty treatment in the mainstream stochastic energy planning optimisation literature. Additionally, the mainstream uncertainty-aware long-term energy planning optimisation literature lacks any kind of model-based decision-support analyses regarding the degree of uncertainty needed to be treated to reach the pre-defined renewable energy development goals – for example, as to the value the target customers place on reliable, resilient, and self-sufficient supply. This indicates that, despite growing recognition of the importance of addressing system-inherent uncertainties, systematic methods to characterise and mitigate multi-dimensional uncertainties remain a significant challenge, particularly for systems that comprise a large number of interacting sub-components.

Furthermore, the uncertainty associated with the power output from the solar PV plant in practically all the relevant reviewed publications has been characterised

based solely on the uncertainty coupled with solar irradiance forecasts. However, to yield more complete representations of the uncertainty inherent in the PV plant's output power, a planning model needs to handle both the uncertainty in solar irradiance and ambient temperature forecasts. Furthermore, previous work has commonly failed to address the uncertainty associated with river streamflow forecasts. Moreover, less attention has been given to determining the uncertain parameters and inputs that contribute most to output variability in the context of MG capacity planning and designing. Notably, this less well-explored area has the potential to significantly improve the understanding of how reducing uncertainty in the parameters of interest would lead to a reduction in output uncertainty (the effects of uncertainty treatment), with the answer to this question implying potentially significant implications for system design and costing – towards best-spent uncertainty budgets. Additionally, by targeting the most sensitive uncertain parameters and managing MG resources in a systematic way, such analyses would offer the opportunity to tailor the MG design towards reducing uncertainty in critical areas yet allowing for flexibility in others – in the post-optimisation phase.

On a wider level, the reviewed publications in Table SM4.1 indicate a relative paucity of comprehensive, high-level uncertainty-aware approaches, where uncertainty is not coarsely accounted for by using confidence factors on the resulting decision variables – as is also the case in many of the studies that did not fit the review criteria. This implies that assuming perfect long-term input data forecasts – or, put differently, ignoring the uncertainty associated with input data forecasts – is common practice in the long-term MG investment planning literature. Accordingly, although their potential benefit in narrowing reality gaps has been demonstrated in several RSES optimisation areas, stochastic models applied to the MG capacity planning problem remain underutilised. That is, the long-term MG investment planning problem in the mainstream literature reviewed in the previous chapters has most commonly been deterministically formulated, where the forecasts of input data, such as meteorological, load demand, and wholesale electricity price time-series, are merely modelled using the expected values of the stochastic input parameters involved. This trend can be explained by the fact that adding a stochastic dimension to the MG capacity optimisation problem potentially makes it

computationally expensive. The reason lies in the need to solve the problem for all possible combinations of data forecasts to represent a multi-variate scenario tree, with the nodes visited by each path (scenario) corresponding to the values assumed for uncertain variables in the model. By the same token, the underlying factor for the alarming paucity of research concurrently addressing multiple sources of data uncertainty is the computational intractability of simulating the associated systems for all the combinatorial data possibilities generated from the discretisation of the corresponding PDFs – that are derived from the relevant historical datasets – when the number of uncertain inputs exceeds a context-specific – and yet nearly always low – critical threshold. Accordingly, the associated computational complexities are the main reason for the limited number of uncertainty sources quantified jointly (especially when using probabilistic multi-variate time-series forecasting approaches based on historical data and/or meta-heuristic optimisation approaches). On the other hand, the algorithmic complexity of mathematically modelled uncertainty quantification approaches increases as the number of uncertainty sources rises.

Table SM4.1, additionally, reveals that the Monte Carlo simulation (MCS) is the mainstream approach in the literature for characterising the model-inherent parametric uncertainties. Particularly, in the relevant meta-heuristic-based solution approaches, there is a consistent tendency towards using the MCS method to represent uncertainties. This is due not only to its straightforward model specifications, but also to its potential to handle multiple uncertain parameters simultaneously. More specifically, the main advantages of MCS for probabilistic analyses – provided that long-term historical data for the uncertain parameters are available – can be summarised as follows [285]: (1) reflecting any sources of nonlinearity or asymmetry in the functional relationships, (2) handling the joint simulation of multi-variate distributions with specific correlations provided that the covariance is incorporated into the input distributions, (3) providing a coverage interval corresponding to the coverage probability, as well as (4) simple foundations and easy implementation.

Accordingly, this study utilises an improved variant of the original MCS-based uncertainty treatment approach. A flowchart of the basic MCS-based

stochastic uncertainty characterisation is depicted in Fig. 4.2. The procedure relies on historical data and uses probabilistically generated pseudo-random numbers based on the associated best-fit distributions. After evaluating the performance of the model for various pseudo-randomly sampled data, the best-fit PDFs of the output decision variables are derived, which contain all the information needed for uncertainty analyses. In the MG planning context, the mean values of the output quantities for the decision variables and objective function are often the only statistical measure used for interpreting the obtained results in terms of forecast uncertainty. That is, according to the law of large numbers, the means of results are considered as uncertainty-aware results.[2]

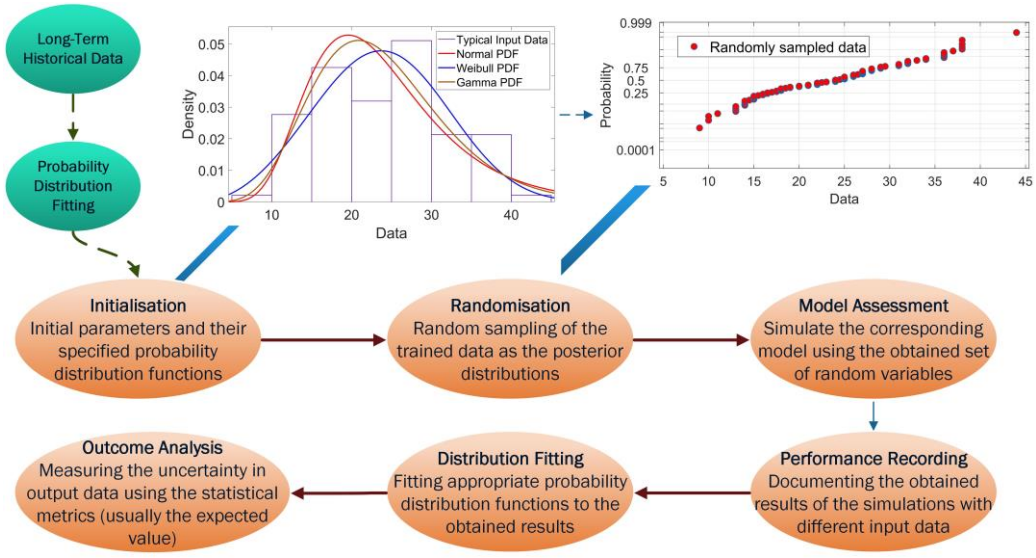


Figure 4.2: Overview of the MCS-based uncertainty quantification approach.

Furthermore, the literature review provides key insights into the uncertain parameters with the highest effect sizes (relative importance) – as indicated by the most commonly characterised uncertain parameters. As Table SM4.1 reveals, the climatic, load demand, and wholesale price forecasts constitute the most widely quantified uncertainty factors, which supports the choice of parametric uncertainties accommodated in this study – in accordance with the structure of the

[2] The law of large numbers states that the arithmetic means of the results derived from a large number of trials will be close to the true value and gets closer the larger the number of trials.

conceptualised test-case system and the non-dispatchable generation resources considered for integration.

In addition, Table SM4.1 is revealing as to the less scholarly attention given to the consideration of arbitrage-aware optimal dispatch strategies (in an integrated way) in the associated stochastic methods focusing on the optimal system configuration and unit sizing of RSESs. More specifically, while around half of the identified relevant articles promote an integrated design and dispatch optimisation approach, the potentially significant profits associated with using the onsite storage for arbitrage operations have been widely overlooked. That is, the table demonstrates that no single article, as far as can be ascertained, has effectively valued the arbitrage economics of energy storage during the long-term strategic investment planning phases of RSESs, whilst quantifying the problem-inherent parametric uncertainties.

### 4.1.3. Objectives and contributions

This chapter aims to contribute to the trends of broadening the scope and level of analysis of the MG equipment-capacity planning and scheduling co-optimisation problem and reducing the systematic – and potentially significant – misalignments between the modelled and actual life-cycle costs of 100%-renewable and reliable RSESs, evident in the summary of the previous work in Table SM4.1, through adding a probabilistic decision-making dimension that is aware of arbitrage opportunities. More specifically, informed by the probabilistic planning-related research gaps highlighted in the previous section, the first main objective of this chapter is to introduce a more integrative MG sizing approach that considers more refined considerations during the long-term energy planning optimisation – in the interest of bridging the potentially significant simulation-to-reality gaps – by systematically broadening the spectrum of input data uncertainty sources characterised concurrently, while retaining the solution accuracy and CPU usage time within acceptable limits. Accordingly, by addressing the glaring research gaps identified in the preceding section in terms of the accuracy of numerical solution approaches to the optimal stochastic investment planning problem of RSESs, the chapter adds new layers of insight and perspective into the collective body of

knowledge in the field by simultaneously quantifying the forecast uncertainty of six input parameters (including two less well-explored uncertain parameters), while optimally planning and designing RSESs. More broadly, the chapter seeks to demonstrate the importance of making systematically sound, strategic, budget-constrained decisions under various parametric uncertainties during the MG infrastructure planning optimisation processes. To this end, it provides in-depth, accurate, and robust energy planning decision-making support under different degrees of tolerable multi-variate data uncertainty – in pursuit of making the simulation results more perceptually representative of real-world scenarios, in line with the designers' expectations.

On the other hand, as demonstrated in the previous section, there exist severe methodological and content gaps in the renewable energy system planning optimisation literature on the coordination of an optimal integrated resource allocation problem with a nested optimal scheduling problem to size individual MG components simultaneously with their operation strategy. In response, the chapter addresses the problem of optimal scheduling of multiple generation technologies, energy storage media, and DR resources in the presence of utility grid, focusing on hourly optimal dispatch to minimise operational costs over a representative year with a moving one-day time horizon as a trade-off between computational burden and solution quality for solving a specifically formulated linear optimal energy management problem via linear programming. In addition to being capable of handling a high-dimensional decision space (without suffering from the so-called '*curse-of-dimensionality*' phenomena), the proposed optimal dispatch framework is novel as it constitutes the first MG scheduling problem of any kind that explicitly accounts for both grid arbitrage and local renewable energy generation arbitrage on a daily basis using the storage devices whose timescales fit the economic daily cycling, with the option for the outer-layer design problem to allocate additional energy storage installations for energy arbitrage reasons alone. To this end, the chapter also, for the first time, implements a large-dimensional optimal dispatch strategy including available DR capacities into a meta-heuristic-based stochastic MG capacity planning optimisation model. Also, on a collective level, the proposed stochastic MG planning and scheduling co-optimisation model is novel in that it

addresses a high-dimensional optimal dispatch problem integrated into the (computationally costly) meta-heuristic-based, large-scale, DR-integrated MG sizing problem under a wide spectrum of multi-variant parametric uncertainties.

As the above discussion indicates, the objective of the chapter is then twofold, namely (i) the budget-constrained uncertainty reduction during the MG investment planning phases, and (ii) determining the portfolio-wide optimal dispatch of the components simultaneously to the system design. In this setting, to address primary research objective 3, the chapter first introduces a general, comprehensive, large-scale, high-level MCS-based, scenario reduction-aided stochastic framework to simultaneously characterise a relatively large number of key input data uncertainties – meteorological data that dictate power outputs from various non-dispatchable generation technologies, power load demand, and wholesale electricity prices – in a systematic and efficient (both computationally and statistically) manner. Notably, the proposed multi-dimensional uncertainty quantification method is able to yield trade-offs between the computational cost and robustness of the solutions – which is of utmost importance for the tractability of determining a globally optimum solution to the computationally expensive long-term energy planning problem using meta-heuristics under various sources of parametric uncertainty. The proposed large-scale, scenario-led, data-driven, coordinated uncertainty characterisation framework that is able to address multiple parametric uncertainties – long-term forecasts of solar irradiance, ambient temperature, wind speed, river streamflow, electricity price, and power load in hourly resolution – at a time is then integrated into the standard meta-heuristic-based MG capacity planning optimisation model. The resulting stochastic MG capacity planning decision-making model makes the following novel contributions to the literature, each addressing one of the three uncertainty-related literature gaps identified in the previous section, towards giving a more realistic grounding to research on the computational simulation-based optimal capacity planning of RSESs:

- It provides a platform to translate uncertainty forecasts into risk analyses; hence, the model is able to furnish decision-makers with a range of possible

MG design alternatives and the corresponding probabilities of occurrence. Also, the impact of extreme risk attitudes – risk-seeking and risk-averse – as well as risk-neutral preferences on the optimal configuration and total discounted cost of grid-connected, sector-coupled, community-scale, 100%-renewable MGs is comprehensively analysed. Put differently, the method provides a platform to assist the associated MG planning decision-making process under different degrees to which uncertainty could be reduced, namely: the best-case, most likely case, and worst-case projections. This modelling of the design process is consistent with high-level modelling approaches where system-level design targets are translated into design specifications by cascading them down to the lowest level of the modelling hierarchy.

- It integrates a mixed-integer linear programming (MILP)-based heuristic scenario clustering technique into the general MCS-based uncertainty characterisation models. The heuristic scenario reduction algorithm yields a statistically representative subset of the original set of multi-dimensional uncertainty scenarios – generated by discretising the corresponding hour-specific PDFs – to effectively reduce running times, while retaining the solution quality (optimality or accuracy) within an acceptable limit. More specifically, the effective MILP-based scenario reduction algorithm is leveraged to determine an optimal scenario subset (of prescribed accuracy) to make the characterisation of a large number of problem-inherent parametric uncertainties – obtained using discrete approximations (probabilistic scenario realisations) of the corresponding probability distributions – computationally tractable.

- It characterises the uncertainties in ambient temperature and river streamflow forecasts for the first time in the long-term energy planning optimisation literature by adequately deriving the PDFs that best fit the corresponding historical datasets, which respectively influence the estimated power outputs from solar PV and micro-hydro power generation plants. More specifically, the uncertainty associated with the power output

from a solar PV plant is characterised in terms of the variability of both solar irradiance and ambient temperature, while the power output from the micro-hydro power plant is estimated probabilistically based on streamflow variability.

Moreover, comprehensive impact analyses illustrate how the proposed uncertainty budgeting approach can help guide RSES designers on how to optimally 'spend' the uncertainty choice towards better-informed uncertainty management efforts and changes in target design. This, consequently, provides a platform for MG asset allocation decision-makers to determine – in the initial design phases – where more resources need to be allocated to strategically meet operational requirements – in accordance with the optimum asset allocation strategy.

To meet the second main objective of the chapter (primary research objective 4), discussed above, a novel linear programming-based dispatch optimisation framework is then nested within the stochastic meta-heuristic-based MG infrastructure capacity allocation model to optimise the operational schedules of the portfolio-wide dispatchable DERs, grid trades, and sectoral DR capacities over a moving 24-hour energy dispatch horizon simultaneously to the system design. The operational planning algorithm provides 24-hour look-ahead strategic foresight to cost-minimally address the dynamic nature of system states – in terms of load demand, local non-dispatchable generation, and wholesale electricity prices. The intelligent dispatch strategy is also designed to be aware of potential daily arbitrage revenues that can be generated by charging energy storage during off-peak hours and discharging during peak hours of the day. Accordingly, the stochastic, coordinated, system-level design and dispatch co-optimisation model implemented over a moving one-day look-ahead period determines the operating schedules of controllable decision variables (for example, the hybrid storage, dispatchable generation, DR utilisation including FCEV2G interventions, and energy exchanges with the grid) at every 24 hours based on the operational cost minimisation subject to the system-wide energy balance and component-specific operational constraints. The optimal schedules obtained, achieved in the baseline year (Year 1), are assumed to hold true for the ensuing years in the project life-cycle, with recurring costs discounted back to the present. A major contribution of the developed dispatch

strategy integrated into the sizing model is that it maximises the daily profit from storage providing arbitrage together with effective internal reserve provision under perfect foresight of hourly local generation, demand, and wholesale prices up to 24 hours (the coming day).

Note that the stochastic, design and dispatch co-optimisation model presented in this chapter builds on – and adds an intelligent, probabilistic layer to – the Stackelberg, non-cooperative game-theoretic, sectoral aggregator-mediated, market-oriented, incentive-based, interruptible DR-integrated MG capacity planning optimisation framework introduced in the previous chapter. In general, the chapter proposes a novel meta-heuristic-based optimal stochastic equipment capacity planning model tailored to grid-connected MG systems, which exploits the benefits of simultaneously optimising the design and portfolio-level operation of smart, integrated RSESs towards developing a holistic optimality perspective. For uncertainty impact analyses, the model is applied to an on-grid system – feeding various customer classes – that integrates solar PV, WT, and micro-hydro non-dispatchable technologies, which could be backed by any dispatchable generation technologies and energy storage systems, as such components are not expected to contribute to the system-level parametric uncertainty. However, given that the proposed uncertainty characterisation approach substantially alleviates the computational burden associated with meta-heuristic-based probabilistic MG sizing processes, it is featured with parametric scalability. Accordingly, it can be readily applied to handling any (reasonable) number of uncertain input parameters desired provided that the historical/synthetically reproduced data streams are available – as necessitated by other MG configurations. Moreover, the presence of a relatively large number of dispatchable devices in the test-case system's configuration results in a high-dimensional MG-level optimal scheduling problem. To surmount the challenge of intractable dimensionality of the sequential series of system-wide one-day optimal operation problems (with a finite time horizon) nested within the meta-heuristic-based stochastic sizing model, they are linearized and solved via linear programming, which ensures global optimality necessary for (algorithmic) generalisability. This, consequently, allows for reduced running time and greater

scalability to enable the application of the model to even larger-scale systems over long periods of time.

## 4.2. Stochastic meta-heuristic-based MG capacity planning and operational scheduling co-optimisation

This section first presents the overall structure of the proposed meta-heuristic-based probabilistic MG design optimisation model that systematically accounts for the most salient problem-inherent parametric forecast uncertainties (Section 4.2.1). As noted above, the model is generalisable to any MG configurations to quantify any set of uncertain parameters desired during the long-term investment planning phase and provide uncertainty budget-constrained energy planning decision support. Accordingly, underlying the proposed model is the view that a designer can tolerate a particular level of uncertainty, which can be characterised by specified acceptable levels of the total discounted system cost. Also, the overarching goal is to provide the decision-maker with important insights into the effect size of budget-constrained uncertainty characterisation and the cost of accounting for the uncertainty in most salient input parameter forecasts.

Given the secondary contributions of the chapter, namely characterising the variability inherent in river streamflow and ambient temperature (in addition to solar irradiance, wind speed, load demand, and wholesale prices), the model is specifically parametrised for the test-case MG 4 presented in the preceding chapter. Although MG 2 induces the same parametric uncertainty set, MG 4 has been selected as the test case in this chapter as it represents the most numerically challenging design problem in this thesis due to: (1) the relatively high degree of seasonality of the load demand the system needs to be specifically designed to handle, which presents additional challenges in terms of the optimal management of the DER portfolio (onsite renewable generation and storage technologies), as well as the dimensionality of the problem, making it least amenable to exact mathematical optimisation algorithm treatments even under strong simplifying assumptions, (2) the significant diversity of the customer segments, which provides useful insights into the value of uninterruptible service to various classes of customers (residential, commercial, industrial, agricultural, and EV-charging loads)

and associated category-specific dynamics, which, in turn, enable realistic and appropriate valuation of sectoral energy at risk necessary for the optimal stochastic MG investment decisions, (3) the considerably larger size of the overall network and equipment capacity required to meet the loads, resulting in more significant findings in terms of the absolute changes in the total discounted system cost (from a more practical perspective and less of a pure optimisation perspective), and (4) that the synthetically generated power load time-series data – which is synthesised due to the lack of reliable hourly-resolved historical datasets – is normalised to the real-world annual peak records and corrected for the country-wide share of sectoral loads,[3] which carries the advantage of more narrow confidence intervals for the associate analyses and interventions pertaining to the system design that optimally serves the particular energy needs of the corresponding community.

The objective function remains to minimise the total NPC of the MG system, as expressed in Equation 3.41, subject to the sets of operational- and planning-level constraints outlined in Section 3.4.2 with the associate data values specified in Table 3.3. Also, the optimisation algorithm consists of an implementation of the MFOA in a single run as explicit, multi-variant, statistically valid evidence has been produced on the distinctly small value of the standard error of the total discounted system cost results returned throughout different simulation runs – or more specifically, the standard deviation of the population of the MG total NPC solutions over 30 independent trials. Furthermore, in accordance with Fig. 3.5, a rule-based Greedy energy dispatch strategy is used in the basic stochastic simulations for storage scheduling because it has shown to be able to cost-minimally maximise a grid-connected MG's self-sufficiency ratio [286]. Recall that, under the Greedy strategy, the onsite renewable power generation first serves the local demand and any excess power charges the internal stationary energy storage system before being

[3] Recall that the GREEN grid dataset [168] relates to power consumption at the household level. That is, it neither accounts for the seasonality effect due to ski tourists, nor includes power consumption across commercial, industrial, agricultural, and e-mobility sectors. Accordingly, in addition to the country-wide share of sectoral loads, the forecasted demand was adjusted for seasonal variations in consumption that arise from the opening of the ski resort and the associated power consumption of ski lodges. To this end, it was assumed that the number of ski tourists during the winter season follows a normal distribution with a peak of 250 people per day (occurring in the mid-winter) with a seasonal cumulative sum of 7,000 people.

exported into the utility grid. On the other hand, any positive net load demand (local load minus onsite generation) is met by discharging the storage first before importing from the grid.

The basic stochastic simulations are then further advanced in Section 4.2.2 by nesting a linear programming-based, forward-looking, dynamic energy scheduling strategy within the proposed meta-heuristic-based, DR-integrated, stochastic sizing model to jointly optimise the design and dispatch of MG systems. By solving the optimal operational scheduling problem over a moving 24-hour time horizon, it provides a platform to more intelligently respond to the dynamic nature of system conditions, thereby minimising the risk of sub-optimality. However, note that the usage of the Greedy energy dispatch algorithm in the basic stochastic simulations is useful in that it allows for a direct comparison of the uncertainty-aware and deterministic results; or, in other words, separately measuring the impact of characterising the system-wide parametric uncertainties and the optimisation-based energy dispatch decisions on the costing and configuration of the conceptual MG system.

### 4.2.1. Probabilistic parametric uncertainty characterisation

To address the most salient case-specific, model-inherent parametric uncertainties (namely the hourly-basis forecasts of solar irradiance, ambient temperature, wind speed, river streamflow, wholesale electricity price, as well as power load demand input data), the proposed deterministic model is transformed into a stochastic formulation using a MCS-based approach through the following steps: (1) derive the associated hourly PDFs of the uncertain inputs based on the corresponding hourly-resolved historical and synthetic datasets, which has been shown to be a sufficient temporal resolution to effectively capture the variability in meteorological, load, and wholesale price time-series data (and hence, the dynamics of RSESs) [287], (2) discretise the hourly PDFs into a number of equal-width regions, (3) generate a set of hourly multi-dimensional scenario vectors based on all possible combinations of the uncertain hourly values in accordance with the discretised PDFs, (4) reduce the number of scenario vectors by solving a MILP problem to alleviate the computational burden, while retaining accuracy within an

acceptable limit, (5) solve the deterministic model for each annual set of reduced scenario vectors, and (6) fit a (cumulative) normal distribution to the obtained results (in accordance with the posterior probabilities assigned by the scenario reduction algorithm) to assist decision-making in designing cost-minimal MGs under different uncertainty budgets. Note that the uncertainty in input data is represented probabilistically, implying that each uncertain variable is considered to be a random variable, the components of which can be described by a PDF.

#### 4.2.1.1. PDF construction

The proposed uncertainty quantification process begins by building the hour-specific PDF of each uncertain variable based on real or synthetic (where appropriate) prior data. The beta and two-parameter Weibull distributions are respectively the most widely accepted distributions for time series solar irradiance and wind speed data. It has also been demonstrated that normal (Gaussian) distributions fit the power load demand, ambient temperature, and wholesale electricity price datasets best in terms of characterising the associated variability. Moreover, the two-parameter gamma distribution has been found to provide the best fit with measured river streamflow data and, therefore, is often used to characterise streamflow regimes [288]–[294]. Accordingly, the best-fitting distributions for the corresponding random variables are utilised to build the PDFs. That is, the PDFs that provide the best fits to the underlying hourly histograms of the historical data are generated. Also note that for load demand and wholesale price data, a time-dependent dummy variable is used to distinguish weekday and weekend data points; it takes a value of 1 if the data point represents a weekday, and 0 otherwise.

The PDF of the beta distribution for a random variable $0 \leq x \leq 1$ and shape parameters $\alpha, \beta > 0$ can be described as follows [295]:

$$f(x;\alpha,\beta) = \frac{\Gamma(\alpha+\beta)}{\Gamma(\alpha)\Gamma(\beta)} x^{\alpha-1}(1-x)^{\beta-1}, \tag{4.1}$$

where $\Gamma(z) = (z-1)!$ denotes the gamma function, while the shape parameters of the distribution can be obtained from Equations 4.2 and 4.3, respectively.

$$\alpha = \frac{\mu.\beta}{1-\mu}, \tag{4.2}$$

$$\beta = (1-\mu)\left(\frac{\mu(1+\mu)}{\sigma^2} - 1\right), \tag{4.3}$$

where $\mu$ and $\sigma^2$ respectively denote the mean and variance of the distribution.

The two-parameter Weibull PDF for a random variable $x \geq 0$ can be expressed as [295]:

$$f(x;c,k) = \frac{k}{c}\left(\frac{x}{c}\right)^{k-1} e^{-\left(\frac{x}{c}\right)^k}, \tag{4.4}$$

where $k > 0$ and $c > 0$ denote the shape and scale parameters of the distribution, which can be approximated by Equations 4.5 and 4.6, respectively.

$$k = \left(\frac{\sigma}{\mu}\right)^{-1.086}, \tag{4.5}$$

$$c = \frac{\mu}{\Gamma\left(1+\frac{1}{k}\right)}. \tag{4.6}$$

The gamma distribution can be parametrised using a shape parameter $\alpha > 0$ and a rate (inverse scale) parameter $\beta > 0$. The PDF of a gamma-distributed random variable $x > 0$ in the shape-rate parametrisation can be expressed as [295]:

$$f(x;\alpha,\beta) = \frac{\beta^\alpha x^{\alpha-1} e^{-\beta x}}{\Gamma(\alpha)}, \tag{4.7}$$

$$\alpha = \frac{\mu^2}{\sigma^2}, \tag{4.8}$$

$$\beta = \frac{\sigma^2}{\mu}. \tag{4.9}$$

The PDF of a normal random variable $x$ with mean $\mu$ and standard deviation $\sigma$ can be formulated as follows [295]:

$$f(x;\mu,\sigma) = \frac{1}{\sqrt{2\pi}\sigma} e^{-\frac{1}{2}\left(\frac{x-\mu}{\sigma}\right)^2}, \tag{4.10}$$

where $\mu$ and $\sigma$ respectively denote the mean and standard deviation of the distribution.

Specifically, the associated PDFs are built based on 20 years' (1999 to 2018) worth of hourly-resolved historical data for the climatic inputs, 10 year's (2010 to 2019) worth of hourly historical data for wholesale prices, as well as 20 independent hourly-basis, one-year synthetic time-series derived for electricity consumption – given the lack of reliable historical load demand time-series data for the case study area with hourly granularity. More specifically, to populate the proposed stochastic model and form the basis for generating hourly PDFs of power load demand, the total forecasted (hourly-basis) load profile for aggregated sectors was synthetically regenerated 19 times (over a one-year period) using a second-order Markov chain model developed specifically following the steps described by McLoughlin et al. [296], whilst employing a time-dependent dummy variable to account for the calendar-time-dependent characteristics of the electric demand data (namely, the weekday versus weekend-day/holiday effects), in the same way as proposed by Lusis et al. [297]. In this light, to improve the quality of characterising the uncertainty associated with power load forecasts, the respective year-long, hourly-basis data streams are first split into 72 subsets, each representing a month- and day-type-specific sub-diurnal timeframe. Accordingly, 3 × 2 × 12 (intra-day timeframes × weekdays/weekends × months) distinct sub-datasets of the power load demand were derived by clustering the year-long, hourly-basis electrical load time-series datasets. More specifically, unlike wholesale price and meteorological time-series datasets (for which only the records for a particular hour of the historical year-round time-series datasets are considered for PDF generations, though considering the weekdays/weekends effects for wholesale prices), each of the 8,760 time-steps of the power load datasets is not treated independently from all the rest. To this end, Table 4.1 provides a determination of the intra-day (sub-diurnal) timeframes within a New Zealand context [298]. The power load data in each of the 72 subsets of the year-long power load datasets (distinct periods of energy use) is

then assigned a normal PDF. Accordingly, the PDFs of load demand data were determined for the specified month- and day-type-specific intra-day time windows within a year.

Table 4.1: Pre-determined weekday-/weekend day-specific sub-diurnal time windows to classify the synthetically augmented power load demand data for each month of the year.

| Day types | Peak hours | Shoulder hours | Off-peak hours |
|---|---|---|---|
| Workdays | 6 a.m. to 10 a.m.<br>5 p.m. to 10 p.m. | 11 a.m. to 4 p.m.<br>11 p.m. to 12 p.m. | 1 a.m. to 5 a.m. |
| Weekends/public holidays | 5 p.m. to 10 p.m. | 6 a.m. to 4 p.m.<br>11 p.m. to 12 p.m. | 1 a.m. to 5 a.m. |

Note that the above-described data partitioning aspect of the model is useful in that it allows adding a higher-level layer of uncertainty modelling to the traditional MCS-based uncertainty quantification by leveraging the data points of the same order of magnitude with the same stochastic order of variability in generating relevant PDFs. That is, the quantity of the relevant historical data, on which the accuracy of the MCS-based uncertainty quantification is highly dependent, is substantially increased. This is expected to compensate, to some extent, for the lack of hourly-resolved historical power load data. Furthermore, the built-in '*normfit*', '*betafit*', '*wblfit*', and '*gamfit*' functions in MATLAB were respectively used to return 95% confidence intervals that estimate the specific parameters of the normal, beta, two-parameter Weibull, and two-parameter gamma PDFs that best fit the corresponding historical and synthetically reproduced time-series data.

#### 4.2.1.2. PDF discretisation

Given a continuous probability distribution-driven stochastic decision-making problem can only be solved when the underlying distributions are divided into discrete data points (due to the practical limits on the size of stochastic models), a finite scenario set with associated probabilities needs to be generated to represent the continuous distributions. Accordingly, discrete approximations of the uncertain parameter-specific hourly PDFs are determined, as illustrated in Fig. 4.3 for the

case where the range of probability densities of a random variable $x$ over a typical representative normal PDF is divided into seven equal-width intervals. As the figure shows, the range of possible values on the uncertain parameter-specific hourly PDFs is divided into a set of mutually exclusive and collectively exhaustive equal-width segments. The intervals are then represented by their means and the associated probabilities of occurrence. Predictably, increasing the granularity step size for PDF discretisation improves the accuracy of approximations. That is, increasing the number of the above-mentioned equal-width intervals, employed to determine discrete approximations of probability distributions, increases the accuracy of the uncertainty characterisation process, but at the cost of increased CPU execution time.

As an illustrative example, suppose that the continuous PDFs are approximated by seven equally sized regions – which are assumed to be sufficient to effectively capture the density of the target functions – on the value axis denoted by $R_1$, $R_2$, $R_3$, $R_4$, $R_5$, $R_6$, $R_7$, which are represented by their means $x_1$, $x_2$, $x_3$, $x_4$, $x_5$, $x_6$, $x_7$. Each of the regions on the value axis represents a variable-specific scenario in the uncertainty quantification process. Additionally, the scenarios are characterised by a probability of occurrence that reflects the chance that the true value of the uncertain variable will be in the interval [299]. Also, the approximation has the same mean as the original continuous probability distribution. Furthermore, the probabilities of the finite sets of scenarios for each uncertainty variable, derived from the corresponding continuous distributions, sum up to 1. Note that it is assumed that all the PDFs of the uncertain variables are discretised by the same number of intervals.

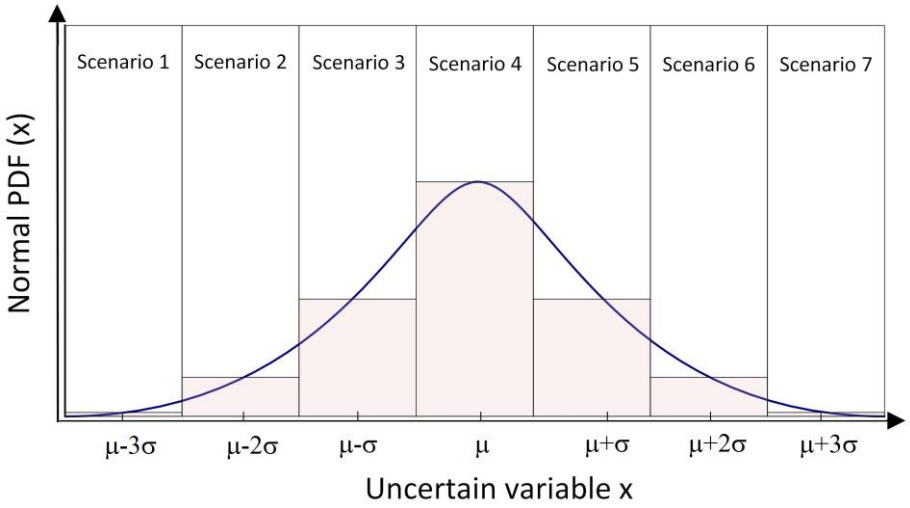


Figure 4.3: Schematic illustration of the process of discretising a typical representative normal PDF based on equal-width intervals.

#### 4.2.1.3. Scenario vector generation

In this setting, the probabilities of occurrence and the associated parameter values (probability-value pairs) obtained from a discrete approximation of the corresponding PDFs (representing a scenario for the realisation of the uncertain variable $x$) are given in Equations 4.11 and 4.12, respectively.

$$p_i = \int_{R_i} PDF(x)dx \quad for\ i = 1, 2, \dots, 7, \tag{4.11}$$

$$x_i = \int_{R_i} x \frac{PDF(x)}{p_i}\, dx \quad for\ i = 1, 2, \dots, 7, \tag{4.12}$$

where $x$ is a representative uncertain variable, $R_i$ denotes the $i$-th region on the corresponding PDF's value axis (in accordance with the specified number of equal-width intervals), $p$ is the associated probability density, and the numeric value 7 represents the total number of scenarios generated for uncertain variable $x$ through PDF discretisation. Then, $7^6$ = 117,649 original independent scenario vectors were generated for each hour of the representative one-year MG operational planning horizon in accordance with all possible combinations of the six uncertain inputs (the so-called '*uncertainty space*') represented by seven equal-width segments of

the relevant PDFs.[4] That is, a full factorial combination of all possible discrete hourly values of the six uncertain parameters represented by seven equal-width discrete regions leads to 117,649 independent, probabilistically generated scenarios. Accordingly, each MG design needs to be evaluated 117,649 times, making the overall problem that involves a typical 8,760-hour annual energy balance analysis computationally infeasible.

Given that multiple uncertain variables are considered in this study, each scenario in the uncertainty characterisation process consists of one state of each of the independent variables. That is, each of $N_i$ separate, multi-dimensional scenarios (for different realisations of the uncertain variables) has a certain overall probability of occurrence. Accordingly, the probability of occurrence of each time-step-specific scenario vector of uncertain variables can be calculated by multiplying the probabilities of occurrence of its constituent uncertain variables (according to the multiplication rule of probability that ensures a unique solution under the assumption of independent distributions), as follows:

$$p_{X_i} = \prod_x p_{x,i} \quad for\ i = 1, 2, \dots, N_i, \tag{4.13}$$

where $N_i$ is the total number of possible combinations of uncertain variable-specific scenarios (i.e., the total number of scenario vectors) for each hour of the MG operation, which can be obtained by:

$$N_i = \prod_x N_x, \tag{4.14}$$

where $N_x$ denotes the scenario realisations for uncertain parameter $x$.

#### 4.2.1.4. Scenario vector reduction

As illustrated above, assuming that all the PDFs of the six uncertain variables considered in this study are discretised by seven intervals, solving the stochastic variant of the MG design optimisation problem that contains all possible scenario

[4] Note that for an uncertainty vector containing $m$ variables, the independent distributions of which are discretised into *N* points, there are $N^m$ distinct paths in the time-step-specific scenario tree [315].

vectors is by no means tractable within the computationally intensive context of meta-heuristic-based MG investment planning. This brings to light the necessity of reducing the uncertainty space using a heuristic scenario reduction algorithm when dealing with multiple uncertain inputs. A scenario reduction algorithm can be employed to identify a minimum subset of a given set of multi-dimensional scenarios with new probabilities such that the probability distribution represented by them is the closest possible to that of the original scenario set. To this end, the multi-dimensional scenarios were reduced to seven using a MILP-based scenario reduction algorithm [300]. The MILP-based heuristic algorithm preserves a scenario subset incorporating the least similar (best representative) and most probable members, whilst simultaneously assigning optimal probabilities to the realisation of the associated reduced scenarios. More specifically, as the underlying principle of the technique for retaining the key statistical characteristics of the original set of scenarios, it ensures that the overall probability of occurrence for a particular realisation (value) of each uncertain input at time-step $t$ in the final (preserved, reduced, or clustered) subset of scenarios equals the probability of the uncertain input taking on that specific value. The associated MILP problem is subject to the constraint that the sum of the probabilities of the reduced scenarios is equal to one. The efficacy of the preserved scenarios in representing the possible outcomes of the uncertain inputs defined by the original scenarios – and, in turn, significantly reducing the running time of the stochastic simulations – is demonstrated by its developers. Specifically, based on comprehensive numeric simulations of a statistically representative set of benchmark test cases, the algorithm's error is found to be in the 0.5–2% range [300]. The validity of this finding for MG capacity planning applications has been verified based on a total of 12 unreported comprehensive statistical preliminary benchmark efficiency tests, considering 4 combinations of problem-inherent uncertainty factors applied to 3 simplified MG sizing problems, which identified an average error of 1.4%.

Mathematically, the scenario reduction heuristic that determines the minimum number of preserved multi-dimensional scenarios – satisfying the criterion that the sum of the probabilities of the new scenarios containing a specific realisation of an uncertain variable is equal to the probability of occurrence of that

particular value for the uncertain variable – can be formulated for the specific test case of interest as follows (assuming that the range of possible values for the six uncertain variables has been divided into seven regions):

$$\min N_{rs} = \sum_{x_1=1}^{7} \sum_{x_2=1}^{7} \dots \sum_{x_6=1}^{7} \omega_{x_1,x_2,\dots,x_6}, \tag{4.15}$$

subject to:

$$\sum_{x_2=1}^{7} \sum_{x_3=1}^{7} \dots \sum_{x_6=1}^{7} p_{rs}(x_1, x_2, \dots, x_6) = p_{1,x_1} \quad for\, x_1 = 1, 2, \dots, 7, \tag{4.16}$$

$$\sum_{x_1=1}^{7} \sum_{x_3=1}^{7} \dots \sum_{x_6=1}^{7} p_{rs}(x_1, x_2, \dots, x_6) = p_{2,x_2} \quad for\, x_2 = 1, 2, \dots, 7, \tag{4.17}$$

.

.

.

$$\sum_{x_1=1}^{7} \sum_{x_2=1}^{7} \dots \sum_{x_5=1}^{7} p_{rs}(x_1, x_2, \dots, x_6) = p_{6,x_6} \quad for\, x_6 = 1, 2, \dots, 7, \tag{4.18}$$

$$\sum_{x_1=1}^{7} \sum_{x_2=1}^{7} \dots \sum_{x_6=1}^{7} p_{rs}(x_1, x_2, \dots, x_6) = 1 \quad \forall x_1, x_2, \dots, x_6, \tag{4.19}$$

$$p_{rs}(x_1, x_2, \dots, x_6) \leq \omega_{x_1,x_2,\dots,x_6} \quad \forall x_1, x_2, \dots, x_6, \tag{4.20}$$

$$0 \leq p_{rs}(x_1, x_2, \dots, x_6) \leq 1 \quad \forall x_1, x_2, \dots, x_6, \tag{4.21}$$

$$\omega_{x_1,x_2,\dots,x_6} \in \{0, 1\} \quad \forall x_1, x_2, \dots, x_6, \tag{4.22}$$

where $N_{rs}$ is the optimal number of reduced scenarios, the numeric value 7 represents the number of equal-width distribution discretisation intervals, $p_{rs}(x_1, x_2, \dots, x_6)$ is the new probability of occurrence assigned to the reduced scenario vector $X^{rs} = [x_1, x_2, \dots, x_6]$ (which contains a specific realisation of the uncertain parameters according to the corresponding PDF approximates), $p_{n,x_n}$ denotes the probability that the $n$-th uncertain parameter takes on the value of $x_n$, while the binary variable $\omega_{x_1,x_2,\dots,x_6}$ corresponds to the presence or absence of the original scenario vector $X^s$ in the optimal subset of scenarios $X^{rs}$; it takes a value of 1 if the original scenario vector exists in the set of new (reduced) scenarios, and a value of 0 otherwise. Note that the problem's uncertain parameters are coded from

1 to 6, while $x_n = i$ indicates that the $n$-th uncertain variable is in the $i$-th scenario realisation, as defined by the equal-width PDF segments – which are represented by their means and the associated probabilities of occurrence. Also, the hourly uncertainty vector of the specific problem at hand for each reduced scenario vector index $rs \in \{1, 2, 3, 4, 5, 6, 7\}$, can be represented as $X^{rs}(t) = [F^{rs}(t), I_G^{rs}(t), T_a^{rs}(t), V_h^{rs}(t), \pi_{im}^{rs}(t), P_L^{rs}(t)]$.

Intriguingly, solving the formulated MILP-based scenario reduction problem using the built-in '*intlinprog*' MATLAB optimisation function yields seven optimal multi-dimensional scenarios with newly assigned (diverse) probabilities for each hour of the MG dispatch, which, in retrospect, explains why the illustrative PDF discretisation example is discussed for the case with seven equal-width distribution segments. In addition, as discussed in detail in Section 4.3 (*Simulation results and discussion*), the employed scenario clustering technique has ensured the computational tractability, whilst retaining an acceptable level of accuracy for the representative bins – which represents the quality of approximations.

#### 4.2.1.5. Model evaluation

The original deterministic model is then solved for each of the seven optimal year-long (8,760-h) sets of reduced hourly scenario vectors – or, put differently, for the time-step-specific reduced sets of year-long multi-dimensional scenarios – with the reduced sample size $N_{rs}$. Then, the modelling results (optimal solutions), as well as the corresponding posterior probabilities of occurrence of the MG designed for the annual sets of reduced hourly multi-dimensional scenarios, are recorded. The posterior probability of each design is calculated by averaging the posterior probabilities of hourly scenario vectors with the same index number over the year-round superset of input data.

#### 4.2.1.6. Outcome analysis

Finally, the (cumulative) normal distribution functions that best approximate (fit) the output histograms of the resulting values of the objective function (total discounted system cost) and decision variables (the optimum capacity of the equipment, power trades with the upstream utility grid, as well as the utilised DR

capacity including FCEV2G operations) are produced and summary statistics are calculated for the obtained solutions. In particular, to more effectively support the associated optimal stochastic MG infrastructure planning decision-making process and provide informed choices of design variable ranges and probable values, three key scenarios of uncertainty management – with the associate levels of risk that can be tolerated (mitigated risk) – are analysed, namely: the most likely (middle-case), best-case, and worst-case projection scenarios. To this end, the expected values (mean values), as well as the $5^{th}$ and $95^{th}$ percentile values[5] of the output (cumulative) normal distributions are respectively calculated. This leads to three distinct probabilistic decision patterns, which quantify the effect of the most salient model-inherent data uncertainties on the decision variables, as well as the associated cost objective, based on different levels of managed risk, evaluated as a function of changes in the distributions of uncertain inputs – or put differently, considering the concept of risk as a function of probability and consequence [301]. To illustrate, the most likely case, best-case, and worst-case projection scenarios represent the risk-neutral, risk-seeking (opportunistic), and risk-averse (conservative or robust) decision-making preferences under high-dimensional, multi-variate parametric uncertainties.

In this context, given that the modelling results are independent and identically distributed, the average values of the model outputs in different hourly scenarios (probability-value pairs) converge almost surely to the expected values, according to the strong law of large numbers. Accordingly, the stochastic modelling results for each output variable $x$ in the most likely case are also frequently referred to as realistic-uncertainty-adjusted results. This can be expressed mathematically as [302]:

$$E_{rs} = \sum\nolimits_{rs \in RS} \gamma_{rs} Y_{rs}, \tag{4.23}$$

[5] The $p^{th}$ percentile of the PDF of a continuous random variable $x$, denoted by $\eta(p)$ is the specific value such that (i) $p$% of the area under the graph of the PDF of $x$ ($f(x)$) lies to the left of $\eta(p)$, and (ii) $(100-p)$% lies to the right. More specifically, if $F(x)$ is the cumulative distribution function of $x$, then $F(p^{th}\text{ percentile}) = p/100$ [316].

where $E_{rs}$ represents the vector of the expected values of the uncertain variables and the returned values of the fitness function ($Y_{rs}$) optimised for the reduced input probability-value pairs ($p_{rs}(t), X^{rs}(t)$) with the same index number over the year-long, hourly-basis MG operation, $\gamma_{rs}$ is the posterior probability of the associated MG design, while $RS$ represents the set of reduced scenario vectors.

It is also noteworthy that the three distinct decision patterns used in the uncertainty budgeting aspect of the proposed system-wide parametric uncertainty characterisation approach – which quantify the effect of uncertain parameters under consideration on the decision variables and returned value of the objective function in accordance with different levels of tolerable risk – correspond to the following three cases in a basic MCS uncertainty quantification setting where pseudo-random numbers used in the MCS process are generated only from specific regions within the respective hourly PDFs of the uncertain parameters: (1) the best-case projection, where samples taken from the upper extreme (above the 95$^{th}$ percentile) of the PDFs of the climatological data and the lower extreme (below the 5$^{th}$ percentile) of the PDFs of the electricity demand and wholesale price data are used to create uncertainty vectors; (2) the middle-case projection, where Monte Carlo sampling is conducted within the range of 5$^{th}$ to 95$^{th}$ percentiles of the PDFs of all the uncertain variables; and (3) the worst-case projection, where the pseudo-random numbers are sampled from below the 5$^{th}$ percentile of the PDFs of the climatological data and above the 95$^{th}$ percentile of the PDFs of the electricity demand and wholesale price data.

#### 4.2.1.7. Overview of the proposed optimal stochastic solution algorithm

Fig. 4.4 illustrates the general structure of the developed solution algorithm for the proposed probabilistic MG capacity optimisation model. First, all input data, including historical load, meteorological, and wholesale power price datasets, techno-economic specifications of the equipment, parameter settings of the meta-heuristic, as well as the project lifetime and interest rate are supplied to the model. As the figure shows, the process of MG planning optimisation is then carried out for each year-long set of the clustered hourly-basis scenario vectors. Recall that the clustered scenario vectors are yielded by solving the relevant MILP problem for the

hour-specific scenario vectors generated using the MCS-based method that considers all possible combinations of parameter-specific realisations – generated using the respective discretised PDFs constructed specifically for each uncertain parameter. Subsequently, the normal density curves that best approximate the corresponding histograms of the optimised decision variables and the associate whole-life MG cost are derived, while the best-case, most likely case, and worst-case solutions are calculated based on the $5^{th}$ percentile values, expected values, and $95^{th}$ percentile values, respectively.

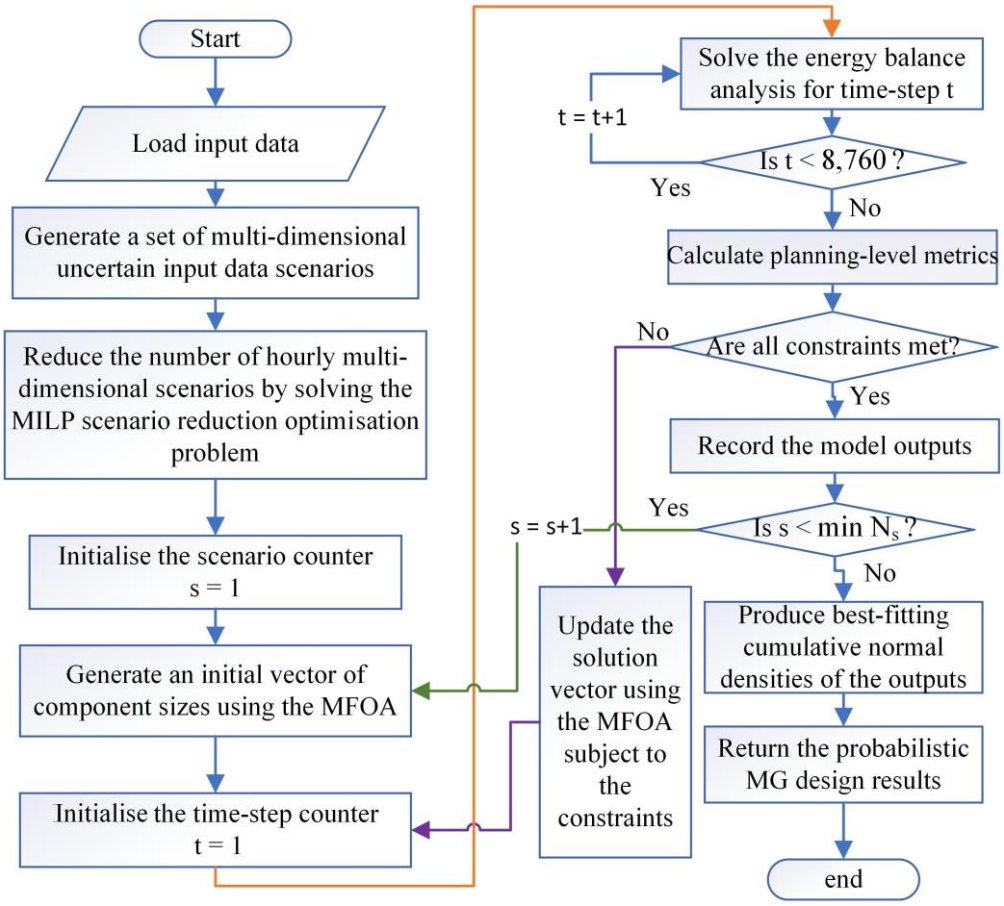


Figure 4.4: Flowchart of the probabilistic, meta-heuristic-based MG design optimisation solution algorithm.

Fig. 4.5 illustrates how the developed uncertainty characterisation layer can be integrated into the general game-theoretic DR-supported meta-heuristic-based MG designing and sizing model, derived in Chapter 3. That is, the figure shows the flowchart of the developed optimal probabilistic variant of the proposed MG

equipment capacity planning method with an integrated game-theoretic DR management scheme. As can be seen from the figure, the algorithm can be partitioned into several sub-programmes highlighted in different colours including (different colours highlight different features of the model): (1) probabilistic characterisation of the considered uncertain parameters in accordance with the uncertainty quantification level adjusted by the designer (the user is prompted in the beginning of the simulation program to enter the uncertainty quantification case), which is assisted by the reduced number of multi-dimensional hourly scenario realisations that best represent the original set of hourly scenarios using the MILP-based scenario reduction algorithm (the green blocks); (2) optimisation of the total NPC of the MG using the MFOA with the following decision variables (the blue blocks): (i) the optimum combination of the size of the MG equipment, (ii) the total grid power exchanges, and (iii) the total FCEV2G capacity utilised; (3) implementation of the proposed game-theoretic day-ahead DR provision framework in the top level of the double-nested energy management function to optimally produce load curtailment decisions in accordance with available (practical or releasable) system-wide DR resources, whilst realistically projecting distributed sectoral customer engagement in incentive-based DR programmes subject to preserving the end-users' comfort and utility levels and providing a fair allocation of the associated overall financial benefits between the sole energy service provider, monopoly responsive load aggregators, and end-consumers (the yellow block); (4) applying the developed rule-based, hourly-basis operational strategy in the bottom level of the double-nested MG operation function (the light coral block); and (5) producing best-fitting (cumulative) normal densities of the outputs (the optimal values of the decision variables and the associate total discounted system cost) optimised for different year-long, hourly-basis sets of reduced multi-dimensional scenarios before returning uncertainty budget-constrained results for the user-defined tolerable risk (uncertainty management) level (the light pink blocks).

Note that the equipment capacity planning problem is solved separately for each year-long set of reduced scenario vectors using the MFOA subject to the imposed constraints, whilst accounting for the outputs of the system-level DR

dispatch game at each iteration of the MFOA. Also, note that the best-fitting (cumulative) normal distributions are produced separately for each decision variable of the optimisation problem (cost-optimal sizes for each technology in the candidate pool, the optimal grid trades, and demand-side flexibility capacity utilisation), as well as the associated total NPC of the system, based on the modelling results obtained for the seven annual reduced scenario vector realisations that build 7 input data matrices of the dimension 6×8,760, where 6 represents the number of uncertain variables and 8,760 is the total number of hourly time-steps. This modelling of the design process is consistent with post-processing-based modelling exercises where the search trajectories associated with the design problem for different values of key inputs are aggregated for a holistic view of the design space.

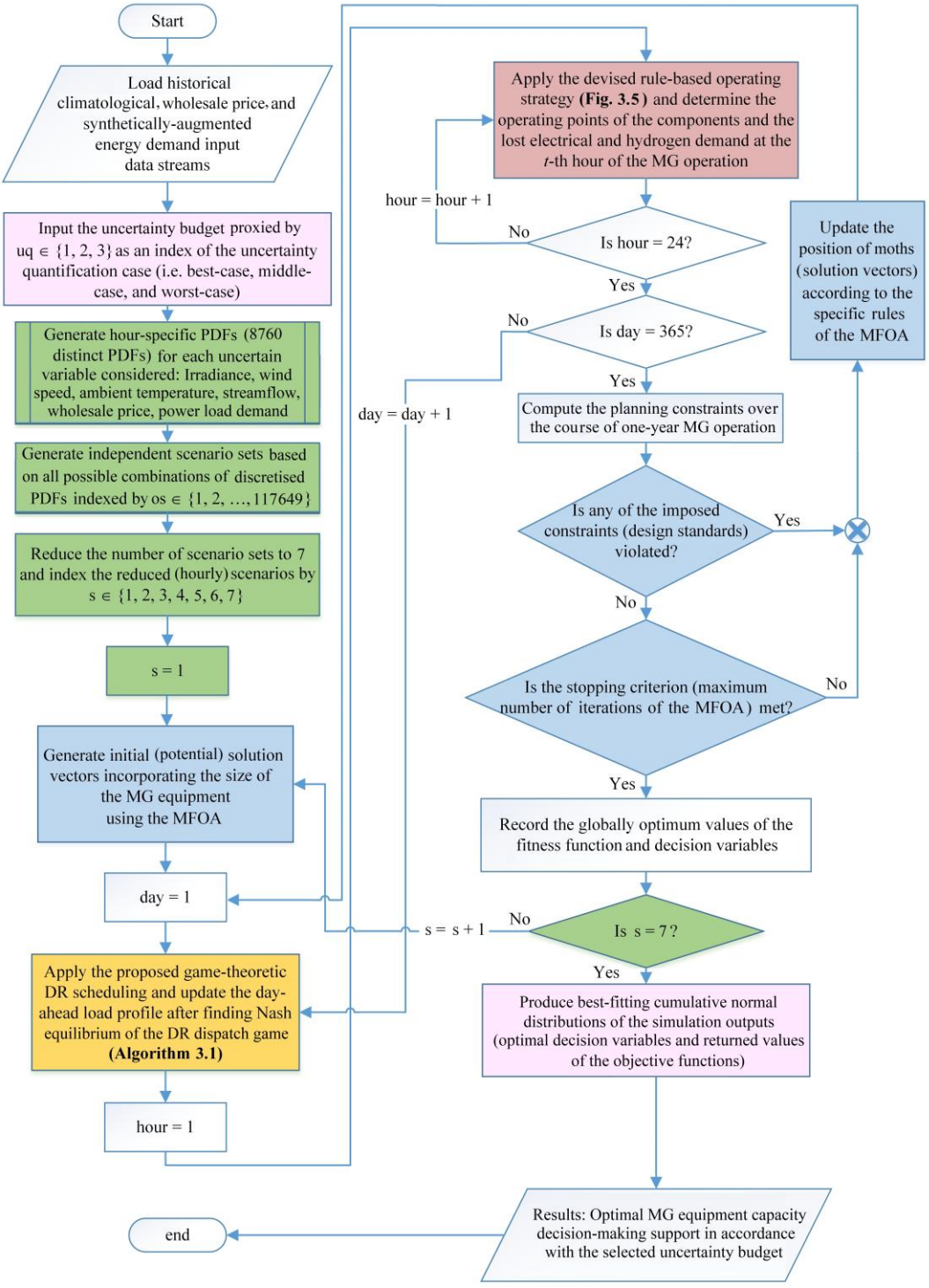


Figure 4.5: Flowchart of the budget-aware stochastic uncertainty characterisation solution algorithm integrated into the proposed DR-adjusted meta-heuristic-based MG capacity planning model.

### 4.2.2. Nested micro-grid scheduling optimisation

Optimising the operational schedules over a look-ahead planning horizon, subject to the operation of dispatchable devices within their limits, is necessary to minimise the risk of sub-optimal investment, as inferior dispatch decisions cascade upward into the optimal sizing problem, thereby impairing the quality of long-term planning solutions. The associated short-term energy management problem requires decision-making over multiple time increments. Ideally, the dispatch problem would be solved simultaneously for the entire analysis period (one year at hourly resolution). However, given that solving the optimal scheduling problem for all time-steps at a time is not computationally tractable within the operations research context, the whole-year time period needs to be broken down (decomposed) into smaller time segments – a series of sequential dispatch decision-making problems solved over a moving time window. Accordingly, the time horizon length is (heuristically) selected to be 24 hours as it adequately captures the diurnal cycle of load demand, wholesale electricity market prices, and renewable energy supplies – and therefore, it best represents how the MG system actually operates.

In this light, in contrast to the rule-based, hourly-basis dispatch strategy commonly employed in the MG design optimisation software packages and most of the existing MG sizing methods in the literature (to charge the storage when excess renewable power is present and to discharge the storage when renewable sources are not satisfying the load demand, for instance for grid-isolated systems), the proposed model accommodates an intelligent scheduling optimisation algorithm to be nested within the optimal sizing problem. The scheduling optimisation is formulated as a linear programming problem solved using the built-in '*linprog*' MATLAB function over a moving 24-hour time horizon with reference to the day-ahead forecasts of onsite variable generation, load demand, and wholesale prices. Notably, the operational planning optimisation problem follows the general arbitrage strategy of 'charge cheaply, discharge discreetly'. That is, the overarching goal of the day-ahead energy management optimisation problem is to maximise the MG's overall profit from power exchanges with the grid. Mathematically, the optimal scheduling problem can be expressed as [303]:

$$\min \boldsymbol{OPEX} = \boldsymbol{P_{im}}\boldsymbol{\pi}^T\Delta t - \boldsymbol{P_{ex}}\boldsymbol{\pi}^T\Delta t + 10^{-6}\|\boldsymbol{u}\|_1, \tag{4.24}$$

subject to:

$$\begin{aligned}\boldsymbol{P_{im}} - \boldsymbol{P_{ex}} = \left(\frac{\boldsymbol{P_L}}{\eta_I}\right) + \left(\frac{\boldsymbol{P_S}}{\eta_S}\right) + \boldsymbol{P_E} - \boldsymbol{P_{PV}} - \boldsymbol{P_{WT}} - \boldsymbol{P_{MH}} - \boldsymbol{P_{BP}} - \boldsymbol{P_{FC}} \\ - \boldsymbol{P_{FCEV2G}} + \boldsymbol{P_{ch}} - \boldsymbol{P_{dch}} - \left(\frac{\boldsymbol{Q_L}}{\eta_I}\right) - \left(\frac{\boldsymbol{Q_{H_2}}}{\eta_S}\right),\end{aligned} \tag{4.25}$$

where $\boldsymbol{OPEX}$ denotes the 24-hour column vector of the daily operational expenditure; $\boldsymbol{P_{im}}$ and $\boldsymbol{P_{ex}}$ respectively denote the 24-hour column vectors of imported power and exported power; $\boldsymbol{\pi}$ is the 24-hour column vector of wholesale electricity price; $\boldsymbol{P_L}$ and $\boldsymbol{P_S}$ respectively represent the 24-hour column vectors of power and hydrogen loads; $\boldsymbol{P_E}$ denotes the 24-hour column vector of power supplied to the electrolyser; $\boldsymbol{P_{PV}}$, $\boldsymbol{P_{WT}}$, $\boldsymbol{P_{MH}}$, and $\boldsymbol{P_{BP}}$ respectively denote the 24-hour column vectors of solar PV, wind turbine, micro-hydro, and biopower plant generation; $\boldsymbol{P_{FC}}$ is the 24-hour column vector of fuel cell power generation; $\boldsymbol{P_{FCEV2G}}$ is the 24-hour column vector of FCEV2G provisions; $\boldsymbol{P_{ch}}$ and $\boldsymbol{P_{dch}}$ are the 24-hour column vectors of the hybrid battery/SC storage system's charging power and discharging power, respectively; while $\boldsymbol{Q_L}$ and $\boldsymbol{Q_{H_2}}$ respectively denote the 24-hour column vectors of unmet power and hydrogen loads. Also, the term $10^{-6}\|\boldsymbol{u}\|_1$ in Equation 4.24 represents the L1-norm of the energy storage schedules over the 24-hour operational horizon that is included to penalise any needless cycling of the storage devices, the intended operational timescales of which can be accommodated within the daily time horizon of the optimisation-based dispatch strategy, namely the battery and SC banks. This is applied separately for the SC and battery banks. More specifically, it penalises the solutions that entail unprofitable battery and SC cycling. To this end, it captures the NPC of the associated storage device deterioration due to cycling in the present 24-hour horizon. The L1-norm of the storage schedules for the applicable storage media is formulated linearly as $\|\boldsymbol{u}\|_1 = \sum_{t=t_1}^{t_1+23}(P_{ch,B}(t) + P_{dch,B}(t))$ for the battery storage and $\|\boldsymbol{u}\|_1 = \sum_{t=t_1}^{t_1+23}(P_{ch,SC}(t) + P_{dch,SC}(t))$ for the SC storage. It should also be noted that a specifically imposed non-strict inequality (greater than or equal) constraint ensures

that the optimum schedules of the hybrid battery/SC bank and the relevant hydrogen-based energy storage system's components (fuel cell and electrolyser) satisfy the associated power relationships defined by the first of the two dedicated consecutive energy filters. However, it does not strictly enforce equality to increase the model's degree of freedom in choosing whether or not to leverage potential long-term and seasonal arbitrage opportunities. This is discussed in more detail in Section 4.3.4 (*Impact of nested optimal dispatch strategy*). Also, the power allocated to the hybrid battery/SC bank is decomposed into the battery and SC charging/discharging power components in accordance with the second first-order passive low-pass filter developed without strictly enforcing equality with the fundamentally same logic mentioned above (refer to Section 3.2.3 for more details on the overall three-timescale energy filter and its parameter settings).

While all the operational-level constraints, presented in Section 3.4.2, essentially remain active for the nested day-ahead MG scheduling strategy, some of them need to be linearized to be able to use linear programming to solve the associated optimisation problem. More specifically, Equation 2.45 that disallows charging the battery/SC bank while simultaneously (at the same time) discharging it, as well as Equation 2.46 that requires the power imports and exports to not occur concurrently (at a single time-step), in line with physical, real-world limitations, need to be reformulated. That is, the charging and discharging of the battery/SC bank, as well as importing/exporting power from/to the utility grid, are mutually exclusive events. To this end, two binary control variables are used for each of the above constraints, which are plugged into the associated original constraints that reflect the maximum charge and discharge power capacities of the overall battery and SC storage systems, as well as the maximum import and export capacities controlled by the transformer size, as follows:

$$0 \leq P_{ch,B}(t) \leq u_{ch,B}(t) \times (N_B \times P_{ch,B}^{max}) \ \ \forall t, \tag{4.26}$$

$$0 \leq P_{dch,B}(t) \leq u_{dch,B}(t) \times (N_B \times P_{dch,B}^{max}) \ \ \forall t, \tag{4.27}$$

$$u_{ch,B}(t) + u_{dch,B}(t) \leq 1 \ \ \forall t, \tag{4.28}$$

$$0 \leq P_{ch,SC}(t) \leq u_{ch,SC}(t) \times (N_{SC} \times P_{ch,SC}^{max}) \ \forall t, \tag{4.29}$$

$$0 \leq P_{dch,SC}(t) \leq u_{dch,SC}(t) \times (N_{SC} \times P_{dch,SC}^{max}) \ \forall t, \tag{4.30}$$

$$u_{ch,SC}(t) + u_{dch,SC}(t) \leq 1 \ \forall t, \tag{4.31}$$

$$0 \leq P_{im}(t) \leq u_{im}(t) \times (N_T \times 0.95 \times P_{T,r}) \ \forall t, \tag{4.32}$$

$$0 \leq P_{ex}(t) \leq u_{ex}(t) \times (N_T \times 0.95 \times P_{T,r}) \ \forall t, \tag{4.33}$$

$$u_{im}(t) + u_{ex}(t) \leq 1 \ \forall t, \tag{4.34}$$

where $u_{ch,B}$ and $u_{dch,B}$ are the binary variables that control the operation mode of the battery bank, $u_{ch,SC}$ and $u_{dch,SC}$ are the binary variables that control the operation mode of the SC bank, $u_{im}$ and $u_{ex}$ are the binary variables that control the exchange of power with the upstream grid, $N_B$ and $N_{SC}$ respectively represent the optimal quantity of battery and SC modules, $N_T$ denotes the optimal capacity of the transformer, $P_{ch,B}^{max}$ and $P_{ch,SC}^{max}$ respectively represent the maximum charge power capacities of the battery and SC modules, $P_{dch,B}^{max}$ and $P_{dch,SC}^{max}$ respectively represent the maximum discharge power capacities of the battery and SC modules, and $P_{T,r}$ denotes the step-size increment of the rated power capacity of the transformer (1 kVA), while the numeric value 0.95 represents the power factor.

Moreover, unlike all the previous analyses, it is assumed here that the MG has a contract with a financially responsible market participant (FRMP), which has financial obligations with respect to their subscribers for energy sold or purchased through the wholesale spot market. This allows the MG to access the wholesale electricity market. Of the various FRMPs working under the existing wholesale market regulatory arrangements, the registered small generator aggregators – which aggregate the outputs of a number of small generating units and dispatch the collective output into the spot market – are particularly well-suited for the purpose of this study. Nevertheless, it is assumed that network constraints do not block the acquisition of resources into the wholesale market. Also, network charges and service fees collected by the FRMP were not taken into account.

Fig. 4.6 illustrates the structure of solving a sequence of day-ahead (24-h) optimal dispatch problems (at an hourly resolution) using the linear programming-based energy scheduling framework. As the figure shows, the optimal dispatch problem is solved over the 24-hour time horizon and then stepped forward in time and re-solved for the next 24-hour subset (of the entire year) until the overall analysis period of interest is completed and the optimal dispatch is estimated over the entire year. Accordingly, for each subset of the overall analysis period (one year), the hourly operational decisions are recorded as part of the year-long optimal dispatch matrix.

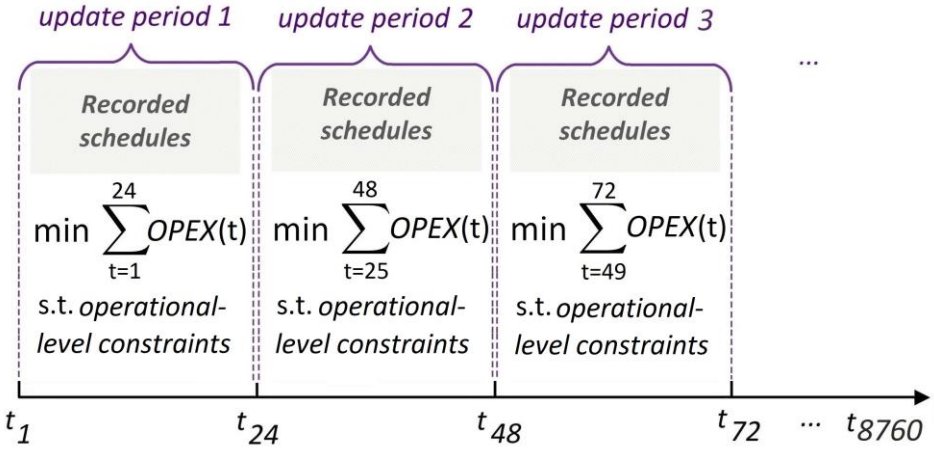


Figure 4.6: Structure of solving a sequence of look-ahead optimal scheduling problems over a moving 24-hour time window.

Accordingly, the flowchart of the budget-aware stochastic uncertainty characterisation solution algorithm integrated into the proposed DR-adjusted meta-heuristic-based MG capacity planning model, presented in Fig. 4.5, can be updated to include the predictive, look-ahead energy scheduling modelling element described above by replacing the blocks responsible for conducting the hourly-basis rule-based operational strategy with a new process block to represent the linear programming-based operational planning, in accordance with Fig. 4.6. That is, the flowchart of the overall structure of the stochastic, DR-integrated investment planning model with a nested (integrated) optimal operation dispatch strategy differs from that in Fig. 4.5 only in that the nested daily MG scheduling optimisation replaces the hourly rule-based, heuristic energy management strategy (the light coral block), as well as its preceding and following blocks, which ensure that the

hourly operation schedule is developed for all the hours of the same day before applying the proposed game-theoretic DR scheduling framework to the next day. Accordingly, both the central energy dispatch and system-level DR procurement planning sub-problems are solved with an update period of 24 hours.

Moreover, on a higher level, the overall structure of the formulated MG investment planning and operational scheduling co-optimisation problem (disregarding the uncertainty quantification and DR procurement modelling elements) can be separated into an outer loop meta-heuristic-based capacity sizing problem, within which daily optimal energy scheduling problems are nested, in accordance with Fig. 4.7. As the figure shows, the optimal sizing problem (outer loop) sends a vector of decision variables (*here-and-now* design variables) to the optimal scheduling problem (inner loop). The decision variables are treated as parameters (held fixed) by the optimal scheduling problem, a solution to which yields the *wait-and-see* decisions (operating schedules). The optimal scheduling problem is solved for every 24-hour period in the baseline year, the solutions of which are returned to the optimal design problem to evaluate each design's fitness (total NPC of the MG) subject to the planning-level constraints. Accordingly, for all the search agents of the MFOA (vectors of decision variables that represent candidate designs) in the inner loop, the optimal daily operating strategy is determined subject to the operational-level constraints until the operating schedules have been developed for the whole representative operation period (one year) and the obtained results are returned to the outer loop to evaluate the associated designs' fitness necessary to update the search agents' positions in the search space following the particular rules and operators of the MFOA. The outer design process then loops iteratively with the updated positions of the dedicated search agents until the termination condition (maximum number of iterations) is met.

Note that the outer optimal investment planning problem is feasible if and only if the inner optimal scheduling problem is feasible. Also, given that the optimal scheduling problem is convex, solving the formalised nested problem structure using linear programming is guaranteed to provide the globally optimum results over the associated operational scheduling horizon. This type of interaction between

two linked optimisation problems is commonly referred to as unidirectional coupling [21].

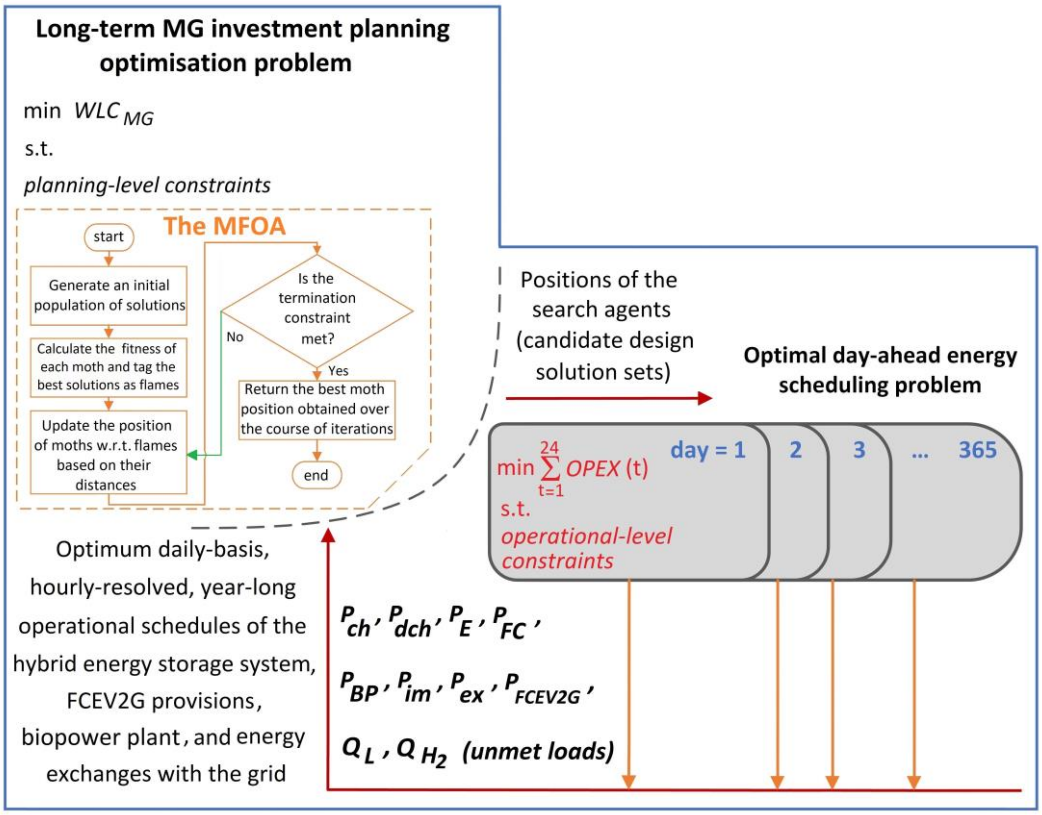


Figure 4.7: Structure of the optimal MG capacity planning problem with nested day-ahead scheduling optimisation sub-problems.

## 4.3. Simulation results and discussion

This section demonstrates the applicability and efficacy of the developed uncertainty budget-aware stochastic MG capacity planning and scheduling co-optimisation model in providing systematic guidance to MG planning decision-makers in quantifying and managing system-wide aleatory uncertainties (which arise from natural randomness), as well as providing a better understating of the comparative effects of parametric uncertainties on the design and costing of MG systems – necessary to make well-informed resource allocation decisions aimed at cost-optimal uncertainty reduction. It also quantifies the relative importance of the nested operational scheduling framework. To this end, it presents and discusses the numeric simulation results obtained by applying the proposed integrated framework

for MG planning and dispatch co-optimisation under uncertainty to an illustrative example. Specifically, the problem setup is defined in Section 4.3.1; the indicative hourly probability-value pairs for reduced scenario vectors (containing probabilistic realisations of the uncertain parameters) generated by the MILP-based scenario clustering algorithm are provided in Section 4.3.2 to confirm the feasibility and validity of the algorithm through scenario testing; and high-level, direct comparative analyses of the fixed-controller deterministic and stochastic (with different levels of mitigated uncertainty) modelling results with associate running (CPU execution) time analyses are detailed in Section 4.3.3 to illustrate the potentially significant and diverse implications of a wide range of uncertainty reduction preferences in terms of system cost and configuration with detailed discussions of the computational complexities of meta-heuristic-based MG sizing under uncertainty (which is prone to the so-called '*curse-of-dimensionality*' phenomena) – with associated explanations of the analytical perspectives and steps of the proposed stochastic optimisation methodology. The analyses are carried out for the case with an integrated system-level DR dispatch game for the optimal coordination of sectoral, aggregator-activated, incentive-responsive loads in a platform-mediated, liberal market. Additionally, a systematic rank order for uncertain input variables is provided through comprehensive analyses of the relative importance (effect size) of quantifying the selected uncertain parameters to develop an understanding of the extent to which various uncertain inputs contribute to the overall quantity of interest (QoI)[6] uncertainty – by which the designer can systematically explore the trade-offs between design modifications and parameter-wise uncertainty management. The presentation and discussion of the numeric simulation results proceed by specifically analysing the impact of MG sizing and scheduling co-optimisation in the most likely stochastic scenario in Section 4.3.4. Then, the stability and robustness of the overall probabilistic MG sizing model in producing optimal uncertainty reduction alternatives and MG design choices is

[6] In the context of probabilistic parametric uncertainty analysis, the term 'quantity of interest' refers to a pre-specified statistical tool applied to the PDF of continuous output variables derived from solving a deterministic model for different realisations of uncertain inputs. It can be a central tendency value (for example, mean or median), a dispersion parameter (for example, standard deviation or coefficient of variation), or more frequently, a percentile – which is often set to be constant.

verified in Section 4.3.5 through two sets of in-depth sensitivity analyses. The first one explores the variation of model outputs to changes in the minimum allowed self-sufficiency ratio – with a particular focus on the actual self-sufficiency ratio of the optimally designed system – while the second one investigates the economics of temporal battery energy arbitrage with the grid. The sensitivity analyses are carried out by solving the stochastic model repeatedly for different values of the sensitivity parameters of interest. For the first set, this consists of solving the model for various minimum allowed self-sufficiency ratios (ranging between 0 and 100), while for the second set this entails solving the model for various combinations of projected battery capital cost and feed-in-tariff. Subsequently, comprehensive financial viability analyses incorporating various capital budgeting metrics are carried out in Section 4.3.6 to systematically compare and contrast the profitability of different uncertainty management scenarios considered, as well as the most likely case with the multi-period optimisation-based dispatch strategy, whilst also benchmarking the resulting metrics against those of the base-case, deterministic modelling results obtained in the previous chapter, with the secondary objective of substantiating the technical competence and economic viability of notional MG 4 optimised for the case of Ohakune.

### 4.3.1. Problem setup: The case of Ohakune

To demonstrate the effectiveness of the model within a community renewable energy project scheme, the model was specifically parametrised for application to test-case MG 4 (see Section 3.2), which is populated for the case of Ohakune. Accordingly, the selected equipment product models and the associate techno-economic specifications – the capital, replacement, and O&M costs, as well as the life-cycle expectancy and efficiency – of the candidate MG technologies for implementation in Ohakune remain the same as those listed for PV panels, micro-hydro turbines, transformer, SC modules, electrolyser and fuel cell stacks, hydrogen tank, and hydrogen refuelling unit in Table 2.2, as well as those provided for the WTs, biopower plant, power loads' inverters, battery packs, and the FCEV2G unit of the hydrogen station in Table 3.1. Recall that the selection of the equipment product models was based on the author's experience – on the technical and cost aspects – from the options available in the Australian and New Zealand renewable

energy asset markets. Also, as mentioned earlier, costs are always cited in 2019 $NZ throughout this thesis. Furthermore, the project lifetime and real interest rate are respectively assumed to be 20 years and 2.45%; the single rate feed-in tariff and per-unit premium tariff rate for V2G power are set to be $0.08/kWh; the total cost associated with the pelletisation of blended biomass feedstocks is considered to be $98/tonne of pellets [271], [272]; while the average social cost of $CO_2$ emissions (from the biopower plant) is considered to be $46/t$CO_2$ [229]. Moreover, the set of key simplifying assumptions, presented in Section 2.3.4, underlie the development of the test-case MG model and the proposed optimal stochastic equipment capacity planning formulation with and without the look-ahead, predictive dispatch strategy. The MG is, additionally, designed to be scheduled using the hourly-basis, rule-based expert system put forward in Section 3.2.5 for the baseline, non-intelligent dispatch-oriented case, while the prescribed order of precision for the size of different components (as defined by the associated size step increments) remains unaltered.

As stated earlier, the climatic time-series data are based on 20 years' (1999 to 2018) worth of hourly historical data retrieved from the CliFlo database [167], while the wholesale price time-series data are based on 10 year's (2010 to 2019) worth of half-hourly historical locational marginal electricity data retrieved from the New Zealand's electricity market database (converted to hourly values to comply with the time-step increment resolution of the devised rule-based and forward-looking operational strategies) [169]. Also, the synthesised overall year-long power load demand time-series data (refer to Section 3.5.3) is regenerated 19 times (refer to Section 4.2.1.1) to achieve statistical representativeness necessary for constructing initial power load probability distributions for each time-step of the representative one-year system operation – since relevant hourly-resolved historical data are lacking and expert elicitation is not applicable in this context. However, for reasons of brevity, the historical one-year profiles for uncertain meteorological and wholesale prices, as well as the synthetically regenerated profiles for load demand data, are not shown explicitly. For a general view of the associated profiles, the reader is referred to Figs. 3.15 and 2.19 that respectively depict the monthly-mean daily profiles for the 20 years' worth of climatic and 10 years' worth of

wholesale price data,[7] as well as Fig. 3.18 (a) that plots the original (non-regenerated) synthetic power load profile derived for the total forecasted electricity consumption at each hour of the MG operation in the representative year. Note that, for better visualisation, the power load profile is also presented vs time-of-day (24 hours) as averaged over the month. It should, however, be emphasised that all the PDFs of uncertain inputs are generated on an hourly basis – and the operational planning sub-problem is solved with hourly granularity. Also, while treated in an hourly-resolved manner in the model, the forecasted monthly averaged profile for biomass availability is displayed in Fig. 3.16. Moreover, the synthesised monthly-mean daily profile for the hydrogen load demand, which, unlike power loads, is assumed not to be subject to uncertainty, is displayed in Fig. 3.18 (b).

Similarly, all the other applicable modelling assumptions, simplifications, procedures, formulations, constraints, and data values (for instance, see Tables 2.2 and 3.1–3.4) for the advanced stochastic model remain the same as those discussed in the relevant previous sections of Chapters 2 and 3 for the base-case, deterministic MG sizing model, as well as the Stackelberg, non-cooperative game-theoretic, aggregator-mediated DSM framework integrated. Again, note that the proposed framework for modelling high-dimensional stochastic variability is added to the interruptible DR-adjusted, meta-heuristic-based optimal MG sizing model formulated in the previous chapter – towards developing a holistic understanding of MG capital investment decision-making processes that systematically account for pre-specified tolerable levels of aggregate input data uncertainty. This also provides a platform to identify key parametric forecast-related drivers of risk in MG investments and their relative weights.

[7] Recall that the hourly-basis, year-long climatic and wholesale price data used in the deterministic model are forecasted by averaging the records of historical data over the same hour of the corresponding 8,760-h time-series (a particular hour of the day in each month over the year-round time-series), whilst employing a time-dependent dummy variable to account for the weekday versus weekend effect in the calculation of the weighted arithmetic means of wholesale price time-series data.

### 4.3.2. Indicative scenario reduction analysis

As explained in Sections 4.2.1.2 and 4.2.1.3, the hourly-basis, uncertain parameter-specific PDFs – generated based on the historical and synthetically augmented data – were first approximated by dividing them into 7 equal-width regions to form the basis for scenario vector generation ($N_x = 7$). Then, solving the scenario reduction problem, formulated in Equations 4.15–4.22, reduced the original number of hourly multi-dimensional scenarios to 7, from the original $7^6$ = 117,649 scenario vectors generated by all possible combinations of the stochastic representations (discrete approximations) of the uncertain inputs – obtained using the associated discretisation of PDFs. Note that the hour-to-hour correlation is not modelled in this study as that would result in an annual scenario vector tree for the operation of the MG incorporating as much as $117{,}649^{8{,}760}$ distinct paths as part of the stochastic sizing simulations with the original scenario vectors and at least $7^{8{,}760}$ distinct paths for the stochastic simulations that solve for the reduced scenario vectors, both of which are by no means computationally tractable.[8] Accordingly, the selected scenario vectors and the new probabilities assigned to them (probability-value pairs associated with the reduced multi-dimensional scenarios) were determined for each hour of the MG operation individually in the baseline year.[9]

To verify the utility and validity of the MILP-based scenario clustering algorithm in optimally minimising the number of original hourly input scenario vectors, an indicative analysis is provided in this section. To this end, Table 4.2 lists the posterior probabilities of occurrence assigned to the selected seven reduced multi-dimensional scenarios for the stochastic realisation of the considered uncertain variables for each hour of the day that represents the most intense peak on the year-round, mean daily load profile (consisting of the mean of the power load demand forecasts over 24 equidistant time-steps in the course of each

[8] However, further work is underway to reduce the total time modelled at the operational analysis level by separating the entire year into a very small number of representative days with adequate accuracy. This would provide a platform to explicitly model the hour-to-hour correlations for the reduced scenario vectors.

[9] Note that these posterior probabilities are assigned to the uncertainty vectors (which contain a joint realisation of the uncertain parameters), rather than to each individual uncertain input realisation.

continuous 24-hour period of the representative year), namely July 21st. As the table demonstrates, for each hour of the representative day, the sum of the individual probabilities of the set of mutually exclusive and collectively exhaustive multi-dimensional scenarios is equal to 1, while a direct comparison of the hourly scenario realisations reveals diverse combinations of individual probabilities. Furthermore, no two of the seven scenario vectors obtained for a specific hour have an equal probability value. These observations, collectively, suggest the validity and adequacy of the employed scenario reduction technique for modelling large-scale, high-dimensional variability associated with input parameters in stochastic MG capacity planning applications where the uncertainty in input parameters is represented probabilistically.

Table 4.2: Posterior probabilities of the seven reduced scenario vectors generated for each hour of the representative day (July 21st).

| Hour of day | Prob. of scenario 1 | Prob. of scenario 2 | Prob. of scenario 3 | Prob. of scenario 4 | Prob. of scenario 5 | Prob. of scenario 6 | Prob. of scenario 7 |
|---|---|---|---|---|---|---|---|
| 1 | 0.45 | 0.24 | 0.09 | 0.08 | 0.07 | 0.05 | 0.02 |
| 2 | 0.26 | 0.20 | 0.17 | 0.16 | 0.12 | 0.06 | 0.03 |
| 3 | 0.25 | 0.21 | 0.19 | 0.16 | 0.09 | 0.08 | 0.02 |
| 4 | 0.41 | 0.30 | 0.10 | 0.08 | 0.06 | 0.04 | 0.01 |
| 5 | 0.27 | 0.24 | 0.18 | 0.12 | 0.09 | 0.08 | 0.02 |
| 6 | 0.24 | 0.20 | 0.16 | 0.14 | 0.13 | 0.10 | 0.03 |
| 7 | 0.35 | 0.18 | 0.16 | 0.13 | 0.09 | 0.06 | 0.03 |
| 8 | 0.24 | 0.21 | 0.20 | 0.15 | 0.14 | 0.05 | 0.01 |
| 9 | 0.25 | 0.19 | 0.16 | 0.15 | 0.12 | 0.09 | 0.04 |
| 10 | 0.28 | 0.25 | 0.17 | 0.12 | 0.09 | 0.05 | 0.04 |
| 11 | 0.23 | 0.18 | 0.17 | 0.16 | 0.13 | 0.10 | 0.03 |
| 12 | 0.55 | 0.19 | 0.11 | 0.09 | 0.03 | 0.02 | 0.01 |
| 13 | 0.30 | 0.21 | 0.16 | 0.14 | 0.11 | 0.05 | 0.03 |
| 14 | 0.26 | 0.25 | 0.17 | 0.13 | 0.09 | 0.07 | 0.03 |
| 15 | 0.24 | 0.22 | 0.21 | 0.14 | 0.09 | 0.08 | 0.02 |
| 16 | 0.33 | 0.23 | 0.13 | 0.11 | 0.10 | 0.06 | 0.04 |
| 17 | 0.26 | 0.22 | 0.14 | 0.13 | 0.10 | 0.08 | 0.07 |
| 18 | 0.37 | 0.30 | 0.17 | 0.09 | 0.04 | 0.02 | 0.01 |
| 19 | 0.41 | 0.20 | 0.15 | 0.10 | 0.06 | 0.05 | 0.03 |
| 20 | 0.31 | 0.24 | 0.13 | 0.12 | 0.11 | 0.05 | 0.04 |

| | | | | | | | |
|---|---|---|---|---|---|---|---|
| 21 | 0.25 | 0.22 | 0.17 | 0.12 | 0.10 | 0.08 | 0.06 |
| 22 | 0.37 | 0.26 | 0.17 | 0.09 | 0.07 | 0.03 | 0.01 |
| 23 | 0.24 | 0.18 | 0.16 | 0.15 | 0.13 | 0.11 | 0.03 |
| 24 | 0.45 | 0.28 | 0.08 | 0.07 | 0.06 | 0.05 | 0.01 |

Also, for greater insight into the dynamics of hourly scenario vectors in terms of the corresponding values of the uncertain parameters, Table 4.3 presents the posterior probabilities and the associated stochastic realisations of uncertain input variables in the reduced multi-dimensional scenarios yielded for the hour at which the annual net morning peak load[10] occurs over the course of representative year-long MG operation, namely 9 a.m., July 21$^{st}$.[11,12] The corresponding average forecasts of the uncertain input parameters (determined by the mean of historical values for a particular time-step in time-series datasets), which are used in the deterministic model, are as follows: solar irradiance = 161 W/m$^2$, ambient temperature = 3.2 °C, wind speed = 3.8 m/s, river streamflow = 4,129 L/s, power load = 6,188 kWh, and wholesale electricity price = $0.23/kWh. As it can be observed from the table, as the probability of occurrence of the scenario vectors decreases, the absolute changes in the probabilistically represented output variables from the corresponding mean values increase – though not strictly necessarily. The detailed representative time-step analyses, additionally, confirm the feasibility and validity of the MILP-based scenario clustering algorithm in accurately representing all possible realisations of forecast uncertainties – the space of all possible combinations of uncertain parameters – and providing realistic estimates of the associated uncertain parameter values in the extreme-case scenarios – in accordance with historical and synthetically regenerated data. Put differently, the seven reduced hourly scenario vectors provide a statistically representative range of possible

[10] More specifically, the annual net morning peak hour refers to the time-step at which the average net load (internal load minus onsite variable generation) is the highest within the subset of the net load time-series dataset containing relevant data points across year-long morning peak hours (refer to Table 4.1).

[11] The annual net peak demand also occurs on July 21$^{st}$ (a winter day in the Southern Hemisphere), where, additionally, the one-day total energy consumption is highest. However, as the annual net peak demand occurs in the evening (specifically, 6 p.m.) when solar PV panels do not generate, it was decided to use the annual net morning peak load for the illustrative example.

[12] Recall that the load characteristics described in Section 3.5.3 lead to a winter peak dominated by space heating, followed by the power consumption of the ski resort.

uncertain input data realisations – governing the dynamic nature of operating conditions of the MG – in accordance with the relevant historical and synthetic statistical data. It is also worth recalling that the input parameters for the identified most probable and dissimilar scenario vectors within the original multi-dimensional scenario set are represented by the means of the evenly spaced regions resulting from equal interval partitioning of the corresponding (hourly) input variable PDFs.

Table 4.3: Indicative probability-value pairs of reduced scenario vectors for the representative annual net morning peak hour (9 a.m., July 21$^{st}$).

| Reduced scenario vector | Probability of occurrence | Uncertain parameter | | | | | |
|---|---|---|---|---|---|---|---|
| | | Solar irradiance [W/m$^2$] | Ambient temperature [°C] | Wind speed [m/s] | River streamflow [L/s] | Power load demand [kWh] | Wholesale price [$/kWh] |
| 1 | 0.25 | 158 | 3.0 | 3.6 | 4,025 | 6,392 | 0.22 |
| 2 | 0.19 | 171 | 3.5 | 3.3 | 3,962 | 5,921 | 0.26 |
| 3 | 0.16 | 145 | 2.7 | 4.3 | 3,877 | 6,540 | 0.28 |
| 4 | 0.15 | 143 | 2.6 | 4.4 | 4,574 | 6,733 | 0.18 |
| 5 | 0.12 | 194 | 4.0 | 3.0 | 3,680 | 6,801 | 0.29 |
| 6 | 0.09 | 197 | 4.1 | 4.6 | 3,616 | 5,538 | 0.30 |
| 7 | 0.04 | 122 | 1.9 | 4.8 | 4,728 | 5,218 | 0.10 |

As Table 4.3 demonstrates, the seven multi-dimensional scenarios have adequately captured the underlying correlations of meteorological, power load, and wholesale price forecasts. For instance, in line with expectations, solar irradiance and ambient temperature are positively correlated. As another instance, river streamflow and locational marginal price data are negatively correlated as at times of higher streamflow, inflows into the nearby (off-site) hydro lakes are higher as well. This leads to lower expected marginal water values that are assigned by the corresponding hydro generators to reflect their opportunity cost of releasing water for electricity dispatch in the context of the New Zealand wholesale electricity market that is dominated by hydroelectric generation [304]. Also, note that the probability of occurrence of reduced scenario vector 7 is as low as 0.04, implying that other system conditions with different combinations of higher or lower possible realisation values for the uncertain parameters of interest – compared to the corresponding long-run average values – can be safely ignored.

### 4.3.3. Comparative deterministic and stochastic MG planning results

To evaluate the impact of the selected system-inherent parametric uncertainties on the overall conceptual configuration of the MG system – represented by the optimal values of the equipment capacity design variables – and the associated whole-life cost of the system, comparative results of the fixed-controller stochastic and deterministic model variants are presented in this section. Also, comprehensive risk analyses are carried out to evaluate the most interesting results (according to designer preferences) from the stochastic simulations adjusted for the perceived levels of risk. The comprehensive forecast uncertainty-driven risk analyses, more specifically, elucidate the comparative impact of various tolerable levels of risk on the optimal MG cost and configuration solution set. Importantly, the associated cost(-risk)-benefit balancing analyses seek to produce best-compromise solutions by balancing the benefits of implementing the MG in a particular configuration against the level of risk it presents in terms of unmet load; the risk tolerated increases proportionately with the magnitude of the unreliability involved, which varies inversely with the associated life-cycle cost incurred. As explained in Section 4.2.1.6, in the post-optimisation phase of the stochastic simulations, three key uncertainty-aware strategic decision-making scenarios are considered that illustrate the financial and design implications of two extreme-case scenarios and one middle-case scenario, namely: (1) a strong risk-averse case, which represents the pessimistic decision-maker's strategy to hedge against the worst-case scenario in a highly conservative and robust manner; (2) a risk-neutral case, where the realistic decision-maker is concerned about the most likely outcome, which carries the highest probability of occurrence; and (3) a strong risk-seeking case, where opportunistic decisions are made in accordance with the most optimistic (best-case) outcomes irrespective of how small the associated probabilities of occurrence are.

Fig. 4.8 displays the convergence process of the MFOA-based solution algorithm for the seven probabilistic sub-models (or, looking from the inside out, deterministically formulated model instances, which are systematically combined to create the overall stochastic model), each addressing one of the seven sets of 8,760 reduced hourly scenario vectors that contain specific probabilistic realisations of the uncertain inputs. The figure reaffirms the adequacy of the selected stopping

criteria (300 iterations) with 50 search agents for the MFOA to optimise a robust solution to the high-dimensional community-scale, sector-coupled MG capacity planning problems tailored to 100%-renewable and -reliable projects. Recall that explicit multi-variant evidence has also been provided in Chapters 2 and 3 supporting the adequacy of a single run of the MFOA.

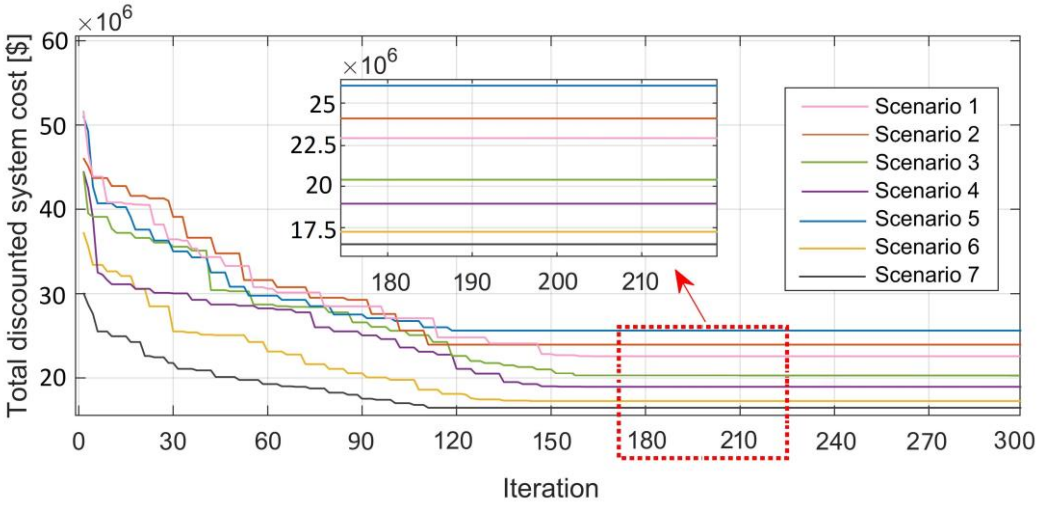


Figure 4.8: Convergence process of the deterministically formulated MFOA-based solution algorithm for the seven annual sets of reduced scenario vectors.

Furthermore, Fig. 4.8 provides useful initial insights into the comparative influence of the six uncertain input parameters under consideration on the total discounted system cost. Specifically, assuming that, at all time-steps of the MG operation, deviations of the uncertain input parameters from the corresponding means of historical data follow the same scenario-specific trends as those provided for the time-step 9 a.m., July 21$^{st}$, the following key insights emerge from a direct comparison of the optimal whole-life costs of the MG, yielded in Fig. 4.8, for the seven sets of 8,760 reduced multi-dimensional scenario vectors:

1. Unlike for all other uncertain parameters, the total discounted system cost has shown a directly inverse relationship with wind speed irrespective of scenario realisations for other uncertainty factors. That is, the greater the mean wind speed in an annual scenario set, the lower the total NPC of the system in spite of scenario realisations for other parameters that have a negative impact on the system cost. This indicates that wind speed is the

most sensitive uncertain parameter, which can be, at least in part, explained by the observed relatively high share of wind generation in the optimal DER investment portfolio in the baseline, deterministic case – as it represents the greatest rate of capacity factor to NPC per kW installed among the non-dispatchable renewables considered in the candidate pool for implementation at the site of interest. To illustrate, wind speed realisations in scenario vectors 1, 2 and 5, which are lower than historical average values, have relatively proportionally led to increased optimal total discounted system costs compared to the deterministic case (NZ$21.72m). On the other hand, higher than historical average wind speed realisations in scenario vectors 3, 4, 6, and 7 have led to approximately proportionally decreased total MG life-cycle costs.

2. Given the comparatively low shares of solar PV and micro-hydro in the optimal combination of technologies for the site under consideration, the positive or negative deviations of solar irradiance, temperature, and streamflow from the corresponding historical average values, even where all the three deviations are associated with the same direction (sign) relative to their associated historical means, do not necessarily result in the deviation of the whole-life MG cost moving in the opposite direction. To illustrate, better than average (higher than normal) irradiance, temperature, and streamflow forecasts, even collectively, do not guarantee reductions in total discounted MG costs due to the relatively insignificant shares of solar PV and micro-hydro plants in the total optimal non-dispatchable power generation capacity. The most notable observation supporting this argument is that, while the values of irradiance, temperature, and streamflow are all reduced in scenario vector 3 compared to the corresponding mean values (which result in lower power outputs from solar PV and micro-hydro technologies) by as much as ~10%, ~16%, and ~6%, respectively, the whole-life cost of the MG for the annual set of input data incorporating that scenario vector is lower than that of the deterministic case by as much as ~6% – indicating that the economic viability of the MG is improved, mainly as a result of higher than average wind speeds.

3. Collectively, relative to irradiance, temperature, and streamflow, the wholesale price has a more pronounced impact on the finances of the system, but it is still significantly less impactful than wind speed. For instance, changes in wholesale price in scenario vectors 2, 4, 5, and 7 (relative to the corresponding historical means) is directly correlated with the associated total system cost. However, an inverse correlation can be seen for scenario vectors 1, 3, and 6. While the above-mentioned direct correlations for scenario vectors 2, 4, 5, and 7 are in line with expectations, the main reason for the observed inverse correlations for scenario vectors 1, 3, and 6 lies in the system dynamics with respect to the minimum allowable self-sufficiency ratio constraint imposed ($SSR^{min}$ = 80%) – a major limiting factor for the influence of wholesale price forecast uncertainty on the total system cost. More specifically, the increase in the estimated system cost following a reduction in the wholesale price in scenario vector 1 can be, to a great extent, explained by the fact that the maximum contribution of utility grid imports to serving the power loads is restricted to be at most 20% and, therefore, the relative impact of the wholesale price uncertainty factor on the variability of the objective function is limited. Also, a major explanation for the reduced MG life-cycle cost following an increase in the corresponding wholesale prices in scenario vectors 3 and 6 is the more dramatic upward changes in wind speed, which significantly contribute to the cost-efficiency of overbuilding WT capacity and exporting excess power during the light-load periods (with negative net loads) back into the grid, rather than importing power to the maximum possible level.

4. Similar to irradiance, temperature, and streamflow, no significant trend can be discerned for the influence of the load demand forecast uncertainty on the performance and cost-optimality of the system, which implies the relatively low overall sensitivity of the system cost against the probable range of load demand variations. This can be mainly explained by the observation that load demand is relatively less subject to variability for the case under consideration. One factor that potentially limits the generalisability of this finding is that the probable range of load demand

variations is determined synthetically using a Markov chain process that systematically regenerates the forecasted hourly-basis, year-long dataset – that is also synthetically profiled – due to the lack of appropriate historical time-series data. Given this limitation, the possibility that the obtained range for load demand variations is not the best representative of actual conditions cannot be ruled out.

The synthetic regeneration of load demand time-series data (which potentially reduces the generalisability of the associated findings), together with the fundamental simplifying assumption of similar patterns of inter-scenario variability at all hours of the system operation, brings to light the importance of a more holistic approach to quantify the relative importance of key uncertain inputs. Such a more holistic approach provides a platform to more effectively assist designers in cataloguing and prioritising which parameters contribute most to the output uncertainty – necessary to target the most sensitive uncertain parameters during the MG design phases and manage resources in a strategic manner. The above analyses on the relative effect size of the uncertain parameters of interest should, therefore, be treated as indicative and useful for gaining initial insights.

Accordingly, to more systematically analyse the relative significance of quantifying the uncertainty in input parameters of interest, the stochastic simulations were run a further six times, each time characterising only one source of parametric uncertainty before applying the three budgets on the acceptable levels of uncertainty in design quantities of interest. To this end, for each set of stochastic simulations, all the uncertain variables except one were fixed at the corresponding historical mean values. The contribution of each uncertainty factor to the overall deviation of the (increased or decreased) MG whole-life cost (compared to that of the corresponding uncertainty budget scenario in the original probabilistic simulations, where all the uncertainty sources are jointly characterised) then serves to quantify the impact of the uncertainty factor that has not been fixed; the larger the deviation of the MG whole-life cost, the more substantial the contribution of that parameter to the propagated uncertainty into model outputs. The comparative uncertainty impact analysis results are presented in Table 4.4, which describe the sensitivity of the main model output (life-cycle cost of the MG) to each uncertain

input. It can be seen, for example, that in the best-case scenario, wind speed forecast uncertainty accounts for a relatively significant 61% of the total decrease (in terms of pooled effect size) in the life-cycle cost of the MG relative to the corresponding probabilistic case where all the uncertain parameters are quantified simultaneously, whereas wholesale electricity market price, solar irradiance, ambient temperature, river streamflow, and power load demand forecast uncertainties make up 15%, 6%, 4%, 8%, 6% of this total, respectively. Moreover, the percentage contribution of each uncertainty factor to the increased MG life-cycle cost in the most likely and worst-case scenarios of stochastic modelling is found to be in the same range as those for the best-case scenario, which verifies the statistical robustness of the findings. In addition, the obtained rank orders of the uncertain input variables – based on how much uncertainty in total discounted system cost would be reduced if only one of the uncertain parameters under consideration was quantified – have demonstrated a rank order that is consistent with those of the indicative preliminary results. This, accordingly, validates the relevant initial findings. The comparatively lower percentage contribution of ambient temperature forecast uncertainty to the uncertainty in MG life-cycle cost also, to some extent, justifies its absence in uncertainty vectors associated with systems integrating solar PV generation in previous work. However, it should be noted that, as demonstrated in Table 4.4, when added to the percentage contribution of irradiance to measure the overall influence of solar PV-related uncertainties as a single factor, ambient temperature has a non-negligible impact on the comparative importance of parametric uncertainty sources. More specifically, in all the cases analysed, characterising the overall uncertainty inherent in solar PV generation forecasts, based on both solar irradiance and temperature, changes the rank order of the aggregate solar PV-related uncertainty on the total NPC of the MG, compared to the case where the associated effect size is quantified solely based on solar irradiance forecast uncertainty. Also, further analyses identified that for the specific case studied, the impacts of the uncertainties in the forecasted power outputs from the non-dispatchable generation technologies are, to a great extent, commensurate with the associated rates of (site-specific) capacity factor to NPC per kW installed.

Table 4.4: Percentage contribution of each uncertainty factor to the total deviation of the MG life-cycle cost across different uncertainty budgets of stochastic simulations.

| Uncertain parameter | Stochastic simulation case | | |
|---|---|---|---|
| | Best-case scenario | Most likely case | Worst-case scenario |
| Wind speed forecasts | 61% (−$3.26m) | 57% ($0.61m) | 55% ($3.13m) |
| Wholesale electricity price forecasts | 15% (−$0.80m) | 17% ($0.19m) | 19% ($1.08m) |
| Solar irradiance forecasts | 6% (−$0.32m) | 8% ($0.09m) | 7% ($0.40m) |
| Ambient temperature forecasts | 4% (−$0.21m) | 4% ($0.04m) | 5% ($0.28m) |
| River streamflow forecasts | 8% (−$0.43m) | 7% ($0.08m) | 10% ($0.57m) |
| Load demand forecasts | 6% (−$0.32m) | 7% ($0.08m) | 4% ($0.23m) |
| Overall impact of forecast uncertainties | 100% (−$5.34m) | 100% ($1.09m) | 100% ($5.69m) |

Fig. 4.9 shows the best cumulative normal distribution function fit to the total discounted system cost data with overlaid deterministic, expected, 5$^{th}$ percentile, and 95$^{th}$ percentile values.

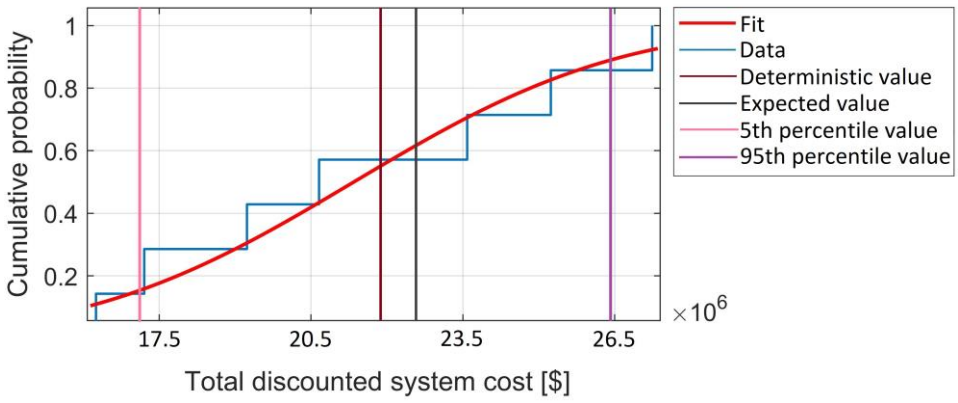


Figure 4.9: Fitting a cumulative normal distribution to the total NPC outputs from the stochastic sub-models.

Furthermore, to improve the (relatively low) degree of the stochastic model outputs' granularity (due to the limited number of reduced scenario realisations, or more specifically, the limited population of the model outputs for only seven

reduced annual scenario vector sets in the stochastic simulations) necessary to more effectively support the associated MG capacity optimisation decision-making processes, the probabilistic modelling results are systematically augmented. To this end, the results are assumed to follow a normal distribution and the built-in MATLAB function '$normrnd(\mu,\sigma)$' was used to generate $N$ = 300,000 random numbers (discrete scenarios) from the normal distribution best fit to the original population distribution of a random output variable $X$ with mean $\mu$ and standard deviation $\sigma$ – containing the resulting seven optimal values of a specific output of the stochastic model (decision variables and the objective function) for the seven annual sets of reduced multi-dimensional hourly scenarios. Accordingly, a synthetically augmented population distribution of $\bar{X}$ was generated to derive the respective normal density curves. The margin of error (with a confidence level of 95%) associated with an output for each of the three stochastic scenario realisations (in accordance with the expected values, as well as the 5$^{th}$ and 95$^{th}$ percentiles of the results) can be determined as follows [305]:

$$MOE = \frac{\sigma(\bar{X})}{\sqrt{N}} t_{m,N}, \tag{4.35}$$

where $t_{m,N}$ is the value of the variable on a Student's $t$-distribution with $N$ degrees of freedom for $m$% right-tailed probability corresponding to the selected uncertainty budget. For the best-case, most likely case, and worst-case scenarios, $m$ is set to 5%, 50%, and 95% respectively.

Fig. 4.10 illustrates this process for the best normal distribution curve fit to the augmented population of the total NPC of the system (based on the optimal cost solutions estimated for the seven annual sets of reduced scenario vectors) with different uncertainty budgets (design quantities of interest) overlaid. The resulting values for the whole-life cost of the system under the three key probabilistic scenarios indicate the following negligibly small $MOE$ values: best-case scenario, 0.157%; most likely case, 0.351%; and worst-case scenario, 0.161%. Notably, not only does this inverse surrogate (auxiliary) modelling approach – which assists in augmenting a set of reference design variables obtained for particular uncertainty realisations – improve data fidelity of the simulation outputs (or in other words,

improve the resolution of discrete output distributions), but it also provides an additional layer of stochasticity to the overall probabilistic modelling processes, which helps minimise the optimality (reality) gap.

Note that similar output-specific normal distribution fits are produced and the relevant quantities of interest are determined for all the decision variables. Accordingly, the expected values, as well as the $5^{th}$ and $95^{th}$ percentiles of the results are determined based on the corresponding normal distribution curves derived for the augmented output data associated with the seven annual sets of reduced hourly scenario vectors.

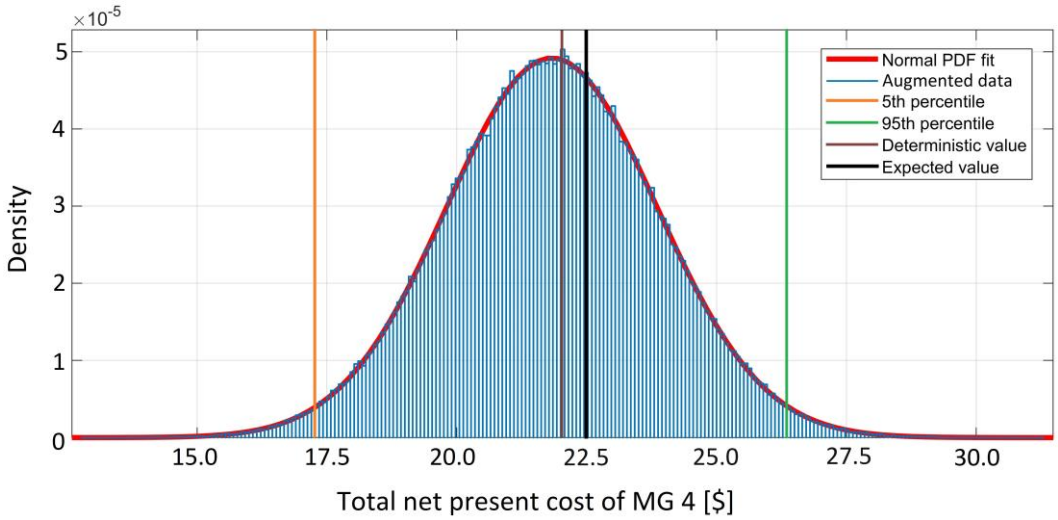


Figure 4.10: Fitting a normal PDF to the augmented optimal MG life-cycle cost histograms with overlaid uncertainty budgets of interest.

Tables 4.5 and 4.6 present the comparative MG investment planning model results under the deterministic and probabilistic cases and provide a breakdown of the total discounted system costs by system components and cost/income output parameters. In particular, the probabilistic case explores three different levels of accepted risk in accordance with three separate uncertainty budgets; specifically, two high impact, low probability scenarios and one low impact, high probability scenario. More specifically, Table 4.5 provides a breakdown of the optimal cost/income components included in the life-cycle analysis of the MG system, while Table 4.6 presents the optimum capacity of the MG equipment along with the share of each component in the total discounted equipment-related cost. The

percentages in parentheses refer to the relative change of the results of the probabilistic cases with respect to the deterministic case results. More specifically, the percentages are referred to as the relative value of the stochastic solution (VSS) in the probabilistic uncertainty characterisation context, which can be mathematically formulated as follows [306]:

$$VSS = z^*_{det} - z^*_{stoch}, \tag{4.36}$$

$$\overline{VSS} = \frac{VSS}{z^*_{det}} \times 100\%, \tag{4.37}$$

where $z^*_{det}$ and $z^*_{stoch}$ respectively denote the optimal solutions to the deterministic and stochastic problems (outputs of the deterministic and stochastic variants of the model).

Table 4.5, additionally, presents the associated CPU usage times of the deterministic and probabilistic simulation cases. Note that the computational cost of the probabilistic simulation case equals the sum of the CPU times associated with solving the model for the seven annual sets of reduced hourly scenario vectors – upon the augmented output data of which the uncertainty budget of interest is applied to derive the relevant information.

Table 4.5: Breakdown of the total discounted system cost under deterministic and budget-constrained probabilistic MG planning simulation cases.

| Cost component | Cost subcomponent | Simulation case | | | |
|---|---|---|---|---|---|
| | | **Deterministic** | **Best case** | **Most likely case** | **Worst case** |
| Total discounted equipment-related costs $((\sum_{c\in C} \underset{20-yr}{NPC_c}) + \underset{20-yr}{NPC_I})$ [$] | | 18.25m | 17.38m (−5%) | 20.16m (+10%) | 26.59m (+46%) |
| Total discounted MG operational costs $(\underset{20-yr}{NPV}(\sum_{t=1}^{8760} OC_{MG}(t)))$ | Total discounted incentive payment to the aggregators $(\underset{20-yr}{NPV}(\sum_{t=1}^{8760} I_{MGO}(t) \sum_{j\in J} D_{LA}^{j}(t)))$ [$] | 3.99m | 2.84m (−29%) | 3.13m (−22%) | 1.12m (−72%) |
| | Total discounted cost of electricity imports $(\underset{20-yr}{NPV}(\sum_{t=1}^{8760} cost_{im}(t)))$ [$] | 0.46m | 0.57m (+24%) | 0.38m (−17%) | 0.11m (−76%) |
| Total discounted FCEV2G electricity provision costs $(\underset{20-yr}{NPV}(\sum_{t=1}^{8760} \pi_{FCEV2G} P_{FCEV2G}(t)))$ [$] | | 0.42m | 0.35m (−17%) | 0.39m (−7%) | 0.30m (−29%) |
| Total discounted operating costs of the biopower plant | Total discounted emission credits $(\underset{20-yr}{NPV}(\sum_{t=1}^{8760} cost_{em}(t)))$ [$] | 0.52m | 0.52m (0%) | 0.52m (0%) | 0.52m (0%) |
| | Total discounted biomass feedstock costs $(\underset{20-yr}{NPV}(0.098\ [\$/kg] \times \sum_{t=1}^{8760} M_{BP}(t)\ [kg]))$ [$] | 0.49m | 0.49m (0%) | 0.49m (0%) | 0.49m (0%) |
| Total discounted income derived from electricity exports $(-\underset{20-yr}{NPV}(\sum_{t=1}^{8760} income_{ex}(t)))$ [$] | | −2.41m | −5.08m (−111%) | −2.56m (−6%) | −2.96m (−23%) |
| Whole-life cost of the system ($WLC$) [$] | | 21.72m | 17.07m (−21%) | 22.51m (+4%) | 26.17m (+20%) |
| CPU usage time [s] | | 82,920 | | 690,950 (+733%) | |

Table 4.6: Comparative deterministic and stochastic (under different uncertainty budgets) optimal MG equipment capacity solution sets.

| Component | | Simulation case | | | |
|---|---|---|---|---|---|
| | | Deterministic | Best case | Most likely case | Worst case |
| PV plant | $N_{PV}$ [no.] | 3,594 | 3,824 (+6%) | 3,801 (+6%) | 4,315 (+20%) |
| | STDEC* [%] | 9.3 | 10.4 (+1.1) | 8.7 (−0.6) | 7.9 (−1.4) |
| Wind plant | $N_{WT}$ [no.] | 4 | 5 (+25%) | 5 (+25%) | 8 (+100%) |
| | STDEC* [%] | 19.5 | 31.0 (+11.5) | 26.0 (+6.5) | 29.0 (+9.5) |
| Micro-hydro power plant | $N_{MH}$ [no.] | 6 | 7 (+17%) | 7 (+17%) | 8 (+33%) |
| | STDEC* [%] | 2.2 | 2.6 (+0.4) | 2.2 (0) | 2.0 (−0.2) |
| Biopower plant | $N_{BP}$ [no.] | 4 | 4 (0%) | 4 (0%) | 4 (0%) |
| | STDEC* [%] | 0.8 | 0.9 (+0.1) | 0.7 (−0.1) | 0.6 (−0.2) |
| Transformer | $N_T$ [kVA] | 310 | 415 (+34%) | 362 (+17%) | 391 (+26%) |
| | STDEC* [%] | 0.3 | 0.4 (+0.1) | 0.3 (0) | 0.2 (−0.1) |
| Hydrogen tank | $N_{HT}$ [kg] | 6,079 | 3,742 (−38%) | 6,179 (+2%) | 7,452 (+23%) |
| | STDEC* [%] | 16.7 | 8.0 (−8.7) | 15.4 (−1.3) | 15.0 (−1.7) |
| Electrolyser | $N_E$ [no.] | 122 | 75 (−39%) | 124 (+2%) | 149 (+22%) |
| | STDEC* [%] | 3.7 | 2.0 (−1.7) | 3.5 (−0.2) | 3.3 (−0.4) |
| Fuel cell | $N_{FC}$ [no.] | 238 | 148 (−38%) | 240 (+1%) | 288 (+21%) |
| | STDEC* [%] | 7.1 | 4.1 (−3.0) | 6.4 (−0.7) | 6.3 (−0.8) |
| Battery bank | $N_{1600}$ [no.] | 2 | 2 (−3%)† | 2 (+3%)† | 2 (+15%)† |
| | $N_{400}$ [no.] | 0 | 0 | 0 | 1 |
| | $N_{100}$ [no.] | 2 | 1 | 3 | 3 |
| | STDEC* [%] | 15.3 | 14.8 (−0.5) | 13.9 (−1.4) | 13.8 (−1.5) |
| Super-capacitor bank | $N_{SC}$ [no.] | 1,982 | 1,922 (−3%) | 1,998 (+1%) | 2,094 (+6%) |

| | | | | | |
|---|---|---|---|---|---|
| | STDEC* [%] | 13.8 | 14.5 (+0.7) | 12.5 (−1.3) | 12.0 (−1.8) |
| FCEV2G setup | $N_{FCEV2G}$ [kW] | 504 | 462 (−8%) | 489 (−3%) | 431 (−14%) |
| | STDEC* [%] | 2.1 | 2.1 (0) | 1.9 (−0.2) | 1.3 (−0.8) |
| Hydrogen station | $N_S$ [kg-$H_2$/h] | 6.14 | 6.14 (0%) | 6.14 (0%) | 6.14 (0%) |
| | STDEC* [%] | 0.5 | 0.6 (+0.1) | 0.5 (0) | 0.4 (−0.1) |
| Inverter | $N_{900}$ [no.] | 5 | 5 (−6%)† | 5 (+1%)† | 5 (+6%)† |
| | $N_{115}$ [no.] | 2 | 0 | 2 | 4 |
| | $N_{33}$ [no.] | 1 | 0 | 2 | 2 |
| | STDEC* [%] | 8.7 | 8.6 (−0.1) | 7.9 (−0.8) | 8.0 (−0.7) |

* STDEC stands for the share of the total discounted equipment-related costs, which can be expressed explicitly in mathematical terms as $((\sum_{c\in C} \underset{20-yr}{NPC_c}) + \underset{20-yr}{NPC_I})$. Also, given that STDEC is measured in percentage points, the associated deviations of the probabilistically optimised decision variables from the corresponding deterministic values are represented by absolute changes, rather than relative changes – to make clear comparisons.

† For the battery bank and multi-mode inverter, the percentage of stochastic results' deviation from the deterministic results refers to the associated optimal overall capacity, rather than the constituent elements alone.

The following key insights emerge collectively from Table 4.5 and Figs. 4.9 and 4.10:

1. The probabilistic model is able to effectively support decision-making in designing cost-optimal MGs under various parametric uncertainties in accordance with the investment planning budget of interest. More specifically, accounting for the forecast uncertainties, the most likely total NPC of the system indicates a relatively significant ~4% (equating to ~NZ$0.79m) uncertainty cost premium above the deterministic modelling results. That is, the life cycle cost of the MG would have been underestimated by as much as ~4% according to the most likely case scenario if the variability inherent in forecast inputs was not factored into the analysis. Also, at the lower (best-case) and upper (worst-case) extremes, the total NPC is found to be ~21% (equating to ~NZ$4.65m) lower and ~20% (equating to ~NZ$4.45m) higher than the deterministic case, respectively. That is, the mean of the population of resulting whole-life MG costs from the stochastic model instances is approximately equal to its median; thus, the corresponding density function is non-skewed. Accordingly, characterising the parametric uncertainties of interest may increase or decrease the system's total NPC depending on the decision-maker's risk attitude. Specifically, the estimated additional cost incurred by strongly risk-averse planning decisions is approximately equal to the expected savings of the corresponding risk-seeking scenario (with the same absolute value for the degree of conservatism desired by the decision-maker dealing with multi-variate forecast uncertainties, but with the opposite sign).

2. The overall computational cost (CPU usage time) of the probabilistic model is found to be 690,950 s, which is ~8.3 times higher than that of the deterministic model (82,920 s). Note that the overall CPU usage time associated with the stochastic simulations for the specific case analysed represents the time required to run the deterministic model for the seven sets of annual reduced scenario vectors. The best-case, most likely case, and worst-case analyses are then made based on the systematically augmented

outputs obtained for these seven sets of inputs. In view of the fact that the optimal MG sizing is an offline, one-time process, such large computational costs associated with the deterministic model are deemed acceptable within the context of computationally intensive meta-heuristic-based MG capacity planning optimisation – in that the year-long energy balance analysis needs to be solved for each of the hundreds of search agents in each of the hundreds of iterations. This is in line with the fact that a solution to the optimal MG sizing problem is intended to generate investment decisions over a multi-decade project lifetime and, thus, relatively long computing times are generally acceptable in this context. However, to keep the computational costs manageable, the computation of probabilistic model instances can be conveniently parallelised. The parallelisation process is deemed convenient as a single-processor calculation needs to be conducted for each of the seven annual sets of hourly reduced scenario vectors supplied to the deterministic model (the deterministic model is run seven independent times). That is, the computations have no data dependencies and need not be carried out in a particular sequence – therefore, the associated processes consisting of a number of completely independent calculations on separate CPUs in parallel are often called *embarrassingly parallel* [307]. This eliminates the need for using supercomputers to be able to solve the stochastic problem within a reasonable computational time. To this end, the parallelisation has been conducted over 7 CPUs of the same specifications (with specifications detailed in Section 2.6) in this study.

3. As expected, most of the CPU time for the simulation of the probabilistic model was in running the deterministic model for the seven independent annual sets of hourly input data, taking 577,410 seconds of computational time. The remainder of the CPU time (i.e., 113,540 s) was in generating hourly PDFs (12,240 s) and solving the hourly MILP scenario reduction problems (101,300 s). More specifically, a standard desktop computer was able to solve the hourly scenario reduction problem within a few seconds of computational time (due to the linearity of the heuristic scenario reduction model). Accordingly, the scenario clustering problem is solved for the 8,760

hours (time-steps) of MG operation in the representative year in 101,300 s. Also, the computational time associated with the deterministic model (82,920 s) – and similarly, each of the seven probabilistic sub-models (around 82,480 s on average, totalling 577,410 s) – incorporates the running time of the non-cooperative game-theoretic DR-integrated model. More specifically, the overall solution time returned for the deterministic case incorporates the whole DR-integrated updating process of the search agents, which entails running the system-level DR dispatch game and conducting the energy balance analysis for each time-step of the hourly-basis, year-long MG operation over the course of iterations (see Fig. 4.5). At each iteration for each search agent, the hourly 8,760-based energy dispatch decisions, which are adjusted for the unique, pure-strategy Nash equilibrium of the DSM game, are determined in approximately 4.7667 seconds of computational time, resulting in: 300 (iterations) × 50 (search agents) × 4.7667 s = 71,500 s. The remainder of the average 82,480 seconds of computation time for each of the probabilistic sub-problems (82,480 s – 71,500 s = 10,980 s, on average) can be attributed to the execution of the MFOA itself (and not the associated energy management function calls). Note that the MATLAB's Parallel Computing Toolbox is used to run element-wise (hourly) operations in parallel on the 6 cores of the CPU to speed up overall simulation runtime. Also note that this is distinct from the so-called '*embarrassingly parallel*' processes mentioned above.

4. A comparison of the total discounted equipment-related costs (which adequately reflect the total capital cost of the system)[13] and the whole-life costs of the system provides important insights into the disproportionate capital expenditure requirements associated with different risk mitigation strategies. To illustrate, the best-case, most likely-case, and worst-case scenarios respectively indicate percentage changes of approximately –5%,

[13] Among the components of the whole-life cost of the MG presented in Table 4.5, the total discounted equipment-related cost is the only component that incurs capital cost. Also, more than 95% of the total discounted equipment-related costs are occupied by capital costs (adjusted for salvage value), on average across all the four cases analysed.

+10%, +46% in the total discounted equipment-related cost compared to the deterministic case, while the corresponding percentage changes in the total life-cycle costs are approximately –21%, +4%, and +20%, respectively. That is, the strong risk-seeking strategy reduces the total NPC of the system to the same extent that the corresponding highly risk-averse attitude increases it (with a difference of around 1% in absolute value terms). However, it is associated with comparatively insubstantial reductions in capital expenditures (~5%). On the other hand, the highly robust decision-making preference induces increases of as much as ~46% in capital outlays. Similar to the worst-case scenario, a realistic designer faces more substantial increases in capital expenditure requirements (~10%) than the whole-life cost of the MG (4%). These observations can be explained by the relevant findings that the proportion of loads served by onsite infrastructure increases as the degree of conservative decision-making increases, whereas the optimistic approach leads to overbuilt capital-intensive generation infrastructure that is significantly attractive in terms of (negative) operational expenditures in that they ultimately (substantially) outbalance the limited reductions in the associated total initial costs. It is also interesting to note that the total NPC of the system in the worst-case scenario approximately equals its total capital investment cost. The overbuilding of the DER assets in the worst-case scenario – with respect to the average historical trends and synthetically regenerated patterns of uncertain input data, and not with respect to the needs of the specific uncertainty budget, as was the case for the best-case scenario mentioned above – which forms a major portion of the uncertainty cost premium, also increases the total net revenue from exchanging power with the utility grid mainly due to the combination of (i) increased frequency and magnitude of remunerative otherwise-curtailed over-generation exports, and (ii) reduced expensive grid imports over the course of the MG operation. Intriguingly, the total net revenue associated with grid traded power is also higher in the best-case scenario compared to the deterministic modelling results. This indicates that better-matched variable supply and demand in the best-case scenario

reduces the number of hours where it is not cost-effective to serve the (most likely reduced, and not the original) loads using (additional) onsite infrastructure – and hence, more frequent and intense surplus energy products are exported. Furthermore, it is important to note that the most likely scenario represents a capital cost increase of ~10% relative to the deterministic case, which indicates salient redesign and refinance requirements for deterministically optimised systems in the interest of highly reliable, resilient, and self-sufficient operations. Favourably, for the specific case study where none of the considered technologies were rejected, the redesign process (assuming that a deterministic approach was taken during the investment planning phase) would essentially involve capacity reinforcement for all the components except the less impactful (on the total NPC) FCEV2G technology, hydrogen station, and biopower plant. However, the possibility of more challenging and costlier redesign needs that would potentially involve uninstalling all or part of less profitable equipment (provided that the associated resale value including labour costs is higher than its contribution to the profitability of the refined plan) and/or adding previously deselected components (from the original technology candidate pool of interest) cannot be ruled out. It should also be noted that the total annual net energy purchased from the grid in the most likely case has yielded the smallest discrepancy relative to the deterministic case, despite the relatively high increase in the total discounted equipment-related costs, given the similar dynamics that are taking place with the system LCOE in the two cases. It, more specifically, represents relatively modestly reduced total annual net electricity exchange costs (2%) compared to the deterministic case, which can be mainly explained by the higher economic viability of storing energy internally for later use. The above analyses, collectively, bring to light the importance of capital expenditure versus operational expenditure considerations for funding MGs.

Furthermore, a direct comparison of the optimal configuration of the MG system yielded in fixed-controller deterministic and stochastic simulation cases (Table 4.6) provides important insights into the impact of the three statistically

representative uncertainty budgets on the dynamics of balancing electricity supply and demand on the internal network in terms of allocating various non-dispatchable renewables, exchanging power with the utility grid, harnessing the potential of DR resources including FCEV2G capacities, and the operation of energy storage assets (tailored to different timescales) with consequent implications for the comparative economics of self-sufficiency under various uncertainty budgets, as follows:

1. The much greater than historical average meteorological forecasts in the best-case scenario have improved the cost-efficiency of variable renewable technologies, thereby increasing their overall share in the total discounted equipment-related costs, despite reduced power loads and wholesale prices compared to the deterministic case. Among the non-dispatchable renewables, WTs have made up the largest share of the total capacity increase, not only due to the associated significantly larger step-size increments of the WT generation capacity, but also more importantly due to the higher rate of site-specific capacity factor to NPC per kW installed. Note that, as detailed in Table 4.5, in view of lower than average wholesale prices, the trade-offs between power imports and distributed sectoral DR elicitation have changed towards increased imports subject to the minimum allowed self-sufficiency ratio. This has reduced the total discounted MG operational costs (as defined by the sum of power import costs and financial incentives paid for load reduction) by a significant ~23% when compared directly to the base-case, deterministic scenario, and by as much as ~14% when the comparison is made in a normalised load setting – or put differently, when correcting for the total variance in the two power load datasets. Furthermore, the comparative optimal combinations of the components indicate reductions in the size of all the energy storage assets in the best-case scenario, and most notably the hydrogen-based energy storage components. This can be attributed to the assumed highly greater than the average potential of variable renewables at the site in this scenario, which makes the overbuilding of them and exporting the excess power during the light-load season a cost-optimal choice (note the more than doubled income from power exports, as shown in Table 4.5), as seasonal storage using locally

produced green, electrolytic hydrogen is found to be not as financially viable as that of the deterministic case. Nevertheless, it is not cost-optimal (in terms of the least-cost resource mix) to address the seasonality of load demand solely by overbuilt renewables. That is, unlike all other cases, in the case where the site under consideration is assumed to be very richly endowed with highly complementary renewable resources (best-case scenario), overbuilding of the renewable capacity forms part of the seasonally-matched optimal integrated resources plan. In other words, the overbuilt capacity is expected to meet a proportion of the winter demand that is met by other seasonally-matched resources – particularly, hydrogen storage – in the other cases considered. Therefore, the need for seasonal storage is reduced, but not totally eliminated as a result of the dynamics that are taking place within the system with respect to the viability of grid power exchanges (both imports and exports), DR capacity procurements, as well as short-duration energy storage installations (the SC and battery banks). More specifically, in the strongly risk-seeking scenario, adding seasonal energy storage capacity is viable if it simultaneously provides short-term energy management benefits – or put differently, to the extent to which the associated renewable and short-duration energy storage infrastructure investment decisions can contribute to reduced imports (in terms of both frequency and intensity) during the periods of highest wholesale prices in the summertime, as well as the avoided dispatch of high-marginal-cost DR resources. The overbuilt renewable capacity also implies substantial export of surplus power during the summer. Consequently, the optimal size of the transformer has increased by ~34%, which implies that it is controlled by exports, rather than imports – mainly as a result of the minimum self-sufficiency ratio constraint imposed. Also, it has been found that the system uses grid imports to the maximum allowable percentage that adheres to the minimum self-sufficiency ratio constraint, despite the presence of overbuilt renewable capacity. This is mainly as a result of significantly low wholesale prices at some time-steps, which are (potentially significantly) lower than the LCOE of the MG and/or the corresponding time-step-specific marginal cost of system-level DR procurement. Moreover, further analyses revealed

that in all the cases, the total curtailed excess power equals zero. This can be explained by a combination of relatively low transformer costs and comparatively high feed-in-tariff, which guarantees adequate compensation and drives the optimal design towards a solution with comparatively overbuilt renewable capacity. Another potential contributing factor to this decision is the assumption that, at all time-steps of the MG operation, the export complies with local export limitation codes in place. Also, the availability of the MG components (defined as $1 - probability\ of\ failure$) is assumed to be 100%. Therefore, no such layers of curtailment occur as well.

2. In the other extreme case, namely the worst-case scenario, the lower than average variable renewable generation power output forecasts, as well as higher than average wholesale prices and power loads, collectively, result in a substantial increase in the total non-dispatchable renewable capacity optimised, whilst additionally considerably increasing the overall energy storage required compared to the deterministic case. Similar to the best-case scenario, the WT generation has undergone the most dramatic change in terms of the optimum capacity. Also, the same rank order observed for the profitability of non-dispatchable renewable generation technologies under consideration confirms the validity of the findings on the site-specific optimal portfolio of generation assets. However, in contrast to the best-case scenario, the hydrogen-based energy storage system components have experienced the highest relative increase in capacity. The primary factors behind such model behaviour are the relatively large discrepancies between the marginal costs of renewable technologies in the best-case and worst-case scenarios. More specifically, decreases in non-dispatchable generation, as well as demand increases, which result in less well-matched variable supply and demand, along with increases in wholesale prices that make imports of more than 9% of total power loads a non-cost-effective solution (therefore, actual self-sufficiency ratio = 91%, despite the minimum allowed constraint of 80%), collectively improve the comparative economics of seasonal energy storage. Also, the increase in the optimum size of both onsite

renewable generation and energy storage technologies reduces the need for DR resources. Accordingly, the total discounted MG operational cost is decreased by as much as ~72%, as can be seen from Table 4.5. Furthermore, the increased size of the transformer relative to the deterministic case (albeit modestly) corroborates the above-mentioned finding that the size of the transformer is controlled by the otherwise-curtailed excess power exports. It is also interesting to note that in both the extreme cases, the total discounted operational MG cost is reduced, though to different extents. Recall that, according to the main objective function in Equation 3.41, the trade-space of MG investment planning and sizing decisions is five-dimensional incorporating the following dimensions that need to be traded off against each other: (1) non-dispatchable renewable capacity, (2) dispatchable renewable capacity, (3) operational costs (including incentivised DR solutions and power imports), (4) power exports, and (5) FCEV2G interventions. In this light, due to the exogeneity of the biopower plant capacity optimisation (as the dispatchable generation technology), whose schedule is treated as an exterior parametric input to the system, as well as the relatively insubstantial impact of the FCEV2G operations on the total discounted system costs, system-wide trade-offs occur most prominently among the other three sets of decision variables. Also note that, as illustrated above, the potential changes in the optimised variables of the dimensions with more than one degree of freedom are neither necessarily proportional to each other, nor necessarily deviate in the same direction due to the strong nonlinearities and non-convexities present in the problem formulation, as well as the disparate step-size increments of the selected components.

3. A comparison of the stochastic model response in the most likely case and worst-case scenarios reveals that rightward deviations from the deterministically derived optimal cost solution (see Figs. 4.9 and 4.10) follow practically the same trend in terms of the optimal integrated resource planning decision, namely increased share of onsite non-dispatchable generation and energy storage infrastructure to decrease reliance on

relatively more expensive power imports, which has direct implications for DR resourcing costs as well as FCEV2G provisions. More specifically, as the degree of conservatism increases, the cost-efficiency of importing electricity and leveraging the potential of site-wide incentive-responsive loads decreases, whilst additionally reducing the (normalised) total exported power – as more local renewable supplies are dispatched to serve the increased load demand and/or stored for later use. On the other hand, as the decision-maker's level of optimism with respect to the system-wide uncertainties increases, the cost-efficiency of importing power increases (which reaches the maximum allowed total power imports in the $28^{th}$ percentile of the normal distribution for the total discounted system cost data obtained for different annual scenario vector sets), the allocated energy storage infrastructure and DR resources decrease, and the opportunity for remunerative power exports increases. However, the effect of different levels of the same overall risk management strategy (risk-seeking or risk-averse) with respect to the uncertainty of input data on the optimal investment planning and sizing decisions is highly nonlinear, but monotonic. Yet, a high degree of multicollinearity exists between the optimal capacity of the electrolyser, hydrogen tank, and fuel cell units obtained for different cases (under a statistically representative range of acceptable levels of risk), which further verifies the effectiveness and robustness of the rule-based operational planning strategy developed. Also, the absolute values of rightward and leftward deviations from the baseline deterministic realisation on the (cumulative) normal distribution function of stochastic total discounted system cost histograms are approximately equal for the same degrees of risk-seeking and risk-aversion. This indicates that the stochastic life-cycle cost realisations are approximately proportional to the level of risk accepted, which is evaluated as a budget on the allowable probability of not meeting design variables. Moreover, the actual self-sufficiency ratio of the system in the most likely scenario is found to be 80%, which equals its minimum allowed value. A comparison of the actual self-sufficiency ratio obtained for the most likely and best-case scenarios indicates that the maximum turning point for the self-sufficiency ratio

occurs in between them. Further analyses identified the location of the maximum turning point to be the deterministic case, the solution set of which represents a self-sufficiency ratio of 89%. Given the identified monotonicity of the model behaviour with respect to the degree of uncertainty reduction under the same overall risk preference (robust or opportunistic), a comparison of the total discounted incentive payment to the aggregators for the scenarios considered implies that DR is modestly overvalued in the deterministic case. Notably, the most likely case indicates a reduction of ~22% in the dispatch of DR resources over the analysis period. Accordingly, the most likely stochastic results provide a more accurate and robust quantitative valuation of DR capacity for the MG operator. This also implies potentially significant consequences for the distribution of expected payoffs to different classes of participating customers and the corresponding aggregators in the long run (in terms of seasonal patterns and the overall benefit allocation among sector-wide sets of players), which in turn, has potential distributional effects on the share of each sector in the total DR capacity delivered.

4. None of the components in any of the scenarios have reached the corresponding pre-defined maximum allowable capacities (see Table 3.3). This observation indicates that the higher net revenues from power exchanges with the utility grid are not able to completely offset the costs of additional infrastructure capacity required if allocated exclusively for exporting back to the grid (in pursuit of improved overall financial viability) even in the best-case scenario; or, put simply, it is by no means cost-optimal to add capacity solely for grid exports at the existing market conditions. Also, the optimal size of the multi-mode (loads') inverter is found to be inversely correlated with the level of risk tolerance; the riskier the integrated resource plan, the lower the overall size of the hybrid inverter – in proportion with the corresponding expected decrease in the peak load demand. Furthermore, the load demand of the hydrogen station is assumed not to be subject to long-term variability; that is, the uncertainty in hydrogen load forecasts is not modelled explicitly. This explains the unaltered optimal

size of the station in different scenarios. Also, the same optimal values obtained for the size of the biopower plant in all the simulation cases can be principally explained by the fact that biopower generation is treated as negative load – whose capacity is limited by the maximum allowable emissions – as well as the fact that the long-term availability of biomass feedstock is assumed to be secure in terms of all the associated elements including supplier agreements, realistic transport distances, and acceptable costs of collection, transport, and storage. It is also noteworthy that in all the analyses above, unless explicitly stated otherwise, the comparisons refer to unnormalised load profiles. For reasons of space, the reader is referred to Table 4.6 for insights into the normalised dynamics of MG configurations tailored to different uncertainty budgets – or, more specifically, changes in the share of each component in the total discounted equipment-related costs.

5. In all the scenarios studied, the model has well-diversified the electricity generation mix essential to energy security. The key underlying reason for such diversity is the potentially significant temporal complementary characteristics of the non-dispatchable RESs at the case study site. Specifically, power outputs from solar PV and WTs complement each other on a daily basis, while streamflow has a complementary seasonal cycle with both solar irradiance and wind speed. These observations also lend further support to the utility and effectiveness of the proposed model in both stochastic and deterministic variants in determining the optimal mix of variable generation technologies that effectively leverage the associated temporal complementarities – and smooth out the variability in aggregate non-dispatchable renewable generation in both short and long timescales, whilst minimising the cost-intensive supply-demand matching resource requirements. Moreover, of the component size variables that are endogenous to the model, none have reached a saturation point (past which added capacity becomes economically unattractive) in any of the probabilistic cases considered. For non-dispatchable renewables, this substantiates the potentially significant impact of the associated temporal complementarities on the economic viability of the system, whereas for the

three-timescale hybrid energy storage system, this reaffirms the validity of the first-order passive low-pass energy filters used as part of the developed energy storage power allocation strategy. In addition, the ratio of the share of the total discounted energy storage-related costs to the total discounted non-dispatchable renewable generation-related costs in the associated overall discounted equipment-related cost components is ~0.99, ~1.83, ~1.40, and ~1.30 in the best-case, deterministic case, most likely case, and worst-case scenarios, respectively. This observation suggests that the risk-seeking and risk-averse MG planning strategies both have a contradictory effect on the above-mentioned two cost sub-components. That is, at the current costs, efficiencies, as well as self-discharge and degradation rates (where applicable) of the storage and non-dispatchable renewable technologies considered, the contribution of storage capacity to managing the total system-wide forecast uncertainty associated with inputs decreases, relative to the variable renewables, as the degree of uncertainty reduction increases under each of the categories of risk preference – though it is more sensitive to the risk-seeking strategy than risk-averse attitude – while optimally allocating DERs.

### 4.3.4. Impact of the nested optimal dispatch strategy

This section quantifies the effectiveness of the optimal scheduling of the MG system using the proposed linear programming formulation – which looks ahead over a series of sequential 24-hour (foresight) horizons with time discretisation in 1-hour increments within the time horizons and the selected step-size between the sequential decision horizons of the length of the time horizon (zero overlaps) – in improving the DR-integrated, stochastic long-term MG investment planning results. However, for reasons of brevity and practical importance, only the most likely scenario has been discussed. Furthermore, the interested reader is referred to the journal paper this chapter is (partly) drawn on for the key insights generated from the application of the proposed design and dispatch co-planning model to the conceptual MG 3 to maintain the overall narrative structure of the chapter, which particularly addresses the notional MG 4. The paper, additionally, provides a

comprehensive comparative evaluation of the performance of the proposed MG designing and dispatch co-planning model and that of the industry-leading pre-feasibility design software for modelling MGs, namely HOMER Pro, using MG 3 as a test case. The comparatively less complex configuration of MG 3 offers the opportunity to analyse the impact of scheduling optimisation on the hourly-basis, daily dynamics of energy balance in greater detail.

A comparison of the most likely stochastic results of the DR-integrated planning case obtained for MG 4 with and without intelligent, look-ahead provisions, presented in Tables 4.7 and 4.8, offers the following key statistically significant and valid insights:

1. The co-optimisation of the day-ahead energy scheduling (over a moving 24-hour horizon for the representative year) and long-term investment planning of the MG reduces the total discounted system cost in the most likely probabilistic case by a significant ~19% (equating to ~NZ$4.3m) compared to the counterpart case that uses a business-as-usual rule-based, Greedy approach to decide the (non-optimal) operation of the system with fixed controllers. The savings stem mainly from the added strategic foresight (the increased MG-level predictability) to look beyond a one-hour energy balance analysis. That is, optimising the storage schedules over a moving 24-hour foresight horizon (at an hourly resolution), over which there is perfect foresight of the community's load demand, non-dispatchable generation, and wholesale prices, has a considerable impact on reducing the total discounted cost of resource procurement – by making the decision-making process more dynamic and appropriate. More specifically, the main reason for the substantially reduced MG whole-life cost is the exploited potential of storing the cheaper daily energy imports or excess variable generation during the off-peak hours in an intelligent, predictive manner for later local use or export back to the grid during the coincident peak hours of the same day – which refer to two distinct realisations of arbitrage, namely 'import low-price, store, export high-price', and 'store the excess, export high-price', as well as two intelligent energy shifting strategies, namely 'buy

low-price, store, use later', and 'store the excess, use later'. Further unreported observations revealed that the above four strategies contribute approximately equally to the effectiveness of the nested look-ahead economic dispatch strategy.

2. Integrating the year-long day-ahead linear programming-based energy scheduling model into the probabilistic, DR-integrated, meta-heuristic-based optimal MG sizing problem increases the CPU usage time by ~143% compared to the counterpart most likely stochastic case with a rule-based dispatch strategy given that the linear programming model needs to run successively for every day in the baseline year under each of the reduced multi-dimensional scenarios for each moth (search agent) in each iteration. More specifically, given the linearity of the optimal energy dispatch model, the standard desktop computer specified above was able to solve the series of sequential daily (24-h) energy dispatch problems (which were parallelised using the MATLAB's Parallel Computing Toolbox) over the representative year in 9.4316 seconds of computational time (on average), yielding an overall year-long, daily-basis scheduling optimisation running time (operational analysis solution time) of ~471 s for the total of moths (search agents) at each of the 300 iterations of each of the 7 stochastic sub-models. That is, 9.4316 (seconds) × 50 (moths) × 300 (iterations) × 7 (annual sets of multi-dimensional hourly scenarios) = ~990,320 s.

3. Except for the size of the battery bank, no statistically significant changes were observed in the size of equipment for the cases with and without a forward-looking dispatch strategy. More specifically, the maximum percentage change in the size of the components other than battery bank was found to be as low as −1.7% (for fuel cells), which is negligible from a practical perspective – even considering the general decreasing size trend for those components and the aggregate savings. However, the relatively significant 11.4% increase in the overall size of the battery bank is attributable to the allocation of an additional 400 kWh battery pack, which is found to be able to contribute to the profitability of the system planned by

the design and dispatch co-optimisation model through leveraging value-enhancing arbitrage services along with foresighted energy management operational decisions. On a wider level, the relatively insubstantial changes in the total discounted equipment-related costs, incentive payments to the aggregators, FCEV2G provisioning costs, as well as the costs associated with the operation of the biopower plant, indicate that the incorporation of optimal dynamic dispatch decisions does not statistically significantly affect the overall MG development plan in terms of portfolio-wide infrastructure allocation versus sectoral aggregator-mediated incentive-response customer DR utilisation balance; nor does it markedly alter the capital outlay estimates. However, it exhibits a major influence on the MG business model in that the total discounted grid import costs and export revenues are respectively increased by ~839% (equating to ~NZ$3.19m) and ~304% (equating to ~NZ$7.79m), which result in a total energy arbitrage trade profit of ~NZ$4.60m when compared to the base-case stochastic simulation that employs a non-arbitrage-aware dispatch strategy. The reason for the practically unchanged MG configuration and unit sizes is, in large part, the identified inadequacy of (1) daily energy arbitrage of any kind alone to provide sufficient revenues to make new energy storage installations (only for arbitrage purposes) economically viable, and/or (2) adding generation infrastructure solely for profitable grid exports. That is, nesting the look-ahead economic dispatch strategy that optimises the dispatch of the components within the main sizing problem generates additional revenue and benefit streams that are practically achievable (but are missed) by the components sized under a rule-based, Greedy dispatch strategy. In other words, design and dispatch co-optimisation delivers the best possible balance of resilience, self-sufficiency, reliability, and total discounted cost.

4. As noted above, a direct comparison of the net grid purchase costs in the two simulation cases of interest indicates a total energy arbitrage trade profit of ~NZ$4.60m. Subtracting the discounted cost of added battery capacity from the total energy arbitrage trade profit, as well as accounting for the reduced total costs of some of the other components and DR incentive

payments, yields a total *net* energy arbitrage trade profit of ~$4.30m. A major contributing factor to the economic profitability of arbitrage opportunities for battery storage is the unaltered size of the bi-directional transformer and multi-mode inverter in the case with an intelligent operational strategy compared to the baseline case. Notably, it was observed that the arbitrage trades occur smoothly over the representative year, implying that sharp charging (during the periods in which spot prices were extremely low) and discharging (during the price spike periods) for energy arbitrage with the grid were generally avoided. Further unreported observations have revealed that grid arbitrage is unprofitable (in expectation) for the trades that incur added inverter and/or transformer capital costs, while added battery storage capacity for daily arbitrage cycling is economically viable if it derives synergy effects for a cost-optimal serving of local loads – or, put simply, if it simultaneously contributes to lower levelised costs of *onsite* energy.

5. A comparison of the obtained MG whole-life cost for the most likely design and dispatch co-optimisation case ($18.21m) with those of the most likely fixed-controller optimisation case ($22.51m), best-case fixed-controller optimisation case ($17.07m), and deterministic fixed-controller optimisation case ($21.72m) indicates that not only is optimising the dispatch simultaneously to the design able to compensate for the costs associated with providing a hedge against the most likely realisations of system-wide parametric uncertainties, it can even yield a total NPC that is highly competitive with the best-case fixed-controller scenario – at the comparatively negligible costs of a real-time controller to be used for forward-looking predictions.

6. The arbitrage with the grid over longer than diurnal timescales, such as long-duration arbitrage (discharge duration >10 hours and <100 hours) and seasonal arbitrage (discharge duration >100 hours) [308] is not explicitly modelled – that is, it is not considered as an optimisation criterion. However, given that the solution approach is based on meta-heuristics, it is inherently

assumed in the outer optimal designing model that there is freedom in choosing values for the sizes of the components that are greater than those are optimal for meeting the local loads exclusively, provided that they result in lower whole-life costs; for example, by cycling the hydrogen-based energy storage system to arbitrage on price differences in the spot electricity market. Yet, despite this degree of freedom, no arbitrage trades were observed over the long-term and seasonal cycles. The reason lies, in large part, in the fact that hydrogen-based energy storage technologies are relatively costly and it is not profitable to allocate any hydrogen storage capacity (in accordance with the three-timescale energy filter developed) for such longer-term arbitrage opportunities. Note that, given that the energy balance analyses are conducted at an hourly temporal resolution, the possible benefits from arbitrage cannot be theoretically captured using the storage media that are associated with hourly and sub-hourly timescales (the battery and SC banks, in this study) without explicitly nesting a specifically developed optimisation model into the upper-level sizing model, which explains the rationale behind the proposed double-layer design and dispatch co-planning model.

Table 4.7: Breakdown of the total discounted system cost under stochastic (most likely), DR-integrated MG equipment capacity planning simulation cases with forward-looking and rule-based dispatch strategies.

| Cost component | Cost subcomponent | Stochastic (most likely), DR-integrated simulation case | |
|---|---|---|---|
| | | With rule-based dispatch | With forward-looking dispatch |
| Total discounted equipment-related costs $((\sum_{c\in C} \underset{20-yr}{NPC_c}) + \underset{20-yr}{NPC_I})$ [$] | | 20.16m | 20.59m (+2%) |
| Total discounted MG operational costs $(\underset{20-yr}{NPV}(\sum_{t=1}^{8760} OC_{MG}(t)))$ | Total discounted incentive payment to the aggregators $(\underset{20-yr}{NPV}(\sum_{t=1}^{8760} I_{MGO}(t) \sum_{j\in J} D_{LA}^{j}(t)))$ [$] | 3.13m | 3.03m (−3%) |
| | Total discounted cost of electricity imports $(\underset{20-yr}{NPV}(\sum_{t=1}^{8760} cost_{im}(t)))$ [$] | 0.38m | 3.57m (+839%) |
| Total discounted FCEV2G provision costs $(\underset{20-yr}{NPV}(\sum_{t=1}^{8760} \pi_{FCEV2G} P_{FCEV2G}(t)))$ [$] | | 0.39m | 0.36m (−8%) |
| Total discounted operating costs of the biopower plant | Total discounted emission credits $(\underset{20-yr}{NPV}(\sum_{t=1}^{8760} cost_{em}(t)))$ [$] | 0.52m | 0.52m (0%) |
| | Total discounted biomass feedstock costs $(\underset{20-yr}{NPV}(0.098\ [\$/kg] \times \sum_{t=1}^{8760} M_{BP}(t)\ [kg]))$ [$] | 0.49m | 0.49m (0%) |
| Total discounted income derived from exports $(-\underset{20-yr}{NPV}(\sum_{t=1}^{8760} income_{ex}(t)))$ [$] | | −2.56m | −10.35m (−304%) |
| Whole-life cost of the system ($WLC$) [$] | | 22.51m | 18.21m (−19%) |
| CPU usage time [s] | | 690,950 | 1,681,270 (+143%) |

Table 4.8: Comparative optimal MG equipment capacity solution sets under stochastic (most likely), DR-integrated MG equipment capacity planning simulation cases with forward-looking and rule-based dispatch strategies.

| Component | | Stochastic (most likely), DR-integrated simulation case | |
|---|---|---|---|
| | | With rule-based dispatch | With forward-looking dispatch |
| PV plant | $N_{PV}$ [no.] | 3,801 | 3,784 (−0.5%) |
| | STDEC [%] | 8.7 | 8.4 (−0.3) |
| Wind plant | $N_{WT}$ [no.] | 5 | 5 (0%) |
| | STDEC [%] | 26.0 | 25.5 (−0.5) |
| Micro-hydro power plant | $N_{MH}$ [no.] | 7 | 7 (0%) |
| | STDEC [%] | 2.2 | 2.1 (−0.1) |
| Biopower plant | $N_{BP}$ [no.] | 4 | 4 (0%) |
| | STDEC [%] | 0.7 | 0.7 (0) |
| Transformer | $N_T$ [kVA] | 362 | 362 (0%) |
| | STDEC [%] | 0.3 | 0.3 (0) |
| Hydrogen tank | $N_{HT}$ [kg] | 6,179 | 6,158 (−0.3%) |
| | STDEC [%] | 15.4 | 15.0 (−0.4) |
| Electrolyser | $N_E$ [no.] | 124 | 122 (−1.6%) |
| | STDEC [%] | 3.5 | 3.4 (−0.1) |
| Fuel cell | $N_{FC}$ [no.] | 240 | 236 (−1.7%) |
| | STDEC [%] | 6.4 | 6.3 (−0.1) |
| Battery bank | $N_{1600}$ [no.] | 2 | 2 (+11.4%) |
| | $N_{400}$ [no.] | 0 | 1 |
| | $N_{100}$ [no.] | 3 | 3 |
| | STDEC [%] | 13.9 | 16.0 (+2.1) |
| Super-capacitor bank | $N_{SC}$ [no.] | 1,998 | 1,992 (−0.3%) |
| | STDEC [%] | 12.5 | 12.2 (−0.3) |
| FCEV2G setup | $N_{FCEV2G}$ [kW] | 489 | 482 (−1.4%) |
| | STDEC [%] | 1.9 | 1.9 (0) |
| Hydrogen station | $N_S$ [kg-$H_2$/h] | 6.14 | 6.14 (0%) |
| | STDEC [%] | 0.5 | 0.5 (0) |
| Inverter | $N_{900}$ [no.] | 5 | 5 (0%) |
| | $N_{115}$ [no.] | 2 | 2 |
| | $N_{33}$ [no.] | 2 | 2 |
| | STDEC [%] | 7.9 | 7.7 (−0.2) |

Furthermore, Fig. 4.11 shows the monthly mean daily profiles for the state-of-charge (SOC) of the battery bank, the optimal size of which has undergone the most drastic change among the storage media considered, as well as all the decision variables (including MG components) more generally. As the figure implies, the linear programming-based intelligent scheduling framework has effectively charged the battery bank using excess power and/or power imports during lower-priced off-peak hours to minimise the daily operational costs – and more cost-efficiently meet the net load demand – by discharging the battery bank to local demand and/or back to the grid during peak times when wholesale prices are higher. More specifically, Fig. 4.11 reveals the following key insights:

1. The optimal size of the battery bank is primarily driven by the daily energy storage requirements during the wintertime (June through August), where not only is the total renewable energy generation output reduced, but also the overall interruptible share of power loads is proportionally lower than that of summer months (December through February) given the disproportional increase in low-temperature domestic heating loads (recall the lower DR supply elasticity of residential loads relative to other load segments), suggesting a negative synergy. Also note that given the minimum self-sufficiency and resilience constraints imposed, lower wholesale prices during the wintertime cannot be extremely leveraged in the interest of a well-distributed operational cost (as defined by the sum of grid import costs and incentive payments for load reduction) throughout the year necessary for optimally balanced capital investment and expected operational costs – such that the marginal benefit of investing in additional capital is balanced to reduce operational costs. The observation of the (relatively) consistently high values of the battery SOC throughout the summer months provides further credence to support the above argument that the size of the battery bank is particularly optimised for short-duration storage capacity needs associated with optimal intra-day energy shifting during the wintertime, as particularly necessitated during prolonged periods (several days) of low solar radiation and low temperature – and thus, low solar PV generation and high domestic heating loads of comparatively low

DR capacity supply elasticity. It should be emphasised that this is not contrasted to the functional roles of the hydrogen-based energy storage system as the battery bank is the only storage device employed to provide energy arbitrage services on a daily timescale. This gives rise to the novel insight that, for grid-connected MGs subject to highly seasonal loads, the additional revenues generated by added battery storage capacity from daily arbitrage during the high season – in addition to the benefit of catering for some portion of loads during the coincident peak periods of the high season, which improves the profitability of capital-intensive seasonal storage investments – is able to yield surpassed capital cost recovery even if underutilised during the light-load months – up to the point where the marginal benefit of added battery capacity is equal to its marginal capital cost. Further evidence supporting the validity of this key insight is the observation that the energy content of the battery bank experiences a minimum state in the evening peak of July for the integrated design and dispatch optimisation case, as shown in Fig. 4.11. Moreover, the fairly similar general patterns of the monthly mean daily battery SOC profiles in terms of the monthly average SOC levels throughout the year for the cases with and without an intelligent operational strategy indicate that the possibility of reducing the size of the capital-intensive hydrogen-based energy storage system (that meets seasonal demand peaks) is alone able to provide sufficient benefit in allocating added battery capacity that is primarily used during the high winter months – albeit to a significantly less dramatic extent in the case with rule-based dispatch compared to the case with predictive control (non-fixed). Note that, although the developed three-timescale energy filter apportions the total hourly load into three distinct components commensurate with the operational timescales of the considered storage technologies, the *non-deterministic* nature of meta-heuristics (that effectively explore the search space) does, though paradoxically, aid in determining the best-compromise solution for the hybrid storage capacity. On the other hand, the differences in the daily patterns of the associated profiles over each month for the cases with model-predictive and rule-based dispatch strategies is attributable to the exploited

potential of storing the cheaper daily energy imports or excess variable generation during the off-peak hours for later local use or export to the grid during the coincident peak hours of the same day explained above. Also, collectively, the above observations imply that fuel cell generations are mainly used to meet part of the seasonal *base-load* customer requirements in winter.

2. In both cases, the minimum daily battery SOC occurs most frequently during the evening peak hours when the MG's net load peak coincides with the more expensive utility grid peak. During these time-steps, the base-case's single-time-period dispatch strategy that cannot plan for future system states and follows fixed rules essentially always decides to discharge the battery bank subject to the maximum allowable power and energy capacities before importing. However, the behaviour of the intelligent model, which is able to strategically plan ahead the battery storage over multiple time-steps is more complex and multi-faceted. To illustrate, the relatively sharper SOC decreases in the economic dispatch-based case during some of the coincident peak periods indicate that the battery is discharged simultaneously to local demand and utility grid to maximise the actual battery profit. As another indication, the optimisation-based model's decision to charge the battery bank using imports during some of the time-steps when there is an onsite shortage, as directed by the decreases in the SOC in the base-case Greedy dispatch scenario, indicates that the forward-looking model is well aware of the future time-steps that necessitate costly imports or offer highly remunerative exports. Furthermore, the constant battery SOC during some of the time-steps in the intelligent model, despite increases or decreases in the battery SOC profiled by the fixed model, suggests that, given the improved foresight of future spot market prices – and future system conditions, more generally – which aids the efficient reserve utilisation, it is most profitable to sell the surplus generation or import the capacity shortfall at those time-steps. Some of the differences between the battery SOC profiles derived by the two models can also be explained by the fact that the look-ahead dispatch model has identified that

battery charging during the upcoming off-peak, lower-priced hours is more economically viable. These observations indicate that the optimal dispatch strategy can well plan for both the excess and shortage of variable renewable energy, whereas the rule-based operating strategy is not able to (optimally) plan ahead for these occurrences by, for example, efficiently scheduling the charging periods to the periods when prices are lowest.

3. The intelligent scheduling design strategy has effectively reduced the peak-to-average ratio of the monthly energy in-store profiles, which drives unused battery capacity reductions (reduced underutilisation) – and not the optimum battery size, which is increased relative to the base-case stochastic model with fixed operational strategy, in pursuit of maximising the opportunities from energy arbitrage. This is achieved in light of the optimisation-based energy management framework's strategic foresight of the daily load demand, local generation, and wholesale prices at an hourly resolution – in contrary to the single-time-step decisions made by the rule-based Greedy energy management approach employed in the base-case most likely stochastic simulations. Consequently, the average charge/discharge schedules of the battery bank are considerably different in the two cases. For instance, the rate of the battery charging during the light-load hours of 0:00 a.m. to 4:00 a.m. in the monthly mean daily battery SOC profile in July is higher for the optimisation-based dispatch case, with the difference coming from the utility grid to more cost-effectively meet the net loads in the remaining hours of the day by discharging the battery to local demand (specifically, during the more expensive peak hours), as well as to generate revenues from increased highly profitable peak exports. Then, during the $5^{th}$ and $6^{th}$ hours, despite the shortage of local generation, the intelligent dispatch strategy continues charging the battery bank because of the relatively lower wholesale price values present – unlike the Greedy algorithm that discharges the battery due to the positive net load available. On the other hand, despite the existence of excess power, which results in battery charging as decided by the Greedy algorithm, the intelligent scheduling framework discharges the battery bank for export during the $9^{th}$

and $10^{th}$ hours. The underlying reason for this observation is that, from a daily operational cost perspective, it is cost-optimal for the MG to export the energy stored during the off-peak hours (in terms of either or both internal loads and wholesale prices) at these time-steps, in addition to the existing over-generation of non-dispatchable renewables. However, note that given the inability of the storage to be charged and discharged simultaneously, it is not possible for the optimisation-based operational strategy to allocate some proportion of the excess power to the internal storage. Accordingly, selecting the excess export strategy over battery charging by the forward-looking dispatch framework during the above-mentioned time-steps can also be explained, in part, by the identified sub-optimal (needless or unprofitable) battery cycling that allocating the entire surplus generation for charging would induce in the remaining time-steps of the day.

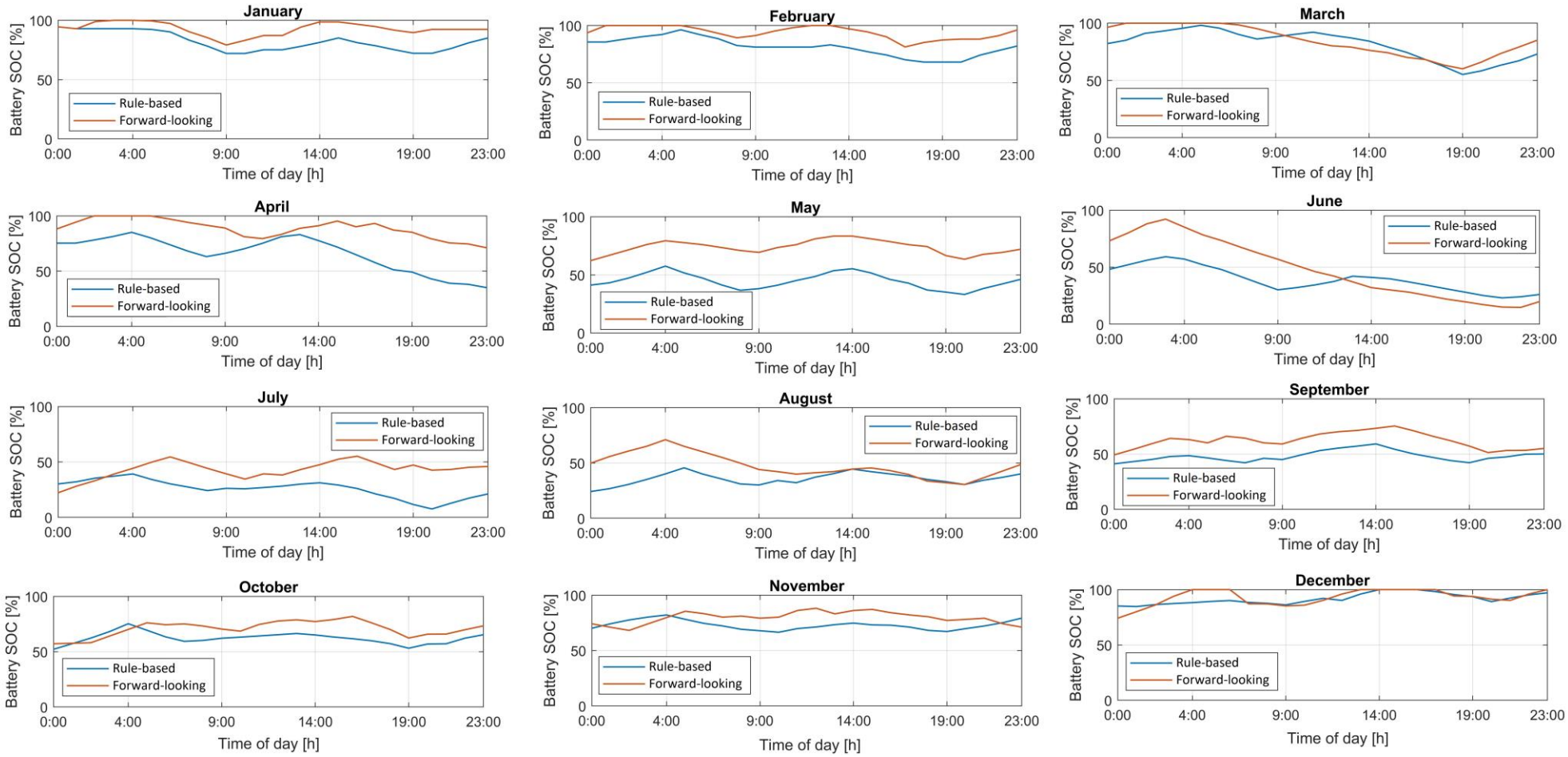


Figure 4.11: Monthly mean daily profiles for the energy content of the battery bank in the most likely stochastic cases with and without a nested scheduling optimisation framework.

### 4.3.5. Sensitivity analyses

Two separate sets of sensitivity analyses are provided in this section to systematically investigate the complex interactions of the model, whilst additionally measuring the robustness of the overall probabilistic MG sizing model in generating optimal MG designs under various expectations of system inputs and future MG operating states. Specifically, the first set of one-way sensitivity analyses evaluates the economics of self-sufficiency under the possible range of minimum allowed self-sufficiency ratio, while the second set of two-way sensitivity analyses measures the economics of daily arbitrage by simultaneously varying the values of feed-in-tariff and expected capital costs of the battery energy storage system. The two-way sensitivity analyses are necessary for the latter case, in which there is a correlation between the associated key input variables – feed-in-tariff and battery capital cost – in terms of contribution to changes in model outputs. That is, varying the associated key input variables independently in univariate sensitivity analyses would potentially offer a misleading view.

#### 4.3.5.1. Economics of self-sufficiency

A sensitivity analysis is provided in this section to understand the robustness of the whole-life cost of the system in the most likely probabilistic scenario to changes in the minimum allowed self-sufficiency ratio, which is treated as a bounded constraint. To this end, the optimisation process was repeated for multiple values of the minimum self-sufficiency ratio ranging from 0% to 100% in intervals of 10%, totalling 11 stochastic optimisation cases. Note that all the model instances are simulated probabilistically, meaning that the relevant 7 sub-problems are first solved independently and then compiled to create uncertainty-aware results. Also, as mentioned above, for reasons of space and tractability, only the most likely case has been discussed. It is not implausible, however, that the dynamics of the model differ significantly between the best-case, most likely case, and worst-case scenarios.

Fig. 4.12 depicts the sensitivity of the total discounted system cost and the optimal system self-sufficiency (the actual self-sufficiency ratio associated with the

optimal solution set) with respect to changes in the value of the imposed minimum allowed self-sufficiency ratio constraint. The following key observations can be made from the figure:

1. Imposing different values for the minimum allowed self-sufficiency ratio does not significantly alter the MG whole-life cost results. The percentage error between the MG net present worth solutions under 0% and 100% minimum allowed self-sufficiency ratio constraints is as low as 12% (equating to ~$2.45m). Interestingly, further analyses revealed that the changes in the size of the storage devices and the total power exchanged with the grid were the major contributors to the differences observed in the total discounted system costs. More specifically, ignoring the minor variations due to the stochastic processes involved, in both scenarios, the optimal mix of the non-dispatchable power generation components were found to include approximately the same share of non-dispatchable renewables. This indicates that it is not cost-optimal to alter the overall mix of non-dispatchable renewables under consideration yielded for the base most likely case solely to meet the altered self-sufficiency constraints, as it best leverages the associated temporal complementary characteristics. Rather, the changes in the self-sufficiency constraint can be more cost-effectively satisfied by refinements in the size of the storage media with associated trade-offs between the shares of total net power imports, internal energy storage capacity allocation, and incentivised DR utilisation.

2. Solving the model instances with the minimum allowed self-sufficiency ratio values ranging from 0% to 60% yields the same least-cost solution. The underlying reason for this is that the optimal solution returns an actual self-sufficiency ratio of approximately 62% in the case with $SSR^{min}$ = 0%, where practically no minimum self-sufficiency constraint is active, which highlights the modest cost of self-sufficiency – as defined by the additional cost incurred to reach the minimum allowable value of 80%.

3. The resulting MG whole-life costs obtained for the cases in between the cases with $SSR^{min}$ = 60% and $SSR^{min}$=100% suggest that there are

important dynamics that are taking place with the corresponding constraint. Specifically, the optimal value of the self-sufficiency ratio of the system was found to be 70% and 80% in the cases with $SSR^{min}$ = 70% and $SSR^{min}$ = 80%. A comparison of the MG net present values obtained under the above two scenarios indicates a relatively sharp cost increase to meet the prescribed minimum self-sufficiency ratios – which can be referred to as 'relative cost of self-sufficiency'. However, the actual self-sufficiency ratio of the case with the imposed constraint of $SSR^{min}$ = 90% was found to be 100%. This can be explained by the fact that the problem is optimised over a mixed-discrete-continuous search space, where the size of generation components, as well as the SC modules, battery packs, and hydrogen-based energy storage system components, vary in discrete intervals. Accordingly, redundant generation and storage capacity increments that are unnecessary for meeting the 90% self-sufficiency target – but unavoidable due to the limited resolution of the generation elements' and storage devices' step lengths – make the 100% self-sufficiency scenario the cost-optimal choice.

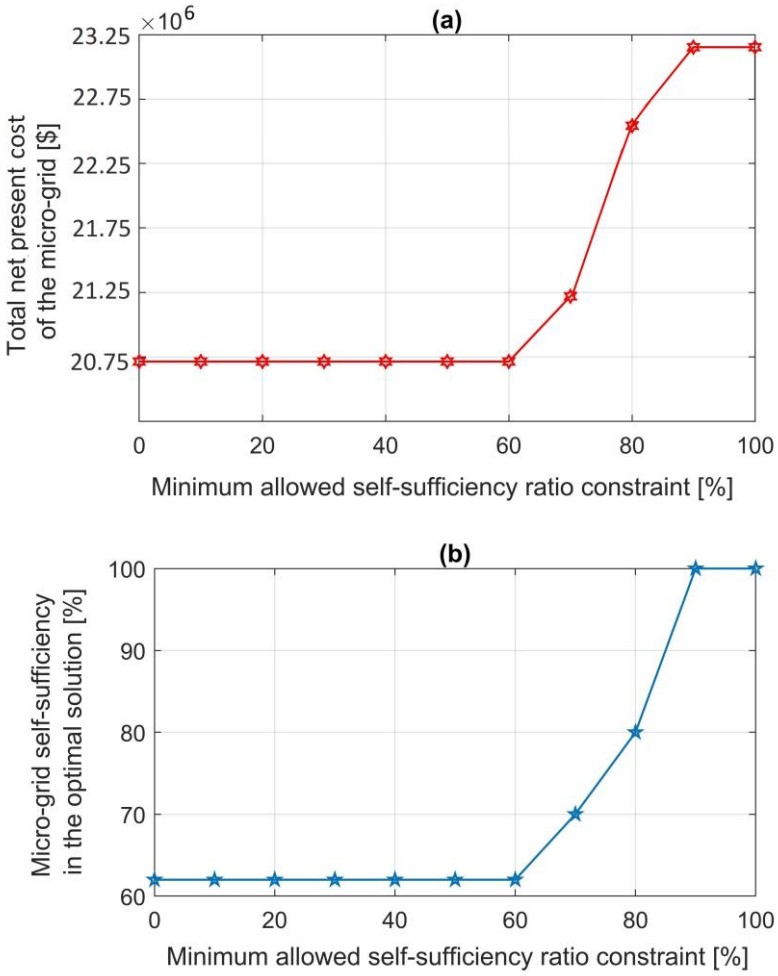


Figure 4.12: Sensitivity analysis with respect to the minimum allowed self-sufficiency ratio: (a) the MG whole-life cost; and (b) the optimal self-sufficiency ratio.

#### 4.3.5.2. Economics of daily energy arbitrage

This section evaluates the economics of daily electricity price and renewable energy arbitrage (using the battery bank) and its robustness to changes in key related parameters. To this end, two-way sensitivity analyses were carried out to estimate the total amount of annual arbitrage trades with respect to a range of incremental buyback rates from the current value of \$0.08/kWh to \$0.43/kWh[14] in intervals of \$0.05/kWh, as well as a range of expected reductions in the capital cost of the selected battery chemistry; specifically, from its current values to 30% of its current

[14] Assuming additional income streams such as frequency control ancillary services, operating reserves, and network support markets.

values in intervals of 10%. Accordingly, 64 combinations of future buyback rates and battery energy storage system capital costs were created and the stochastic model was solved for each of them. Note that, for practical reasons, all the analyses in this section represent the most likely case of stochastic simulations. Also recall that, according to the comprehensive impact analyses of the nested operational scheduling optimisation (Section 4.3.4), (i) energy arbitrage over inter-seasonal cycles is not profitable using the electrolytic, green hydrogen-based energy storage system at the present costs and technologies, (ii) the optimal capacity of the SC bank is not effectively influenced by the altered system dynamics due to the daily arbitrage processes with the grid, and (iii) overbuilding of non-dispatchable renewables for energy arbitrage functional roles is also found to be economically inviable as that would generate a reasonable profit stream only during the summer months when the difference between the minimum and maximum daily wholesale prices is larger, implying that the MG would have to sell a significant proportion of over-generation capacity at less remunerative spot market prices during the wintertime (though load is larger) – which, consequently, results in a rejection of the overbuilt renewable capacity strategy for leveraging potential benefits from arbitrage, demonstrating that the associated arbitrage revenue expectations from overbuilt renewable capacity fall short of the revenue requirements necessary for capital cost recovery.

Furthermore, given the computational expensiveness of simulating the proposed model, a reduced variant of the model was used to conduct the sensitivity analyses. To this end, the hourly-basis, one-year input time-series were averaged to a lower resolution, namely monthly mean 24-hour data streams. Accordingly, the typical 8,760-h annual energy balance analysis was reduced to a 288-h (12 months × 24 hours) analysis.[15] It is also noteworthy that, in this study, temporal energy

[15] Such data compression-based model reduction is found to have an insignificant impact (< 5%) on the optimality of the MG investment planning solutions with the results published in the following paper:

• **S. Mohseni**, A.C. Brent, and D. Burmester, "A demand response-centred approach to the long-term equipment capacity planning of grid-independent micro-grids optimized by the moth-flame optimization algorithm," *Energy Conversion and Management*, vol. 200, p. 112105, 2019.

arbitrate not only refers to buying energy at a low price, storing it, and selling it later at a higher price, but it also incorporates the strategy of storing the excess onsite generation for later, more remunerative exports (using renewables to charge storage when electricity prices are low and then discharging it when demand and prices are higher), as well as later discharge of the energy stored by lower-priced imports and excess generation to local loads during the coincident peak periods. Moreover, to ensure the computational tractability of the two-way sensitivity analyses, the assumption on the agreement of the MG system with an FRMP to access the wholesale spot market in the original MG planning and scheduling co-optimisation model was considered inactive – and the sensitivity analyses were run under the basic single-tier feed-in-tariff export settlement format. In this setting, the later more remunerative exports principally reflect the technical impossibility of simultaneously charging and discharging the batteries, as well as importing and exporting at the same time. Put differently, the general arbitrage strategy of 'buy low, sell high' followed in the original co-optimisation simulations to take advantage of future price variations turns into 'buy low, sell reasonably', or in battery energy management terms, 'charge cheaply, discharge foresightedly', which essentially prioritise taking advantage of low market prices for maximum imports over non- to slightly-profitable exports for the model instances with fixed, low to moderate feed-in-tariff rates. On the other hand, the model instances with relatively high feed-in-tariff rates (higher than yearly mean wholesale prices) seek to maximise exports subject to the battery discharge power capacity, whilst maximising the imports during the lowest wholesale prices subject to the battery charge power capacity. Accordingly, for the sake of fair comparative analyses, the baseline most likely co-optimisation case for business-as-usual conditions was re-run under the new assumptions and input time-series data resolution.

The resulting two-way sensitivity analyses are depicted in Fig. 4.13. As the figure shows, at the existing fixed feed-in-tariff rate, the capital costs of the 0.5 C vanadium redox flow battery bank need to be reduced by at least 30% so that the

---

However, for reasons of space, those analyses are not included in this thesis and the reader is referred to the above-mentioned journal article for detailed discussions. Also, further input data reduction efficacy improvements are planned for future work.

volume of profitable energy arbitrage trades increases approximately linearly with the associated battery cost reductions. On the other hand, at the current costs of the considered storage technology, the fixed buyback rate needs to be increased by at least 190% for the energy arbitrage trades to become an increasing linear function of feed-in-tariff. As a whole, given the New Zealand's remarkably green grid, the buyback rate is highly improbable to be increased to that large an extent in the future (even considering additional value streams from operating reserve and frequency control ancillary services markets, as well as further not-yet-monetised network services[16]). Yet, despite this limitation, as the analyses indicate, it is likely that the community-scale behind-the-meter battery systems are able to reach exceptionally large profitability levels, especially when used for energy arbitrage reasons in conjunction with the onsite backup provision, in a few years' time – in view of the projected cost reductions for the vanadium redox flow battery chemistry [309], [310]. The two-way sensitivity analyses, additionally, show that the energy arbitrage trade reaches a saturation point when/if the feed-in-tariff is increased to \$0.43/kWh and the battery capital costs are reduced by at least 70%. The arbitrage trade saturation point is limited by the upper bound imposed on the size of the battery bank. This implies that the return on any potential investment made at the feed-in-tariff above \$0.43/kWh and battery capital costs lower than 30% of the existing costs would be a strictly increasing linear function of the battery investment cost.

[16] Examples of such network support services include network congestion relief, network resource adequacy, network upgrade deferral, as well as keeping the low voltage grid operational during outages or maintenance [317].

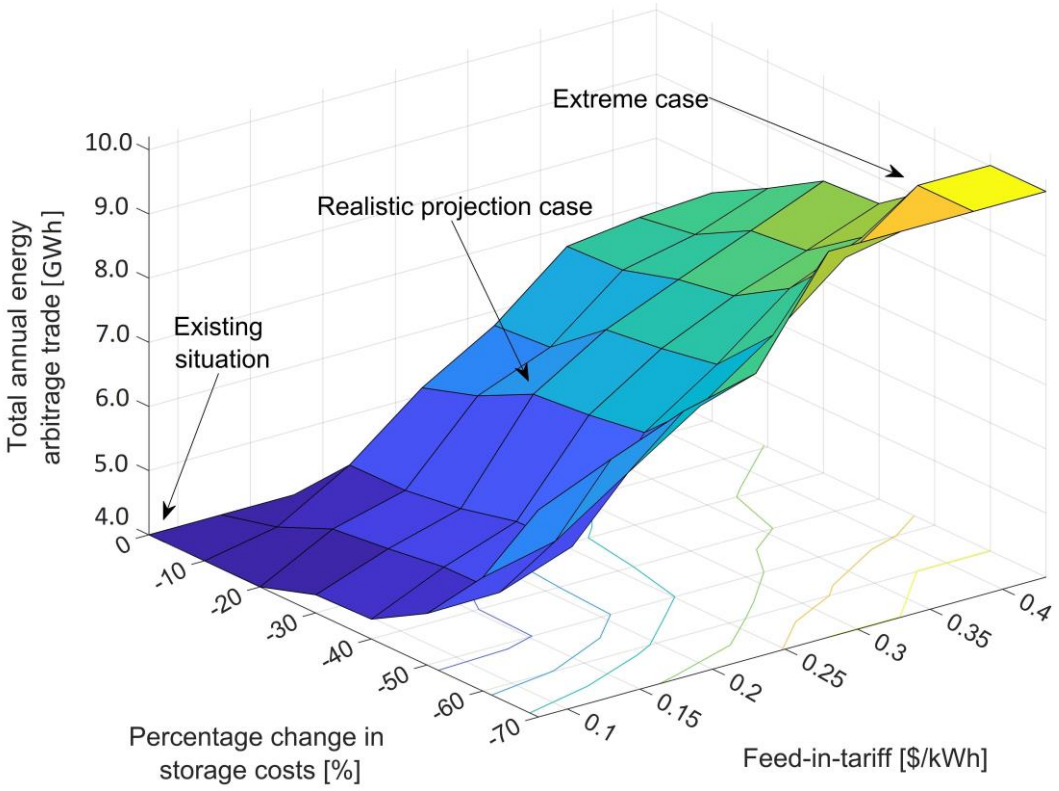


Figure 4.13: Sensitivity of the total arbitrage trade with respect to changes in the buyback rate and the capital cost of the battery energy storage system.

To further analyse the impact of the variations in the feed-in-tariff and the battery capital cost on the optimal combination of the MG components, as well as the exchanged power with the grid, Table 4.9 details the cost-optimal solutions obtained for the three cases marked in Fig. 4.13, namely: the existing situation (business-as-usual case), a realistic projection case (where the feed-in-tariff is increased to \$0.18/kWh and the battery capital cost is reduced by 40%), and an extreme case (where the feed-in-tariff is increased to \$0.43/kWh and the battery capital cost is reduced by 70%). For reasons of greater focus, the table only reports the variations in the optimal capacities of the battery bank, transformer, and multi-mode inverter, which have undergone the most important changes from an arbitrage perspective, compared to the other decision variables including component sizes, dispatched DR capacity, FCEV2G operations, and non-arbitrage-related grid power exchanges. That is, although the operational dynamics of the system slightly vary as the values of the sensitivity parameters of interest vary (especially in terms of utilised DR resources and non-arbitrage-related grid trades) with associated

planning-level implications, it was decided, for clarity and space considerations, to avoid such level of detail.

The particularly small changes observed in Table 4.9 in the key relevant output variables of the stochastic (most likely) design and dispatch co-optimisation case under the new modelling and data assumptions for the business-as-usual battery capital cost and feed-in-tariff scenario compared to the original most likely planning and scheduling co-optimisation case (see Tables 4.7 and 4.8) are revealing in important ways, namely: (i) the convergence of the arithmetic means of the outputs of the model instances with a statistically representative range of fixed feed-in-tariffs to the expected values of the outputs of the model instance with access to the spot market for exports, and (ii) the validity of the high accuracy of the employed data reduction method that reduces the hourly-basis, year-long time-series data into 12 representative days.

Also, as an illustration of the dynamics that are taking place within the system, which yield the associated total net energy arbitrage trade profit in the business-as-usual battery capital cost and feed-in-tariff case, multiplying the associated total annual arbitrage trade (~4.03 GWh), shown in Fig. 4.13, by the average hourly difference in per-unit import and export rates of ~$0.0537/kWh (accounting for the total net discounted cost of additional equipment capacity by converting the associated annualised costs into hourly operating basis), and then multiplying the result by the number of years in the planning horizon (20 years) yields a total net energy arbitrage trade profit of ~$4.33m. Table 4.9, furthermore, provides important insights into the statistically significant impact of the above-mentioned 'realistic' and 'extreme-case' projections of feed-in-tariff and battery capital costs. As can be seen from the table, a further battery capacity of ~1.8 MWh, a further transformer capacity of ~329 kVA, and a further inverter capacity of ~300 kW have been allocated for arbitraging on electricity tariffs under the realistic projection case scenario, which increase to ~16.1 MWh, ~1,636 kVA, and ~1.6 MW under the extreme case scenario, respectively.

Expectedly, the comparative results indicate that the opportunity for exploiting the difference in import and export rates increases as the battery costs

decrease and/or feed-in-tariffs increase. Accordingly, the battery capacity becomes a strictly increasing function of feed-in-tariff and battery capital cost beyond the aforementioned thresholds in feed-in-tariff increment and battery capital cost reduction. The battery capacity has also reached its maximum allowable limit (as defined in Table 3.3) just in the extreme-case projection scenario (as can be inferred from Fig. 4.13), which explains, in retrospect, the choice of the feed-in-tariff upper bound and battery capital cost lower bound for the bivariate sensitivity analyses. The comparatively less dramatic changes in the size of the transformer and inverter (which are found to be multicollinear by the power factor), additionally, indicate generally smooth increases in power trades across the entire representative operational period, rather than spikes in exchanges during the most remunerative time-steps – or, put differently, sharp charging and discharging for energy arbitrage with the grid. Most notably, a significant total discounted system cost reduction of ~16% (equating to ~NZ$2.92m) has been found for the realistic projection scenario, which is around double the increased (net) capital expenditure of the system. Note that the projected decreases in battery costs in the realistic scenario are expected to be realised within a couple of years in accordance with the relevant extrapolated 'learning curves' [309], [310], while the associated more than doubled average feed-in-tariff ($0.18/kWh) is also deemed to be feasible when payments for the network services provided by large-scale batteries are established (apart from the current existence of energy retailers that compensate $0.16/kWh for the first 50 kWh exported per fortnight at the site under consideration [311]).

Moreover, note that vanadium redox flow batteries are 100%-DOD-capable, have a long calendar life of at least 20 years with an unlimited cycle life, and are associated with negligible self-discharge and minimal degradation rates, which make them an ideal choice for daily energy arbitrage [312]. It should also be noted that the observation that the size of the transformer is in the kVA range, while the capacity of the inverter is in the MW range, can be explained by the fact that the hybrid inverter is utilised in both on- and off-grid modes, implying that its optimum size is primarily dictated by the magnitude of peak loads, rather than grid trade decisions – while the associated multicollinearity identified between the sizes of the inverter and transformer indicates that the additional inverter capacity is

fundamentally used for arbitrage services using the battery storage. It is also noteworthy that no considerable reductions are projected for the capital costs of power electronics devices and transformers for the near future [286].

Table 4.9: Comparative modelling results under the existing situation, realistic projection case, and the extreme case scenarios generated for the most likely case probabilistic analyses.

| Model output | Scenario | | |
|---|---|---|---|
| | Business-as-usual case* | Realistic projection | Extreme-case projection |
| Total NPC [$m] | 18.18 | 15.26 (−16%) | 7.51 (−59%) |
| Total net energy arbitrage trade profit [$m] | 4.33 | 6.9 (+165%) | 29.7 (+1,042%) |
| Optimal battery bank size [MWh] | 3.9 | 5.7 (+46%) | 20.0 (+413%) |
| Bi-directional transformer capacity† [kVA] | 362 | 691 (+91%) | 1,998 (+452%) |
| Multi-mode inverter capacity† [MW] | 4.8 | 5.1 (+6%) | 6.4 (+33%) |

* The small changes in some of the model outputs relative to the base-case, most likely planning and scheduling co-optimisation results are attributable to the down-sampled input data, as well as deactivating the MG system's access to the wholesale spot market through an FRMP.

† The overall battery bank and hybrid inverter capacities are allocated to the corresponding three different product models (with different nominal capacities), in accordance with the strategy devised in Chapter 3 (see Equations 3.4–3.6) – which gives priority to higher-rated product models as they carry lower per-unit costs whilst minimising unused capacities.

In addition, further unreported results revealed that as the feed-in-tariff increases and/or the battery capital cost decreases, the total non-arbitrage-related net energy purchased in the optimal solution set increases, whilst adhering to the minimum required self-sufficiency ratio. The underlying reason for this observation is that the increased optimal battery capacity – as a result of improved arbitrage profitability – increases the opportunity to store the off-peak energy purchased from the grid – at costs lower than the system's LCOE – for later internal use, to cost-optimally supplement the power generated by onsite non-dispatchable renewables – in addition to the increased frequency and volume of arbitrage-related exports.

### 4.3.6. Budget-constrained financial viability analyses

To develop a better understanding of the long-term financial implications of the uncertainty reduction and associate risk mitigation targets during the planning phases of sector-coupled, community-scale MGs, this section presents the comprehensive financial viability analyses carried out based on various capital budgeting metrics. This provides a platform to systematically compare and contrast the profitability of the three key uncertainty management scenarios – with associate risk attitudes – explored using the baseline non-intelligent-dispatch-integrated stochastic model, along with that of the system optimised by the designing and scheduling co-optimisation model under the most likely uncertainty realisation scenario. The financial appraisal metrics yielded for the stochastic modelling results are, furthermore, benchmarked against those of the base-case, deterministic modelling results obtained in the previous chapter. Note that all the processes involved in calculating the capital budgeting metrics, including those used for decomposing the LCOE into levelised costs of electricity and hydrogen, remain the same as those discussed in Sections 2.6.4 and 3.6.6.

Table 4.10 summarises the resulting capital budgeting metrics for the investigated representative uncertainty reduction cases (explored as part of the baseline probabilistic simulations), as well as a further most likely case with a nested liner programming-based operational strategy, which are benchmarked against those of the deterministic model. Interestingly, the comparative results reveal that, while, as expected, the deterministic and most likely case scenarios achieve practically the same level of profitability, dramatic changes occur in the economic viability of the system in the best-case and worst-case scenarios. More specifically, the MG's LCOE ranges from \$0.08/kWh (best-case) to \$0.13/kWh (worst-case), which respectively realise dynamic payback periods of 5.56 years and 8.45 years. This indicates that the proposed sustainable energy project is able to yield high returns on investment even under strongly conservative assumptions – in view of the existing average retail domestic electricity price of \$0.22/kWh at the site. While this thesis aims not to recommend a specific risk attitude (and in turn, a corresponding MG design choice), the connection of the test-case system to a highly

green[17] and reliable utility grid might justify favouring higher than normal levels of tolerable risk margin. An important remark that arguably gives further credence to taking such risk-seeking strategies – especially where capital resource budgets are limited – is that a high minimum self-sufficiency ratio of 80% is met in all the scenarios explored, which indicates that the potential risks of unreliability could be readily hedged against using additional grid imports, provided that a higher transformer capacity (than that optimised for the best-case scenario) is available. However, as the parametric uncertainty quantification analyses have shown and in line with expectations, it is likely that the optimal resource allocation strategies with such narrow budgets on the system-wide uncertainty reduction, which potentially require a redesign to a higher-performing design in a non-systematic way in the post-optimisation phase to decrease the risk of not meeting system requirements – for example, by reinforcing the transformer capacity for the specific case under consideration for potential increases in imports relative to the estimates for the best-case realisation – do not produce globally cost-optimal solutions. Yet, on a higher level, developing an understanding of the impact of a complete spectrum of uncertainty management scenarios using the proposed uncertainty budgeting framework is able to effectively enable iterative multi-stage MG infrastructure planning decisions, wherein per stage of the design process a particular level of uncertainty and risk can be tolerated – providing designers with the necessary tools to adopt a dynamic approach to MG development decision-making by setting phased targets for MG redesign and uncertainty reduction. In addition, as Table 4.10 demonstrates, while the economic viability of the project increases by as much as around 23% on average across all the capital budgeting metrics for the most likely design and dispatch co-optimisation case compared to the most likely non-intelligent-dispatch-integrated case, it does not reach (albeit close to) the profitability levels expected in the highly risk-seeking non-intelligent-dispatch-integrated case. Recall that, for practical reasons, the stochastic design and dispatch co-optimisation model is analysed only under the most likely probabilistic conditions.

[17] Over 80% of electricity is generated by renewable sources of energy in New Zealand [258].

Furthermore, the comprehensive financial viability analyses collectively provide another layer of evidence that lends further support to the core theme salient in the results of Chapters 2 and 3 on the financial sustainability of using hydrogen as an energy carrier in smart, integrated, decentralised community energy systems.

Table 4.10: Comparative summary of the capital budgeting analyses for the deterministic and stochastic model variants populated for the Ohakune test-case system.

| Model variant | Capital budgeting metric | | | | | |
|---|---|---|---|---|---|---|
| | LCOE* | LCOEE | LCOH | DPP | MIRR | DPI |
| Deterministic | \$0.11/ kWh | \$0.10/ kWh | \$5.27/ (kg-$H_2$) | 7.04 years | 10.1% | 2.66 |
| Best baseline stochastic case | \$0.08/ kWh | \$0.07/ kWh | \$4.16/ (kg-$H_2$) | 5.56 years | 12.7% | 3.37 |
| Most likely baseline stochastic case | \$0.12/ kWh | \$0.11/ kWh | \$5.48/ (kg-$H_2$) | 7.46 years | 9.7% | 2.56 |
| Worst baseline stochastic case | \$0.13/ kWh | \$0.12/ kWh | \$6.27/ (kg-$H_2$) | 8.45 years | 8.4% | 2.22 |
| Most likely co-planning† | \$0.09/ kWh | \$0.08/ kWh | \$4.42/ (kg-$H_2$) | 5.92 years | 12.0% | 3.17 |

* Note that the levelised cost of energy calculations for the estimated uncertainty budget-based MG whole-life costs are conducted with respect to the annual sets of reduced hourly scenario vectors that provide the lowest, highest, and medium power loads (in terms of the total sum of hourly values) respectively in the best-case, worst-case, and most likely case scenarios. This, together with the fact that the uncertainty in hydrogen loads is not characterised explicitly, explains the resulting somewhat disproportionate capital budgeting metrics obtained for the three stochastic cases compared to the base deterministic case.

† The most likely stochastic planning and scheduling co-optimisation case.

## 4.4. Chapter summary

In accordance with Part III of the research, this chapter has continued the process of expanding the basic structure of the meta-heuristic-based, high-dimensional community MG equipment capacity planning optimisation model, presented in Chapter 2, to include more realistic modelling aspects that are expected to have greater validity and give more detailed and accurate results, but at the expense of increased model complexity, as well as more computational resource requirements – in pursuit of developing a better understanding of the underlying operational dynamics of MGs towards making simulation results at the planning level more perceptually representative of real-world scenarios. To this end, the chapter has re-

used the general meta-heuristic-based high-dimensional MG sizing model, formulated in Chapter 2, as well as the game-theoretic, aggregator-mediated, distributed, sectoral, incentive-based, interruptible DR flexibility procurement modelling aspects, developed in Chapter 3, and added a large-scale, data-driven, coordinated, clustered scenario-led parametric uncertainty characterisation dimension that enables the simultaneous handling of multiple uncertain inputs, including, but not limited to, ambient temperature and river streamflow, which are not well explored in the mainstream optimal MG sizing literature, whilst simultaneously optimising the dispatch strategy. More specifically, the chapter has developed a novel meta-heuristic-based, non-cooperative game-theoretic DR-integrated, optimal stochastic equipment capacity planning and scheduling model tailored to highly self-sufficient and resilient, 100%-renewable, grid-connected MG systems that cost-minimally meet residential power loads subject to a set of operational- and planning-level constraints, in alignment with the designer's overall budget of system-wide parametric uncertainty. The developed model is able to comprehensively and concurrently account for at least six sources of probabilistic uncertainty associated with input data, for the first time in the long-term MG capacity planning optimisation literature, whilst preserving the range of the original solution space – in pursuit of improving the accuracy of (stochastic) modelling results and minimising the associated simulation-to-reality gaps.

A novel uncertainty budgeting approach has also been developed to more effectively support stochastic MG design decisions. Specifically, the proposed stochastic model provides tailored strategic MG infrastructure asset allocation decision-making support under two extreme-case (deviant) uncertainty budgets and one middle-case (realistic) uncertainty budget. To this end, three key scenarios have been considered, namely the best-case, most likely case, and worst-case. The best-case and worst-case scenarios respectively represent the $5^{th}$ and $95^{th}$ percentile values of the normal distributions fit to the decision variables (including the onsite equipment capacity, exchanged power with the grid, as well as the dispatched incentive-responsive sectoral DR and FCEV2G capacity) and the associated life-cycle cost results optimised for the clustered stochastic scenarios, while the most likely case represents the expected values of the probabilistic modelling outputs.

That is, specific MG resource allocation strategies that balance the total discounted cost and uncertainty mitigation level have been analysed to support MG designers in deciding which uncertain parameters – that govern the operation of MG components – require particular attention for maximum benefit. However, this chapter aims not to recommend a specific decision-making risk attitude, but rather to provide a general framework by which the MG designing community can systematically explore the associated trade-offs between the economic viability of a renewable energy project and the extent of model-inherent parametric uncertainty bounds narrowed.

To further improve the accuracy of long-term DR-integrated probabilistic strategic MG development plans through the integration of fundamentally new modelling elements in a deductive reasoning setting, the chapter then formalised a linear programming operational scheduling optimisation model that is aware of the potential revenue streams associated with energy arbitrage from the spot market with the utility grid (buy low, sell high) using the storage systems with daily and sub-daily timescales, whilst additionally accounting for renewable energy arbitrage (storing local generation when prices are low and returning it when high). The chapter then showed how this economic dispatch strategy could be implemented into a probabilistic, DR-integrated, meta-heuristic-based MG investment planning and capacity allocation optimisation model. Accordingly, a nested optimisation problem was formulated to integrate the day-ahead, forward-looking, intelligent energy dispatch planning optimisation framework into the optimal probabilistic resource allocation model developed – in pursuit of the co-optimisation of the long-term investment planning and short-term operational scheduling processes. The introduced more integrative approach to energy planning optimisation and business case analyses, which systematically captures the diurnal nature of load demand, wholesale prices, and non-dispatchable renewable energy supplies – and builds on the proposed stochastic, DR-centred, meta-heuristic-based model – has the potential to more effectively support the robust, informed, and adaptive decision-making under multiple, highly correlated parametric uncertainties in the presence of a large portfolio share of sectoral DR capacity. Notably, the developed solution algorithm accounts for two nested iterations, namely the day-ahead DSM operations and

dispatchable component management, which both gradually change the total operational cost (as defined by the sum of grid import costs and incentive payments). More specifically, the integration of the optimal dispatching problem into the MG sizing formulation makes the planning decisions aware of how the system would be actually operated in practice, which in turn, is expected to make the numeric simulation results more realistic.

The application of the proposed stochastic MG planning model to the most complex MG system conceptualised in this thesis (MG 4), which is populated for the highly challenging and interesting case of Ohakune, has demonstrated the computational tractability of the model in simultaneously quantifying at least six sources of forecast uncertainty during the long-term MG investment planning phases, whilst statistically preserving the range of the original solution space. Specifically, the applicability and validity of a MILP-based scenario clustering algorithm, which adequately addresses the prohibitive computational cost associated with the execution of all possible scenario realisations by producing annual sets of reduced hourly scenario vectors – that can be used as inputs for the deterministic MG planning model – have been verified. The numerical stochastic simulation results obtained from the case example of Ohakune by producing normal distributions that best fit the systematically augmented model outputs of the seven annual hourly scenario vector sets, and then applying the designer-specified budget on the allowable risk probability, have provided high-level, in-depth, accurate, and robust strategic renewable energy infrastructure planning decision-making support under system-wide parametric uncertainties in accordance with a complete and holistic range of uncertainty budgets. This has addressed another glaring gap in the mainstream stochastic MG design optimisation literature, namely focusing merely on determining a single 'optimal system' which meets a specific statistic of the QoI (most commonly, mean and percentile values).

Also, several novel, relevant, and encompassing insights have been generated into the significance of a comprehensive approach to system-wide parametric uncertainty management. Specifically, it is shown that the proposed probabilistic approach towards MG planning incurs an additional percentage cost of ~4%

(equating to ~NZ$0.79m) and ~20% (equating to ~NZ$4.45m) above the deterministic MG whole-life cost estimates in the most likely (risk-neutral) and worst-case (strong risk-aversion) scenarios, respectively. On the other hand, a highly risk-seeking decision-maker who selects the least theoretically feasible future infrastructure mix for the region (in terms of meeting the load with 100% reliability and 80% self-sufficiency without additional imports) could expect a ~21% (equating to ~NZ$4.65m) reduction in total discounted system costs. Put differently, failure to effectively quantify the most salient model-inherent parametric uncertainties results in at least a ~4% and ~20% underestimation of the total discounted system cost in the most likely case and worst-case scenarios, whereas the best-case stochastic results are found to be at least ~21% lower than the deterministic model. This indicates that the absolute change in the total discounted system cost is approximately the same for the best-case and worst-case scenarios. Also, a comparison of the stochastic modelling results towards the two extremes of the continuum of uncertainty mitigation strategies shows statistically robust changes in the optimal cost solution yielded for the opportunistic and robust (conservative) scenarios of different risk mitigation targets. This is consistent with the comprehensive capital budgeting-based financial viability analyses conducted, which have demonstrated that the impact of a risk-seeking attitude on the financial sustainability of the project is approximately by the same relative value positive as is negative for the counterpart risk-averse strategy. This is because, expectedly, the deterministic whole-life MG cost lies at around the peak of the corresponding output normal distribution curve. The financial viability analyses have, additionally, substantiated the technical competence and economic viability of using hydrogen as an energy vector in smart, integrated, sector-coupled, community RSESs.

The indicative uncertainty factor relative impact analyses that measure the sensitivity of the whole-life system cost, as well as the robustness of the MG configuration, to variations in different input data forecast uncertainties have also illustrated how the proposed uncertainty budgeting approach can help guide RSES designers on how to optimally ‘spend’ the uncertainty choice towards better-informed uncertainty management efforts and changes in the target design. This,

consequently, provides an effective platform for MG asset allocation decision-makers to screen for the input parameters with the highest influence on the objective function and system architecture, and determine – in the initial design phases – where more resources need to be allocated to strategically meet operational and planning requirements – in accordance with the optimum asset allocation strategy. The results of the uncertainty factor relative importance analyses can also be used to exclude the characterisation of parameters with relatively minor impacts from the uncertainty set to speed up the optimisation process by reducing the degrees of freedom with consequent positive implications on the accuracy of scenario reduction. For the specific largely wind-driven case studied, as shown by the stochastic annual scenario vector set impact analyses, the results of which are corroborated by the so-called '*deterministic sensitivity analyses*' – where the deterministic model is solved repeatedly for each of the annual scenario realisations of uncertain parameters independently with associate uncertainty budgeting processes – wind speed forecast uncertainty has been found to have the largest influence on the optimal MG whole-life cost solution, while the interaction between river streamflow and wholesale price forecast uncertainties is also responsible for a considerable part of the overall impact of parametric uncertainties on the total system life-cycle cost estimate. This indicates that, under high resilience, self-sufficiency, sustainability, and reliability constraints, meteorological sources of data uncertainty are (collectively) of the highest importance among the system-wide parametric uncertainties, with the relative importance of climatic data uncertainties against each other largely depending on the share of the associated non-dispatchable technologies in the optimal energy generation mix, which is mainly controlled by the site-specific potential of renewable energy. However, no significant influence on the overall conceptual MG architecture has been identified under any of the uncertainty budgets analysed, given the strong non-dispatchable power generation complementarities present. This observation indicates that, notwithstanding the varying effect sizes of different meteorological data uncertainties on the optimal cost solution, the best strategy for the specific problem analysed is to 'spend' the uncertainty budget by targeting proportional forecast uncertainty reductions for the variable climatic parameters studied; or in other words, the best strategy is not to allocate the uncertainty budget in an exogenous fashion for meteorological data –

to be able to fully leverage the above-mentioned complementary characteristics. On a wider level, the comparative relative importance analyses of uncertainty factors revealed that for the highly self-sufficient, resilient, reliable, and renewable case considered, larger weights, in proportionate terms, are *implicitly* assigned to meteorological input data (in aggregate) than wholesale electricity market prices and power loads during the associated uncertainty reduction efforts. Note that this is a different concept from the above-mentioned uncertainty budget spending strategy in that it is beyond the decision-maker's control – and is driven primarily by the dynamics of renewable energy supply, energy storage, grid exchanged power, and DR resource availability. More specifically, for the particular problem setup studied and the notional MG model conceptualised, in descending order, the most influential parametric uncertainties are found to be wind speed, wholesale prices, river streamflow, solar irradiance, load demand, and ambient temperature (ranked based on their average rank orders when quantified separately under the three uncertainty budgets studied). Also, in all the cases, more than half (~59%) of the overall uncertainty impact is found to be attributable to wind speed forecasts, around one-sixth is contributed by wholesale price forecasts, with the remaining ~25% occupied collectively by the other four uncertain parameters.

Importantly, the proposed stochastic approach for system-wide data uncertainty characterisation, which adds a probabilistic layer to the standard meta-heuristic-based MG equipment capacity planning problem, is featured with parametric scalability, as it substantially alleviates the computational burden associated with high-dimensional, large-scale, scenario-led, data-driven uncertainty quantification processes. That is, the proposed computationally effective model for uncertainty-budget-constrained optimal MG sizing can be readily generalised to address any (reasonable) number of uncertain input parameters desired, provided that the corresponding historical/synthetically reproduced data streams are available – as necessitated by MG configurations of interest. Moreover, the stability and robustness of the overall probabilistic MG sizing model in producing optimal uncertainty reduction alternatives and MG design choices are verified through in-depth sensitivity analyses exploring the variation of model outputs to changes in the minimum allowable self-sufficiency ratio constraint.

Aimed at a holistic approach to deriving the globally optimum MG investment planning solutions, the advanced version of the stochastic design formulation with a nested predictive, day-ahead economic dispatch framework – that results in a two-loop optimisation problem structure for each of the seven model instances associated with the annual sets of reduced hourly scenario vectors used in probabilistic simulations – is also demonstrated to be able to improve the optimality of long-term MG planning solutions through making effective use of forward-looking predictions that well represent how smart RSESs are operated in practice. More specifically, the developed stochastic design and dispatch co-optimisation model's application under the most likely uncertainty realisation case to the notional MG 4 populated for the case of Ohakune has shown its effectiveness in generating savings of up to a significant ~19% (equating to ~NZ$4.30m) compared to the counterpart case where a conventional rule-based, Greedy, cycle-charging scheduling strategy is used to sequentially decide the operation of the system at hourly intervals, linked to other time increments solely through the boundary conditions of the energy contents of storage media – and thus, without systematically planning energy storage for future time increments. The savings from the greater flexibility – enabled by the ability to forecast future scenarios – are also found to be fairly equally attributable to (distinct) realisations of daily grid and renewables arbitrage, namely 'import low-price, store, export high-price', and 'store the excess, export high-price' as well as two intelligent energy shifting strategies, namely 'buy low-price, store, use later', and 'store the excess, use later', which are highly inter-dependent in that the latter two strategies have a direct influence on the total net energy arbitrage trade profit from the former two.

Also, the balanced capital investment and operational MG costs by coordinating the optimal stochastic, DR-integrated sizing problem with a nested operational scheduling optimisation problem – to develop an integrated resource plan that simultaneously plans ahead the storage for variations in the operating conditions – are found to have a significant impact on the MG's operating business model, but not on the total capital cost as it does not result in considerably downsized components, aside from the modestly increased battery capacity. The co-optimisation model has also produced a novel insight on the inefficacy of long-

term and seasonal arbitrage given that the dedicated hydrogen-based energy storage systems (used in this study to provide such services) are comparatively costly and unprofitable with present technologies. Further analyses have also revealed that profits solely from daily energy arbitrage, without consideration of internal energy balance benefits, are insufficient to achieve additional battery capacity capital cost recovery. That is, at the existing costs of battery storage systems, daily energy arbitrage alone is not a viable market niche for storage; rather, it can be regarded as a value-enhancing service if accompanied by an economic dispatch strategy tailored to managing the battery storage capacity in a forward-looking manner that would otherwise remain underutilised within the MG context. Moreover, the arbitrage trades have also been found to remain as smooth and gentle as possible to avoid capacity additions necessary for sharper arbitrage-related power exchanges. In addition, comprehensive capital budgeting analyses have confirmed the significance of an integrated design and dispatch optimisation approach in improving the economic viability of the project. Notably, it was shown that a coordinated, system-level design and dispatch co-optimisation model – that considers the capacity planning optimisation of individual dispatchable DER components within the candidate pool simultaneously with their optimal operational scheduling strategy – whilst quantifying the system-wide parametric uncertainties under the most likely scenario, yields capital budgeting metrics that well outperform those of a baseline most likely stochastic case – and are highly competitive with those of a baseline best-case stochastic scenario – that uses conventional heuristics to decide (and not optimise) the operating schedules of battery storage without explicitly planning it for future time-steps. In particular, the LCOE and dynamic payback period of the project are significantly reduced to NZ$0.09/kWh and 5.92 years in the most likely co-optimisation case, from NZ$0.12/kWh and 7.46 years in the counterpart baseline case.

While the proposed stochastic, DR-integrated meta-heuristic-based model, especially with a nested dispatch optimisation framework, is rather computationally intensive to simulate (though completely tractable and of high accuracy), the decision-making processes it is intended to support involve the allocation of significant, capital-intensive resources for MGs that are typically designed for

multi-decade life-cycles. Thus, in view of its demonstrated multi-million-dollar impact on the whole-life cost estimates of sector-coupled, community MGs, the relatively long running times associated with such one-time numerical simulations could be expected to be acceptable to designers. It should also be noted that the test-case system studied, for which the general probabilistic co-optimisation model is parametrised and the set of uncertain factors is defined, is arguably one of the most numerically complex and comprehensive systems in the literature. That is, the commonly lower numbers of decision variables and/or uncertain parameters considered during the design processes of smaller-scale community MG systems (especially in off-grid topologies), which in turn reduce the dimensionality of the associated problems, warrant lower computational costs.

To explore the variation of model outputs to changes in the minimum allowed self-sufficiency ratio, sensitivity analysis was performed by running the most likely stochastic co-optimisation model repeatedly for different minimum allowed self-sufficiency values ranging between 0 and 100 in intervals of 10 to yield a continuous optimal total cost versus self-sufficiency ratio curve. The results indicated a roughly linear increase in the whole-life cost for increasing levels of the minimum allowed self-sufficiency ratio from 60% to 90%. Also, the model instances optimised subject to the minimum allowed self-sufficiency ratios equal to or lower than 60% returned the same optimal MG portfolio that was associated with an *actual* self-sufficiency ratio of around 62%. That is, even if the minimum allowable self-sufficiency ratio constraint is inactive and without explicitly assigning a lower bound for self-sufficiency, the optimal solution set is associated with a relatively large self-sufficiency ratio. This further substantiates the economic viability of the MG development proposal against the current practice of importing the community's entire electricity needs from the national grid as it indicates a relatively insubstantial cost of self-sufficiency (within the realm of planning for self-sufficiency). Furthermore, comprehensive two-way sensitivity analyses were carried out to understand the robustness of the total net energy arbitrage trade profit to simultaneous variations in key related parameters, namely the capital cost of 0.5 C vanadium redox flow batteries and feed-in-tariff. Notably, the bivariate sensitivity analyses have indicated that under a realistic projection scenario, where

the feed-in-tariff is increased to $0.18/kWh – assuming additional payments from frequency control ancillary services and operating reserves, as well as the network services that have not yet been monetised, such as keeping the low voltage grid operational during planned or unplanned outages, network congestion relief, network resource adequacy, and network upgrade deferral – and the battery capital cost is simultaneously reduced by 40%, a significant total discounted system cost reduction of ~16% (equating to ~NZ$2.92m) compared to the status quo could be expected from arbitrage opportunities, which is around double the estimated increase in the capital expenditure of the system mainly due to the added battery, transformer, and inverter capacities of 1.8 MWh (+46%), 329 kVA (+91%), and 300 kW (+6%), respectively. From a broader perspective, the associated one-way and two-way sensitivity analyses that involve repeated evaluation of the proposed stochastic, DR-integrated design and dispatch co-optimisation model using a wide and statistically representative range of inputs assigned to the dedicated sensitivity variables – defined as input variables for which multiple values are specified – collectively offer additional evidence supporting the model's robustness in determining the cost-optimal solution under various input data scenarios. They, additionally, further verify the viability of hydrogen and fuel cell technologies in facilitating the sector-coupled community-level integration of renewables by providing an effective platform for seasonal storage and transportation sector electrification interventions, with the latter also benefitting from increased ability to manage grid peaks and fluctuations through specifically developed vehicle-to-grid (FCEV2G) opportunities.

Also, as far as the results from the chapter are concerned, the efficacy of the basic structure of the proposed meta-heuristic-based solution algorithm in optimising a robust solution to the MG sizing problem, as well as the statistically significant contribution of the specifically developed Stackelberg, non-cooperative game-theoretic, platform-mediated sectoral DR marketplace to the profitability of the MG development plans, have shown to remain valid under a comprehensive range of time-series input data, which indicates the robustness and effectiveness of the proposed general DR-integrated, meta-heuristic-based MG planning approach. On a different level, the efficacy of the model in producing a well-diversified

integrated resource mix has also been substantiated. The economic viability and technical feasibility of using hydrogen as an energy vector in niche transportation and inter-seasonal storage applications have, additionally, been corroborated.

In conclusion, this chapter has systematically broadened the scope and methodological complexity of business-as-usual approaches for stochastic, DR-integrated renewable energy investment planning and operational scheduling co-optimisation under multiple sources of parametric uncertainty considering a relatively large number of dispatchable resources, with the ultimate goal of formulating an advanced model that adopts a holistic approach to deriving the uncertainty-adjusted globally optimum energy planning solutions that account for the potentially significant arbitrage interventions. It has, furthermore, provided an insightful knowledge base to inform energy and climate change policy, business models for renewable energy, and the wider sustainable energy system modelling community of significant opportunities that more advanced, stochastic energy planning optimisation approaches hold for tailoring highly renewable, self-sufficient, reliable, and resilient community energy systems to different uncertainty budgets governing the associated adequacy and security reference margins – and consequently, driving their deployment, especially in sector-coupled community-scale applications. Community batteries that are managed to simultaneously provide onsite power reserves and daily energy arbitrage services with the wider network are, additionally, found to provide an effective platform to increase energy equity by reducing the system's estimated LCOE, thereby generating substantial savings that can eventually be passed onto the end-consumers – thus, allowing low-income sectoral customers, who otherwise would not have the required financial or technical means, to access reliable clean energy and benefit from the transition to a sector-coupled renewable energy economy. Further sensitivity analyses have also shown that obtaining sufficient revenue for the distribution network service provider-owned community battery storage solely from arbitrage opportunities – without necessarily absorbing locally generated renewable energy – is both feasible and realistic when the required trading platforms to unlock the community battery storage's access to the network service markets are established with the accompanying realisation of the projected battery capital cost reductions.

In terms of relevance for policy implications, the findings indicate that the image of sustainable energy potentially becomes tarnished in the eyes of the public if they lead to more expensive energy prices than those promised during the pre-feasibility and design phases, or more severely, if they largely fail to deliver the desired reliability, security, adequacy, self-sufficiency, sustainability, robustness, or resilience targets[18] – or do not yield the expected profitability levels from the investors' perspective. To surmount this challenge, this chapter has established a solid foundation for a more realistic projection of the total discounted cost of MG systems under high-dimensional parametric uncertainties during the associated long-term strategic investment planning optimisation processes, upon which more sophisticated models can be built as demonstrated for the integration of a forward-looking, predictive, intelligent economic dispatch model (the nested optimal dispatch problems). That is, the proposed computationally tractable, meta-heuristic-based, probabilistic, DR-integrated MG planning and scheduling co-optimisation model lays fundamentally novel and innovative new foundations for specific renewable energy policy objectives.

[18] The value that a community places on reliable, secure, adequate, self-sufficient, green, robust, or resilient supply/service can be highly context-dependent.

# Chapter 5: Conclusions and Future Work

To effectively manage the integration of significant volumes of non-dispatchable renewable generation into electricity networks, as well as the ever-increasing growth in electricity demand due to the emerging end-use sector-coupling efforts,[1] the electricity industry is on the cusp of transformation to the 'grid of grids' paradigm where the unified network is set to collapse into a collection of smaller, highly renewable networks that can operate in concert or independently within the smart grid milieu. On the other hand, the rapidly declining costs of DERs (particularly, solar PV and battery storage systems) are facilitating the achievement of the United Nation's sustainable development goal of providing universal energy access by 2030, via its "Sustainable Energy for All" initiative through the proliferation of autonomous and semi-autonomous clean, reliable, low-voltage, low-inertia local renewable energy networks.

Yet, despite substantial technological advancements, as well as improved regulatory and institutional policies, the wider strategic long-term renewable energy planning optimisation literature has failed to adequately address a number of important methodological, topological, and social/behavioural gaps. The gaps disconnect the relevant optimal MG equipment capacity planning methods from reality, and make it difficult to see how they can be directly applied to real-world strategic sector-coupled community renewable energy system planning problems. Strategic distributed energy planning models yield the whole-life cost-optimal mix of the sizes of the candidate DERs and power conversion devices that meet the energy demand at a pre-specified reliability level. While demonstrating some encouraging positive research trends towards more holistic approaches, the systematic literature review in Chapter 1 has revealed a number of glaring thematic

[1] End-use sector-coupling involves the integration and electrification of major energy-consumers – residential, commercial, industrial, agricultural, and transportation sectors – while reinforcing the interactions between electricity supply and demand necessary to unlock transformational synergies between substantial increases in the use of electricity and renewable power generation – in the efforts toward economy-wide deep decarbonisation [3], [6].

knowledge gaps in terms of the methodological complexity of business-as-usual approaches, which lead to potentially significant optimality shortcomings. In response, this research has focused on developing a better understanding of globally optimum long-term distributed renewable energy planning based on multi-faceted quantitative decision support analyses, whilst using an integrative approach that links the associated conceptual, theoretical, and practical framings.

Accordingly, the research has made distinct and significant contributions to address seven of the most salient gaps in the renewable energy system capacity planning optimisation literature, namely: (i) paucity of state-of-the-art meta-heuristic optimisation algorithms, (ii) poor understanding of the social/behavioural aspects of DR procurement in the long run, especially in aggregator-mediated, double-sided market platforms, (iii) lack of comprehensive, high-level stochastic programming approaches and underutilisation of scenario reduction algorithms, (iv) underrepresented usage of joint operational and investment planning optimisation methods, (v) techno-economic limits in developing 100%-renewable energy systems, (vi) lack of hybridising different energy storage technologies tailored to operating on different timescales, and (vii) negligence of the potential of V2G services and power-to-gas interventions for the cost-effective integration of variable renewable energy generation.

Examining the potential of state-of-the-art meta-heuristics in improving the quality of solutions to the long-term strategic MG designing and capacity planning optimisation problem, Chapter 2 has provided descriptive statistically robust quantitative evidence supporting the proposition that using newly developed meta-heuristics in MG sizing applications carries the potential to significantly improve the economics of MG systems, which can be in large part attributed to the non-deterministic nature of meta-heuristics. This indicates that efficiency testing of meta-heuristics during MG investment planning phases is an ever-continuing area of research. More specifically, based on comprehensive, multi-case-study statistical analyses of the performance of 20 meta-heuristic optimisation algorithms, including well-established and state-of-the-art single and hybrid techniques embedded in a specifically developed meta-heuristic-based solution approach to the standard total net present cost-oriented MG size optimisation problem, the study has provided

statistically significant evidence on the superiority of the MFOA to the other 19 candidate meta-heuristic optimisers. The 20 top-performing optimisers were selected based on comprehensive preliminary meta-heuristic efficiency testing in simplified MG designing simulations involving a total of 226 algorithms. Furthermore, two novel generalisations of the standard MG capacity planning are introduced, namely: (i) using more diversified portfolios of variable generation technologies with complementary characteristics together with a sustainable share of dispatchable RESs ensures the cost-optimal dispatchability of future RSESs, and (ii) optimal hybridisation of different energy storage technologies in compliance with the timescale relevant to the technical capabilities of each technology, particularly the duration of energy storage capacity per unit of power capacity, is able to substantially improve the economics of MG systems. Accordingly, the chapter has addressed research gaps 1, 5, 6, primary objective 1, and secondary objectives 1 and 2 defined in Section 1.5.

Chapter 3 has demonstrated the potential of aggregator-mediated, incentive-based, market-driven DSM programmes tailored to small- to medium-scale end-consumers in improving the economic viability of community-scale, sector-coupled MG systems. To this end, a specifically developed DSM market design, which systematically and effectively characterises the strategic interactions between the MG operator, monopoly DRAs, and end-consumers using tools borrowed from non-cooperative game theory and endogenous Stackelberg leader-follower relationships, is integrated into the meta-heuristic-based optimal MG sizing model proposed in Chapter 2. Accordingly, Chapter 3 expands the boundaries of knowledge and understanding of the positive impacts of altering the energy consumption behaviour of different classes of electrical loads on the cost-optimal design of MG systems. Also, a secondary objective of the chapter has been to ascertain the technological competence and cost-competitiveness of EV fleet trip level energy management and V2G connectivity in the context of sustainable energy system operation and planning. The chapter has also substantiated the efficacy of first-order passive low-pass energy filter-based approaches to scheduling hybrid energy storage systems, as well as the technical feasibility and financial viability of utilising hydrogen as an energy vector in community-scale

MGs for niche applications – inter-seasonal energy storage to meet seasonal demand, and hydrogen mobility to decarbonise the transport sector. Accordingly, the chapter has addressed research gaps 2, 5, 6, 7, primary objective 2, and secondary objective 3, whilst additionally corroborating the validity of the contributions put forward (in Chapter 2) to achieve secondary objectives 1 and 2 defined in Section 1.5.

Chapter 4 has gone further and added a computationally tractable probabilistic dimension to the proposed sectoral DR-integrated meta-heuristic-based MG configuration planning optimisation model presented in Chapter 3. Importantly, the chapter has demonstrated the significant role of using optimisation-based scenario clustering techniques that yield a statistically representative subset of the original set of multi-dimensional uncertainty representation scenarios in increasing the number of uncertainty factors characterised simultaneously, and thereby improving the solution quality. To this end, a novel data-driven MCS-based uncertainty quantification layer has been added to the meta-heuristic-based, sectoral DR-aware MG energy planning optimisation model, which is able to produce different energy planning decisions in accordance with the uncertainty budget of interest. Moreover, the uncertainties coupled with ambient temperature (for potential solar PV) and river streamflow (for potential micro-hydropower) have been adequately quantified for the first time in the long-term energy planning optimisation literature. Chapter 4 has then proceeded to further improve the proposed sectoral DR-integrated, uncertainty-aware MG energy planning optimisation model by nesting a novel linear programming-based energy management optimisation framework within the meta-heuristic-based stochastic energy infrastructure capacity allocation approach to optimise the operational schedules of dispatchable DERs over a moving 24-h energy dispatch horizon simultaneously to the system design. The operational planning algorithm provides 24-h look-ahead foresight to cost-minimally address the dynamic nature of system states – in terms of load demand, local non-dispatchable generation, and wholesale electricity prices (where appropriate). To this end, the overall problem has been formulated as an outer loop stochastic capacity planning optimisation problem, within which daily energy management optimisation problems are nested. In the

simulation process, component sizes have been treated as '*here-and-now*' variables and the operating schedules have served as '*wait-and-see*' variables. As far as the relative importance of MG design and dispatch co-optimisation is concerned, the chapter has shown that a smart, dynamic scheduling framework with 24-h look-ahead periods for the dispatch of MG components is able to substantially reduce the associated total MG life-cycle cost in the most likely uncertainty characterisation scenario as compared to the counterpart case with a business-as-usual rule-based Greedy energy dispatch strategy. Accordingly, the chapter has addressed research gaps 3 and 4 in accordance with primary objectives 3 and 4 defined in Section 1.5.

Collectively, Chapters 2–4 have produced a number of detailed and generalised insights, which have important financial and technical implications for robust renewable energy prior techno-economic feasibility and business case analyses. Methodologically, the chapters support the main research proposition that not only is it technically feasible to implement smart, sector-coupled, 100%-renewable and -reliable community-scale energy systems optimised by the introduced meta-heuristic-based, DR-integrated, stochastic energy planning and scheduling co-optimisation model, but they also surpass unsubsidised retail parity at existing renewable energy technology costs in New Zealand. The main three reasons behind observed improvements in the optimality of the long-term MG energy planning solutions compared to business-as-usual approaches are: (i) employing a new population-based meta-heuristic optimisation algorithm that systematically rebalances exploration for improved exploitation of the search space for potential solutions by using an adequate set of sub-spaces, whereby the probability of exploiting a local optimum that is located near the global optimum increases, (ii) producing optimal trade-offs between importing electricity from the main grid (where appropriate), eliciting sectoral, elasticity-aware, personalised DR resources, and investing in renewable energy generation and hybrid energy storage systems, and (iii) reducing the degree of conservatism by making effective use of an innovative new, double-sided market-based, behaviourally-characterised, aggregator-mediated DR flexibility provisioning design, a novel scenario reduction-oriented high-dimensional parametric uncertainty quantification framework able to provide uncertainty budget-ware decision-making support, as

well as a novel distributed energy planning optimisation formulation that couples the optimal sizing and dispatch problems in a systematic way. Accordingly, Chapters 2–4 have generated novel insights into developing cost-minimal, 100%-renewable and -reliable sector-coupled local energy systems supplying multi-vector loads (including hydrogen as a transportation fuel and electricity for low-temperature heat) tailored towards grid-connected and isolated community-scale MG development projects by refining some of the key common (simplifying) assumptions underpinning the long-term distributed renewable energy investment planning, as well as adding new features to the standard MG equipment capacity planning solution algorithms, which make the numerical simulation results more accurate.

## 5.1. Major contributions

The major contributions of the research, which are put forward to achieve the four primary research objectives are recapitulated in Table 5.1. The major contributions of the research have led to the production of several main novel generalisations of the standard long-term strategic MG equipment capacity planning and designing problem, which contribute to addressing seven glaring content gaps and previously neglected factors – in pursuit of broadening the scope and level of analysis of integrated MG resource planning and optimal infrastructure allocation problem.

Table 5.1: Recapitulation of the major contributions of the thesis mapped against primary research objectives.

| Primary research objective (PRO) | Contributions |
|---|---|
| ***PRO1. Formulating a robust meta-heuristic-based, highly dimensional MG equipment capacity planning optimisation model tailored towards community-scale, sector-coupled, multi-energy-storage-technology, 100%-renewable and -reliable energy projects and identifying the superior*** | • Developing a descriptive statistics-based comparative meta-heuristic performance analysis scheme for MG capacity planning applications that adequately accounts for varying efficiencies of meta-heuristics when applied to structurally different MG systems, as well as their initialisation-directed stochasticity in different simulation trials.<br>• Proposing a first-order, passive, low-pass energy filter-based operational planning algorithm for efficient scheduling of multiple energy storage technologies integrated into grid-connected and isolated MG systems.<br>• Devising an efficient energy management strategy for the coordinated integration of light-duty fuel cell electric commuter |

| | |
|---|---|
| ***meta-heuristic in MG sizing applications*** | vehicles, as well as medium-duty fuel cell electric vessels, heavy-duty tractors, and heavy-freight trucks. |
| ***PRO2. Formalising a sectoral aggregator-mediated, EV-charging-load-addressable, market-driven interruptible DR scheduling framework to give a realistic grounding to research on distributed DSM planning and integrating it into the proposed MG sizing model*** | • Devising a bi-level Stackelberg, non-cooperative game-theoretic DSM plan to characterise the strategic interactions of the MG operator (utility), intermediary sectoral DRAs, and end-customers in day-ahead, incentive-based DR programmes in a robust, equitable, transparent, market-driven manner.<br>• Developing an iterative, privacy-preserving distributed algorithm able to handle non-linearities in actors' payoff functions to determine the unique, pure-strategy Nash equilibrium of the DR dispatch game, whilst capturing the price elasticity of DR supply across different load segments to improve the forecast quality of load type-dependent DR participation.<br>• Designing a stochastic load disaggregation technique to break down the forecasted total sectoral electricity consumption into any individual number of end-users, whilst accounting for the diverse sector-wide customer behaviours and strategies, as well as the corresponding sectoral aggregator payoff profiles. |
| ***PRO3. Large-scale, data-driven, scenario-led, multi-dimensional quantification of various problem-inherent parametric uncertainties based on the discretisation of the corresponding PDFs and developing different energy planning decisions in accordance with different energy uncertainty budgets*** | • Proposing a large-scale MCS-based stochastic framework to simultaneously characterise a relatively large number of input data uncertainties – power outputs from various non-dispatchable generation technologies, load power demand, and wholesale electricity prices.<br>• Applying a MILP-based scenario clustering technique that yields a statistically representative subset of the original set of multi-dimensional uncertainty scenarios to reduce running times, while retaining the solution quality (optimality) within an acceptable limit.<br>• Characterising the uncertainties in ambient temperature and river streamflow forecasts by adequately deriving the PDFs that best fit the corresponding historical datasets, which respectively influence the estimated power outputs from solar PV and micro-hydro power generation plants. |
| ***PRO4. Coordinated, system-level hybrid-energy-storage-technology MG design and dispatch co-optimisation, whilst accounting for the total incentive-responsive V2G resource capacity in the integrated resource plan, as well as various arbitrage opportunities*** | • Introducing a linear programming-based, arbitrage-aware, dynamic, look-ahead, predictive dispatch strategy for the optimal scheduling of MG systems – charging/discharging of energy storage systems and energy exchanges with the main power grid – over a moving 24-h dispatch horizon.<br>• Nesting the developed forward-looking operational planning problem – formulated to optimally respond to the dynamic nature of system conditions over a moving one-day period – within the proposed meta-heuristic-based, DR-integrated, stochastic MG sizing model to jointly optimise the design and dispatch of MG systems. |

## 5.2. Best practice insights

Despite their demonstrated reliability, resilience, and sustainability benefits, communities and electric utilities may face various key financial, technical, computational, ICT-integration, and perception barriers and challenges to implementing community MG systems. Accordingly, based on the novel insights gleaned from the in-depth multi-case-study-oriented analyses carried out in this research, a number of leading practices have been developed. That is, the primary aim of this section is to enable MG design and planning practitioners to incorporate the associated novel best practices into new community MG development projects necessary for successful implementation. The proposed practices for MG developers and decision-makers to consider when addressing financial, technical, computational, ICT-integration, and perception barriers can be summarised as follows:

1. *Limited availability of capital*: Communities and sectoral energy consumers may suffer from limited capital resources to invest in community MGs, particularly low-income communities – and especially, in view of current expenses to manage the COVID-19 pandemic. Accordingly, in light of the demonstrated attractiveness of community MG projects for third-party investment in this study, business models and value chains, such as EaaS and resilience-as-a-service are suggested, which (i) eliminate or minimise the need for customers to invest in potentially significant upfront capital for installing community MGs, (ii) simplify operations, (iii) provide modularity in implementation (in the interest of phased targets), and (iv) strategically account for the specific value the target community places on unserved energy.

2. *Significance of energy diversification:* Not only does the diversification of renewable energy mix improve the energy security and reduce the relative cost of a highly resilient and self-sufficient scheme, but it also provides an effective platform to reduce the estimated total discounted system cost through leveraging the associated temporal complementarities in non-dispatchable supplies. Accordingly, all the potentially significant variable

RESs at a case study site (along with the dispatchable resources, such as biomass) are recommended to be included in the technology candidate pool for optimisation during techno-economic feasibility analyses.

3. *Importance of hybrid energy storage systems:* The optimal hybridisation of different energy storage technologies across a broad spectrum of disparate timescales, in compliance with the timescale relevant to the technical capabilities of each technology, is particularly useful in minimising the risk of MG design sub-optimality. More specifically, multi-energy-storage-technology MGs benefit from reduced overall cost, minimum excess curtailment, and improved system efficiency. A technically viable and financially sustainable hybridisation choice for multi-energy, sector-coupled community MGs is found to be the SC-battery-hydrogen combination.

4. *Relatively insubstantial cost of self-sufficiency:* For the cases that have access to the national grid, the whole-life cost of the system is not expected to be exceedingly sensitive to the choice of the minimum allowed self-sufficiency ratio. That is, the relative cost of self-sufficiency is not prohibitively high. The reason lies in the fact that, even without assigning a lower limit to the desired self-sufficiency level, the optimally sized systems are, to a great extent (at least 60%), self-sufficient, which implies the significant cost-efficiency of grid-connected community MGs compared to the base-case of importing the entire electricity needs from the wider network. Also, except where it simultaneously contributes to meeting high self-sufficiency constraints, oversizing of renewables (for an 'exports-only' revenue stream) is viable only to the point that it does not necessitate additional inverter and transformer capacities.

5. *Relative weight of parametric uncertainties:* MG developers may lack computational resources, and more strikingly financial resources, to conservatively hedge against the long-term parametric (forecast) uncertainties. In such cases, the characterisation of meteorological forecast data needs to be prioritised. Also, from an optimality perspective, it is best

practice to assign equal weights to the quantification of the uncertainty associated with the power outputs from non-dispatchable technologies of interest – as that preserves the temporal supply complementarities involved. However, even where there are severe computational resource limitations (in terms of processing power, with consequent tediously, though not intractably, long running times), treating the forecast uncertainty associated with the non-dispatchable technology that has the largest portfolio share is of utmost importance and should not be neglected. Avoiding to do so is shown to significantly impair the optimality of total cost estimates, despite having little to no effect on the optimal system type (configuration). That is, a fully deterministic MG design approach would expectedly entail salient redesign and refinance requirements in the interest of highly reliable, resilient, and self-sufficient operations. Moreover, on a higher level, developing an understanding of the impact of a complete spectrum of uncertainty management scenarios using the proposed uncertainty budgeting framework is able to effectively enable iterative multi-stage MG infrastructure planning decisions, wherein per stage of the design process a particular level of uncertainty and risk can be tolerated – providing designers with the necessary tools to adopt a dynamic approach to MG development decision-making by setting phased targets for redesign and uncertainty reduction.

6. *Sectoral elasticity of DR supply capacity:* The long-run incentive price elasticity of supply of DR capacity from different customer classes is a useful tool for prioritising the integration of sectoral DR capacities. The DR elasticity across different sectors, can be ranked, in ascending order of value, as residential, commercial, industrial, agricultural, and EV-charging loads. Accordingly, where the financial and technical means are insufficient for the simultaneous integration of the total MG-wide sectoral DR capacity, it is recommended to begin the integration process with EV-charging loads and end with residential loads, which respectively represent the lowest and highest cost of acquiring DR capacity during the coincidental peak periods. Also, the costs of advanced, multi-layered information and communications

platforms – as enabling technologies and prerequisites for the implementation of the proposed two-sided, platform-mediated DR flexibility marketplace that systematically accounts for the heterogeneous willingness of end-users to participate in interruptible DR activities – may represent a substantial financial barrier. For such cases, the results from this research suggest that leveraging direct load control services, which are associated with significantly less expensive communications platforms, is a viable strategy to facilitate customer enrolment in DR programmes. The main numerical evidence in support of the above argument is that, to a considerable extent, overpayment for DR products is found to less negatively affect the trade-off operational cost solution (between grid imports and DR incentivisation) than the lack of flexible DR resources in the integrated resource plan. Moreover, given the potentially significant contribution of the V2G interventions to the dispatchability of MGs, and in view of the relatively high costs of the associated enabling infrastructure, it is a real option for the MG stakeholders to incentivise or subsidise the installation of V2G-enabled chargers in the form of rebates or discounts on approved items – to, at least partially, address the cost premiums that exist between standard EV chargers and V2G-enabled chargers.

7. *Economics of energy arbitrage:* At the existing costs of battery storage systems, daily energy arbitrage alone is not a viable market niche for storage; rather, it can be regarded as a value-enhancing service if accompanied by an economic dispatch strategy tailored to managing the battery storage capacity in a forward-looking manner that would otherwise remain underutilised within the MG context. Also, the community-scale behind-the-meter battery systems are able (in expectation) to reach exceptionally large profitability levels, especially when used for energy arbitrage reasons in conjunction with the onsite backup provision and not-yet-commoditised network services, in a few years' time – especially in view of the projected cost reductions for the vanadium redox flow battery chemistry that is well-suited for the task. However, the arbitrage with the grid over longer than diurnal timescales, such as long-duration arbitrage

(discharge duration >10 hours and <100 hours) and seasonal arbitrage (discharge duration >100 hours) using the hydrogen-based energy storage system is not expected to be profitable, at least substantially, even if the added capacity simultaneously contributes to procuring seasonal onsite energy reserves.

## 5.3. Way forward

There exist several research opportunities to improve the practical utility of the proposed model. Accordingly, further work is planned (and to a large extent, it is already underway), which can be summarised as follows:

1. Quantifying the effect and relative importance of time resolution (granularity) of input data time-series on finances and scheduling decisions of DR-integrated MG systems under uncertainty. Accordingly, further work could seek to explore the best-compromise trade-offs between simulation accuracy and computational speed by evaluating the robustness of the optimality gap against the (i) time-series fidelity, (ii) number of design/dispatch variables, (iii) number of uncertain parameters characterised concurrently, (iv) number of end-consumers participating in aggregator-mediated interruptible DR programmes, and (v) time horizon of the associated multi-period dispatch problem – that uses expectations of system inputs and future MG states – based on comprehensive one- and multi-way sensitivity analyses.

2. Carrying out high-level impact analyses of parametric uncertainty factors (holistic ranking of the effect size of uncertain input data) in a more systematic, statistically representative, and valid multi-test-case-oriented way that generates greater insight into the ranking of the relative impact of various input data forecast uncertainties, whilst factoring various climatic, meteorological, and electricity price conditions, as well as different MG topologies/layouts (off- versus on-grid) and configurations (constituent generation and storage components) into the comparative analyses – similar to the processes followed in Chapter 2 for the ranking of meta-heuristics.

Given that the probabilistic model is somewhat computationally costly (though tractable) to evaluate, an advanced, machine learning-based input data reduction approach that produces typical representative days (with more than 98% accuracy) is under development for use for such large-scale sensitivity analyses. This would also provide a platform to explicitly model the hour-to-hour correlations for the reduced scenario vectors.

3. Carrying out population-based field experiments to gather high-frequency, granular real-world data pertaining to the patterns of dissatisfaction cost of various DR capacity suppliers at different scales for use in big data-driven analyses of habitual energy consumption, as well as deriving the associated sectoral elasticity of supplying DR capacity. This would entail conducting empirical work at the individual DR resource level with appliance-fidelity to produce statistically representative datasets on the response attributes of a wide range of DR units across residential, commercial, industrial, agricultural, and electrified transport sectors, which would provide a robust and reliable platform to replace the "lumpiness" of the proposed DSM model with the finer-grained response patterns of specific DR-enabled end-uses, while operating and designing local MG systems.

4. Advancing the proposed aggregator-mediated sectoral DR framework to accurately quantify the magnitude of energy service price elasticities relevant to both direct and indirect rebound effects (which postulate that an effective decline in the cost of energy services, as a result of improved energy efficiency, induces a measurable increase in energy services demand), whilst addressing the associated behavioural drivers of consumer response to changes in energy efficiency and energy prices.

5. Investigating the relative importance and computational complexity of modelling the associated behavioural DR attributes over long-term investment planning horizons by analysing the solution quality and CPU usage time of energy planning optimisation results yielded under various combinations of behavioural DR attributes considered, whilst additionally carrying out comparative quantitative analyses of uniform (non-

discriminatory) and pay-as-bid (discriminatory) settlement formats [195] for different DR service auctions in a systematic way.

6. Developing innovative near-real-time emergency DR interventions, where load curtailments are carried out extremely quickly (seconds to 10 minutes) in response to unforeseen system-wide contingencies, contributing to the provisioning of spinning reserves as an additional revenue stream for MGs.

7. Adopting a micro-meso-macro approach [313] to DR management, where tools borrowed from micro-, meso-, and macro-economics on different levels of analysis are used in a coordinated way in order to develop a better understanding of the recursive linkages, feedback effects, interactions, and complementarities that may exist between utility- and customer-centric approaches to the quantification of DR benefits.

8. Executing the simulation of the original, non-reduced version of the stochastic, DR-integrated, meta-heuristic-based MG sizing and economic dispatching model on parallel computing facilities, such as grids, clusters, and massively parallel processing systems to speed up the simulations.

In addition, further sensitivity analyses are planned for future work to explore the economics of arbitrage over long-duration and inter-seasonal cycles using the hydrogen-based energy storage system with respect to the projected reductions in the associated hydrogen technology capital costs and increments in feed-in-tariff rates that account for other augmenting value streams such as capacity payments that are of potentially greater value than the average energy value. In inverse sensitivity analysis terms, this translates into identifying cost and performance targets for hydrogen storage to become profitable for long-duration and seasonal arbitrage interventions, while additionally (in a bundled manner) contributing to smoothing seasonal variations in net load (the local load seasonality). On a wider level, research is also planned to identify when battery and hydrogen energy storage technologies are expected to become viable business options – to be formulated as an optimal timing problem – as energy products for providing arbitrage services in the presence or absence of intra-hour balancing and network support services

(where arbitrage value and potential external network services are decoupled from any other internal network services that could potentially be bundled) with or without additional renewable energy generation capacity specifically dedicated to the task, provided that robust and reliable projections of the associated capital cost reductions, as well as market value estimates of such external network services, as modelling parameters, are available – and are considered as *a priori* known input.

Most of all, on many occasions throughout this research, public- and private-sector energy stakeholders and decision-makers, as well as renewable energy scholars, have voiced their concerns over the accuracy of MG design optimisation and long-term investment planning software tools available in the literature and industry. Accordingly, a new commercial MG capacity planning optimisation software package, named SMOULDER (Stochastic Micro-grid Optimisation under Uncertainties in Loads and Distributed Energy Resources), is under development based on the novel scientific findings of this research. Two phases of acceptance testing have also been planned for the software package, namely: (i) an internal acceptance (alpha) testing by an independent test team at Victoria University of Wellington's commercialisation office Wellington Univentures – Te Paewai, and (ii) an external user acceptance (beta) testing by releasing the software package to a number of expert practitioners across academia and industry to ensure that the (eventual) product has no faults or bugs and that the most important function points work as expected.

## 5.4. Final reflection

The research presented in this thesis provides a variety of general novel methodological insights into how MG system integration of non-dispatchable renewables can cost-optimally be achieved through a combination of important contributions to long-term strategic MG planning within the broader context of socio-techno-economic approaches to energy transitions, namely: (i) leveraging fundamentally new meta-heuristic optimisation algorithms, (ii) behaviourally-founded integration of sectoral aggregator-mediated, individualised, interruptible DR resources via platform-mediated, two-sided, elasticity-aware, EV-charging-load-addressable DSM markets, (iii) in-depth, data-driven, multi-dimensional

parametric uncertainty analyses, and (iv) formulating advanced combined sizing and scheduling frameworks with a daily basis moving horizon. It has, furthermore, provided an insightful multi-variant evidence base – which is validated through comprehensive capital budgeting and financial appraisal analyses, as well as comparative analyses of the resulting levelised costs of energy of the conceptualised MG systems with existing retail electricity tariffs [$/kWh] – to inform energy and climate change policy, business models for renewable energy, and the wider sustainable energy system modelling and optimisation community of significant opportunities that more integrative energy planning optimisation approaches hold for reducing the adequacy and security reference margins of highly renewable sector-coupled community energy systems – and consequently, driving their deployment. The developed long-term MG energy planning optimisation decision-making framework is able to yield optimal trade-offs between grid power exchanges (for grid-connected systems), sectoral DR resource utilisation (including FCEV2G interventions), as well as renewable generation and hybrid energy storage system capacity allocations subject to the associated technical feasibility and social acceptability constraints, whilst adequately addressing the numerical challenges in the size optimisation of a highly diversified mix of non-dispatchable renewable generation assets supported by multiple energy storage media – with associated temporal complementary characteristics – present in the candidate pool. In conclusion, the proposed holistic MG energy planning optimisation model has derived substantial implications for the (cost-minimal) deployment of smart, integrated RSESs in both green- and brown-field sites – as part of the universal clean, reliable, affordable energy access and the wider economy-wide deep decarbonisation efforts.

# Bibliography


[1] International Energy Agency (IEA), "*World Energy Outlook 2020*," Paris, France, 2020. [Online]. Available: https://www.iea.org/reports/world-energy-outlook-2020 [Accessed: 11-Apr.-2021].

[2] United Nations – Climate Change, "*The Paris Agreement*," Paris, France, 2016. [Online]. Available: https://unfccc.int/process-and-meetings/the-paris-agreement/the-paris-agreement [Accessed: 11-Apr.-2021].

[3] International Renewable Energy Agency (IRENA), "*Electrification with Renewables*," Abu Dhabi, UAE, 2019. [Online]. Available: https://www.irena.org/publications/2019/Jan/Electrification-with-Renewables [Accessed: 11-Apr.-2021].

[4] V. C. Gungor *et al.*, "Smart grid technologies: Communication technologies and standards," *IEEE Trans. Ind. informatics*, vol. 7, no. 4, pp. 529–539, 2011.

[5] International Renewable Energy Agency (IRENA), "*Power system flexibility for the energy transition*," Abu Dhabi, UAE, 2018. [Online]. Available: https://irena.org/publications/2018/Nov/Power-system-flexibility-for-the-energy-transition [Accessed: 11-Apr.-2021].

[6] T. Brown, D. Schlachtberger, A. Kies, S. Schramm, and M. Greiner, "Synergies of sector coupling and transmission reinforcement in a cost-optimised, highly renewable European energy system," *Energy*, vol. 160, pp. 720–739, 2018.

[7] International Renewable Energy Agency (IRENA), "International Renewable Energy Agency (IRENA), "*Power system flexibility for the energy transition*," Abu Dhabi, UAE, 2019. [Online]. Available: https://www.irena.org/-/media/Files/IRENA/Agency/Publication/2019/Dec/IRENA_Demand-side_flexibility_2019.pdf [Accessed: 11-Apr.-2021].

[8] Power Advisory LLC, "*Integration of Variable Output Renewable Energy Sources – The Importance of Essential Reliability Services*," St. Andrews by-the-Sea, New Brunswick, 2017. [Online]. Available: https://www.nrcan.gc.ca/sites/www.nrcan.gc.ca/files/emmc/pdf/17-0071-Essential-Reliability-Services-access-EN.pdf [Accessed: 11-Apr.-2021].

[9] C. Burger, A. Froggatt, C. Mitchell, and J. Weinmann, *Decentralised Energy: A Global Game Changer*. Ubiquity Press, 2020.

[10] D. Ockwell and R. Byrne, *Sustainable energy for all: Innovation, technology and pro-poor green transformations*. Taylor & Francis, 2016.

[11] J. D. McCalley. *Introduction to System Operation, Optimization, and Control*. Iowa State University. [Online]. Available: http://home.engineering.iastate.edu/~jdm/ee553/Intro.pdf [Accessed: 11-Apr.-2021].

[12] C. S. Lai, G. Locatelli, A. Pimm, X. Wu, and L. L. Lai, "A review on long-term electrical power system modeling with energy storage," *J. Clean. Prod.*, p. 124298, 2020.

[13] P. A. Trotter, N. J. Cooper, and P. R. Wilson, "A multi-criteria, long-term energy planning optimisation model with integrated on-grid and off-grid electrification–The case of Uganda," *Appl. Energy*, vol. 243, pp. 288–312, 2019.

[14] F. H. Clarke, "Generalized gradients and applications," *Trans. Am. Math. Soc.*, vol. 205, pp. 247–262, 1975.

[15] G. J. Woeginger, "Exact algorithms for NP-hard problems: A survey," in *Combinatorial*

*Optimization*, Springer, 2003, pp. 185–207.

[16] W. Peng, A. Maleki, M. A. Rosen, and P. Azarikhah, "Optimization of a hybrid system for solar-wind-based water desalination by reverse osmosis: Comparison of approaches," *Desalination*, vol. 442, pp. 16–31, 2018.

[17] S. Burger, J. P. Chaves-Ávila, C. Batlle, and I. J. Pérez-Arriaga, "The Value of Aggregators in Electricity Systems," *MIT Center for Energy and Environmental Policy Research*, 2016. [Online]. Available: https://energy.mit.edu/wp-content/uploads/2016/01/CEEPR_WP_2016-001.pdf [Accessed: 11-Apr.-2021].

[18] N. Good, K. A. Ellis, and P. Mancarella, "Review and classification of barriers and enablers of demand response in the smart grid," *Renew. Sustain. Energy Rev.*, vol. 72, pp. 57–72, 2017.

[19] C. M. Weiller and M. G. Pollitt, "Platform markets and energy services," *Smart grid Handb.*, pp. 1–23, 2016.

[20] Y. Feng and S. M. Ryan, "Scenario construction and reduction applied to stochastic power generation expansion planning," *Comput. Oper. Res.*, vol. 40, no. 1, pp. 9–23, 2013.

[21] J. W. Whitefoot, "Optimal Co-Design of Microgrids and Electric Vehicles: Synergies, Simplifications and the Effects of Uncertainty," PhD thesis, University of Michigan, Ann Arbor, 2012.

[22] E. L. V Eriksson and E. M. Gray, "Optimization and integration of hybrid renewable energy hydrogen fuel cell energy systems – A critical review," *Appl. Energy*, vol. 202, pp. 348–364, 2017.

[23] Z. K. Pecenak, M. Stadler, and K. Fahy, "Efficient multi-year economic energy planning in microgrids," *Appl. Energy*, vol. 255, p. 113771, 2019.

[24] W. Feng *et al.*, "A review of microgrid development in the United States–A decade of progress on policies, demonstrations, controls, and software tools," *Appl. Energy*, vol. 228, pp. 1656–1668, 2018.

[25] H.-K. Ringkjøb, P. M. Haugan, and I. M. Solbrekke, "A review of modelling tools for energy and electricity systems with large shares of variable renewables," *Renew. Sustain. Energy Rev.*, vol. 96, pp. 440–459, 2018.

[26] HOMER Energy. HOMER (Hybrid Optimization Models for Energy Resources) [Computer software], Boulder, CO. https://www.homerenergy.com/

[27] Natural Resources CAMNET Energy Technology. RETScreen [Computer software]. https://www.nrcan.gc.ca/maps-tools-publications/tools/data-analysis-software-modelling/retscreen/7465/

[28] J. W. Whitefoot, A. R. Mechtenberg, D. L. Peters, and P. Y. Papalambros, "Optimal component sizing and forward-looking dispatch of an electrical microgrid for energy storage planning," in *International Design Engineering Technical Conferences and Computers and Information in Engineering Conference*, 2011, vol. 54822, pp. 341–350.

[29] J. P. Vielma, "Mixed integer linear programming formulation techniques," *Siam Rev.*, vol. 57, no. 1, pp. 3–57, 2015.

[30] HOMER Energy. HOMER Pro (Hybrid Optimization Models for Energy Resources Pro) [Computer software], Boulder, CO. https://www.homerenergy.com/

[31] National Renewable Energy Lab and the University of Massachusetts Amherst. Hybrid2 [Computer software]. https://www.umass.edu/windenergy/research/topics/tools/software/hybrid2/

[32] National Renewable Energy Lab. SAM (System Advisor Model) [Computer software]. https://sam.nrel.gov/

[33] XENDEE [Computer software]. https://xendee.com/

[34] National Renewable Energy Lab. REopt [Computer software]. https://reopt.nrel.gov/

[35] Grid Integration Group, Berkeley Lab. DER-CAM (Distributed Energy Resources-Customer Adoption Model) [Computer software]. https://gridintegration.lbl.gov/der-cam/

[36] C. Gamarra and J. M. Guerrero, "Computational optimization techniques applied to microgrids planning: A review," *Renew. Sustain. Energy Rev.*, vol. 48, pp. 413–424, 2015.

[37] A. H. Fathima and K. Palanisamy, "Optimization in microgrids with hybrid energy systems - A review," *Renew. Sustain. Energy Rev.*, vol. 45, pp. 431–446, 2015.

[38] D. Emad, M. A. El-Hameed, M. T. Yousef, and A. A. El-Fergany, "Computational methods for optimal planning of hybrid renewable microgrids: a comprehensive review and challenges," *Arch. Comput. Methods Eng.*, vol. 27, pp. 1297–1319, 2020.

[39] S. Sinha and S. S. Chandel, "Review of recent trends in optimization techniques for solar photovoltaic-wind based hybrid energy systems," *Renew. Sustain. Energy Rev.*, vol. 50, pp. 755–769, 2015.

[40] M. A. Hannan, M. Faisal, P. Jern Ker, R. A. Begum, Z. Y. Dong, and C. Zhang, "Review of optimal methods and algorithms for sizing energy storage systems to achieve decarbonization in microgrid applications," *Renew. Sustain. Energy Rev.*, vol. 131, p. 110022, 2020.

[41] Y. Yang, S. Bremner, C. Menictas, and M. Kay, "Battery energy storage system size determination in renewable energy systems: A review," *Renew. Sustain. Energy Rev.*, vol. 91, pp. 109–125, 2018.

[42] A. Mellit and S. A. Kalogirou, "MPPT-based artificial intelligence techniques for photovoltaic systems and its implementation into field programmable gate array chips: Review of current status and future perspectives," *Energy*, vol. 70, pp. 1–21, 2014.

[43] M. H. Shoreh, P. Siano, M. Shafie-khah, V. Loia, and J. P. S. Catalão, "A survey of industrial applications of Demand Response," *Electr. Power Syst. Res.*, vol. 141, pp. 31–49, 2016.

[44] A. R. Jordehi, "Optimisation of demand response in electric power systems, a review," *Renew. Sustain. Energy Rev.*, vol. 103, pp. 308–319, 2019.

[45] F. Shariatzadeh, P. Mandal, and A. K. Srivastava, "Demand response for sustainable energy systems: A review, application and implementation strategy," *Renew. Sustain. Energy Rev.*, vol. 45, pp. 343–350, 2015.

[46] G. Mavromatidis, K. Orehounig, and J. Carmeliet, "A review of uncertainty characterisation approaches for the optimal design of distributed energy systems," *Renew. Sustain. Energy Rev.*, vol. 88, pp. 258–277, 2018.

[47] R. H. A. Zubo, G. Mokryani, H. S. Rajamani, J. Aghaei, T. Niknam, and P. Pillai, "Operation and planning of distribution networks with integration of renewable distributed generators considering uncertainties: A review," *Renew. Sustain. Energy Rev.*, vol. 72, pp. 1177–1198, 2017.

[48] M. Aien, A. Hajebrahimi, and M. Fotuhi-Firuzabad, "A comprehensive review on uncertainty modeling techniques in power system studies," *Renew. Sustain. Energy Rev.*, vol. 57, pp. 1077–1089, 2016.

[49] C. H. Glock and S. Hochrein, "Purchasing Organization and Design: A Literature Review," *Bus. Res.*, vol. 4, no. 2, pp. 149–191, 2011.

[50] D. Moher, A. Liberati, J. Tetzlaff, D. G. Altman, and P. Grp, "Preferred Reporting Items for Systematic Reviews and Meta-Analyses: The PRISMA Statement (Reprinted from Annals of Internal Medicine)," *Phys. Ther.*, vol. 89, no. 9, pp. 873–880, 2009.

[51] D. E. Goldberg and J. H. Holland, "Genetic algorithms and machine learning," *Mach. Learn.*, vol. 3, pp. 95–99, 1988.

[52] J. Kennedy and R. Eberhart, "Particle swarm optimization," *1995 IEEE Int. Conf. Neural Networks*, vol. 4, pp. 1942–1948, 1995.

[53] D. Karaboga, "*An idea based on honey bee swarm for numerical optimization*," Technical Report-TR06, Erciyes University, Engineering Faculty, Computer Engineering Department, 2005.

[54] K. Deb, A. Pratap, S. Agarwal, and T. Meyarivan, "A fast and elitist multiobjective genetic algorithm: NSGA-II," *IEEE Trans. Evol. Comput.*, vol. 6, pp. 182–197, 2002.

[55] J. Stewart, H. Haeri, and L. Garth, "*Demand Response Elasticities Analysis*," The Cadmus Group LLC, 2018. [Online]. Available: https://www.bpa.gov/EE/Technology/demand-response/Documents/180301_BPA_DR_Elasticities_Analysis_Report.pdf [Accessed: 11-Apr.-2021].

[56] N. Rujeerapaiboon, K. Schindler, D. Kuhn, and W. Wiesemann, "Scenario Reduction Revisited: Fundamental Limits and Guarantees," *Math. Prog., Ser. B*, 2018.

[57] P. Denholm and T. Mai, "Timescales of energy storage needed for reducing renewable energy curtailment," *Renew. Energy*, vol. 130, pp. 388–399, 2019.

[58] F. Mwasilu, J. J. Justo, E.-K. Kim, T. D. Do, and J.-W. Jung, "Electric vehicles and smart grid interaction: A review on vehicle to grid and renewable energy sources integration," *Renew. Sustain. energy Rev.*, vol. 34, pp. 501–516, 2014.

[59] GlobalData Energy, "*Traditional fuels to remain prominent despite AFV sales growth*," Offshore Technology, 2021. [Online]. Available: https://www.offshore-technology.com/comment/surge-alternative-fuel-vehicles-traditional-fuels/ [Accessed: 11-Apr.-2021].

[60] J. Mouton, *How to succeed in your master's and doctoral studies: A South African guide and resource book*. Van Schaik Publishers, 2011.

[61] E. Antona, "Mathematical models and their use in engineering," in *Applied Mathematics in Aerospace Science and Engineering*, Springer, 1994, pp. 395–433.

[62] E. Turban and J. R. Meredith, *Fundamentals of Management Science*. Richard D. Irwin, 1994.

[63] G. Marion and D. Lawson, "An introduction to mathematical modelling," *Edinburgh Bioinforma. Stat. Scotland, Univ. Bristol*, 2008.

[64] R. S. Prawat and R. E. Floden, "Philosophical perspectives on constructivist views of learning," *Educ. Psychol.*, vol. 29, no. 1, pp. 37–48, 1994.

[65] Butte College, "Deductive, Inductive and Abductive Reasoning," 2019. [Online]. Available: http://www.butte.edu/departments/cas/tipsheets/thinking/reasoning.html [Accessed: 11-Apr.-2021].

[66] M. Young, L. Varpio, S. Uijtdehaage, and E. Paradis, "The spectrum of inductive and deductive research approaches using quantitative and qualitative data," *Acad. Med.*, vol. 95, no. 7, p. 1122, 2020.

[67] P. Rule and V. M. John, "A necessary dialogue: Theory in case study research," *Int. J. Qual. Methods*, vol. 14, no. 4, 2015.

[68] J. Nash, "Non-Cooperative Games," *Ann. Math.*, vol. 54, no. 2, pp. 286–295, 1951.

[69] R. Amir and I. Grilo, "Stackelberg versus Cournot equilibrium," *Games Econ. Behav.*, vol. 26, no. 1, pp. 1–21, 1999.

[70] B. Wauters and D. Beach, "Process tracing and congruence analysis to support theory-based impact evaluation," *Evaluation*, vol. 24, no. 3, pp. 284–305, 2018.

[71] J. Meredith, "Theory building through conceptual methods," *Int. J. Oper. Prod. Manag.*, vol. 13, no. 5, 1993.

[72] V. A. Thurmond, "The point of triangulation," *J. Nurs. Scholarsh.*, vol. 33, no. 3, pp. 253–258, 2001.

[73] P. D. Leedy and J. E. Ormrod, *Practical research: planning and design*. Pearson College Div, 2004.

[74] B. Succar and M. Kassem, "Point of Adoption," *Facilities Management Industry*, 2016. [Online]. Available: https://www.fmindustry.com/en/2017/best_practice/1790/Point-of-Adoption-building-information-modelling-BIM-implementation-performance-assessment-innovation-diffusion-FM-Magazine-White-Papers--Briefings.htm [Accessed: 11-Apr.-

2021].

[75] W. Ongsakul and V. N. Dieu, *Artificial intelligence in power system optimization*. CRC Press, Inc., 2013.

[76] J. Zhao, H. S. Ramadan, and M. Becherif, "Metaheuristic-based energy management strategies for fuel cell emergency power unit in electrical aircraft," *Int. J. Hydrogen Energy*, vol. 44, no. 4, pp. 2390–2406, 2019.

[77] A. Tabanjat, M. Becherif, D. Hissel, and H. S. Ramadan, "Energy management hypothesis for hybrid power system of H2/WT/PV/GMT via AI techniques," *Int. J. Hydrogen Energy*, vol. 43, no. 6, pp. 3527–3541, 2018.

[78] P. B. de M. Oliveira and J. B. Cunha, "Blending Artificial Intelligence into PID Controller Design: A Biomedical Engineering Experiment," *IFAC-PapersOnLine*, vol. 49, no. 6, pp. 366–371, 2016.

[79] R. B. Hiremath, S. Shikha, and N. H. Ravindranath, "Decentralized energy planning; modeling and application–a review," *Renew. Sustain. Energy Rev.*, vol. 11, no. 5, pp. 729–752, 2007.

[80] S. Mohseni and S. M. Moghaddas-Tafreshi, "A multi-agent system for optimal sizing of a cooperative self-sustainable multi-carrier microgrid," *Sustain. Cities Soc.*, vol. 38, pp. 452–465, 2018.

[81] N. D. Hatziargyriou, D. Škrlec, T. Capuder, P. S. Georgilakis, and M. Zidar, "Review of energy storage allocation in power distribution networks: applications, methods and future research," *IET Gener. Transm. Distrib.*, vol. 10, no. 3, pp. 645–652, 2016.

[82] A. Maleki and A. Askarzadeh, "Comparative study of artificial intelligence techniques for sizing of a hydrogen-based stand-alone photovoltaic/wind hybrid system," *Int. J. Hydrogen Energy*, vol. 39, no. 19, pp. 9973–9984, 2014.

[83] B. Khan and P. Singh, "Selecting a Meta-Heuristic Technique for Smart Micro-Grid Optimization Problem: A Comprehensive Analysis," *IEEE Access*, vol. 5, pp. 13951–13977, 2017.

[84] A. Maleki and F. Pourfayaz, "Optimal sizing of autonomous hybrid photovoltaic/wind/battery power system with LPSP technology by using evolutionary algorithms," *Sol. Energy*, vol. 115, pp. 471–483, 2015.

[85] M. A. M. Ramli, H. R. E. H. Bouchekara, and A. S. Alghamdi, "Optimal sizing of PV/wind/diesel hybrid microgrid system using multi-objective self-adaptive differential evolution algorithm," *Renew. Energy*, vol. 121, pp. 400–411, 2018.

[86] S. Mohseni, A. Brent, D. Burmester, and A. Chatterjee, "Optimal Sizing of an Islanded Micro-Grid Using Meta-Heuristic Optimization Algorithms Considering Demand-Side Management," *2018 Australasian Universities Power Engineering Conference (AUPEC)*, 2018, pp. 1–6.

[87] S. Sharma, S. Bhattacharjee, and A. Bhattacharya, "Grey wolf optimisation for optimal sizing of battery energy storage device to minimise operation cost of microgrid," *IET Gener. Transm. Distrib.*, vol. 10, no. 3, pp. 625–637, 2016.

[88] A. Maleki and F. Pourfayaz, "Sizing of stand-alone photovoltaic/wind/diesel system with battery and fuel cell storage devices by harmony search algorithm," *J. Energy Storage*, vol. 2, pp. 30–42, 2015.

[89] S. Singh, M. Singh, and S. C. Kaushik, "Feasibility study of an islanded microgrid in rural area consisting of PV, wind, biomass and battery energy storage system," *Energy Convers. Manag.*, vol. 128, pp. 178–190, 2016.

[90] A. Fetanat and E. Khorasaninejad, "Size optimization for hybrid photovoltaic-wind energy system using ant colony optimization for continuous domains based integer programming," *Appl. Soft Comput. J.*, vol. 31, pp. 196–209, 2015.

[91] M. Kefayat, A. Lashkar Ara, and S. A. Nabavi Niaki, "A hybrid of ant colony optimization and artificial bee colony algorithm for probabilistic optimal placement and sizing of

distributed energy resources," *Energy Convers. Manag.*, vol. 92, pp. 149–161, 2015.

[92] A. L. Bukar, C. W. Tan, and K. Y. Lau, "Optimal sizing of an autonomous photovoltaic/wind/battery/diesel generator microgrid using grasshopper optimization algorithm," *Sol. Energy*, vol. 188, pp. 685–696, 2019.

[93] M. Tolba, H. Rezk, A. A. Z. Diab, and M. Al-Dhaifallah, "A Novel Robust Methodology Based Salp Swarm Algorithm for Allocation and Capacity of Renewable Distributed Generators on Distribution Grids," *Energies*, vol. 11, no. 10, p. 2556, 2018.

[94] E. S. Ali, S. M. Abd Elazim, and A. Y. Abdelaziz, "Optimal allocation and sizing of renewable distributed generation using ant lion optimization algorithm," *Electr. Eng.*, vol. 100, no. 1, pp. 99–109, 2018.

[95] D. H. Wolpert and W. G. Macready, "No free lunch theorems for optimization," *IEEE Trans. Evol. Comput.*, vol. 1, no. 1, pp. 67–82, 1997.

[96] S. Obara, R. Hamanaka, and A. G. El-Sayed, "Design methods for microgrids to address seasonal energy availability–A case study of proposed Showa Antarctic Station retrofits," *Appl. Energy*, vol. 236, pp. 711–727, 2019.

[97] Y. T. Kao and E. Zahara, "A hybrid genetic algorithm and particle swarm optimization for multimodal functions," *Appl. Soft Comput. J.*, vol. 8, no. 2, pp. 849–857, 2008.

[98] M. Dorigo, G. D. Di Caro, and L. Gambardella, "Ant Colony Optimization: A New Meta-Heuristic," *Proc. Congr. Evol. Comput.*, vol. 2, pp. 1470–1477, 1999.

[99] P. Ganeshkumar, C. Rani, D. Devaraj, and T. Aruldoss Albert Victoire, "Hybrid ant bee algorithm for fuzzy expert system based sample classification," *IEEE/ACM Trans. Comput. Biol. Bioinforma.*, vol. 11, no. 2, pp. 347–360, 2014.

[100] S. Mirjalili, "The ant lion optimizer," *Adv. Eng. Softw.*, vol. 83, pp. 80–98, 2015.

[101] M. Mahdavi, M. Fesanghary, and E. Damangir, "An improved harmony search algorithm for solving optimization problems," *Appl. Math. Comput.*, vol. 188, no. 2, pp. 1567–1579, 2007.

[102] O. K. Erol and I. Eksin, "A new optimization method: Big Bang-Big Crunch," *Adv. Eng. Softw.*, vol. 37, no. 2, pp. 106–111, 2006.

[103] S. Mirjalili, "Moth-flame optimization algorithm: A novel nature-inspired heuristic paradigm," *Knowledge-Based Syst.*, vol. 89, pp. 228–249, 2015.

[104] S. Mirjalili, "SCA: A Sine Cosine Algorithm for solving optimization problems," *Knowledge-Based Syst.*, vol. 96, pp. 120–133, 2016.

[105] S. Mirjalili, S. M. Mirjalili, and A. Hatamlou, "Multi-Verse Optimizer: a nature-inspired algorithm for global optimization," *Neural Comput. Appl.*, vol. 27, no. 2, pp. 495–513, 2016.

[106] A. Kaveh and T. Bakhshpoori, "Water Evaporation Optimization: A novel physically inspired optimization algorithm," *Comput. Struct.*, vol. 167, pp. 69–85, 2016.

[107] S. Mirjalili, S. M. Mirjalili, and A. Lewis, "Grey Wolf Optimizer," *Adv. Eng. Softw.*, vol. 69, pp. 46–61, 2014.

[108] X.-S. Yang and S. Deb, "Engineering Optimisation by Cuckoo Search," *Int. J. Math. Model. Numer. Optim.*, vol. 1, no. 4, pp. 330–343, 2010.

[109] S. Mirjalili, A. H. Gandomi, S. Z. Mirjalili, S. Saremi, H. Faris, and S. M. Mirjalili, "Salp Swarm Algorithm: A bio-inspired optimizer for engineering design problems," *Adv. Eng. Softw.*, vol. 114, pp. 163–191, 2017.

[110] S. Saremi, S. Mirjalili, and A. Lewis, "Grasshopper Optimisation Algorithm: Theory and application," *Adv. Eng. Softw.*, vol. 105, pp. 30–47, 2017.

[111] S. Mirjalili, "Dragonfly algorithm: a new meta-heuristic optimization technique for solving single-objective, discrete, and multi-objective problems," *Neural Comput. Appl.*, vol. 27, no. 4, pp. 1053–1073, 2016.

[112] X.-S. Yang, "A new metaheuristic bat-inspired algorithm," in *Nature inspired cooperative*

*strategies for optimization NISCO 2010, studies in computational intelligence, vol. 284*, J. R. Gonzalez and E. Al., Eds. Berlin: Springer, 2010, pp. 65–74.

[113] X.-S. Yang, *Nature-inspired metaheuristic algorithms*. Luniver Press, 2008.

[114] C. Li *et al.*, "Evaluation of wind energy resource and wind turbine characteristics at two locations in China," *Technol. Soc.*, vol. 47, pp. 121–128, 2016.

[115] M. H. Amrollahi and S. M. T. Bathaee, "Techno-economic optimization of hybrid photovoltaic/wind generation together with energy storage system in a stand-alone micro-grid subjected to demand response," *Appl. Energy*, vol. 202, pp. 66–77, 2017.

[116] M. M. V. Leme, M. H. Rocha, E. E. S. Lora, O. J. Venturini, B. M. Lopes, and C. H. Ferreira, "Techno-economic analysis and environmental impact assessment of energy recovery from Municipal Solid Waste (MSW) in Brazil," *Resour. Conserv. Recycl.*, vol. 87, pp. 8–20, 2014.

[117] L. Xu, X. Ruan, C. Mao, B. Zhang, and Y. Luo, "An Improved Optimal Sizing Method for Wind-Solar-Battery Hybrid Power System," *IEEE Trans. Sustain. Energy*, vol. 4, no. 3, pp. 774–785, 2013.

[118] Eaton Corporation. XLR-48 Supercapacitor, Feb. 2019, Technical Data 10510. [Online]. Available: https://datasheet.octopart.com/XLR-48R6167-R-Eaton-datasheet-130052459.pdf [Accessed: 21-May-2020].

[119] F. Xu, J. Liu, S. Lin, Q. Dai, and C. Li, "A multi-objective optimization model of hybrid energy storage system for non-grid-connected wind power: A case study in China," *Energy*, vol. 163, pp. 585–603, 2018.

[120] H-TEC Systems. The core of electrolysis: PEM electrolyser stacks – Designed for ideal integration in systems, 2019, H-TEC Series-S: S 30/30. [Online]. Available: https://www.h-tec-systems.com/fileadmin/Content/PDFs/19022019/H-TEC_SYSTEMS_Datenblatt_Stacks_SE30_30_EN.PDF [Accessed: 21-May-2020].

[121] Ballard Power Systems Inc. FCgen–1020ACS, 2015, SPC5101559-0H. [Online]. Available: https://www.ballard.com/docs/default-source/spec-sheets/fcgen-1020-acs-v2.pdf?sfvrsn=c3ebc380_4 [Accessed: 21-May-2020].

[122] S. M. Hakimi and S. M. Moghaddas-Tafreshi, "Optimal sizing of a stand-alone hybrid power system via particle swarm optimization for Kahnouj area in south-east of Iran," *Renew. Energy*, vol. 34, no. 7, pp. 1855–1862, 2009.

[123] T. Hübert, L. Boon-Brett, and W. Buttner, *Sensors for safety and process control in hydrogen technologies*. CRC Press, 2016.

[124] J. D. T. Graham, A. J. Mulvenna, W. E. Mufford, J. G. Borck, J. Ko, and M. A. M. Harper, "Hydrogen fueling station," Google Patents, 02-Nov-2004.

[125] H. Takagi, *Queueing analysis: a foundation of performance evaluation*, vol. 1. North-Holland Amsterdam, 1991.

[126] U. Mukherjee *et al.*, "Techno-economic, environmental, and safety assessment of hydrogen powered community microgrids; case study in Canada," *Int. J. Hydrogen Energy*, vol. 42, no. 20, pp. 14333–14349, 2017.

[127] G. Dispenza *et al.*, "Development of a solar powered hydrogen fueling station in smart cities applications," *Int. J. Hydrogen Energy*, vol. 42, no. 46, pp. 27884–27893, 2017.

[128] C. He, H. Sun, Y. Xu, and S. Lv, "Hydrogen refueling station siting of expressway based on the optimization of hydrogen life cycle cost," *Int. J. Hydrogen Energy*, vol. 42, no. 26, pp. 16313–16324, 2017.

[129] F. Grüger, L. Dylewski, M. Robinius, and D. Stolten, "Carsharing with fuel cell vehicles: Sizing hydrogen refueling stations based on refueling behavior," *Appl. Energy*, vol. 228, pp. 1540–1549, 2018.

[130] Pure Energy Centre Limited. Hydrogen fueling station, 2019. [Online]. Available: https://pureenergycentre.com/hydrogen-fueling-station/ [Accessed: 21-May-2020].

[131] Anonymous. Hydrogenesis Passenger Ferry. [Online]. Available: https://www.ship-technology.com/projects/hydrogenesis-passenger-ferry/ [Accessed: 21-May-2020].

[132] S. M. Moghaddas-Tafreshi, S. Mohseni, M. E. Karami, and S. Kelly, "Optimal energy management of a grid-connected multiple energy carrier micro-grid," *Appl. Therm. Eng.*, vol. 152, pp. 796–806, 2019.

[133] H. Qin and J. W. Kimball, "Solid-state transformer architecture using AC-AC dual-active-bridge converter," *IEEE Trans. Ind. Electron.*, vol. 60, no. 9, pp. 3720–3730, 2013.

[134] Canadian Solar Inc. CS6K-270|275|280P, 2017, PV Module Product Datasheet V5.552_EN. [Online]. Available: https://www.collectiu-solar.cat/pdf/2-Panel-Canadian_Solar-Datasheet-CS6K.pdf [Accessed: 21-May-2020].

[135] M. R. Patel, *Wind and solar power systems: design, analysis, and operation*. CRC Press, 2005.

[136] Meteonorm. Bern, Switzerland: Genossenschaft Meteotest; 2018. Version 7.3.0.

[137] Sunceo Hydro. XJ50-100SCTF6-Z, 2015. [Online]. Available: https://www.micro-hydro-power.com/100kw-hydro-turbine-generator/ [Accessed: 21-May-2020].

[138] M. T. Gatte and R. A. Kadhim, "Hydro power," *Energy Conserv.*, vol. 9, no. 51000, pp. 95–124, 2012.

[139] Anonymous, "New Holland's NH2 fuel cell powered tractor to enter service," *Fuel Cells Bull.*, vol. 2012, no. 1, pp. 3–4, 2012.

[140] Anonymous, "Hyundai and H2 Energy to launch world's first fleet of Fuel Cell Truck," 2018.

[141] C. Brunetto and G. Tina, "Optimal hydrogen storage sizing for wind power plants in day ahead electricity market," *IET Renew. Power Gener.*, vol. 1, no. 4, pp. 220–226, 2007.

[142] AWS HC Wind Turbine – Performance Series. [Online]. Available: https://80349778-823f-498f-9402-994883b1a929.filesusr.com/ugd/3830e3_1e1e44ed6ca14fa29155b9c81feaaa81.pdf [Accessed: 21-May-2020].

[143] R. Kaiser, "Optimized battery-management system to improve storage lifetime in renewable energy systems," *J. Power Sources*, vol. 168, no. 1, pp. 58–65, 2007.

[144] Y. Shi, B. Xu, Y. Tan, and B. Zhang, "A convex cycle-based degradation model for battery energy storage planning and operation," *2018 Annual American Control Conference (ACC)*, 2018, pp. 4590–4596.

[145] MathWorks®, *Rainflow counts for fatigue analysis*. [Online]. Available: https://au.mathworks.com/help/signal/ref/rainflow.html [Accessed: 21-May-2020].

[146] Y. Wang *et al.*, "Research on capacity planning and optimization of regional integrated energy system based on hybrid energy storage system," *Appl. Therm. Eng.*, vol. 180, p. 115834, 2020.

[147] F. F. Nerini, O. Broad, D. Mentis, M. Welsch, M. Bazilian, and M. Howells, "A cost comparison of technology approaches for improving access to electricity services," *Energy*, vol. 95, pp. 255–265, 2016.

[148] D. Gandini and A. T. de Almeida, "Direct current microgrids based on solar power systems and storage optimization, as a tool for cost-effective rural electrification," *Renew. Energy*, vol. 111, pp. 275–283, 2017.

[149] My Solar Quotes. Solar Battery Storage – Product Comparison, 2020. [Online]. Available: https://www.mysolarquotes.co.nz/about-solar-power/residential/solar-battery-storage---product-comparison/ [Accessed: 21-May-2020].

[150] A. C. Duman and Ö. Güler, "Techno-economic analysis of off-grid PV/wind/fuel cell hybrid system combinations with a comparison of regularly and seasonally occupied households," *Sustain. Cities Soc.*, vol. 42, pp. 107–126, 2018.

[151] L. Viktorsson, J. T. Heinonen, J. B. Skulason, and R. Unnthorsson, "A Step towards the Hydrogen Economy—A Life Cycle Cost Analysis of A Hydrogen Refueling Station," *Energies*, vol. 10, no. 6, p. 763, 2017.

[152] D. Thomas, O. Deblecker, and C. S. Ioakimidis, "Optimal design and techno-economic analysis of an autonomous small isolated microgrid aiming at high RES penetration," *Energy*, vol. 116, pp. 364–379, 2016.

[153] M. Soshinskaya, W. H. J. Crijns-Graus, J. van der Meer, and J. M. Guerrero, "Application of a microgrid with renewables for a water treatment plant," *Appl. Energy*, vol. 134, pp. 20–34, 2014.

[154] M. R. B. Khan, R. Jidin, J. Pasupuleti, and S. A. Shaaya, "Optimal combinations of PV, wind, micro-hydro and diesel systems for a seasonal load demand," *2014 IEEE International Conference on Power and Energy (PECon)*, 2014, pp. 171–176.

[155] A. Chauhan and R. P. Saini, "Techno-economic optimization based approach for energy management of a stand-alone integrated renewable energy system for remote areas of India," *Energy*, vol. 94, pp. 138–156, 2016.

[156] M. Naderi, S. Bahramara, Y. Khayat, and H. Bevrani, "Optimal planning in a developing industrial microgrid with sensitive loads," *Energy Reports*, vol. 3, pp. 124–134, 2017.

[157] S. Mohseni and S. M. Moghaddas-Tafreshi, "A multi-agent approach to optimal sizing of a combined heating and power microgrid," *arXiv Prepr.*, arXiv:1812.11076, 2018.

[158] Trading Economics. New Zealand − Real Interest Rate. [Online]. Available: https://tradingeconomics.com/new-zealand/real-interest-rate-percent-wb-data.html/ [Accessed: 21-May-2020].

[159] HOMER Energy, *Salvage Value*. [Online]. Available: https://www.homerenergy.com/products/pro/docs/latest/salvage_value.html [Accessed: 21-May-2020].

[160] D. Brigo and F. Mercurio, *Interest rate models−theory and practice: with smile, inflation and credit*. Springer Science & Business Media, 2007.

[161] HOMER Energy, *Generator Operational Life*. [Online]. Available: https://www.homerenergy.com/products/pro/docs/latest/generator_operational_life.html [Accessed: 21-May-2020].

[162] HOMER Energy, *Battery Bank Life*. [Online]. Available: https://www.homerenergy.com/products/pro/docs/latest/battery_bank_life.html [Accessed: 21-May-2020].

[163] E. Ofry and A. Braunstein, "The Loss of Power Supply Probability as a Technique for Designing Stand-Alone Solar Electrical (Photovoltaic) Systems," *IEEE Power Eng. Rev.*, vol. PER-3, no. 5, pp. 34–35, 1983.

[164] Y. Zhang, A. Lundblad, P. E. Campana, F. Benavente, and J. Yan, "Battery sizing and rule-based operation of grid-connected photovoltaic-battery system: A case study in Sweden," *Energy Convers. Manag.*, vol. 133, pp. 249–263, 2017.

[165] T. Ma, H. Yang, and L. Lu, "A feasibility study of a stand-alone hybrid solar–wind–battery system for a remote island," *Appl. Energy*, vol. 121, pp. 149–158, 2014.

[166] New Zealand Lifelines Council Members, "New Zealand Lifelines Infrastructure Vulnerability Assessment: Stage 1," 2017. [Online]. Available: https://www.civildefence.govt.nz/assets/Uploads/lifelines/National-Vulnerability-Assessment-Stage-1-September-2017.pdf [Accessed: 21-May-2020].

[167] CliFlo: New Zealand's national climate database. [Online]. Available: http://cliflo.niwa.co.nz/ [Retrieved: 9-Jan.-2020].

[168] B. Anderson, D. Eyers, R. Ford, D. G. Ocampo, R. Peniamina, J. Stephenson, K. Suomalainen, L. Wilcocks, and M. Jack. *New Zealand GREEN grid household electricity demand study 2014-2018*. Colchester, Essex: UK Data Service.

[169] The Electricity Market Information. *The New Zealand electricity authority's wholesale*

*database.* [Online]. Available: https://www.emi.ea.govt.nz/Wholesale/Reports/ [Retrieved: 9-Jan.-2020].

[170] MATLAB. Natick, MA: The MathWorks Inc; 2018. R2018b, Version 9.5.

[171] U.S. Energy Information Administration. *Levelized Cost and Levelized Avoided Cost of New Generation Resources in the Annual Energy Outlook 2020*.

[172] J. Aldersey-Williams and T. Rubert, "Levelised cost of energy – A theoretical justification and critical assessment," *Energy Policy*, vol. 124, pp. 169–179, 2019.

[173] I. Fisher, *The theory of interest, as determined by impatience to spend income and opportunity to invest it*. New York: Macmillan, 1930.

[174] D. L. Whitman and R. E. Terry, "Fundamentals of engineering economics and decision analysis," *Synth. Lect. Eng.*, vol. 7, no. 1, pp. 1–219, 2012.

[175] D. Fioriti, S. Pintus, G. Lutzemberger, and D. Poli, "Economic multi-objective approach to design off-grid microgrids: A support for business decision making," *Renew. Energy*, vol. 159, pp. 693–704, 2020.

[176] New Zealand's Ministry of Business Innovation & employment. *Quarterly survey of domestic electricity prices – nominal indicators on 15 August 2020*. [Online]. Available: https://www.mbie.govt.nz/assets/Uploads/qsdep-report-15aug2020.pdf [Accessed: 21-May-2020].

[177] Concept Economics Pty Ltd. *Hydrogen in New Zealand Report 1 – Summary*, 2019. [Online]. Available: http://www.concept.co.nz/uploads/2/5/5/4/25542442/h2_report1_summary_v4.pdf [Accessed: 21-May-2020].

[178] Concept Economics Pty Ltd. *Hydrogen in New Zealand Report 2 – Analysis*, 2019. [Online]. Available: https://www.concept.co.nz/uploads/1/2/8/3/128396759/h2_report2_analysis_v4.pdf [Accessed: 21-May-2020].

[179] A. P. Agalgaonkar, C. V. Dobariya, M. G. Kanabar, S. A. Khaparde, and S. V. Kulkarni, "Optimal sizing of distributed generators in MicroGrid," *2006 IEEE Power India Conf.*, 2005, pp. 901–908.

[180] Y. Cheng, N. Zhang, D. S. Kirschen, W. Huang, and C. Kang, "Planning multiple energy systems for low-carbon districts with high penetration of renewable energy: An empirical study in China," *Appl. Energy*, vol. 261, p. 114390, 2020.

[181] C. Dortans, M. W. Jack, B. Anderson, and J. Stephenson, "Lightening the load: quantifying the potential for energy-efficient lighting to reduce peaks in electricity demand," *Energy Effic.*, vol. 13, pp. 1105–1118, 2020.

[182] Y. Matsuo, S. Endo, Y. Nagatomi, Y. Shibata, R. Komiyama, and Y. Fujii, "Investigating the economics of the power sector under high penetration of variable renewable energies," *Appl. Energy*, vol. 267, p. 113956, 2020.

[183] M. Jin, W. Feng, P. Liu, C. Marnay, and C. Spanos, "MOD-DR: Microgrid optimal dispatch with demand response," *Appl. Energy*, vol. 187, pp. 758–776, 2017.

[184] W. Huang, N. Zhang, C. Kang, M. Li, and M. Huo, "From demand response to integrated demand response: review and prospect of research and application," *Prot. Control Mod. Power Syst.*, vol. 4, no. 1, p. 12, 2019.

[185] H. Hui, Y. Ding, Q. Shi, F. Li, Y. Song, and J. Yan, "5G network-based Internet of Things for demand response in smart grid: A survey on application potential," *Appl. Energy*, vol. 257, p. 113972, 2020.

[186] E. Koliou, C. Eid, J. P. Chaves-Ávila, and R. A. Hakvoort, "Demand response in liberalized electricity markets: Analysis of aggregated load participation in the German balancing mechanism," *Energy*, vol. 71, pp. 245–254, 2014.

[187] A. Obermeier, C. Windmeier, E. Esche, and J.-U. Repke, "A Discrete-time Scheduling Model for Continuous Power-intensive Processes Considering Fatigue of Equipment," *28*

*European Symposium on Computer Aided Process Engineering*, vol. 43, A. Friedl, J. J. Klemeš, S. Radl, P. S. Varbanov, and T. B. Wallek, Eds. Elsevier, 2018, pp. 955–960.

[188] S. Abapour, B. Mohammadi-Ivatloo, and M. Tarafdar Hagh, "Robust bidding strategy for demand response aggregators in electricity market based on game theory," *J. Clean. Prod.*, vol. 243, p. 118393, 2020.

[189] Y. Chen, W. S. Lin, F. Han, Y.-H. Yang, Z. Safar, and K. J. R. Liu, "Incentive compatible demand response games for distributed load prediction in smart grids," *APSIPA Trans. Signal Inf. Process.*, vol. 3, 2014.

[190] U.S. Department of Energy, "*Benefits of Demand Response in Electricity Markets and Recommendations for Achieving Them*," A report to the United States congress pursuant to Section 1252 of the Energy Policy Act 2005, 2006.

[191] A. C. Chapman, G. Verbič, and D. J. Hill, "A healthy dose of reality for game-theoretic approaches to residential demand response," *2013 IREP Symposium Bulk Power System Dynamics and Control-IX Optimization, Security and Control of the Emerging Power Grid*, 2013, pp. 1–13.

[192] T. Roughgarden, "Algorithmic game theory," *Commun. ACM*, vol. 53, no. 7, pp. 78–86, 2010.

[193] N. Nisan and A. Ronen, "Algorithmic mechanism design," *Games Econ. Behav.*, vol. 35, no. 1–2, pp. 166–196, 2001.

[194] M. O. Jackson, "Mechanism theory," *MIT Press*, 2000.

[195] M. J. Morey, "*Power Market Auction Design: Rules and Lessons In Market-based Control for the New Electricity Industry*," Edison Electric Institute (EII), 2001.

[196] M. Yu and S. H. Hong, "Incentive-based demand response considering hierarchical electricity market: A Stackelberg game approach," *Appl. Energy*, vol. 203, pp. 267–279, 2017.

[197] J. Wang, H. Zhong, Z. Ma, Q. Xia, and C. Kang, "Review and prospect of integrated demand response in the multi-energy system," *Appl. Energy*, vol. 202, pp. 772–782, 2017.

[198] Y. Chen, P. Xu, J. Gu, F. Schmidt, and W. Li, "Measures to improve energy demand flexibility in buildings for demand response (DR): A review," *Energy Build.*, vol. 177, pp. 125–139, 2018.

[199] J. Von Neumann and O. Morgenstern, *Theory of games and economic behavior (commemorative edition)*. Princeton University Press, 2007.

[200] H. Ren *et al.*, "Optimal scheduling of an EV aggregator for demand response considering triple level benefits of three-parties," *Int. J. Electr. Power Energy Syst.*, vol. 125, p. 106447, 2021.

[201] İ. Şengör, A. Çiçek, A. K. Erenoğlu, O. Erdinç, and J. P. S. Catalão, "User-comfort oriented optimal bidding strategy of an electric vehicle aggregator in day-ahead and reserve markets," *Int. J. Electr. Power Energy Syst.*, vol. 122, p. 106194, 2020.

[202] H. Zhong, L. Xie, and Q. Xia, "Coupon incentive-based demand response: Theory and case study," *IEEE Trans. Power Syst.*, vol. 28, no. 2, pp. 1266–1276, 2012.

[203] S. O. Sobhani, S. Sheykhha, and R. Madlener, "An integrated two-level demand-side management game applied to smart energy hubs with storage," *Energy*, vol. 206, p. 118017, 2020.

[204] C. Feng, Z. Li, M. Shahidehpour, F. Wen, and Q. Li, "Stackelberg game based transactive pricing for optimal demand response in power distribution systems," *Int. J. Electr. Power Energy Syst.*, vol. 118, p. 105764, 2020.

[205] J. Vuelvas, F. Ruiz, and G. Gruosso, "Limiting gaming opportunities on incentive-based demand response programs," *Appl. Energy*, vol. 225, pp. 668–681, 2018.

[206] A. S. Gazafroudi, M. Shafie-Khah, F. Prieto-Castrillo, J. M. Corchado, and J. P. S. Catalão, "Monopolistic and Game-based Approaches to Transact Energy Flexibility," *IEEE Trans.*

*Power Syst.*, vol. 35, no. 2, pp. 1075–1084, 2019.

[207] Y. Li, C. Wang, G. Li, and C. Chen, "Optimal scheduling of integrated demand response-enabled integrated energy systems with uncertain renewable generations: a Stackelberg game approach," *Energy Convers. Manag.*, vol. 235, p. 113996, 2021.

[208] J. Niu, Z. Tian, J. Zhu, and L. Yue, "Implementation of a price-driven demand response in a distributed energy system with multi-energy flexibility measures," *Energy Convers. Manag.*, vol. 208, p. 112575, 2020.

[209] A. Ihsan, M. Jeppesen, and M. J. Brear, "Impact of demand response on the optimal, techno-economic performance of a hybrid, renewable energy power plant," *Appl. Energy*, vol. 238, pp. 972–984, 2019.

[210] A. Modarresi Ghazvini and J. Olamaei, "Optimal sizing of autonomous hybrid PV system with considerations for V2G parking lot as controllable load based on a heuristic optimization algorithm," *Sol. Energy*, vol. 184, pp. 30–39, 2019.

[211] Z. Jing, J. Zhu, and R. Hu, "Sizing optimization for island microgrid with pumped storage system considering demand response," *J. Mod. Power Syst. Clean Energy*, vol. 6, no. 4, pp. 791–801, 2018.

[212] H. Kim, J. Bae, S. Baek, D. Nam, H. Cho, and H. J. Chang, "Comparative Analysis between the Government Micro-Grid Plan and Computer Simulation Results Based on Real Data: The Practical Case for a South Korean Island," *Sustainability*, vol. 9, no. 2, 2017.

[213] V. Amir and M. Azimian, "Dynamic Multi-Carrier Microgrid Deployment Under Uncertainty," *Appl. Energy*, vol. 260, p. 114293, 2020.

[214] L. Gelazanskas and K. A. A. Gamage, "Demand side management in smart grid: A review and proposals for future direction," *Sustain. Cities Soc.*, vol. 11, pp. 22–30, 2014.

[215] H. T. Haider, O. H. See, and W. Elmenreich, "A review of residential demand response of smart grid," *Renew. Sustain. Energy Rev.*, vol. 59, pp. 166–178, 2016.

[216] B. P. Esther and K. S. Kumar, "A survey on residential Demand Side Management architecture, approaches, optimization models and methods," *Renew. Sustain. Energy Rev.*, vol. 59, pp. 342–351, 2016.

[217] F. C. Robert, G. S. Sisodia, and S. Gopalan, "A critical review on the utilization of storage and demand response for the implementation of renewable energy microgrids," *Sustain. Cities Soc.*, vol. 40, pp. 735–745, 2018.

[218] M. Behrangrad, "A review of demand side management business models in the electricity market," *Renew. Sustain. Energy Rev.*, vol. 47, pp. 270–283, 2015.

[219] S. Kahrobaee, S. Asgarpoor, and W. Qiao, "Optimum sizing of distributed generation and storage capacity in smart households," *IEEE Trans. Smart Grid*, vol. 4, no. 4, pp. 1791–1801, 2013.

[220] L. Yu, Y. P. Li, G. H. Huang, and C. J. An, "A robust flexible-probabilistic programming method for planning municipal energy system with considering peak-electricity price and electric vehicle," *Energy Convers. Manag.*, vol. 137, pp. 97–112, 2017.

[221] F. Varasteh, M. S. Nazar, A. Heidari, M. Shafie-khah, and J. P. S. Catalão, "Distributed energy resource and network expansion planning of a CCHP based active microgrid considering demand response programs," *Energy*, vol. 172, pp. 79–105, 2019.

[222] G. Cardoso *et al.*, "Optimal investment and scheduling of distributed energy resources with uncertainty in electric vehicle driving schedules," *Energy*, vol. 64, pp. 17–30, 2013.

[223] H. Hosseinnia, D. Nazarpour, and V. Talavat, "Multi-objective optimization framework for optimal planning of the microgrid (MG) under employing demand response program (DRP)," *J. Ambient Intell. Humaniz. Comput.*, vol. 10, no. 7, pp. 2709–2730, 2019.

[224] S. M. Moghaddas-Tafreshi, M. Jafari, S. Mohseni, and S. Kelly, "Optimal operation of an energy hub considering the uncertainty associated with the power consumption of plug-in hybrid electric vehicles using information gap decision theory," *Int. J. Electr. Power Energy Syst.*, vol. 112, pp. 92–108, 2019.

[225] Ö. Okur, N. Voulis, P. Heijnen, and Z. Lukszo, "Aggregator-mediated demand response: Minimizing imbalances caused by uncertainty of solar generation," *Appl. Energy*, vol. 247, pp. 426–437, 2019.

[226] All Power Labs. Old PP20 vs New PP30 Cogen-CS: Technical Specifications & Comparisons, 2019, Rev 03. [Online]. Available: http://www.allpowerlabs.com/wp-content/uploads/2019/07/PP30-vs-PP20-Spec-Sheet-Public-2019-Rev-03-current-July-2019.pdf [Accessed: 4-Mar.-2020].

[227] R. Chen *et al.*, "Life cycle energy and greenhouse gas emission effects of biodiesel in the United States with induced land use change impacts," *Bioresour. Technol.*, vol. 251, pp. 249–258, 2018.

[228] O. Y. Ahmed, M. J. Ries, and W. F. Northrop, "Emissions factors from distributed, small-scale biomass gasification power generation: Comparison to open burning and large-scale biomass power generation," *Atmos. Environ.*, vol. 200, pp. 221–227, 2019.

[229] Interagency Working Group on Social Cost of Greenhouse Gases, United States Government, "*Technical Support Document: Technical Update of the Social Cost of Carbon for Regulatory Impact Analysis Under Executive Order 12866*," The August 2016 revision of the 2013 Technical Support Document on the Social Cost of Carbon. [Online]. Available: https://www.epa.gov/sites/production/files/2016-12/documents/sc_co2_tsd_august_2016.pdf [Accessed: 4-Mar.-2020].

[230] Leonics Co. Apollo GTP-500, 2018, P.LEN.BRO.INV.156 Rev. 12.00. [Online]. Available: http://www.leonics.com/product/renewable/inverter/dl/GTP-500-156.pdf [Accessed: 4-Mar.-2020].

[231] A. S. Jacob, R. Banerjee, and P. C. Ghosh, "Sizing of hybrid energy storage system for a PV based microgrid through design space approach," *Appl. Energy*, vol. 212, pp. 640–653, 2018.

[232] F. Mazda, *Telecommunications engineer's reference book*, Focal Press, 2013.

[233] CellCube Energy Storage Systems Inc. Use your own power grid: Intelligent storage systems based on vanadium redox flow technology, 2018, D6144/0714ND3. [Online]. Available: https://static1.squarespace.com/static/5b1198ada2772c6585959926/t/5b57363f88251b71261fc4a1/1532442177499/CellCube+-+Use+Your+Own+Power+Grid.pdf [Accessed: 4-Mar.-2020].

[234] C. B. Robledo, V. Oldenbroek, F. Abbruzzese, and A. J. M. van Wijk, "Integrating a hydrogen fuel cell electric vehicle with vehicle-to-grid technology, photovoltaic power and a residential building," *Appl. Energy*, vol. 215, pp. 615–629, 2018.

[235] Anonymous, "Riversimple Rasa two-seater FCEV unveiled, 20-car trial this year," Fuel Cells Bull., vol. 2016, no. 3, p. 2, 2016.

[236] Riversimple. Designing the Rasa, 2017. [Online]. Available: https://www.riversimple.com/the-design-of-the-rasa/ [Accessed: 4-Mar.-2020].

[237] Alstom. Ecotècnia ECO 48/750 Datasheet, Aug. 2014. [Online]. Available: https://en.wind-turbine-models.com/turbines/791-ecot-cnia-eco-48-750#datasheet/ [Accessed: 21-May-2020].

[238] V. Oldenbroek, G. Smink, T. Salet, and A. J. M. van Wijk, "Fuel cell electric vehicle as a power plant: Techno-economic scenario analysis of a renewable integrated transportation and energy system for smart cities in two climates," *Appl. Sci.*, vol. 10, no. 1, 2020.

[239] V. Oldenbroek, V. Hamoen, S. Alva, C. B. Robledo, L. A. Verhoef, and A. J. M. van Wijk, "Fuel Cell Electric Vehicle-to-Grid: Experimental Feasibility and Operational Performance as Balancing Power Plant," *Fuel Cells*, vol. 18, no. 5, pp. 649–662, 2018.

[240] S. S. Farahani, R. van der Veen, V. Oldenbroek, F. Alavi, E. H. P. Lee, N. van de Wouw et al., "A hydrogen-based integrated energy and transport system: The design and analysis of the car as power plant concept," *IEEE Trans. Syst. Man. Cybern. Mag.*, vol. 5, no. 1, pp. 37–50, 2019.

[241] D. M. Steward, "*Critical Elements of Vehicle-to-Grid (V2G) Economics*," No. NREL/TP-5400-69017, National Renewable Energy Lab (NREL), Golden, CO, USA, 2017.

[242] T. Basar and G. J. Olsder, "Dynamic noncooperative game theory," *Classics in Applied Mathematics*, revised SIAM Classics Edition, vol. 23, 1999.

[243] E. Pacuit and O. Roy, *Epistemic foundations of game theory*. The Stanford Encyclopedia of Philosophy (Summer 2017 Edition), Edward N. Zalta, Ed. [Online]. Available: https://seop.illc.uva.nl/entries/epistemic-game/ [Accessed: 4-Mar.-2020].

[244] K. Madani and J. R. Lund, "A Monte-Carlo game theoretic approach for Multi-Criteria Decision Making under uncertainty," *Adv. Water Resour.*, vol. 34, no. 5, pp. 607–616, May 2011.

[245] H. von Stackelberg, *Marktform und gleichgewicht*. Springer, 1934. Eng. transl. H. v. Stackelberg, *Theory of the market economy*. Oxford University Press, 1952.

[246] S. Jørgensen, S.-P. Sigue, and G. Zaccour, "Stackelberg leadership in a marketing channel," *Int. Game Theory Rev.*, vol. 3, no. 01, pp. 13–26, 2001.

[247] R. S. Gibbons, *Game theory for applied economists*. Princeton University Press, 1992.

[248] M. Fahrioglu and F. L. Alvarado, "Designing incentive compatible contracts for effective demand management," *IEEE Trans. Power Syst.*, vol. 15, no. 4, pp. 1255–1260, 2000.

[249] M. Fahrioglu and F. L. Alvarado, "Using utility information to calibrate customer demand management behavior models," *IEEE Trans. Power Syst.*, vol. 16, no. 2, pp. 317–322, 2001.

[250] R. Stafford, "Random vectors with fixed sum," MATLAB Central File Exchange, 2006. [Online]. Available: https://au.mathworks.com/matlabcentral/fileexchange/9700-random-vectors-with-fixed-sum/ [Accessed: 4-Aug.-2020].

[251] S. Chowdhury, J. Zhang, and A. Messac, "Avoiding premature convergence in a mixed-discrete particle swarm optimization (MDPSO) algorithm," *53rd AIAA/ASME/ASCE/AHS/ASC Structures, Structural Dynamics and Materials Conference 20th AIAA/ASME/AHS Adaptive Structures Conference 14th AIAA*, 2012, p. 1678.

[252] Anonymous, *Ohakune Useful Information*. 2011. [Online]. Available: http://www.visitohakune.co.nz/page/ohakune-useful-information/12/ [Accessed: 4-Mar.-2020].

[253] National Institute of Water and Atmospheric Research (NIWA), *Statistical analysis of river flow data in the Horizons Region*, NIWA Client Report: CHC2006-154. [Online]. Available: https://www.horizons.govt.nz/HRC/media/Media/One%20Plan%20Documents/Statistical-analysis-of-river_ta-in-the-Horizons-Region.pdf?ext=.pdf [Accessed: 4-Mar.-2020].

[254] E. Jarvis, *Understanding Microgrid Categories and Business Models*. 2017. [Online]. Available: https://blog.se.com/renewable-energy/2017/12/15/understanding-microgrid-categories-business-models/ [Accessed: 4-Aug.-2020].

[255] Environmental Protection Authority, *Summary and Analysis – Carrots and Parsnips*. No. APP201045, 2012. [Online]. Available: https://www.epa.govt.nz/assets/FileAPI/hsno-ar/APP201045/fb604d3064/APP201045-Summary-and-Analysis-Carrot-and-Parsnip.pdf [Accessed: 4-Mar.-2020].

[256] P. Hall and M. Jack, *Bioenergy options for New Zealand – Analysis of large-scale bioenergy from forestry*. No. 1124-2019-3124, Scion – Next Generation Biomaterials, 2009. [Online]. Available: https://niwa.co.nz/sites/niwa.co.nz/files/imported/__data/assets/pdf_file/0007/95668/Large-scale-forestry-for-bioenergy.pdf [Accessed: 4-Mar.-2020].

[257] J. Anderson, "Pulling the Plug on Network Congestion," B.A. dissertation, Department of Economics, University of Otago, Dunedin, New Zealand, 2009.

[258] New Zealand's Ministry of Business, Innovation, and Employment. *Energy in New Zealand 19.* [Online]. Available: https://www.mbie.govt.nz/dmsdocument/7040-energy-in-new-zealand-2019/ [Accessed: 4-Aug.-2020].

[259] B. Anderson, *NZ GREEN Grid Household Electricity Demand Data: EECA Data Analysis*

*(Part C) Upscaling Advice Report v1.0*, 2019.

[260] EU SCIENCE HUB, *Individual mobility: From conventional to electric cars*, 2015. [Online]. Available: https://ec.europa.eu/jrc/en/publication/eur-scientific-and-technical-research-reports/individual-mobility-conventional-electric-cars/ [Accessed: 4-Aug.-2020].

[261] B. Anderson, R. Parker, D. Myall, H. Moller, and M. Jack, "Will flipping the fleet f**k the grid?," *7th IAEE Asia-Oceania Conference*, 2020, pp. 1–8.

[262] New Zealand's Ministry of Transport, *New Zealand Household Travel Survey 2010-2013*, 2014. [Online]. Available: https://www.transport.govt.nz/assets/Uploads/Research/Documents/Drivers-2014-y911-Final-v3.pdf [Accessed: 4-Aug.-2020].

[263] O. Tayan, Y. M. Alginahi, M. N. Kabir, and A. M. Al Binali, "Analysis of a Transportation System With Correlated Network Intersections: A Case Study for a Central Urban City With High Seasonal Fluctuation Trends," *IEEE Access*, vol. 5, pp. 7619–7635, 2017.

[264] Electricity Authority, *Investigation into the Value of Lost Load in New Zealand – Report on methodology and key findings*, 2013. [Online]. Available: https://www.ea.govt.nz/dmsdocument/15385-electricity-authority-investigation-into-the-value-of-lost-load-in-new-zealand-report-on-methodology-and-key-findings-23-july-2013 [Accessed: 4-Aug.-2020].

[265] X. Xi and R. Sioshansi, "Using Price-Based Signals to Control Plug-in Electric Vehicle Fleet Charging," *IEEE Trans. Smart Grid*, vol. 5, no. 3, pp. 1451–1464, 2014.

[266] N. I. Nwulu and X. Xia, "Multi-objective dynamic economic emission dispatch of electric power generation integrated with game theory based demand response programs," *Energy Convers. Manag.*, vol. 89, pp. 963–974, 2015.

[267] N. I. Nwulu and X. Xia, "Implementing a model predictive control strategy on the dynamic economic emission dispatch problem with game theory based demand response programs," *Energy*, vol. 91, pp. 404–419, 2015.

[268] U.S. Energy Information Administration, *Annual Electric Power Industry Report, Form EIA-861 detailed data files*. [Online]. Available: https://www.eia.gov/electricity/data/eia861/ [Retrieved: 10-Feb.-2020].

[269] İ. Şengör, O. Erdinç, B. Yener, A. Taşcıkaraoğlu, and J. P. S. Catalão, "Optimal Energy Management of EV Parking Lots Under Peak Load Reduction Based DR Programs Considering Uncertainty," *IEEE Trans. Sustain. Energy*, vol. 10, no. 3, pp. 1034–1043, 2019.

[270] Concept Economics Pty Ltd, *Investigation of the value of unserved energy – Stage 1*. No. ABN 73 129 990 530, Prepared for Electricity Commission, 2008. [Online]. Available: https://www.researchgate.net/profile/Deb_Chattopadhyay/publication/322255908_Investigation_of_the_Value_of_Unserved_Energy/links/5a4e8ff5458515e71b085a3f/Investigation-of-the-Value-of-Unserved-Energy.pdf [Accessed: 19-Dec.-2020].

[271] V. Karkania, E. Fanara, and A. Zabaniotou, "Review of sustainable biomass pellets production - A study for agricultural residues pellets' market in Greece," *Renew. Sustain. Energy Rev.*, vol. 16, pp. 1426–1436, 2012.

[272] S. Mani, S. Sokhansanj, X. Bi, and A. Turhollow, "Economics of producing fuel pellets from biomass," *Appl. Eng. Agric.*, vol. 22, no. 3, pp. 421–426, 2006.

[273] H. R. Baghaee, M. Mirsalim, and G. B. Gharehpetian, "Multi-objective optimal power management and sizing of a reliable wind/PV microgrid with hydrogen energy storage using MOPSO," *J. Intell. Fuzzy Syst.*, vol. 32, no. 3, pp. 1753–1773, 2017.

[274] B. Li, R. Roche, D. Paire, and A. Miraoui, "Sizing of a stand-alone microgrid considering electric power, cooling/heating, hydrogen loads and hydrogen storage degradation," *Appl. Energy*, vol. 205, pp. 1244–1259, 2017.

[275] B. Kampman *et al.*, "BUBE: Better Use of Biomass for Energy - Background Report to the Position Paper of IEA RETD and IEA Bioenergy," *IEA RETD and IEA Bioenergy*, p. 151, 2010.

[276] S. Mohseni, A. C. Brent, and D. Burmester, "A Reliability-Oriented Cost Optimisation Method for Capacity Planning of a Multi-Carrier Micro-Grid: A Case Study of Stewart Island, New Zealand," *arXiv Prepr.*, arXiv:1906.09544, 2019.

[277] International Energy Agency. *The Future of Hydrogen – Seizing today's opportunities*. Tech Rep., 2019. [Online]. Available: https://www.iea.org/reports/the-future-of-hydrogen/ [Accessed: 4-Mar.-2020].

[278] The Lines Company. *2018 Asset Management Plan*. Mar 2018. [Online]. Available: https://www.thelinescompany.co.nz/site/uploads/Disclosures/AssetManagementPlans/2018-Asset-Management-Plan.pdf [Accessed: 4-Mar.-2020].

[279] T. Ersal *et al.*, "Coupling between component sizing and regulation capability in microgrids," *IEEE Trans. Smart Grid*, vol. 4, no. 3, pp. 1576–1585, 2013.

[280] K. P. Kumar and B. Saravanan, "Recent techniques to model uncertainties in power generation from renewable energy sources and loads in microgrids – A review," *Renew. Sustain. Energy Rev.*, vol. 71, pp. 348–358, 2017.

[281] Y. Lu, S. Wang, C. Yan, and Z. Huang, "Robust optimal design of renewable energy system in nearly/net zero energy buildings under uncertainties," *Appl. Energy*, vol. 187, pp. 62–71, 2017.

[282] A. Ioannou, A. Angus, and F. Brennan, "Risk-based methods for sustainable energy system planning: A review," *Renew. Sustain. Energy Rev.*, vol. 74, pp. 602–615, 2017.

[283] S. Abedi, A. Alimardani, G. B. Gharehpetian, G. H. Riahy, and S. H. Hosseinian, "A comprehensive method for optimal power management and design of hybrid RES-based autonomous energy systems," *Renew. Sustain. Energy Rev.*, vol. 16, no. 3, pp. 1577–1587, 2012.

[284] A. Ehsan and Q. Yang, "Optimal integration and planning of renewable distributed generation in the power distribution networks: A review of analytical techniques," *Appl. Energy*, vol. 210, pp. 44–59, 2018.

[285] I. Farrance and R. Frenkel, "Uncertainty in measurement: a review of Monte Carlo simulation using Microsoft Excel for the calculation of uncertainties through functional relationships, including uncertainties in empirically derived constants," *Clin. Biochem. Rev.*, vol. 35, no. 1, p. 37, 2014.

[286] S. I. Sun, B. D. Smith, R. G. A. Wills, and A. F. Crossland, "Effects of time resolution on finances and self-consumption when modeling domestic PV-battery systems," *Energy Reports*, vol. 6, pp. 157–165, 2020.

[287] D. Wu, X. Ma, S. Huang, T. Fu, and P. Balducci, "Stochastic optimal sizing of distributed energy resources for a cost-effective and resilient Microgrid," *Energy*, vol. 198, p. 117284, 2020.

[288] H. Li, P. Liu, S. Guo, B. Ming, L. Cheng, and Z. Yang, "Long-term complementary operation of a large-scale hydro-photovoltaic hybrid power plant using explicit stochastic optimization," *Appl. Energy*, vol. 238, pp. 863–875, 2019.

[289] N. Lu, R. Diao, R. P. Hafen, N. Samaan, and Y. V Makarov, "A comparison of forecast error generators for modeling wind and load uncertainty," *2013 IEEE Power & Energy Society General Meeting*, 2013, pp. 1–5.

[290] Z. Qin, W. Li, and X. Xiong, "Incorporating multiple correlations among wind speeds, photovoltaic powers and bus loads in composite system reliability evaluation," *Appl. Energy*, vol. 110, pp. 285–294, 2013.

[291] E. Khmaladze, "Statistical analysis of electricity prices," *J. Data Sci.*, vol. 5, no. 1, pp. 103–129, 2007.

[292] D. Villanueva, A. E. Feijóo, and J. L. Pazos, "An analytical method to solve the probabilistic load flow considering load demand correlation using the DC load flow," *Electr. Power Syst. Res.*, vol. 110, pp. 1–8, 2014.

[293] B. S. Borowy and Z. M. Salameh, "Optimum photovoltaic array size for a hybrid wind/PV

system," *IEEE Trans. energy Convers.*, vol. 9, no. 3, pp. 482–488, 1994.

[294] P. D. Domanski and M. Gintrowski, "Alternative approaches to the prediction of electricity prices," *Int. J. Energy Sect. Manag.*, vol. 11, no. 1, pp. 3–27, 2017.

[295] H. Jeffreys, *The theory of probability*. OUP Oxford, 1998.

[296] F. McLoughlin, A. Duffy, and M. Conlon, "The generation of domestic electricity load profiles through Markov chain modelling," *Euro-Asian J. Sustain. Energy Dev. Policy*, vol. 3, p. 12, 2010.

[297] P. Lusis, K. R. Khalilpour, L. Andrew, and A. Liebman, "Short-term residential load forecasting: Impact of calendar effects and forecast granularity," *Appl. Energy*, vol. 205, pp. 654–669, 2017.

[298] C. Dortans, B. Anderson, M. Jack, and J. Stephenson, "*Estimating the Technical Potential for Residential Demand Response in New Zealand*," Renewable Energy and the Smart Grid (GREEN Grid) Technical Report, University of Otago, 2018.

[299] A. C. Miller and T. R. Rice, "Discrete approximations of probability distributions," *Manage. Sci.*, vol. 29, no. 3, pp. 352–362, 1983.

[300] R. Karuppiah, M. Martín, and I. E. Grossmann, "A simple heuristic for reducing the number of scenarios in two-stage stochastic programming," *Comput. Chem. Eng.*, vol. 34, no. 8, pp. 1246–1255, 2010.

[301] M. M. J. Opgenoord and K. E. Willcox, "Sensitivity analysis methods for uncertainty budgeting in system design," *AIAA J.*, vol. 54, no. 10, pp. 3134–3148, 2016.

[302] S. E. Ahmadi and N. Rezaei, "A new isolated renewable based multi microgrid optimal energy management system considering uncertainty and demand response," *Int. J. Electr. Power Energy Syst.*, vol. 118, p. 105760, 2020.

[303] A. J. Pimm, J. Palczewski, R. Morris, T. T. Cockerill, and P. G. Taylor, "Community energy storage: A case study in the UK using a linear programming method," *Energy Convers. Manag.*, vol. 205, p. 112388, 2020.

[304] A. Philpott and Z. Guan, "*Benchmarking wholesale hydroelectricity markets: 2017 update*," Technical report, Electric Power Optimization Centre, University of Auckland, 2020.

[305] L. Urbanucci and D. Testi, "Optimal integrated sizing and operation of a CHP system with Monte Carlo risk analysis for long-term uncertainty in energy demands," *Energy Convers. Manag.*, vol. 157, pp. 307–316, 2018.

[306] J. R. Birge and F. Louveaux, *Introduction to stochastic programming*. Springer Science & Business Media, 2011.

[307] G. C. Fox, "Parallel computing comes of age: Supercomputer level parallel computations at Caltech," *Concurr. Pract. Exp.*, vol. 1, no. 1, pp. 63–103, 1989.

[308] O. J. Guerra, "Beyond short-duration energy storage," *Nature Energy*, vol. 6, pp. 460–461, 2021.

[309] CSIRO, "*GenCost 2019-20: preliminary results for stakeholder review*," 2019. [Online]. Available: https://www.aemo.com.au/-/media/Files/Electricity/NEM/Planning_and_Forecasting/Inputs-Assumptions-Methodologies/2019/CSIRO-GenCost2019-20_DraftforReview.pdf [Accessed: 25-Jul.-2020].

[310] O. Schmidt, S. Melchior, A. Hawkes, and I. Staffell, "Projecting the future levelized cost of electricity storage technologies," *Joule*, vol. 3, no. 1, pp. 81–100, 2019.

[311] Solar Power New Zealand. *Solar Power Buy Back Rates New Zealand.* 2021. [Online]. Available: https://solar-power.co.nz/residential-solar-power-buy-back-rates-nz/ [Accessed: 25-Jul.-2020].

[312] Pacific Northwest National Laboratory, "*National Assessment of Energy Storage for Grid Balancing and Arbitrage: Phase 1. WECC*," Technical report PNNL-21388, Prepared for

the U.S. Department of Energy, 2012.

[313] K. Dopfer, J. Foster, and J. Potts, "Micro-meso-macro," *J. Evol. Econ.* vol. 14, pp. 263–729, 2004.

[314] N. G. Mankiw, *Principles of economics*. Cengage Learning, 2014.

[315] K. Høyland and S. W. Wallace, "Generating scenario trees for multistage decision problems," *Manage. Sci.*, vol. 47, no. 2, pp. 295–307, 2001.

[316] A. M. Mood, *Introduction to the Theory of Statistics*. McGraw-Hill, 1950.

[317] M. Shaw, "*Community batteries: a cost/benefit analysis*," Technical report, Research School of Chemistry, The Australian National University, 2020.

# Supplementary Material[1]

## Supplementary Material 1. Overview of the identified articles from the systematic literature review

Table SM1.1: Overview of the studies on the long-term, DR-integrated optimal planning and designing of RSESs (listed in chronological order).

| Ref. | Technologies in the candidate pool | Multi-temporal storage/ reserve allocation | DSM strategy | Responsive load sector(s) | Uncertain-ty treatment technique | Parametric uncertainty source(s) | Optimisa-tion algorithm | Decision criteria | Nested operational planning | Geographi-cal scope |
|---|---|---|---|---|---|---|---|---|---|---|
| [1] | Wind, non-renewables, main grid | × | ICSs | Residential | MCS | Renewable generation, load | GA | Economic | × | Town |
| [2] | Unspecified renewables, main grid | × | ICSs | Unspecified | PEM | Load demand | SP | Economic | × | Region |
| [3] | Wind, BESS, main grid | × | RTP | Residential | MCS | Renewable generation, load, wholesale prices | PSO | Economic | × | Building |
| [4] | Solar PV, solar thermal, BESS, | × | DLC | E-mobility | MCS | Load demand | MILP | Economic | ✓ | Neighbour-hood |

[1] As some of the materials do not form an essential part (core) of the thesis (compared to the ones featured in the main text) with regards to meeting the research aim and objectives – and can best be categorised as additional useful background information, as well as non-key results, which support and complement the main text – and in order to maintain a reasonable overall length of the thesis that complies with the maximum allowable word count, they are included in Supplementary Material.

| | | | | | | | | | | |
|---|---|---|---|---|---|---|---|---|---|---|
| | non-renewables, main grid | | | | | | | | | |
| [5] | Wind, solar PV, non-renewables, main grid | × | DLC | E-mobility | MCS | Renewable generation, load | NSGA-II | Economic, GHG emissions | × | City |
| [6] | Wind, solar PV, BESS, non-renewables, main grid | × | Demand bidding | Residential, commercial, industrial | MCS | Renewable generation | NLP | Economic | × | Town |
| [7] | Wind, non-renewables, main grid | × | ICSs | Residential | MCS | Renewable generation, load | Decomposi-tion-based analytics | Economic | × | Region |
| [8] | Solar PV, BESS, SC, main grid | ✓ | ICSs | Residential | Interval analysis | Renewable generation, load | PSO | Economic | × | Subdivision |
| [9] | Wind, main grid | × | ICSs | E-mobility | PEM | Renewable generation, wholesale prices | DP | Economic | × | Region |
| [10] | Wind, non-renewables, main grid | × | ICSs | E-mobility | MCS | Renewable generation | ABC | Economic | × | Region |
| [11] | Wind, non-renewables, main grid | × | RTP | Residential | MCS | Renewable generation, load, wholesale prices | SP | Economic | ✓ | Rural community |
| [12] | Wind, solar PV, main grid | × | ICSs | Residential | MCS | Renewable generation, load, wholesale prices | MILP | Economic | × | Rural community |

| | | | | | | | | | | |
|---|---|---|---|---|---|---|---|---|---|---|
| [13] | Solar PV, main grid | ✓ | CPP | Residential | MCS | Load demand | Ad-hoc peak load-based | Economic | × | Rural community |
| [14] | Unspecified renewables, main grid | × | ICSs | Unspecified | MCS | Load demand | LP | Economic | × | Generic |
| [15] | Wind, BESS, main grid | × | RTP | Unspecified | MCS | Renewable generation, load | SP | Economic | ✓ | City |
| [16] | Wind, solar PV, non-renewables, main grid | × | CPP | E-mobility | MCS | Load demand | RO | Economic | × | Region |
| [17] | Wind, BESS, non-renewables, main grid | × | ToU | Unspecified | MCS | Renewable generation, load | MINLP | Economic, reliability | × | Town |
| [18] | Wind, solar PV, non-renewables, main grid | × | ICSs | Unspecified | MCS | Renewable generation, load | DP | Economic | × | Region |
| [19] | Wind, solar PV, main grid | × | ICSs | Residential | Interval analysis | Renewable generation | SP | Economic | × | Neighbour-hood |
| [20] | Unspecified renewables, BESS, non-renewables, main grid | × | ToU | Unspecified | MCS | Load, wholesale prices | MIP | Economic | × | City |
| [21] | Wind, solar PV, BESS, non-renewables, main grid | × | ToU | Residential | MCS | Renewable generation, load | MILP | Economic, customer satisfaction | × | Town |
| [22] | Wind, solar PV, BESS, TS, bioenergy, non-renewables, main grid | × | ToU | Residential | MCS | Renewable generation | LP | Economic | ✓ | Rural community |

| | | | | | | | | | | |
|---|---|---|---|---|---|---|---|---|---|---|
| [23] | Wind, solar PV, BESS, hydro, bioenergy, geothermal, non-renewables, main grid | × | ToU | Residential | MCS | Economic parameters | Ad-hoc peak load-based | Economic | × | Rural community |
| [24] | Wind, solar PV, BESS, main grid | × | CPP | Undefined | PEM | Renewable generation, wholesale prices | RO | Economic | ✓ | Town |
| [25] | Solar PV, CHP, boiler, non-renewables, main grid | × | ToU | Residential | Interval analysis | Renewable generation, load | LP | Economic | ✓ | Subdivision |
| [26] | Solar PV, BESS, non-renewables, main grid | × | DLC | Commer-cial | Interval analysis | Renewable generation, load, wholesale prices | MILP | Economic | ✓ | Campus |
| [27] | Unspecified renewables, main grid | × | RTP | Unspecified | PEM | Renewable generation, load | MILP | Economic | × | Generic |
| [28] | Wind, solar PV, BESS, non-renewables, main grid | × | Demand bidding | Unspecified | MCS | Renewable generation | MILP | Economic | × | Region |
| [29] | Wind, solar PV, BESS, non-renewables, main grid | × | ICSs | Residential | MCS | Renewable generation, load | PSO | Economic | × | Town |
| [30] | Solar PV, BESS, non-renewables | × | DLC | Residential, e-mobility | CCM | Renewable generation, load | MINLP | Economic | ✓ | Remote community |

| | | | | | | | | | | |
|---|---|---|---|---|---|---|---|---|---|---|
| [31] | Wind, solar PV, BESS | × | RTP | Industrial, residential, commercial | MCS | Renewable generation, load | MINLP | Economic | × | Remote community |
| [32] | Solar PV, solar thermal, CHP, BESS, main grid | × | ICSs | Industrial, residential, commercial | MCS | Renewable generation, load | MILP | Economic, value-at-risk | ✓ | Neighbour-hood |
| [33] | Wind, solar PV, MT, BESS, main grid | × | ICSs | Industrial, residential | MCS | Renewable generation, load, wholesale prices | MILP | Economic | × | City |
| [34] | Wind, BESS, non-renewables, main grid | × | ToU | Residential | MCS | Renewable generation, load | MIP | Economic, reliability | × | Rural community |
| [35] | Wind, solar PV, PHS | × | ToU | Unspecified | MCS | Renewable generation | PSO | Economic | × | Region |
| [36] | Wind, solar PV, BESS, non-renewables, main grid | × | RTP | Residential | MCS | Renewable generation, load | MILP | Economic | ✓ | Building |
| [37] | Wind, solar PV, BESS | × | RTP-ICSs | Residential | MCS | Renewable generation | MILP | Economic | × | Remote community |
| [38] | Solar PV, CHP, BESS, TS, main grid | × | RTP-ICSs | Unspecified | MCS | Renewable generation, load, wholesale prices | NSGA-II | Economic, GHG emissions | ✓ | City |
| [39] | Solar PV, CHP, boiler, BESS, main grid | × | ToU | Unspecified | MCS | Renewable generation, load | MINLP | Economic | ✓ | Neighbour-hood |

| | | | | | | | | | | |
|---|---|---|---|---|---|---|---|---|---|---|
| [40] | Wind, CHP, boiler, BESS, TS, main grid | × | ToU | Unspecified | MCS | Renewable generation, load | MINLP | Economic | ✓ | Neighbour-hood |
| [41] | Wind, solar PV, BESS, TS, non-renewables, main grid | × | ICSs | Residential | Interval analysis | Renewable generation, load | NSGA-II | Economic, GHG emissions | ✓ | Town |
| [42] | Wind, CHP, main grid | × | RTP | Industrial, residential, commercial | MCS | Renewable generation, load | SP | Economic | ✓ | Town |

Key: ABC = Artificial Bee Colony, BESS = Battery Energy Storage System, CCM = Chance-Constrained Method, CHP = Combined Heat and Power, CPP = Critical Peak Pricing, DLC = Direct Load Control, DP = Dynamic Programming, DSM = Demand-Side Management, GA = Genetic Algorithm, GHG = Green-House Gas, ICSs = Interruptible/Curtailable Services, LP = Linear Programming, MCS = Monte Carlo Simulation, MILP = Mixed-Integer Linear Programming, MINLP = Mixed-Integer Nonlinear Programming, MIP = Mixed-Integer Programming, MT = Micro-Turbine, NLP = Nonlinear Programming, NSGA-II = Non-dominated Sorting Genetic Algorithm II, PEM = Point Estimate Method, PHS = Pumped Hydro Storage, PSO = Particle Swarm Optimisation, PV = Photovoltaic, RO = Robust Optimisation, RTP = Real-Time Pricing, SC = Super-Capacitor, SP = Stochastic Programming, ToU = Time-of-Use, TS = Thermal Storage.

# Supplementary Material 2. Detailed results of the customer-specific optimal DR provision

This supplementary material presents detailed results of the customer-specific optimal DR provision estimated by the proposed Stackelberg, non-cooperative game-theoretic, aggregator-mediated, incentive-driven DSM market framework tailored towards distributed sectoral interruptible DR flexibility resources for the two indicative extreme-case time-steps of the operation of MG 4, namely: 5 p.m. representative summer day, and 6 p.m. representative winter day.

Table SM2.1: Detailed results of the inflow and outflow of incentives on the residential customers' side for the two illustrative extreme-case time-steps: 5 p.m. summer day, and 6 p.m. winter day.

| Cust. no. | $c_1$ [\$/kWh$^2$] | $c_2$ [\$/kWh] | $d_{full}$ [kWh] | $d_{ncr}$ [kWh] | Customer utility [\$] | | Customer discomfort [\$] | | Procured load reduction [kWh] | |
|---|---|---|---|---|---|---|---|---|---|---|
| | | | | | 5 p.m. summer day | 6 p.m. winter day | 5 p.m. summer day | 6 p.m. winter day | 5 p.m. summer day | 6 p.m. winter day |
| 1 | 1.08 | 11.55 | 22.71 | 3.57 | 0.09 | 0.12 | 0.10 | 0.13 | 1.73 | 2.71 |
| 2 | 1.10 | 11.68 | 10.94 | 4.51 | 0.10 | 0.15 | 0.11 | 0.16 | 1.34 | 3.23 |
| 3 | 1.14 | 11.54 | 8.47 | 3.81 | 0.11 | 0.16 | 0.11 | 0.16 | 1.66 | 2.60 |
| 4 | 1.13 | 11.57 | 20.32 | 3.54 | 0.09 | 0.14 | 0.11 | 0.16 | 1.93 | 2.89 |
| 5 | 1.09 | 11.51 | 14.62 | 6.99 | 0.13 | 0.19 | 0.13 | 0.20 | 3.17 | 5.11 |
| 6 | 1.12 | 11.62 | 28.67 | 9.26 | 0.17 | 0.25 | 0.19 | 0.26 | 4.50 | 7.34 |
| 7 | 1.12 | 11.53 | 29.58 | 9.55 | 0.18 | 0.27 | 0.19 | 0.29 | 4.10 | 7.16 |
| 8 | 1.10 | 11.50 | 14.31 | 4.16 | 0.11 | 0.16 | 0.12 | 0.17 | 2.28 | 3.46 |
| 9 | 1.11 | 11.64 | 25.62 | 6.12 | 0.16 | 0.24 | 0.17 | 0.26 | 2.39 | 4.65 |
| 10 | 1.15 | 11.56 | 27.71 | 5.32 | 0.15 | 0.22 | 0.15 | 0.23 | 2.42 | 4.04 |
| 11 | 1.08 | 11.63 | 21.15 | 6.43 | 0.16 | 0.24 | 0.19 | 0.25 | 2.21 | 4.19 |
| 12 | 1.12 | 11.57 | 27.45 | 4.49 | 0.13 | 0.19 | 0.14 | 0.21 | 1.11 | 3.01 |
| 13 | 1.10 | 11.62 | 28.76 | 3.01 | 0.11 | 0.16 | 0.12 | 0.17 | 1.91 | 2.19 |
| 14 | 1.11 | 11.49 | 20.08 | 5.77 | 0.16 | 0.24 | 0.17 | 0.25 | 2.41 | 4.19 |
| 15 | 1.15 | 11.68 | 24.02 | 3.80 | 0.11 | 0.16 | 0.12 | 0.17 | 1.41 | 2.69 |
| 16 | 1.09 | 11.66 | 20.69 | 2.70 | 0.07 | 0.09 | 0.07 | 0.10 | 1.15 | 2.25 |
| 17 | 1.13 | 11.65 | 17.57 | 7.66 | 0.18 | 0.27 | 0.19 | 0.28 | 4.18 | 7.14 |
| 18 | 1.12 | 11.66 | 17.82 | 5.73 | 0.15 | 0.22 | 0.16 | 0.24 | 2.13 | 4.05 |
| 19 | 1.13 | 11.57 | 22.22 | 9.71 | 0.17 | 0.25 | 0.18 | 0.26 | 4.53 | 7.88 |
| 20 | 1.15 | 11.62 | 19.47 | 8.22 | 0.16 | 0.24 | 0.16 | 0.25 | 3.35 | 6.25 |
| 21 | 1.14 | 11.61 | 16.19 | 2.56 | 0.10 | 0.14 | 0.10 | 0.16 | 1.55 | 1.75 |

| | | | | | | | | | | |
|---|---|---|---|---|---|---|---|---|---|---|
| 22 | 1.10 | 11.60 | 28.62 | 7.60 | 0.13 | 0.19 | 0.13 | 0.20 | 3.11 | 5.68 |
| 23 | 1.09 | 11.55 | 26.25 | 7.79 | 0.12 | 0.17 | 0.13 | 0.19 | 3.23 | 5.72 |
| 24 | 1.08 | 11.54 | 26.68 | 7.34 | 0.12 | 0.17 | 0.13 | 0.19 | 3.61 | 5.68 |
| 25 | 1.11 | 11.58 | 16.20 | 6.64 | 0.12 | 0.17 | 0.14 | 0.19 | 3.19 | 5.15 |
| 26 | 1.13 | 11.54 | 21.05 | 4.14 | 0.10 | 0.14 | 0.11 | 0.16 | 1.53 | 3.05 |
| 27 | 1.14 | 11.66 | 27.20 | 8.29 | 0.14 | 0.20 | 0.15 | 0.21 | 3.12 | 6.20 |
| 28 | 1.10 | 11.70 | 28.54 | 4.21 | 0.10 | 0.14 | 0.12 | 0.15 | 1.66 | 3.10 |
| 29 | 1.15 | 11.50 | 22.71 | 5.28 | 0.11 | 0.16 | 0.13 | 0.16 | 2.17 | 4.11 |
| 30 | 1.12 | 11.60 | 22.55 | 9.18 | 0.15 | 0.22 | 0.17 | 0.22 | 3.75 | 6.58 |
| 31 | 1.09 | 11.51 | 22.38 | 8.92 | 0.15 | 0.23 | 0.17 | 0.24 | 3.93 | 6.38 |
| 32 | 1.13 | 11.66 | 11.59 | 5.52 | 0.10 | 0.15 | 0.10 | 0.16 | 2.12 | 4.20 |
| 33 | 1.12 | 11.70 | 16.95 | 4.89 | 0.10 | 0.15 | 0.10 | 0.17 | 2.13 | 3.72 |
| 34 | 1.13 | 11.50 | 22.67 | 7.06 | 0.12 | 0.18 | 0.12 | 0.19 | 3.02 | 5.37 |
| 35 | 1.15 | 11.69 | 28.54 | 9.33 | 0.13 | 0.20 | 0.13 | 0.22 | 4.11 | 7.19 |
| 36 | 1.14 | 11.49 | 25.84 | 9.32 | 0.13 | 0.20 | 0.15 | 0.22 | 4.91 | 7.18 |
| 37 | 1.10 | 11.63 | 18.66 | 6.94 | 0.12 | 0.18 | 0.14 | 0.19 | 3.60 | 5.67 |
| 38 | 1.12 | 11.65 | 24.65 | 4.99 | 0.10 | 0.15 | 0.10 | 0.16 | 2.55 | 3.59 |
| 39 | 1.10 | 11.60 | 18.18 | 8.90 | 0.11 | 0.17 | 0.11 | 0.18 | 3.22 | 6.36 |
| 40 | 1.11 | 11.68 | 29.38 | 5.82 | 0.09 | 0.13 | 0.10 | 0.15 | 2.37 | 4.12 |
| 41 | 1.15 | 11.68 | 29.74 | 9.28 | 0.13 | 0.18 | 0.13 | 0.21 | 4.71 | 7.35 |
| 42 | 1.08 | 11.62 | 27.01 | 2.75 | 0.06 | 0.09 | 0.08 | 0.11 | 1.91 | 2.19 |
| 43 | 1.12 | 11.52 | 16.56 | 6.49 | 0.10 | 0.15 | 0.11 | 0.16 | 2.10 | 4.33 |
| 44 | 1.11 | 11.54 | 18.00 | 7.87 | 0.11 | 0.17 | 0.12 | 0.18 | 3.21 | 5.68 |
| 45 | 1.15 | 11.53 | 13.43 | 3.84 | 0.07 | 0.10 | 0.08 | 0.11 | 1.13 | 2.22 |
| 46 | 1.13 | 11.50 | 25.26 | 5.02 | 0.09 | 0.13 | 0.10 | 0.13 | 2.07 | 3.62 |
| 47 | 1.15 | 11.51 | 27.42 | 3.91 | 0.07 | 0.12 | 0.08 | 0.13 | 1.46 | 2.77 |
| 48 | 1.14 | 11.62 | 28.10 | 4.91 | 0.06 | 0.11 | 0.08 | 0.12 | 2.02 | 3.53 |
| 49 | 1.10 | 11.69 | 20.28 | 5.53 | 0.08 | 0.14 | 0.09 | 0.15 | 2.36 | 4.60 |
| 50 | 1.12 | 11.56 | 21.18 | 6.61 | 0.09 | 0.15 | 0.10 | 0.16 | 3.03 | 5.72 |
| 51 | 1.13 | 11.67 | 29.70 | 9.04 | 0.12 | 0.22 | 0.14 | 0.22 | 3.64 | 7.57 |
| 52 | 1.13 | 11.70 | 27.79 | 6.65 | 0.09 | 0.15 | 0.11 | 0.16 | 3.19 | 3.15 |
| 53 | 1.15 | 11.69 | 17.91 | 4.56 | 0.08 | 0.14 | 0.10 | 0.16 | 2.12 | 3.37 |
| 54 | 1.14 | 11.63 | 12.52 | 4.31 | 0.08 | 0.14 | 0.10 | 0.16 | 1.81 | 3.18 |
| 55 | 1.10 | 11.70 | 27.79 | 4.32 | 0.08 | 0.14 | 0.10 | 0.16 | 2.19 | 3.48 |
| 56 | 1.09 | 11.65 | 24.78 | 3.66 | 0.07 | 0.12 | 0.07 | 0.13 | 1.71 | 2.68 |
| 57 | 1.08 | 11.56 | 27.41 | 9.67 | 0.13 | 0.22 | 0.13 | 0.22 | 4.39 | 7.15 |
| 58 | 1.11 | 11.63 | 24.27 | 9.52 | 0.13 | 0.22 | 0.14 | 0.22 | 4.68 | 7.14 |
| 59 | 1.13 | 11.54 | 22.81 | 8.64 | 0.12 | 0.20 | 0.13 | 0.20 | 3.92 | 6.37 |
| 60 | 1.14 | 11.55 | 22.61 | 7.96 | 0.11 | 0.19 | 0.12 | 0.20 | 3.79 | 6.15 |
| 61 | 1.13 | 11.63 | 10.70 | 3.82 | 0.07 | 0.12 | 0.08 | 0.14 | 1.82 | 2.70 |
| 62 | 1.08 | 11.60 | 16.96 | 5.20 | 0.09 | 0.15 | 0.10 | 0.16 | 2.41 | 3.85 |

| | | | | | | | | | | |
|---|---|---|---|---|---|---|---|---|---|---|
| 63 | 1.12 | 11.58 | 14.06 | 3.92 | 0.07 | 0.12 | 0.08 | 0.13 | 1.87 | 2.78 |
| 64 | 1.10 | 11.62 | 23.77 | 2.51 | 0.06 | 0.11 | 0.08 | 0.12 | 1.13 | 1.71 |
| 65 | 1.11 | 11.65 | 14.23 | 4.87 | 0.10 | 0.17 | 0.11 | 0.17 | 2.20 | 3.50 |
| 66 | 1.15 | 11.61 | 27.72 | 7.75 | 0.13 | 0.22 | 0.13 | 0.23 | 3.51 | 5.69 |
| 67 | 1.09 | 11.61 | 26.18 | 7.19 | 0.13 | 0.22 | 0.13 | 0.23 | 3.32 | 5.36 |
| 68 | 1.13 | 11.61 | 16.58 | 6.57 | 0.13 | 0.22 | 0.14 | 0.23 | 2.45 | 4.59 |
| 69 | 1.12 | 11.60 | 18.95 | 5.79 | 0.11 | 0.19 | 0.12 | 0.20 | 2.08 | 4.30 |
| 70 | 1.09 | 11.51 | 23.29 | 4.66 | 0.09 | 0.15 | 0.10 | 0.15 | 1.98 | 3.14 |
| 71 | 1.12 | 11.64 | 26.36 | 6.26 | 0.10 | 0.17 | 0.11 | 0.19 | 2.84 | 4.56 |
| 72 | 1.15 | 11.70 | 21.41 | 8.21 | 0.12 | 0.20 | 0.13 | 0.22 | 3.98 | 6.14 |
| 73 | 1.13 | 11.56 | 20.64 | 8.22 | 0.12 | 0.20 | 0.13 | 0.21 | 3.99 | 6.15 |
| 74 | 1.12 | 11.69 | 15.17 | 6.82 | 0.10 | 0.17 | 0.11 | 0.19 | 3.55 | 5.08 |
| 75 | 1.13 | 11.56 | 18.04 | 8.11 | 0.12 | 0.20 | 0.13 | 0.22 | 3.14 | 6.06 |
| 76 | 1.15 | 11.68 | 23.70 | 7.34 | 0.11 | 0.19 | 0.11 | 0.21 | 3.33 | 5.38 |
| 77 | 1.14 | 11.59 | 27.46 | 3.42 | 0.07 | 0.12 | 0.08 | 0.14 | 1.74 | 2.40 |
| 78 | 1.10 | 11.58 | 23.86 | 6.28 | 0.11 | 0.19 | 0.12 | 0.21 | 2.84 | 4.57 |
| 79 | 1.09 | 11.54 | 12.41 | 5.10 | 0.10 | 0.17 | 0.11 | 0.19 | 2.61 | 3.68 |
| 80 | 1.08 | 11.52 | 22.85 | 3.19 | 0.07 | 0.12 | 0.08 | 0.14 | 1.59 | 2.32 |
| 81 | 1.11 | 11.55 | 17.65 | 3.61 | 0.07 | 0.12 | 0.08 | 0.14 | 1.92 | 2.54 |
| 82 | 1.11 | 11.64 | 17.63 | 3.99 | 0.08 | 0.14 | 0.09 | 0.16 | 1.38 | 3.13 |
| 83 | 1.12 | 11.65 | 20.57 | 7.54 | 0.12 | 0.20 | 0.12 | 0.22 | 3.12 | 5.53 |
| 84 | 1.11 | 11.64 | 25.92 | 5.74 | 0.10 | 0.17 | 0.11 | 0.19 | 2.80 | 5.16 |
| 85 | 1.15 | 11.49 | 15.15 | 7.71 | 0.12 | 0.20 | 0.13 | 0.22 | 3.40 | 6.66 |
| 86 | 1.13 | 11.67 | 13.42 | 4.43 | 0.09 | 0.15 | 0.10 | 0.17 | 1.90 | 3.17 |
| 87 | 1.15 | 11.68 | 15.54 | 2.57 | 0.06 | 0.11 | 0.07 | 0.14 | 1.05 | 1.75 |
| 88 | 1.14 | 11.65 | 16.27 | 6.49 | 0.11 | 0.19 | 0.11 | 0.21 | 2.84 | 4.73 |
| 89 | 1.10 | 11.50 | 20.02 | 4.60 | 0.08 | 0.14 | 0.09 | 0.16 | 1.98 | 3.30 |
| 90 | 1.12 | 11.57 | 20.36 | 9.60 | 0.18 | 0.30 | 0.19 | 0.32 | 4.44 | 8.40 |
| 91 | 1.12 | 11.64 | 16.71 | 4.30 | 0.10 | 0.16 | 0.11 | 0.18 | 2.12 | 3.37 |
| 92 | 1.08 | 11.64 | 16.76 | 5.45 | 0.09 | 0.14 | 0.10 | 0.16 | 2.62 | 4.04 |
| 93 | 1.08 | 11.54 | 19.34 | 2.69 | 0.06 | 0.10 | 0.07 | 0.12 | 1.03 | 2.05 |
| 94 | 1.09 | 11.55 | 22.47 | 7.54 | 0.08 | 0.13 | 0.09 | 0.15 | 3.14 | 5.23 |
| 95 | 1.15 | 11.63 | 28.92 | 8.78 | 0.14 | 0.22 | 0.15 | 0.24 | 3.78 | 7.47 |
| 96 | 1.13 | 11.59 | 23.89 | 9.79 | 0.19 | 0.30 | 0.20 | 0.32 | 4.84 | 8.24 |
| 97 | 1.11 | 11.62 | 16.80 | 2.93 | 0.06 | 0.10 | 0.07 | 0.12 | 1.28 | 2.13 |
| 98 | 1.14 | 11.54 | 26.30 | 5.88 | 0.08 | 0.13 | 0.08 | 0.15 | 2.56 | 5.27 |
| 99 | 1.12 | 11.53 | 16.96 | 6.87 | 0.11 | 0.18 | 0.11 | 0.20 | 3.07 | 6.12 |
| 100 | 1.10 | 11.66 | 9.33 | 3.65 | 0.07 | 0.11 | 0.08 | 0.13 | 1.54 | 2.57 |
| 101 | 1.09 | 11.65 | 9.85 | 3.90 | 0.07 | 0.11 | 0.07 | 0.13 | 1.66 | 2.76 |
| 102 | 1.08 | 11.69 | 11.61 | 4.38 | 0.09 | 0.14 | 0.09 | 0.14 | 2.00 | 3.33 |
| 103 | 1.08 | 11.51 | 15.13 | 6.95 | 0.10 | 0.16 | 0.11 | 0.17 | 3.17 | 5.28 |

| | | | | | | | | | | |
|---|---|---|---|---|---|---|---|---|---|---|
| 104 | 1.09 | 11.53 | 14.64 | 5.30 | 0.09 | 0.14 | 0.09 | 0.15 | 2.42 | 4.03 |
| 105 | 1.15 | 11.51 | 8.26 | 3.86 | 0.07 | 0.11 | 0.07 | 0.13 | 1.64 | 2.73 |
| 106 | 1.13 | 11.59 | 19.88 | 3.37 | 0.07 | 0.11 | 0.07 | 0.13 | 1.86 | 2.26 |
| 107 | 1.11 | 11.53 | 10.10 | 2.93 | 0.05 | 0.08 | 0.05 | 0.10 | 1.88 | 2.13 |
| 108 | 1.08 | 11.68 | 11.22 | 4.85 | 0.10 | 0.16 | 0.12 | 0.17 | 1.17 | 3.29 |
| 109 | 1.09 | 11.51 | 21.89 | 4.64 | 0.08 | 0.13 | 0.09 | 0.14 | 1.78 | 3.13 |
| 110 | 1.15 | 11.50 | 26.91 | 6.96 | 0.09 | 0.14 | 0.10 | 0.15 | 3.55 | 5.09 |
| 111 | 1.13 | 11.61 | 29.43 | 9.72 | 0.16 | 0.26 | 0.16 | 0.27 | 4.35 | 7.09 |
| 112 | 1.11 | 11.65 | 20.56 | 3.89 | 0.07 | 0.11 | 0.08 | 0.12 | 1.50 | 2.06 |
| 113 | 1.14 | 11.56 | 29.93 | 3.95 | 0.08 | 0.13 | 0.09 | 0.14 | 1.30 | 3.00 |
| 114 | 1.10 | 11.53 | 20.18 | 5.06 | 0.08 | 0.13 | 0.08 | 0.15 | 2.21 | 3.75 |
| 115 | 1.10 | 11.56 | 19.34 | 9.50 | 0.13 | 0.21 | 0.14 | 0.23 | 4.17 | 7.12 |
| 116 | 1.13 | 11.53 | 15.28 | 5.43 | 0.10 | 0.16 | 0.11 | 0.17 | 2.02 | 4.03 |
| 117 | 1.15 | 11.60 | 17.46 | 4.55 | 0.09 | 0.14 | 0.10 | 0.15 | 1.14 | 3.06 |
| 118 | 1.14 | 11.68 | 18.82 | 3.64 | 0.07 | 0.11 | 0.08 | 0.12 | 1.20 | 2.17 |
| 119 | 1.10 | 11.62 | 9.56 | 4.48 | 0.10 | 0.16 | 0.11 | 0.17 | 1.52 | 3.20 |
| 120 | 1.12 | 11.51 | 27.53 | 5.31 | 0.11 | 0.18 | 0.12 | 0.20 | 2.92 | 4.04 |
| 121 | 1.12 | 11.57 | 9.42 | 3.48 | 0.08 | 0.13 | 0.10 | 0.15 | 1.98 | 2.64 |
| 122 | 1.08 | 11.50 | 17.60 | 5.76 | 0.11 | 0.18 | 0.12 | 0.19 | 2.11 | 4.18 |
| 123 | 1.08 | 11.60 | 26.19 | 3.19 | 0.07 | 0.11 | 0.08 | 0.13 | 1.17 | 2.12 |
| 124 | 1.09 | 11.58 | 16.68 | 7.11 | 0.13 | 0.21 | 0.14 | 0.23 | 3.58 | 5.30 |
| 125 | 1.11 | 11.70 | 21.50 | 2.58 | 0.06 | 0.10 | 0.07 | 0.12 | 1.16 | 1.76 |
| 126 | 1.11 | 11.66 | 26.01 | 6.80 | 0.15 | 0.24 | 0.16 | 0.26 | 3.64 | 5.07 |
| 127 | 1.11 | 11.59 | 27.50 | 8.42 | 0.15 | 0.24 | 0.15 | 0.26 | 3.82 | 6.20 |
| 128 | 1.11 | 11.68 | 28.48 | 4.27 | 0.10 | 0.16 | 0.11 | 0.17 | 1.19 | 3.15 |
| 129 | 1.09 | 11.50 | 24.90 | 6.70 | 0.11 | 0.18 | 0.12 | 0.19 | 3.65 | 5.09 |
| 130 | 1.10 | 11.57 | 13.69 | 5.77 | 0.10 | 0.16 | 0.10 | 0.18 | 2.13 | 4.39 |
| 131 | 1.10 | 11.68 | 27.75 | 2.96 | 0.07 | 0.11 | 0.08 | 0.13 | 1.95 | 2.25 |
| 132 | 1.14 | 11.68 | 21.05 | 6.22 | 0.12 | 0.19 | 0.13 | 0.20 | 2.98 | 4.13 |
| 133 | 1.13 | 11.64 | 19.08 | 7.32 | 0.13 | 0.21 | 0.14 | 0.23 | 3.10 | 5.16 |
| 134 | 1.09 | 11.62 | 21.48 | 4.16 | 0.11 | 0.18 | 0.12 | 0.20 | 1.94 | 3.06 |
| 135 | 1.12 | 11.56 | 26.03 | 8.78 | 0.14 | 0.22 | 0.15 | 0.23 | 3.18 | 6.47 |
| 136 | 1.12 | 11.69 | 19.70 | 9.78 | 0.17 | 0.27 | 0.17 | 0.28 | 4.80 | 7.33 |
| 137 | 1.10 | 11.52 | 22.45 | 8.85 | 0.15 | 0.24 | 0.17 | 0.25 | 3.52 | 6.53 |
| 138 | 1.09 | 11.64 | 17.99 | 6.29 | 0.13 | 0.21 | 0.15 | 0.22 | 2.97 | 4.28 |
| 139 | 1.08 | 11.63 | 17.41 | 4.59 | 0.13 | 0.21 | 0.15 | 0.22 | 1.45 | 3.09 |
| 140 | 1.10 | 11.66 | 29.25 | 8.10 | 0.14 | 0.22 | 0.14 | 0.23 | 3.84 | 6.06 |
| 141 | 1.13 | 11.57 | 21.64 | 4.28 | 0.10 | 0.16 | 0.11 | 0.18 | 1.99 | 3.15 |
| 142 | 1.15 | 11.65 | 23.30 | 9.68 | 0.13 | 0.21 | 0.14 | 0.22 | 4.56 | 7.26 |
| 143 | 1.14 | 11.67 | 23.84 | 7.15 | 0.10 | 0.16 | 0.12 | 0.17 | 3.10 | 5.33 |
| 144 | 1.10 | 11.56 | 15.63 | 7.00 | 0.10 | 0.16 | 0.11 | 0.17 | 3.17 | 5.12 |

| | | | | | | | | | | |
|---|---|---|---|---|---|---|---|---|---|---|
| 145 | 1.11 | 11.61 | 19.37 | 3.79 | 0.06 | 0.10 | 0.06 | 0.11 | 1.15 | 2.58 |
| 146 | 1.11 | 11.70 | 20.25 | 3.18 | 0.06 | 0.10 | 0.07 | 0.11 | 1.17 | 2.12 |
| 147 | 1.14 | 11.61 | 11.44 | 4.41 | 0.08 | 0.13 | 0.08 | 0.13 | 1.83 | 3.05 |
| 148 | 1.13 | 11.56 | 20.37 | 8.94 | 0.14 | 0.22 | 0.15 | 0.23 | 3.91 | 6.19 |
| 149 | 1.14 | 11.62 | 23.29 | 9.33 | 0.15 | 0.24 | 0.16 | 0.24 | 4.35 | 7.09 |
| 150 | 1.15 | 11.57 | 17.38 | 7.75 | 0.12 | 0.19 | 0.13 | 0.19 | 3.13 | 5.89 |
| 151 | 1.15 | 11.65 | 26.40 | 7.94 | 0.12 | 0.19 | 0.14 | 0.19 | 3.92 | 6.03 |
| 152 | 1.08 | 11.58 | 24.09 | 4.22 | 0.08 | 0.13 | 0.08 | 0.13 | 1.47 | 3.11 |
| 153 | 1.10 | 11.59 | 15.92 | 6.82 | 0.11 | 0.18 | 0.12 | 0.18 | 3.15 | 5.08 |
| 154 | 1.09 | 11.64 | 17.99 | 7.58 | 0.13 | 0.21 | 0.14 | 0.21 | 3.14 | 5.56 |
| 155 | 1.15 | 11.69 | 16.50 | 5.53 | 0.10 | 0.16 | 0.11 | 0.16 | 2.26 | 4.10 |
| 156 | 1.13 | 11.56 | 25.06 | 9.91 | 0.17 | 0.27 | 0.18 | 0.27 | 4.20 | 7.33 |
| 157 | 1.11 | 11.67 | 24.15 | 3.17 | 0.06 | 0.10 | 0.07 | 0.11 | 1.13 | 2.21 |
| 158 | 1.14 | 11.65 | 17.47 | 4.91 | 0.08 | 0.13 | 0.09 | 0.13 | 2.16 | 3.43 |
| 159 | 1.12 | 11.69 | 23.26 | 6.34 | 0.10 | 0.16 | 0.12 | 0.16 | 2.55 | 4.42 |
| 160 | 1.10 | 11.50 | 28.79 | 2.95 | 0.06 | 0.10 | 0.06 | 0.10 | 1.38 | 2.14 |
| 161 | 1.09 | 11.56 | 25.25 | 7.94 | 0.12 | 0.19 | 0.12 | 0.19 | 3.72 | 6.03 |
| 162 | 1.08 | 11.63 | 23.52 | 6.67 | 0.10 | 0.16 | 0.10 | 0.16 | 3.34 | 5.07 |
| 163 | 1.08 | 11.55 | 10.41 | 3.47 | 0.06 | 0.10 | 0.07 | 0.10 | 1.98 | 2.64 |
| 164 | 1.09 | 11.54 | 17.58 | 8.72 | 0.14 | 0.22 | 0.14 | 0.22 | 3.48 | 6.63 |
| 165 | 1.08 | 11.64 | 21.00 | 8.94 | 0.14 | 0.22 | 0.16 | 0.22 | 4.17 | 6.79 |
| 166 | 1.11 | 11.62 | 18.11 | 8.42 | 0.14 | 0.22 | 0.17 | 0.22 | 3.74 | 6.40 |
| 167 | 1.11 | 11.61 | 9.11 | 4.88 | 0.07 | 0.11 | 0.08 | 0.12 | 2.33 | 3.71 |
| 168 | 1.12 | 11.63 | 13.03 | 5.89 | 0.09 | 0.14 | 0.09 | 0.15 | 2.49 | 4.48 |
| 169 | 1.11 | 11.50 | 26.35 | 8.14 | 0.13 | 0.21 | 0.14 | 0.22 | 3.81 | 6.19 |
| 170 | 1.15 | 11.56 | 8.34 | 3.32 | 0.07 | 0.11 | 0.08 | 0.12 | 1.81 | 2.52 |
| 171 | 1.13 | 11.58 | 27.00 | 9.32 | 0.20 | 0.32 | 0.21 | 0.33 | 6.21 | 7.02 |
| 172 | 1.13 | 11.54 | 10.72 | 4.52 | 0.07 | 0.11 | 0.08 | 0.12 | 1.98 | 3.14 |
| 173 | 1.13 | 11.64 | 22.72 | 6.43 | 0.12 | 0.19 | 0.13 | 0.19 | 2.81 | 4.19 |
| 174 | 1.14 | 11.67 | 19.00 | 9.79 | 0.16 | 0.26 | 0.17 | 0.26 | 4.18 | 7.14 |
| 175 | 1.15 | 11.55 | 12.80 | 5.83 | 0.06 | 0.10 | 0.07 | 0.10 | 2.68 | 4.13 |
| 176 | 1.10 | 11.64 | 20.58 | 4.84 | 0.05 | 0.08 | 0.06 | 0.08 | 1.11 | 3.18 |
| 177 | 1.10 | 11.52 | 10.69 | 4.69 | 0.05 | 0.08 | 0.06 | 0.09 | 1.94 | 3.06 |
| 178 | 1.15 | 11.67 | 22.77 | 8.88 | 0.13 | 0.21 | 0.14 | 0.21 | 3.15 | 6.25 |
| 179 | 1.13 | 11.52 | 21.19 | 9.34 | 0.14 | 0.22 | 0.15 | 0.22 | 4.48 | 7.30 |
| 180 | 1.15 | 11.61 | 9.23 | 3.29 | 0.07 | 0.11 | 0.08 | 0.13 | 1.51 | 2.19 |
| 181 | 1.14 | 11.57 | 9.24 | 4.42 | 0.08 | 0.13 | 0.08 | 0.15 | 1.80 | 3.16 |
| 182 | 1.10 | 11.66 | 11.36 | 3.16 | 0.07 | 0.11 | 0.08 | 0.13 | 0.74 | 1.40 |
| 183 | 1.12 | 11.60 | 8.43 | 2.79 | 0.06 | 0.10 | 0.06 | 0.12 | 0.77 | 1.12 |
| 184 | 1.12 | 11.59 | 17.57 | 6.89 | 0.13 | 0.21 | 0.13 | 0.23 | 2.14 | 4.24 |
| 185 | 1.10 | 11.67 | 26.31 | 9.61 | 0.15 | 0.24 | 0.16 | 0.26 | 3.98 | 6.30 |

| | | | | | | | | | | |
|---|---|---|---|---|---|---|---|---|---|---|
| 186 | 1.11 | 11.56 | 21.58 | 2.96 | 0.06 | 0.10 | 0.07 | 0.11 | 0.55 | 1.25 |
| 187 | 1.11 | 11.58 | 19.44 | 6.88 | 0.14 | 0.22 | 0.15 | 0.23 | 3.34 | 5.23 |
| 188 | 1.08 | 11.69 | 27.01 | 4.64 | 0.09 | 0.14 | 0.10 | 0.16 | 2.22 | 3.53 |
| 189 | 1.09 | 11.50 | 10.15 | 4.71 | 0.09 | 0.14 | 0.09 | 0.15 | 2.95 | 3.58 |
| 190 | 1.08 | 11.69 | 27.98 | 3.93 | 0.06 | 0.10 | 0.06 | 0.11 | 1.49 | 1.99 |
| 191 | 1.09 | 11.53 | 10.38 | 4.82 | 0.08 | 0.13 | 0.08 | 0.14 | 2.18 | 3.46 |
| 192 | 1.11 | 11.63 | 19.37 | 5.45 | 0.11 | 0.18 | 0.11 | 0.19 | 2.32 | 4.04 |
| 193 | 1.15 | 11.61 | 11.15 | 5.70 | 0.13 | 0.21 | 0.13 | 0.23 | 2.68 | 4.13 |
| 194 | 1.08 | 11.63 | 20.31 | 7.58 | 0.16 | 0.26 | 0.17 | 0.28 | 3.14 | 5.56 |
| 195 | 1.12 | 11.57 | 8.10 | 3.06 | 0.07 | 0.11 | 0.08 | 0.13 | 1.48 | 2.13 |
| 196 | 1.10 | 11.62 | 24.87 | 4.89 | 0.09 | 0.14 | 0.09 | 0.15 | 2.25 | 3.42 |
| 197 | 1.11 | 11.66 | 26.67 | 3.50 | 0.06 | 0.10 | 0.07 | 0.12 | 1.16 | 2.26 |
| 198 | 1.15 | 11.49 | 28.17 | 7.54 | 0.14 | 0.22 | 0.14 | 0.23 | 3.90 | 5.33 |
| 199 | 1.09 | 11.51 | 29.71 | 6.78 | 0.13 | 0.21 | 0.13 | 0.23 | 3.93 | 5.05 |
| 200 | 1.08 | 11.69 | 19.11 | 3.77 | 0.07 | 0.11 | 0.07 | 0.13 | 1.84 | 2.57 |
| 201 | 1.11 | 11.63 | 13.97 | 3.61 | 0.07 | 0.11 | 0.08 | 0.13 | 1.78 | 2.64 |
| 202 | 1.13 | 11.54 | 10.22 | 4.07 | 0.08 | 0.13 | 0.09 | 0.15 | 1.65 | 3.09 |
| 203 | 1.14 | 11.57 | 19.17 | 9.31 | 0.15 | 0.24 | 0.15 | 0.26 | 4.55 | 7.08 |
| 204 | 1.14 | 11.52 | 20.88 | 6.64 | 0.13 | 0.21 | 0.14 | 0.22 | 3.43 | 5.05 |
| 205 | 1.13 | 11.55 | 25.78 | 8.75 | 0.18 | 0.29 | 0.19 | 0.31 | 5.71 | 6.69 |
| 206 | 1.14 | 11.54 | 9.83 | 2.90 | 0.06 | 0.10 | 0.06 | 0.10 | 1.42 | 2.20 |
| 207 | 1.15 | 11.56 | 22.56 | 8.54 | 0.16 | 0.26 | 0.17 | 0.28 | 3.57 | 6.29 |
| 208 | 1.15 | 11.52 | 19.37 | 5.89 | 0.12 | 0.19 | 0.12 | 0.21 | 2.87 | 4.28 |
| 209 | 1.08 | 11.56 | 11.76 | 5.37 | 0.13 | 0.21 | 0.14 | 0.23 | 2.21 | 4.18 |
| 210 | 1.10 | 11.52 | 28.65 | 8.42 | 0.16 | 0.26 | 0.17 | 0.28 | 3.72 | 6.20 |
| 211 | 1.09 | 11.68 | 20.99 | 5.23 | 0.12 | 0.19 | 0.13 | 0.21 | 1.78 | 2.97 |
| 212 | 1.15 | 11.51 | 17.69 | 6.49 | 0.14 | 0.22 | 0.15 | 0.24 | 2.36 | 3.93 |
| 213 | 1.13 | 11.69 | 28.72 | 7.84 | 0.16 | 0.26 | 0.17 | 0.28 | 2.98 | 4.96 |
| 214 | 1.12 | 11.57 | 22.43 | 9.04 | 0.21 | 0.34 | 0.22 | 0.36 | 3.32 | 5.87 |
| 215 | 1.12 | 11.50 | 17.94 | 4.97 | 0.09 | 0.14 | 0.10 | 0.16 | 2.97 | 3.78 |
| 216 | 1.11 | 11.56 | 26.47 | 7.38 | 0.15 | 0.24 | 0.16 | 0.26 | 3.17 | 5.61 |
| 217 | 1.08 | 11.64 | 19.72 | 9.81 | 0.16 | 0.26 | 0.17 | 0.28 | 4.78 | 7.46 |
| 218 | 1.11 | 11.66 | 20.19 | 3.07 | 0.06 | 0.10 | 0.07 | 0.12 | 1.90 | 2.33 |
| 219 | 1.14 | 11.60 | 22.96 | 6.90 | 0.11 | 0.18 | 0.12 | 0.20 | 3.04 | 5.24 |
| 220 | 1.12 | 11.63 | 16.08 | 5.60 | 0.08 | 0.13 | 0.09 | 0.15 | 2.10 | 4.16 |
| 221 | 1.10 | 11.68 | 13.26 | 4.82 | 0.10 | 0.16 | 0.10 | 0.17 | 2.04 | 3.56 |
| 222 | 1.09 | 11.50 | 20.74 | 4.48 | 0.09 | 0.14 | 0.09 | 0.14 | 1.58 | 3.30 |
| 223 | 1.08 | 11.55 | 27.07 | 8.19 | 0.15 | 0.24 | 0.15 | 0.26 | 3.67 | 6.12 |
| 224 | 1.08 | 11.50 | 16.95 | 8.96 | 0.15 | 0.24 | 0.15 | 0.26 | 3.97 | 6.61 |
| 225 | 1.09 | 11.53 | 10.48 | 3.90 | 0.07 | 0.11 | 0.08 | 0.12 | 1.66 | 2.76 |
| 226 | 1.15 | 11.64 | 17.76 | 7.36 | 0.15 | 0.24 | 0.16 | 0.26 | 3.29 | 5.49 |

| | | | | | | | | | | |
|---|---|---|---|---|---|---|---|---|---|---|
| 227 | 1.13 | 11.64 | 14.60 | 3.97 | 0.08 | 0.13 | 0.10 | 0.14 | 1.71 | 3.02 |
| 228 | 1.11 | 11.67 | 16.83 | 5.94 | 0.09 | 0.14 | 0.10 | 0.15 | 2.11 | 4.51 |
| 229 | 1.08 | 11.61 | 26.33 | 8.52 | 0.15 | 0.24 | 0.16 | 0.25 | 3.99 | 6.48 |
| 230 | 1.09 | 11.50 | 16.88 | 5.68 | 0.12 | 0.19 | 0.13 | 0.21 | 2.49 | 4.32 |
| 231 | 1.10 | 11.68 | 16.58 | 7.97 | 0.16 | 0.26 | 0.17 | 0.27 | 3.80 | 6.16 |
| 232 | 1.15 | 11.66 | 15.93 | 6.24 | 0.13 | 0.21 | 0.14 | 0.23 | 2.62 | 4.54 |
| 233 | 1.15 | 11.55 | 11.09 | 5.57 | 0.12 | 0.19 | 0.13 | 0.21 | 2.58 | 4.13 |
| 234 | 1.14 | 11.60 | 13.72 | 5.17 | 0.11 | 0.18 | 0.12 | 0.20 | 2.14 | 3.73 |
| 235 | 1.14 | 11.70 | 9.91 | 3.05 | 0.06 | 0.10 | 0.06 | 0.12 | 1.87 | 2.12 |
| 236 | 1.12 | 11.64 | 17.45 | 6.93 | 0.12 | 0.19 | 0.12 | 0.19 | 3.10 | 5.17 |
| 237 | 1.11 | 11.67 | 13.66 | 6.33 | 0.11 | 0.18 | 0.13 | 0.20 | 2.71 | 4.51 |
| 238 | 1.15 | 11.58 | 14.55 | 3.95 | 0.08 | 0.13 | 0.08 | 0.14 | 1.82 | 3.03 |
| 239 | 1.08 | 11.59 | 17.35 | 5.74 | 0.09 | 0.14 | 0.09 | 0.15 | 2.29 | 4.31 |
| 240 | 1.12 | 11.61 | 10.62 | 4.12 | 0.08 | 0.13 | 0.10 | 0.15 | 1.18 | 2.13 |
| 241 | 1.10 | 11.55 | 18.89 | 2.79 | 0.06 | 0.10 | 0.07 | 0.12 | 1.91 | 2.02 |
| 242 | 1.11 | 11.65 | 23.54 | 9.60 | 0.15 | 0.24 | 0.16 | 0.28 | 4.16 | 7.10 |
| 243 | 1.15 | 11.60 | 13.36 | 6.23 | 0.10 | 0.16 | 0.11 | 0.18 | 1.72 | 4.53 |
| 244 | 1.09 | 11.63 | 25.27 | 6.69 | 0.10 | 0.16 | 0.11 | 0.18 | 2.05 | 5.08 |
| 245 | 1.13 | 11.55 | 9.63 | 3.88 | 0.05 | 0.08 | 0.06 | 0.09 | 1.65 | 2.75 |
| 246 | 1.12 | 11.52 | 16.67 | 6.23 | 0.09 | 0.14 | 0.10 | 0.15 | 2.56 | 4.43 |
| 247 | 1.15 | 11.59 | 8.07 | 3.38 | 0.07 | 0.11 | 0.07 | 0.13 | 1.80 | 2.67 |
| 248 | 1.08 | 11.57 | 12.85 | 5.96 | 0.12 | 0.19 | 0.14 | 0.20 | 2.18 | 4.53 |
| 249 | 1.12 | 11.66 | 8.03 | 2.91 | 0.03 | 0.10 | 0.04 | 0.11 | 0.83 | 1.41 |
| 250 | 1.10 | 11.65 | 12.16 | 3.72 | 0.05 | 0.11 | 0.07 | 0.12 | 1.20 | 1.83 |
| Total | – | – | – | – | 26.7 | 42.6 | 28.9 | 45.9 | 654.5 | 1,092.0 |

Table SM2.2: Detailed results of the inflow and outflow of incentives on the commercial customers' side for the two illustrative extreme-case time-steps: 5 p.m. summer day, and 6 p.m. winter day.

| Cust. no. | $c_1$ [\$/kWh$^2$] | $c_2$ [\$/kWh] | $d_{full}$ [kWh] | $d_{ncr}$ [kWh] | Customer utility [\$] | | Customer discomfort [\$] | | Procured load reduction [kWh] | |
|---|---|---|---|---|---|---|---|---|---|---|
| | | | | | 5 p.m. summer day | 6 p.m. winter day | 5 p.m. summer day | 6 p.m. winter day | 5 p.m. summer day | 6 p.m. winter day |
| 1 | 1.06 | 11.43 | 60.17 | 20.02 | 0.20 | 0.41 | 0.19 | 0.39 | 2.55 | 11.09 |
| 2 | 1.05 | 11.47 | 68.87 | 10.95 | 0.12 | 0.32 | 0.11 | 0.30 | 2.22 | 6.80 |
| 3 | 1.07 | 11.42 | 92.00 | 29.90 | 0.36 | 0.65 | 0.35 | 0.62 | 5.66 | 19.96 |
| 4 | 1.05 | 11.31 | 35.47 | 8.75 | 0.08 | 0.26 | 0.07 | 0.25 | 1.52 | 5.11 |
| 5 | 1.05 | 11.32 | 80.35 | 21.40 | 0.29 | 0.51 | 0.28 | 0.48 | 4.33 | 16.61 |
| 6 | 1.05 | 11.35 | 47.70 | 11.08 | 0.11 | 0.32 | 0.10 | 0.31 | 3.99 | 9.52 |
| 7 | 1.06 | 11.39 | 53.49 | 12.28 | 0.10 | 0.31 | 0.09 | 0.30 | 2.10 | 7.02 |

| | | | | | | | | | | |
|---|---|---|---|---|---|---|---|---|---|---|
| 8 | 1.06 | 11.33 | 32.46 | 6.41 | 0.07 | 0.26 | 0.06 | 0.25 | 1.93 | 4.58 |
| 9 | 1.06 | 11.31 | 85.52 | 15.38 | 0.15 | 0.38 | 0.14 | 0.37 | 3.42 | 12.13 |
| 10 | 1.07 | 11.43 | 69.99 | 11.34 | 0.11 | 0.30 | 0.10 | 0.29 | 3.01 | 8.74 |
| 11 | 1.07 | 11.37 | 79.08 | 14.81 | 0.12 | 0.31 | 0.11 | 0.30 | 3.59 | 9.82 |
| 12 | 1.06 | 11.44 | 84.41 | 21.36 | 0.21 | 0.46 | 0.21 | 0.45 | 4.02 | 13.83 |
| 13 | 1.07 | 11.38 | 45.38 | 8.56 | 0.09 | 0.26 | 0.08 | 0.25 | 1.85 | 5.49 |
| 14 | 1.04 | 11.38 | 96.06 | 24.51 | 0.34 | 0.57 | 0.34 | 0.56 | 8.06 | 19.85 |
| 15 | 1.04 | 11.32 | 59.81 | 12.95 | 0.12 | 0.33 | 0.11 | 0.32 | 3.50 | 9.84 |
| 16 | 1.05 | 11.32 | 80.41 | 16.81 | 0.17 | 0.42 | 0.16 | 0.41 | 3.70 | 13.21 |
| 17 | 1.06 | 11.33 | 79.39 | 17.69 | 0.20 | 0.45 | 0.20 | 0.44 | 3.84 | 13.60 |
| 18 | 1.06 | 11.41 | 86.49 | 16.09 | 0.18 | 0.42 | 0.17 | 0.41 | 3.68 | 13.16 |
| 19 | 1.07 | 11.35 | 52.52 | 16.35 | 0.11 | 0.33 | 0.10 | 0.32 | 3.01 | 8.45 |
| 20 | 1.06 | 11.45 | 56.58 | 5.05 | 0.06 | 0.22 | 0.05 | 0.21 | 0.91 | 2.56 |
| 21 | 1.05 | 11.46 | 69.45 | 28.75 | 0.13 | 0.33 | 0.12 | 0.32 | 8.52 | 23.51 |
| 22 | 1.04 | 11.44 | 68.10 | 30.00 | 0.12 | 0.38 | 0.11 | 0.37 | 9.21 | 27.89 |
| 23 | 1.06 | 11.39 | 86.81 | 15.34 | 0.10 | 0.29 | 0.09 | 0.28 | 2.69 | 7.01 |
| 24 | 1.04 | 11.35 | 91.63 | 8.44 | 0.09 | 0.27 | 0.08 | 0.26 | 2.33 | 5.71 |
| 25 | 1.06 | 11.35 | 66.60 | 15.72 | 0.20 | 0.39 | 0.20 | 0.38 | 4.42 | 11.43 |
| 26 | 1.04 | 11.40 | 66.62 | 14.69 | 0.15 | 0.42 | 0.14 | 0.39 | 4.04 | 10.34 |
| 27 | 1.05 | 11.44 | 88.39 | 25.48 | 0.32 | 0.58 | 0.32 | 0.57 | 4.57 | 11.64 |
| 28 | 1.05 | 11.37 | 32.79 | 6.84 | 0.09 | 0.24 | 0.08 | 0.23 | 1.44 | 4.05 |
| 29 | 1.05 | 11.39 | 90.83 | 20.50 | 0.18 | 0.42 | 0.17 | 0.39 | 3.57 | 7.88 |
| 30 | 1.06 | 11.42 | 52.62 | 14.93 | 0.13 | 0.36 | 0.14 | 0.35 | 3.83 | 9.91 |
| 31 | 1.05 | 11.47 | 32.91 | 8.40 | 0.10 | 0.26 | 0.09 | 0.25 | 2.05 | 5.77 |
| 32 | 1.05 | 11.34 | 79.69 | 18.48 | 0.21 | 0.43 | 0.21 | 0.42 | 4.72 | 10.26 |
| 33 | 1.05 | 11.43 | 32.39 | 18.61 | 0.10 | 0.32 | 0.09 | 0.31 | 5.17 | 10.54 |
| 34 | 1.05 | 11.41 | 31.51 | 8.21 | 0.10 | 0.32 | 0.09 | 0.31 | 2.01 | 5.93 |
| 35 | 1.05 | 11.38 | 68.48 | 8.85 | 0.12 | 0.32 | 0.11 | 0.31 | 2.23 | 5.98 |
| 36 | 1.07 | 11.46 | 40.36 | 8.79 | 0.09 | 0.26 | 0.08 | 0.25 | 1.56 | 5.50 |
| 37 | 1.05 | 11.38 | 45.93 | 8.36 | 0.10 | 0.28 | 0.09 | 0.27 | 2.67 | 6.38 |
| 38 | 1.05 | 11.34 | 52.14 | 5.00 | 0.07 | 0.26 | 0.06 | 0.25 | 1.52 | 2.86 |
| 39 | 1.05 | 11.42 | 52.51 | 10.21 | 0.11 | 0.27 | 0.10 | 0.26 | 2.06 | 5.63 |
| 40 | 1.07 | 11.42 | 50.90 | 13.19 | 0.15 | 0.38 | 0.14 | 0.37 | 3.07 | 5.91 |
| 41 | 1.05 | 11.37 | 68.78 | 10.56 | 0.11 | 0.28 | 0.10 | 0.27 | 2.32 | 5.79 |
| 42 | 1.07 | 11.45 | 33.35 | 10.44 | 0.10 | 0.26 | 0.09 | 0.25 | 2.18 | 5.12 |
| 43 | 1.06 | 11.48 | 35.05 | 6.14 | 0.08 | 0.24 | 0.07 | 0.23 | 1.44 | 4.04 |
| 44 | 1.05 | 11.48 | 27.57 | 5.08 | 0.07 | 0.27 | 0.06 | 0.26 | 0.95 | 2.66 |
| 45 | 1.07 | 11.33 | 45.85 | 7.65 | 0.10 | 0.28 | 0.09 | 0.27 | 2.04 | 5.73 |
| 46 | 1.06 | 11.35 | 81.57 | 13.02 | 0.14 | 0.36 | 0.13 | 0.35 | 3.13 | 8.79 |
| 47 | 1.05 | 11.31 | 38.73 | 7.27 | 0.09 | 0.25 | 0.08 | 0.24 | 1.56 | 5.51 |
| 48 | 1.06 | 11.41 | 79.23 | 5.00 | 0.06 | 0.26 | 0.05 | 0.25 | 0.93 | 2.34 |

| | | | | | | | | | | |
|---|---|---|---|---|---|---|---|---|---|---|
| 49 | 1.07 | 11.33 | 75.43 | 15.77 | 0.12 | 0.33 | 0.11 | 0.32 | 3.37 | 8.92 |
| 50 | 1.05 | 11.38 | 85.93 | 20.24 | 0.23 | 0.44 | 0.21 | 0.43 | 4.90 | 13.29 |
| 51 | 1.05 | 11.46 | 86.24 | 15.13 | 0.15 | 0.38 | 0.13 | 0.37 | 3.63 | 9.63 |
| 52 | 1.06 | 11.40 | 43.47 | 9.33 | 0.08 | 0.26 | 0.07 | 0.25 | 2.66 | 6.06 |
| 53 | 1.07 | 11.37 | 44.75 | 10.56 | 0.10 | 0.28 | 0.09 | 0.27 | 2.08 | 7.25 |
| 54 | 1.06 | 11.35 | 61.84 | 11.14 | 0.13 | 0.34 | 0.11 | 0.33 | 3.10 | 8.98 |
| 55 | 1.05 | 11.38 | 46.02 | 10.94 | 0.12 | 0.38 | 0.11 | 0.37 | 2.76 | 8.04 |
| 56 | 1.06 | 11.47 | 86.55 | 5.03 | 0.10 | 0.27 | 0.09 | 0.26 | 1.17 | 3.85 |
| 57 | 1.07 | 11.33 | 84.82 | 17.65 | 0.19 | 0.49 | 0.20 | 0.48 | 5.28 | 14.28 |
| 58 | 1.06 | 11.39 | 64.56 | 15.03 | 0.20 | 0.36 | 0.18 | 0.35 | 3.47 | 9.74 |
| 59 | 1.06 | 11.46 | 41.04 | 5.21 | 0.07 | 0.11 | 0.06 | 0.10 | 0.93 | 2.62 |
| 60 | 1.05 | 11.32 | 74.45 | 10.21 | 0.13 | 0.25 | 0.11 | 0.24 | 2.74 | 7.69 |
| 61 | 1.04 | 11.43 | 38.69 | 9.20 | 0.10 | 0.28 | 0.09 | 0.27 | 2.40 | 6.74 |
| 62 | 1.05 | 11.48 | 56.51 | 10.13 | 0.10 | 0.29 | 0.10 | 0.28 | 2.99 | 8.39 |
| 63 | 1.04 | 11.36 | 50.77 | 8.00 | 0.10 | 0.29 | 0.09 | 0.28 | 2.12 | 5.68 |
| 64 | 1.04 | 11.43 | 99.34 | 8.42 | 0.09 | 0.16 | 0.09 | 0.15 | 1.98 | 5.55 |
| 65 | 1.06 | 11.39 | 44.60 | 17.80 | 0.12 | 0.29 | 0.09 | 0.28 | 5.95 | 14.95 |
| Total | – | – | – | – | 8.5 | 21.7 | 8.1 | 20.9 | 205.0 | 577.1 |

Table SM2.3: Detailed results of the inflow and outflow of incentives on the industrial customers' side for the two illustrative extreme-case time-steps: 5 p.m. summer day, and 6 p.m. winter day.

| Cust. no. | $c_1$ [\$/kWh$^2$] | $c_2$ [\$/kWh] | $d_{full}$ [kWh] | $d_{ncr}$ [kWh] | Customer utility [\$] | | Customer discomfort [\$] | | Procured load reduction [kWh] | |
|---|---|---|---|---|---|---|---|---|---|---|
| | | | | | 5 p.m. summer day | 6 p.m. winter day | 5 p.m. summer day | 6 p.m. winter day | 5 p.m. summer day | 6 p.m. winter day |
| 1 | 1.03 | 11.85 | 115.17 | 29.78 | 0.73 | 0.91 | 0.67 | 0.84 | 12.83 | 25.05 |
| 2 | 0.99 | 11.75 | 181.30 | 32.50 | 0.83 | 0.89 | 0.71 | 0.75 | 17.25 | 28.53 |
| 3 | 1.03 | 11.73 | 106.16 | 39.04 | 0.90 | 1.03 | 0.79 | 1.00 | 19.82 | 33.08 |
| 4 | 1.02 | 11.73 | 155.83 | 36.28 | 0.85 | 1.01 | 0.77 | 0.93 | 21.81 | 34.60 |
| 5 | 0.99 | 11.75 | 186.80 | 30.01 | 0.75 | 0.92 | 0.65 | 0.78 | 18.24 | 28.91 |
| 6 | 1.00 | 11.84 | 125.98 | 20.95 | 0.60 | 0.77 | 0.54 | 0.69 | 11.53 | 19.75 |
| 7 | 1.02 | 11.75 | 113.76 | 43.23 | 0.92 | 1.14 | 0.80 | 0.96 | 19.67 | 38.82 |
| 8 | 1.03 | 11.83 | 193.88 | 49.39 | 0.94 | 1.19 | 0.86 | 1.10 | 31.95 | 48.21 |
| 9 | 1.01 | 11.73 | 191.40 | 36.20 | 0.84 | 1.05 | 0.73 | 0.87 | 10.27 | 33.53 |
| 10 | 1.02 | 11.85 | 167.42 | 33.18 | 0.83 | 1.00 | 0.75 | 0.83 | 18.53 | 32.02 |
| Total | – | – | – | – | 8.2 | 9.9 | 7.3 | 8.8 | 181.9 | 322.5 |

Table SM2.4: Detailed results of the inflow and outflow of incentives on the agricultural customers' side for the two illustrative extreme-case time-steps: 5 p.m. summer day, and 6 p.m. winter day.

| Cust. no. | $c_1$ [$/kWh$^2$] | $c_2$ [$/kWh] | $d_{full}$ [kWh] | $d_{ncr}$ [kWh] | Customer utility [$] | | Customer discomfort [$] | | Procured load reduction [kWh] | |
|---|---|---|---|---|---|---|---|---|---|---|
| | | | | | 5 p.m. summer day | 6 p.m. winter day | 5 p.m. summer day | 6 p.m. winter day | 5 p.m. summer day | 6 p.m. winter day |
| 1 | 0.97 | 11.26 | 64.29 | 34.81 | 0.28 | 0.21 | 0.18 | 0.15 | 5.67 | 5.18 |
| 2 | 0.97 | 11.27 | 45.36 | 13.72 | 0.08 | 0.06 | 0.04 | 0.03 | 1.73 | 1.59 |
| 3 | 0.98 | 11.29 | 33.89 | 23.03 | 0.17 | 0.15 | 0.12 | 0.10 | 3.53 | 3.71 |
| 4 | 0.95 | 11.25 | 39.03 | 16.93 | 0.10 | 0.08 | 0.06 | 0.05 | 2.31 | 1.93 |
| 5 | 0.96 | 11.25 | 44.31 | 27.14 | 0.21 | 0.16 | 0.12 | 0.09 | 4.60 | 3.95 |
| 6 | 0.95 | 11.26 | 50.82 | 21.88 | 0.16 | 0.13 | 0.07 | 0.05 | 3.47 | 3.32 |
| 7 | 0.98 | 11.28 | 39.18 | 23.31 | 0.18 | 0.12 | 0.13 | 0.10 | 4.29 | 2.65 |
| 8 | 0.95 | 11.29 | 51.10 | 32.21 | 0.26 | 0.21 | 0.13 | 0.11 | 6.24 | 4.84 |
| 9 | 0.97 | 11.28 | 54.89 | 11.84 | 0.07 | 0.06 | 0.04 | 0.04 | 1.65 | 1.36 |
| 10 | 0.95 | 11.27 | 63.80 | 14.70 | 0.09 | 0.05 | 0.05 | 0.03 | 1.82 | 1.81 |
| 11 | 0.98 | 11.28 | 34.11 | 19.42 | 0.14 | 0.11 | 0.08 | 0.07 | 2.96 | 2.56 |
| 12 | 0.95 | 11.26 | 40.38 | 24.80 | 0.19 | 0.15 | 0.12 | 0.11 | 4.42 | 3.58 |
| 13 | 0.96 | 11.29 | 41.16 | 28.18 | 0.22 | 0.16 | 0.14 | 0.11 | 4.13 | 4.05 |
| 14 | 0.96 | 11.26 | 44.85 | 23.00 | 0.16 | 0.14 | 0.09 | 0.07 | 3.00 | 3.20 |
| 15 | 0.97 | 11.28 | 47.78 | 24.62 | 0.19 | 0.13 | 0.11 | 0.08 | 3.78 | 3.04 |
| 16 | 0.96 | 11.26 | 32.99 | 14.41 | 0.08 | 0.06 | 0.05 | 0.05 | 1.73 | 1.38 |
| 17 | 0.98 | 11.27 | 39.19 | 20.55 | 0.14 | 0.11 | 0.10 | 0.08 | 3.47 | 2.53 |
| 18 | 0.96 | 11.28 | 58.04 | 34.54 | 0.27 | 0.22 | 0.21 | 0.17 | 6.20 | 5.20 |
| 19 | 0.96 | 11.29 | 31.02 | 13.32 | 0.08 | 0.06 | 0.06 | 0.05 | 1.61 | 1.58 |
| 20 | 0.95 | 11.25 | 62.51 | 28.87 | 0.23 | 0.19 | 0.13 | 0.11 | 4.61 | 4.63 |
| 21 | 0.95 | 11.30 | 55.56 | 34.43 | 0.28 | 0.23 | 0.20 | 0.15 | 6.71 | 5.52 |
| 22 | 0.98 | 11.29 | 47.10 | 32.33 | 0.26 | 0.19 | 0.11 | 0.08 | 6.34 | 4.35 |
| 23 | 0.97 | 11.27 | 50.25 | 16.23 | 0.11 | 0.08 | 0.05 | 0.05 | 2.47 | 2.15 |
| 24 | 0.97 | 11.27 | 38.30 | 14.48 | 0.09 | 0.08 | 0.03 | 0.03 | 1.78 | 1.92 |
| 25 | 0.95 | 11.27 | 46.06 | 24.97 | 0.18 | 0.14 | 0.07 | 0.06 | 3.35 | 3.67 |
| 26 | 0.98 | 11.27 | 63.71 | 15.99 | 0.10 | 0.07 | 0.05 | 0.05 | 2.39 | 1.76 |
| 27 | 0.97 | 11.28 | 49.14 | 11.14 | 0.06 | 0.05 | 0.03 | 0.03 | 1.33 | 1.19 |
| 28 | 0.96 | 11.28 | 48.24 | 29.64 | 0.24 | 0.17 | 0.09 | 0.07 | 5.91 | 4.49 |
| 29 | 0.97 | 11.29 | 38.11 | 20.87 | 0.16 | 0.13 | 0.09 | 0.08 | 2.95 | 3.37 |
| 30 | 0.96 | 11.29 | 47.11 | 32.42 | 0.27 | 0.22 | 0.10 | 0.08 | 5.96 | 5.35 |
| 31 | 0.95 | 11.28 | 51.84 | 16.67 | 0.11 | 0.08 | 0.04 | 0.04 | 2.20 | 2.09 |
| 32 | 0.96 | 11.27 | 53.77 | 22.91 | 0.17 | 0.14 | 0.10 | 0.08 | 4.05 | 3.71 |
| 33 | 0.95 | 11.29 | 43.84 | 26.13 | 0.21 | 0.18 | 0.15 | 0.11 | 4.06 | 4.35 |

| | | | | | | | | | | |
|---|---|---|---|---|---|---|---|---|---|---|
| 34 | 0.96 | 11.28 | 42.86 | 24.36 | 0.20 | 0.15 | 0.15 | 0.11 | 4.22 | 3.55 |
| 35 | 0.96 | 11.27 | 64.58 | 15.47 | 0.10 | 0.08 | 0.06 | 0.05 | 2.08 | 2.00 |
| 36 | 0.96 | 11.30 | 31.32 | 19.94 | 0.14 | 0.11 | 0.10 | 0.09 | 3.33 | 2.92 |
| 37 | 0.95 | 11.29 | 60.98 | 32.57 | 0.26 | 0.23 | 0.15 | 0.11 | 5.91 | 5.87 |
| 38 | 0.98 | 11.28 | 61.97 | 23.17 | 0.18 | 0.12 | 0.10 | 0.07 | 3.50 | 2.87 |
| 39 | 0.98 | 11.28 | 57.87 | 16.68 | 0.11 | 0.08 | 0.05 | 0.04 | 2.22 | 2.05 |
| 40 | 0.96 | 11.28 | 33.45 | 14.99 | 0.10 | 0.08 | 0.05 | 0.04 | 1.89 | 2.14 |
| 41 | 0.96 | 11.26 | 39.17 | 26.87 | 0.21 | 0.15 | 0.11 | 0.08 | 4.77 | 3.71 |
| 42 | 0.96 | 11.27 | 41.74 | 14.22 | 0.09 | 0.07 | 0.03 | 0.03 | 1.98 | 1.73 |
| 43 | 0.98 | 11.27 | 53.79 | 30.63 | 0.24 | 0.19 | 0.17 | 0.13 | 4.61 | 4.48 |
| 44 | 0.96 | 11.26 | 34.78 | 17.92 | 0.11 | 0.08 | 0.04 | 0.04 | 2.09 | 1.79 |
| 45 | 0.95 | 11.29 | 55.24 | 23.46 | 0.18 | 0.15 | 0.09 | 0.07 | 3.84 | 3.44 |
| 46 | 0.97 | 11.26 | 33.74 | 20.40 | 0.13 | 0.10 | 0.09 | 0.07 | 3.17 | 2.25 |
| 47 | 0.96 | 11.26 | 52.88 | 18.81 | 0.12 | 0.09 | 0.06 | 0.05 | 2.62 | 2.19 |
| 48 | 0.96 | 11.26 | 47.30 | 20.17 | 0.15 | 0.11 | 0.09 | 0.07 | 2.73 | 2.43 |
| 49 | 0.96 | 11.26 | 57.27 | 31.60 | 0.27 | 0.20 | 0.18 | 0.13 | 4.96 | 4.22 |
| 50 | 0.95 | 11.27 | 55.03 | 19.28 | 0.14 | 0.10 | 0.10 | 0.08 | 3.31 | 2.52 |
| 51 | 0.96 | 11.26 | 31.15 | 14.90 | 0.10 | 0.08 | 0.07 | 0.06 | 2.12 | 1.76 |
| 52 | 0.98 | 11.30 | 61.18 | 34.39 | 0.29 | 0.24 | 0.12 | 0.09 | 6.00 | 5.32 |
| 53 | 0.98 | 11.27 | 41.70 | 25.56 | 0.20 | 0.16 | 0.09 | 0.07 | 4.71 | 3.62 |
| 54 | 0.97 | 11.26 | 54.46 | 22.04 | 0.17 | 0.15 | 0.12 | 0.09 | 3.49 | 3.64 |
| 55 | 0.95 | 11.30 | 36.92 | 10.44 | 0.06 | 0.05 | 0.04 | 0.04 | 1.30 | 1.13 |
| Total | – | – | – | – | 8.9 | 7.1 | 5.2 | 4.2 | 195.6 | 171.6 |

Table SM2.5: Detailed results of the inflow and outflow of incentives on the FCEV-refuelling customers' side for the two illustrative extreme-case time-steps: 5 p.m. summer day, and 6 p.m. winter day.

| Cust. no. | $c_1$ [\$/kWh$^2$] | $c_2$ [\$/kWh] | $d_{full}$ [kWh] | $d_{ncr}$ [kWh] | Customer utility [\$] | | Customer discomfort [\$] | | Procured load reduction [kWh] | |
|---|---|---|---|---|---|---|---|---|---|---|
| | | | | | 5 p.m. summer day | 6 p.m. winter day | 5 p.m. summer day | 6 p.m. winter day | 5 p.m. summer day | 6 p.m. winter day |
| 1 | 0.94 | 11.47 | 8.35 | 4.46 | 0.01 | 0.01 | 0.00 | 0.00 | 0.20 | 0.21 |
| 2 | 0.94 | 11.46 | 5.77 | 4.24 | 0.01 | 0.01 | 0.00 | 0.00 | 0.18 | 0.20 |
| 3 | 0.93 | 11.43 | 28.48 | 16.73 | 0.08 | 0.07 | 0.02 | 0.02 | 1.42 | 1.60 |
| 4 | 0.92 | 11.50 | 12.53 | 8.53 | 0.02 | 0.02 | 0.01 | 0.01 | 0.37 | 0.40 |
| 5 | 0.93 | 11.44 | 12.39 | 9.78 | 0.03 | 0.03 | 0.01 | 0.01 | 0.47 | 0.52 |
| 6 | 0.91 | 11.41 | 13.32 | 8.39 | 0.02 | 0.02 | 0.01 | 0.01 | 0.33 | 0.35 |
| 7 | 0.92 | 11.53 | 16.68 | 11.82 | 0.04 | 0.03 | 0.01 | 0.01 | 0.70 | 0.78 |
| 8 | 0.92 | 11.44 | 21.20 | 15.42 | 0.08 | 0.06 | 0.02 | 0.02 | 1.55 | 1.62 |
| 9 | 0.93 | 11.50 | 20.10 | 14.80 | 0.09 | 0.08 | 0.03 | 0.02 | 1.46 | 1.62 |

| | | | | | | | | | | |
|---|---|---|---|---|---|---|---|---|---|---|
| 10 | 0.92 | 11.52 | 26.06 | 18.15 | 0.11 | 0.10 | 0.03 | 0.03 | 1.97 | 2.28 |
| 11 | 0.92 | 11.46 | 18.98 | 10.11 | 0.05 | 0.04 | 0.02 | 0.01 | 0.87 | 0.91 |
| 12 | 0.91 | 11.53 | 26.35 | 20.56 | 0.12 | 0.10 | 0.04 | 0.03 | 2.22 | 2.41 |
| 13 | 0.93 | 11.47 | 13.70 | 7.62 | 0.02 | 0.02 | 0.01 | 0.01 | 0.34 | 0.38 |
| 14 | 0.92 | 11.52 | 16.15 | 9.36 | 0.03 | 0.03 | 0.01 | 0.01 | 0.55 | 0.59 |
| 15 | 0.93 | 11.52 | 6.36 | 4.70 | 0.01 | 0.01 | 0.00 | 0.00 | 0.18 | 0.20 |
| 16 | 0.93 | 11.48 | 9.43 | 6.09 | 0.02 | 0.02 | 0.01 | 0.01 | 0.37 | 0.40 |
| 17 | 0.93 | 11.40 | 21.57 | 15.76 | 0.06 | 0.05 | 0.02 | 0.01 | 1.07 | 1.18 |
| 18 | 0.91 | 11.46 | 13.27 | 8.21 | 0.02 | 0.02 | 0.01 | 0.01 | 0.32 | 0.35 |
| 19 | 0.91 | 11.47 | 27.46 | 15.98 | 0.06 | 0.05 | 0.02 | 0.01 | 1.08 | 1.13 |
| 20 | 0.92 | 11.45 | 7.95 | 4.06 | 0.01 | 0.01 | 0.00 | 0.00 | 0.18 | 0.19 |
| 21 | 0.93 | 11.43 | 29.71 | 20.86 | 0.11 | 0.10 | 0.03 | 0.03 | 1.81 | 1.98 |
| 22 | 0.93 | 11.54 | 18.50 | 11.63 | 0.04 | 0.03 | 0.01 | 0.01 | 0.71 | 0.77 |
| 23 | 0.92 | 11.47 | 22.67 | 14.41 | 0.06 | 0.05 | 0.02 | 0.01 | 1.07 | 1.20 |
| 24 | 0.93 | 11.55 | 29.99 | 20.48 | 0.11 | 0.10 | 0.03 | 0.03 | 2.00 | 2.30 |
| 25 | 0.93 | 11.47 | 12.20 | 6.32 | 0.02 | 0.02 | 0.01 | 0.01 | 0.38 | 0.41 |
| 26 | 0.94 | 11.53 | 15.36 | 9.14 | 0.03 | 0.03 | 0.01 | 0.01 | 0.56 | 0.60 |
| 27 | 0.93 | 11.47 | 16.62 | 12.16 | 0.05 | 0.04 | 0.02 | 0.01 | 0.97 | 1.03 |
| 28 | 0.92 | 11.54 | 24.10 | 17.09 | 0.08 | 0.08 | 0.02 | 0.02 | 1.30 | 1.54 |
| 29 | 0.91 | 11.53 | 25.46 | 13.69 | 0.06 | 0.05 | 0.02 | 0.01 | 1.01 | 1.09 |
| 30 | 0.93 | 11.46 | 7.51 | 4.05 | 0.01 | 0.01 | 0.00 | 0.00 | 0.18 | 0.20 |
| 31 | 0.93 | 11.44 | 9.45 | 4.99 | 0.01 | 0.01 | 0.00 | 0.00 | 0.20 | 0.21 |
| 32 | 0.92 | 11.53 | 13.99 | 7.03 | 0.03 | 0.03 | 0.01 | 0.01 | 0.57 | 0.63 |
| 33 | 0.91 | 11.56 | 6.42 | 4.02 | 0.01 | 0.01 | 0.00 | 0.00 | 0.18 | 0.19 |
| 34 | 0.92 | 11.46 | 18.05 | 12.57 | 0.06 | 0.05 | 0.02 | 0.01 | 1.04 | 1.16 |
| 35 | 0.91 | 11.51 | 13.40 | 9.61 | 0.04 | 0.04 | 0.01 | 0.01 | 0.65 | 0.72 |
| 36 | 0.92 | 11.47 | 9.39 | 6.19 | 0.02 | 0.02 | 0.01 | 0.01 | 0.38 | 0.41 |
| 37 | 0.92 | 11.54 | 10.22 | 5.44 | 0.01 | 0.01 | 0.00 | 0.00 | 0.18 | 0.19 |
| 38 | 0.93 | 11.53 | 27.63 | 19.05 | 0.10 | 0.09 | 0.03 | 0.03 | 1.68 | 1.77 |
| 39 | 0.92 | 11.43 | 21.88 | 11.77 | 0.05 | 0.04 | 0.02 | 0.01 | 0.89 | 0.98 |
| 40 | 0.94 | 11.55 | 16.71 | 9.03 | 0.03 | 0.03 | 0.01 | 0.01 | 0.50 | 0.55 |
| 41 | 0.93 | 11.57 | 27.80 | 14.72 | 0.07 | 0.06 | 0.02 | 0.02 | 1.33 | 1.39 |
| 42 | 0.94 | 11.49 | 7.60 | 4.12 | 0.01 | 0.01 | 0.00 | 0.00 | 0.17 | 0.19 |
| 43 | 0.93 | 11.55 | 23.64 | 13.01 | 0.06 | 0.05 | 0.02 | 0.01 | 1.19 | 1.33 |
| 44 | 0.94 | 11.50 | 23.41 | 13.08 | 0.06 | 0.05 | 0.02 | 0.01 | 0.96 | 1.02 |
| 45 | 0.92 | 11.43 | 19.05 | 11.34 | 0.05 | 0.04 | 0.02 | 0.01 | 0.97 | 1.06 |
| 46 | 0.93 | 11.43 | 9.60 | 5.71 | 0.01 | 0.01 | 0.00 | 0.00 | 0.19 | 0.20 |
| 47 | 0.92 | 11.47 | 19.93 | 11.27 | 0.05 | 0.04 | 0.02 | 0.01 | 0.91 | 0.96 |
| 48 | 0.93 | 11.53 | 12.50 | 7.19 | 0.03 | 0.03 | 0.01 | 0.01 | 0.56 | 0.62 |
| 49 | 0.93 | 11.54 | 8.35 | 6.41 | 0.02 | 0.02 | 0.01 | 0.01 | 0.38 | 0.42 |
| 50 | 0.91 | 11.53 | 10.32 | 7.34 | 0.02 | 0.02 | 0.01 | 0.01 | 0.25 | 0.26 |

| | | | | | | | | | | |
|---|---|---|---|---|---|---|---|---|---|---|
| 51 | 0.92 | 11.45 | 27.37 | 18.25 | 0.05 | 0.05 | 0.02 | 0.02 | 0.98 | 1.06 |
| 52 | 0.92 | 11.49 | 6.79 | 3.77 | 0.01 | 0.01 | 0.00 | 0.00 | 0.08 | 0.09 |
| 53 | 0.93 | 11.42 | 11.06 | 6.23 | 0.01 | 0.01 | 0.01 | 0.01 | 0.17 | 0.09 |
| 54 | 0.94 | 11.42 | 6.34 | 3.32 | 0.01 | 0.01 | 0.00 | 0.00 | 0.09 | 0.09 |
| 55 | 0.92 | 11.42 | 16.04 | 12.42 | 0.03 | 0.03 | 0.01 | 0.01 | 0.59 | 0.64 |
| 56 | 0.93 | 11.52 | 5.33 | 3.80 | 0.01 | 0.01 | 0.00 | 0.00 | 0.08 | 0.09 |
| 57 | 0.93 | 11.48 | 27.43 | 18.31 | 0.05 | 0.05 | 0.02 | 0.02 | 0.92 | 0.98 |
| 58 | 0.91 | 11.43 | 9.92 | 5.89 | 0.01 | 0.01 | 0.01 | 0.01 | 0.19 | 0.20 |
| 59 | 0.93 | 11.48 | 7.33 | 4.03 | 0.01 | 0.01 | 0.00 | 0.00 | 0.10 | 0.10 |
| 60 | 0.92 | 11.43 | 12.68 | 8.71 | 0.02 | 0.02 | 0.01 | 0.01 | 0.29 | 0.31 |
| 61 | 0.94 | 11.41 | 16.40 | 13.06 | 0.02 | 0.02 | 0.01 | 0.01 | 0.33 | 0.36 |
| 62 | 0.91 | 11.54 | 7.54 | 4.16 | 0.01 | 0.01 | 0.00 | 0.00 | 0.10 | 0.10 |
| 63 | 0.92 | 11.50 | 29.88 | 17.25 | 0.04 | 0.04 | 0.01 | 0.01 | 0.73 | 0.80 |
| 64 | 0.92 | 11.56 | 13.30 | 8.23 | 0.02 | 0.02 | 0.01 | 0.01 | 0.28 | 0.30 |
| 65 | 0.92 | 11.52 | 12.43 | 6.49 | 0.01 | 0.01 | 0.01 | 0.01 | 0.17 | 0.19 |
| 66 | 0.93 | 11.50 | 6.55 | 4.62 | 0.01 | 0.01 | 0.00 | 0.00 | 0.09 | 0.10 |
| 67 | 0.92 | 11.54 | 12.46 | 7.73 | 0.01 | 0.01 | 0.01 | 0.01 | 0.19 | 0.20 |
| 68 | 0.93 | 11.55 | 6.16 | 4.90 | 0.01 | 0.01 | 0.00 | 0.00 | 0.10 | 0.11 |
| 69 | 0.92 | 11.57 | 17.64 | 10.95 | 0.02 | 0.02 | 0.01 | 0.01 | 0.36 | 0.38 |
| 70 | 0.91 | 11.40 | 24.04 | 16.50 | 0.03 | 0.03 | 0.01 | 0.01 | 0.49 | 0.53 |
| 71 | 0.92 | 11.55 | 20.78 | 11.35 | 0.03 | 0.02 | 0.01 | 0.01 | 0.41 | 0.45 |
| 72 | 0.93 | 11.50 | 7.25 | 4.45 | 0.01 | 0.01 | 0.00 | 0.00 | 0.10 | 0.11 |
| 73 | 0.92 | 11.57 | 7.02 | 3.85 | 0.01 | 0.01 | 0.00 | 0.00 | 0.10 | 0.11 |
| 74 | 0.91 | 11.49 | 24.43 | 17.77 | 0.04 | 0.03 | 0.01 | 0.01 | 0.66 | 0.73 |
| 75 | 0.92 | 11.48 | 27.63 | 21.04 | 0.05 | 0.05 | 0.02 | 0.02 | 0.87 | 0.96 |
| 76 | 0.93 | 11.54 | 18.34 | 11.10 | 0.03 | 0.02 | 0.01 | 0.01 | 0.50 | 0.54 |
| 77 | 0.92 | 11.44 | 7.73 | 5.45 | 0.01 | 0.01 | 0.00 | 0.00 | 0.09 | 0.10 |
| 78 | 0.93 | 11.48 | 25.65 | 15.09 | 0.03 | 0.03 | 0.01 | 0.01 | 0.60 | 0.62 |
| 79 | 0.92 | 11.55 | 13.45 | 8.87 | 0.02 | 0.02 | 0.01 | 0.01 | 0.25 | 0.26 |
| 80 | 0.94 | 11.50 | 12.35 | 9.26 | 0.03 | 0.03 | 0.01 | 0.01 | 0.50 | 0.56 |
| 81 | 0.92 | 11.54 | 23.66 | 16.07 | 0.05 | 0.04 | 0.02 | 0.01 | 0.96 | 1.06 |
| 82 | 0.93 | 11.53 | 5.26 | 3.16 | 0.01 | 0.01 | 0.00 | 0.00 | 0.20 | 0.22 |
| 83 | 0.92 | 11.50 | 6.21 | 3.66 | 0.01 | 0.01 | 0.00 | 0.00 | 0.19 | 0.21 |
| 84 | 0.92 | 11.44 | 21.70 | 13.80 | 0.06 | 0.05 | 0.02 | 0.01 | 1.03 | 1.11 |
| 85 | 0.91 | 11.51 | 20.09 | 12.59 | 0.05 | 0.04 | 0.02 | 0.01 | 0.83 | 0.89 |
| 86 | 0.93 | 11.41 | 18.15 | 11.03 | 0.04 | 0.04 | 0.01 | 0.01 | 0.78 | 0.82 |
| 87 | 0.93 | 11.51 | 23.24 | 15.51 | 0.07 | 0.06 | 0.02 | 0.02 | 1.34 | 1.43 |
| 88 | 0.93 | 11.51 | 22.68 | 16.39 | 0.10 | 0.09 | 0.03 | 0.03 | 1.71 | 1.78 |
| 89 | 0.92 | 11.52 | 24.53 | 15.39 | 0.09 | 0.09 | 0.03 | 0.03 | 1.52 | 1.64 |
| 90 | 0.93 | 11.55 | 12.20 | 7.67 | 0.02 | 0.02 | 0.01 | 0.01 | 0.35 | 0.37 |
| 91 | 0.93 | 11.57 | 22.31 | 11.99 | 0.05 | 0.04 | 0.02 | 0.01 | 0.97 | 1.08 |

| | | | | | | | | | | |
|---|---|---|---|---|---|---|---|---|---|---|
| 92 | 0.93 | 11.53 | 18.92 | 9.60 | 0.03 | 0.03 | 0.01 | 0.01 | 0.58 | 0.63 |
| 93 | 0.93 | 11.50 | 14.91 | 8.75 | 0.03 | 0.02 | 0.01 | 0.01 | 0.55 | 0.61 |
| 94 | 0.94 | 11.56 | 6.54 | 3.89 | 0.01 | 0.01 | 0.00 | 0.00 | 0.18 | 0.19 |
| 95 | 0.92 | 11.50 | 24.50 | 17.05 | 0.08 | 0.07 | 0.02 | 0.02 | 1.37 | 1.48 |
| 96 | 0.93 | 11.40 | 13.44 | 10.58 | 0.04 | 0.03 | 0.01 | 0.01 | 0.75 | 0.83 |
| 97 | 0.92 | 11.42 | 20.20 | 15.77 | 0.08 | 0.07 | 0.02 | 0.02 | 1.53 | 1.71 |
| 98 | 0.91 | 11.55 | 23.53 | 15.00 | 0.08 | 0.07 | 0.02 | 0.02 | 1.42 | 1.54 |
| 99 | 0.93 | 11.48 | 7.62 | 4.36 | 0.01 | 0.01 | 0.00 | 0.00 | 0.18 | 0.20 |
| 100 | 0.92 | 11.54 | 8.20 | 5.98 | 0.02 | 0.02 | 0.01 | 0.01 | 0.36 | 0.40 |
| 101 | 0.92 | 11.44 | 18.74 | 13.64 | 0.06 | 0.05 | 0.02 | 0.01 | 1.03 | 1.12 |
| 102 | 0.93 | 11.49 | 17.13 | 12.37 | 0.06 | 0.05 | 0.02 | 0.01 | 1.12 | 1.25 |
| 103 | 0.93 | 11.51 | 27.26 | 19.71 | 0.10 | 0.10 | 0.03 | 0.03 | 1.96 | 2.17 |
| 104 | 0.92 | 11.41 | 24.97 | 13.28 | 0.08 | 0.07 | 0.02 | 0.02 | 1.57 | 1.75 |
| 105 | 0.93 | 11.50 | 23.36 | 16.46 | 0.10 | 0.10 | 0.03 | 0.03 | 1.90 | 2.07 |
| 106 | 0.92 | 11.46 | 6.28 | 4.01 | 0.01 | 0.01 | 0.00 | 0.00 | 0.17 | 0.18 |
| 107 | 0.94 | 11.41 | 6.82 | 3.84 | 0.01 | 0.01 | 0.00 | 0.00 | 0.19 | 0.20 |
| 108 | 0.93 | 11.48 | 7.21 | 3.82 | 0.01 | 0.01 | 0.00 | 0.00 | 0.17 | 0.19 |
| 109 | 0.92 | 11.43 | 24.96 | 18.65 | 0.13 | 0.12 | 0.04 | 0.03 | 2.14 | 2.23 |
| 110 | 0.93 | 11.42 | 28.58 | 15.79 | 0.10 | 0.09 | 0.03 | 0.03 | 1.68 | 1.77 |
| 111 | 0.93 | 11.43 | 22.09 | 12.13 | 0.07 | 0.06 | 0.02 | 0.02 | 1.16 | 1.25 |
| 112 | 0.93 | 11.42 | 8.30 | 5.81 | 0.01 | 0.01 | 0.00 | 0.00 | 0.18 | 0.20 |
| 113 | 0.91 | 11.50 | 29.27 | 16.83 | 0.13 | 0.12 | 0.04 | 0.03 | 2.12 | 2.21 |
| 114 | 0.92 | 11.41 | 7.76 | 5.08 | 0.01 | 0.01 | 0.00 | 0.00 | 0.19 | 0.21 |
| 115 | 0.92 | 11.51 | 7.94 | 5.64 | 0.01 | 0.01 | 0.00 | 0.00 | 0.19 | 0.21 |
| 116 | 0.91 | 11.45 | 21.02 | 11.48 | 0.06 | 0.05 | 0.02 | 0.01 | 1.18 | 1.24 |
| 117 | 0.94 | 11.49 | 13.22 | 10.39 | 0.05 | 0.04 | 0.02 | 0.01 | 0.90 | 0.97 |
| 118 | 0.93 | 11.52 | 21.35 | 14.14 | 0.08 | 0.07 | 0.02 | 0.02 | 1.49 | 1.58 |
| 119 | 0.92 | 11.48 | 23.73 | 16.70 | 0.09 | 0.09 | 0.03 | 0.03 | 1.76 | 1.97 |
| 120 | 0.93 | 11.49 | 19.58 | 10.00 | 0.03 | 0.03 | 0.01 | 0.01 | 0.54 | 0.59 |
| 121 | 0.93 | 11.48 | 23.50 | 17.45 | 0.10 | 0.10 | 0.03 | 0.03 | 1.71 | 1.81 |
| 122 | 0.93 | 11.42 | 10.87 | 7.88 | 0.03 | 0.03 | 0.01 | 0.01 | 0.60 | 0.63 |
| 123 | 0.93 | 11.48 | 23.37 | 12.53 | 0.07 | 0.06 | 0.02 | 0.02 | 1.13 | 1.22 |
| 124 | 0.93 | 11.55 | 29.26 | 19.24 | 0.12 | 0.12 | 0.04 | 0.03 | 2.08 | 2.30 |
| 125 | 0.93 | 11.55 | 26.67 | 15.94 | 0.10 | 0.07 | 0.03 | 0.02 | 1.99 | 2.20 |
| 126 | 0.94 | 11.45 | 7.16 | 4.75 | 0.01 | 0.01 | 0.00 | 0.00 | 0.17 | 0.19 |
| 127 | 0.92 | 11.44 | 14.16 | 8.77 | 0.03 | 0.02 | 0.01 | 0.01 | 0.52 | 0.55 |
| 128 | 0.91 | 11.50 | 14.23 | 8.89 | 0.03 | 0.03 | 0.01 | 0.01 | 0.49 | 0.53 |
| 129 | 0.91 | 11.51 | 22.13 | 12.26 | 0.06 | 0.04 | 0.02 | 0.01 | 1.18 | 1.31 |
| 130 | 0.91 | 11.47 | 19.95 | 11.50 | 0.05 | 0.04 | 0.02 | 0.01 | 0.83 | 0.87 |
| 131 | 0.92 | 11.44 | 24.73 | 12.52 | 0.06 | 0.04 | 0.02 | 0.01 | 1.04 | 1.15 |
| 132 | 0.92 | 11.56 | 14.19 | 11.03 | 0.05 | 0.04 | 0.02 | 0.01 | 0.98 | 1.09 |

| | | | | | | | | | | |
|---|---|---|---|---|---|---|---|---|---|---|
| 133 | 0.92 | 11.41 | 10.15 | 7.07 | 0.02 | 0.02 | 0.01 | 0.01 | 0.36 | 0.38 |
| 134 | 0.93 | 11.42 | 7.17 | 5.59 | 0.01 | 0.01 | 0.00 | 0.00 | 0.18 | 0.19 |
| 135 | 0.93 | 11.42 | 24.30 | 13.34 | 0.06 | 0.04 | 0.02 | 0.01 | 1.10 | 1.19 |
| 136 | 0.93 | 11.43 | 10.14 | 7.87 | 0.03 | 0.02 | 0.01 | 0.01 | 0.56 | 0.62 |
| 137 | 0.94 | 11.51 | 14.71 | 10.86 | 0.04 | 0.03 | 0.01 | 0.01 | 0.64 | 0.69 |
| 138 | 0.94 | 11.50 | 18.79 | 12.65 | 0.05 | 0.04 | 0.02 | 0.01 | 0.91 | 0.98 |
| 139 | 0.92 | 11.41 | 10.72 | 6.78 | 0.02 | 0.02 | 0.01 | 0.01 | 0.32 | 0.35 |
| 140 | 0.91 | 11.56 | 21.05 | 12.15 | 0.06 | 0.04 | 0.02 | 0.01 | 1.16 | 1.22 |
| 141 | 0.93 | 11.52 | 17.11 | 12.41 | 0.06 | 0.04 | 0.02 | 0.01 | 1.04 | 1.09 |
| 142 | 0.91 | 11.53 | 8.80 | 5.00 | 0.01 | 0.01 | 0.00 | 0.00 | 0.19 | 0.21 |
| 143 | 0.93 | 11.41 | 24.55 | 12.75 | 0.07 | 0.06 | 0.02 | 0.02 | 1.19 | 1.30 |
| 144 | 0.93 | 11.55 | 7.52 | 5.49 | 0.02 | 0.02 | 0.01 | 0.01 | 0.37 | 0.39 |
| 145 | 0.94 | 11.56 | 12.35 | 8.66 | 0.03 | 0.03 | 0.01 | 0.01 | 0.59 | 0.65 |
| 146 | 0.92 | 11.57 | 10.93 | 7.81 | 0.02 | 0.02 | 0.01 | 0.01 | 0.32 | 0.33 |
| 147 | 0.92 | 11.55 | 18.27 | 12.65 | 0.07 | 0.06 | 0.02 | 0.02 | 1.14 | 1.23 |
| 148 | 0.93 | 11.53 | 7.29 | 4.56 | 0.01 | 0.01 | 0.00 | 0.00 | 0.16 | 0.18 |
| 149 | 0.93 | 11.49 | 15.13 | 9.34 | 0.04 | 0.03 | 0.01 | 0.01 | 0.75 | 0.80 |
| 150 | 0.93 | 11.43 | 7.62 | 5.68 | 0.02 | 0.02 | 0.01 | 0.01 | 0.37 | 0.40 |
| 151 | 0.91 | 11.53 | 10.32 | 7.34 | 0.02 | 0.02 | 0.01 | 0.01 | 0.25 | 0.26 |
| 152 | 0.92 | 11.45 | 27.37 | 18.25 | 0.05 | 0.05 | 0.02 | 0.02 | 0.98 | 1.06 |
| 153 | 0.92 | 11.49 | 6.79 | 3.77 | 0.01 | 0.01 | 0.00 | 0.00 | 0.08 | 0.09 |
| 154 | 0.93 | 11.42 | 11.06 | 6.23 | 0.01 | 0.01 | 0.01 | 0.01 | 0.17 | 0.09 |
| 155 | 0.94 | 11.42 | 6.34 | 3.32 | 0.01 | 0.01 | 0.00 | 0.00 | 0.09 | 0.09 |
| 156 | 0.92 | 11.42 | 16.04 | 12.42 | 0.03 | 0.03 | 0.01 | 0.01 | 0.59 | 0.64 |
| 157 | 0.93 | 11.52 | 5.33 | 3.80 | 0.01 | 0.01 | 0.00 | 0.00 | 0.08 | 0.09 |
| 158 | 0.93 | 11.48 | 27.43 | 18.31 | 0.05 | 0.05 | 0.02 | 0.02 | 0.92 | 0.98 |
| 159 | 0.91 | 11.43 | 9.92 | 5.89 | 0.01 | 0.01 | 0.01 | 0.01 | 0.19 | 0.20 |
| 160 | 0.93 | 11.48 | 7.33 | 4.03 | 0.01 | 0.01 | 0.00 | 0.00 | 0.10 | 0.10 |
| 161 | 0.92 | 11.43 | 12.68 | 8.71 | 0.02 | 0.02 | 0.01 | 0.01 | 0.29 | 0.31 |
| 162 | 0.94 | 11.41 | 16.40 | 13.06 | 0.02 | 0.02 | 0.01 | 0.01 | 0.33 | 0.36 |
| 163 | 0.91 | 11.54 | 7.54 | 4.16 | 0.01 | 0.01 | 0.00 | 0.00 | 0.10 | 0.10 |
| 164 | 0.92 | 11.50 | 29.88 | 17.25 | 0.04 | 0.04 | 0.01 | 0.01 | 0.73 | 0.80 |
| 165 | 0.92 | 11.56 | 13.30 | 8.23 | 0.02 | 0.02 | 0.01 | 0.01 | 0.28 | 0.30 |
| 166 | 0.92 | 11.52 | 12.43 | 6.49 | 0.01 | 0.01 | 0.01 | 0.01 | 0.17 | 0.19 |
| 167 | 0.93 | 11.50 | 6.55 | 4.62 | 0.01 | 0.01 | 0.00 | 0.00 | 0.09 | 0.10 |
| 168 | 0.92 | 11.54 | 12.46 | 7.73 | 0.01 | 0.01 | 0.01 | 0.01 | 0.19 | 0.20 |
| 169 | 0.93 | 11.55 | 6.16 | 4.90 | 0.01 | 0.01 | 0.00 | 0.00 | 0.10 | 0.11 |
| 170 | 0.92 | 11.57 | 17.64 | 10.95 | 0.02 | 0.02 | 0.01 | 0.01 | 0.36 | 0.38 |
| 171 | 0.91 | 11.40 | 24.04 | 16.50 | 0.03 | 0.03 | 0.01 | 0.01 | 0.49 | 0.53 |
| 172 | 0.92 | 11.55 | 20.78 | 11.35 | 0.03 | 0.02 | 0.01 | 0.01 | 0.41 | 0.45 |
| 173 | 0.93 | 11.50 | 7.25 | 4.45 | 0.01 | 0.01 | 0.00 | 0.00 | 0.10 | 0.11 |

| | | | | | | | | | | |
|---|---|---|---|---|---|---|---|---|---|---|
| 174 | 0.92 | 11.57 | 7.02 | 3.85 | 0.01 | 0.01 | 0.00 | 0.00 | 0.10 | 0.11 |
| 175 | 0.91 | 11.49 | 24.43 | 17.77 | 0.04 | 0.03 | 0.01 | 0.01 | 0.66 | 0.73 |
| 176 | 0.92 | 11.48 | 27.63 | 21.04 | 0.05 | 0.05 | 0.02 | 0.02 | 0.87 | 0.96 |
| 177 | 0.93 | 11.54 | 18.34 | 11.10 | 0.03 | 0.02 | 0.01 | 0.01 | 0.50 | 0.54 |
| 178 | 0.92 | 11.44 | 7.73 | 5.45 | 0.01 | 0.01 | 0.00 | 0.00 | 0.09 | 0.10 |
| 179 | 0.93 | 11.48 | 25.65 | 15.09 | 0.03 | 0.03 | 0.01 | 0.01 | 0.60 | 0.62 |
| 180 | 0.92 | 11.55 | 13.45 | 8.87 | 0.02 | 0.02 | 0.01 | 0.01 | 0.25 | 0.26 |
| Total | – | – | – | – | 6.8 | 6.0 | 2.1 | 1.7 | 121.9 | 132.4 |

# Supplementary Material 3. Identified LCOEs for the comparable community renewable energy projects to MG 4

Table SM3.1: Comprehensive comparative evaluation of the LCOE and renewable fraction values of MG 4 for the case of Ohakune against those of the comparable international projects.

| Reference | Renewable energy system architecture | Case study site(s) | Climatic conditions | Unsubsidised LCOE [$/kWh][*, †] | Renewable fraction [%] |
|---|---|---|---|---|---|
| Isa et al., 2016 [43] | A grid-tied PV/WT/FC/micro-CHP MG | The Universiti Kebangsaan Malaysia Medical Centre, Malaysia | Tropical rainforest | 0.13 | 82 |
| Hosseinalizadeh et al., 2016 [44] | An on-grid PV/WT/BESS/FC MG | Four villages in Iran, namely Moaleman, Ghadamgah, Marvdasht, and Nikouyeh | Diverse climatic conditions | 0.76–0.96 | 100 |
| Shang et al., 2016 [45] | An insular PV/WT/BESS/DG MG | An unnamed island near Singapore | Tropical/equatorial | 0.17 | 100 |
| Boussetta et al., 2017 [46] | A grid-connected PV/WT/BESS MG | The city of Dakhla, Morocco | Moderate and subtropical | 0.14 | 72.5 |
| Akinyele, 2017 [47] | A non-grid-connected PV/WT/BESS/DG nano-grid | A village in Gwagwalada-Abuja, Nigeria | Tropical | 0.44–0.76 | 70 |
| Chauhan and Saini, 2017 [48][‡] | A stand-alone PV/WT/BESS/DG/BP/MHPP MG | Chamoli district, Uttarakhand state, India | Warm temperate | 0.11–0.15 | 100 |
| Zheng et al., 2018 [49][‡] | A grid-tied PV/BP/boiler MG | Davis, CA, USA | Mediterranean | 0.08–0.30 | N/A[§] |
| Fu et al., 2018 [50] | Stand-alone solar PV systems | U.S.-wide | Diverse climatic conditions | 0.16–0.20 | 100 |
| Phurailatpam et al., 2018 [51] | A grid-connected PV/WT/BESS MG | A village in Palari Tehsil, India | Tropical monsoon | 0.31 | 69.1 |
| Ramli et al., 2018 [52] | An off-grid PV/WT/BESS/DG MG | The city of Yanbu, Saudi Arabia | Hot dry | 0.08–0.12 | 95.6 |
| Li, 2019 [53] | A grid-independent PV/BESS/FC MG | A community centre in Kunming, China | Humid subtropical | 0.98 | 100 |
| Ghenai and Bettayeb, 2019 [54] | An off-grid PV/BESS/FC MG | The University of Sharjah's administration building, United Arab Emirates | Desert | 0.25 | 75.8 |

| | | | | | |
|---|---|---|---|---|---|
| Adefarati and Bansal, 2019 [55] | A stand-alone PV/WT/BESS/DG MG | An unspecified rural community in South Africa | Mediterranean | 0.15–0.25 | N/A[§] |
| Rezk et al., 2019 [56] | A grid-independent PV/FC hybrid renewable energy system | The city of Minya, Egypt | Mediterranean | 0.09 | 100 |
| Nagapurkar and Smith, 2019 [57] | A grid-connected PV/WT/BESS/BG/FC MG | Three U.S. cities, namely Tucson, AZ, Lubbock, TX, and Dickinson, ND | Diverse climatic conditions | 0.37–0.46 | N/A[§] |
| Subramanyam et al., 2020 [58] | A grid-connected PV/WT/BESS MG | Four cities, namely Wellington in New Zealand, Aswan in Egypt, Yuma in AZ, and San Francisco in CA | Diverse climatic conditions | 0.05–0.15 | N/A[§] |
| Al-Ghussain et al., 2020 [59] | A grid-tied PV/WT/PHSS/FC MG | Middle East Technical University Northern Cyprus Campus in Guzelyurt, Cyprus | Mediterranean | 0.21 | 91.8 |
| This study (MG 4) | A grid-tied PV/WT/MHPP/BP/FC/BESS/SC MG | The town of Ohakune, New Zealand | Temperate | 0.14 | 100 |

Key: AZ = Arizona state, BESS = Battery Energy Storage System, BG = Biodiesel Generator, BP = Biopower Plant, CA = California state, CHP = Combined Heat and Power, DG = Diesel Generator, FC = Fuel Cell, MG = Micro-Grid, MHPP =Micro-Hydro Power Plant, ND = North Dakota state, PHSS = Pumped-Hydro Storage System, PV = Photovoltaic, SC = Super-Capacitor, TX = Texas state, WT = Wind Turbine.

[*] For cases where different configurations of the proposed system are investigated, or the conceptualised system is optimised under different climatic conditions, or the optimisation process is carried out in a multi-objective search space or in a stochastic way, the value of LCOE is reported as a range, rather than a certain value.

[†] Where appropriate, the LCOE values were adjusted to 2019 NZ dollars.

[‡] Only two of the previous studies focusing on the DR-integrated optimal planning of renewable energy systems, which fit the selected criteria for benchmarking studies, have provided information on their proposed systems' LCOE values.

[§] N/A stands for not available.

## Supplementary Material 4. Summary of the previous work on the stochastic capacity planning optimisation of MGs

Table SM4.1: Summary of the most notable previous studies on the optimal stochastic investment planning of RSESs.

| Reference (authors, year of publication) | System architecture | Uncertainty quantification technique | Uncertain factor(s) | Operational scheduling (with arbitrage) | Optimisation approach |
|---|---|---|---|---|---|
| Martins and Borges, 2011 [60] | An active distribution network with a high penetration of renewables | MCS | WSFs, SIFs, LDFs, load growth | × (×) | GA |
| Kahrobaee et al., 2013 [3] | A smart home with distributed energy resources | MCS | WSFs, SIFs, LDFs, EPFs | × (×) | PSO |
| Cardoso et al., 2014 [4] | A grid-tied MG incorporating PV and ST panels, ICEs, MTs, GTs, FCs, HEs, ACs, and SESS | MCS | EV driving patterns | ✓ (×) | DER-CAM tool |
| Hassanzadeh-Fard et al., 2015 [8] | A grid-connected PV/FC/BESS/SC MG | MATLAB's white noise block | WSFs, SIFs, LDFs | × (×) | PSO |
| Atia and Yamada, 2016 [12] | An on-grid PV/WT/BESS MG | MCS | WSFs, SIFs | × (×) | MILP |
| Pazouki and Haghifam, 2016 [11] | An energy hub equipped with WTs, CHP units, boilers, BESS, and a thermal energy storage system | MCS | WSFs, LDFs, EPFs | ✓ (×) | MINLP |
| Schachter et al., 2016 [13] | A smart distribution network with deep penetration of DERs | MCS | DR events, peak load demand growth | × (×) | Simple matching of supply and demand |
| Hussain et al., 2017 [61] | A tri-generation network incorporating CHP units, DGs, and boilers | Scenario analysis | LDFs | ✓ (×) | PSO |

| | | | | | |
|---|---|---|---|---|---|
| Yu et al., 2017 [16] | A municipal energy system equipped with coal, gas, wind, solar, and biomass generation plants | MCS | LDFs, techno-economic variables, EV charging schedules | × (×) | RFP |
| Nojavan et al., 2017 [62] | A representative highly renewable distribution grid | MCS | WSFs, LDFs | × (×) | MIP |
| Nojavan et al., 2017 [17] | A grid-connected MG adapted from the standard IEEE 33-bus with a high share of renewables | MCS | WSFs, LDFs | × (×) | MINLP |
| Chen et al., 2018 [21] | A grid-tied PV/WT/BESS MG | MCS | WSFs, SIFs, LDFs | × (×) | MILP |
| Xiao et al., 2018 [63] | A modified standard IEEE 33-bus distribution system | MCS | WSFs, LDFs | ✓ (×) | MBGO |
| Zheng et al., 2018 [22] | An on-grid multiple-energy-carrier MG integrating WTs, PV panels, a BP, a BESS, a boiler, and a thermal energy storage system | MCS | WSFs, SIFs, techno-economic variables | ✓ (×) | LP |
| Zheng et al., 2018 [49] | A grid-connected multi-carrier MG accommodating PV panels, a BP, and a boiler | MCS | WSFs, SIFs, LDFs, techno-economic variables | ✓ (×) | LP |
| Prathapaneni and Detroja, 2019 [30] | An off-grid solar PV/BESS/diesel MG | CCP | WSFs, SIFs, LDFs | ✓ (×) | MINLP |
| Mansouri et al., 2020 [39] | An energy hub integrating CHP units, solar PV panels, BESS, boilers, and chillers | MCS | SIFs, LDFs | ✓ (×) | PSO |
| Masoumi et al., 2020 [64] | A grid-tied MG integrating wind and solar PV resources, as well as BESS | ANN | SIFs, WSFs, LDFs | × (×) | PSO |
| Amir and Azimian, 2020 [38] | A grid-connected multi-carrier MG incorporating solar PV generation, thermal storage, CHP units, and BESS | MCS | SIFs, LDFs, EPFs | ✓ (×) | GA |

| | | | | | |
|---|---|---|---|---|---|
| Wu et al., 2020 [65] | A grid-connected MG integrating solar PV generation and BESS | Interval analysis | SIFs, LDFs | ✓ (×) | MILP |
| Barbaro and Castro, 2020 [66] | An off-grid solar PV/WT/geothermal/DG/BESS MG | MCS | WSFs, LDFs | × (×) | PSO |
| Wei et al., 2020 [67] | A grid-tied multi-energy MG integrating WTs, solar PV panels, BESS, CHP units, and thermal storage | IGDT | WSFs, SIFs, LDFs | ✓ (×) | MILP |
| This study | A grid-tied solar PV/WT/MHPP/BP/FC/BESS/SC MG | MCS | WSFs, SIFs, ATFs, RSFs, LDFs, EPFs | ✓ (✓) | MFOA |

Key: ACs = Absorption Chillers, ANN = Artificial Neural Network, ATFs = Ambient Temperature Forecasts, BESS = Battery Energy Storage System, BP = Biopower Plant, CCP = Chance-Constrained Programming, CHP = Combined Heat and Power, DER-CAM = Distributed Energy Resources-Customer Adoption Model, DERs = Distributed Energy Resources, DG = Diesel Generator, DR = Demand Response, EPFs = Electricity Price Forecasts, EV = Electric Vehicle, FC = Fuel Cell, GA = Genetic Algorithm, GTs = Gas Turbines, HEs = Heat Exchangers, ICEs = Internal Combustion Engines, IGDT = Information Gap Decision Theory, LDFs = Load Demand Forecasts, LP = Linear Programming, MBGO = Metamodel-Based Global Optimisation, MCS = Monte Carlo Simulation, MFOA = Moth-Flame Optimisation Algorithm, MG = Micro-Grid, MHPP = Micro-Hydro Power Plant, MILP = Mixed-Integer Linear Programming, MINLP = Mixed-Integer Nonlinear Programming, MIP = Mixed-Integer Programming, MTs = Micro-Turbines, PSO = Particle Swarm Optimisation, PV = Photovoltaic, RFP = Robust Flexible Programming, RSFs = River Streamflow Forecasts, SC = Super-Capacitor, SESS = Stationary Electricity Storage System, SIFs = Solar Irradiance Forecasts, ST = Solar Thermal, WSFs = Wind Speed Forecasts, WTs = Wind Turbines.

# Bibliography (Supplementary Material)


[1] V. F. Martins and C. L. T. T. Borges, "Active Distribution Network Integrated Planning Incorporating Distributed Generation and Load Response Uncertainties," *IEEE Trans. Power Syst.*, vol. 26, no. 4, pp. 2164–2172, 2011.

[2] A. Ehrenmann and Y. Smeers, "Stochastic equilibrium models for generation capacity expansion," in *Stochastic optimization methods in finance and energy*, Springer, 2011, pp. 273–310.

[3] S. Kahrobaee, S. Asgarpoor, and W. Qiao, "Optimum sizing of distributed generation and storage capacity in smart households," *IEEE Trans. Smart Grid*, vol. 4, no. 4, pp. 1791–1801, 2013.

[4] G. Cardoso *et al.*, "Optimal investment and scheduling of distributed energy resources with uncertainty in electric vehicle driving schedules," *Energy*, vol. 64, pp. 17–30, 2013.

[5] M. F. Shaaban and E. F. El-Saadany, "Accommodating High Penetrations of PEVs and Renewable DG Considering Uncertainties in Distribution Systems," *IEEE Trans. Power Syst.*, vol. 29, no. 1, pp. 259–270, 2014.

[6] A. Zakariazadeh, S. Jadid, and P. Siano, "Smart microgrid energy and reserve scheduling with demand response using stochastic optimization," *Int. J. Electr. Power Energy Syst.*, vol. 63, pp. 523–533, 2014.

[7] C. Li, Z. Dong, G. Chen, F. Luo, and J. Liu, "Flexible transmission expansion planning associated with large-scale wind farms integration considering demand response," *IET Gener. Transm. Distrib.*, vol. 9, no. 15, pp. 2276–2283, 2015.

[8] H. Hassanzadeh-Fard, S. M. Moghaddas-Tafreshi, and S. M. Hakimi, "Optimization of grid-connected microgrid consisting of PV/FC/UC with considered frequency control," *Turkish J. Electr. Eng. Comput. Sci.*, vol. 23, no. 1, pp. 1–16, 2015.

[9] S. Behboodi, D. P. Chassin, C. Crawford, and N. Djilali, "Renewable resources portfolio optimization in the presence of demand response," *Appl. Energy*, vol. 162, pp. 139–148, 2016.

[10] C. Rathore and R. Roy, "Impact of wind uncertainty, plug-in-electric vehicles and demand response program on transmission network expansion planning," *Int. J. Electr. Power Energy Syst.*, vol. 75, pp. 59–73, 2016.

[11] S. Pazouki and M. R. Haghifam, "Optimal planning and scheduling of energy hub in presence of wind, storage and demand response under uncertainty," *Int. J. Electr. Power Energy Syst.*, vol. 80, pp. 219–239, 2016.

[12] R. Atia and N. Yamada, "Sizing and Analysis of Renewable Energy and Battery Systems in Residential Microgrids," *IEEE Trans. Smart Grid*, vol. 7, no. 3, pp. 1204–1213, 2016.

[13] J. A. Schachter, P. Mancarella, J. Moriarty, and R. Shaw, "Flexible investment under uncertainty in smart distribution networks with demand side response: Assessment framework and practical implementation," *Energy Policy*, vol. 97, pp. 439–449, 2016.

[14] J. A. Schachter and P. Mancarella, "Demand Response Contracts as Real Options: A Probabilistic Evaluation Framework Under Short-Term and Long-Term Uncertainties," *IEEE Trans. Smart Grid*, vol. 7, no. 2, pp. 868–878, 2016.

[15] J. Comden, Z. Liu, and Y. Zhao, "Harnessing flexible and reliable demand response under customer uncertainties," *8th Int. Conf. Future Energy Systems*, 2017, pp. 67–79.

[16] L. Yu, Y. P. Li, G. H. Huang, and C. J. An, "A robust flexible-probabilistic programming method for planning municipal energy system with considering peak-electricity price and electric vehicle," *Energy Convers. Manag.*, vol. 137, pp. 97–112, 2017.

[17] S. Nojavan, M. Majidi, and N. N. Esfetanaj, "An efficient cost-reliability optimization model for optimal siting and sizing of energy storage system in a microgrid in the presence of responsible load management," *Energy*, vol. 139, pp. 89–97, 2017.

[18] R. Hejeejo and J. Qiu, "Probabilistic transmission expansion planning considering distributed generation and demand response programs," *IET Renew. Power Gener.*, vol. 11, no. 5, pp. 650–658, 2017.

[19] A. S. Kocaman, E. Ozyoruk, S. Taneja, and V. Modi, "A stochastic framework to evaluate the impact of agricultural load flexibility on the sizing of renewable energy systems," *Renew. Energy*, vol. 152, pp. 1067–1078, 2020.

[20] M. Majidi, S. Nojavan, and K. Zare, "Optimal Sizing of Energy Storage System in A Renewable-Based Microgrid Under Flexible Demand Side Management Considering Reliability and Uncertainties," *J. Oper. Autom. Power Eng.*, vol. 5, no. 2, pp. 205–214, 2017.

[21] J. Chen *et al.*, "Optimal sizing for grid-tied microgrids with consideration of joint optimization of planning and operation," *IEEE Trans. Sustain. Energy*, vol. 9, no. 1, pp. 237–248, 2018.

[22] Y. Zheng, B. M. Jenkins, K. Kornbluth, and C. Træholt, "Optimization under uncertainty of a biomass-integrated renewable energy microgrid with energy storage," *Renew. Energy*, vol. 123, pp. 204–217, 2018.

[23] M. Husein and I.-Y. Chung, "Optimal design and financial feasibility of a university campus microgrid considering renewable energy incentives," *Appl. Energy*, vol. 225, pp. 273–289, 2018.

[24] F. S. Gazijahani and J. Salehi, "Reliability constrained two-stage optimization of multiple renewable-based microgrids incorporating critical energy peak pricing demand response program using robust optimization approach," *Energy*, vol. 161, pp. 999–1015, 2018.

[25] Y. Zheng, B. M. Jenkins, K. Kornbluth, A. Kendall, and C. Træholt, "Optimization of a biomass-integrated renewable energy microgrid with demand side management under uncertainty," *Appl. Energy*, vol. 230, pp. 836–844, 2018.

[26] V. B. Hau, M. Husein, I.-Y. Chung, D.-J. Won, W. Torre, and T. Nguyen, "Analyzing the impact of renewable energy incentives and parameter uncertainties on financial feasibility of a campus microgrid," *Energies*, vol. 11, no. 9, p. 2446, 2018.

[27] M. Asensio, P. M. de Quevedo, G. Muñoz-Delgado, and J. Contreras, "Joint Distribution Network and Renewable Energy Expansion Planning Considering Demand Response and Energy Storage—Part I: Stochastic Programming Model," *IEEE Trans. Smart Grid*, vol. 9, no. 2, pp. 655–666, 2018.

[28] M. BiazarGhadikolaei, M. Shahabi, and T. Barforoushi, "Expansion planning of energy storages in microgrid under uncertainties and demand response," *Int. Trans. Electr. Energy Syst.*, vol. 29, no. 11, p. e12110, 2019.

[29] S. M. Hakimi, A. Hasankhani, M. Shafie-khah, and J. P. S. Catalão, "Optimal sizing and siting of smart microgrid components under high renewables penetration considering demand response," *IET Renew. Power Gener.*, vol. 13, no. 10, pp. 1809–1822, 2019.

[30] D. R. Prathapaneni and K. P. Detroja, "An integrated framework for optimal planning and operation schedule of microgrid under uncertainty," *Sustain. Energy, Grids Networks*, vol. 19, p. 100232, 2019.

[31] T. Khalili, A. Jafari, M. Abapour, and B. Mohammadi-Ivatloo, "Optimal battery technology selection and incentive-based demand response program utilization for reliability improvement of an insular microgrid," *Energy*, vol. 169, pp. 92–104, 2019.

[32] Z. Guo, G. Li, M. Zhou, and W. Feng, "Resilient Configuration Approach of Integrated Community Energy System Considering Integrated Demand Response Under Uncertainty," *IEEE Access*, vol. 7, pp. 87513–87533, 2019.

[33] A. Nazari and R. Keypour, "A two-stage stochastic model for energy storage planning in a microgrid incorporating bilateral contracts and demand response program," *J. Energy Storage*, vol. 21, pp. 281–294, 2019.

[34] P. Salyani, M. Abapour, K. Zare, and T. Babri, "Optimal Stochastic Planning of DERs in a Game Theory Framework Considering Demand Response and Pollution Issues," in *Demand Response Application in Smart Grids: Concepts and Planning Issues - Volume 1*, S. Nojavan and K. Zare, Eds. Cham: Springer International Publishing, 2020, pp. 193–214.

[35] M. Basu, "Optimal generation scheduling of hydrothermal system with demand side management considering uncertainty and outage of renewable energy sources," *Renew. Energy*, vol. 146, pp. 530–542, 2020.

[36] M. Farrokhifar, F. H. Aghdam, A. Alahyari, A. Monavari, and A. Safari, "Optimal energy

management and sizing of renewable energy and battery systems in residential sectors via a stochastic MILP model," *Electr. Power Syst. Res.*, vol. 187, p. 106483, 2020.

[37] M. Sugimura *et al.*, "Optimal sizing and operation for microgrid with renewable energy considering two types demand response," *J. Renew. Sustain. Energy*, vol. 12, no. 6, p. 65901, 2020.

[38] V. Amir and M. Azimian, "Dynamic Multi-Carrier Microgrid Deployment Under Uncertainty," *Appl. Energy*, vol. 260, p. 114293, 2020.

[39] S. A. Mansouri, A. Ahmarinejad, M. S. Javadi, and J. P. S. Catalão, "Two-stage stochastic framework for energy hubs planning considering demand response programs," *Energy*, vol. 206, p. 118124, 2020.

[40] S. A. Mansouri, A. Ahmarinejad, M. Ansarian, M. S. Javadi, and J. P. S. Catalao, "Stochastic planning and operation of energy hubs considering demand response programs using Benders decomposition approach," *Int. J. Electr. Power Energy Syst.*, vol. 120, p. 106030, 2020.

[41] X. Yang, Z. Chen, X. Huang, R. Li, S. Xu, and C. Yang, "Robust capacity optimization methods for integrated energy systems considering demand response and thermal comfort," *Energy*, vol. 221, p. 119727, 2021.

[42] B. Zeng, Y. Liu, F. Xu, Y. Liu, X. Sun, and X. Ye, "Optimal demand response resource exploitation for efficient accommodation of renewable energy sources in multi-energy systems considering correlated uncertainties," *J. Clean. Prod.*, vol. 288, p. 125666, 2021.

[43] N. M. Isa, H. S. Das, C. W. Tan, A. H. M. Yatim, and K. Y. Lau, "A techno-economic assessment of a combined heat and power photovoltaic/fuel cell/battery energy system in Malaysia hospital," *Energy*, vol. 112, pp. 75–90, 2016.

[44] R. Hosseinalizadeh, H. S. G, M. S. Amalnick, and P. Taghipour, "Economic sizing of a hybrid (PV–WT–FC) renewable energy system (HRES) for stand-alone usages by an optimization-simulation model: Case study of Iran," *Renew. Sustain. Energy Rev.*, vol. 54, pp. 139–150, 2016.

[45] C. Shang, D. Srinivasan, and T. Reindl, "An improved particle swarm optimisation algorithm applied to battery sizing for stand-alone hybrid power systems," *Int. J. Electr. Power Energy Syst.*, vol. 74, pp. 104–117, 2016.

[46] M. Boussetta, R. El Bachtiri, M. Khanfara, and K. El Hammoumi, "Assessing the potential of hybrid PV–Wind systems to cover public facilities loads under different Moroccan climate conditions," *Sustain. Energy Technol. Assessments*, vol. 22, pp. 74–82, 2017.

[47] D. Akinyele, "Techno-economic design and performance analysis of nanogrid systems for households in energy-poor villages," *Sustain. Cities Soc.*, vol. 34, pp. 335–357, 2017.

[48] A. Chauhan and R. P. Saini, "Size optimization and demand response of a stand-alone integrated renewable energy system," *Energy*, vol. 124, pp. 59–73, 2017.

[49] Y. Zheng, B. M. Jenkins, K. Kornbluth, A. Kendall, and C. Træholt, "Optimization of a biomass-integrated renewable energy microgrid with demand side management under uncertainty," *Appl. Energy*, vol. 230, pp. 836–844, 2018.

[50] R. Fu, D. J. Feldman, and R. M. Margolis, "*US solar photovoltaic system cost benchmark: Q1 2018*," National Renewable Energy Lab. (NREL), Golden, CO (United States), 2018.

[51] C. Phurailatpam, B. S. Rajpurohit, and L. Wang, "Planning and optimization of autonomous DC microgrids for rural and urban applications in India," *Renew. Sustain. Energy Rev.*, vol. 82, pp. 194–204, 2018.

[52] M. A. M. Ramli, H. R. E. H. Bouchekara, and A. S. Alghamdi, "Optimal sizing of PV/wind/diesel hybrid microgrid system using multi-objective self-adaptive differential evolution algorithm," *Renew. Energy*, vol. 121, pp. 400–411, 2018.

[53] C. Li, "Techno-economic study of off-grid hybrid photovoltaic/battery and photovoltaic/battery/fuel cell power systems in Kunming, China," *Energy Sources, Part A Recover. Util. Environ. Eff.*, vol. 41, no. 13, pp. 1588–1604, 2019.

[54] C. Ghenai and M. Bettayeb, "Modelling and performance analysis of a stand-alone hybrid solar PV/Fuel Cell/Diesel Generator power system for university building," *Energy*, vol. 171, pp. 180–189, 2019.

[55] T. Adefarati and R. C. Bansal, "Reliability, economic and environmental analysis of a microgrid system in the presence of renewable energy resources," *Appl. Energy*, vol. 236, pp. 1089–1114, 2019.

[56] H. Rezk *et al.*, "Fuel cell as an effective energy storage in reverse osmosis desalination plant powered by photovoltaic system," *Energy*, vol. 175, pp. 423–433, 2019.

[57] P. Nagapurkar and J. D. Smith, "Techno-economic optimization and environmental Life Cycle Assessment (LCA) of microgrids located in the US using genetic algorithm," *Energy Convers. Manag.*, vol. 181, pp. 272–291, 2019.

[58] V. Subramanyam, T. Jin, and C. Novoa, "Sizing a renewable microgrid for flow shop manufacturing using climate analytics," *J. Clean. Prod.*, vol. 252, p. 119829, 2020.

[59] L. Al-Ghussain, R. Samu, O. Taylan, and M. Fahrioglu, "Sizing renewable energy systems with energy storage systems in microgrids for maximum cost-efficient utilization of renewable energy resources," *Sustain. Cities Soc.*, vol. 55, p. 102059, 2020.

[60] V. F. Martins and C. L. T. Borges, "Active distribution network integrated planning incorporating distributed generation and load response uncertainties," *IEEE Trans. Power Syst.*, vol. 26, no. 4, pp. 2164–2172, 2011.

[61] A. Hussain, S. M. Arif, M. Aslam, S. Danial, and A. Shah, "Optimal Siting and Sizing of Tri-Generation Equipment for Developing an Autonomous Community Microgrid Considering Uncertainties," *Sustain. Cities Soc.*, vol. 32, pp. 318–330, 2017.

[62] S. Nojavan, M. Majidi, and K. Zare, "Stochastic multi-objective model for optimal sizing of energy storage system in a microgrid under demand response program considering reliability: A weighted sum method and fuzzy satisfying approach," *J. Energy Manag. Technol.*, vol. 1, no. 1, pp. 61–70, 2017.

[63] H. Xiao, W. Pei, Z. Dong, and L. Kong, "Bi-level planning for integrated energy systems incorporating demand response and energy storage under uncertain environments using novel metamodel," *CSEE J. power energy Syst.*, vol. 4, no. 2, pp. 155–167, 2018.

[64] A. Masoumi, S. Ghassem-Zadeh, S. H. Hosseini, and B. Z. Ghavidel, "Application of neural network and weighted improved PSO for uncertainty modeling and optimal allocating of renewable energies along with battery energy storage," *Appl. Soft Comput.*, vol. 88, p. 105979, 2020.

[65] D. Wu, X. Ma, S. Huang, T. Fu, and P. Balducci, "Stochastic optimal sizing of distributed energy resources for a cost-effective and resilient Microgrid," *Energy*, vol. 198, p. 117284, 2020.

[66] M. Barbaro and R. Castro, "Design optimisation for a hybrid renewable microgrid: Application to the case of Faial island, Azores archipelago," *Renew. Energy*, vol. 151, pp. 434–445, 2020.

[67] J. Wei, Y. Zhang, J. Wang, X. Cao, and M. A. Khan, "Multi-period planning of multi-energy microgrid with multi-type uncertainties using chance constrained information gap decision method," *Appl. Energy*, vol. 260, p. 114188, 2020.